SGP-TR-60

CONF-821214--

PROCEEDINGS
EIGHTH WORKSHOP
GEOTHERMAL RESERVOIR ENGINEERING

December 14-16, 1982

Stanford Geothermal Program
INTERDISCIPLINARY RESEARCH
IN ENGINEERING AND EARTH SCIENCES
Stanford University, Stanford, California

MASTER

DISTRIBUTION OF THIS DOCUMENT IS UNLIMITED

CONF-821214--

STANFORD GEOTHERMAL PROGRAM
STANFORD UNIVERSITY
STANFORD, CALIFORNIA 94305

SGP-TR-60

SGP-TR--60

DE83 015865

PROCEEDINGS OF THE EIGHTH WORKSHOP

ON

GEOTHERMAL-RESERVOIR ENGINEERING

NOTICE
PORTIONS OF THIS REPORT ARE ILLEGIBLE.
It has been reproduced from the best available copy to permit the broadest possible availability.

Stanford University

Stanford, California

December 14-16, 1982

DISCLAIMER

This report was prepared as an account of work sponsored by an agency of the United States Government. Neither the United States Government nor any agency thereof, nor any of their employees, makes any warranty, express or implied, or assumes any legal liability or responsibility for the accuracy, completeness, or usefulness of any information, apparatus, product, or process disclosed, or represents that its use would not infringe privately owned rights. Reference herein to any specific commercial product, process, or service by trade name, trademark, manufacturer, or otherwise does not necessarily constitute or imply its endorsement, recommendation, or favoring by the United States Government or any agency thereof. The views and opinions of authors expressed herein do not necessarily state or reflect those of the United States Government or any agency thereof.

SPONSORED BY

THE GEOTHERMAL AND HYDROPOWER TECHNOLOGIES DIVISION

OF THE DEPARTMENT OF ENERGY

STANFORD-DOE CONTRACT NO. DE-AT03-80SF11459

MASTER

DISTRIBUTION OF THIS DOCUMENT IS UNLIMITED

TABLE OF CONTENTS

Page

Preface . . . . . -vii-

Introduction

The DOE Geothermal Research and Development Program - R.S.H. Toms 1

Hydrothermal Systems

Geothermal Reservoirs in Hydrothermal Convection Systems - M.L. Sorey 5

Geologic and Preliminary Reservoir Data on the Los Humeros Geothermal System, Puebla, Mexico - H. Ferriz 19

A Fieldwide Reservoir Engineering Analysis of the Pilgrim Springs, Alaska, Geothermal Reservoir - M.J. Economides, C.A. Ehlig-Economides, J.F. Kunze and B. Lofgren 25

Engineering and Geological Analyses of the Geothermal Energy Potential of Selected Sites in the State of Alaska - M.J. Economides, J.A. Ansari, G.N. Arce and J.W. Reeder 31

Hydrothermal Alteration and Tectonic Setting of Intrusive Rocks from East Brawley, Imperial Valley: An Application of Petrology to Geothermal Reservoir Analysis - M. Keskinen and J. Sternfeld 39

Chemical and Isotopic Studies of the Coso Geothermal Area R.O. Fournier and J.M. Thompson 45

Field Development

Overview of Cerro Prieto Studies - M.J. Lippmann 49

Hydrologic Changes at Tauhara Field due to Exploitation of Wairakei Field - R.G. Allis 67

Reservoir Characterization of the Ribeira Grande (Azores) Field L. Mete and J. Rivera-R. 73

Well Testing

Interpretation of Redondo Creek Field Pressure Buildup Tests J.B. Fallon 91

Evaluation of Injection Test Data from a Baca Well T.D. Riney and S.K. Garg 97

Interpretation of Nonisothermal Step-Rate Injection Tests S. Benson 103

The Measurement of Permeability by Injection Tests - M.A. Grant 111

Toward A Two-Equation Method for Geothermal Simulation of Fractured Porous Reservoirs - D.E. Dougherty and G.F. Pinder 115

Well Test Analysis for Naturally Fractured Reservoirs - G. DaPrat 119

Page

Two-Phase Flow

An Experiment in Relative Permeabilities and Two-Phase Transient Theory - M.A. Grant, R.B. Glover and M.W. Killup 127

A Modified Gas Correction for the Lip-Pressure Method M.A. Grant, R. James and P.F. Bixley 133

Estimating Reservoir Properties and Well Performance using Surface Production Data - V.T. Hoang 137

Flashing Flow in Fractured Geothermal Reservoirs A.J. Menzies, J.S. Gudmundsson and R.N. Horne 143

Description of a Geothermal Reservoir Simulator 'NSCGREATS' and a Preliminary Simulation of the Kirishima Field - M. Tachimori 149

A Numerical Simulation Model for Vertical Flow in Geothermal Wells M. Tachimori 155

Geophysics and Well Logging

Resistivity Monitoring of Fluid Migration at the Cerro Prieto Field N.E. Goldstein, K. Pruess, M.J. Wilt and G.S. Bodvarsson 161

The Movement of Geothermal Fluid in the Cerro Prieto Field as Determined from Well Logs and Reservoir Engineering Data S.E. Halfman, M.J. Lippmann, R. Zelwer 171

Monitoring Fluid Depletion at The Geysers by the Gravity Change/Subsidence Ratio - R.G. Allis 177

Comparison of Subsidence at Wairakei, Broadlands and Kawerau Fields, New Zealand - R.G. Allis 183

Resistivity Logging of Fractured Basalt - V. Stefansson, G. Axelsson, O. Sigurdsson 189

Effects of Temperature and Stress on the Compressibilities, Thermal Expansivities, and Porosities of Cerro Prieto and Berea Sandstone to 9000 psi and 280 °C - E. Contreras, E. Iglesias and F. Bermejo 197

Effects of Contamination by Geothermal Drilling Mud on Laboratory Determinations of Sandstone Pore Properties: An Evaluation H. Arenas, E. Iglesias, G. Izquierdo, M. Guevara, R. Oliver and S. Santoyo 205

Simulation

Modeling Studies of the Natural State of the Krafla Geothermal Field, Iceland - G.S. Bodvarsson, K. Pruess, V. Stefansson and E.T. Eliasson 211

Proximity Functions for Modeling Fluid and Heat Flow in Reservoirs with Stochastic Fracture Distributions - K. Pruess and K. Karasaki 219

Page

Quasi-Three-Dimensional Model Applied to Geothermal Reservoirs Systems with Heat Flow from Deeper Zones - S. Hirakawa and M. Ichikawa 225

Reservoir Simulation Studies on the Cerro Prieto Geothermal Field: Preliminary Results - M. Castaneda, A. Abril, V. Arellano and R. Marques 231

Petrothermal and Geopressured Energy

The Stimulation of a Hot-Dry-Rock Geothermal Reservoir in the Cornubian Granite, England - A.S. Batchelor 237

Recent Results: Los Alamos Hot-Dry-Rock Project - D.W. Brown 249

Heat Extraction Modeling of the Stanford Hydrothermal Reservoir Model - A. Hunsbedt, S.T. Lam, P. Kruger and K. Pruess 255

Analysis of Sweet Lake Geopressured-Geothermal Aquifer M. Andrade, F. Rago, H. Ohkuma, K. Sepehrnorri, E. Peters and M. Dorfman 261

Problems Associated with Application of a Wellbore Heat Transmission Computer Code - Z.V. Dash and G.A. Zyvoloski 269

Reinjection

Hydrothermal Injection Experiments at the Raft River KGRA, Idaho W.F. Downs, R.E. McAtee, R.M. Capuano and W. Still 275

Response of RRGI and RRGI 7 to Injection during the 5 MW Plant Operations March 25-June 15, 1982 - P.A. Skiba 279

Dispersion in Fracture Networks - L.C. Hull and K.N. Koslow . . . . . .

Retention of Chemical Tracers in Geothermal Reservoirs R.N. Horne, K.A. Breitenbach and M.P. Fossum 289

Reservoir Chemistry

Fluid Geochemistry Applications in Reservoir Engineering (Vapor-Dominated System) - F. D'Amore, R. Celati and C. Calore 295

A Summary of the Chemical Characteristics of the HGP-A Well: Puna, Hawaii - D.M. Thomas 309

Interpretation of Radon Concentration in the Serrazzano Zone of the Larderello Geothermal Field - L. Semprini, P. Kruger and F. D'Amore 315

Geochemical Evidence of Natural Recharge in Larderello and Castelnuovo Areas - C. Calore, R. Celati, F. D'Amore and P. Noto 323

Thermal Waters and the Effect of Their Use on the Environment I.M. Dvorov and V.I. Dvorov 329

List of Participants 335

PREFACE

The Eighth Workshop on Geothermal Reservoir Engineering was held at Stanford University 14-16 December 1982. The attendance was the highest ever with 123 participants of which 17 were from 6 foreign countries.

The purposes of the Workshop were to bring together researchers, engineers and managers involved in geothermal reservoir studies and developments, and to provide for prompt and open reporting of progress and the exchange of ideas. There were 39 technical papers presented at the Workshop and 7 additional papers appear in these Proceedings.

This year three experts in their fields were invited to give keynote presentations at the Workshop. They were M.L. Sorey on "Geothermal Reservoirs in Hydrothermal Convection Systems," A.J. Batchelor on "The Stimulation of a Hot-Dry-Rock Reservoir in the Cornubian Granite, England" and F. D'Amore on "Fluid Geochemistry Applications in Reservoir Engineering: Vapor Dominated Systems." The keynote speakers provided the highlights of the Workshop. This format will be retained for the 1983 Workshop.

The introductory speech was given by R.S.H. Toms of the U.S. Department of Energy and the banquet speaker was R.P. Wischow of Pacific Gas and Electric Company.

An important contribution was made to the Workshop by the Chairmen of the technical sessions. They were D.E. White (Hydrothermal Systems), C. Bufe (Field Development), H.J. Ramey, Jr. (Well Testing), J.R. Counsil (Two-Phase Flow), P.M. Wright (Geophysics and Well Logging), P.G. Atkinson (Simulation), A.S. Abou-Sayed (Petrothermal and Geopressured Energy), S.M. Benson (Reinjection), D.K. Bird (Reservoir Chemistry) and P. Kruger (Special Topics). Active discussion by the majority of the participants was apparent both in and outside the Workshop arena.

The Proceedings of previous Workshops are now out of print. There is still a great demand for these so the Stanford Geothermal Program is having the first six volumes reprinted in two books. These should become available by the middle of 1983.

The Workshop was organized by the Stanford Geothermal Program faculty, staff and students. We would like to thank Jean Cook, Joanne Hartford, Terri Ramey, Amy Osugi, and Marilyn King for their valuable help with the Workshop and the Proceedings, and Avrami Sageev and other students for arranging and operating the audio-visual equipment.

The Workshop was supported by the U.S. Department of Energy through Contract DE-AT03-80SF11459. We are certain that all the participants join us in our appreciation of this continued support.

January 1983
H.J. Ramey, Jr.; P. Kruger; R.N. Horne; W.E. Brigham; F.G. Miller; J.S. Gudmundsson

DISCLAIMER

This report was prepared as an account of work sponsored by an agency of the United States Government. Neither the United States Government nor any agency Thereof, nor any of their employees, makes any warranty, express or implied, or assumes any legal liability or responsibility for the accuracy, completeness, or usefulness of any information, apparatus, product, or process disclosed, or represents that its use would not infringe privately owned rights. Reference herein to any specific commercial product, process, or service by trade name, trademark, manufacturer, or otherwise does not necessarily constitute or imply its endorsement, recommendation, or favoring by the United States Government or any agency thereof. The views and opinions of authors expressed herein do not necessarily state or reflect those of the United States Government or any agency thereof.

DISCLAIMER

Portions of this document may be illegible in electronic image products. Images are produced from the best available original document.

Proceedings Eighth Workshop Geothermal Reservoir Engineering
Stanford University, Stanford, California, December 1982
SGP-TR-60

THE DOE GEOTHERMAL RESEARCH AND DEVELOPMENT PROGRAM

Ronald S. H. Toms

Department of Energy
1000 Independence Avenue, S.W.
Washington, D.C. 20585

ABSTRACT

The author reviews the progress of geothermal development since the Geothermal Steam Act of 1970 and discusses the present status of geothermal technology and the recent accomplishments of the DOE geothermal program. He then describes the present DOE budget picture and program planned by DOE, giving a context for reservoir engineering research and development.

INTRODUCTION

I am pleased to be here today at the 8th Annual Reservoir Engineering Workshop to review for you the DOE geothermal program. As you are aware, DOE has reevaluated its program priorities across the board. This has required a realistic appraisal of our energy options and needs and a redefinition of the Federal role in research and development, in line with the Administration's policy of reducing Federal deficits and reducing interference in the free market.

The Fiscal Year 1983 program is being finalized by Congress and the President and it reflects a transfer of commercialization activities to the private sector and an emphasis on the critical long-range high-risk research and development that industry is not expected to undertake alone.

HISTORICAL REVIEW

To give a context for the present program, I will review briefly the geothermal program of the last twelve years.

In 1970 when the Geothermal Steam Act was passed giving leasing access to public land that contained more than half the geothermal resources, geothermal activity was very small in the United States. Boise and Klamath Falls had rather old district heating systems and Pacific Gas and Electric Company was producing 78 megawatts at The Geysers steam field with no hydrogen sulfide control and with the liquid effluent discharging into a creek. About 100 exploratory wells had been drilled in the Western United States and at that time the key technical barriers were a) the limited knowledge of the nature and extent of the resource, b) the limited knowledge of reservoir behavior under production conditions, c) the high risk and cost of geothermal drilling, d) the unknown cost and the technical challenge of meeting environmental concerns, e) the large total investment cost, f) the unknown economical potential for exploiting geopressured resources and hot dry rock.

The progress in resolving the technical problems, with the help of the USGS, industry, the universities and the DOE Labs has been considerable. Some highlights are:

1. National maps of the potential resource have been produced, with detailed maps for the Western states.

2. About 25% of the resource is considered (by the USGS) to be discovered. Improved geophysical techniques have assisted greatly in this determination.

3. About 600 wells have been drilled. Drilling costs have been reduced by about 25% but still remain high. Fracture zones are still much harder to drill than matrix-permeable rocks.

4. Reservoir models for production capacity and longevity are being used with limited success.

5. Air quality concerns are being met at fairly high cost but injection of spent brine remains a problem area.

6. Binary systems, low cost materials and components, and chemical treatments are becoming available to reduce total power plant cost up to 25% but further reductions are needed.

7. The economic potential of hot dry rock and geopressured are still not known.

A major goal of the Federal program in the last decade was to stimulate the growth of industry and this has resulted in the availability of a number of commercial items in the private sector. These include:

1. Magnetotelluric and passive seismic exploration techniques.

2. Precipitators/clarifiers and scale inhibitors to handle high salinity corrosive brine.

3. Wellhead size flash, total flow and binary power systems.

4. High-temperature elastomers and polymer concretes.

5. Improved drag and roller-bit drills using polycrystalline diamonds and new seals and bearings.

6. Water and mud-driven turbo-drills for directional drilling.

7. Cavitating water-jet cleaning for piping and heat exchangers.

8. High-temperature electronics and sensors for well logging.

CURRENT STATUS

Industry reports that there are now several hundred industrial firms of various sizes involved in geothermal field development and power plant design and construction. Recent estimates show that the U.S. private sector investment in geothermal energy development exceeded $230 million in the year 1981. There are now 19 power plants on line--totalling 902 MW at The Geysers, 30 MW at the Imperial Valley and 3 MW in Hawaii. Forty-three new power plants are planned to be on line by 1990 adding an additional 2234 MW. Direct heat uses totalling 12.5 trillion BTU per year are now operational and a similar amount of additional capacity is in the planning stage.

During the past fiscal year, the DOE program has accomplished a number of important activities including:

1. Completing the proof-of-concept experiment for the hot dry rock system at Fenton Hill.

2. Completing short term tests of the geopressured resource characteristics of nine existing oil and gas wells on the Gulf Coast.

3. Completing negotiations on the final design and long lead time procurement for the 50 MW binary geothermal demonstration project at Heber, California.

4. Completing the operational tests and shut down of the 5 MW pilot plant at Raft River.

5. Developing lost-circulation zone mapping techniques.

6. Completing the evaluation of the helical screw expander in Italy, and transferring it to New Zealand where tests are now well under way.

7. Developing the design and completing the fabrication of carbon dioxide and pH probes for monitoring brines in hydrothermal power systems.

8. Completing the user-coupled hydrothermal resource definition drilling program.

9. Testing seismic and electromagnetic exploration techniques in the geothermal environment for injection monitoring.

Summarizing the present status of the technology and economics of geothermal development, the present picture seems to be:

1. The generation of electricity from vapor-dominated resources is cost-competitive and presents no significant technical problems, other than finding a cost-effective method for H_2S control.

2. The exploitation of liquid-dominated resources is economically marginal except at a few high grade sites.

3. Drilling and completion technology has improved and advanced approaches offering lower costs are emerging.

4. Reservoir uncertainty remains a major problem and it is compounded by the lack of adequate low cost exploration techniques, logging instrumentation and reservoir engineering.

5. The available materials and geochemical techniques are not yet adequate to provide economic solutions for injection of fluids and prevention of corrosion.

6. Environmental control technology is available for air and water emission but only at significantly high cost and the control of subsidence is still an uncertainty.

7. Stimulation of poorly producing wells has proved to be an expensive and uncertain technique.

PRESENT BUDGET PICTURE

In planning the DOE geothermal program for the current fiscal year, we have followed policy guidelines which place an emphasis on research

and development--but without abandoning on-going projects that represent firm earlier commitments. For example, we plan to continue the Heber demonstration plant and to complete the work on the direct heat field experiments. We plan to complete the second-phase loop operation of the hot dry rock research at Fenton Hill and to conclude our work on geopressured well testing.

In fiscal year 1983, we plan to continue working in energy conversion technology associated with moderate temperature resources, including the development of direct contact binary technology and research on the binary fluid equations-of-state and transport properties. We will also continue development of temperature and corrosion resistant materials and conduct research on scale control and slurry elimination. In the geosciences, we plan to continue development and field testing of advanced geoscience technologies to enhance exploration success and reservoir management through improved geophysical and geochemical techniques.

Reservoir engineering is and will continue to be one of the most important aspects of the DOE geothermal technology development program. In the present program structure, we are carrying reservoir engineering under the category of geoscience technology, where we emphasize both resource definition and injection technology. Both of these items fit well within the new priorities and they clearly both require considerable development in the discipline of reservoir engineering.

CONCLUDING REMARKS

I have not attempted to review in any detail the contribution made to geothermal development by reservoir engineering because I can see how well it will be covered in the program before us. I still find it remarkable that we are able to make any conclusions from the scant data we are able to obtain about the phenemona occurring in the unseen depths of the earth. It is through the powerful, theoretical work and the extensive practical work performed by many of the experts here at this conference that we have achieved the present level of understanding and can hope to reach the goals we have set for ourselves. I wish this workshop every success.

Proceedings Eighth Workshop Geothermal Reservoir Engineering
Stanford University, Stanford, California, December 1982
SGP-TR-60

GEOTHERMAL RESERVOIRS IN HYDROTHERMAL CONVECTION SYSTEMS

Michael L. Sorey

U.S. Geological Survey, Menlo Park, California

Abstract Geothermal reservoirs commonly exist in hydrothermal convection systems involving fluid circulation downward in areas of recharge and upwards in areas of discharge. Because such reservoirs are not isolated from their surroundings, the nature of thermal and hydrologic connections with the rest of the system may have significant effects on the natural state of the reservoir and on its response to development. Conditions observed at numerous developed and undeveloped geothermal fields are discussed with respect to a basic model of the discharge portion of an active hydrothermal convection system. Effects of reservoir development on surficial discharge of thermal fluid are also delineated.

Introduction Geothermal reservoirs containing concentrations of recoverable thermal energy exist under a variety of geologic and hydrologic conditions. This paper focuses on reservoirs in hydrothermal convection systems (HCS), in which heat transfer by fluid movement is the dominant process for concentrating thermal energy in reservoirs at exploitable depths. Geothermal reservoirs in conduction-dominated systems which do not involve significant vertical fluid movement are discussed in Muffler (1979), Smith (1978), and Sorey and others (1983), and Batchelor (this volume).

Development of an adequate understanding of basic relationships between fluid, rock, and heat in HCS requires synthesis of information generated in various types of investigations. These include studies of geologic structure and volcanic history, geophysical properties of the subsurface, geochemistry of surface and subsurface fluids, and hydrology. Coupling of results from such studies with data from drilling and well testing provides the best means for locating geothermal reservoirs and evaluating their potential for energy development. The importance of this synthesis is often overlooked, as is the comparison of similarities and differences between HCS in different areas.

The principal components of a HCS are the heat source, the working fluid(s), and the means for moving fluid through the system (permeable rock and pressure gradients). Although differences in the nature of these components give rise to significant variations in detail among HCS, it is possible to identify a simple basic model that describes the essential features of heat and fluid flow in and through reservoirs in most HCS. Various types of HCS discussed in the literature, for example, hot-water, liquid-dominated, vapor-dominated, high-temperature, low-temperature, can be compared and elucidated with reference to this basic model. The model is also useful for discussing changes in HCS accompanying fluid production for energy development.

The existence of HCS is commonly indicated by surficial discharge of hot water or steam. The thermodynamic and chemical states of these surface fluids are related to those of the underlying reservoir fluid. Care must be taken, however, in interpreting subsurface conditions based on the locations and the nature of surficial discharge features. In addition, the possibility of alteration or cessation of surface discharge in response to geothermal development may be an important limiting factor in such development, as discussed below.

Thermal Settings The thermal setting within which a HCS occurs refers to the nature of the heat source at depth and the interactions between circulating fluid and the heat source. Studies of regional conductive heat flow provide the background from which to identify anamolous heat flow and

temperature gradients related to shallow crustal heat sources and/or convective heat transfer (Sass and others, 1981). On a regional scale, it is unlikely that conductive heat flow derived from mantle and lower crustal sources and radioactivity of the upper crust can exceed 3 HFU (130 mW/m^2), or would fall below about 1 HFU (40 mW/m^2). Local areas with heat flow outside this range could be considered anamolous and indicative of the factors noted above.

Shallow crustal heat sources are formed by silicic magma bodies whose residence time can be substantial (10^5 -10^6 years), especially where resupply of magma from deeper levels occurs. Long residence time may also be a requirement for the establishment of extensive HCS and associated geothermal reservoirs. Magma chambers underlying HCS have been delineated at many locations in the western United States, including the Rio Grande Rift and Valles Caldera in New Mexico (Sanford and Einarsson, 1982), Yellowstone Caldera in Wyoming (Iyer, 1979), Long Valley Caldera in California (Steeples and Iyer, 1976), and The Geysers in California (Iyer and others 1979). Depths to such chambers range from about 5 to 10 km; areal extents are on the order of 100 km^2. Magma bodies at shallower levels support HCS in ocean rift environments, as in Iceland (Einarsson, 1978) and Hawaii (Furumoto, 1978), and may function similarly in the Cascade Range in Oregon and California (Muffler and others, 1982, and MacLeod and Sammel, 1982).

Conductive heat flow in regions underlain by shallow crustal heat sources for periods exceeding 10^5 years should be greater than 3 HFU. For 800 °C magma at 8 km, for example, conductive heat flow would approach 5 HFU for average crustal rock thermal conductivities (5 mcal/scm°C). Where a HCS exists above such a heat source, the heat flux calculated by integrating convective and conductive heat output over the total area of the system will exceed 5 HFU. Thus, hydrothermal circulation decreases the "effective depth" to magma, or the depth that would be implied by heat flow observations if convection were absent.

A useful relation was developed by Lachenbruch and Sass (1977) for the "effective depth", He, as a function of mean thermal conductivity, K, magmatic temperature, T, and measured heat flux, q, assuming steady-state conditions:

$$H_e = K\ T\ /\ q \qquad (1)$$

In the case of the Long Valley caldera, q = 13 HFU and from (1), H_e = 3 km for K = 5 mcal/scm°C and T = 800°C. This implies that if hydrothermal circulation has been continuous at near present-day rates for 10^5 years or more, circulation must extend downward to within about 3 km of the magma chamber or to depths of 3-5 km. More detailed numerical simulations indicate that if the present HCS were more recently developed, depths of fluid circulation could be shallower (Sorey, Lewis, and Olmsted, 1978).

Hydrothermal convection systems also develop in regions where shallow crustal heat sources are absent. Most of the identified HCS within the Basin and Range Province occur in regions of slightly elevated crustal heat flow (2-3 HFU) and extentional tectonics. In such systems fluid circulation cannot significantly increase the average crustal heat flow, and under steady-state conditions, average surficial heat flow from conduction and convection cannot exceed the regional value. This places significant constraints on the depth of circulation and the areal extent of HCS.

The area, A, over which circulating fluid must adsorb a portion of the regional heat flow, Δq, can be calculated for steady-state conditions as

$$A = Q\ \Delta T\ c\ /\ \Delta q \qquad (2)$$

where Q = total mass throughflow, ΔT = increase in fluid temperature between recharge and discharge areas, and c = average fluid specific heat. For parameters typical of high-temperature HCS in the Basin and Range (Q = 10 kg/s, ΔT = 200°C, Δq = 2 HFU), an area of 100 km^2 is obtained. Such results tend to preclude circulation systems restricted to a single fault conduit, except for convective activity of short duration or great depth (Welch, Sorey, and Olmsted, 1981).

Estimates of depths of fluid circulation in HCS supported by regional conductive heat flow are dependent on knowledge of the areal extent and the duration of convective activity. Minimum depths of circulation, D_{min}, are given by

$$D_{min} = K\ \Delta T\ /\ q \qquad (3)$$

For K = 5 mcal/scm°C, ΔT = 200°C, and q = 3 HFU, D_{min} = 3.3 km. Downward circulation depresses the temperature distribution relative to the

conduction-only isotherms; upflow has the opposite effect. With reference to (2), values of A decrease as the depth of circulation increases because Δq increases.

Hydrologic Settings Although HCS occur within a variety of geologic and thermal settings, several aspects appear common to those within continental regimes. The dominant source of fluid is of meteoric origin. Studies of stable oxygen and hydrogen isotopes in thermal and non-thermal fluids in many systems demonstrate the meteoric source and in many cases delineate potential recharge areas (Craig, Boato, and White, 1956; Arnason, 1976; Sorey, Lewis, and Olmsted, 1978). Enrichment of He^3 relative to He^4 in thermal fluids (water and/or steam) indicates a component of magmatic origin in HCS in Iceland (Mamyrin and others, 1972), Yellowstone National Park and Lassen Volcanic National Park (Craig and others, 1978), and at Cerro Prieto (Welham and others, 1979). Enrichment of He from magmatic sources is commonly observed in submarine HCS associated with spreading ridges (Lupton, 1979).

An active HCS is one in which fluid circulation is presently occuring, downward in recharge areas and upward toward discharge areas. Because of the potential for chemical self-sealing in discharge areas, HCS can become inactive, in some cases leaving behind reservoirs of stored thermal energy in so-called blind anamolies (Flynn and Trexler, 1982; Phillips Petroleum Co., unpublished data on Desert Peak, NV). In active HCS, secondary permeability created by faulting plays an important role in the establishment of fluid circulation to substantial depths and maintenance of permeability at shallow depths. As noted in the previous section, depths of circulation for high-temperature HCS (>150 °C) can be several kilometers or more. Permeable connections for lateral flow between recharge and discharge areas may also be provided by faulting, although in some cases other mechanisms may be effective (e.g. carbonate and clastic formations and brecciated contact zones). In the extreme, hydrothermal circulation through and above cooling plutons appears to have occurred at depths of up to 10 km through fractures created by differential thermal expansion and thermal fluid pressurizing (Norton and Taylor, 1979; Stefansson and Bjornsson, 1982).

Pressure gradients for moving fluid through HCS are provided by a combination of thermally induced density differences and elevation differences between recharge and discharge areas. Density differences producing pressure differences of tens to hundreds of bars can drive HCS associated with shallow magmatic heat sources. In regional conductive environments, elevation differences appear to be required to initiate convective flow that in turn sets up density differences and additional pressure gradients.

Rates of throughflow under natural conditions are usually limited by overall differences in pressure or head and by rock permeability rather than by recharge potential. Typical throughflow rates for HCS in various areas are listed below.

1. Dixie Valley, NV - 5 kg/s
2. Beowawe, NV - 6 kg/s
3. Grass Valley, NV - 10 kg/s
4. Valles Caldera, NM - 20 kg/s
5. Steamboat Springs, NV - 60 kg/s
6. Long Valley, CA - 250 kg/s
7. Wairakei, NZ - 400 kg/s
8. Yellowstone Caldera, WY - 3000 kg/s

In general, flow rates for HCS with magmatic heat sources (4 - 8) exceed those for HCS in regional conductive environments (1 - 3). Although the magnitude and perhaps the duration of this natural flow provide some indication of thermal and hydrologic conditions at depth, they are by no means definitive. For example, low flow rates may result from low permeability at shallow depths in discharge areas below which high permeability reservoirs may exist.

For high-temperature HCS, depths of fluid curculation where maximum temperatures are attained are generally too great to be drilled directly. Consequently, exploitable reservoirs in such systems (and in many lower-temperature systems) must be fed or charged by upward flow and subsequent lateral leakage of thermal water. In some cases upward flow may be restricted to narrow fault zones and no lateral leakage may have occurred. In HCS where laterally extensive reservoirs do exist, fluid production during development can be expected to induce changes in the natural rate of inflow and outflow that may singificantly affect reservoir response.

Reservoirs in the Natural State The general features of the initial fluid

states within the discharge portions of active HCS can be discussed with reference to the basic model suggested by Donaldson and Grant (1981) and shown in figure 1. The reservoir is pictured as a vertical cylinder containing hot fluid and surrounded by relatively cold water. Under undisturbed conditions, there is an upflow of fluid from below, M_b, and a discharge of fluid at the surface, M_f. Hence, the natural state is dynamic, not static; this upflow is largely responsible for the observed predevelopment pressures, temperatures, and enthalpies. For high-enthalpy inflow, the upflowing fluid boils when its pressure falls to the saturation pressure for its temperature and a zone of two-phase flow extends from that depth to a near-surface zone involving mixing with cold groundwater.

The boundaries of each zone are idealized here. In the field they are diffuse and irregular. Inflow at the base may be locallized along major fault structures, some of which may continue to transmit fluid to the surface. At the margins of the field there usually are intrusions of cold water and outflows of hot water, so that the temperature pattern may be quite disturbed. The single-phase/two-phase boundary can also show considerable uneveness that tends to follow distributions of temperature and gas content. The upper boundary where cold water overlies hotter fluid and where cold water may enter the reservoir under production is often the least regular. Within this zone, large variations in temperature near conduits carrying hot water and steam to the surface would be expected.

Most of these boundary irregularities are caused by variability in the permeability of the rock. In general, the spatial scale of these variations is usually sufficiently small that field-scale computations of initial conditions and effects of production can be accomplished by treating the rock as more uniformly permeable and the boundaries as smooth and regular. Permeability variations cannot, however, be neglected in more detailed exploration and development activities.

The general distributions of pressure and temperature with depth in the basic model are shown in figure 2. The pressure distribution OMA is nearly linear and super-hydrostatic, as would be required to drive the upflow to the surface. Gradients approximately 110 percent of hydrostatic have been measured in several New Zealand fields and in the Redondo Creek field in the Valles caldera (Grant, 1979a; Grant and Garg, 1981). Alternatively, in the case of the Redondo Creek reservoir, the measured pressure gradient of 79 bars/km (0.348 psi/ft) could be considered to correspond to a hydrostatic gradient for water at 260 °C so that fluid upflow is implied in regions where temperature exceeds 260 °C. The temperature distribution in figure 2 is isothermal along CD, and above the depth of boiling, B, temperatures following a boiling point-for-depth curve along OC. Localized effects of cool, near-surface groundwater on these profiles are indicated by the linear portion along OC (commonly much more irregular).

The pressure distribution in the two-phase zone OM remains superhydrostatic as long as both phases flow upward. This is the essential criterion for a liquid -dominated HCS. Pre-exploitation conditions at Wairakei matched those in figure 2, with the boiling level approximately 400 m below land surface and nearly uniform reservoir temperatures near 250 °C. Surficial discharge included both hot springs and fumaroles, with a total outflow of about 400 kg/s (Donaldson and Grant, 1981).

Terms like liquid-dominated and vapor-dominated HCS are actually overly restrictive. Many HCS contain both liquid- and vapor-dominated zones and transitions from one type to another may occur during the lifetime of the system. For example, Grant (1979a) discusses a model that accounts for different physical states within many HCS in mountainous terrain, such as occur in the Valles caldera, Lassen Volcanic National Park, and the Tongonan thermal area in the Philippines. As shown in figure 3, within the upflow region where boiling occurs there is a separation of phases. Liquid flows laterally to discharge as chloride hot springs at lower elevations, and steam rises through a parasitic vapor-dominated zone to discharge as fumaroles or steam-heated springs at higher elevations. Corresponding pressure distributions show liquid-dominated conditions in the region of choride spring discharge and beneath the vapor zone. Vapor-static conditions in the steam zone are overlain by a near-surface condensate layer where pressures are hydrostatic. Note that pressures in and below the two-phase zone are controlled by the elevation of the chloride springs and appear subhydro-

static with respect to elevations of the steam-heated springs.

Unpublished numerical simulations indicate that the flow system pictured in figure 3a could develop from an initial state involving high-enthalpy, liquid-dominated upflow to the surface. Necessary conditions appear to be (1) opening of an outlet for liquid at lower elevations and (2) low permeability near-surface rocks. Condition (2) is analogous to a low-permeability caprock above the two-phase reservoir and is required to prevent liquid from recharging and quenching the reservoir after the low-elevation outlet is created. Based on data for the Valles system (Union Oil Co., 1978) and the Tongonan system (Whittome and Smith, 1979), these conditions appear reasonable.

Additional variations on the basic model in figure 1 make it more applicable to other geothermal fields. The enthalpy and flow rate of the base inflow are critical parameters in this regard. For low enthalpy inflow, or higher enthalpy inflow at low flow rates, boiling may only occur near the surface or be non-existent. Such systems, as occuring at Raft River, Idaho, and Klamath Falls, Oregon, have been termed low- or intermediate-temperature systems. With high enthalpy inflow, the reservoir can be two-phase down to exploitable drilling depths. In addition, the presence of significant concentrations of non-condensible gas lowers the range of reservoir temperatures for which boiling occurs and so tends to increase the depth of boiling (Pritchett and others, 1981). Such conditions exist in New Zealand fields at Broadlands (boiling to 1.5 km) and Ngawha (boiling to 4 km).

Hydrothermal convection systems in which extensive vapor-dominated conditions prevail throughout the drillable depths and minimal surficial fluid discharge is observed fit the usual description of a vapor-dominated reservoir. As observed at The Geysers in California, Larderello in Italy, and Kawah Kamojang in Indonesia, circulation of steam and slightly mobile liquid occurs within the reservoir in the natural state; giving rise to relatively large heat flow at the surface.

Conditions leading to the development of vapor-dominated reservoirs are conjectural. White, Muffler, and Truesdell (1971) suggest evolution from an early hot-water stage as net discharge exceeds recharge and steam boils from a declining water table. Pruess and Truesdell (1980) attempted to numerically model this type of development by applying a potent heat source (190 HFU) to the base of a cylinder whose upper boundary was held at 1 bar and 10°C. During a transient period lasting for 93,000 years, convection under all-liquid conditions gave way to two-phase conditions beneath a low-permeability caprock layer. The establishment of vapor-dominated conditions, however, could not be determined from the results presented. Alternatively, the model presented in figure 3 suggests that vapor-dominated reservoirs could evolve in HCS with lateral outflow of liquid and upward migration of steam. Once a vapor zone is established, chemical deposition could act to restrict upflow, while continued lateral outflow induces boiling and expansion of the vapor zone.

Reservoir Exploitation The response of a geothermal reservoir in an active HCS to exploitation involves changes in mass and energy storage within the reservoir and motion of boundaries connecting the reservoir with the rest of the system. The basic model (figure 1) provides a useful reference for discussion of these effects.

The initial response to production is a decline in reservoir pressure in the production zone. With time pressure declines spread horizontally and vertically. Pressure declines can be expected to extend downward roughly twice the depth of the production zone (Grant, 1977a). In figure 1, induced inflow of cooler water from the sides of the reservoir is indicated by the inward bow of the dashed lines along the sides of the reservoir. An increase in base inflow, M_b, is not indicated in figure 1 because in most high-temerature HCS pressure drops accompanying production remain small compared with total pressure differences driving the throughflow. In practice, it is difficult to distinguish between recharge induced from cooler regions surrounding the reservoir and any enhancement of throughflow since both reach the production zone as hot water (until cold-water breakthrough occurs).

Reductions in reservoir pressure tend to cause reductions in the surface discharge, M_f, resulting in an increase in the net inflow of thermal water to the reservoir ($M_b - M_f$). The effects of this increase in inflow on reservoir productivity (discharge/

pressure decline) depend on the relative magnitude of M_b compared with well discharge, M_w. Data listed previously for throughflow rates in HCS indicate that in most cases $M_w >> M_b$. However, if a large fraction of the well discharge is injected into the reservoir, capturing the natural throughflow by reducing M_f to zero could significantly increase reservoir productivity.

Where a near-surface zone of cold groundwater overlies the reservoir, the potential exists for cold water to be drawn downward into production zones. Differences in the extent and timing of this cold-water fingering at various developed fields suggest that it may be more important for reservoirs in sedimentary rocks (like at Cerro Prieto, Mexico) than for reservoirs in fractured rocks (like Wairakei) (Grant and others, 1981), although other factors may be involved.

Motion of the cold side boundaries occurs as water from surrounding regions pushes hot water toward the production area and mines heat from the reservoir rocks. The rate of inward movement is considerably slower than the actual fluid velocity; in uniformly permeable rocks, tens to hundreds of years may be required for cold water to reach production zones (Robinson, 1977). In some fractured reservoirs, more rapid quenching of wells along high-permeability channels can occur (Horne, 1981).

The magnitude of induced recharge depends primarily on reservoir pressure declines and permeabilities in the surrounding region. In general, such permeabilities are much lower than reservoir values - in vapor-dominated reservoirs, the former may be effectively zero. At Wairakei, reservoir permeabilities on the order of 100 md (10^{-9}cm^2) exist within a region of permeability on the order of 10 md (Fradkin, Sorey, and McNabb, 1981; Mercer and Faust, 1979). Models of the response of the Wairakei reservoir to production and repeat gravity measurements (Hunt, 1977) indicate that with approximately 30 bars of reservoir pressure decline the rate of induced recharge is nearly equal to well discharge.

Within the exploited reservoir, pressure declines induce changes in fluid properties. Production from single-phase zones (liquid or steam) causes a decrease in fluid density, ρ_f, and a decrease in rock porosity, ϕ. The associated change in fluid mass per unit reservoir volume is given by

$$\Delta M = \rho_f \, \phi (c_r + c_f) \, \Delta P$$

where c_r = rock compressibility $(\phi^{-1} \partial\phi / \partial P)$ and c_f = fluid compressibility $(\rho_f^{-1} \partial \rho_f / \partial P)$. Values of c_r for reservoirs in porous rocks are roughly the same magnitude as values of c_f for liquid but less than c_f for steam. For reservoirs in many fractured rocks, $c_r << c_f$. The product of ΔM times reservoir volume gives an estimate of reservoir productivity in the absence of induced recharge.

The speed of transmission of pressure changes induced by production is also an important aspect of reservoir response. It is proportional to the hydraulic diffusivity, D, given under single-phase conditions by

$$D = \frac{k}{\phi \, \mu_f (c_r + c_f)}$$

where μ_f = fluid dynamic viscosity. From observations of the time, t, required for measurable pressure changes to occur at a distance L from the production zone, the following relations can be derived for D:

$$D \approx \frac{L^2}{t} \qquad \text{(radial flow)}$$

$$D \approx \frac{L^2}{4t} \qquad \text{(linear flow)}$$

Values of D for liquid reservoirs are relatively high because $(C_r + C_f)$ is relatively low. Under such conditions, pressure changes can propogate over distances of several kilometers in periods of months.

Production from two-phase reservoirs induces boiling and accompanying temperature declines as heat is removed from the rock to vaporize liquid. The change in fluid mass per unit of reservoir volume is then given approximately by

$$\Delta M = \rho_s \, \phi \, c_2 \Delta P$$

where ρ_s = steam density and c_2 = effective compressibility due to phase change. The expression derived by Grant and Sorey (1979) for c_2 as a function of latent heat of water and heat capacities of rock and water indicates that c_2 is 100 to 1,000 times larger than values of compressibility for steam and liquid, re-

spectively. Thus, for the same P, changes in mass per unit reservoir volume are roughly 100 times larger under two-phase conditions than under single-phase conditions. This difference tends to result in larger reservoir productivity with boiling than under single-phase conditions. However, under two-phase conditions with both phases mobile, low relative permeabilities tend to force large pressure and temperature drops to maintain production. Under vapor-dominated conditions, production is maintained by boiling without the negative effects of low relative permeabilities.

Values of diffusivity under two-phase conditions are given by

$$D = \frac{k}{\phi \mu_2 c_2}$$

where μ_2 = total dynamic viscosity of two-phase flow (Grant and Sorey, 1979). Pressure transmission tends to be much slower than under single-phase conditions because $c_2 >> c_f$. This tends to minimize interference between wells but also restricts the inducement of recharge from surrounding regions.

In HCS for which the basic model (figure 1) applies, optimum reservoir response may be realized if well production from the deeper single-phase region induces expansion of the overlying two-phase zone with accompanying downward drainage of liquid. The Wairakei reservoir appears to have responded in this manner. With an initial boiling level at a depth of about 400 m, most production bores were drillled to depths of 0.5 - 1.5 km. During over 20 years of production at an average rate near 2000 kg/s, most of the discharge has entered the wells from liquid-filled portions of the reservoir. This is evidenced by relatively uniform discharge enthalpy and rapid tranmission of pressure changes across the reservoir (Fradkin, Sorey, and McNabb, 1981; Bolton, 1970). Measurements in shallow bores indicate that the overlying two-phase zone has expanded laterally and vertically and become drier. The boiling level has fallen about 200 m, implying drainage of liquid in amounts sufficient to supply approximately 10 years of production (McNabb, 1975). The resultant rate of reservoir pressure decline with discharge for the Wairakei reservoir is lower by a factor of about 50 than would be expected in the absence of two-phase conditions (Pritchett, Rice, and Garg, 1979). In effect, the reservoir response appears much more compressible than under single-phase conditions.

Concurrent with changes in storage within the two-phase zone at Wairakei, pressure declines in the production zone have been transmitted out to the sides of the field where recharge of colder water has been induced. The relative contributions of induced recharge and storage changes (drainage) have been delineated from repeat gravity surveys (Hunt, 1977) and modeling simulations of the reservoir pressure history (Mercer and Faust, 1979; Prittchet, Rice, and Garg, 1980; Fradkin, Sorey, and McNabb, 1981). These studies show that drainage effects were most significant in the early stages of field development, and that recharge has increased as reservoir pressures have declined to the point where over 90 percent of current production is supplied by recharge. As noted previously, lateral boundaries are not likely to be uniformly permeable and induced recharge would not be uniformly distributed around the reservoir. Such is the case at Wairakei, as evidenced by the variability in pressure response in cold peripheral wells and pressure drawdowns in wells in the adjacent Tauhara field (Grant, 1978).

To a large extent, the near-optimal response of the Wairakei reservoir results from its relatively high permeability-thickness ($kh=10^5$ md-m). In fields where kh is significantly lower than at Wairakei, or in fields with similar kh produced at significantly greater rates, two-phase conditions may invade production zones that were initially single-phase. For example, at the Redondo Creek field in the Valles caldera, where kh values appear to be near 2×10^3 md-m, well tests and modeling simulations predict extensive development of two-phase conditions in the reservior accompanying production at rates near 400 kg/s for 50 MW_e (Bodvarsson and others, 1980). Corresponding decreases in total dynamic viscosity with two-phase flow at Redondo Creek would necessitate large pressure drops to maintain a constant production rate, although this effect can be partially offset by reinjection and by the need for less total production to supply 50 MW_e as the field dries out. The two-phase Ohaki reservoir at Broadlands, NZ, on the other hand has $kh = 2 \times 10^4$ md-m and may be able to sustain production at 100 MW_e if re-

charge from surrounding liquid-filled regions can be induced (Grant, 1977b; Donaldson and Grant, 1981).

Effects on Surface Features Surface dischages of thermal fluid in active HCS vary considerably in their physical and chemical characteristics, and studies of these characteristics have provided much of our current understanding of HCS (White, 1970; Truesdell, 1976; Ellis and Mahon, 1977). The potential for alteration of the natural rate of fluid discharge during reservoir exploitation was noted previously. Because this effect may significantly influence the development of geothermal resources (from both physical and regulatory standpoints), this issue is discussed in more detail here.

The nature and magnitude of changes in flow rate, temperature, and chemistry of hot springs and fumaroles accompanying reservoir exploitation depend in part on how such discharge features are connected with the reservoir and the rest of the HCS. In the simplest case (1), a hot spring contains fluid of chemical composition similar to that of the reservoir fluid and is fed simply by upflow along one or more conduits from the reservoir to the surface. Hot springs with high chloride, neutral pH waters typify this situation. A slight variation (2) involves the mixing of reservoir fluid with cooler, more dilute water within the upflow conduit. In some cases (3), warm springs represent shallow groundwater heated by conduction from an underlying convective anomaly, and therefore contain no water from a geothermal reservoir (Goff and others, 1982). In other cases (4) shallow groundwater may be heated by addition of steam from a deeper vapor-dominated zone, producing low-chloride, acid-sulphate hot springs. Steam discharge in fumaroles (5) commonly occurs along with steam-heated springs and both features may be indicative of vapor-dominated reservoirs or of parasitic vapor zones in active HCS (figure 3).

In the natural state, pressure gradients within and above the reservoir drive thermal fluid toward the surface. Fluid production during exploitation causes a reduction in reservoir pressure and in the vertical pressure gradient. As a consequence, the rate and temperature of liquid discharging at the surface (as in cases 1 and 2) will decrease, although the time scale over which such changes occur varies with the properties of rock and fluid in the upflow conduits. Within zones of two-phase flow or vapor flow, however, vertical pressure gradients may exceed vapor-static conditions during exploitation and increased steam mobility can result in increased upflow of steam (Grant, 1979b). Thus, in cases (4) and (5) reservoir production may result in additional fumarolic activity and temperature increases in steam-heated springs. Discharge rates and temperatures of warm springs (case 3) should be the least affected by reservoir exploitation.

Most of the effects described above have been observed at Wairakei during its 30-year production history. Significant fluid withdrawal began around 1953 and reductions in natural discharge were observed by 1954 (Grant, 1979b). By 1962 major reductions in the discharge of high-chloride hot springs in Geyser Valley, located 1 km northeast of the production field, were found (Glover, 1977). By 1968, the activity in Geyser Valley had changed from mainly flowing springs and active geysers to steam-heated non-flowing pools, mudpots, and fumaroles. During the same period (1955-1968), rates of heat and mass flow from thermal areas to the west, north, and south of the production field increased due to the expansion of vapor-dominated conditions above the reservoir in those areas (Allis, 1980). By 1979, total mass outflow from thermal areas had declined by about 60 percent, from 440 kg/s to 180 kg/s. A change from mainly liquid discharge to mainly steam discharge, however, resulted in an increase in natural heat discharge from 400 MW to 600 MW. The estimated net heat flow loss from the field of 700 MW_t in 1979 (including production and recharge) would produce an average thermal rundown of the two-phase zone of 1.5 °C/yr, and further reduction in the mass outflow from thermal areas (Allis, 1980).

Changes in surficial discharge of thermal fluid due to reservoir exploitation in other active HCS can be expected to be of a similar nature to those observed at Wairakei. However, the timing and magnitude of such changes depend on several factors. These include reservoir and caprock permeability and diffusivity, production rates and depths of producing intervals, distances from production zones to discharge areas, and locations of reinjection wells. Significant reductions or cessation of natural liquid discharge following

reservoir testing or development has been observed in geothermal areas in Mexico (Cerro Prieto), Japan (Otake), Iceland (Hveragerdi), and the United States (Beowawe and Steamboat Springs, Nevada). However, quantitative analyses that account for the factors noted above are generally lacking except for preliminary results for the Rotorua-Whakarewarew field in New Zealand (Donaldson, 1980) and the Valles Caldera (unpublished reports by Union Oil Company and Geotrans, Inc.).

It should be noted that some amount of reservoir pressure drawdown will accompany fluid production, even at rates below that of the natural throughflow. This drawdown tends to reduce liquid outflow, as does any increase in boiling in the two-phase zone (which reduces liquid relative permeability). Reinjection of waste liquid offers possibilities for reservoir pressure maintainance and increased recovery of stored thermal energy. Short-term effects of reinjection may include increased reservoir production, increased natural discharge of liquid, and reduction in natural discharge of steam. However, long term effects may be detrimental to the borefield production enthalpy in fields like Wairakei where induced hot liquid inflow from depth supplies most of the heat extracted from the reservoir.

Summary Consideration of geothermal reservoirs as existing within larger hydrothermal convection systems goes a long way toward explaining the general thermal, chemical, and hydrologic observations made in explored geothermal fields. Information on the characteristics of HCS can guide exploration for geothermal reservoirs and the analysis of energy recovery from such reservoirs. In addition to indications provided by surficial discharges of thermal fluid, regions of upflow of thermal water delineated from temperature measurements in shallow or intermediate-depth wells may offer attractive targets for deeper drilling. The response of developed fields in active HCS has also been shown to depend on the nature of the boundaries between the reservoir and the rest of the system. The consequences of changes in flow across these boundaries during development may vary for different fields and additional experience and analysis is required before predictions can confidently be made for undeveloped fields.

Studies of HCS offer unique opportunities for the blending of information from a variety of disciplines and specialties. With such input, geothermal reservoir engineering can evolve from more narrowly defined limits imposed by previous experiences restricted to fields like petroleum engineering and groundwater hydrology. In addition, knowledge gained in the study of geothermal reservoirs should be applicable to other efforts such as volcanic hazards assessment and mineral recovery from ore deposits associated with fossil hydrothermal systems and submarine hydrothermal systems.

References

Allis, R.G., 1980, Possible effects of reinjection at Warrakai Geothermal Field: Geothermal Resources Council, TRANSACTIONS, v. 4, p. 389-392.

Arnason, B., 1976, Groundwater systems in Iceland traced by deuterium: Societas Scientiarium Islandica, v. 42, 236 p.

Bodvarsson, G.S., Vonder Haar, S.P., Wilt, M.J., and Tsang, C.F., 1980, Preliminary estimation of the reservoir capacity and the longevity of the Baca geothermal field, New Mexico: Society of Petroleum Engineers SPE 9273, Paper presented at 55th Annual Fall Technical Conference, Dallas, Texas.

Bolton, R.S., 1970, The behavior of the Wairakei geothermal field during exploitation: paper presented at U.N. Symposium on Development and Utilization of Geothermal Resources, United Nations, Pisa, Italy, Sept. 22 - Oct. 1, 1970.

Craig, H., Boato, G., and White, D.E., 1956, Isotopic geochemistry of thermal waters, in Nuclear processes in geologic settings, National Research Council Committee Nuclear Science, Nuclear Science Series Report 19, p. 29-38.

Craig, H., Lupton, J.E., Welham, J.A., and Poreda, R., 1978, Helium isotope ratios in Yellowstone and Lassen Park volcanic gases: Geophysical Research Letters, 5, p. 897-900.

Donaldson, I.G., 1980, Geothermal energy resources can also be tourist resources: lessons from Wairakei and Rotorua - Whakarewa-

rewa, New Zealand: Proceedings Sixth Workshop Geothermal Reservoir Engineering, Stanford University, p. 41-48.

Donaldson, I.G., and Grant, M.A., 1981, Heat extraction from geothermal reservoirs: in Geothermal Systems: Principals and Case Histories, ed. by L. Rybach and L.J.P. Muffler, John Wiley and Sons, p. 145-179.

Einarsson, P., 1978, S-wave shadows in the Krafla Caldera in NE Iceland, evidence for a magma chamber in the crust: Bulletin of Volcanology, v. 41, p. 1-9.

Ellis, A.J., and Mahon, W.A.J., 1977, Chemistry and Geothermal Systems; Academic Press, New York, 392 p.

Flynn, T. and Trexler, D.T., 1982, The Kemp Thermal Anamoly: A newly discovered geothermal resource in Pumpernickle Valley, Nevada: Geothermal Resources Council Transactions, v. 6, p. 121-124.

Fradkin, L. Jr., Sorey, M.L., and McNabb, A., 1981, On identification and validation of some geothermal models: Water Resources Research, v. 17, no. 4, p. 929-936.

Furumoto, A.S., 1978, The relationship of a geothermal reservoir to the geological structure of the East Rift of Kilauea Volcano, Hawaii: Geothermal Resources Council Transactions, v. 2, p. 199-201.

Glover, R.B., 1977, Chemical and Physical Changes at Geyser Valley, Wairakei, and their relationship to changes in borefield performance: New Zealand Dept. of Scientific and Industrial Research DSIR Bulletin 218, p. 19-26.

Goff, F., McCormick, T., Trujillo, P.E. Jr., Counce, D., and Grigsby, C.O., 1982, Geochemical data for 95 thermal and nonthermal waters from the Valles caldera - Southern Jemez Mountains region, New Mexico: Report LA-9367-OBES, Los Alamos National Lab, Los Alamos, New Mexico, 51 p.

Grant, M.A., 1977a, Approximate calculations based on the simple one-phase model of a geothermal system: New Zealand Journal of Science, v. 20, p. 19-25.

Grant, M.A., 1977b, Broadlands - a gas-dominated geothermal field: Geothermics, v. 6, p. 9-29.

Grant, M.A., 1978, Two-phase linear geothermal pressure transients: A comparison with single-phase transients: New Zealand Journal of Science, v. 21, p. 355-364.

Grant, M.A., 1979a, Interpretation of downhole measurements at Baca: Proceeding of Fifth Workshop Geothermal Reservoir Engineering, Stanford University, p. 261-268.

Grant, M.A., 1979b, Fluid state at Wairakei: Proceedings of the New Zealand Geothermal Workshop, University of Auckland, p. 79-84.

Grant, M.A., and Sorey, M.L., 1979, The compressibility and hydraulic diffusivity of a water-steam flow: Water Resources Research, v. 15, no. 3, p. 684-686.

Grant, M.A., Truesdell, A.H., Manon, A., 1981, Production induced boiling and cold water entry in the Cerro Prieto geothermal reservoir indicated by chemical and physical measurement: Proceedings, 3rd Symposium on the Cerro Prieto Geothermal Field, p. 221-247: Geothermics (in press).

Grant, M.A., and Garg, S.K., 1981, Interpretation of downhole data from the Baca geothermal field: Status as of June 1981: Geothermal Resources Council Transactions, v. 5, p. 337-340.

Horne, R.N., 1981, Geothermal injection experience in Japan: Society of Petroleum Engineers SPE9925, Paper presented at 1981 California Regional Meeting in Bakersfield, California, p. 423-433.

Hunt, T.M., 1977, Recharge of water in the Wairakei geothermal field determined from repeat gravity measurements: New Zealand Journal of Geology and Geophysics, v. 20, p. 303-317.

Iyer, H.M., 1979, Deep structure under Yellowstone National Park, U.S.A., A continental "hot spot": Tectonophysics, v. 56, p. 165-197.

Iyer, H.M., Oppenheimer, D.H., Hitchcock, T., 1979, Large teleseismic P-wave delays in the Geysers - Clear Lake geothermal

area, California; Science, v. 204, p. 425-427.

Lachenbruch, A.H., and Sass, J.H., 1977, Heat flow in the United States and the thermal regime of the crust: American Geophysical Union Geophysical Monograph 20, p. 626-675.

Lupton, J.E., 1979, Helium - 3 in the Guaymas Basin; Evidence for injection of mantle volatiles in the Gulf of California: Journal of Geophysical Research, v. 84, p. 7446-7452.

MacLeod, N.S., and Sammel, E.A., 1982, Newberry Volcano, Oregon, A Cascade Range geothermal prospect: California Geology, November, p. 235-244.

Mamyrin, B.A., Tolstikhin, I.N., Anufriev, G.S., and Kamensky, I.G., 1972, Isotopic composition of helium in thermal springs of Iceland: Geokhimiya, no. 11, p. 1396.

McNabb, A., 1975, A model of the Wairakei geothermal field: unpublished report, Applied Mathematics Division, Department of Scientific and Industrial Research, Wellington, NZ.

Mercer, J.W., and Faust, C.R., 1979, Geothermal reservoir simulation: 3. Application of liquid- and vapor-dominated hydrothermal modeling techniques to Wairakei, New Zealand: Water Resources Research, v. 15, no. 3, p. 653-671.

Muffler, L.J.P., 1979, Assessment of geothermal resources of the United States - 1978: U.S. Geological Survey Circular 790, 163 p.

Muffler, L.J.P., Bacon, C.R., and Duffield, W.A., 1982, Geothermal systems of the Cascade Range: Proceedings of Pacific Geothermal Conference 1982 and 4th New Zealand Geothermal Workshop, Part 2, p. 349-356.

Norton, D. and Taylor, H.P., Jr., 1979, Quantitative Simulation of the hydrothermal systems of crystallizing magmas on the basis of transport theory and oxygen isotope data: an analysis of the Skaergard intrusion: Journal of Petrology, v. 20, p. 421-486.

Pritchett, J.W., Rice, L.F., and Garg, S.K., 1979, Summary of reservoir engineering data: Wairakei geothermal field, New Zealand: Report LBL-8669 GREMP-2, Lawrence Berkeley Lab., University of California, Berkeley.

Pritchett, J.W., Rice, L.F., and Garg, S.K., 1980, Reservoir simulation studies: Wairakei geothermal field, New Zealand: Report LBL-11497, GREMP-11, Lawrence Berkeley Lab., University of California, Berkeley.

Pritchett, J.W., Rice, M.H., and Riney, T.D., 1981, Effects of CO content on geothermal systems: Implications for the Baca reservoir: Geothermal Resources Council Transactions, v. 5, p. 369-372.

Pruess, K., and Truesdell, A.J., 1980, A numerical simulation of the natural evolution of vapor-dominated hydrothermal systems: Proceedings, Sixth Workshop Geothermal Reservoir Engineering, Stanford University, p. 194-203.

Robinson, J.L., 1977, An estimate of the lifetime of the Wairakei geothermal field: New Zealand Journal of Science, v. 20, p. 27-29.

Sanford, A.R., and Einarsson, P., 1982, Magma chambers in rifts, in Palmason, G., ed., Continental and oceanic rifts: AGU Geodynamic Series, v. 8.

Sass, J.H., Blackwell, D.D., Chapman, D.S., Costain, J.K., Decker, E.R., Lawver, L.A., and Swanberg, C.A., 1981, Heat flow from the crust of the Unted States; in Toulokian, Y.S., Judd, W.R., and Roy, R.F., eds., Physical properties of rocks and minerals: New York, McGraw-Hill, p. 503-548.

Smith, M.C., 1978, Heat extraction from hot, dry, crustal rocks: Pure and Applied Geophysics, v. 117.

Sorey, M.L., Lewis, R.E., and Olmsted, F.H., 1978, The hydrothermal system of Long Valley caldera, California: U.S. Geological Survey Prof. Paper 1044-A, 60 p.

Sorey, M.L., Nathenson, M., Smith, C., 1983, Methods for assessing low-temperature geothermal resources; in Reed, M.J., ed., Assessment of low-temperature geothermal resources of the United States -

1981: U.S. Geological Circular (in press).

Steeples, D.W., and Iyer, H.M., 1976, Low velocity zone under Long Valley as determined from teleseismic events: Journal of Geophysical Research, v. 81, p. 849-860.

Stefansson, V., and Bjornsson, S., 1982, Physical aspects of hydrothermal systems, in Palmason, G., ed., Continental and oceanic rifts, AGU Geodynamics Series, v. 8, p. 123-145.

Truesdell, A.H., 1976, Summary of Section III: Geochemical techniques in exploration: Proceedings of the 2nd United Nations Symposium on the development and use of geothermal resources, v. 1, p. Iiii-Ixxix.

Union Oil Company, of California and Public Service Company of New Mexico, 1978, Geothermal demonstration plant: Technical and Management Proposal to DOE.

Welch, A.H., Sorey, M.L., and Olmsted, F.H., 1981, The hydrothermal system in southern Grass Valley, Pershing County, Nevada: U.S. Geological Survey Open-file Report 81-915, 193 p.

Welham, J.A., Poreda, R., Lupton, J.E., and Craig, H., 1979, Gas chemistry and helium isotopes at Cerro Prieto: Geothermics, v. 8, p. 241-244.

White, D.E., 1970, Geochemistry applied to the discovery, evaluation, and exploitation of geothermal energy resources, in United Nations symposium on development and utilization of geothermal resources, Pisa 1970, v. 1, pt. 2: Geothermics, Special Issue 2, p. 50-80.

White, D.E., Muffler, L.J.P., and Truesdell, A.H., 1971, Vapor-dominated hydrothermal systems compared with hot-water systems: Economic Geology, v. 66, p. 75-97.

Whittome, A.J., and Smith, E.W., 1979, A model of the Tongonan Geothermal field: Proceedings of the New Zealand Geothermal Workshop, University of Aukland, p. 141-147.

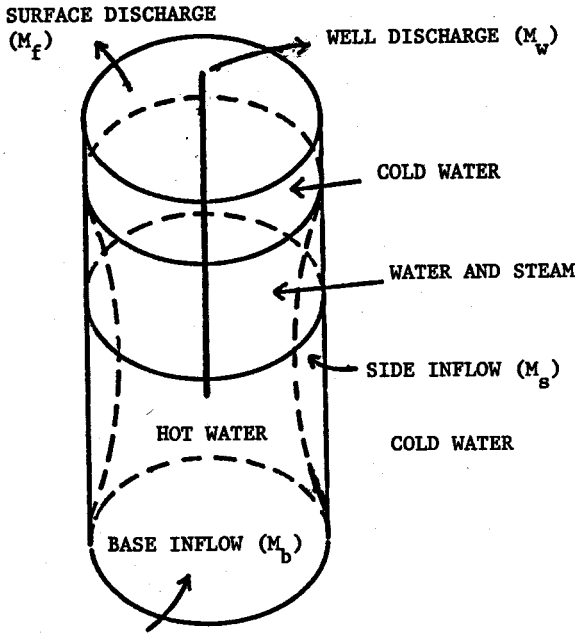

Figure 1. Basic model of a geothermal reser-reservoir in the discharge portion of an active hydrothermal convection system (adapted from Donaldson and Grant, 1981).

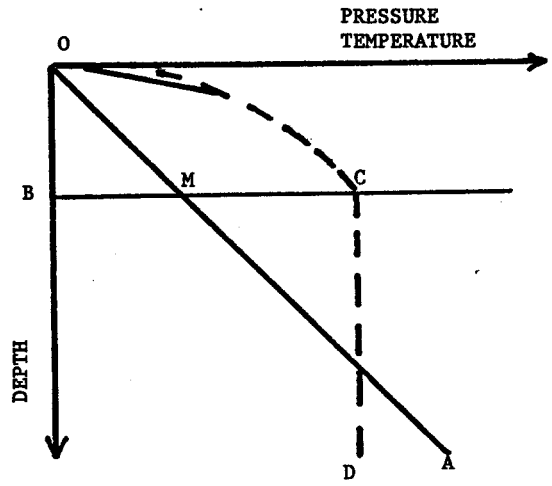

Figure 2. Generalized distributions of temperature and pressure with depth in the basic model of figure 1 (adapted from McNabb, 1975)

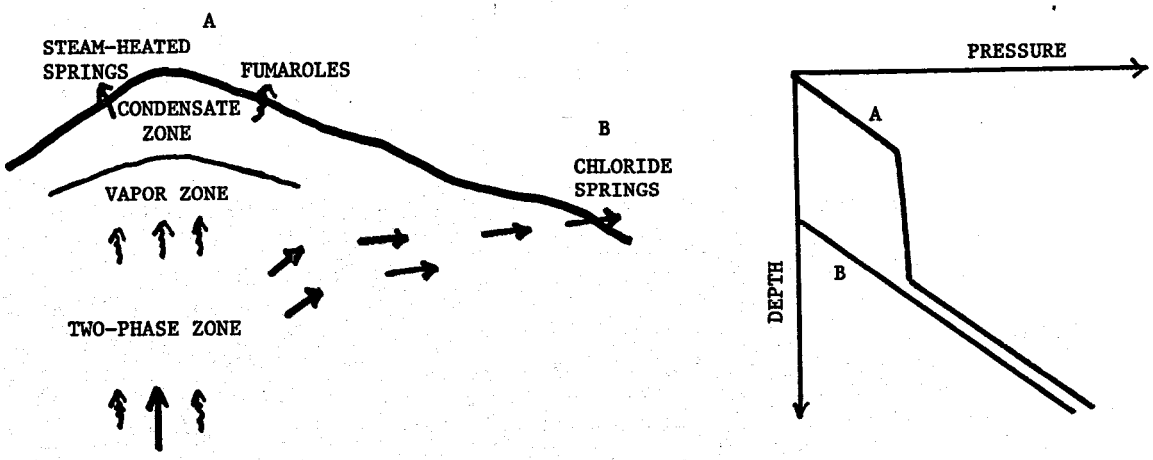

Figure 3. Conceptual model of hydrothermal convection systems in regions of high relief in which phase separation occurs in the upflow zone, producing a vapor-dominated zone above and a zone of lateral outflow of liquid. Generalized pressure distributions with depth in region A (upflow zone) and region B (outlfow zone) are shown at right (adapted from Grant, 1979a).

Proceedings Eighth Workshop Geothermal Reservoir Engineering
Stanford University, Stanford, California, December 1982
SGP-TR-60

GEOLOGIC AND PRELIMINARY RESERVOIR DATA ON THE LOS HUMEROS GEOTHERMAL SYSTEM, PUEBLA, MEXICO.

Horacio Ferriz

Dept. of Applied Earth Sciences
Stanford University
Stanford, CA 94305

ABSTRACT

Exploratory drilling has confirmed the existence of a geothermal system in the Los Humeros volcanic center, located 180 km east of Mexico City. Volcanic activity in the area began with the eruption of andesites, followed by two major caldera-forming pyroclastic eruptions. The younger Los Potreros caldera is nested inside the older Los Humeros caldera. At later stages, basaltic andesite, dacite, and olivine basalt lavas erupted along the ring-fracture zones of both calderas.

Geologic interpretation of structural, geophysical, and drilling data suggests that: (1) The water-dominated geothermal reservoir is hosted by the earliest andesitic volcanic pile, is bounded by the ring-fracture zone of the Los Potreros caldera, and is capped by the products of the oldest caldera-forming eruption. (2) Permeability within the andesitic pile is provided by faults and fractures related to intracaldera uplift. (3) The geothermal system has potential for a large influx of meteoric water through portions of the ring-fracture zones of both calderas. (4) Volcanic centers with similar magmatic and structural conditions can be found in the eastern Cascades, U.S.A.

INTRODUCTION

The Los Humeros volcanic center (LHVC) is located in the eastern end of the Mexican Neovolcanic Belt, 20 km northwest of Perote, Veracruz. Mild fumarolic activity sparked interest in the geothermal potential of the area in the mid-1960's. Preliminary geological and geophysical reconaissance surveys (Mooser, 1964; Pérez, 1978; Alvarez, 1978) led Mexico's Comisión Federal de Electricidad to undertake an extensive exploration program that included regional geologic mapping (Yáñez and Casique, 1980), detailed geologic mapping of the volcanic center (Ferriz and Yáñez, 1981), resistivity, self-potential, and aeromagnetic surveys (Palacios and Garcia, 1981), geochemical surveys (Molina, 1979), and exploration drilling (Rivera, 1982; López, 1982a; Gutiérrez, 1982).

This paper integrates some of the information collected during the exploration program, under the framework of detailed geologic mapping, to provide preliminary data on the characteristics of the geothermal reservoir.

REGIONAL GEOLOGY AND LOCAL "BASEMENT"

The Quaternary Mexican Neovolcanic Belt is an irregular belt of large andesitic stratovolcanoes, cinder-cone fields, and a few silicic centers, which bisects central Mexico in an east-west direction. Molnar and Sykes (1969) suggested that magmatism along this belt is related to the subduction of the Cocos Plate below Mexico along the Middle America Trench. LHVC is one of several silicic centers located in the "back-arc" portion of the belt. Two other of these silicic centers, Los Azufres and La Primavera (Mahood, 1980), also host significant geothermal systems.

The local basement of LHVC is formed by a Mesozoic sedimentary sequence and Tertiary intrusions and andesites. The Mesozoic rocks (Viniegra, 1965; Yáñez and Casique, 1980) can be divided in a Triassic to Middle Jurassic clastic sequence, and a Middle Jurassic to Upper Cretaceous sequence of marls and limestones of inferred low permeability.

GEOLOGIC HISTORY

The oldest exposed rocks at Los Humeros are dense porphyritic to sparsely porphyritic andesite and basalt flows of the Teziutlán Formation. K-Ar age determinations on these flows range from 3.5 ± 0.3 to 1.6 ± 0.07 Ma. These flows crop out in the northern portion of LHVC, but similar rock types have been found during drilling in its central and southern portions. Similar rock fragments are common in all the younger pyroclastic units. Thus, these andesite and basalts seem to have covered most of the area now occupied by LHVC. Mapping of flow directions, breccia pipes, and fossil hydrothermal alteration zones indicates that the vents for these flows were located in the area now occupied by LHVC. This inference is reinforced by an increase in the thickness of the Teziutlán Formation from 60 m in the northern outcrops to more than 1000 m in a borehole drilled in the central portion of LHVC (H-4 in Figure 1). It is in these dense and brittle rocks that fluid production has been found during exploration drilling.

The onset of silicic volcanism is marked by the intrusion of two high-silica rhyolite domes, one of which has been K-Ar dated at 0.5 ± 0.03 Ma. Later eruption of the 180 km^3 rhyolitic (76% SiO_2) to rhyodacitic (71% SiO_2) Xáltipan Ignimbrite led to the collapse of the Los Humeros caldera (LHC in Figure 1). The rim of this 21 by 15 km caldera is covered by younger volcanic rocks, so its configuration has been determined by the location of ring-fracture volcanism, as well as by topographic expression. Given the volume of magma equivalent to the Xáltipan Ignimbrite (≈90 km^3) and the area of the caldera, one can estimate the average amount of collapse as 350 m. Nowhere is the Xáltipan Ignimbrite exposed inside the Los Humeros caldera, but a 200 m-thick moderately welded ignimbrite found at 965 m depth in the H-1 borehole could be its intracaldera equivalent.

After collapse, several high-silica rhyolite domes were emplaced along the northwestern, northern, and southern (?) portions of the inferred ring-fracture zone. Their emplacement was followed by the eruption of more than 2 km^3 of rhyodacitic (72-69% SiO_2) air-fall tuffs.

The eruption of the 20 km^3 rhyodacitic (70% SiO_2) to andesitic (59% SiO_2) Zaragoza Ignimbrite resulted in the formation of the 10-km-diameter Los Potreros caldera (LPC in Figure 1), nested within the older Los Humeros caldera. Its eastern and western topographic walls can still be recognized in the field, but the northern and southern portions of the caldera rim have been obliterated by younger ring-fracture volcanism. A minimum of 200 m of collapse has been estimated from reconstruction of precaldera topography. Outflow sheets of the Zaragoza Ignimbrite tilted up to 12°, and postcaldera lavas that flowed radially away from Los Potreros caldera, indicate doming of the caldera and its surroundings shortly after collapse.

Although stratigraphic relations are unclear, it seems that after collapse a small basaltic and andesitic volcanic edifice occupied the central portion of the Los Potreros caldera. This edifice was later intruded by a biotite rhyodacite dome.

After the emplacement of the Zaragoza Ignimbrite an arc of basaltic andesite scoria cones developed along the southern ring-fracture zone of the Los Humeros caldera (Figure 1). The cinder cones fed approximately 4 km^3 of basaltic andesite (56-59% SiO_2) lava that flowed south of LHVC. Similar lavas erupted from two small shield volcanoes located between the eastern and northeastern rims of the two nested calderas. The lavas from these volcanoes, which flowed radially away from the Los Potreros caldera, have a total volume of ≈2 km^3.

Activity continued with the eruption of 10 km^3 of dacitic (68-69% SiO_2) flows from centers located along the northern, eastern, and southern portions of the ring-fracture zone of the Los Potreros caldera. The simultaneous venting of dacitic and andesitic tephra, approximately coeval with the eruption of the earliest dacite flows, led to the collapse of the 1.7-km-diameter El Xalapazco caldera along the south-southeastern ring-fracture zone of the Los Potreros caldera. This eruption was followed by minor fault-bounded uplift of the southeastern quadrant of the Los Potreros caldera, perhaps due to upward movement of magma.

The final stage of volcanic activity at LHVC is represented by the eruption of olivine basalts (49% SiO_2) on the floor of the Los Potreros and El Xalapazco calderas, and along the southwestern ring-fracture zone of the Los Humeros caldera. The total volume represented by these basalts is ≈0.25 km^3.

The apparent erratic composition of the products of LHVC appears to represent tapping of different levels of a magma chamber that was zoned from rhyolite to basaltic andesite in composition, and probably underplated by olivine basalts. This tapping of different levels would be possible only because of the existence of two nested collapse structures of significantly different size, the ring-fracture zone of the larger structure tapping deeper levels of the magma chamber than that of the smaller structure. Perhaps more relevant for the development of the geothermal system is that: (1) the mere existence of the collapse structures suggests that the magma chamber was lodged at a shallow depth, (2) the volume of the eruptive products indicates that the magma chamber was a voluminous one, (3) the long magmatic history implies a prolongued period of heating of the rocks that hosted the magma chamber, (4) the ring-fracture zones of both calderas have persisted as zones of structural weakness or discontinuity for an extended period of time, thus providing favourable structural conditions for the development of a hydrothermal system.

GEOPHYSICAL DATA

Aeromagnetic surveys of the area (Flores et al., 1978; J. Ruiz in Palacios and García, 1981) show a change in polarity along the southern ring-fracture zone of the Los Humeros caldera, and a major bipolar anomaly on the northeastern quadrant of the Los Potreros caldera. The center of this bipolar anomaly corresponds with a small gravity high (Mena and González, 1978) and, from what is known about the geology of LHVC, could correspond to a swarm of basaltic dikes, to the thick central portion of the eruptive center(s) that fed the Teziutlán andesites, or to an intracaldera intrusion.

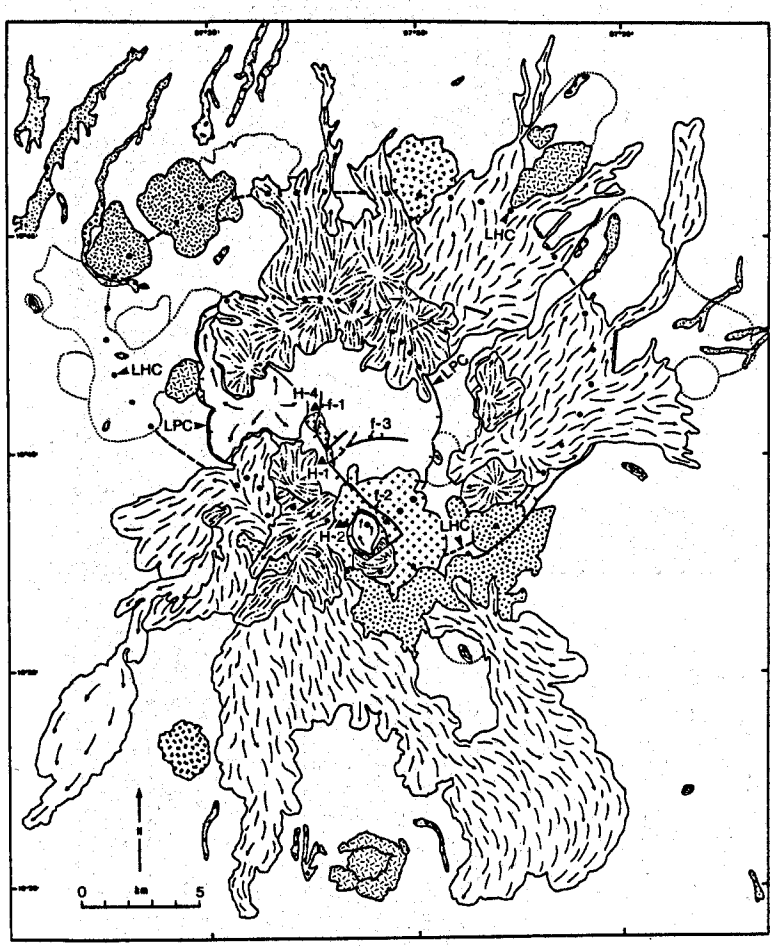

Figure 1. Simplified geologic map of the Los Humeros volcanic center. LHC, Los Humeros caldera rim; LPC, Los Potreros caldera rim; caldera rims discontinuous where inferred, dotted where buried. Heavy lines, faults. Triangles, boreholes. Sandstone pattern, Xáltipan Ignimbrite; boulder pattern, Zaragoza Ignimbrite; dashes and "v" patterns, rhyolite and dacite domes; breccia pattern, scoria cones; dash-arrow pattern, basaltic andesites; dash-dot and cross patterns, dacites; arrow pattern, olivine basalts; blank, tuffs younger than the Zaragoza Ignimbrite.

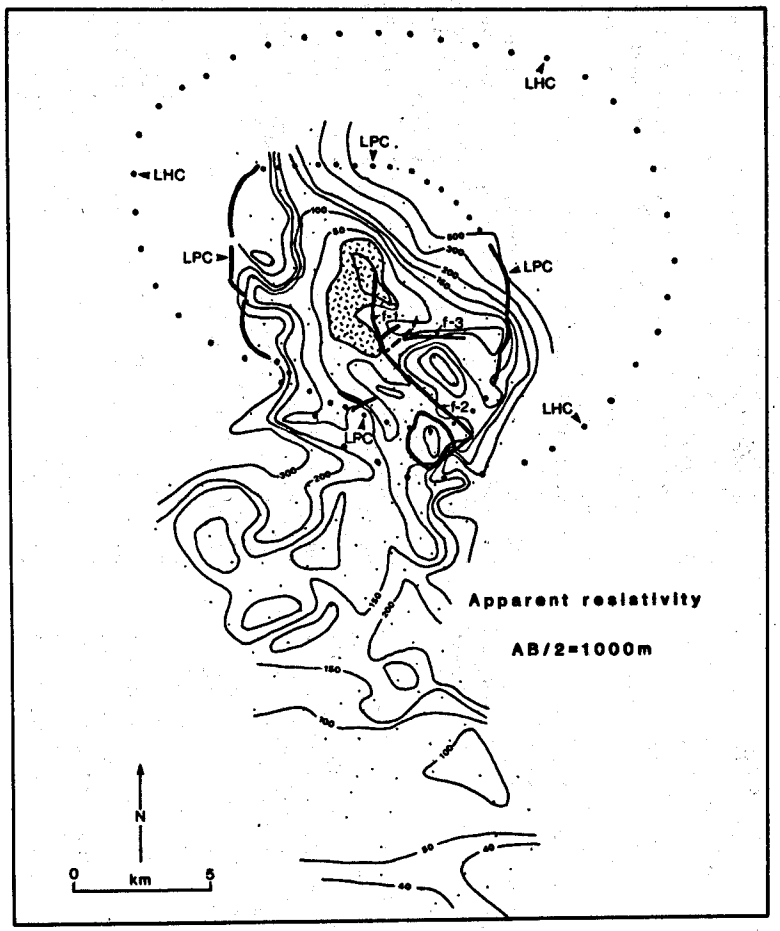

Figure 2. Apparent resistivity isopleth map for AB/2 = 1 km. Resistivities in ohm-m. LHC, Los Humeros caldera; LPC, Los Potreros caldera. Heavy lines, faults. Dash pattern, area enclosed by the 20 ohm-m apparent resistivity contour. Light dots, center of sounding. Modified from Palacios and García, 1981).

The LHVC corresponds with a broad negative low in the residual anomaly gravity map of Mena and González (1978), which they modelled as a ≤ 1-km-thick accumulation of material with an average density of 2.35 g/cm^3 and a density contrast of 0.32 g/cm^3 with respect to the surrounding rocks. An average thickness of 1 km for low-density intracaldera deposits is not unreasonable in the light of the results of boreholes H-1 and H-4 (Figure 1), in which the dense Teziutlán andesites were cut at depths of 1155 m and 874 m respectively. Other negative anomalies around LHVC are attributed to thick accumulations of the outflow sheets of the Xáltipan Ignimbrite.

Palacios and García (1981) reported the results of 184 Schlumberger vertical electric soundings with maximum electrode spacings (AB/2) of 2 km, and 32 soundings with maximum spacings of 4 km. Their results have been used to construct the simplified isopleth map of apparent resistivities, for an AB/2 spacing of 1 km, shown in Figure 2; the major structural features defined by geologic mapping are also shown as heavy lines and dots. A zone of low resistivity, delineated by the 20 ohm-m contour, occupies the central portion of the Los Potreros caldera; the general shape of the low seems to be controlled by fault f-1 and by the northwestward projection of fault f-2. Fault control in the central portion of the Los Potreros caldera seems to be better expressed by the 50 ohm-m contour, spurs of which are aligned along faults f-2 and f-3; however, the major southern spur of this contour does not correspond to any mappable fault or fracture zone. Apparent resistivities increase abruptly toward the rim of the Los Potreros caldera, except at the southern caldera rim and along a narrow "channel" through the northwestern rim. Thus, the Los Potreros ring-fracture zone seems to constitute an impermeable barrier that partially bounds the geothermal system, except for the southward and northwestern "openings", which, as discussed below, may represent zones of meteoric water influx into the system. Structural control by intracaldera faults can still be recognized in apparent resistivity maps with AB/2 of 1.5 and 2 km (Palacios and García,1981) but, in addition, the southern ring-fracture zone of the Los Potreros caldera seems to become a major controlling structure.

BOREHOLE DATA

Three boreholes have been completed in the area (Figure 1). The data obtained during drilling have been reported by Gutiérrez (1982), López (1982a,1982b), and Rivera (1982a).

The first exploratory borehole, H-1 in Figure 1, was sited near the intersection of faults f-1 and f-2. In its 1458 m it cut 700 m of intracaldera lavas and tuffs, 265 m of lithic tuff that may correlate with the upper Zaragoza Ignimbrite, 190 m of Xáltipan Ignimbrite, and 303 m of Teziutlán andesites. Two permeable zones, found at 1250 m and 1400 m depth, probably represent the down-hole intersections of faults f-1 and f-2. Maximum temperatures of 270° to 276° C were measured at the depth of the lower permeable zone during initial production tests in September,1981 (López,1982a).

The H-1 well is currently producing a 200 tonne/hr steam-water mixture at a wellhead pressure of 14 kg/cm^2 and with an enthalpy of 300 kcal/kg. One analysis of brine collected at atmospheric pressure (López,1982a) shows, in ppm, Na(I)=265, K(I)=31, Li(I)=5, Ca(II)=1.9, Mg(II)=0.2, B=195, NH_4=7, F(I)=0.4, Cl(I)=100, HCO_3(I)=270, CO_3(II)=120, SO_4(II)=115, SiO_2=480, and pH=8.5. Incondensable gases collected at the wellhead form 0.5% by volume of the steam phase; their analysis (López,1982a) shows, in mole %, CO_2=87.1, H_2S=0.03, H_2=0.03, and CH_4=0.4.

Borehole H-2 is located near, but on the outside, of the inferred rim of the Los Potreros caldera. According to Gutiérrez (1982), in its 2301 m it cut 495 m of postcaldera lavas and tuffs, 245 m of ignimbrite, 400 m of Teziutlan andesites, and 1161 m of Mesozoic marls. Although bottom temperatures as high as 280° C were recorded no permeable zones were found in this borehole.

Borehole H-4 is located near the northern end of fault f-1, on the down-thrown side of the fault. According to Rivera (1982b), in its 1880 m the borehole cut 108 m of postcaldera tuffs, 766 m of ignimbrite (which may represent the aggregate thickness of the Xáltipan and Zaragoza ignimbrites), and 1006 m of Teziutlán andesites. Because several intervals of circulation loss were found at depths greater than 1000 m, production casing was installed between 1100 m and 1880 m depth. A bottom temperature of 299° C was recorded prior to the start of production tests. The well began producing dry steam at a pressure of 116 kg/cm^2 by September,1982; pressure soon stabilized at 17 kg/cm^2 and the dry steam flow rate stabilized at 160 tonne/hr. After a short period, however, pressure and flow rate began declining again and, by mid-November,1982, had values of 4.6 kg/cm^2 and 47 tonne/hr respectively (López,1982b). The field operators have attributed this decline to plugging of the well during production tests.

Incondensable gases, analyzed during the stage of stable pressure, formed 2.9% by volume of the steam. Their analysis (López,1982b) shows, in mole %, CO_2=78.5, H_2S=9.4, H_2=11.9, CH_4=0.04, and N_2=0.15.

DISCUSSION

The preliminary geophysical and drilling data can be interpreted in light of the detailed geologic study (Ferriz and Mahood, in prep.) to estimate some of the parameters needed in reservoir engineering, namely the boundaries of the system; the location, nature, and extent of the major permeability controls; and the potential water influx into the system. These parameters will support and complement those obtained through transient pressure analyses once more boreholes are drilled. In the meantime they may prove useful in siting exploration boreholes.

It has already been suggested that the system is bounded laterally by the ring-fracture zone of the Los Potreros caldera. Of the major units found inside the caldera only the Xáltipan and Zaragoza ignimbrites could be expected to have significant primary permeabilities. However, production zones in wells H-1 and H-4 are within the very dense Teziutlán andesites, suggesting that the hot-water aquifer is confined to steeply dipping zones of secondary permeability such as fault f-1. Although mapped faults cut both andesites and ignimbrites, open fractures would be more likely to persist in the brittle andesites than in the moderately consolidated overlying ignimbrites. In addition, hydrothermal alteration will tend to reduce the primary permeability of the ignimbrites, which would then operate as a semi-impermeable cap for the reservoir. The restriction of mild fumarolic activity to the trace of fault f-1 implies the existence of such a cap. In summary, the geothermal system seems to be hosted by the essentially homogeneous Teziutlán andesites, and capped by impermeable intracaldera ignimbrite, within the Los Potreros caldera.

The resistivity surveys (Figure 2), and the results obtained from wells H-1 and H-4, suggest that permeable zones are controlled by the faults that bound the uplifted southeastern quadrant of the Los Potreros caldera (faults f-1, f-2, and f-3). If this uplift is indeed the result of magma intrusion, its boundary faults would not be expected to propagate beyond the inferred rim of the Los Potreros caldera, as has been confirmed by geologic mapping. The location of at least a group of permeable zones seems thus to be well constrained. However, spurs in the contours of the apparent resistivity maps (Figure 2 and Palacios and García, 1981) suggest fracture control in areas within the Los Potreros caldera in which no evidence of such fracture zones can be found in the surface. To confirm the existence of such zones, and to characterize them, is one of the tasks faced by the field operator. These inferred fractures are perhaps related to the regional doming experienced by the Los Potreros caldera shortly after its collapse, and thus would have been formed much earlier than the faults associated with the uplift of the southeastern quadrant of the caldera. Tensional faulting and fracturing related to somewhat similar doming has been documented in other caldera systems (Smith and Bailey, 1968); the faults thus formed are commonly parallel and do not extend beyond the boundaries of the caldera.

The apparent resistivity isopleths of Figure 2 suggest that there could be flow of fluid into or outwards from the geothermal system through the northwestern rim of the Los Potreros caldera; the idea that flow is into the system is favoured due to the lack of thermal indicators in the northern portion of LHVC. Peculiar regional topographic conditions cause precipitation in the northern portion of LHVC to be more intense than in the southern portion; an average of 1200 and 600 mm/yr respectively (Reyes, 1979). Precipitation infiltrates quickly through the permeable unconsolidated and unaltered pyroclastic deposits, but not so through the unfractured domes and lava flows. Taking into account the distribution of impermeable lavas shown in Figure 1, and the difference in precipitation intensity, a larger infiltration rate would be expected in the northwestern portion of LHVC. Assuming 50% evapotranspiration a potential water influx of 10^7 m^3/yr might be expected from the area enclosed by the northwest ring-fracture zones of both calderas into the Los Potreros caldera.

Another potential source of water influx is groundwater from the closed basin that extends south of LHVC, which forms its northern boundary. The basin has an area of approximately 5250 km, and an average annual precipitation of 620 mm; 40% of the precipitation infiltrates to later move outwards from the basin to the north (Reyes, 1979), where the groundwaters could be intercepted by the plumbing system of the volcanic center. Water influx would explain the "opening" in the resistivity contours south of the Los Potreros caldera (Figure 2). Alternatively, such "opening" could indicate migration of fluids from the geothermal system into the hydrologic system of the closed basin.

CONCLUSIONS

I currently see the geothermal reservoir as a water-dominated system bounded by the Los Potreros caldera, hosted by the Teziutlán andesites, and capped by the Xáltipan Ignimbrite and younger volcanic units. Permeable zones are controlled by the fault zones that bound an intracaldera uplift. Additional permeable zones are perhaps provided by fractures related to post-collapse doming of the caldera area; these fractures are not expected to propagate beyond the rim of the Los Potreros caldera. The heat that is now being tapped by the geothermal fluid was

probably derived from a compositionally zoned magma chamber that developed in a shallow level of the crust within the last 0.5 Ma. A potentially large influx of water into the system may be structurally controlled by portions of the ring-fracture zones of the Los Humeros and Los Potreros calderas.

The conclusions obtained through geologic, geophysic, and hydrologic studies of this center, coupled with the development of the reservoir, shall be of interest for the exploration and development of reservoirs hosted by volcanic centers in the eastern Cascades. Centers such as the Newberry and Medicine Lake volcanoes have many similarities with Los Humeros, such as similar tectonic environment, complex magmatic histories, the potential for nested collapse structures and post-collapse doming and fracturing, and potentially high influx of cold water into the systems.

ACKNOWLEDGMENTS

I want to thank the technical personnel of Mexico's Comisión Federal de Electricidad for their continuing support and access to unpublished data, in particular to C. García, C. Yáñez, C. Fernández, J.M. López, L.C.A. Gutiérrez, and O. Rivera. G. Mahood, J. Gudmundsson, P. Bartos, and J. Ortiz reviewed the manuscript and made useful suggestions. Acknowledgment is made to Mexico's Comisión Federal de Electricidad, and Consejo Nacional de Ciencia y Tecnología, and to the Donors of the Petroleum Research Fund, administred by the American Chemical Society, for the support of this research.

REFERENCES

Alvarez,R. (ed.) (1968), "Los Humeros caldera special issue", Geof. Internacional, v.17, p.407-478.

Ferriz,H.; Yáñez,C. (1981), "Mapa geologico del centro volcánico de Los Humeros, Edición preliminar", Comisión Federal de Electricidad, Mexico (map). Copies can be obtained from H. Ferriz, AES, Stanford University, Stanford CA 94305.

Flores,C.; Alvarez,R.; Singh,S.K.; Urrutia,J. (1978) "Aeromagnetic survey of Los Humeros caldera, Mexico", Geof. Internacional, v.17, p.415-428.

Gutiérrez,L.C.A. (1982) "Litología y zoneamiento hidrotermal en los pozos H-1 y H-2 del campo geotérmico de Los Humeros, Puebla", Comisión Federal de Electricidad, Mexico, 45p.

López,J.M. (1982a) "Geoquímica del agua y gases separados del Pozo Humeros-1, campo geotérmico de Los Humeros, Puebla, Mexico", Comisión Federal de Electricidad, Mexico, 15p.

López,J.M. (1982b) "Geoquímica de gases separados del Pozo Humeros-4, campo geotérmico de Los Humeros, Puebla, Mexico", Comisión Federal de Electricidad, Mexico.

Mahood,G.A. (1980) "Geological evolution of a Pleistocene rhyolitic center - Sierra La Primavera, Jalisco, Mexico", J. Volcanol. Geotherm. Res., v.8, p.199-230.

Mena,M.; González,T. (1978) "Regional gravity of Los Humeros volcanic area", Geof. Internacional, v.17, p.429-444.

Molina,R. (1979) "Geoquímica de los gases de la región geotérmica Los Humeros - Las Derrumbadas, Puebla", Comisión Federal de Electricidad, Mexico, 33p.

Molnar,P.; Sykes,L.R. (1969) "Tectonics of the Caribbean and Middle America regions from focal mechanisms and seismicity", Geol. Soc. Am. Bull., v.80, p.1639-1684.

Mooser,F. (1964) "Geología de la Cuenca de Oriental", (map), Comisión Hidrológica Cuenca Valle de México, 99p.

Palacios,L.H.; García,H. (1981) "Informe geofísico del proyecto geotérmico Los Humeros - Derrumbadas, Puebla y Veracruz", Comisión Federal de Electricidad, Mexico, 99p.

Pérez,J. (1978) "Geología y petrografía de la caldera de Los Humeros", Geomimet, No.91, p.97-106.

Reyes,M. (1979) "Geología de la Cuenca de Oriental, estados de Puebla, Veracruz, y Tlaxcala", Colección Científica INAH, Mexico, v.71, 62p.

Rivera,O. (1982a) "Reporte geológico del Pozo Humeros-1, campo geotérmico de Los Humeros, Puebla", Comisión Federal de Electricidad, Mexico.

Rivera,O. (1982b) Personal communication.

Smith,R.L.; Bailey,R.A. (1968) "Resurgent cauldrons", Geol. Soc. Am. Mem. 116, p.613-662.

Viniegra,F. (1965) "Geología del Macizo de Teziutlán y la Cuenca Cenozoica de Veracruz", Bol. Asoc. Mexicana Geol. Petr., v.17, p.101-163.

Yáñez,C.; Casique,J. (1980) "Informe geológico del proyecto geotérmico Los Humeros - Derrumbadas, estados de Puebla y Veracruz", Comisión Federal de Electricidad, Mexico, 59p.

Proceedings Eighth Workshop Geothermal Reservoir Engineering
Stanford University, Stanford, California, December 1982
SGP-TR-60

A FIELDWIDE RESERVOIR ENGINEERING ANALYSIS OF THE PILGRIM SPRINGS, ALASKA, GEOTHERMAL RESERVOIR

Michael J. Economides[1], Christine A. Ehlig Economides[1]
Jay F. Kunze[2], Ben Lofgren[3]

[1]University of Alaska, [2]Energy Services Inc., [3]Woodward-Clyde Consultants

INTRODUCTION

In an attempt to identify the geothermal potential of the Pilgrim Springs area in the Seward Peninsula, Alaska, exploratory drilling was undertaken in the Summer of 1982. A total of four wells were drilled through a State appropriation. The Division of Energy and Power Development acted as the Project Manager while Woodward-Clyde Consultants were selected as the principal contractor. Two other shallow wells were drilled in 1979. The six wells were completed at various depths ranging from approximately 70 ft to 1000 ft.

The drilling activity followed an extensive geological and geophysical assessment done by Forbes et al. (1979), Turner and Forbes (1980) and Wescott and Turner (1981). Their work indicated the existence of an extensive, liquid dominated, shallow geothermal reservoir in the area. The shallow reservoir, confirmed by the 1979 drilling, was delineated within a 1 to 1.5 km^2 area, bounded by permafrost at least 350 ft thick.

The results of the 1979 drilling were presented by Kline (1981). Table 1 is a summary of the well completion data. Figure 1 shows the well locations. Wells PS1 and PS2 were drilled to 150 ft. Air-lifted flowrate was estimated at 200 GPM and 350 GPM, respectively, with a flowing wellhead temperature of 91°C. The wells were then filled with mud and cemented until 1982 when they were reopened. The mud settled at 105 ft in both wells, making them inaccessible below that depth. They were perforated using shape charges at the interval 70-100 ft (PS1) and 60-90 ft (PS2). The unaided flowrate never exceeded 30 GPM in PS1 and 65 GPM in PS2.

The first well, drilled in 1982 was PS3 at a total depth of 260 ft. A 3-inch slotted liner was installed between 155 and 255 ft. The completed interval produced 60 GPM at over 65°C.

Wells PS4 and PS5 were attempts towards an intermediate depth. They were drilled to 881 ft and 1001 ft respectively. Well PS4 is an open hole completion from 186 ft and below. A flowrate of 100 GPM and a wellhead temperature of 46°C were recorded. Well PS5 was completed below 540 ft with a 3" slotted liner. This interval presented siginificant problems during drilling. The formations encountered were often very hard materials. The total flowrate in Well PS5 was only 10 GPM, with a temperature of 35°C.

A sixth well, MI1, was drilled in land owned by Mary's Igloo. It was completed between 227 and 307 ft using 3" slotted liner. The flowrate was 120 GPM at 25°C.

The successively lower flowing temperatures observed in the deeper completions were later explained by the data from temperature versus depth surveys. Interpretation of the temperature surveys will be discussed in detail in this article.

REGIONAL GEOLOGY

The thermal activity at Pilgrim Springs is located in the Pilgrim River Valley, a tectonic depression (graben) bounded by Precambrian amphibolites and Mesozoic plutons. In some areas it is overlain and overthrust by Paleozoic carbonates. Potassium-Argon dating done by Turner and Swanson (1981) indicated a cooling age of 84 m.y. suggesting igneous intrusive activity in mid-Cretaceous time.

Gravity surveys conducted in the region by Kienle and Lockhart (1980) suggest that Pilgrim Springs is near the intersection of two possible fault zones which form the corner of a

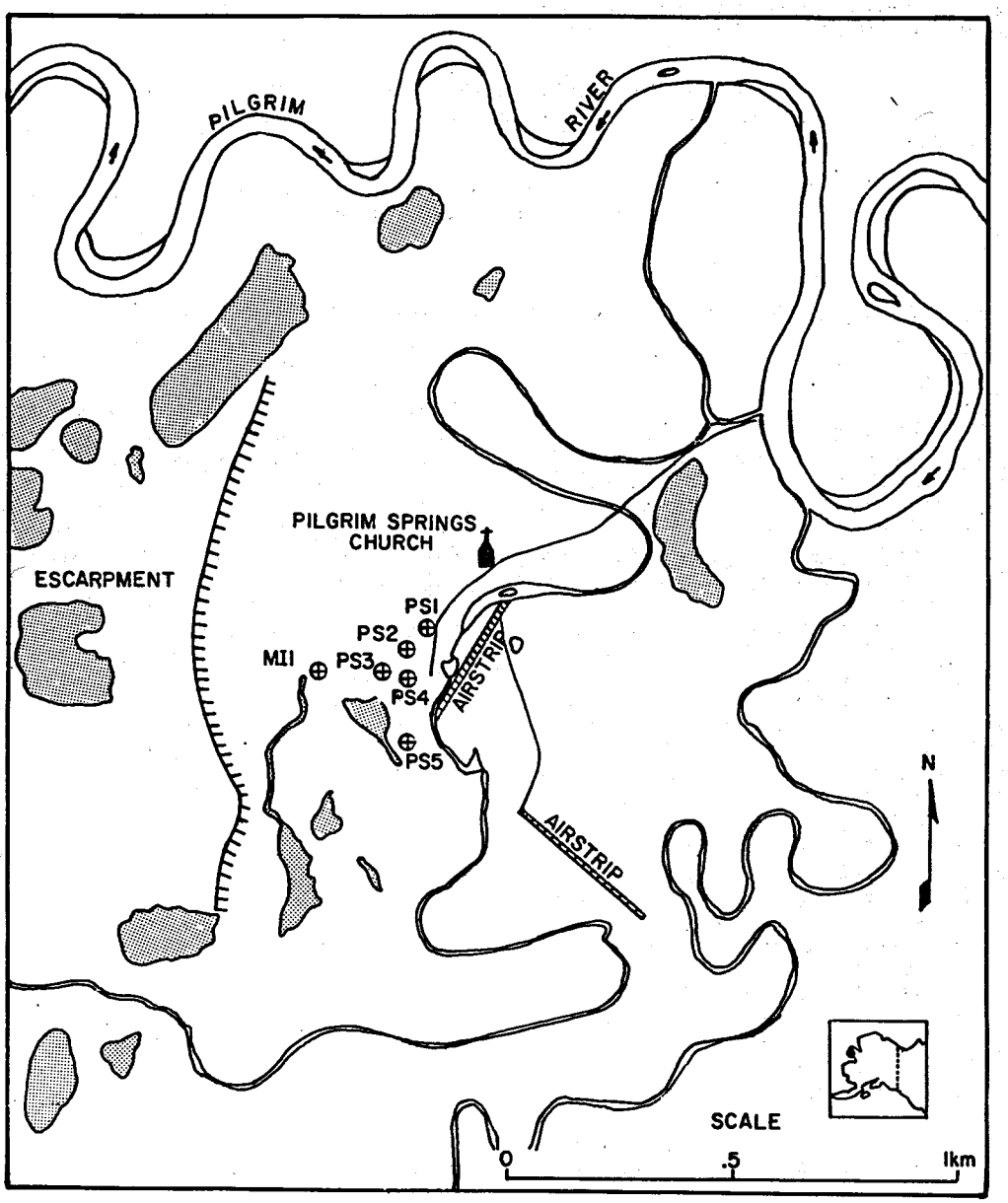

Figure 1. Drill Sites in the Pilgrim Springs Geothermal Reservoir

downdropped basement block. Other faults in the area have been verified by seismic data and geologic mapping, and one or more of these faults could provide a deep conduit for the geothermal anomaly.

The possible existance of a major rift system is of significance for the regional geothermal potential. A helium survey was conducted to test this rift model, and nine out of eleven helium anomalies occur near the proposed rift segments and suggest abnormally high heat flow in these areas. Furthermore, extensive basaltic fields north of Pilgrim Springs area have been interpreted as resulting from eruption in a zone of crustal weakness produced by the general north-south extension (Turner and Swanson, 1981).

The amount of separation along this proposed rift is less than the widths of the Quaternary depressions which have probably been enlarged by normal faulting and marginal subsidence, along with rifting. Potassium-argon dating indicates that volcanism which

Table 1

WELL-COMPLETION SUMMARY, PILGRIM SPRINGS, ALASKA

Well	Drilling Date	Drilled Depth	Remarks
PS-1 1982	Fall'79	150	Cemented from 1979-1982. Perforated in 1982 between 60-90 ft.
PS-2	Fall'79	150	Cemented from 1979-1982. Perforated in 1982 between 70-100 ft.
PS-3	Sum.'82	260	Static head 12 ft. above land surface. Artesian flow- 60 GPM
PS-4	Sum.'82	881	76 feet of drill stem stuck in bottom. Static Head -12 ft. Latest artesian flow- 250 GPM at 114°F.
PS-5	Sum.'82	1001	Latest artesian flow-10 GPM at 98oF
MI-1	Sum.'82	307	Static head - 11 ft. above land surface. Latest artesian flow--100 GPM at 78°F very soft, sweet

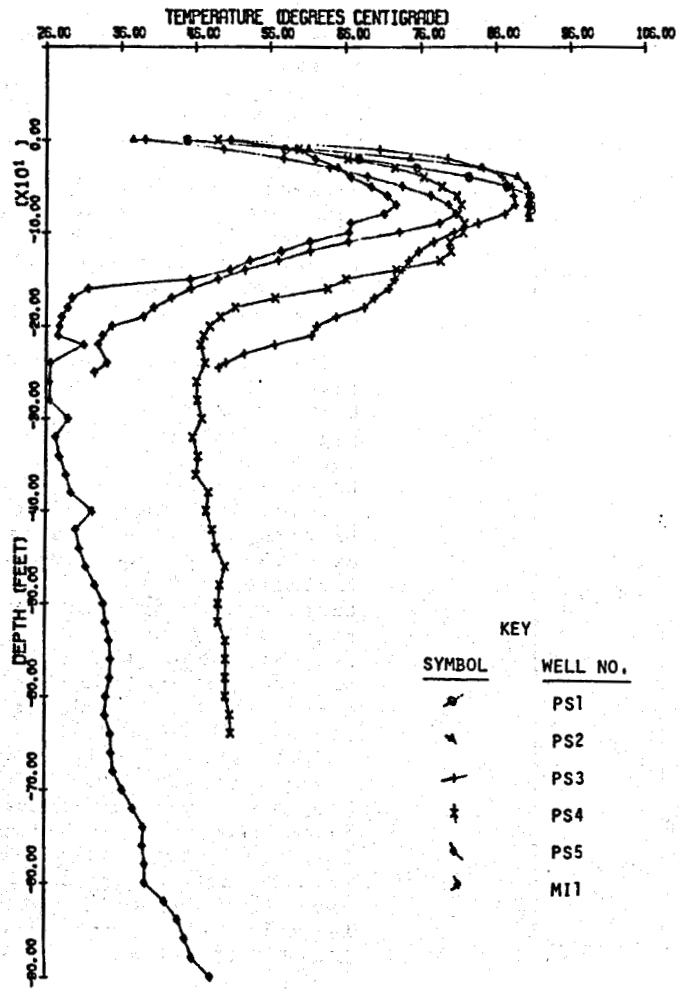

Figure 2. Temperature Versus Depth Profiles of the Pilgrim Springs Wells

was associated with rifting began in the Upper Miocene (Turner and Swanson, 1981).

Finally, a permafrost boundary, enclosing a 1 to 1.5 km^2 area has been identified. The thickness of the permafrost is over 350 ft.

TEMPERATURE DATA INTERPRETATION

Previous temperature data were limited to shallow depth, (4.5 meters) by Wescott and Turner (1981), soil Helium surveys by Turner and Forbes (1980), and geothermometry by Motyka et al. (1980) Motyka's estimate for the source water temperature using Na-K-Ca as the temperature indicator was $150^{\circ}C \pm 10^{\circ}C$. The data of Wescott and Turner indicated a regional geothermal anomaly and suggested that the well sites chosen for PS3, PS4 and PS5 were likely locations for the source fluid.

The temperature data for this study were taken from temperature versus depth data recorded in the wells drilled in the Pilgrims Springs region.

Two months after completion of the last well, temperature surveys were run in all six wells. The temperature versus depth profiles for all wells were identical in shape, as shown in Fig. 2. All showed a trend toward a maximum temperature at depths from 40 to 100 feet, followed by a sharp decrease in temperature with depth from 100 to 250 ft, followed by a constant geothermal gradient ranging from $1.8^{\circ}C$ to $2.1^{\circ}C$ per 100 ft that was recorded down to 900 ft in the deepest well. The two wells, drilled deep enough to determine the geothermal gradient at depth (PS4 and PS5) show temperature trends that would intersect at about $155^{\circ}C$ at a depth of 4875 ft. Hence, the geothermometer temperature estimate of $150^{\circ}C$ is corroborated by the latest findings. In addition, and more importantly, the data suggest that all of the wells overlay the source reservoir at the 4875 ft depth.

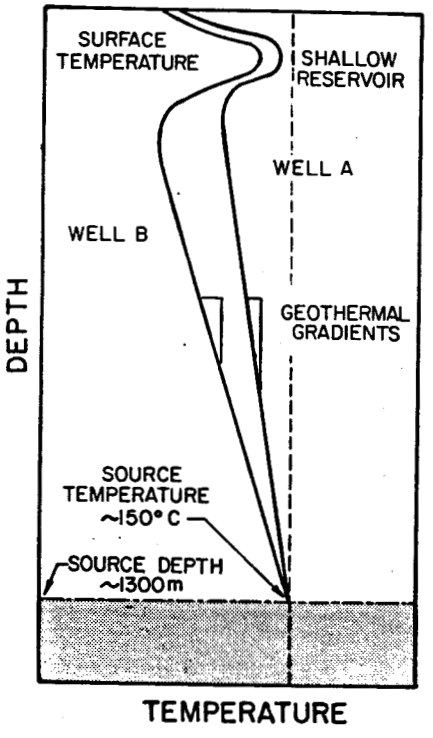

Figure 3. Conceptual Representation of the Shallow and Deep Reservoirs at Pilgrim Springs.

Figure 3 is a schematic representation of the temperature versus depth profile that would be expected at a well (A) near the source from depth of the hot water flowing in the shallow zone. Well B, further away from the source, shows a lower maximum temperature in the shallow zone which grades to a lower temperature at the base of the shallow temperature anomaly and results in a higher geothermal gradient to reach the source temperature at depth.

The shallow temperature anomaly observed in all the wells suggests that somewhere in the immediate region, water from the hot source at depth is flowing upwards through a fissure or fault which extends vertically from a depth of about 50 feet to the 4875 foot depth identified as the source depth. Aerial variations in the maximum recorded temperature for the six wells are contoured in Figure 4. These data suggest that the hot source fluid enters the shallow formation at some point to the north of the six well sites. The fluid then flows radially and laterally away from the fissure source towards springs such as the Pilgrim Springs or perhaps in the surrounding stream beds, thus creating a steady state flow pattern for the shallow hot water zone. Locating the hot water source for the shallow zone is relatively unimportant, since the fluid at depth provides a high temperature source formation extending aerially at least as far as the total area drilled. The temperature data provide a most compelling

justification for deeper drilling in the area.

SHALLOW FORMATION PROPERTIES

Core samples were taken from the 87 to 95 foot depth interval in Well PS4. Three plugs were taken and analyzed for porosity and permeability. The uppermost sample was a large-grained, poorly cemented, primarily quartz sandstone with a porosity of 40% and air permeability in excess of 4 Darcys. This sample is believed to be representative of the shallow hot water zone. The middle sample was a fine grained, well cemented, quartz sandstone with a porosity of 28% and exceptionally low permeability. The deepest sample was a loose conglomerate with a porosity of 24%. The permeability of this sample could not be determined. The middle sample could represent the impermeable base for the shallow hot water zone.

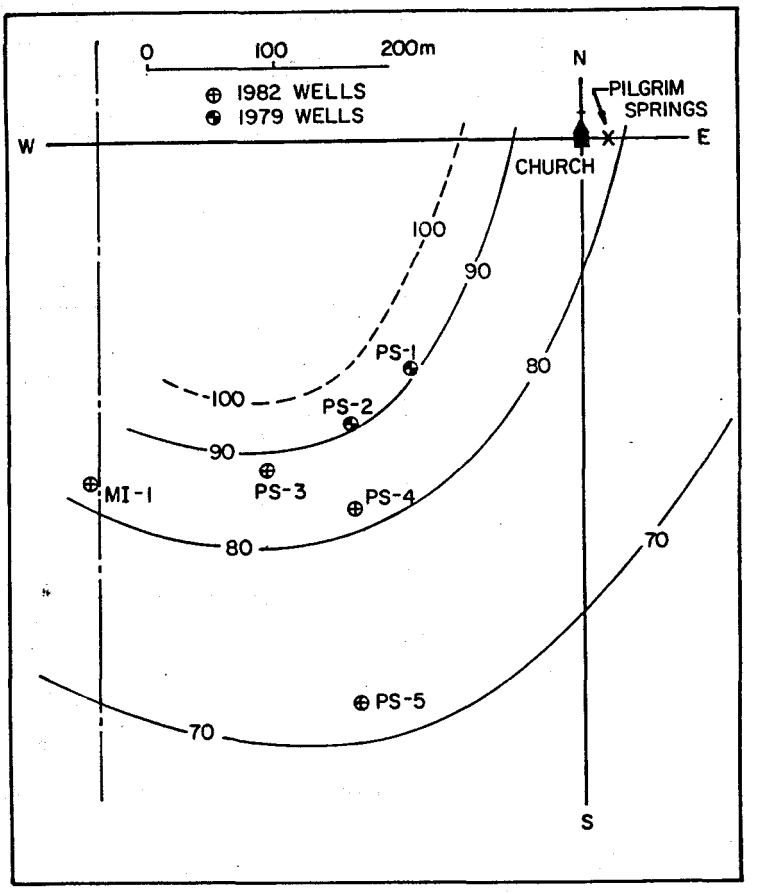

Figure 4. Temperature Contours in the Shallow Reservoir.

Data from an interference well test are shown in Table 2. Shut-in pressures were recorded in PS2 while PS1 was flowing at a rate of 30-35 GPM. A log-log graph of the drawdown pressures in Well PS2 versus time was analyzed by type curve matching with the line source solution, as shown in Fig. 5. From the pressure match, the permeability is estimated at 4.5 Darcys. The time match gives a porosity compressibility product of 5.4×10^{-6} psi^{-1}, which results in an estimate of 14×10^{-6} psi^{-1} for the compressibility, if the porosity is assumed to be 40%. The results of the interference test agree with the core analysis data from Well PS4 and suggest that the shallow hot water zone has similar properties throughout the region of the six wells.

CONCLUSIONS

The wells drilled in the region of the geothermal anomaly near Pilgrim Springs provide considerable insight into the general characteristics of the geotherml system. Previous work, including resistivity studies and geothermometry are corroborated by the temperature profiles observed in the six wells. The existence of a hot

Table 2

Pressure Interference Data Between Wells PS1 and PS2

PS1 (flowing), q = 30-35 GPM

PS2 (wellhead pressures recorded)

Time(min)	p(psig)	Time(min)	p(psig)
0	3.5	20	1.6
8	2.9	22	1.5
12	2.4	24	1.3
14	2.3	27	1.1
16	2.1	29	1.0
17	2.0	30	0.9
18	1.9	31	0.8

Distance between wells = 269 ft
Water viscosity = 1 cp
Reservoir porosity = 40%
Reservoir thickness = 60 ft

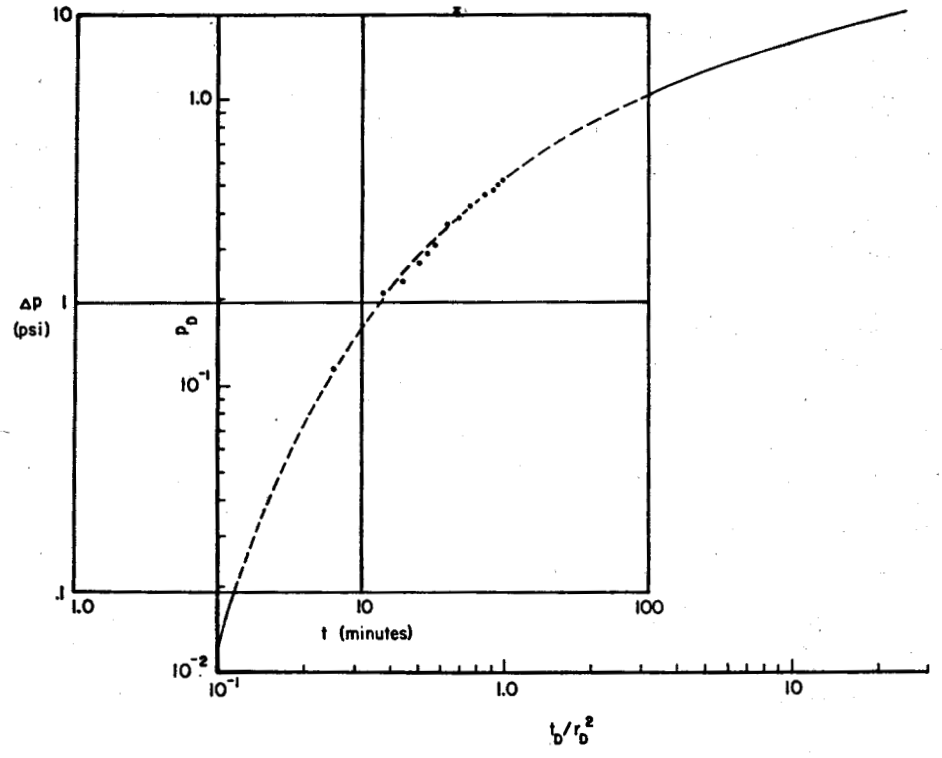

Figure 5. Type-Curve Matching of the Pressure Interference Data Between Wells PS1 and PS2.

water zone of about 150°C and at a depth of around 5000 ft is now virtually certain.

Acknowledgements

The authors wish to thank the State of Alaska through its Department of Energy and Power Development for funding to do this study and to present our findings. We also wish to acknowledge the effects of Mr. Paul Chamberlin to keep an accurate record of all the tests run and the data taken during drilling and completion of the new wells.

REFERENCES

Forbes, R.B., Wescott, E.M., Turner, D.L., Kienle, J., Ostercamp, T., Hawkins, D.B., Kline, J.T., Swanson, S., Reger, R.D. and Harrison, W.: "A Geological and Geophysical Assessment of the Geothermal Potential of Pilgrim Springs, Alaska", Geophysical Institute, UAF and Alaska D.G.G.S. Preliminary Rept., 39 pp., 1979.

Kienle, J. and Lockhart, A. in Turner, D.L. and Forbes, R.B. (Eds), 1980.

Kline, J.T.: "Surficial Geology of the Lower Pilgrim Valley and Vicinity, Western Seward Peninsula, Alaska", Alaska D.G.G.S., AOF-140, 1981.

Motyka, R., Moorman, M. and Forbes, R.B. in Turner, D.L. and Forbes, R.B. (Eds), 1980.

Turner, D.L. and Forbes, R.B. (Eds): "A Geological and Geophysical Study of the Geothermal Energy Potential of Pilgrim Springs, Alaska", Geophysical Institute, UAF, Report UAG R-271, 166 pp., 1980.

Turner, D.L. and Swanson, S.E. in Wescott, E.M. and Turner, D.L. (Eds), 1981.

Turner, D.L. (and 13 other authors): "Summary of Results of a Geological and Geophysical Investigation of the Geothermal Energy Potential of the Pilgrim Springs KGRA, Alaska," Geothermal Resources Council, Trans. v.4, pp. 93-95, 1980.

Wescott, E.M. and Turner, D.L. (Eds): "Geothermal Reconnaissance Survey of the Central Seward Peninsula, Alaska", Geophysical Institute, UAF, Report UAG. R-284, 123 pp., 1981.

Proceedings Eighth Workshop Geothermal Reservoir Engineering
Stanford University, Stanford, California, December 1982
SGP-TR-60

ENGINEERING AND GEOLOGICAL ANALYSES OF THE GEOTHERMAL ENERGY POTENTIAL OF SELECTED SITES IN THE STATE OF ALASKA

Michael J. Economides[1], Jamal Ansari[1],
Gary N. Arce[1] and John W. Reeder[2]

[1]University of Alaska, [2]Division of Geological and Geophysical Surveys

INTRODUCTION

Resource assessment of a variety of locations in Alaska has demonstrated that the State owns significant geothermal sites. Certain reservoirs have already been identified and they could be utilized for either direct space heating or (probably) for power generation. While several of these reservoirs would have been quite attractive elsewhere, extremely high contruction costs, the sparsity of the Alaskan population and the remoteness from urban markets, indicate unfavorable economics in most cases. The State owns some of the largest petroleum, natural gas and coal resources in the U.S.A. There is an enormous potential for hydroelectric power.

Hence, the demonstration of the desirability of geothermal energy utilization in Alaska faces highly adverse odds. The sites where this mode of energy could compare favorably with other available options are prima facie few.

For example, the Aleutian volcanic arc represents a favorable setting, due to the existence of possible shallow magma bodies and deep tectonic fractures for a "vapor dominated" geothermal reservoir as defined by White et al. (1971). Three 1500 ft temperature gradient wells, drilled on Unalaska in the Summer of 1982, have revealed extraordinary geothermal temperature gradients. A reservoir yet to be discovered would be of a quality to produce significant amounts of electric power. Yet, its desirability must be demonstrated against the presently used diesel. Obscuring the issue are future (real or projected) uses. The future price of fossil fuels is difficult to assess. New markets may emerge or expand such as a major bottom fish industry or other heavy users of power.

Although "vapor dominated" reservoirs are expected to be rare (or non-existent) in the rest of Alaska, hot water reservoirs are presumed quite common. The State contains an impressive collection of natural hot springs. Limited drilling activity has produced very encouraging results in at least one site (Prilgrim Springs), while geological and geophysical surveys of a large number of sites have indicated good potential.

It is the purpose of this report to produce ideas and/or options on how geothermal resources might be actually developed assuming a given geological data base for several geothermal prospect areas in Alaska. The possibility of geothermal energy utilization could be weighed against existing (or proposed) modes of energy. The economic attractiveness or lack thereof, will be demonstrated using a common means of comparison among the options.

Six geothermal prospect sites have been selected for this study:

a) Tenakee Springs
b) Sitka Region (Goddard Hot Springs)
c) Pilgrim Springs
d) The Klawasi Region of Copper Valley
e) Summer Bay on Unalaska
f) The Makushin Volcanic Region of Unalaska.

Figure 1 positions the six sites on the map of Alaska. All of these have been the target of general geothermal interest in the past few years. They were included in the July 1980 Alaska Geothermal Implementation Plan (Reeder et al., 1980). Their selection provides a geographic diversity spanning the entire State. With the exception of Tenakee Springs, they are in relative proximity with population centers which, by virtue of their

remoteness, pay a premium price for diesel. The attractiveness of geothermal energy utlization is more probable in these sites than elsewhere.

TENAKEE SPRINGS

The thermal springs at Tenakee occur in Cretaceous granitic rocks (Brew and Morrell, 1980) which are cut by numerous high-angle joints. The two most prominent orientations are N50E and N40W. Silurian hornblende and biotite synenite are exposed just south of Tenakee, and have been interpreted (Loney et al., 1975) to bound the granodiorite by an east-west fault which would be located just offshore.

The liquid-dominated hydrothermal system at Tenakee may derive its fluids from connate waters associated with extensive sedimentary units located at depth. The prominent joint sets in the granitic rocks provide an avenue for transporting the heated fluids to the surface. The east-west fault likely serves as a lateral boundary on the reservoir.

Subsurface reservoir temperatures, based on silica and Na-K-Ca geothermometry, have been calculated to be between 101 to 110°C (I. Barnes, personal commun.). During the drilling of seven shallow wells in 1981, temperatures of 100°F were measured at a depth of 180 ft (Miller, 1981). Very small flowrates were obtained through these wells.

The most obvious consumer of the geothermal resource would be the village of Tenakee. Since the springs are located within the community, direct utilization for purposes other than power generation could be easily accomplished. If a deeper high-temperature reservoir were to be discovered, the closest significant population center would be Sitka. A power line route from Tenakee under Tenakee Inlet to Kadashan Bay, over the Moore Mountains (elevation 200 ft), under Peril Strait and onto Baranof Island at Duffield Peninsula is the most direct path. This distance is roughly 50 miles.

Tenakee could be a target for direct utilization. The heating needs of its 50 houses and other structures can be estimated at 1.5 X 10^6 BTU/hrs. on an average year-round basis. The 1981 drilling produced a geothermal gradient of 13°C/100 ft. and with a surface temperature of 16°C. The predicted source temperature of approximately 100°C can be expected at a depth of about 700 ft. If a well, drilled at this depth were to encounter a reservoir, it would need a flowrate of 37500 lbs/hour (for a 40°F useful temperature drop in th heat system). This flowrate can be translated to 70 GPM. The drilling costs are estimated at one million dollars while the distribution system would need another $1.5 million (including pumps). With operating costs of $80,000 ($40,000 for a technician plus $40,000 for pumping costs) and if no taxes or rates of return infringe on the scheme, a 20 year useful life of the system would result in a cost of $15.6/million BTU or an average monthly bill of $340 per household, significantly higher than the present rates. Electric power generation would prove even more costly, compared to diesel generation, since drilling and power plan costs would be very large. Tenakee, with its small market, does not appear to be an attractive target for geothermal utilization even in the most favorable scenario.

SITKA (GODDARD SPRINGS)

One of the more common rock types in this portion of Southeast Alaska is the Sitka Graywacke, a steeply dipping or overturned series of inner submarine fan turbidites. The Sitka Graywacke is prominently jointed and has been regionally metamorphosed to prehnite-pumpellyite facies. Tonalites and granodiorites are exposed south and west of Redoubt Lake, and potassium-argon ages on biotite range from 42 to 46 m.y. This indicates a middle Eocene age of intrusion (Loney and others, 1975). Numerous alkali-olivine diabase dikes are exposed near the hot springs, and range in thickness from centimeters to meters.

Structurally, southeast Alaska is a complex area, cut by numerous high-angle faults. One of the more prominent is the Fairweather-Queen Charlotte system, 190 km in length. This right-lateral, steeply dipping fault is the boundary between the North American and Pacific lithospheric plates. Also of notable size is the Chatam Strait Fault, 400 km long, which has experienced 190 meters of right-lateral movement since the Cretaceous (Loney and others, 1975).

Goddard and Baranof Hot Springs occur in Lower Cenozoic granodiorite

(Brew and Morrell, 1980). High-angle joint sets are common at orientations of N50E and N40W. Goddard Hot Springs are located very near the northwest-trending Redoubt Lake Fault, and Baranof Hot Springs fall on the trace of the Medvejie Lake Fault (Loney and others, 1975).

The shallow liquid-dominated system at Goddard Hot Springs is interpreted to be of very limited extent, based on EM-31 surveys (R. Reifenstuhl, personal commun.) This hydrothermal system is probably quite similar to the Tenakee system, with connate waters associated with sedimentary rocks acting as the fluid source. Extensive exposures of Cretaceous argillite and graywacke are common throughout the Sitka region, but these units are not likely to act as reservoir rocks due to their low permeability and discontinuous jointing.

Subsurface reservoir temperatures for Goddard and Baranof Hot Springs have been calculated at 147°C and 118°C, respectively, based on silica and alkali geothermometry (I. Barnes, personal commun.). If a power plant were constructed near the Goddard Springs, the nearest population center is Sitka. In this case, a possible route for powerlines would be northeastward (parallel to Redoubt Lake) for several miles, then northwest around Mt. Granishinikof, and finally underwater across the Eastern Channel of Sitka Sound (a distance of about 5 miles) to Sitka. The total distance would be approximatley 21 miles.

The distance between the Goddard Springs and Sitka precludes direct utilization even if a reservoir of sufficient proportions were found. A deep water reservoir at 150°C could produce enough power either in a flash or a binary system plant. Transmission of power would be feasible.

Figure 2 presents an economic comparison between diesel and geothermal generated electrical costs. An economic model was written that used a rate of return as a comparing yardstick between geothermal and diesel generation. The high investment costs of geothermal development are eventually offset by the high operating costs associated with diesel fuel. The calculation of the rate of return did not take into account the in-town standard administrative and maintenance costs associated with either option. Hence, the R.O.R. should be used for what is intended, i.e., comparison. The market size and the demand for eventual payoff is of course important. As can be seen, the two curves intersect at a plant capacity (or market demand) of 27 MW. If the electrical demand for Sitka is above this level, geothermal becomes more atractive. Yet, the uncertainty of the existence of the geothermal reservoir and the recent committment towards hydroelectric power cast a doubtful light over geothermal energy development.

PILGRIM SPRINGS

The thermal activity at Pilgrim Springs is located in the Pilgrim River Valley, a fault-bounded tectonic depression (graben). Precambrian amphibolites and Mesozoic plutons are the common rock types in the area, with local exposures of conformable and unconformable (overthrust) Paleozoic carbonates. Potassium-argon dating by Turner and Swanson (1981) indicates a cooling age of 84 m.y., which suggests intrusive igneous activity in the Upper Cretaceous.

Gravity surveys conducted in the region by Kienle et al. (1980) indicate that Pilgrim Springs is located near the intersection of two possible fault zones which form the corner of a downdropped basement block. Other faults in the area have been verified by seismic data and geologic mapping, and one or more of these faults could provide deep conduits for the geothermal anomaly.

It has been suggested (Wescott and Turner, 1982) that the Pilgrim River Valley graben may represent an incipient rift extending 250 kilometers across the central Seward Peninsula and offshore into the Bering Sea. Based on this hypothesis, the anomalous heat flow in the Pilgrim Springs area is due to tensional tectonics and active rifting.

The possible existence of a major rift system is significant for the regional geothermal potential. A helium survey was conducted to test this rift model, and nine out of eleven helium anomalies occur near the proposed rift segments and suggest abnormally high heat flow in these areas. Futhermore, extensive basaltic fields north of the Pilgrim Springs area have been interpreted as resulting from eruption in a zone of crustal weakness produced by the general north-south extension (Turner

and Swanson, 1982).

The amount of separation along this proposed rift is less than the widths of the Quaternary depressions which have probably been enlarged by normal faulting and marginal subsidence, along with rifting. Potassium-argon dating indicates that extrusive volcanism which was associated with rifting began in the Upper Miocene (Turner and Swanson, 1981).

Finally, a permafrost boundary has been identified which encloses an area of 1 to 1.5 km^2. The thickness of this permafrost is over 350 ft.

Temperature data at Pilgrim Springs was previously limited to shallow depth (4.5 meters) temperature readings (Turner and Forbes, 1980), Helium soil surveys (Wescott and Turner, 1981), and geothermometry (Motyka and others, 1980). The temperature data for this study were taken from temperature versus depth curves recorded in six exploration wells. These curves showed a trend toward a maximum temperature at depths from 40 to 100 ft, followed by a rapid temperature decrease at depths from 100 to 250 ft, and finally by a constant geothermal gradient ranging from 1.8°C to 2.1°C per 100 ft, down to a depth of 900 ft. Two deep wells (PS4 and PS5) show temperature trends that would intersect at 155°C at a depth of 4875 ft, suggesting that all the wells overlay the source reservoir at a depth of 4875 ft.

The shallow temperature anomaly observed in all the wells suggests that, somewhere in the immediate vicinity, hot water is flowing upward through a fault or fissure system which extends vertically from a depth of about 50 ft to the deep source reservoir at a depth of 4875 ft.

If a power plant were constructed at Pilgrim Springs, the closest major consumer of that electricity would be the community of Nome. One possible route for powerlines would be westward from Pilgrim Springs to the Cobblestone River Valley, crossing the Kigluaik Mountains at Mosquito Pass, and then south to Jensens Camp and along the road to Nome. This distance is roughly 55 miles. The next closest significant settlement is at Teller, which would be a distance of 45 miles.

The Pilgrim Springs geothermal site has a proven intermediate temperature and shallow reservoir capable of producing 300 GPM of 90°C (at the wellhead) artesian water. Induced air lifted flowrates may reach 1500 GPM. A much hotter and hence deeper reservoir has been postulated. However, the distance between Pilgrim Springs and Nome prohibits the consideration of a hot water pipeline while power generation is also quite doubtful. The depth of the reservoir, the length of the transmission line, and transmission line losses preclude a reasonable calculation.

The presence, though, of a significant amount of hot water could aid in two areas: a) development of a large resort area on site and, b) use of the water as a mineral leaching or permafrost thawing medium in present or contemplated mining operations. Such speculative uses are beyond the scope of this report.

COPPER VALLEY

The tectonic framework of the Copper River Basin is dominated by east-west trending orogenic arcs which are concave to the south, and by the Wrangell Mountains to the east. The regional aeromagnetic map of the Copper River Basin suggests that the andesitic and basaltic lavas of the Wrangell massif underlie the mud volcanoes of the Klawasi hydrothermal springs at a relatively shallow depth (Andreason and others, 1964). A rapid decrease in the magnetic gradient westward from Mt. Drum probably indicates that the lavas are thinner and more deeply buried under the alluvium of the Copper River.

The Moore Creek exploration well drilled by the Pan American Petroleum Corporation penetrated olivine basalt of the Talkeetna Formation after passing through 7500 ft of Cretaceous sedimentary rocks. These units probably extend underneath the Wrangell volcanic pile. The Moose Creek Well encountered high pressure water in bentonitic shale at a depth of 5430 ft.

The hydrothermal reservoirs in the Klawasi area are probably artesian aquifers lying at depths of up to 7000 ft within the sedimentary sequence. A significant amount of cooling and mixing occurs during the upward migration of these fluids, especially in passing through glacial till and permafrost. Nichols and Yehle (1961) report surface temperatures of 12 to 30°C and flow rates up to 10 GPM for the Klawasi springs.

For a power plant constructed at

Upper Klawasi Spring, the Lower Klawasi and Shrub Springs are at distances of roughly five and seven miles, respectively, so heat loss during piping of the fluids could be significant. Glennallen is about 20 miles west of Upper Klawasi Spring, and the other community in the area is Copper Center, roughly 15 miles southwest of Upper Klawasi Spring. Either of these two communities would be a likely recipient of the geothermal engery.

An economic comparison of diesel versus geothermal utilization is presented in Figure 2. (A description of the model is included in the Sitka section.) The point of intersection is 22 MW, within the range of forecasted needs in the Copper Valley region. A vigorous geothermal exploration and subsequent drilling (if indicated) is recommended for the Copper Valley region.

SUMMER BAY, UNALASKA ISLAND

The rocks of Unalaska Island consist of three main groups. The oldest and most extensive is the lower Tertiary Unalaska Formation, composed of interbedded igneous and sedimentary members. This formation has been extensively folded, faulted and metasomatically altered. Upper Tertiary calc-alkaline plutons comprise the second lithologic category. These plutons have been emplaced by such mechanisms as assimilation, stoping, and forceful intrusion. The third group consists of basalt and andesite flows of the Quaternary Makushin Volcanics (Drewes and others, 1961).

The first of the two major hydrothermal areas is at Summer Bay. A large normal fault striking N45W and dipping 60 to 75° south is well exposed along the coast just south of Summer Bay. This fault may be projected across Summer Bay Lake and through the Summer Bay warm spring, although exposures are poor. Therefore, joints trending N45W are highly suspected as controlling the source waters of the springs (Reeder, 1981). The largest of the springs has a temperature of 35°C and a dishcarge of 2 GPM. Two shallow exploration wells were drilled in 1980 and encountered temperatures of 43 to 50°C. Silica geothermometry indicates a subsurface reservoir temperature of 86°C (Motyka and others, 1981). It is not clear what lithologic unit is acting as a cap for this aquifer, because no impermeable material was detected during drilling. A very thin layer consisting mainly of mineral precipitates, derived from the warm waters, may exist above the aquifer. Schlumberger electric soundings, EM-31 Geonics surveys, and Dipole-Dipole resistivity surveys indicate that the shallow aquifer is fairly limited in extent. Data from a Helium soil survey suggests that the hydrothermal source is derived from volcanic rocks, and not from acidic igneous or metamorphic rocks found at such places as Tenakee or Goddard Hot Springs. Summer Bay is approximately 5 miles overland to Dutch Harbor or half the distance if an underwater route is employed.

The Summer Bay reservoir at 86°C could be an interesting find. The city of Unalaska presently has 200 customers with an estimated average heat demand of 20,000 BTU/hr per house. Total use on the island is then 4 X 10^6 BTU/hr. The five mile distance will result in a reduction of 25°C from the wellhead temperature. Hence, in the best of cases, a useful temperature drop of 10°F can be contemplated within a proposed system. The flow rate demand will be 400,00 lbs/hr or 800 GPM. At least four (shallow) wells would be needed for such a flowrate, costing $4 million. The pipeline and distribution system would cost another $8 million (using standard engineering economic figures) for a total of $12 million for capital expenditures. The annual operating costs are expected to top $300,000. If a 20 year useful life were to be considered and if no taxes or rates of return were to be imposed, then a cost consideration of $26 per million BTU can be calculated. An average heating bill of $375/month must be assessed on households in order to recover the investment. Such a figure is quite unattractive considering the present (or projected) costs.

MAKUSHIN VOLCANO

The second major hydrothermal area on Unalaska Island is at Makushin Volcano. The rock contacts between the Unalaska Formation and the granitic plutons in the Makushin region are commonly near vertical and irregular, with the intrusive bodies interfingering into the highly altered sediments. Joints are common in these rocks with orientations of N60E and N55W, and the fumarole activity at Fields 2 and 3 appears to follow the N60E joint system. High-angle faults are also common, along with dikes.

Most of the faults appear to be normal faults and strike N55W and N35E. One of these N55W faults trends directly into Fumarole Field 5, and two other faults with N55W orientations bound Fumarole Field 2 (Reeder, 1981).

Large, vapor-dominated hydrothermal systems, are postulated to exist beneath the eastern and southern flanks of Makushin Volcano, where their eastern extent is marked by Field 1 and their western extent delineated by Fields 2 and 3. Such systems are probably driven by dike-like magma bodies located several kilometers beneath the fumaroles. The dominant gases being discharged from most of the fumaroles are CO_2, N_2, SO_2, and H_2S. Motyka and others (1982) estimated reservoir temperatures of between 232 to 278°C, based on gas geothermometry. Three temperature gradient wells drilled during the summer of 1982 encountered maximum bottomhole temperatures of 200°C at a depth of 1500 feet in the plutonic rocks.

Preliminary gravity modeling suggests that the plutonic rocks and the Unalaska Formation extend beneath the Makushin volcanic pile with no major fault displacements. Such lithologies, if highly fractured, could contain large, vapor-dominated, systems at depths greather than about 1 kilometer.

Should a power plant be constructed to utilize the resource, the plant would need to be close to the wells to minimize the loss in quality when transporting steam. Powerlines could follow Makushin Valley for roughly 6 miles to Broad Bay, where underwater cable could transport the electricity to Dutch Harbor, or an overland route around Captains Bay could be constructed. The safest location for power plant construction from a volcanic hazards viewpoint, would be roughly 4 miles east of Field 1 behind the north-trending massif of Vista Ridge (Arce and Economides, 1982).

Unalaska is a major site of geothermal exploration activities in the State. Figure 2 indicates a juncture between the diesel and the geothermal curves at 32MW. Present projections suggest an electric power demand of 50 MW by the year 2000. Geothermal development is indicated if the enormous logistical costs associated with the terrain and the weather are kept in check.

CONCLUSIONS

Of the six sites examined, only two (Copper Valley and Unalaska/Makushin Volcano) appear to be attractive candidates for geothermal development. In both cases, sufficient reservoirs must be discovered. While the geothermal anomalies (and temperatures) are there, the fluid is yet to be discovered. The only means of verification is drilling. The attractiveness of geothermal development depends largely on capital expenditures. Significant overruns beyond the estimates used in this study shift the market size requirements upwards. Such an event would prove geothermal economically unattractive. A high escalation of diesel costs would have the opposite effect.

REFERENCES

Andreassen, G.E., Granty, A., Zietz, I. and Barnes, D.F.: "Geologic Interpretation of Magnetic and Gravity Data in the Copper River Basin, Alaska", U.S.G.S. Prof. Paper 316-H, 1964.

Arce, G.N. and Economides, M.J.: "Analysis of Volcanic Hazards from Makushin Volcano, Unalaska Island, Proc. IV New Zealand Geothermal Workshop pp. 93-99, 1982.

Brew, D.A. and Morrell, R.P.: "Intrusive Rocks and Plutonic Belts of Southeastern Alaska, U.S.A.", U.S.G.S. Open-File Report 80-78, pp 34, 1980.

Drews, H. Fraser, G.D., Snyder, G.L. and Barnett, H.F., Jr.: "Geology of Unalaska Island and adjacent insular shelf, Aleutian Islands, Alaska", U.S.G.S. Bull. 102B-S, pp 583-676, 1961.

Kienle, J., Lockhart, A. and Peace, J.: "Seismic refraction survey of the Pilgrim Springs geothermal area, Alaska", in Turner, D.L. and Forbes, R.B. (Eds.) A Geological and Geophysical study of the Geothermal Energy Potential of Pilgrim Springs, Alaska, UAF Geophysical Institute Report, UAG R-271, 1980.

Loney, R.A., Brew, D.A., Muffler, L.J. and Pomeroy, J.S.: "Reconnaissance Geology of Chichagof, Baranof and Kruzof Islands, Southeastern Alaska", U.S.G.S. Prof. Paper 792, pp. 105, 1975.

Miller, D.S.: "Final Completion Report, Tenakee Drilling Project",

prepared for the State of Alaska, Division of Energy and Power Development, 1981.

Motyka, R.T., Moorman, M.R. and Forbes, R.B.: in Turner, D.L. and Forbes, R.B.. (Eds.): "A Geological and Geophysical Study of the Geothermal Energy Potential of Pilgrim Springs, Alaska", UAF Geophysical Institute Report UAG R-271, 1980.

Motyka, R.J., Moorman, M.A. and Poreda, R.: "Fluid geochemistry of the Makushin geothermal area, Unalaska Island, Alaska", 1982.

Nichols, D.R. and Yehle, L.A.: "Mud Volcanoes in the Copper River Basin, Alaska", In: Raasch, G.O. (Ed.) Geology of the Arctic, International Symposium, Arctic Geology, Calgary, 1960. Proceedings, v.2, pp. 1063-1087, 1961.

Reeder, J.W., Coonrod, P.L., Bragg, N.J., Denig-Chakroff, D. and Markle, D.R.: "Alaska Geothermal Implementation Plan" Report by the State of Alaska to D.O.E., Contract DE-FGS1-79R000074, pp. 108, 1980.

Reeder, J.W.: "Vapor-dominated hydrothermal manifestations of Unalaska Island and their geologic and tectonic setting, " 1981 IAVCEI Symosium-Arc Volcansm, Volcanological Society of Japan and the IAVCEI, pp. 297-298, 1981.

Turner, D.L. and Forbes, R.B. (Eds.): "A Geological and Geophysical Study of the Geothermal Energy Potential of Pilgrim Springs, Alaska", UAF Geophysical Institute Report, UAG R-271 1980.

Turner, D.L. and Swanson, S.E.: "Continental rifting - a new tectonic model for the Central Seward Peninsula", in Wescott, E.M., and Turner, D.L. (Eds.), Geothermal Reconnaissance Survey of the Central Seward Peninsula, Alaska, UAF Geophysical Institute Report UAG R-284, 1981.

Wescott, E.M. and Turner, D.L., (Eds.): "Geothermal Reconnaissance Survey of the Central Seward Peninsula, Alaska," UAF Geophysical Institute Report UAG R-284, 1981.

Wescott, E.M. and Turner, D.L.: "Geothermal Energy Resource Assessment of Parts of Alaska, final report to the Division of Geothermal Energy, D.O.E., pp. 69, 1982.

White, D.E., Muffler, L.P.J. and Truesdell, A.H.: "Vapor-dominated hydrothermal systems compared with hot-water systems", Economic Geology, v.66, no.1, pp. 75-97, 1971.

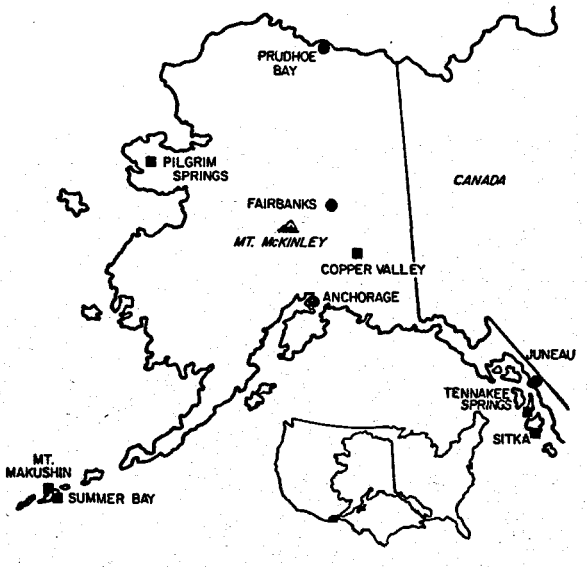

Figure 1. Geothermal Sites in Alaska.

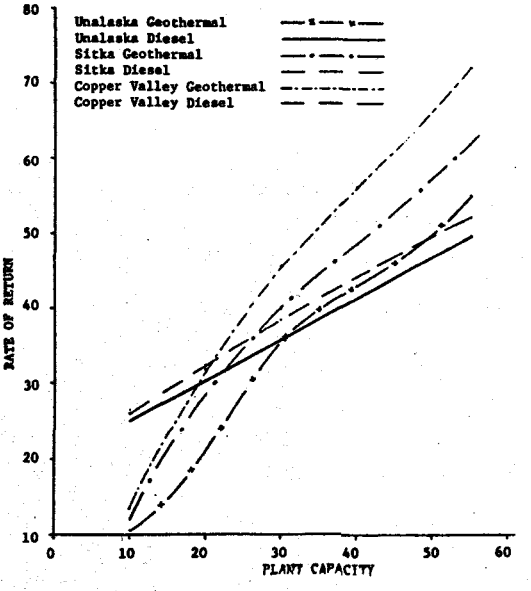

Figure 2. Economic Comparison of Geothermal and Diesel Power Generation in Selected Sites in Alaska.

Proceedings Eighth Workshop Geothermal Reservoir Engineering
Stanford University, Stanford, California, December 1982
SGP-TR-60

HYDROTHERMAL ALTERATION AND TECTONIC SETTING OF INTRUSIVE ROCKS FROM EAST BRAWLEY, IMPERIAL VALLEY: AN APPLICATION OF PETROLOGY TO GEOTHERMAL RESERVOIR ANALYSIS

Mary Keskinen and Jeffrey Sternfeld

Occidental Research Corporation
2100 S.E. Main Street
Irvine, CA 92714

INTRODUCTION

Petrologic and geochemical analysis of subsurface materials can be important in assessment of the potential of a geothermal well and in construction of an appropriate reservoir model for the resource. Qualitative information can be gained relating to the reservoir's thermal evolution, the nature and distribution of fluid flow at depth, and the geologic/tectonic environment controlling the underlying geometry and mechanisms of heat and mass transfer in the reservoir. Geologic models based on petrologic analysis of the Salton Sea and Cerro Prieto geothermal fields (e.g., Younker, et al., 1982; Elders, et al., 1982) have clearly proven the value of such geologic imput in efficient and accurate field assessment and development. In addition to providing data for production and drilling decisions, geologic characterization of the resource can assist in appropriate parameter selection for numerical reservoir modelling and aid in interpretation of geophysical, geochemical, and well log data.

The Imperial Valley lies within the Salton Trough (Fig. 1), a tectonic depression which represents an extension of the spreading center underlying the Gulf of California. During the Cenozoic this basin was filled by a thick sequence of predominantly fluviatile, lacustrine, and deltaic sediments derived from the Colorado River system. The Salton Trough is an area of crustal thinning and extension, characterized by active tectonism, Quaternary silicic and basaltic magmatism, and high regional heat flow (Elders, 1979), leading to its high potential as a geothermal resource. The magmatic activity in the Imperial Valley has few surface manifestations other than the Cerro Prieto and Salton Sea volcanics (Fig. 1), and descriptions of subsurface igneous intrusives from geothermal drillholes have previously been limited and/or proprietary.

Recently, a geothermal well near East Brawley intersected a series of thin (3-35m) diabasic to dioritic intrusives. The petrology and chemistry of these meta-igneous rocks can provide insight into the thermal and fluid chemical characteristics of the reservoir and into the processes of magma generation at depth. A description of the rock types and their hydrothermal alteration is presented in order to increase the petrologic data base relating to this important facet of the geothermal potential of the Salton Trough and to provide a case study illustrating how detailed petrologic examination of well cuttings can provide important input in the construction of a geothermal reservoir model.

PETROCHEMISTRY OF THE INTRUSIVES

The presence of hornfelsic margins both above and below these thin igneous units and their fine to moderate grain size suggest a shallow intrusive origin. The intrusives, which cut thinly interbedded deltaic calcareous sandstones, siltstones, and claystones, are generally calc-alkaline in their chemical affinities (Fig. 2) and similar to diabasic sills from the Salton Sea and Heber areas and to Cenozoic Gulf of California volcanics. These units are slightly more K-rich and alkaline than typical basalts from oceanic spreading ridges (Kay, et al., 1970).

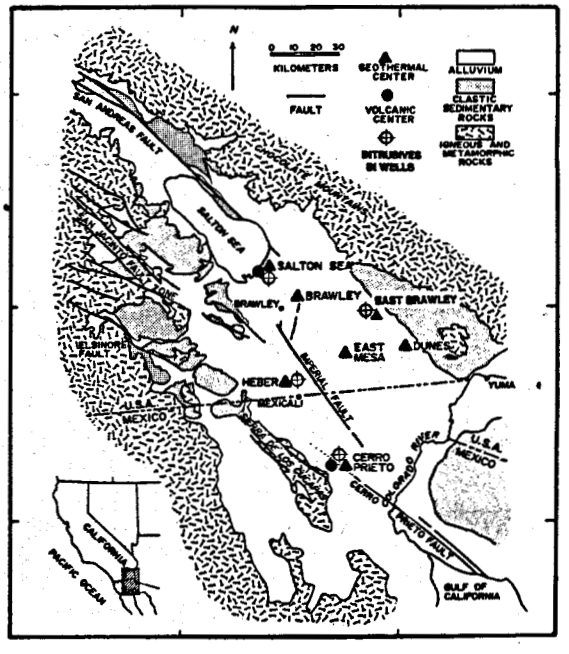

Figure 1. Generalized geologic map of the Salton Trough, modified from Elders, 1979. Locations of reported Quaternary igneous intrusive and volcanic rocks are indicated.

In hand specimen, the dikes are fine to medium grained black to dark green equigranular igneous material, with moderate amounts of calcite, chlorite, and quartz veining suggesting post-solidification fracturing. Texturally, the intrusives originally ranged from glass + crystals (hypocrystalline - now recrystallized to very fine grained crystalline matrix) to equigranular, holocrystalline coarser diabasic material. The very fine grained chips may represent more rapidly chilled thinner intrusives or chilled rims on thicker bodies - vertical control from well cuttings is not precise enough to distinguish between these possibilities.

These rocks had an original mineralogy of euhedral plagioclase (phenocrysts up to 4mm and fine swallowtail laths) + skeletal magnetite + ilmenite + pyroxene + olivine in a fine grained to glassy matrix. This assemblage is appropriate for their normative classification based on ICP analyses (Table 1) ranging from andesite to latite andesite to basalt (Fig. 3). Microprobe analyses permit more precise identification of the opaques as ilmenite + titanmagnetite, of the pyroxenes as augite, and of the few unaltered feldspars as oligoclase, consistent with a diorite to diabase composition.

K-Ar AGE DATES

To distinguish whether the igneous material in this well is related to relatively young Quaternary volcanism (associated with crustal spreading and rifting within the Salton Trough) or represents the older Tertiary to pre-Cambrian basement complex, K-Ar age dates were obtained for three samples (Table 2). The dates are quite consistent (8.1-10.5 million years) and indicate a Pliocene age. The sediments at depths below 10,000 feet in the Imperial Valley may be Miocene or older (Elders, 1979), and hence these intrusions can be related to volcanism which occurred after rifting and sedimentation in the Salton Trough were well established.

TABLE 2: K-Ar Age Dates for Igneous Intrusives from East Brawley

	Age Range (Millions of Years)	% K
Quartz Latite Andesite 1	8.1 ± 0.9	0.624
Basalt/Diabase 5	10.5 ± 0.9	0.870
Diabase 10	8.2 ± 0.8	0.920

K-Ar dates can be affected by slow cooling rates of the intrusion and by later metamorphism, and hence should be regarded as minimum ages. Although the intrusives do show considerable alteration, the plagioclase, which is the probable host for most of the K and Ar, is relatively fresh in these three units. The concordant dates for all three intrusions - much older than the downhole alteration due to the present hydrothermal system - lend credibility to the age dating.

Although no similar dike materials have been reported from other deep wells in the Brawley area, similar diabasic sills and dikes have been encountered during drilling in Cerro Prieto, the Salton Sea geothermal area, and from Heber (Elders, 1979; Robinson et al., 1976; Bird and Norton, 1981; Browne, 1977). Young volcanoes in Cerro Prieto and near the Salton Sea (<1 million years old) also attest to the presence of continued igneous activity in the area.

HYDROTHERMAL ALTERATION OF THE DIKE ROCKS

The dike rocks have been pervasively altered to Greenschist facies mineral assemblages similar to those described by Browne (1977) for the Heber diabase intrusives. Although appearing relatively fresh in the chips, in thin section the mafic minerals and the glassy matrix can be seen to be extensively replaced by chlorite + calcite + amphibole + epidote + sphene. Plagioclase and magnetite appear less

TABLE 1: Whole Rock Chemical Analyses of Igneous Intrusives from the Salton Trough

	East Brawley Intrusive Rocks										Cerro Prieto	Salton Sea			
wt. %	1	2	3	4	5	6	7	8	9	10	11	12	13	14	15
SiO_2	54.1	53.1	54.9	55.6	51.3	53.1	56.2	55.3	51.1	51.7	68.6	73.6	52.2	71.4	51.9
Al_2O_3	13.7	14.4	15.2	13.5	12.9	13.7	15.6	15.0	14.4	12.7	15.6	13.5	14.7	12.8	14.1
FeO	8.9	11.9	8.5	11.1	9.8	11.1	5.6	7.4	12.2	11.6	3.6	1.8	6.2	4.9	11.8
MgO	3.7	4.0	3.7	3.6	3.3	3.7	3.8	3.9	4.5	3.9	0.9	0.2	6.8	0.6	4.8
MnO	<.1	0.2	0.1	0.2	0.1	0.1	<0.1	0.1	0.1	0.2	0.1	0.1	0.2	-	0.1
CaO	7.3	7.7	6.9	5.9	9.9	7.0	6.5	7.0	8.7	7.0	4.7	0.9	10.4	8.8	6.0
K_2O	1.8	1.3	0.7	1.3	1.3	1.3	2.9	2.3	1.0	0.9	1.3	4.1	0.4	5.4	3.1
Na_2O	2.8	2.7	4.9	4.3	3.4	3.6	2.7	2.9	3.5	3.2	2.7	4.5	3.6	3.1	4.4
TiO_2	1.4	2.6	1.9	2.3	1.9	2.2	0.7	1.2	2.4	2.3	0.5	0.04	1.8	0.5	2.4
P_2O_5	0.2	0.3	0.3	0.5	0.3	0.3	0.2	0.2	0.3	0.5	-	-	-	0.1	0.2
BaO	<0.1	<0.1	<0.1	0.7	<0.1	<0.1	0.1	<0.1	0.3	0.9	-	-	-	0.2	0.1
ppm															
Zn	85	118	75	83	84	79	76	71	76	86	-	-	-	-	-
Pb	25	11	<10	<10	<10	<10	<10	<10	<10	<10	-	-	-	-	7
Cu	32	23	5	28	14	17	14	17	26	33	-	-	-	55	30
Ni	18	16	16	36	12	12	16	18	17	17	-	-	-	81	82
Zr	71	118	91	210	88	107	49	75	77	164	-	-	-	500	240

1-10: Analyses by inductively coupled plasma spectroscopy.
FeO: Total Fe.
1,2,7: Quartz-latite-andesite.
8: Quartz monzodiorite.
3,5,10: Basalt/diabase.
4,9: Latite-basalt.
6: Monzodiorite.

11. Average of 2, from Elders, 1979.
12. Average of 4 samples from Obsidian Butte, from Elders, 1979.
13. Average of 5 basaltic xenoliths, from Elders, 1979.
14. Average of 5 subsurface silicic rocks, from Robinson, et al., 1976.
15. Average of 6 subsurface basalts, from Robinson, et al., 1976.

altered, although microprobe/optical analyses indicate incomplete albitization of the feldspars. Secondary growth of white mica, pyrite, hematite, chalcopyrite, rutile, and sphalerite has also been noted. Textural associations of sphene, Ti-magnetite/ilmenite, and chlorite represent the breakdown of Ti-bearing pyroxenes. By analogy with theoretical/experimental data on mineral stability and by comparison with mineralogical and textural zonation with temperature determined by Elders and his coworkers, these rocks correspond to temperatures in the range of 300-320°C - the Calc-Aluminum Silicate Zone of Elders (1979).

Epidote is never present in the great abuncance reported from metasediments from other

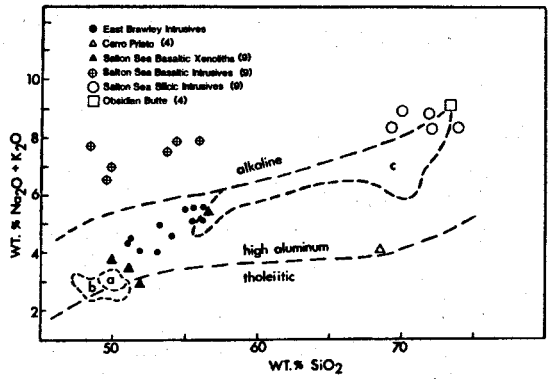

Figure 2. Classification of igneous rock types (in terms of total alkali versus wt. percent silica) from the Salton Trough and Gulf of California. Rock association boundaries are from Gastil, et al., 1979. Numbers in parentheses refer to source of the data in the reference list. Fields "a" and "b" provide average values for Juan de Fuca and Mid-Atlantic ridge basalts from Kay, et al., 1970. Field "c" represents rocks from the Pleistocene Gulf of California volcanic province (Gastil, et al., 1979).

geothermal areas in this temperature range. Its presence in the meta-diabase proves that temperatures were adequate for its stability, and its is believed that inappropriate fluid composition (high fugacity of CO_2, low fugacity of O_2) in the sediments (as evidenced by the persistence of calcite to these depths) inhibits the development of epidote and other calcium aluminum silicates. This suggestion is supported by both theoretical and experimental work on the stability of calcium aluminum silicates (e.g., Allen & Fawcett, 1982). Estimates of f_{S2} and f_{O2} based on the coexistence of anhydrite + hematite + pyrite + magnetite in the dike rocks can also be used to corroborate geochemical estimates from brine analyses and as an indicator of whether the observed mineral assemblages and the brine are in thermal and chemical equilibrium.

FRACTURE ASSEMBLAGES

The petrologic features of the East Brawley reservoir result from the superimposition of flow features on mineralogical/textural changes in response to the high geothermal

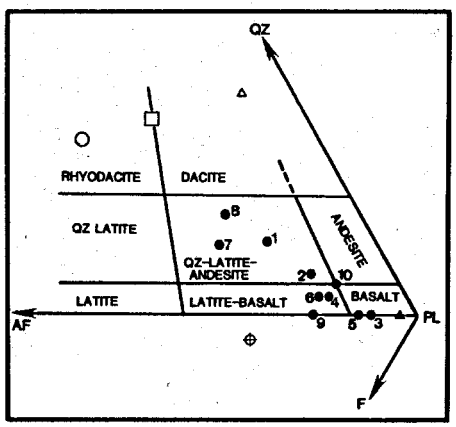

Figure 3. Normative classification of East Brawley intrusive rock types based on ICP analyses shown in Table 1. Symbols for other Salton Sea rocks (some are averages) are shown in Figure 2. AF = Alkali feldspar; F = Feldspathoids; QZ = Quartz; PL = Plagioclase feldspar.

gradient. As such it does not correspond directly to simple models proposed in the literature for other fields.

Production or flow zones in the subsurface can be recognized from well cuttings by diagnostic mineral features. In the shallower metasediments, thick aquifer-type sandstone units bear evidence for significant hot-water flow by the presence of abundant chlorite. SEM photographs of sandstones reveal both euhedral overgrowths on detrital grains (Fig. 4) and dissolution features indicative of dynamic response to flow at depth.

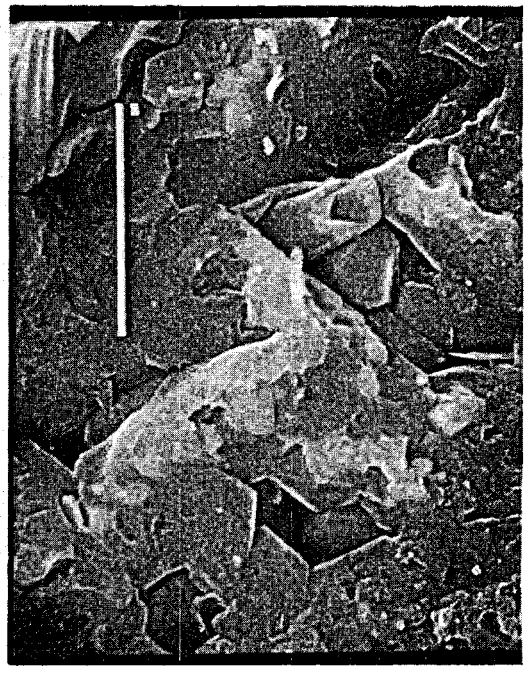

Figure 4. SEM photograph of quartz overgrowths in sandstone/quartzite from a geothermal flow zone at East Brawley. Bar = 10 microns.

Figure 5. Authigenic albite (center) and euhedral quartz crystals in fracture-dominated flow zone from East Brawley. Bar = 1 micron.

Although with increasing depth primary porosity in the reservoir is, in general, decreased as the result of alteration, zones of euhedral quartz crystals (mm-size) within the metasediments and the dike rocks suggest that fracturing (renewable porosity) provides the dominant control on deep subsurface flow. Authigenic albite (Fig. 5), adularia, pyrite, calcite, quartz, and chlorite, all in apparent equilibrium with the present flow system, can further define the chemical characteristics of the geothermal fluids by permitting activity constraints to be calculated. Abundant chlorite in veins and silicification in the sediments adjacent to the dikes further attest to equilibrium between these rocks and the present hydrothermal system. SEM and thin section textural relations suggesting concurrent (simultaneous) growth for most of these vein/fracture minerals are in agreement with fluid inclusion-derived temperature and salinity data.

RELATION OF IGNEOUS ACTIVITY TO THE GEOTHERMAL RESOURCE

These basaltic/dioritic intrusives at depth appear to have a significant relationship to the productivity of the well. Intrusives with ages greater than 8 million years cannot be invoked as direct heat sources for the reservoir. They are, however, probably directly related to deeper continuing dike injection associated with rifting in the Salton Trough. Composition, age, and spatial associations - when compared to basalts from the Gulf of California and from other oceanic spreading centers - suggest that these intrusives are part of a dike swarm (sheeted dike complex) typical of such a tectonic environment.

The change in physical properties with depth due to hydrothermal alteration and local contact metamorphism/silicification (increased density and competence) results in a transition from flow regimes controlled by primary (sandstone) porosity in the upper portion of the reservoir to combined dissolution/matrix porosity to fracture-dominated (secondary) flow at depth. These fractures, which are not easily resealed by mineralization and remobilization of carbonates and sulfates, provide an efficient conduit system which may permit upwelling of thermal solutions and an increase in the local geothermal gradient (a "thermal bulge") in the East Brawley area.

REFERENCES

1. Allen, J.M. and Fawcett, J.J. (1982), Zoisite-Anorthite-Calcite Stability Relations in H_2O-CO_2 Fluids at 5000 Bars: An Experimental and SEM Study: Journal of Petrology, v. 23, 215-239.

2. Bird, D.K. and Norton, D.L. (1981), Theoretical Prediction of Phase Relations Among Aqueous Solutions and Minerals: Salton Sea Geothermal System: Geochim. Cosmochim. Acta, v. 45, 1479-1493.

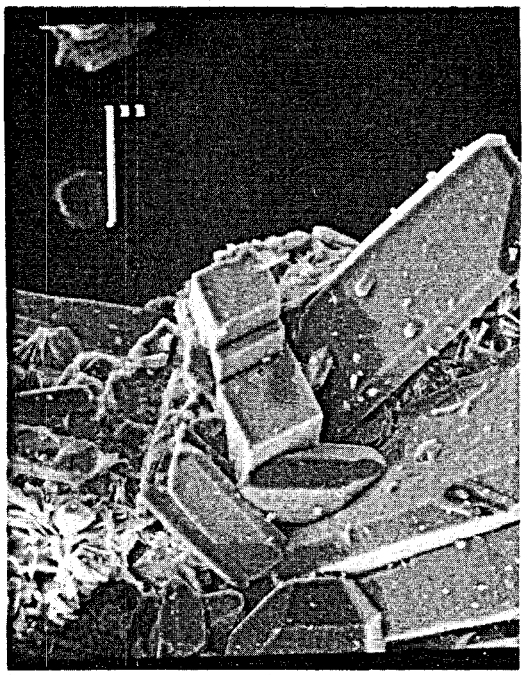

Figure 6. Euhedral quartz crystals, calcite rhombs, and leafy aggregates of chlorite (lower left) indicate equilibrium growth in assemblages lining fractures. Bar = 100 microns.

3. Browne, P.R.L. (1977), Occurrence and Hydrothermal Alteration of Diabase, Heber Geothermal Field, Imperial Valley, California: University of California, Riverside, Institute of Geophysics and Planetary Physics Publication UCR/IGPP-77/9, 70 p.

4. Elders, W.A. (1979), The Geological Background of the Geothermal Fields of the Salton Trough: Guidebook-Geology and Geothermics of the Salton Trough. UCR Campus Museum Publication No. 5, p. 1-19.

5. Elders, W.A., Hoagland, J.R., McDowell, S.D., and Cobo R., J.M. (1979),Hydrothermal Mineral Zones in the Geothermal Reservoir of Cerro Prieto: Guidebook-Geology and Geothermics of the Salton Trough. U.C. Riverside Campus Museum Contribution No. 5, 36-43.

6. Elders, W.A., Bird, D.K., Williams, A.E., and Schiffman, P. (1982), A Model for the Heat Source of the Cerro Prieto Magma-Hydrothermal System, Baja California, Mexico: Proceedings of the Fourth Symposium on the Cerro Prieto Geothermal Field (in press).

7. Gastil, G., Krummenacher, D., and Minch, J. (1979), The Record of Cenozoic Volcanism Around the Gulf of California: Geol. Soc. Amer. Bull., v. 90, 839-857.

8. Kay, R., Hubbard, N.J., and P.W. Gast (1970), Chemical Characteristics and Origin of Oceanic Ridge Volcanic Rocks: J. Geophys. Res., v. 85, 1585-1613.

9. Robinson, P.T., Elders, W.A., and Muffler, L.J.P. (1976), Quaternary Volcanism in the Salton Sea Geothermal Field, Imperial Valley, California: Geol. Soc. Amer. Bull., v. 87, 347-360.

10. Younker, L.W., Kasameyer, P.W., and Tewhey, J.D. (1982), Geological, Geophysical, and Thermal Characteristics of the Salton Sea Geothermal Field, California: Journal of Volcanology and Geothermal Research, v. 12, 221-258.

Proceedings Eighth Workshop Geothermal Reservoir Engineering
Stanford University, Stanford, California, December 1982
SGP-TR-60

CHEMICAL AND ISOTOPIC STUDIES OF THE COSO GEOTHERMAL AREA

R. O. Fournier and J. M. Thompson

U.S. Geological Survey, Menlo Park, CA 94025

ABSTRACT

Wellhead and downhole water samples were collected and analyzed from a 114.3-m well at Coso Hot Springs (Coso No. 1) and a 1477-m well (CGEH No. 1) 3.2 km to the west. The same chloride concentration is present in hot waters entering both wells (about 2350 mg/kg), indicating that a hot-water-dominated geothermal system is present. The maximum measured temperatures are 142°C in the Coso No. 1 well and 195°C in the CGEH No. 1 well. Cation and sulfate isotope geothermometers indicate that the reservoir feeding water to the Coso Hot Spring well has a temperature of about 240-250°C, and the reservoir feeding the CGEH well has a temperature of about 205°C. The variation in the chemical composition of water from the two wells suggests a model in which water-rock chemical equilibrium is maintained as a convecting solution cools from about 245° to 205°C by conductive heat loss.

A total of 39 water samples collected from the Coso geothermal area and vicinity and were analyzed for major chemical constituents, δD and $\delta^{18}O$. Nonthermal ground waters from the Coso Range were found to be isotopically heavier than those from the Sierra Nevada to the west. The similarity of the δD value for the deep thermal water at Coso to that of the Sierra water suggests that the major recharge for the hydrothermal system comes from the Sierra Nevada rather than from local precipitation on the Coso Range. The $\delta^{18}O$ values of the thermal water are about 7‰ heavier than those of the Sierra water. This shift in $\delta^{18}O$ is the result of water-rock reaction at high temperatures, and the magnitude of the shift indicates that the ratio of rock to total water has been large for the system up to its present stage of development. The isotopic data are compatible with the chemical model.

INTRODUCTION

The Coso Geothermal Area is located in east central California on land included in the U. S. Naval Weapons Center, China Lake. The surface expression of hydrothermal activity at Coso is hot ground, fumaroles, and acid-sulfate springs with low rates of discharge. No chloride-rich springs are present. This type of surface expression is typical of vapor-dominated systems, but is not diagnostic.

In 1978 water samples were collected and analyzed from two wells (Fournier and others, 1980). The first well (Coso No. 1) was drilled in 1967, in altered alluvium and granitic rock to a depth of 114.3 m at Coso Hot Springs. The second well (CGEH) No. 1) is located approximately 3.2 km west of Coso Hot Springs and 1.9 km north of Devil's Kitchen. It was drilled in 1977 to a total depth of 1477 m in granitic and metamorphic rocks. On the basis of chemical data obtained from downhole samples, Fournier and others (1980) concluded that a single parental water supplies both wells and that the compositional variations in the waters collected at the wellheads were the result of (1) different amounts of boiling in the wells during upflow and (2) a higher reservoir temperature in the vicinity of the Coso No. 1 well (245°C) than in the vicinity of the CGEH No. 1 well (205°C). These reservoirs are places in the rock where fracturing is locally more extensive than elsewhere, so that permeability and the water/rock ratio are higher there than in the surrounding rock.

In the model of Fournier and others (1980), the water cannot boil as it moves laterally from the 245°C to the 205°C reservoir; if the water had boiled, then the chloride concentrations in the downhole samples from the two wells would have differed. The fact that these two chloride concentrations are nearly identical indicates very slow natural flow and conductive cooling of thermal water as the water moves from the vicinity of the Coso No. 1 well towards the CGEH No. 1 well. The slowness of the flow could be due to very low permeability within the rock connecting the two reservoirs. Alternatively, the permeability could be high (essentially a single reservoir of small vertical extent and with a horizontal temperature gradient) and the convective flow limited by low permeability in the outflow part of the convection system. A

study was then undertaken to determine if the isotopic compositions of the well waters were compatible with the above model, and to determine the recharge area for the hydrothermal system.

Smith and others (1979) measured the deuterium concentrations in rain and snow collected at 26 stations in California and Nevada during the exceptionally wet 1968-69 season. Their results showed that the winter precipitation upon the Sierra Nevada was isotopically slightly lighter than the summer and fall precipitation on the nearby Mojave Desert; most of the Sierra ground-water recharge comes from winter storms moving generally from west to east. These winter storms drop most of their moisture before reaching the Coso Range, which is directly east of the Sierra Nevada. In contrast, most of the Coso Range recharge is from large but infrequent tropical storms moving from south to north. Therefore, the isotopic composition of normal, nonthermal ground water in the vicinity of the Coso geothermal field is slightly lighter than that of nearby Sierra waters.

SAMPLES STUDIED

A total of 39 samples from 37 different sources were collected and analyzed. Of these samples 11 were of cold ground waters flowing from springs and wells in the Coso Range, north and east of Coso Hot Springs within the China Lake Naval Weapons Center; 8 were of Sierra Nevada ground water, collected through a 40-km-long region west and northwest of the Coso area; and 5 were from wells in alluvium of Rose Valley, between the Coso Range and the Sierra Nevada. Fournier and others (1980, table 1) previously reported on the details of the collection and chemical analyses of two samples of thermal water from the CGEH No. 1 well (CC77-4 and CF78-1). Two downhole samples from the Coso No. 1 well (CF79-1 at -50 m and CF79-2 at -95 m) were collected for the present study using a modified version of the Fournier and Morganstern (1971) sampling tool designed for use on wireline equipment.

RESULTS AND DISCUSSION

A plot of δD versus $\delta^{18}O$ (Fig. 1) shows that cold ground waters flowing from the Sierra Nevada and the well waters from Rose Valley all plot near the average meteoric water line of Craig (1961) and have δD values less (more negative) than -100°/oo. The δD values of the Sierra waters generally become more negative to the north (Smith and others, 1979). The cold ground waters collected from springs and wells within the Coso Range also plot near the meteoric-water line (Fig. 1) but have δD values larger (more positive) than -100°/oo, averaging -94°/oo. This difference in isotopic composition between the Sierra ground water and that of the Coso Range reflects the different types of storm systems contributing the major recharge in these two areas, as discussed above.

The two water samples from the CGEH No. 1 well, CC77-4 and CF78-1, plot far to the right of the meteoric-water line (Fig. 1), as do the thermal waters from most geothermal systems throughout the world (White, 1970). As meteoric water flows into a geothermal system and becomes heated, its oxygen exchanges with the isotopically heavy oxygen in the surrounding rock, so that the oxygen in the water becomes isotopically heavier and that in the rock becomes lighter. Hydrogen reacts similarly. However, because the rock contains abundant oxygen and only a small amount of hydrogen, the oxygen-isotopic composition of the water changes considerably while the hydrogen isotopic composition changes only slightly. Therefore, the degree of ^{18}O shift away from the meteoric-water line indicates the relative amount of meteoric water that has reacted with rock, whereas the δD value indicates the δD of the meteoric recharge water. The very large shift in ^{18}O of 7°/oo for samples CC77-4 and CF78-1 indicates that relatively little water has moved through the system (Fig. 1).

The δD value of the CGEH No. 1 water suggests that recharge for the hydrothermal system comes predominantly from the Sierra Nevada to the west with little or no component of recharge from the Coso Range. However, the data do not rule out the possibility that recharge may be a mixture of isotopically light water from parts of the Sierra Nevada north of Coso and isotopically heavy locally derived Coso Range water. The isotopic data unambiguously indicate that recharge for the CGEH No. 1 thermal water is not entirely from locally derived ground water, nor could recharge be from Owens Lake, which is isotopically very heavy because of extensive evaporation (Friedman and others, 1976).

The two samples from the shallow Coso No. 1 well (CF79-1 and CF79-2) also plot far to the right of the meteoric-water line (Fig. 1), but at δD values of -15 and -99°/oo, respectively. The sample from near the top of the water table in this well (CF79-1 at -50 m) contains about twice the total dissolved solids and is isotopically much heavier than the sample from near the bottom of the well (CF79-2 at -95 m). Evaporation from the top of a freestanding column of water in the well accounts for these differences very nicely.

If the model of Fournier and others (1980) is correct, the isotopic composition of the water entering the two wells should be about

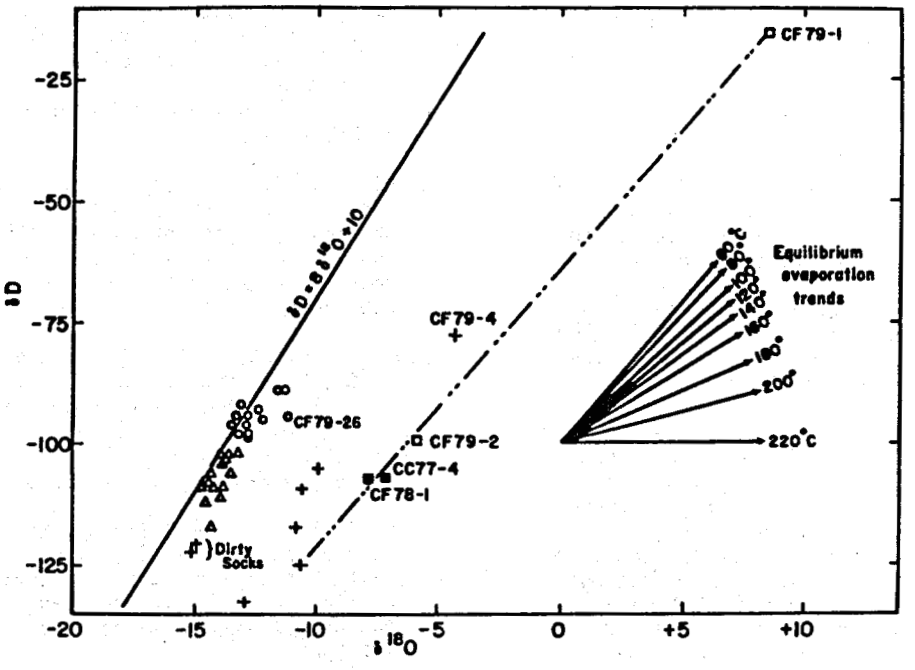

Figure 1. δD versus $\delta^{18}O$ for thermal and nonthermal waters from Coso geothermal area. Circles, nonthermal waters from Sierra Nevada and Rose Valley; solid squares, waters from CGEH No. 1 well; squares, waters from Coso No. 1 well; crosses, other thermal waters and steam condensates..

the same before any boiling or evaporation during upward movement after leaving the respective local reservoirs (if little water-rock isotopic reequilibration takes place because of very slow reaction rates as the temperature changes from 245° to 205°C). The slight difference in the observed isotopic compositions of the downhole samples from the Coso No. 1 well (CF79-2) and the CGEH No. 1 well (CF78-1) appears to reflect slight contamination by evaporated water from the top of the Coso No. 1 well (CF79-1), as shown by the straight-line relation in Fig. 1 for samples from these wells.

CONCLUSIONS

The average meteoric water falling on the Coso Range is isotopically slightly heavier than that falling on the Sierra Nevada to the west. The deuterium concentration in the deep geothermal water is similar to that in the Sierra Nevada ground water and is different from that in the Coso Range water. Therefore, recharge into the deep part of the geothermal system probably comes predominantly from the Sierra Nevada. The main upflow in the hydrothermal system appears to be along a north-northeast-trending fault zone along which Coso Hot Springs is situated. The large shift in ^{18}O of about 7‰ in the thermal water indicates that the rock/water ratio is large and suggests very slow movement of new water into and of old water out of the convection system. The isotopic data are compatible with the geochemical model of Fournier and others (1980), in which some of the chloride-rich hot water ascending along faults that pass through the Coso Hot Springs area encounters other permeable zones and flows laterally toward the CGEH No. 1 well, cooling conductively and reacting chemically with the surrounding rock as it travels. The top of the chloride-rich water remains below ground, and, where underground boiling occurs, fumaroles, acid-sulfate pools, and acid-altered rock occur at the surface.

REFERENCES

Craig, Harmon, 1961, Isotopic variations in meteoric waters: Science, v. 133, p. 1702-1703.

Fournier, R. O., and Morganstern, J. C., 1971, A device for collecting down-hole water and gas samples in geothermal wells, in Geological Survey research 1971: U.S. Geological Survey Professional Paper 750-C, p. C151-C155.

Fournier, R. O., Thompson, J. M., and Austin,C.F., 1980, Interpretation of chemical analyses of waters collected from two geothermal wells at Coso, California: Journal of Geophysical Research, v. 85, p. 2405-2410.

Friedman, Irving, Smith, G. I., and Hardcastle, K. G., 1976, Studies of Quaternary saline lakes-II. Isotopic and compositional changes during desiccation of the brines in Owens Lake, California, 1969-1971: Geochimica et Cosmochimica Acta, v. 40, p. 501-511.

Smith, G. I., Friedman, Irving, Klieforth, Harold, and Hardcastle, K. G., 1979, Areal distribution of deuterium in Eastern California precipitation, 1968-1969: Journal of Applied Meteorology, v. 18, p. 172-188.

White, D. E., 1970, Geochemistry applied to the discovery, evaluation and exploitation of geothermal energy resources: Geothermics Special Issue 2, v. 1, p. 58-80.

Proceedings Eighth Workshop Geothermal Reservoir Engineering
Stanford University, Stanford, California, December 1982
SGP-TR-60

OVERVIEW OF CERRO PRIETO STUDIES

Marcelo J. Lippmann
Earth Sciences Division
Lawrence Berkeley Laboratory
University of California
Berkeley, California 94720

ABSTRACT

The studies performed on the Cerro Prieto geothermal field, Mexico, since the late 1950's are summarized. Emphasis is given to those activities leading to the identification of the sources of heat and mass, the fluid flow paths, and the phenomena occurring in the field in its natural state and under exploitation.

INTRODUCTION

The purposes of this paper are: (1) to review the studies conducted on the Cerro Prieto geothermal field, located about 20 miles south of the city of Mexicali, Baja California, Mexico; and (2) to discuss recent models of the processes in the reservoir and the circulation of geothermal fluids in the system.

The Comisión Federal de Electricidad (CFE), which manages and operates the field, carried out the first studies and surveys, and still continues to evaluate the resource as new wells are drilled and data from existing wells are collected and analyzed.

In 1977 a five-year agreement was signed between CFE and the U. S. Energy Research and Development Administration, now the U. S. Department of Energy (DOE), to conduct a cooperative study of Cerro Prieto (Witherspoon et al., 1978). This agreement resulted in a more intensive study of the reservoir; a wide variety of standard and new geological, geochemical, geophysical and reservoir engineering techniques were carried out. Because of the success of this cooperative program preliminary discussions have been held to sign a new DOE/CFE agreement to study Cerro Prieto and other geothermal areas in Mexico.

STUDIES SPONSORED BY CFE

PRE-1977 STUDIES

Exploration for geothermal resources began in the Mexicali Valley in the late 1950's. Photo and field geologic surveys were concentrated near the Cerro Prieto volcano in an area characterized by numerous hot springs, fumaroles and mud volcanos. Between 1959 and 1961 three relatively shallow wells (up to 755 m deep) were drilled east of the volcano. Only one (well M-1A, Figure 1) produced geothermal fluids, but these were of low enthalpy (Alonso, 1966).

To determine the subsurface structure of the Cerro Prieto area, seismic refraction (GEOCA, 1962) and gravimetric surveys (Velasco, 1963) were carried out. These studies indicated a block-faulted basement, with blocks generally becoming deeper towards the east and major faults striking northwest-southeast. Based on the new subsurface interpretation, four deep exploration wells were drilled in 1964 to intercept some of the inferred faults, reach the geothermal resource and penetrate the basement. Well M-3 encountered relatively hot (~270°C) fluids from about 650 to 900 m depth. Only this well reached basement, at 2532 m. Well M-5 was the discovery well for this field; it produced fluids hotter than 300°C from about 1100 to 1300 m depth (Alonso, 1966).

In 1965 fifty shallow wells were drilled for heat flow determination (Mañón et al., 1978a). In 1966 a geochemical study of the hot springs and fumaroles was completed. Between 1966 and 1968, 15 development wells were drilled in the Cerro Prieto area. After successful well tests were completed the first 75 MW plant was planned. Commercial production of electricity from two 37.5 MW turbogenerators began in 1973 (Alonso, 1978).

On the basis of the geochemical study of the surface manifestations and on the geological and geochemical data from the wells completed at that time, Mercado (1968) presented the first hydrogeologic model of the field showing the circulation of geothermal fluids in the subsurface (Figure 2). The model indicated the entrance from the northeast of cold Colorado River water, which was heated by magmatic gases ascending through the center of the field (between wells M-5 and M-10). Then, deflected by a clay cap rock, the heated fluids moved westward towards the area of well M-6, an area of high-permeability sandstones. There, the fluids leaked to the surface through a fault zone.

In 1968 a study began of the ^{18}O, ^{14}C and deuterium contents in the ground waters of the Mexicali Valley and Cerro Prieto, in particular. The data indicated that these waters originated as Colorado River water altered by evaporation (Crosby et al., 1972).

A regional aeromagnetic survey of the area was completed in 1971 to determine the basement configuration of the Mexicali Valley. The location of a number of strike-slip and normal faults was revealed from this study (Evans, 1972).

Between 1972 and 1975 detailed resistivity surveys of the area were made (García, 1976). The results showed that the field was associated with a large resistivity low which later was found to be due to highly conductive and altered sediments near the surface. (Goldstein and Razo, 1978). A number of faults were identified, including a major one striking northwest-southeast, parallel to the railroad tracks.

To replace damaged wells and to find additional steam to increase power production in the future, 14 new wells were drilled at Cerro Prieto between 1972 and 1974. One of the wells (M-53) was located about 1.5 km northeast of the production area at that time. Its purpose was to explore the eastern region where geophysical data indicated a deep extension of the reservoir. A hot (340°C) reservoir was found at about 1900 m depth (about 600 m deeper than in the western area) which seemed to confirm the existence of an important fault parallel to the railroad tracks.

In 1976 Mercado presented a revised model showing the movement of geothermal fluids in the field (Figure 3). It was a refinement of his 1968 model and was based on new geothermometric and reservoir engineering data. The fluid circulation patterns and temperature distributions shown, especially in the western part of the field, in general have been confirmed by subsequent studies.

Passive seismic studies in the area of Cerro Prieto were carried out in 1974-75 using portable stations. In 1977 five permanent stations were established in the area. The results indicated right-lateral strike-slip faulting parallel to the northwest-southeast striking Cerro Prieto-Imperial transform fault system, and dip-slip faulting along some of the faults oblique to that system (Albores et al., 1978).

1977-1982 STUDIES

Geophysics

Because of their success in the limited area southeast of the Cerro Prieto volcano, CFE in 1977 began a series of geophysical studies in the Mexicali Valley to define the extent of the Cerro Prieto field and to locate other geothermal anomalies. Schlumberger resistivity surveys identified in the area of the field a resistivity low which at that time was assumed to be closely associated with the so-called Cerro Prieto basement horst which had been inferred from gravity data (Razo et al., 1978). Later it was shown that this resistivity low was due to surface effects related to highly conductive near-surface materials (Wilt et al., 1978). On the other hand, Lyons and van de Kamp (1980) indicated that there does not seem to be any convincing geophysical evidence for a basement horst underlying the field.

Gravity, magnetic, and reflection seismic surveys carried out in 1977 enabled Fonseca and Razo (1979) to construct a structural map of the basement. There exists now disagreement about this map since some of the data seem to reflect the alteration of the sediments or the presence of volcanic layers in the valley fill (Lyons and van de Kamp, 1980). However, these studies identified a number of northeast-southwest faults which, at least partially, were confirmed by well log correlation studies. The data gathered were very useful for understanding the subsurface geology at Cerro Prieto (e.g. Lyons and van de Kamp, 1980; Majer and McEvilly, 1982). For example, the magnetic study showed a high centered about 5 km east of the power plant, which later was interpreted as evidence of a basalt/gabbro intrusion which might be related to the heat source for the field (Elders et al., 1982, Goldstein et al., 1982b).

After the 1977 surveys, CFE carried out additional geophysical studies in the Mexicali Valley, most of them to locate new geothermal areas. Only a heat flow study (Díaz, 1978) and a few lines of a 1980 seismic reflection survey (Fonseca, et al., 1981) covered parts of the field. All this time, the monitoring and analysis of the seismic activity continued to study the structure and tectonics of the region (Reyes and Razo, 1979, Reyes et al., 1982; Wong and Frez, 1982).

Geology

In 1978 Puente and de la Peña, and in 1979 de la Peña et al., presented a geologic model of the field based mainly on surface geophysical data and well cutting lithologies. They showed a complex horst-and-graben basement structure and faulting of the sedimentary fill. In their analysis, great weight was given to the A/B contact between unconsolidated (Unit A) and consolidated (Unit B) sediments. This contact was used as a stratigraphic marker horizon. Later, it was found that this was misleading since the A/B contact is an induration boundary that cuts across sedimentary layers, suggesting postdepositional alteration (Elders et al., 1978; Lyons and van de Kamp, 1980; Halfman et al., 1982a).

The cuttings from new wells have been carefully studied by CFE, using mainly a binocular microscope to determine the appearance of key minerals which indicate the presence of high subsurface temperatures. These studies, which are useful to establish well completion depths, have produced lithologic columns and cross section showing the distribution of sand percentage and mineral zones in the field (Cobo, 1981; Cobo and Bermejo, 1982).

Over the years the interpretation of geophysical well logs has been performed by several Mexican authors with the purpose of developing a geologic model of the system (Abril and Noble, 1978; Prian, 1978, 1979, 1981; Díaz et al.,1981).

An ambitious drilling program to establish new production and to define the extent of the geothermal anomaly started in 1977. Between that year and 1982 more than 75 wells were completed at Cerro Prieto (Cobo and Bermejo, 1982). Thirteen of these were planned to be large step-out wells to help define the field boundaries, i.e., wells M-92, M-96, Prian, G-1 (not indicated in Figure 1) and S-262 are now known to be clearly outside the field; wells M-172, H-2, NL-1, M-189 and 0-473 defined approximately the boundaries of the system; wells Q-757 and M-94 are marginal producers; and well E-1, in the western part of the field, discovered a deeper reservoir. This reservoir (B or β) is at about 1550-1800 m depth, and has a temperature of about

335°C, compared to the shallower reservoir (A or α), exploited since 1973, which is about 1000-1400 m depth and has a temperature of about 285°C. After well E-1 was completed, a number of deeper wells (E-series, Figure 1) were drilled in the western part of the field confirming the existence of this excellent geothermal aquifer.

Only two of these 13 exploration wells penetrated basement, well S-262 at 1473 m and well M-96 at 2719 m, even though one well, H-2, was drilled to 3540 m. The cuttings of wells H-2, M-189 and NL-1 indicated that they had drilled through a series of basic and silicic dikes at depths between 2500 and 3540 m (These were also found in production well T-366) Elders et al., 1981; Goldstein et al., 1982b).

Geochemistry

Data on the production characteristics of the Cerro Prieto wells and the chemistry of the fluids produced have been collected and analyzed since the mid-1960's.

Details on the chemical and physical characteristics of the fluids produced by the different wells, the reservoir temperatures computed on the basis of geothermometers, the composition of the reservoir fluids, and their spatial and temporal variations have been discussed by several Mexican authors (Mañón et al., 1978b; Mercado and Samaniego, 1978; Fausto et al., 1979 and 1981; Nieva et al., 1982). A general decrease of reservoir temperatures with time, localized boiling near the wells, and the recharge of colder waters from the west and hot waters from the northeast have been indicated by these studies.

Subsidence

Between 1977 and 1979 three first-order leveling surveys were carried out in the area of Cerro Prieto. The network used in these studies was tied to stations north of the border. In the production area of the field increased ground subsidence was observed. However, it was not clear how much of it was due to fluid extraction and how much to ground shaking related to the strong (6.2 M_L) June 8, 1980 "Victoria" earthquake (de la Peña, 1981).

Reservoir Engineering

In the mid 1970's CFE began carrying out two-rate flow and interference tests in Cerro Prieto wells. A few papers describing the data and results have been published (e.g., Rivera and Ramey, 1977; Rivera et al., 1978; Abril and Molinar, 1979; Abril and Vargas, 1981). The reported permeability-thickness products vary between 3.6 and 40 darcy-meters.

The results of CFE's downhole pressure measurements and the pressure drawdowns observed in the field have been discussed by Bermejo et al. (1979) and Sánchez and de la Peña (1981). The distribution of temperatures in the field have been given by several authors. The latest and most complete set of data is by Navarro et al. (1982), and Rivera et al. (1982).

Over the years CFE has used commercial laboratories to measure hydraulic properties of cores. Recently the Instituto de Investigaciones Eléctricas (IIE) installed a high temperature rock mechanics laboratory for testing samples from geothermal areas. Permeability and porosity data on Cerro Prieto cores have recently been reported by IIE (Contreras et al., 1982a, 1982b).

A number of modeling studies and analysis of production data have been made by CFE and its contractors; part of the results have been reported. Rivera (1977) indicated that the behavior of the Cerro Prieto reservoir and wells could be described using decline curve analysis. In 1978 Rivera described how a graphic procedure could be used for forecasting production. Liguori (1979) simulated the evolution of Cerro Prieto using a mathematical model. He found that a very low heat transfer coefficient between rocks and fluids was adequate to match observed values which he attributed to flow through microfractures as well as pores. His results showed a good match in the steam production rate, but the computed rate of water production was low and the enthalpy too high. Liguori indicated that this was caused by the vertical leakage of colder waters into the reservoir which was not considered by his model.

Saltuklaroglu (1979) analyzed the interference effects between wells. From observation well data he established an average rate of water level drop of 0.56×10^{-6} meter/cumulative ton of discharge. Later this value was used by Grant et al. (1981) to suggest that the α reservoir, the shallow reservoir in the western part of the field, is unconfined.

Based on a simplified reservoir model Molinar et al. (1979), calculated a 20-year production life for Cerro Prieto at an electric power production capacity of 1500 MWe. Using standard groundwater analysis techniques, Sánchez and de la Peña (1981) showed that the α reservoir is very permeable and is recharged from all sides. A permeability-thickness value of 3.4×10^{-3} m^2/s, equivalent to 353 darcy-meters, is given in the paper. According to their data, these authors maintain that the α and β reservoirs in the western part of the field are not connected, at least not locally. The hydrological model of Halfman et al. (1982b) disagrees with this conclusion.

Reinjection

In August 1979 injection of untreated 175-180°C brines began in well M-9. The rate varied between 8 and 80 tons per hour at about constant wellhead pressure. The injection operation has been described in detail by Cortez et al. (1982). It is worthwhile to indicate that a sudden increase in reinjection rate was observed after the June 1980 earthquake; it jumped from about 30 to 70 tons/hr, slowly decreasing with time.

Previously, several treatment methods for colder (about 100°C) brines were evaluated (Hurtado et al., 1981) for possible future use if larger-scale injection operation should begin.

STUDIES SPONSORED BY DOE

PRE-1978 STUDIES

One of the activities carried out before the signing of the 1977 DOE/CFE agreement was to collect available data on Cerro Prieto to incorporate in an open-file data bank (Lippmann et al., 1977). New information is still being added to this bank, which is being maintained by the Earth Sciences Division of the Lawrence Berkeley Laboratory (LBL).

Geochemical studies on Cerro Prieto also began before the formal agreement was signed. In close cooperation with CFE the geochemical data gathered on Cerro Prieto since 1966 were summarized and interpreted by Mañón et al. (1977), and Mazor and Mañón (1978). On the basis of early CFE and U. S. Geological Survey (USGS) data and fluid samples collected between 1977 and 1978, Truesdell et al. (1978a) concluded that production-related drawdown caused the leaking of lower chloride (colder) fluids into the reservoir from above and boiling, with excess steam reaching the producing wells.

In 1977 a preliminary model of the structure of the field was developed by Noble et al. using geophysical well logs, temperature logs, and production and geochemical data.

A self-potential survey conducted in late 1977 detected a large-amplitude, long-wavelength anomaly over the field. In 1978 a more detailed study defined a dipolar self-potential anomaly running through the center of the production field (Figure 4). The source of it appeared to correspond to a north-trending fault, and be caused, possibly, by a electrokinetic (streaming-potential) mechanism (Corwin et al., 1978; Fitterman and Corwin, 1982).

Other 1977 geophysical studies were restricted to the interpretation of CFE Schlumberger resistivity and gravity data using numerical modeling techniques. The gravity interpretation gave clear evidence of a north-northwest trending fault and several trending northeast. The data showed a "basement" high in the production which was interpreted to be the result of a shallow zone of densified sediments (Goldstein, 1977).

The first paper on the hydrothermal alteration of Cerro Prieto sediments was by Reed (1976) of the USGS. In 1977, Elders and his group at the University of California at Riverside (UCR) began thorough petrological and light isotope studies of well cuttings and cores. A number of regularly distributed metamorphic mineral zones were recognized in the field. The progressive changes in mineralogy indicated a systematic relationship with reservoir temperatures (Elders et al., 1978). They also showed that the A/B contact (Puente and de la Peña, 1978) was a postdepositional feature. The isotope studies indicated that the $\delta^{18}O$ for calcite in sandstones could be used to estimate stable reservoir temperatures and that the same parameter in shales could indicate the extent and distribution of subsurface flow (Olson, 1978).

Other results of this work indicated that the Cerro Prieto hydrothermal system is relatively open to fluid flow.

1978-1982 STUDIES

The work pace under the DOE/CFE cooperative program increased in 1978 and did not slow down until quite recently at the expiration of the agreement in July 1982.

Geology

The analysis of cuttings and cores continued at UCR over the entire five-year cooperative program adding vitrinite, fission-track annealing and geophysical well log studies to the petrologic and light isotope work begun earlier (Elders et al., 1979; Barker et al., 1981; Sanford and Elders, 1981; Seamount and Elders, 1981; Williams, 1982). Mainly on the basis of the results of these studies, Elders et al. (1981) developed a model for the natural (pre-production) flow regime at Cerro Prieto (Figure 5). A heat source for the hydrothermal system was suggested to lie to the northeast in an area where wells drilled through basic and silicic dikes. From that source an inclined plume of hot water ascends toward the southwest, boiling in places and precipitating minerals which tend to seal the rock pores. The plume discharges upward and horizontally to the southwest creating surface manifestations and shallow zones of temperature reversals. The model also shows cold water recharge from the northeast which may also seal the reservoir pores as these waters are heated.

In 1978, a study of the paleomagnetism of the rhyodacitic rocks of the Cerro Prieto volcano was made. Magnetic polarity and paleopole position data suggested that the volcanism was initiated about 110,000 years ago. The youngest volcanics reaching the surface cooled about 10,000 years ago (De Boer, 1979).

The analysis of geophysical well logs was conducted during the entire length of the program as new wells were completed. Noble and Abril (1978) described the problems found in interpreting logs obtained from Cerro Prieto wells. Later, and along the same line Ershaghi et al. (1978), Lyons and van de Kamp (1980), Ershaghi and Ghaemian (1980a, 1980b, 1981), and Seamount and Elders (1981) studied the effects of salinity and mineralogy in estimating the parameters of the Cerro Prieto reservoir.

Using mainly wireline well logs and surface geophysical data Lyons and van de Kamp (1980) developed a geologic model of the area that was significantly more detailed than any of the earlier models. They proposed three groups of faults of different ages, and presented a depositional model for the reservoir that showed a transition from a delta environment in the east, to a marine environment in the west. These authors gave well log evidence that disputed the basement-horst structural model; they showed that the gravity high over the reservoir is due

to the high densities of the indurated shales of Unit B. They also showed that the reservoir is not overlain by a laterally continuous low-permeability layer, that the reservoir sandstones present secondary porosity, and that the production intervals in the wells generally straddle or underlie the top of the high-density (and high-resistivity) shales. Lyons and van de Kamp seem to have been the first to suggest that the positive magnetic anomaly, about 5 km east of the power plant, was related to the presence of igneous dikes within the basin fill.

The structural framework of the Mexicali Valley and the Cerro Prieto field was analyzed by Vonder Haar and Howard (1979). The degree and distribution of hydrothermal alteration, and the origin and distribution of dissolution (secondary) porosity in the field were discussed by Vonder Haar (1980, 1981). In 1981, Teilman and Cordon briefly described how the geologic model of Cerro Prieto evolved as new exploration data became available.

A fault map for the field was developed during an internal DOE/CFE workshop (Figure 6) (Lippmann and Mañón, 1980). It showed two types of faults: (1) the NW-SE Cerro Prieto system of strike-slip faults, and (2) the NE-SW Volcano system of normal faults. The existence of a continuous fault near and parallel to the railroad tracks (Michoacán fault) was considered doubtful. On the basis of new data, this map was somewhat modified during a second workshop (Zelwer, 1982).

Recently a micropaleontological analysis of 30 core samples was completed (Ingle, 1982). The distributed patterns of ostracodes and foraminifera together with the lithofacies studies of Lyons and van de Kamp (1980) indicated that the sediments at Cerro Prieto represent a complex of alluvial, deltaic, estuarine and shallow marine environments. These sediments were deposited along the front of the Colorado River delta as it prograded across the Salton Trough during the Pliocene and Pleistocene. Tentative correlation of the Cerro Prieto section with the Palm Spring Formation of the Imperial Valley suggests that the Pliocene/Pleistocene boundary occurs at about 2000 m depth in the area of well M-93. Ingle also found evidence that a sand/shale unit usually present between 700 and 1100 m depth represents a significant mid-Pleistocene marine incursion. The existence of reworked Cretaceous specimens confirmed that a significant part of the deltaic sediments in the area derived from the Colorado Plateau.

After an extensive analysis of geophysical and lithological well logs, Halfman et al. (1982a, 1982b) have recently extended and improved the geologic model developed by Lyons and van de Kamp (1980). By superimposing on the model downhole temperature and well completion data it was possible to establish the movement of the geothermal fluid in the field, prior to its exploitation (Figure 7). The hot fluid appears to enter the system from the southeast, from the area where igneous dikes are believed to have intruded into the valley fill (Lyons and van de Kamp, 1980b; Elders et al., 1982; Goldstein et al., 1982b). Then, the fluid moving westward through permeable layers ascends gradually to shallower depths by flowing upward through faults and sandy gaps in shaly layers acting as local cap rocks. Eventually, in the western part of the field, part of the geothermal fluid leaks to the surface and the rest mixes with colder groundwaters.

Halfman's model seems to indicate that the Michoacán fault (Figure 6), assumed to run parallel to the railroad tracks, does not exist or does not continue southeast of the general area of well M-114. This study has identified three faults (called H, L, and S on Figure 8) which have an important role in controlling the subsurface flow of geothermal fluids. Reflection seismic data (Majer and McEvilly, 1982), the location of boiling zones in the reservoir (Nehring and D'Amore, 1982), and the result of numerical modeling studies (Lippmann and Bodvarsson, 1982) have substantiated the existence of these faults.

The model has also shown, confirming the conclusions of others, that there is no laterally continuous cap rock at Cerro Prieto which prevents the leakage of geothermal fluids from the reservoir. The model indicates that in the general area of well M-10, reservoirs α and β are communicating through a sandy gap in the shale layers.

Geophysics

In 1978, the first LBL detailed seismological study was conducted at Cerro Prieto; two others were made in 1980 and 1981 (Majer and McEvilly, 1979, 1981, 1982). In addition, in late 1980 a downhole geophone was installed in a 100-meter-deep well near well M-6. The purpose of this work was to determine the relation of wave propagation characteristics and microearthquake activity to the production zone, recharge areas, heat source and general lithology and structure of the field. It was found that in the immediate production zone seismicity had increased from 1-2 events/day ($M_L > 1$) in 1978 to 7-8 events/day in 1981, and that these events appeared to be production related. The events registered in 1978 indicated strike-slip movement along northwest-southeast trending faults. The results of later surveys did not permit establishing the type of faulting associated to the monitored events.

The 1980 seismic events were clustered near the center of the production area, at depths from 2 to 5 km, on a fairly well defined north-south plane extending from well M-101 to the power plant. On the other hand, the 1981 events were distributed in a rather diffuse pattern concentrated on the western edge of the field. The diffuse pattern of the 1981 events and the increase in seismicity may indicate that the area is undergoing a transformation from aseismic creep to stick-slip behavior, which is accelerated by the extraction of fluids from the field (Majer and McEvilly, 1982).

During the 1978-1981 period four precision gravity surveys were conducted at Cerro Prieto to study the possibility of geothermally induced subsidence (Chase et al., 1978; Grannell et al., 1981, 1982). Comparison of results from year to year showed subsidence clearly associated with the June 1980 earthquake. Also, significant changes were observed at several stations in the western (older) part of the field. The pattern of these latter changes is elliptical in a northwest-southeast direction parallel to the structural grain and faulting in the region. By correlating precision gravity and leveling data, Zelwer and Grannell (1982) concluded that changes in gravity and surface elevation correlate well, and were primarily produced by compaction that occurred in response to the June 1980 earthquake. However, Grannell et al. (1982) also suggest that this subsidence is probably of geothermal origin because they considered that the natural recharge of the field is not keeping pace with production. Zelwer and Grannell (1982) also indicated that a density increase is taking place in the reservoir zone because of mineral precipitation or the entrance of cooler, denser, waters. Further analysis of the data will be required to clarify the importance of fluid extraction on the subsidence observed at Cerro Prieto.

The first LBL dipole-dipole resistivity survey at Cerro Prieto was completed in 1978. A two-dimensional vertical resistivity model along a northeast-southwest line across the field (line E-E') was developed (Wilt et al., 1978). It showed that the production region is characterized by high resistivity (4 ohm-m) relative to the surrounding region (1 to 2 ohm-m). The higher resistivity is assumed to be related to the densification of the shales in Unit B.

The 1979 studies improved the resistivity model for the eastern part of the field (Wilt and Goldstein, 1979). It revealed that the 4 ohm-m body associated with the producing zone dips eastward at 30 to 50 degrees to a depth greater than 2 km (Figure 9). A narrow, steeply dipping 1.5 ohm-m zone immediately to the east was interpreted as a possible zone of recharge or faulting.

Repetitive high-precision dipole-dipole resistivity measurements taken during the period 1979-1981 over line E-E' showed a consistent pattern of apparent resistivity changes. A zone of increasing resistivity is related to the production region; above and flanking this region are zones of decreasing resistivities. These changes were interpreted as near-surface effects due to changing irrigation patterns and deeper effects due to lateral recharge of cooler, less saline fluids into the shallow western α reservoir. There is also an unresolved component that might relate to ascending hot fluids at the eastern edge of the producing zone (Wilt and Goldstein, 1982).

The changes in apparent resistivities detected at Cerro Prieto from the dipole-dipole monitoring surveys were studied by Pruess et al. (1982) and Goldstein et al. (1982a) using reservoir modeling techniques combined with dc resistivity calculations. Based on schematic one- and two-dimensional reservoir simulations, assuming the existence of waters of different salinity and temperature, changes in formation resistivity were computed which were then transformed into changes in apparent resistivity that would be observed at the surface.

Over a period of three years starting in 1978, three magnetotelluric (MT) studies were made in the area of the field. The initial purpose of the MT soundings was to provide additional and deeper subsurface resistivity data to supplement the dipole-dipole and Schlumberger surveys conducted in the region. Subsurface resistivity models developed jointly from the dipole-dipole resistivity and MT data sets helped define the deep resistivity structure of the field. The models also showed: (a) the inferred position of faults in the system; (b) a front of cooler, less saline Colorado River water entering from the east; and (c) the A/B contact between nonconsolidated and consolidated sediments (Gamble et al., 1979; Goubau et al., 1981). Later MT studies were conducted to help delineate a possible boundary on the south side of the thermal area.

Recently Goldstein et al. (1982b) analyzed the broad magnetic anomaly observed about 5 km east of the power plant. Their modeling studies, coupled with the analysis of cuttings of mafic dikes recovered from well NL-1, and viewed in conjunction with other geological and geophysical data, gave further support to the hypothesis that Cerro Prieto is located in a pull-apart basin like others in the Salton Trough and the Gulf of California (Lomnitz et al., 1970; Elders et al., 1972), into which igneous basic rocks are being emplaced. These authors estimate that the top of the main magnetic source body is about 3.5 km below the surface, and that the present melt zone may be at 10-12 km depth, as determined from seismic (earthquake) observations and a Curie isotherm analysis.

On the basis of preliminary thermal modeling results, Elders et al. (1982) suggested that the present subsurface temperature distribution determined from deep wells can be fitted approximately to a single stage of magmatic intrusion in the form of a funnel-shaped gabbroic body, some 4 km across at the top at a depth of 5 km. The model age for such an event is 30,000 to 40,000 years, which is in the range of the age for the volcanic activity at Cerro Prieto (de Boer, 1979). The depth is quite shallower than the 10-12 km depth of the present magma inferred by Goldstein et al. (1982b). Above the intrusive, Elders postulated the existence of a sheeted dike complex which would correspond to the dikes found in some of the deep wells in the eastern part of the field.

Subsidence

Measurement of horizontal ground-surface movements in the northern part of the Mexicali Valley and around Cerro Prieto began in 1978 (Massey, 1978, 1979, 1981). Inward movement toward the center of the production area was

observed during the 1978-81 study period. The movement, probably not exceeding 6 or 7 cm, occurred mainly between 1978 and 1979 and was confined to the production area. A consistent change in the length of the survey lines crossing the well field, similar to the general shortening detected in 1978-79, was not observed over the 1978-81 period.

Massey (1981) indicated that the ground-surface movements in the production area were due to fluid extraction. However, an increase in the rate of deformation resulting from the continuous exploitation of the field was not evident for the longer time period. Outside the well field ground deformation, excluding earthquake related movements, was small.

Lisowsky and Prescott (1982) studied ground deformations near the epicenter of the June 1980 (M_L = 6.2) Victoria earthquake, located about 30 km southeast of Cerro Prieto. Their analysis showed that production-induced deformations at the field could not be observed or were masked by earthquake-related changes.

In 1978 cores from Cerro Prieto were studied in the laboratory to determine the permeability, thermal conductivity and deformation properties of reservoir rocks. The tests made at that time indicated large changes in properties occurring with temperature and stress (Somerton, 1978, Martínez, 1978). Later, cores were tested under simulated in situ conditions to measure porosity reduction and establish short- and long-term compaction triggered by reservoir drawdown (Abou-Sayed et al., 1979; Schatz, 1982).

It was found that the rocks behaved as expected with respect to instantaneous compaction, and that they present a tendency to compact further with time (creep). The results obtained when extrapolated to a reservoir life of 20 to 30 years showed that reductions of several percent in porosity and several tens of percent in permeability are possible. Instantaneous compaction-related subsidence might be small; however, creep-related subsidence might be significant at Cerro Prieto (Schatz, 1982).

Geochemistry

The scope of geochemical studies on Cerro Prieto geothermal fluids also increased in 1978 as a result of the DOE/CFE agreement. A review of the studies carried out both by U. S. and Mexican scientists has been made by Truesdell et al. (1982).

The 1978 isotopic studies indicated local recharge from the area immediately to the west of the field and leakage of shallower waters into the reservoir. The tritium and ^{14}C contents in the fluids could only suggest an average age between 50 and 10,000 yrs. (Truesdell et al., 1978b).

The work by Mazor and Mañón (1978) indicated regularities and correlations between different ions in the Cerro Prieto fluids, indicating concentration-dilution processes, such as steam loss or mixing with condensed steam and possibly fresher waters from shallower aquifers. The data also suggested that the deep brine has a chloride content of about 10,000 ppm, that no significant reactions occur during the ascent of fluids through the wells, and that temperature zonation existed in the reservoir. This zonation makes the reactive K and SiO_2 ions useful as geothermometers at Cerro Prieto.

The study of the composition of the gases produced from the wells began in 1977 (Nehring and Fausto, 1978). By analyzing the spatial distribution of different gases in the field and using gas geothermometers, Nehring and D'Amore (1982) interpreted that in 1977 a large boiling zone existed in the center of the production area. Changes between 1977 and 1982 seem to indicate that some colder groundwater is leaking into the reservoir, and that the boiling zone is not expanding and possibly receding because some of the wells have been taken out of production.

On the basis of computed deuterium and chloride concentrations in the reservoir brines and measured Cl/Br ratios, Truesdell et al. (1979) concluded that the geothermal fluids are a mixture of Colorado River water and a saline brine of seawater origin. The study showed that this mixture circulated deeply and was extensively altered compositionally by high-temperature reactions involving reservoir rocks.

The surface manifestations were studied by Valette-Silver and others. Five types of surface emissions, each of different chemical characteristics, were identified along the western edge of the production area. A similarity in isotopic composition and ratios of major elements was observed between the hot springs and the producing wells, suggesting that the geothermal reservoir and the springs are closely related. This relationship is also indicated by the chemical changes observed in the hot springs after fluid production began in the field (Valette and Esquer-Patiño, 1979).

The hydrothermal alteration of the sediments associated with the surface manifestations appears to be controlled by the type of emanation. However, most of the sediments in contact with the geothermal fluids show an increase in quartz and potassium feldspar. Below 180°C similar trends in mineralogy changes are observed in the reservoir and in the surface manifestations (Valette-Silver et al., 1981a). Preliminary attempts at modeling the chemical processes and study the reactions between sediments and fluids of the surface manifestations using chemical equilibrium calculations were made by Valette-Silver et al. (1981b).

Nehring and Valette-Silver (1982) studied the differences in gas composition between well and surface manifestation samples. They found that with respect to the wells the surface features show a loss of H_2S because of reaction with metal ions or air and an increase of nitrogen due to mixing of ground and geothermal waters as the latter move toward the surface.

Mazor and Truesdell (1981) used radiogenic and atmospheric noble gases as tracers to develop a dynamic model for the field. They suggested that the geothermal fluids are dominated by meteoric waters which have penetrated to more than 2500 m depth and then mixed with radiogenic helium and argon-40 formed in the reservoir rocks. Afterwards small amounts of steam are lost by continuous removal as it forms (a Raleigh process) and mixing occurs with shallow colder waters.

The radon and ammonia concentrations in the produced fluids were analyzed by Semprini and Kruger (1981, 1982). The data show that a correlation exists between the radon content and the specific volume of the reservoir fluids. They studied the variations in time and space of the radon concentration to determine changes in the field due to exploitation. Supported by other reservoir data, their analysis indicates an expansion of the two-phase zone in the northeastern part of the field and a decrease in the southeast.

Grant et al. (1981) analyzed chemical, production and reservoir engineering data to study the processes within the relatively shallow western α reservoir. Their model indicates that this reservoir is bounded below by low-permeability rocks and above and to the sides by an interface with cooler water; there is no continuous permeability barrier around or immediately above the reservoir, and permeability within the reservoir is predominantly intergranular. They also show that in the natural state, reservoir cooling takes place mainly by mixing of cooler water with the hot water, rather than by boiling. Production has caused displacement of hot water by cooler water rather than by vapor. Local boiling occurs near most wells in response to pressure decreases, but no extended vapor zone has formed (Figure 10).

Recently on the basis of stable water isotopes, tritium values and chemical composition data Makdisi et al. (1982) concluded that: (1) groundwater in the northern and central regions of the Mexicali Valley originates from the Colorado River; (2) near Cerro Prieto, groundwater originates from a mixture of Colorado River water and geothermal brines; (3) other western groundwaters reflect a mixture of Colorado River water and water from a paleoequivalent to the present Salton Sea; (4) variations in the groundwater chemistry within a given region results from mineral-water reactions dependent on the lithology of the reservoir rocks, as well as evaporation and mixing; and (5) higher groundwater temperatures in the southern and western areas of the Mexicali Valley probably increase rates of ion exchange reactions that produce higher salinities.

The chemical equilibrium between Cerro Prieto geothermal fluid and detrital and alteration minerals of the reservoir were studied by Truesdell and Henley (1982). The fluid appears to be in equilibrium with aquifer minerals. On the other hand, the dissolved gases CO_2, H_2S, H_2, N_2, and NH_3 are in equilibrium with each other, although CH_4 equilibria are apparently frozen in at temperatures somewhat above those of the reservoir.

The variations of ^{13}C in Cerro Prieto fluids were studied by Janik et al. (1982). It was found that the changes in the ^{13}C content in CO_2 over time and location within the field indicated the deposition of calcite in near-well boiling zones and subsequent re-solution. They indicated that the source of the carbon may be of magmatic or sedimentary origin, and that the CO_2 from some surface manifestations is heavily influenced by decomposition of organic matter.

Des Marais et al. (1982) measured the hydrocarbon abundance and stable carbon isotope composition in fluids from various Cerro Prieto wells. Parallel measurements were made on gases from laboratory pyrolysis of coal obtained from samples of one of the wells, in an attempt to simulate the production of the geothermal hydrocarbons. The best correlation between the laboratory and well data was obtained when laboratory produced gases from experiments at 400°C and 600°C were mixed. This suggested that the wells are sampling hydrocarbons produced over a range of depths and temperatures in the sediments.

Reservoir Engineering

The only long-term well-interference and build-up tests conducted by DOE-sponsored groups at Cerro Prieto were described by Schroeder et al. (1978). In one of these tests, interference was observed between wells M-10 and M-53, completed in the α and β reservoirs, respectively. The communication between these aquifers was confirmed by the geological model of Halfman et al. (1982b).

In 1979 a two-rate flow test was carried out using a downhole tool modified by Sandia Laboratories for high-temperature wells. No results were reported as the tool failed after 12 hours in a 340°C well. Castañeda and Horne (1981) described the use of pressure gradient techniques to locate feed zones and internal flows in Cerro Prieto wells.

Since 1979 the characteristics of the Cerro Prieto production wells have been studied at LBL. Using known wellhead data, Goyal et al. (1980, 1981) calculated downhole pressures, temperatures, and saturations in flowing wells. The data show that during the period 1973 to 1980 the pressures and temperatures decreased by about 15 bars and 20°C, and the steam saturations had increased slightly in the near-well regions. The studies confirmed the fact that computed downhole pressures are very sensitive to measured wellhead conditions and to changes in inside well diameter.

Heat and mass production data for the period 1973 to 1980 were analyzed by Goyal et al. (1981). It was found that the production of individual wells generally decreased with time due to relative permeability effects, a reduc-

tion in permeability, and/or a reduced pressure gradient in the reservoir. The average enthalpy of the produced fluids has varied over the years. The increases in enthalpy were usually the result of bringing higher-enthalpy wells on line. The decrease in the average enthalpy was thought to be due to the mixing of relatively colder water with the geothermal reservoir fluids.

Goyal et al. (1982) studied the distribution of heat and mass production in the field to determine the initial state of the α and β geothermal reservoirs and the behavior of these aquifers under exploitation. They also analyzed the changes in production characteristics in different wells and the interference effects between wells, establishing the existence of flow barriers and cold boundaries in the reservoirs.

Preliminary reservoir modeling studies of the field's behavior were carried out by Lippmann et al. (1978) and Lippmann and Goyal (1979). Westwood and Castanier (1981) used a lumped-parameter model to gain insight into the physical processes in the reservoir and its response to production. The results suggested that the producing zone became two-phase early in the production history of the field and that strong radial, or spherical, recharge of 260°C water exists.

On the basis of the temperature data given by Castillo et al. (1981), Lippmann (1982) computed the amount of heat stored in the field. A mineable heat of 23.8×10^{13} kcal was obtained using 200°C as the lowest temperature of interest, 3000 m as maximum depth, and assuming that 25% of the total heat stored could be extracted. Taking into consideration the efficiency for electrical conversion (Brook, et al., 1979), a total capacity of 3.16×10^4 MWe-yr, or about 1050 MWe for 30 years, was calculated. This value is similar to the one given by Molinar et al. (1979).

Observed chemical and thermal changes in the reservoir were used by Grant and O'Sullivan (1982) to study the recharge characteristics of the old (western) production field. Based on pressure changes the permeability of the layer overlying the reservoir was calculated. It was found that it was considerably less permeable than the producing aquifer but not sufficiently impermeable to exclude inflow of cooler waters from above. The authors concluded that the α reservoir in the old field is best considered as a leaky aquifer. They estimated that one-quarter to one-half of its recharge derives from cooler rock immediately above it.

A two-dimensional distributed-parameter model was used by Lippmann and Bodvarsson (1982) to study the natural flow of heat and mass through the Cerro Prieto system and the impact of fluid production on the behavior of the field. The results indicated that the Halfman et al. (1982a, 1982b) hydrogeological model is reasonable and consistent with the mass and heat flows in the system. It is shown that the field in its natural state is recharged from the east with hot (about 255°C) water as well as with colder (between 50° and 150°C) waters from shallower aquifers, especially from the west. Some boiling occurs as the hot water ascends through a sandy gap in the shaly layers.

The study of the reservoir response to exploitation showed that most of the fluid recharge to the α reservoir comes from the west and from shallow waters flowing through Fault L. The recharge from the east seemed to be minor due to the presence of a two-phase zone in the sandy gap communicating the α and β reservoirs, near well M-10. Because of the large fluid recharge no extensive two-phase zone develops in the shallow α reservoir.

Reinjection

In support of CFE reinjection tests, the chemistry of silica in Cerro Prieto brines was studied theoretically and in the laboratory (Iglesias and Weres, 1979; Weres et al., 1980). It was established that part of the dissolved silica quickly polymerizes to form suspended colloidal silica. Raising the pH of the brine and stirring produces a rapid and complete flocculation and settling; these results were confirmed by field tests (Hurtado et al., 1981). Weres and his colleagues also developed a simple preinjection treatment for the Cerro Prieto brines, analyzed their equilibrium chemistry and studied the rate of deposition of silica scale from synthetic brines.

The response of the Cerro Prieto field to reinjection was simulated numerically by Tsang et al. (1978, 1979, 1981, 1982). These studies confirmed that the breakthrough of the injected cold water into the production zone is strongly dependent on the location and completion of the injection wells, indicating the need of a carefully planned and monitored production-injection operation to optimize the extraction of the heat stored in the reservoir rocks.

Tsang et al. (1982) incorporated into their model some of the geologic features desribed by Halfman et al. (1982b). The results showed that significant pressure-sustaining effects can be obtained in the producing reservoir by injecting 30% of the fluid extracted.

SUMMARY AND CONCLUSIONS

The present model for the natural (pre-exploitation) circulation of geothermal fluids in Cerro Prieto can be summarized as:

- Waters of Colorado River and seawater origin penetrate deeply into the sedimentary fill of the Mexicali Valley.

- These brines are heated by a thermal source consisting of diabase dikes and gabbroic cummulates presumed to have intruded the eastern part of the field 10^3 to 10^4 years ago. A melt zone and magmatic injection at 10 to 12 km depth may be active presently.

- In response to pressure gradients and bouyancy effects the hot fluids move toward the west through a sandy unit (Reservoir β) overlain by a thick shaly layer.

- The geothermal fluids hydrothermally alter the sedimentary rocks, decreasing their primary porosity. In sandstones some of this effect is offset by the removal by solution of unstable grains and cements (Lyons and van de Kamp, 1980).

- During circulation the composition of the fluids is extensively altered by high-temperature reactions with reservoir rocks.

- As they move westward toward the present production area, the geothermal fluids tend to flow upward through faults and permeable gaps in the overlying shaly layers. During the ascent and because of pressure reduction, some boiling and mineral deposition occurs.

- In the general area of well M-10, where a major sandy gap interrupts the lateral continuity of the shaly materials, some of the geothermal fluids mix with colder waters at shallower depths causing secondary mineral precipitation and porosity reduction. However, most of the hot fluids move into the α and β reservoirs in the western part of Cerro Prieto.

- Along the western edge of the field colder groundwaters are in lateral contact and mix with the geothermal fluids; precipitation of minerals occurs.

- Also in the western areas of the field some of the hot fluids ascend to shallower depths through fault zones, eventually reaching ground level. This is evidenced by the abundant surface manifestations observed along the western edges of the producing area.

A general decrease of pressure and temperature has been observed in the reservoir since fluid production began in 1973. However, because of the open nature of the reservoir, only localized boiling has occurred near the wells. An extensive two-phase zone does not develop, as ample recharge of colder, less saline waters from shallower layers and from the western edges exists. The near-well boiling causes enthalpy excesses in the produced fluids that decrease or disappear with time as the boiling front stabilizes. The boiling results in silica deficiencies in the produced fluids and deposition of quartz near the wells (Grant et al., 1981). Other changes in the characteristics of the produced fluids and interference effects between wells have also been detected (Truesdell et al., 1982).

Great advances have been made toward understanding Cerro Prieto. We hope that many of the studies initiated under the 1977-1982 DOE/CFE agreement will continue and add important new information as the field is expanded. (CFE plans to increase the electrical power output from the present 180 MWe to 620 MWe before the end of 1984.) For example, more needs to be known about the hydraulic properties of the sandy and shaly layers; the hydrogeological model should be updated as new results and field data become available; and the general monitoring of the behavior of the field should continue, especially as new areas come under production.

ACKNOWLEDGEMENTS

This paper would not have been possible without the cooperation of the personnel of the Coordinadora Ejecutiva de Cerro Prieto of CFE who, over the years, have provided the necessary data and assistance. Special thanks are due to Norman Goldstein (LBL) and Alfred Truesdell (USGS) for the stimulating discussions and invaluable suggestions.

This work was supported by the Assistant Secretary for Conservation and Renewable Energy, Office of Renewable Technology, Division of Geothermal and Hydropower Technologies of the United States Department of Energy under Contract No. DE-AC03-76SF00098.

REFERENCES

To avoid repetitions the proceedings of the symposia on Cerro Prieto will be referenced using the following abbreviations:

CPI: Proceedings of the First Symposium on the Cerro Prieto Geothermal Field, September 20-22, 1978, San Diego, California; Lawrence Berkeley Laboratory report LBL-7098.

CPII: Proceedings of the Second Symposium on the Cerro Prieto Geothermal Field, October 17-19, 1979, Mexicali, Baja California, Mexico, Comisión Federal de Electricidad.

CPIII: Proceedings of the Third Symposium on the Cerro Prieto Geothermal Field, March 24-26, 1981, San Francisco, California; Lawrence Berkeley Laboratory report LBL-11967.

CPIV: Proceedings of the Fourth Symposium on the Cerro Prieto Geothermal Field, August 10-12, 1982, Guadalajara, Mexico, Comisión Federal de Electricidad (in preparation).

Abou-Sayed, A.S., J.F. Schatz, and K.M. Wolgemuth, 1979. Compaction and permeability of Cerro Prieto cores: A Laboratory Evaluation. CPII, pp. 263-268.

Abril, A. and R. Molinar, 1979. Description and interpretation of transient well pressure tests at the Cerro Prieto geothermal field. CPII, pp. 513-520.

Abril, A., and J.E. Noble, 1978. Geophysical well log correlations along various cross sections of the Cerro Prieto geothermal field. CPI, pp. 41-48.

Abril, A. and C. Vargas, 1981. Results of the latest transient well pressure tests at Cerro Prieto. CPIII, pp. 504-511.

Albores, A., C.A. Reyes, J.N. Brune, J. Gonzalez, L. Garcilazo, and F. Suárez, 1978. Seismicity studies in the region of the Cerro Prieto geothermal field. CPI, pp. 227-238.

Alonso, H., 1966. La zona geotérmica de Cerro Prieto, Baja California. Bol. Soc. Geol. Mex., v. 29, pp. 17-47.

Alonso, H., 1978. The Cerro Prieto geothermal field - Present and future. CPI, pp. 409-410.

Barker, C.E., M.J. Pawlewicz, N.H. Bostick, and W.A. Elders, 1981. Evolution of the Cerro Prieto geothermal system as interpreted from vitrinite reflectance under isothermal conditions. CPIII, pp. 88-96.

Bermejo, F.J., F.X. Navarro, F. Castillo, C.A. Esquer, and C. Cortez, 1979. Pressure variations at the Cerro Prieto reservoir during production. CPII, pp. 473-496.

Brook, C.A., R.H. Mariner, D.R. Mabey, J.R. Swanson, M. Guffanti, and L.J.P. Muffler, 1979. Hydrothermal convection systems with reservoir temperatures > 90°C. U.S. Geological Survey Circular 790, pp. 18-85.

Castañeda, M. and R.N. Horne, 1981. Location of production zones with pressure gradient logging. Geoth. Resour. Council Trans., v. 5, pp. 275-278.

Castillo, F., F.J. Bermejo, B. Domínguez, C.A. Esquer, and F.J. Navarro, 1981. Temperature distribution in the Cerro Prieto geothermal field. CPIII, pp. 474-483.

Chase, D.S., R.C. Clover, R.B. Grannell, R.M. Leggewie, F. Eppink, D.W. Tarman, and N.E. Goldstein, 1978. Precision gravity studies at Cerro Prieto. CPI, pp. 249-257.

Cobo, J.M., 1981. Configuration of the mudstones, gray-and coffee-colored shale lithologic units, zones of silica and epidote, and their relation to the tectonics of the Cerro Prieto geothermal field. CPIII, pp. 29-45.

Cobo, J.M. and F.J. Bermejo, 1982. Analysis of the exploration wells in the Cerro Prieto field and Mexicali Valley. CPIV.

Contreras, E., E. Iglesias and F. Bermejo, 1982a. Effects of temperature and stress on the compressibilities, thermal expansivities, and porosities of Cerro Prieto and Berea sandstones to 9000 psi and 280°C. Proc. 8th Workshop Geoth. Reserv. Engr., (this volume).

Contreras, E., E. Iglesias, and J. Sánchez, 1982b. High-temperature permeability studies of Cerro Prieto cores. CPIV.

Cortez, C., P. Pérez, S. Godínez, and E. Carreño, 1982. Summary of geothermal brine reinjection tests without previous treatment at well M-9 of the Cerro Prieto geothermal field. CPIV.

Corwin, R.F., H.F. Morrison, S. Díaz, and J. Rodríguez, 1978. Self-potential studies at the Cerro Prieto geothermal field. CPI, pp. 204-210.

Crosby, J.W., R.M. Chatters, J.V. Anderson, and R. L. Fenton, 1972. Hydrogeologic evaluation of the Cerro Prieto geothermal system utilizing isotopic techniques. Pullman, Wash., Washington State Univ., College of Engr., report 72/11-5.

de Boer, J., 1979. Paleomagnetism of the Quaternary Cerro Prieto, Crater Elegante, and Salton Buttes volcanic domes in the northern part of the Gulf of California rhombochasm. CPII, pp. 91-98.

de la Peña, A., 1981. Results of the first order leveling surveys in the Mexicali Valley and at the Cerro Prieto field. CPIII, pp. 281-291.

de la Peña, A., I. Puente, and E. Díaz, 1979. Geologic model of the Cerro Prieto geothermal field. CPII, pp. 29-56.

Des Marais, D.J., M.L. Stallard, N.L. Nehring, and A.H. Truesdell, 1982. Hydrocarbon production in the Cerro Prieto geothermal field. CPIV.

Díaz, E., 1978. Pozos de gradiente Cerro Prieto Oeste. Comision Federal de Electricidad internal report.

Díaz, S., I. Puente, and A. de la Peña, 1981. Proposed geologic model based on geophysical well logs. CPIII, pp. 46-61.

Elders, W.A., D.K. Bird, A.E. Williams, and P. Schiffman, 1982. A model for the heat source of the Cerro Prieto magma-hydrothermal system, Baja California, Mexico. CPIV.

Elders, W.A., J.R. Hoagland, S.D. McDowell, and J.M. Cobo, 1978. Hydrothermal mineral zones in the geothermal reservoir of Cerro Prieto. CPI, pp. 68-75.

Elders, W.A., J.R. Hoagland, and A.E. Williams, 1979. Distribution of hydrothermal mineral zones in the Cerro Prieto geothermal field of Baja California, Mexico. CPII, pp. 57-65.

Elders, W.A., R.W. Rex, T. Meidav, P.T. Robinson, and S. Biehler, 1972, Crustal spreading in southern California. Science, v. 178, p. 15-24.

Elders, W.A., A.E. Williams, and J.R. Hoagland, 1981. An integrated model for the natural flow regime in the Cerro Prieto hydrothermal system based upon petrological and isotope geochemical criteria. CPIII, pp. 102-109.

Ershaghi, I., and S. Ghaemian, 1980a. Detection of hydrothermal alteration in a sedimentary type geothermal system using well logs. Presented at the 55th Annual Fall Tech. Conf. Soc. Petrol. Engr. of AIME, Sept. 21-24, 1980. Dallas, Texas, SPE 9499.

Ershaghi, I. and S. Ghaemian, 1980b. Well log interpretation of the Cerro Prieto field. Proc. 6th Workshop Geoth. Reserv. Engr., Stanford Geothermal Program report SGP-TR-50, pp. 258-263.

Ershaghi, I. and S. Ghaemian, 1981. Estimation of Q_v profile in sedimentary type geothermal reservoir. Presented at 1981 Calif. Reg. Mtg. Soc. Petrol. Engr. of AIME, March 25-26, 1981. Dallas, Texas, SPE 9927.

Ershaghi, I., E.L. Dougherty, H. Ucok, and F. Ghassemi, 1978. Problems in estimation of salinity profile in liquid dominated geothermal systems. Geoth. Resour. Council Trans., v. 2, pp. 181-183.

Evans, K.R. 1972. Aeromagnetic study of the Mexicali-Cerro Prieto geothermal area. Univ. Arizona, Dept. Geosciences, M.S. thesis.

Fausto, J.J., M.E. Jiménez, and I. Esquer, 1981. Current state of the hydrothermal geochemistry studies at Cerro Prieto. CPIII, pp. 188-220.

Fausto, J.J., A. Sánchez, M.E. Jiménez, I. Esquer, and F. Ulloa, 1979. Hydrothermal geochemistry of the Cerro Prieto geothermal field. CPII, pp. 199-223.

Fitterman, D.V. and R.F. Corwin, 1982. Inversion of self-potential data from the Cerro Prieto geothermal field, Mexico. Geophysics, v. 47, pp. 938-945.

Fonseca, H. and A. Razo, 1979. Gravity, magnetics and seismic reflection studies at the Cerro Prieto geothermal field. CPII, pp. 303-328.

Fonseca, H., A. de la Peña, I. Puente, and E. Díaz, 1981. Extension of the Cerro Prieto field, and zones in the Mexicali Valley with geothermal possibilities in the future. CPIII, pp. 384-421.

Gamble, T.D., W.M. Goubau, N.E. Goldstein, R. Miracky, M. Stark, and J. Clarke, 1979. Magnetotelluric studies at Cerro Prieto, CPII, pp. 405-413.

García, S., 1976. Geoelectric study of the Cerro Prieto geothermal area, Baja California, Mexico. Proc. 2nd U.N. Symp. Devel. and Use Geoth. Resour., San Francisco, Calif., May 1975, pp. 1003-1011.

GEOCA, 1962. Levantamiento sismológico de refracción en la zona geotérmica de Cerro Prieto. Internal report prepared for Comisión Federal de Electricidad.

Goldstein, N.E., 1977. Modeling of CFE gravity data on the Mexicali-Cerro Prieto area. Lawrence Berkeley Laboratory internal report.

Goldstein, N.E. and A. Razo, 1978. General overview of geophysical studies at Cerro Prieto. CPI, pp. 161-163.

Goldstein, N.E., K. Pruess, M.J. Wilt, and G.S. Bodvarsson, 1982a. Resistivity monitoring of fluid migration at the Cerro Prieto field. Proc. 8th Workshop Geoth. Reserv. Engr. (this volume).

Goldstein, N.E., M.J. Wilt, and D.J. Corrigan, 1982b. Analysis of the Nuevo León magnetic anomaly and its possible relation to the Cerro Prieto magmatic-hydrothermal system. CPIV.

Goubau, W.M., N.E. Goldstein, and J. Clarke, 1981. Magnetotelluric studies at the Cerro Prieto geothermal field. CPIII, pp. 357-367.

Goyal, K.P., S.E. Halfman, A.H. Truesdell, and J.H. Howard, 1982. Production characteristics of some Cerro Prieto wells. CPIV.

Goyal, K.P., C.W. Miller, and M.J. Lippmann, 1980. Effect of measured wellhead parameters and well scaling on the computed downhole conditions in Cerro Prieto wells. Proc. 6th Workshop Geoth. Reser. Engr., Stanford Geothermal Program report SGP-TR-50, pp. 130-138.

Goyal, K.P., C.W. Miller, M.J. Lippmann, and S.P. Vonder Haar, 1981. Analysis of Cerro Prieto production data. CPIII, pp, 496-500.

Grannell, R.B., R.C. Kroll, R.M. Wyman, and P.S. Aronstam, 1981. Precision gravity studies at Cerro Prieto - A progress report. CPIII, pp. 329-333.

Grannell, R.B., R.M. Wyman, R.M. Leggewie, and G.A. Randall, 1982. Subsidence detection at the Cerro Prieto geothermal field by precision gravity studies. CPIV.

Grant, M.A. and M.J. O'Sullivan, 1982. The old field at Cerro Prieto considered as a leaky aquifer. CPIV.

Grant, M.A., A.H. Truesdell, and A. Mañón, 1981. Production induced boiling and cold water entry in the Cerro Prieto geothermal reservoir indicated by chemical and physical measurements. CPIII, pp. 221-237.

Halfman, S.E., M.J. Lippmann, and R. Zelwer, 1982a. The movement of geothermal fluid in the Cerro Prieto field as determined from well log and reservoir engineering data. Proc. 8th Workshop Geoth. Reserv. Engr. (this volume).

Halfman, S.E., M.J. Lippmann, R. Zelwer, and J.H. Howard, 1982b. Fluid flow model of the Cerro Prieto geothermal field based on well log interpretation. CPIV.

Hurtado, R., S. Mercado, E. Rocha, H. Gamiño, and F. Garibaldi, 1981. Treatment of the Cerro Prieto I brines for use in reinjection. 2. Results of the pilot plant tests. CPIII, pp. 513-533.

Iglesias, E.R. and O. Weres, 1979. Theoretical studies of Cerro Prieto brines chemical equilibria. CPII, pp. 254-258.

Ingle, J.C., 1982, Microfaunal evidence of age and depositional environments of the Cerro Prieto section (Plio-Pleistocene), Baja California, Mexico. Lawrence Berkeley Laboratory report LBL-13897.

Janik, C.J., N.L. Nehring, M.A. Huebner, and A.H. Truesdell, 1982. Carbon-13 variations in fluids from the Cerro Prieto geothermal system. CPIV.

Liguori, P.E., 1979. Simulation of the Cerro Prieto geothermal field using a mathematical model. CPII, pp. 521-526.

Lippmann, M.J., 1981. Capacity of the Cerro Prieto field, in Zelwer, R., ed., Minutes Second Cerro Prieto Internal DOE/CFE Workshop. Lawrence Berkeley Laboratory internal report.

Lippmann, M.J. and G.S. Bodvarsson, 1982. Modeling studies on Cerro Prieto. CPIV.

Lippmann, M.J. and K.P. Goyal, 1979. Numerical modeling studies of the Cerro Prieto reservoir. CPII, pp. 497-507.

Lippmann, M.J. and A. Mañón, eds., 1980. Minutes of the Cerro Prieto internal DOE/CFE workshop, Menlo Park, Calif. March 10-12, 1980. Lawrence Berkeley Laboratory internal report.

Lippmann, M.J., G.S. Bodvarsson, P.A. Witherspoon, and J. Rivera, 1978. Preliminary simulation studies related to the Cerro Prieto field. CPI, pp. 375-383.

Lippmann, M.J., B. Domínguez, H.A. Wollenberg, and P.A. Witherspoon, 1977. Open file data on the Cerro Prieto geothermal field. Lawrence Berkeley Laboratory report LBL-6321.

Lisowski, M. and W.H. Prescott, 1982. Deformation near the epicenter of the 9 June 1980 M_L = 6.2, Victoria, Mexico, earthquake. CPIV.

Lomnitz, C., F. Mooser, C.R. Allen, J.N. Brune, and W. Thatcher, 1970. Seismicity and tectonics of the northern Gulf of California region, Mexico - Preliminary results. Geofísica Internacional, v. 10, no. 2, p. 37-48.

Lyons, D.J. and P.C. van de Kamp, 1980. Subsurface geological and geophysical study of the Cerro Prieto geothermal field, Baja California, Mexico. Lawrence Berkeley Laboratory report LBL-10540.

Majer, E.L. and T.V. McEvilly, 1979. Earthquake monitoring at the Cerro Prieto geothermal field. CPII, pp. 369-371.

Majer, E.L. and T.V. McEvilly, 1981. Detailed microearthquake studies at the Cerro Prieto geothermal field. CPIII, pp. 347-352.

Majer, E.L. and T.V. McEvilly, 1982. Seismological studies at the Cerro Prieto field: 1978-1982. CPIV.

Makdisi, R.S., A.H. Truesdell, J.M. Thompson, T.B. Coplen, and J. Sánchez, 1982. Geochemical evolution of Mexicali Valley groundwaters. CPIV.

Manón, A., A. de la Peña, and I. Puente, 1978a. El campo geotérmico de Cerro Prieto (Estudios realizados y programas futuros). Organ. Lat. Amer. de Energía, Serie Docum. no. 2, pp. 219-262.

Manón, A., E. Mazor, M. Jiménez, A. Sánchez, J. Fausto, and C. Zenizo, 1977. Extensive geochemical studies in the geothermal field of Cerro Prieto, Mexico. Lawrence Berkeley Laboratory report LBL-7019.

Manón, A., A. Sánchez, J.J. Fausto, M.E. Jiménez, A. Jacobo, and I. Esquer, 1978b. Preliminary geochemical model of the Cerro Prieto geothermal field. CPI, pp. 83-94.

Martínez, L.F., 1978. Thermal conductivity of core samples from the Cerro Prieto geothermal field: Experimental results and an improved prediction method. CPI, pp. 342-351.

Massey, B.L., 1978. Regional and local networks of horizontal control, Cerro Prieto geothermal area. CPI, pp. 151-155.

Massey, B.L., 1979. Measured crustal strain, Cerro Prieto field, Baja California, Mexico. CPII, pp. 294-298.

Massey, B.L., 1981. Measured ground-surface movements, Cerro Prieto geothermal field. CPIII, pp. 299-305.

Mazor, E. and A. Manón, 1978. Geochemical tracing in producing geothermal fields: A case study at Cerro Prieto. CPI, pp. 102-109.

Mazor, E. and A.H. Truesdell, 1981. Dynamics of a geothermal field traced by noble gases: Cerro Prieto, Mexico. CPIII, pp. 163-173.

Mercado, S., 1968. Localización de zonas de máxima actividad hidrotermal por medio de proporciones químicas, campo geotérmico de Cerro Prieto, B.C. Presented III Congr. Mex. Quím. Pura y Aplic., March 21-23, 1968, Guadalajara, México, Sociedad Química de México.

Mercado, S., 1976. Migración de fluidos geotérmicos y distribución de temperaturas en el subsuelo del campo geotérmico de Cerro Prieto, Baja California, México. Proc. 2nd U.N. Symp. Devel. and Use Geoth. Resour., San Francisco, Calif., May 1975, pp. 487-492.

Mercado, S. and F. Samaniego, 1978. An example of fluid migration between the layers on the Cerro Prieto geothermal field. Proc. 2nd. Invit. Well-testing Symp., Lawrence Berkeley Laboratory report LBL-8883, pp. 95-107.

Molinar, R., P. Flores, and A. Manón, 1979. Evaluation of the Cerro Prieto geothermal field. CPII, pp. 527-552.

Navarro, F.X., F.J. Bermejo, F. Castillo, and R. Rivera, 1982. Update of temperature behavior and distribution in Cerro Prieto I. CPIV.

Nehring, N.L. and F. D'Amore, 1982. Gas chemistry and thermometry of the Cerro Prieto, Mexico, geothermal field. Submitted to Geothermics.

Nehring, N.L. and J.J. Fausto, 1978. Gases in steam from Cerro Prieto geothermal wells. CPI, pp. 127-128.

Nehring, N.L. and J.N. Valette-Silver, 1982. Gas reactions in the Cerro Prieto reservoir. CPIV.

Nieva, D., J.J. Fausto, J. González, and F. Garibaldi, 1982. Vapor flow into the feeding zone of Cerro Prieto I wells. CPIV.

Noble, J.E. and A. Abril, 1978. Analysis of Cerro Prieto well logs: Some results and problems. CPI, pp. 57-63.

Noble, J.E., A. Manón, M.J. Lippmann, and P.A. Witherspoon, 1977. A study of the structural control of fluid flow within the Cerro Prieto geothermal field, Baja California, Mexico. Presented at 52nd Annual Fall Tech. Conf. Soc. Petrol. Engr. of AIME, October 9-12, 1977. Dallas, Texas, SPE-6763.

Olson, E.R., 1978. Oxygen and carbon isotope studies of calcite from the Cerro Prieto geothermal field. CPI, pp. 119-123.

Prian, R., 1979. Development possibilities at the Cerro Prieto geothermal area, Baja California Norte. CPII, pp. 146-161.

Prian, R., 1981. Drilling rate for the Cerro Prieto stratigraphic sequence. CPIII, pp. 77-87.

Pruess, K., M.J. Wilt, G.S. Bodvarsson, and N.E. Goldstein, 1982. Simulation and resistivity modeling of a geothermal reservoir with waters of different salinity. CPIV.

Puente, I., and A. de la Peña, 1978. Geology of the Cerro Prieto geothermal field. CPI, pp. 17-40.

Razo, A., F. Arellano, and H. Fonseca, 1978. CFE resistivity studies at Cerro Prieto. CPI, pp. 167-178.

Reed, M.J., 1976. Geology and hydrothermal metamorphism in the Cerro Prieto geothermal field, Mexico. Proc. 2nd. U.N. Symp. Devel. and Use Geoth. Resour., San Francisco, Calif., May 1975, pp. 539-547.

Reyes, A. and A. Razo, 1979. Microtectonic and potential field anomaly studies at the Cerro Prieto geothermal field. CPII, pp. 374-389.

Reyes, A., A. Chang, and A. Albores, 1982. Attenuation and origin of the coda waves in the Cerro Prieto geothermal field. CPIV.

Rivera, J., 1977. Decline curve analysis - A useful reservoir engineering tool for predicting the performance of geothermal wells. Geoth. Resour. Council Trans., v. 1, pp. 257-259.

Rivera, J., 1978. Application of type curve procedures for the analysis of production data from geothermal wells. Geoth. Resour. Council Trans., v. 2, pp. 575-578.

Rivera, J. and H. J. Ramey, 1977. Application of two-rate flow tests to the determination of geothermal reservoir parameters. Presented at 52nd Annual Fall Tech. Conf. Soc. Petrol. Engr. of AIME, October 9-12, 1977. Dallas, Texas, SPE-6887.

Rivera, J., F. Samaniego, and R.C. Schroeder, 1978. Pressure transient testing at the Cerro Prieto geothermal field. CPI, pp. 366-371.

Rivera, R., F. Bermejo, F. Castillo, H. Pérez, and A. Abrajan, 1982. Update of temperature behavior and distribution in Cerro Prieto II and III. CPIV.

Saltuklaroglu, M., 1979. Interference effect of producing wells on observation wells in a geothermal field (Cerro Prieto). Proc. 5th Workshop Geoth. Reserv. Engr., Stanford Geothermal Program report SGP-TR-40, pp. 49-59.

Sánchez, J. and A. de la Peña, 1981. Geohydrology of the Cerro Prieto geothermal field. CPIII, pp. 309-327.

Sanford, S.J. and W.A. Elders, 1981. Dating thermal events at Cerro Prieto using fission track annealing. CPIII, pp. 114-119.

Schatz, J.F., 1982. Laboratory measurement related to subsidence potential - Cerro Prieto geothermal field. CPIV.

Schroeder, R.C., C.B. Goranson, S.M. Benson, and M.J. Lippmann, 1978. Well interference tests at the Cerro Prieto geothermal field. CPI, pp. 357-362.

Seamount, D.T., and W.A. Elders, 1981. Use of wireline logs at Cerro Prieto in the identification of the distribution of hydrothermally altered zones and dike locations, and their correlation with reservoir temperatures. CPIII, pp. 123-133.

Semprini, L. and P. Kruger, 1981. Radon and ammonia transects across the Cerro Prieto field. CPIII, pp. 248-256.

Semprini, L. and P. Kruger, 1982. Relationship of radon concentration to spatial and temporal variations of reservoir thermodynamic conditions in the Cerro Prieto geothermal field. CPIV.

Somerton, W.H., 1978. Some physical properties of Cerro Prieto cores. CPI, pp. 333-338.

Teilman, M.A. and U.J. Cordon, 1981. Exploration and development of Cerro Prieto. CPIII, pp. 17-25.

Truesdell, A.H. and R.W. Henley, 1982. Chemical equilibria in the Cerro Prieto hydrothermal fluid. CPIV.

Truesdell, A.H., A. Mañón, M.E. Jiménez, A. Sánchez, and J.J. Fausto, 1978a. Geochemical evidence of drawdown in the Cerro Prieto geothermal field. CPI, pp. 130-135.

Truesdell, A.H., N.L. Nehring, J.M. Thompson, C.J. Janik, and T.B. Coplen, 1982. A review of progress in understanding the fluid geochemistry of the Cerro Prieto geothermal system. CPIV.

Truesdell, A.H., R.O. Rye, F.J. Pearson, E.R. Olson, N.L. Nehring, M.A. Huebner, and T.B. Coplen, 1978b. Preliminary isotopic studies of fluids from the Cerro Prieto geothermal field. CPI, pp. 95-99.

Truesdell, A.H., J.M. Thompson, T.B. Coplen, N.L. Nehring, and C.J. Janik, 1979. The origin of the Cerro Prieto geothermal brine. CPII, pp. 224-234.

Tsang, C.F., G.S. Bodvarsson, M.J. Lippmann, and J. Rivera, 1978. Some aspects of the response of geothermal reservoirs to brine reinjection with application to the Cerro Prieto field. CPI, pp. 396-401.

Tsang, C.F., D.C. Mangold, C. Doughty, and M.J. Lippmann, 1981. The Cerro Prieto reinjection tests: Studies of a multilayer system. CPIII, pp. 537-547.

Tsang, C.F., D.C. Mangold, C. Doughty, and M.J. Lippmann, 1982. Prediction of reinjection effects in the Cerro Prieto geothermal system. CPIV.

Tsang, C.F., D.C. Mangold, and M.J. Lippmann, 1979. Simulation of reinjection at Cerro Prieto using an idealized two-reservoir model. CPII, pp. 599-606.

Valette, J.N. and I. Esquer-Patiño, 1979. Geochemistry of the surface emissions in the Cerro Prieto geothermal field. CPII, pp. 241-250.

Valette-Silver, J.N., I. Esquer, W.A. Elders, P.C. Collier, and J.R. Hoagland, 1981a. Hydrothermal alteration of sediments associated with surface emissions from the Cerro Prieto geothermal field. CPIII, pp. 140-145.

Valette-Silver, J.N., J.M. Thompson, and J.W. Ball, 1981b. Relationship between water chemistry and sediment mineralogy in the Cerro Prieto geothermal field: A preliminary report. CPIII, pp. 263-273.

Velasco, J., 1963. Levantamiento gravimétrico. Zona geotérmica de Mexicali, Baja California. Consejo Recursos Naturales No Renovables internal report.

Vonder Haar, S., 1980. Geology of the Cerro Prieto geothermal field. Earth Sciences Division Newsletter, Lawrence Berkeley Laboratory, v. 3, no. 2, pp. 1-5.

Vonder Haar, S., 1981. A structural and sedimentological study of the Cerro Prieto geothermal field, Baja California, Mexico. Lawrence Berkeley Laboratory report LBL-12187.

Vonder Haar, S. and J.H. Howard, 1979. Intersecting faults and sandstone stratigraphy at the Cerro Prieto geothermal field. CPII, pp. 118-130.

Weres, O., L. Tsao, and E. Iglesias, 1980. Chemistry of silica in Cerro Prieto brines. Lawrence Berkeley Laboratory report LBL-10166.

Westwood, J.D. and L.M. Castanier, 1981. Application of a lumped parameter model to the Cerro Prieto geothermal field. Proc. 7th Workshop Geoth. Reserv. Engr., Stanford Geothermal Program report SGP-TR-55, pp. 23-28.

Williams, A.E., 1982. Stable isotope systematics of oxygen and carbon in and around the Cerro Prieto geothermal anomaly, Baja California, Mexico. CPIV.

Wilt, M.J. and N.E. Goldstein, 1979. Resistivity monitoring at Cerro Prieto. CPII, pp. 419-428.

Wilt, M.J. and N.E. Goldstein, 1982. Interpretation of dipole-dipole resistivity monitoring data at Cerro Prieto. CPIV.

Wilt, M.J., N.E. Goldstein, and A. Razo, 1978. LBL resistivity studies at Cerro Prieto. CPI, pp. 179-188.

Witherspoon, P.A., H. Alonso, M.J. Lippmann, A. Mañón, and H.A. Wollenberg, 1978. Mexican-American cooperative program at the Cerro Prieto geothermal field. Lawrence Berkeley Laboratory report LBL-7095.

Wong, V. and J. Frez, 1982. Inference about the structure based on two aftershocks in the Mexicali-Imperial Valley. CPIV.

Zelwer, R., ed., 1982. Minutes of the second Cerro Prieto internal DOE/CFE workshop, San Felipe, Baja California, January 19-21, 1982. Lawrence Berkeley Laboratory internal report.

Zelwer, R. and R.B. Grannell, 1982. Correlation between precision gravity and subsidence measurements at Cerro Prieto. CPIV.

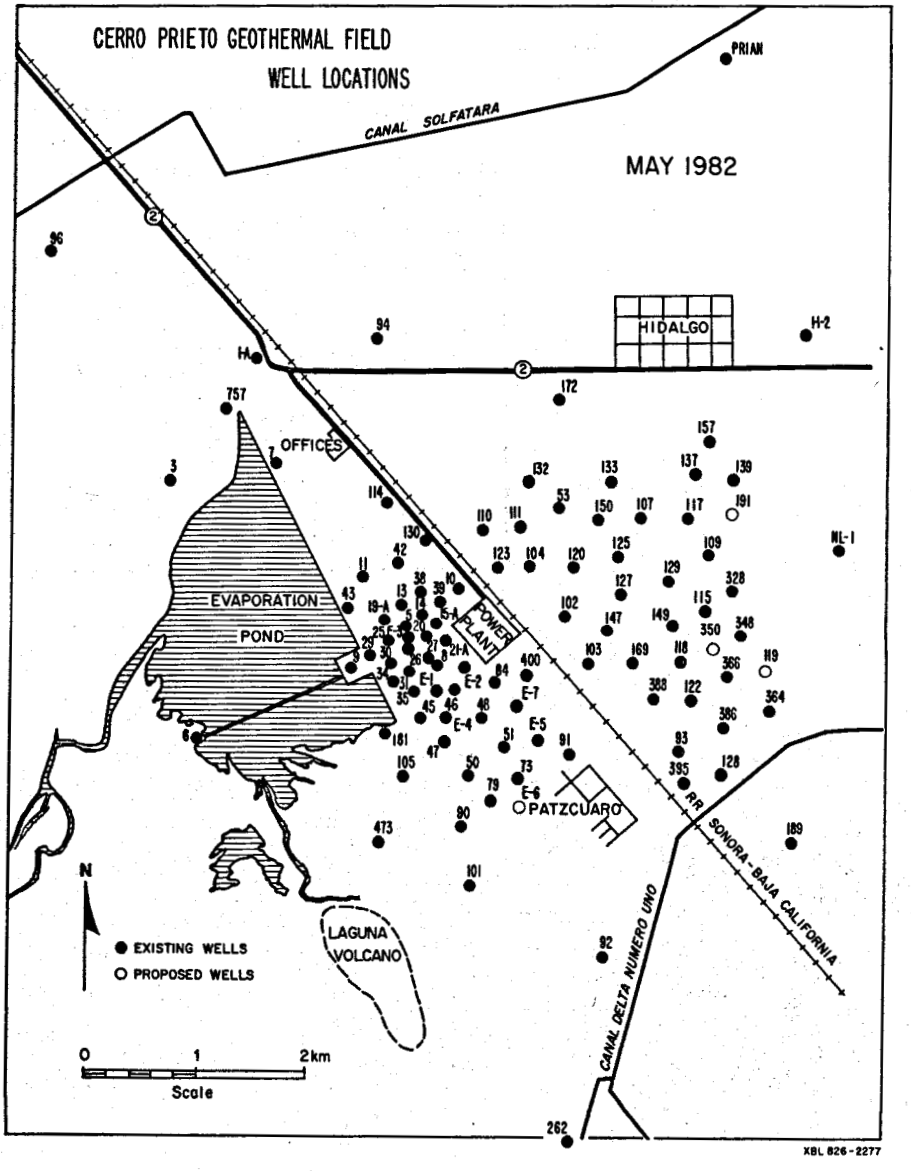

Figure 1. Location of geothermal wells in the Cerro Prieto field.

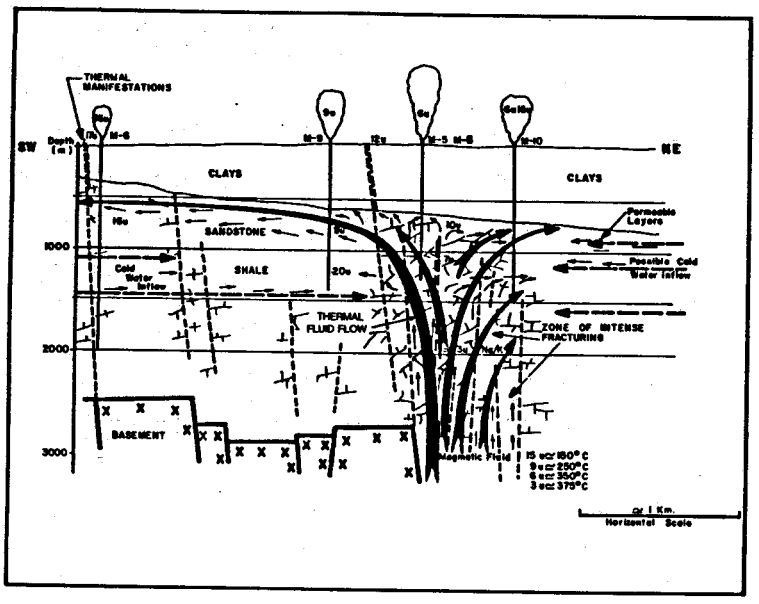

Figure 2. Mercado's (1968) convective model for the Cerro Prieto field.

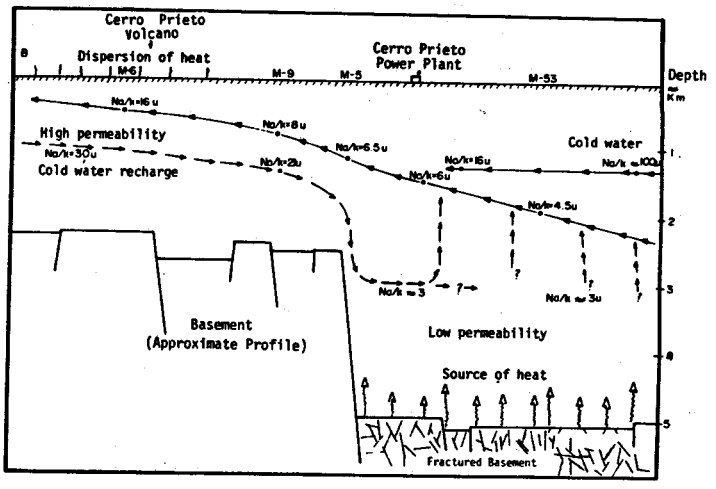

Figure 3. Mercado's (1976) convective model for the Cerro Prieto field.

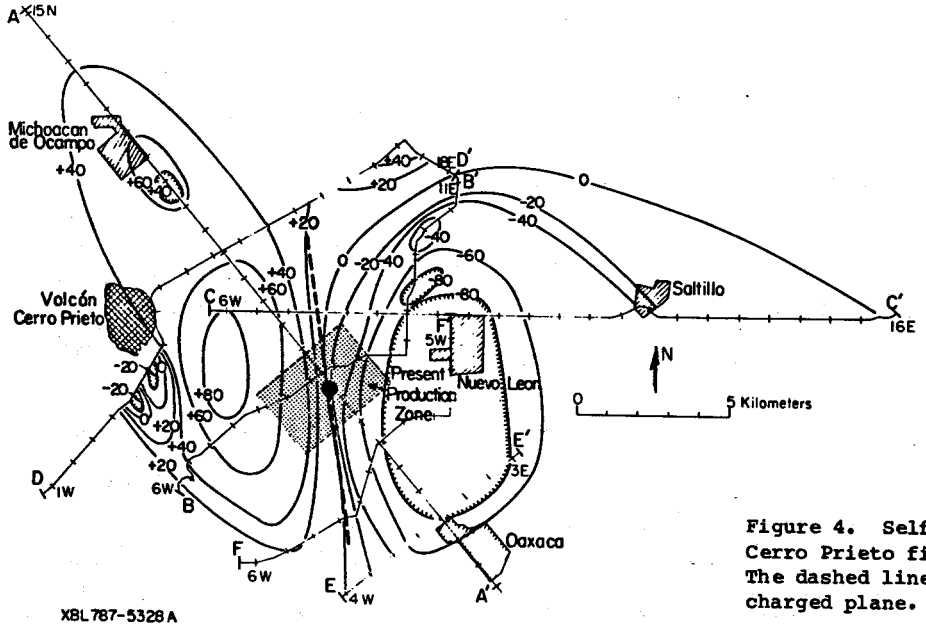

Figure 4. Self-potential anomaly over the Cerro Prieto field (from Corwin et al., 1978). The dashed line indicates the position of the charged plane.

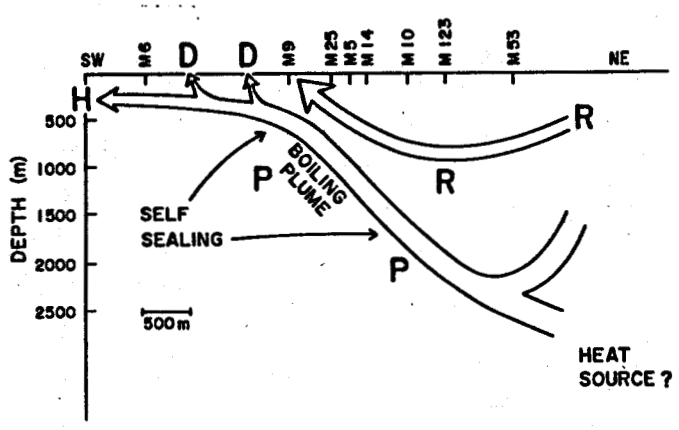

Figure 5. Southwest-northeast section across the Cerro Prieto field showing the flow regime proposed by Elders et al. (1981). R: recharge zone; P: thermal zone; D: discharge zone; H: horizontal flow zone.

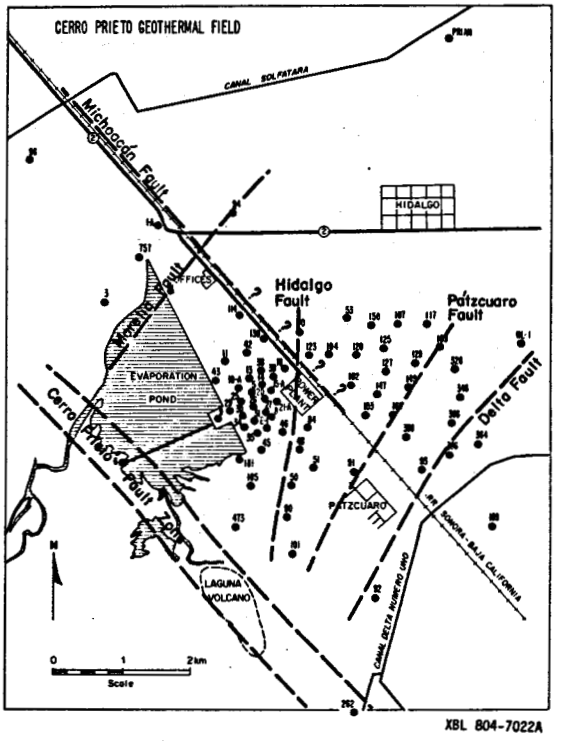

Figure 6. Fault map for the Cerro Prieto region developed at the first DOE/CFE workshop (Lippmann and Mañón, 1980).

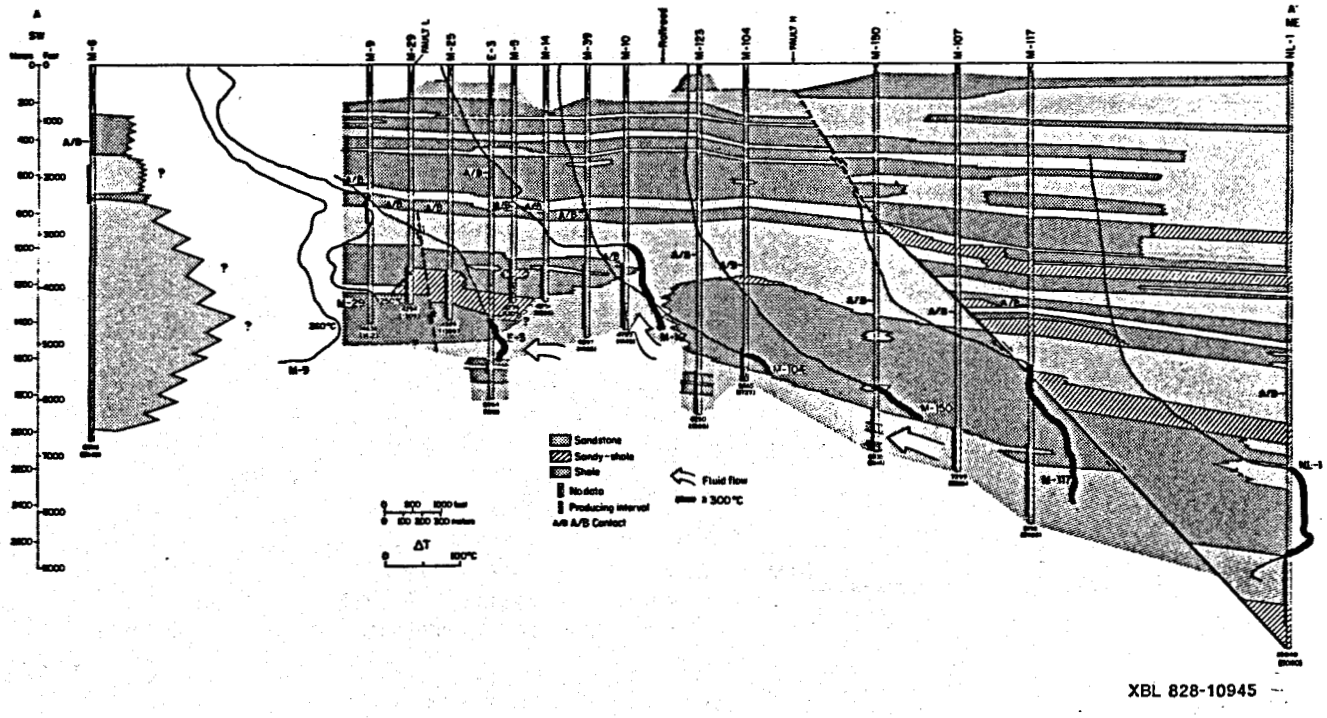

Figure 7. Southwest-northeast cross section of the Cerro Prieto field showing schematically the flow of geothermal fluids in the system (from Halfman et al., 1982a).

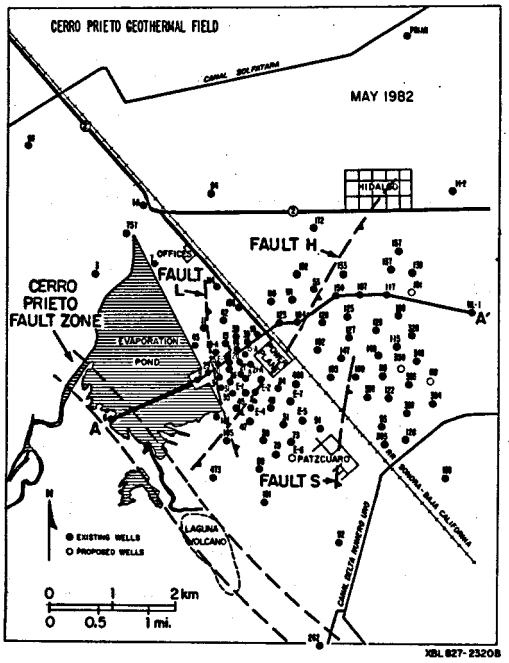

Figure 8. Location of the main faults controlling the subsurface flow of geothermal fluids in the Cerro Prieto field (from Halfman et al., 1982a). Also shown is the position of cross-section A-A' given in Figure 7.

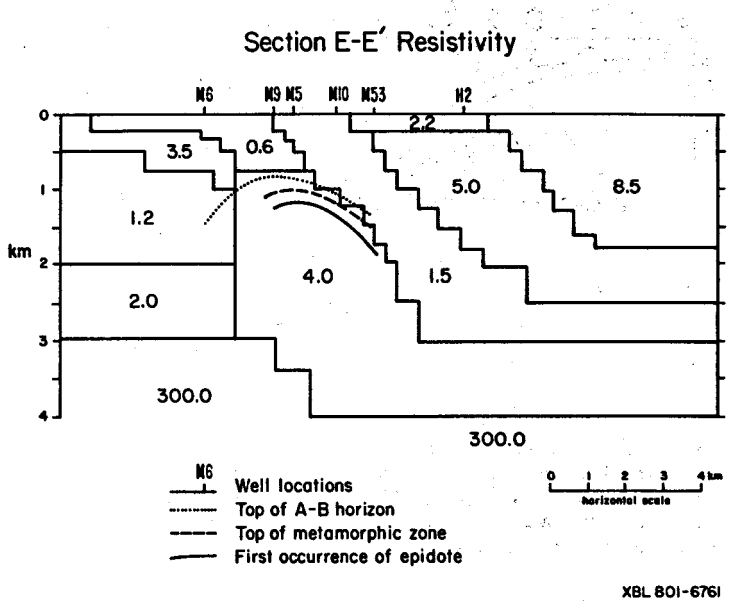

Figure 9. Two-dimensional resistivity model for a southwest-northeast line crossing the Cerro Prieto field (Line E-E'; Wilt and Goldstein, 1979). Shown are also the position of the A/B contact, the top of the metamorphic zone, and the first occurrence of the mineral epidote.

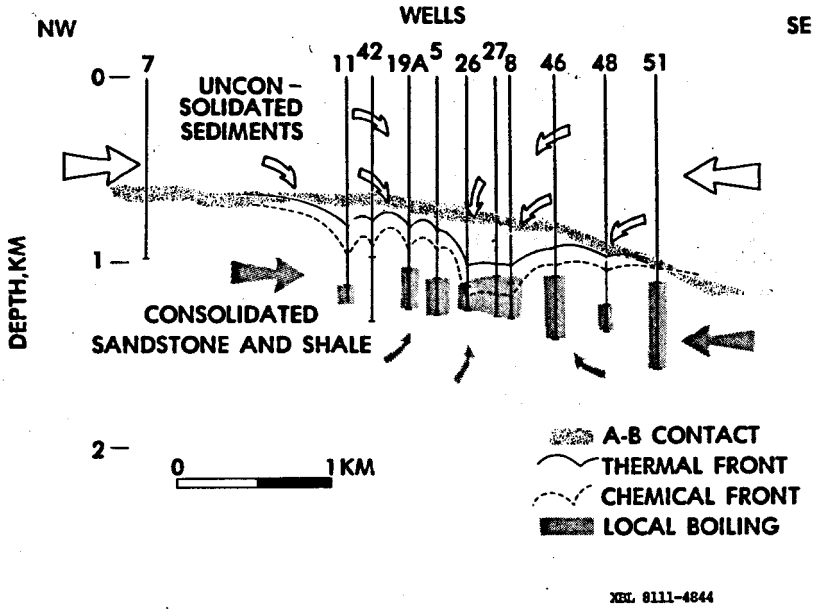

Figure 10. Schematic section across the western part of the Cerro Prieto field, showing movement of hot water (gray arrows) and cold water (white arrows) toward the producing wells, the chemical and thermal fronts, and zones of near-well boiling (from Grant et al., 1981).

Proceedings Eighth Workshop Geothermal Reservoir Engineering
Stanford University, Stanford, California, December 1982
SGP-TR-60

HYDROLOGIC CHANGES AT TAUHARA FIELD DUE TO EXPLOITATION OF WAIRAKEI FIELD

R.G. Allis

Geophysics Division, D.S.I.R.,
Wairakei, New Zealand.

ABSTRACT

The major thermal areas of Tauhara field are situated around the town of Taupo, about 8 km from the Wairakei production borefield. Within Taupo, over 400 wells have been drilled to between 30 and 150 m depth, tapping the near-surface hot water of Tauhara field for domestic heating. Analysis of many measurements made since the 1950's in both domestic wells and the hot springs of Tauhara field has failed to find evidence of a widespread decline in water level or near-surface aquifer pressure. However, a significant increase in both temperature of the near-surface aquifer, and heat flow from thermal areas of Tauhara field has occurred since the mid-1960's. This has resulted in a spread of steaming ground and 3 hydrothermal eruptions on the outskirts of Taupo.

A study of pressure changes in deep wells of Tauhara field suggests a decline of around 18 bars has occured at >400 m depth, due to exploitation at Wairakei. The deep reservoir pressure of Tauhara field is now about 7 bars higher than that of Wairakei field, and significant flow towards Wairakei production borefield is probably occurring. The lack of a significant pressure drop in the surface aquifer of Tauhara field is due to the presence of low permeability lacustrine mudstone layers covering most of the field between 100 and 400 m depth. Deep drawdown of the field has caused a steam zone to form beneath the mudstone layers, and this in turn has caused the increase in steam-heating of the surface aquifer.

INTRODUCTION

Tauhara geothermal field is situated at the base of Mt Tauhara, a rhyo-dacite volcano near Lake Taupo, New Zealand. Apparent resistivity mapping indicates that the field has a 20 km^2 area, and that it merges with Wairakei field in the vicinity of the Waikato River (Fig. 1). The main thermal areas of Tauhara field are about 8 km from the centre of Wairakei production borefield. Prior to 1950, the surface thermal activity of Tauhara field could be divided into 3 areas. At Spa Sights on the Waikato River, there was an outflow of hot chloride water (approx. 1500 ppm Cl) in the form of geysers and springs; in the Waipahihi-Terraces area, dilute chloride (<500 ppm Cl) seeps and springs occurred; and at higher elevation (towards Mt Tauhara) steam heated thermal activity was present. Domestic wells tapping the shallow groundwater at that time confirmed that hot water was restricted to the eastern half of Taupo town, and that where encountered, it varied from a dilute chloride water to sulphate and bicarbonate waters (Thompson, B.N., 1951; Sarbutt, 1964).

The first recorded changes in the thermal activity of Tauhara field occurred in the early 1950's when hydro-electric developments on the Waikato River caused the river level at Spa Sights to fall, and geyser activity became intermittent. Although exploitation of Wairakei field began in 1952, and changes in surface activity of Wairakei field were evident by 1954, similar changes in Tauhara field were not observed until the mid-late 1960's (Fisher, 1965; Dickinson, 1968; Allis, 1981). Existing steam-heated thermal areas expanded in size and increased in intensity, and 3 hydrothermal eruptions have occured since 1974. The magnitude of the increase in heat flow is controversial (Dickinson, 1976; Allis, 1979), but it has clearly been at least 100 MW.

The relatively constant chemistry of springs and well waters in the Waipahihi-Terraces area indicates few changes have occurred to the near-surface water in this part of Tauhara field (Henley and Stewart, 1982). However elsewhere a decline in chloride concentrations, increasing sulphate and silica values, and enrichment of oxygen and deuterium isotopes have occurred. These changes reflect both an increase in steam-heating of the near-surface waters, and also increased steam loss from these waters (Henley and Stewart, 1982).

This paper summarizes the hydrologic changes that have occurred in Tauhara field. A more detailed presentation and discussion of the data is given in Allis (1982a). Additional data on water levels and temperature in domestic wells, and shallow resistivity sounding results have appeared in Dawson and Thompson, (1981). Wooding (1981,1982) has mathematically modelled the pressure response of deep Tauhara wells, and Donaldson (1982) has recently reviewed all of the above papers.

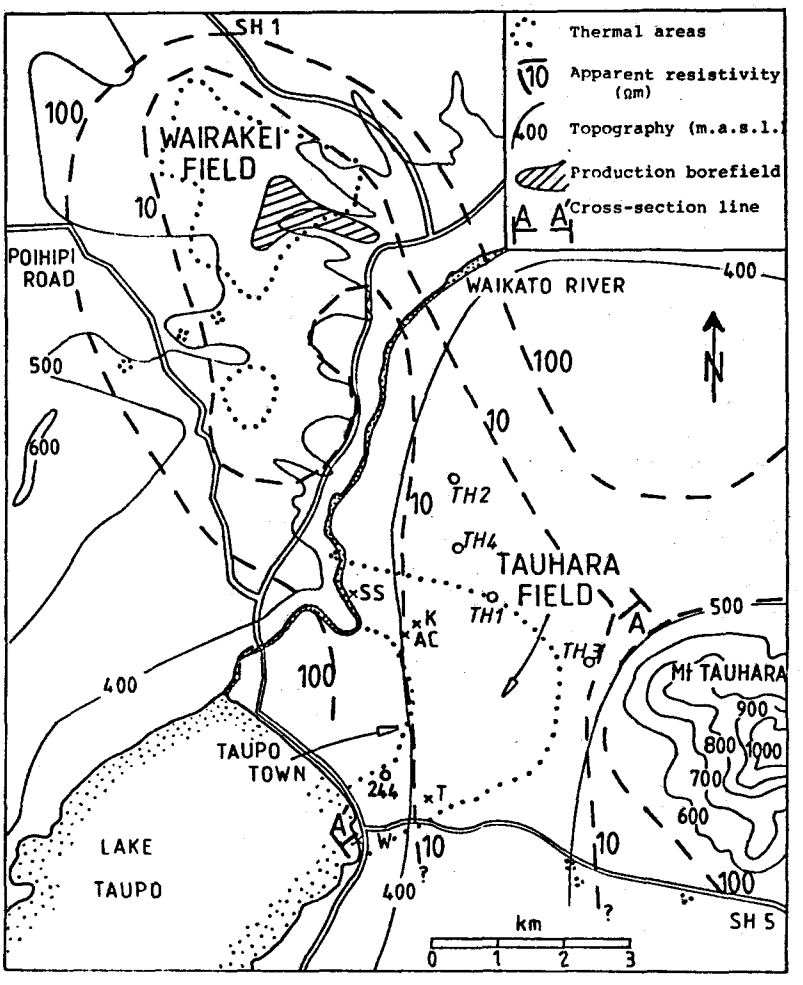

Fig. 1: Map of Tauhara and Wairakei fields. Crosses mark thermal areas of Tauhara field referred to in text: SS = Spa Sights; K = Kathleen Spring; A.C. = A.C. Spring; T = Terraces Springs; W = Waipahihi Springs. o are wells mentioned in text.

SHALLOW HYDROLOGIC CHANGES

Springs Probably the best indicators of hydrologic change at shallow depth are springs. Small changes in aquifer pressure can cause large fluctuations in flow, and changes in heat flow from depth can be precisely monitored by measuring temperature as well. A summary of the thermal changes at several Tauhara springs is shown in Fig. 2. A.C. and Kathleen Springs tap relatively low chloride water in the central part of Tauhara field; Iron Bath and the source of the Waipahihi Stream are dilute chloride springs in the Terraces area near the southern side of the field. Measurements of flow have only been made on the A.C. and Kathleen springs, and these were in 1951, 1963, 1967 and 1982. The A.C. spring flow has remained constant at 10-11 l/s, while the flow of Kathleen spring has remained constant at 22-23 l/s since 1963 at least (V-notch measurements). The 1951 flow measurement of Kathleen spring was 30 l/s, but the accuracy of this measurement is unknown.

Iron Bath spring is now pumped for a nearby baths complex, and its water level has fallen to about 1 m below ground level. There has been no obvious change in flow of the source of the Waipahihi stream since 1951.

The apparently constant mass flow of all springs since at least the early 1960's implies there has been little change in water level or shallow aquifer pressure during this time.

The temperature rise of both Kathleen and A.C. springs has been over 30°C. The start of the increasing temperature trend is known to be 1966, because A.C. Baths management noted increased supply temperature at this time. The small rise in Kathleen spring since 1975 is due to the spring temperature reaching the boiling point of water. A further increase in heat flow of this spring probably occurred through increased steam loss from the groundwater. Enriched oxygen and deuterium concentrations compared to A.C. springs are

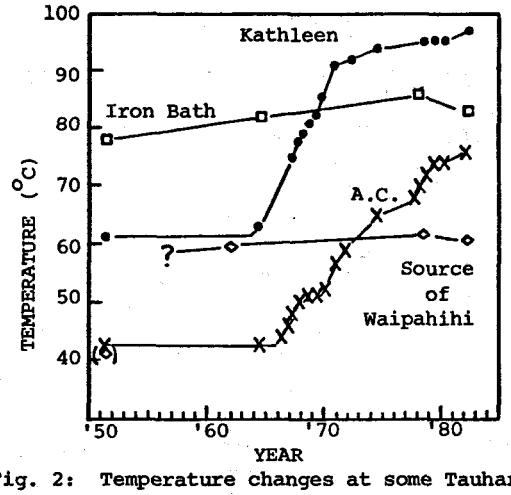

Fig. 2: Temperature changes at some Tauhara Springs.

consistent with such steam loss. Combining temperature with mass flow shows that the heat flow of Kathleen spring has risen from between 4-6 MW prior to 1970, to about 8 MW in 1982 (relative to 15°C). A.C. spring heat flow has risen from just over 1 MW to nearly 3 MW.

Shallow Wells In 1950 there were close to 50 domestic wells in Taupo. Since the sharp rise in the cost of home heating during the early 1970's, the number of wells has increased greatly. Today (1982) the number of wells is probably around 500. The wells are normally between 30 and 150 m deep and tap groundwater up to 120°C. Most water pumped from the ground is returned to shallow (<10 m deep) soak holes after use.

A careful study of repeat water level measurements, and water levels from nearby wells, has failed to find a consistent pattern of water level changes since the first measurements in 1950 (Allis, 1982a). Most water levels (irrespective of date) can be contoured as one water table which reflects the topographic gradient from Mt Tauhara towards Lake Taupo and the Waikato River. However the water table does not have a uniform gradient. Near the western edge of Tauhara field (and roughly parallel to it) there is a 30-40 m step, occurring over less than 100 m of horizontal distance in places. On the low side of the step, water levels range from lake level to about 10 m above lake level. On the high side of the step water levels are typically 40-50 m above Lake Taupo. Wells drilled close to this step, and on the high water level side, often have downflows with water level being dependent on well depth. It will be shown below that the step is due to two near-surface aquifers separated by a mudstone aquiclude. The upper aquifer (in Wairakei pumice breccia) becomes progressively perched as water flows westwards. In addition the mudstone wedges out to the west, with the sudden change in water level marking the western edge of the mudstone aquiclude. Below this aquiclude is the Huka pumice breccia aquifer.

In general, shallow well temperatures have increased with time. Most of the increase occurred during the late 1960's and early 1970's. A good example of this is well 244 located near the Waipahihi seeps (Fig. 3). The greatest temperature increase has occurred near the water level, causing a negative temperature gradient to develop in the well. This indicates that the heat source for the groundwater is not beneath well 244, but must be further east, towards the steam-heated, central area of Tauhara field.

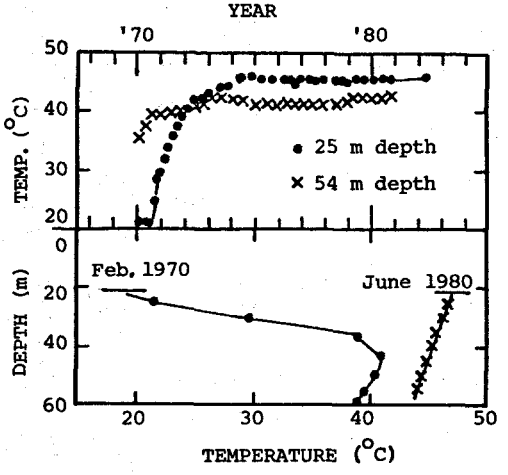

Fig. 3: Temperature changes in well 244, about 500 m north of Waipahihi springs as marked on Figure 1.

DEEP HYDROLOGIC CHANGES

Pressure changes at >400 m depth in Tauhara field are known only from 4, 1-km-deep wells (TH1-4, locations shown on Fig. 1). The first deep well was drilled in 1964, so deep pressure changes before this time have not been measured. Assuming the deep pressure trend measured in TH1 to be typical of that for the whole field, the pressure drop since late 1964 has been 9 bars. This compares with a pressure drop of 7 bars at Wairakei field during this time (Fig. 4; pressure at -152 m R.L.). The pressure drop in both fields since 1970 has been 2 bars. This suggests that deep Tauhara field pressures have followed the Wairakei pressure trend closely, and that any time delay is unlikely to be more than about 2 years.

The only way of estimating the initial pressure of Tauhara field is from the height to which chloride water (from the deep reservoir) rose within the field. Chloride - bearing springs range in elevation from 360-410 m R.L. (metres above sea level). However because of the lateral pressure gradient away from Mt Tauhara, shallow wells east of the springs contain chloride water at a higher elevation. The highest measured chloride water level is at 430 m R.L. Extrapolating downwards from this

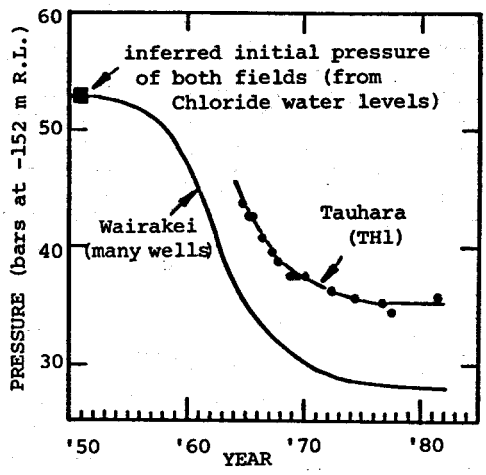

Fig. 4: Comparison of pressure changes in Tauhara field and Wairakei field. Pressure trends are at -152 m R.L., or about 550 m depth.

elevation, assuming a hydrostatic pressure gradient for boiling point conditions, gives a pressure of 48 bars at -152 m R.L. When allowance is made for the initial gradient being about 10% above hydrostatic (to drive the chloride water to the surface; Grant, 1979), the initial pressure must have been close to that at Wairakei before exploitation (i.e. 53 bars at -152 m R.L., Fig. 4). By comparison, chloride springs at Wairakei field ranged in elevation from 370-390 m R.L. in Geyser Valley, to 440 m R.L. in the upper Waiora Valley (Gregg and Laing, 1951). The similarity in the maximum height of chloride water at Wairakei and Tauhara field confirms their initial pressure profiles were also probably similar.

The deep drawdown of Tauhara field has therefore been around 18 bars, compared to about 25 bars at Wairakei. This means there is now a horizontal pressure gradient from Tauhara to Wairakei field, and some of the recharge to Wairakei is probably from Tauhara field.

VERTICAL PRESSURE PROFILE - 1982

To examine the hydrological relationship between shallow domestic wells and springs, and deep wells, a composite pressure-depth plot was compiled by Allis (1982a)(Fig. 5.) This involves plotting aquifer pressure at the pressure-controlling point for each well. Some of the data points from shallow wells date back to the late 1960's. However others in the same depth range suggest little pressure change, so most points are though to be within 1-2 bars of 1982 pressures. The date of measurement is shown with the deep well measurements because of the much larger pressure changes that have occurred at depth. The presence of single phase (liquid) or 2-phase conditions is also shown on Fig. 5.

Tauhara field now seems to have 3 distinct pressure lines, or aquifers. The upper two

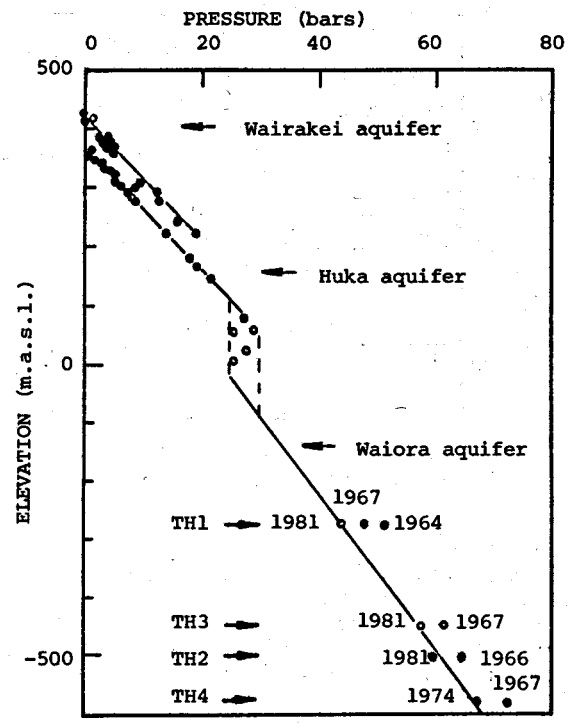

Fig. 5: Vertical pressure trends in Tauhara field (1982).

aquifers represent water tapped by domestic wells. The uppermost aquifer has a zero-pressure intercept of around 410 m R.L., which is close to the elevation of the Terraces, Kathleen and A.C. springs. The intermediate depth aquifer has an intercept at around 360 m R.L., which is a few metres above the level of Lake Taupo and Spa Sights. The overlap of these two lines between 360 and 220 m R.L. is caused by geographic separation and the presence of a lateral pressure gradient away from Mt Tauhara.

Beneath the two shallow aquifers is a region with a very low, subhydrostatic gradient. The points in this zone are 2-phase with both the shut-in fluid state, and the discharge enthalpy of the wells showing strong evidence of steam-zone. Fig. 5 indicates that the steam zone is at least 100 m thick, and that it is at 25-30 bars pressure (230°C approximately). Its elevation coincides with the base of the lower Huka mudstones, and the upper Waiora pumice breccia. This is the same as the initial location of the steam zone at Wairakei (Allis, 1982b). It appears to be a consequence of the relatively low permeability of the lacustrine mudstone compared to the underlying pumice breccia. The mudstone layers in and above the Huka formation have prevented the pressure decline propagating to shallow depth, and have also caused the two shallow aquifers to be present beneath Taupo. This is clearly illustrated in the cross-section shown in Fig. 6. This extends southwest from well TH3 on the northwest flank of Mt Tauhara, to Lake

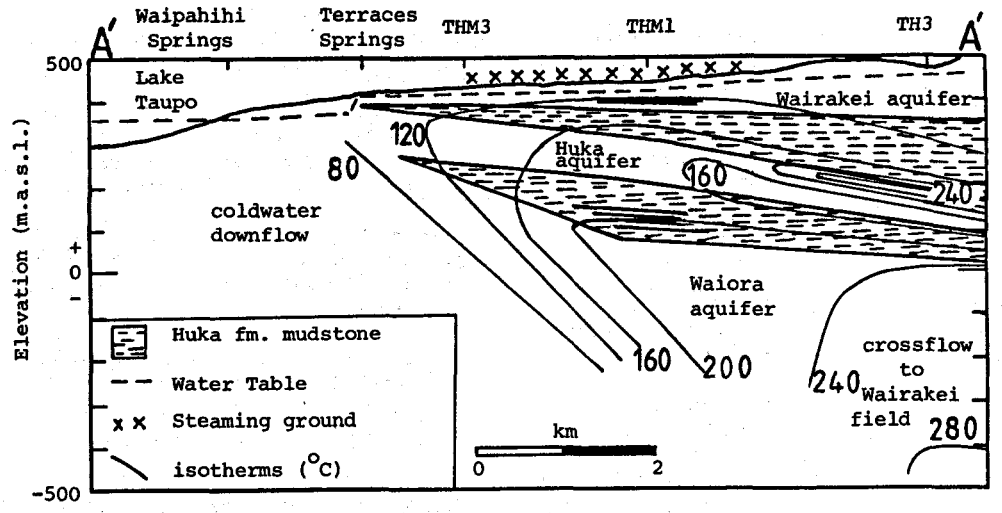

Fig. 6: NE-SW cross-section of Tauhara field showing locations of the 3 aquifers and intervening mudstone aquicludes.

Taupo. TH3 is the hottest well in Tauhara field (temperature >280°C) and it may be close to the field's deep upflow region.

Prior to drawdown, chloride water rose into the shallow aquifers and mixed with cold water flowing westwards. With drawdown, a steam zone has formed beneath the lower mudstone layer, and now steam is flowing up into the shallow aquifers instead of chloride water. A small steam zone may have also formed in the top of the intermediate depth Huka aquifer in the vicinity of TH3. The change to steam-heating has caused increased temperature of the groundwater, and increased heat flow from thermal areas. It has probably also triggered the hydrothermal eruptions. The location of the upflowing steam into the shallow aquifers is uncertain. It could be through faults in the mudstone near TH3, or it could be further east beneath Mt Tauhara where volcanism has disrupted the mudstone layer.

CONCLUSIONS

Drawdown of Tauhara field due to exploitation of Wairakei field has caused a steam zone to form beneath the Huka formation. The pressure of the steam zone has probably not changed greatly since it was first formed in the late 1950's or early 1960's, and it therefore marks the upper limit of significant drawdown in Tauhara field.

This contrasts with the situation beneath the Wairakei production borefield where a steady pressure decline has occurred in the steam zone (due to production), causing the top of the steam zone to migrate to shallower depth. (Fig. 7). In addition, drawdown has propagated into the surface aquifer in this area of the field, and water levels in shallow wells have declined by more than 10 m (Allis, 1982b). West of the production borefield the steam zone pressure rises to about 25 bars. Changes in the surface thermal activity were apparent at Wairakei by the mid-1950's (Thompson, G.E.K., 1960; Allis, 1980). Similar changes in the thermal activity of Tauhara field were not noted until the mid-1960's.

These differences are not attributable to a delay in the pressure drop reaching Tauhara field. The delay, if any, is unlikely to have been more than a few years. The main reason for the differences is the presence of relatively thick (>200 m), presumably competent, lacustrine mudstone layers over most of Tauhara field causing highly anisotropic permeability.

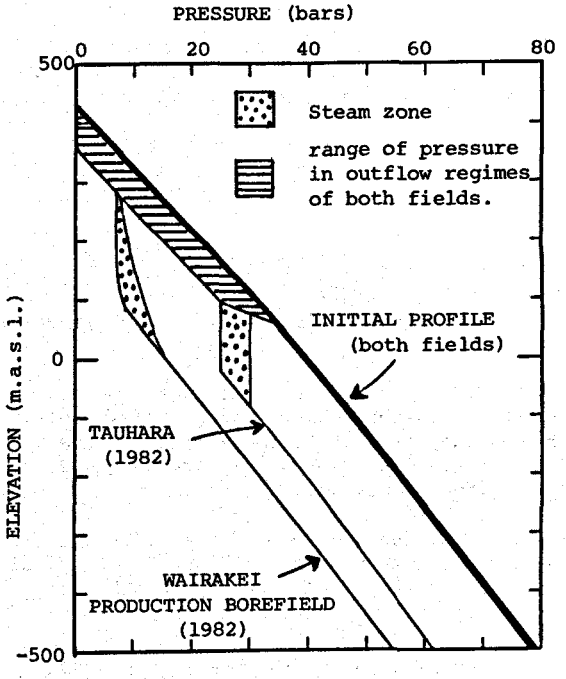

Fig. 7: Comparison of the 1982 pressure-depth trends beneath Tauhara field and the Wariakei production borefield, as a result of exploitation of Wairakei field.

In contrast, across the central portion of Wairakei field, from Geyser Valley in the north to Karapiti thermal area in the south, the thickness of the Huka formation is less than 60 m (Grindley, 1965). The mudstone layers at Wairakei are also severely faulted by the Taupo Fault Belt. These faults control the locations of many of the thermal areas, and because of this the thermal areas of Wairakei field have responded rapidly to changes at depth.

Most of the heat and mass flow from thermal areas of Tauhara field has reached the surface after considerable lateral flow though permeable layers within and above the Huka formation. Since the source region is inferred to be beneath northern Mt Tauhara, the length of the subhorizontal flow path may be at least 2 km. With drawdown of the deep Tauhara aquifer beginning during the 1950's, the mode of heat transport in the source region changed from upflowing chloride water to a steam flux. The temperature of the upflowing fluid may not have changed greatly however. This change in the heat and mass flow into the surface aquifers did not become immediately apparent in the thermal areas and domestic wells of Taupo because of both the length of the outflow path and, to a lesser extent, initial buffering due to storage effects of the rock. These factors are also responsible for the very slow chloride depletion observed in the surface aquifers, and the 50-100 year residence time deduced from tritium analyses (Henley and Stewart, 1982; Allis, 1982a).

REFERENCES

Allis, R.G. 1979: Heat flow and temperature investigations in thermal ground. Report 135, Geophysics Division, D.S.I.R., Wellington, N.Z.

Allis, R.G. 1981: Changes in heatflow associated with exploitation of Wairakei geothermal field, New Zealand. N.Z. Journal of Geology and Geophysics, v. 24, p 1-19.

Allis, R.G. 1982a: Hydrologic changes at Tauhara geothermal field. Geophysics Division Report in prep., D.S.I.R., Wellington, N.Z.

Allis, R.G. 1982b: Geologic controls on shallow hydrologic changes at Wairakei field. proceedings, Pacific Geothermal Conference 1982 and 4th N.Z. Geothermal Workshop 1982, University of Auckland, N.Z.

Dawson, G.B. and Thompson, G.E.K. 1981: Groundwater survey at Taupo, Part 1; Physical data and hydrology. Report 153, Geophysics Division, D.S.I.R., Wellington, N.Z.

Dickinson, D.J. 1968: Temperature survey of the Kathleen Springs. Report 51, Geophysics Division, D.S.I.R., Wellington, N.Z.

Dickinson, D.J. 1976: The 1972 and 1975 infra-red surveys, Taupo area. Unpublished report, Geophysics Division, D.S.I.R., Wellington, N.Z.

Donaldson, I.G. 1982: Comments on the hydrology of the Tauhara geothermal system. Physics and Engineering Laboratory Report in prep., D.S.I.R., Lower Hutt, N.Z.

Fisher, R.G. 1965: Shallow heat flow surveys of Taupo Borough and adjacent country. N.Z. Journal of Geology and Geophysics, v. 7, p 725-771.

Grant, M.A. 1979: Pressure and fluid state at Wairakei. Proceedings of the N.Z. Geothermal Workshop 1979. Part 1, p 79-84. Auckland University, N.Z.

Gregg, D.R. and Laing, A.C.M. 1951: Hot springs of sheet N94/4 with notes on other springs of N94. in Results of geothermal investigations, Wairakei-Taupo Area. unpublished D.S.I.R. Report, p 31-49, Wellington, N.Z.

Grindley, G.W. 1965: The geology, structure and exploitation of the Wairakei geothermal field, Taupo, New Zealand. N.Z. Geological Survey Bulletin n.s. 75, D.S.I.R., Lower Hutt, N.Z.

Henley, R.W. and Stewart, M.K. 1982: Chemical and isotopic change in the hydrology of the Tauhara geothermal field due to exploitation at Wairakei. Journal of Geothermal and Volcanological Research, in press.

Sarbutt, J.V. 1964: A chemical survey of the hot spring and drillhole waters of Taupo Borough. N.Z. Journal of Science. v. 7, p 491-505.

Thompson, B.N. 1951: Interim report on Taupo drillholes, in Results of geothermal investigations, Wairakei-Taupo area. unpublished D.S.I.R. report, p 104-124, Wellington N.Z.

Thompson, G.E.K. 1960: Recent variations of chloride content and spring activity at Wairakei Geyser Valley. N.Z. Journal of Geology and Geophysics, v. 3, p 265-270.

Wooding, R.A. 1981: Aquifer models of pressure drawdown in the Wairakei-Tauhara geothermal region. Water Resources Research, v. 17, p 83-92.

Wooding, R.A. 1982: On transient flow in stratified aquifers with high horizontal permeability. Mathematics and Models in Engineering Science, D.S.I.R. 1982, p 169-177.

Proceedings Eighth Workshop Geothermal Reservoir Engineering
Stanford University, Stanford, California, December 1982
SGP-TR-60

RESERVOIR CHARACTERIZATION OF THE RIBEIRA GRANDE (AZORES) FIELD

Mete, Luigi, Aquater, Spa, Italy

Rivera-Rodríguez, Jesús, Universidad Nacional Autónoma de México

ABSTRACT

A description is made of the geothermal system located at the Ribeira Grande area in San Miguel Island at Azores. To date, three deep wells have been drilled, two of them are considered to be productive and the other one, although capable of production, has been used as an observation well due to completion problems.

One of the wells is presently connected to a 3 MW-portable power plant. A series of tests including both production and well testing, have been conducted in order to provide a reservoir characterization of the system. Several injection falloff, two rate and multiple rate tests have been carried out, as well as a preliminary interference--type test. A description of results obtained is provided.

INTRODUCTION

Once a geothermal field has been located and confirmed by drilling several wells, it is convenient to establish several reservoir and fluid parameters which can be used in order to define the main characteristics of the geothermal system. These data are obtained from geological, geophysical, geochemical and reservoir engineering studies. All the information obtained from these studies should be considered in order to define a preliminary model of the system. Based upon this model and taking into account the main features and anisotropies of the system, as well as fluid characteristics, pressure and temperature, it is possible to come out with a reasonable preliminar assessment of the electrical potential of the geothermal field. This paper summarizes the results of the reservoir engineering studies and test performed on the existing wells of the Ribeira Grande Field in order to characterize the known portion of the system.

References and illustrations at end of paper.

GENERAL BACKGROUND

The Ribeira Grande Field is located in the Sao Miguel Island at Azores (Fig. 1). Three deep wells have been drilled to date, the depth of these wells is 811, 887 and 1229 m, respectively. The geothermal system is located within igneous rocks. a Typical sequence found during drilling in the area under development includes alternate layers of lavas and pyroclastic products of trachytic composition in the shallowest zone, going through alternate layers of lavas and pyroclastites of intermediate composition, which then changes to alternate layers of lavas and pyroclastites of basaltic composition found at the production zone.

In the Ribeira Grande area there are many thermal manifestations, as well as in several places around the island. These features are related to tectonic activity and are located near faults and fractured zones. Two of the deep wells were located near one of such

manifestations. Figure 2 illustrates the location of wells and the main fault system in the area under exploitation.

Figure 3 shows the completion of well PV_1 as well as static pressure and temperature profiles and the main lithologic characteristics found while drilling this well. The Ribeira Grande reservoir is a liquid-dominated system whose production zone is located below 450 m in PV_1. The main production is thought to come through fractures.

At the beginning of the project and in spite of the fact that three deep wells had already been drilled, there was not a proper knowledge of what the reservoir was nor the thickness and the location of the producing intervals. There were only scarse and very preliminary data about the producing capacity of the wells available and the characteristics of their fluids, Therefore, it was the aim of the study undertaken to perform tests and data gathering to collect information realiable enough so as to come out with a proper characterization of the geothermal system. Geological, geophysical, geochemical, geohydrological and well testing studies were carried out. From all of them, this paper deals only with results obtained from the latter.

WELL TESTING PROGRAM

The well testing program for this field was designed according to the following objectives: To locate depth and thickness of the producing zone(s) for each one of the wells available; to obtain the capacity (kh product) of the formation and to determine as occurate as possible both the productivity and the optimum orifice-size production diameter for each well, taking into account that they should be connected to a 3 MW-portable power plant, with a specified inlet steam pressure. An additional task defined during the progress of the field work was to establish even in a very rough manner, the connectivity of that part of the reservoir laying in between the wells available. Unfortunately, this aim could only be partially completed, as will be described later.

Additional restrictions to the type of well testing procedures available, that could be applied to this field were imposed by limitations in equipment availability at the well site, both in quantity and diversity. On the other hand, there were strong indications of a rapid scaling growth in the wells with hot brine production.

Among all pressure transient analysis techniques published in the literature[1], and keeping in mind, all restrictions mentioned above and the objectives pursued, it was decided to perform injection-falloff[2] and two-rate[3] and multiple-rate production testing. This program was carried out in conjunction with well-productivity tests.

INJECTION-FALLOFF TESTS

Injection tests were carried out for two reasons, first to determine the location and thickness of permeable zones within the wellbore open interval, and second for measuring formation capacity (kh). Fig. 4 shows temperature distribution in well PV_1, before injection and also the distribution found from a temperature survey conducted 6 hours after water injection ended. Analyzing this figure permeable zones become apparent.

Injection tests were performed following well-established techniques[1,2]. Just for the sake of completeness, a brief description follows. The standard procedure was to inject fresh water to a prefixed rate for a period of three to four hours, recording changes in bottom-hole pressure by means of a standard bourdon-tube type pressure bomb. Immediately after injection stops, bottom-hole, pressure was recorded during the fallof period for at least twice the injection time. Therefore, it was possible to perform the analysis using

both injection and falloff data in order to check results obtained. Interpretation techniques are well-known and the reader is refered elsewhere[1,2] for futher detail. Fig. 5 shows data for an injection-falloff test performed in well PV_1.

Once the duration of wellbore storage effects[1,4] were determined by means of type-curve procedures, semi-log analysis techniques were carried out. As far as type-curve procedures is concerned, those presented by Agarwal et al[5] and Gringarten et al[6] were performed. These techniques were used only as cheking devices for results obtained by means of analytical methods or when conditions for an adequate application of these methods were not reached.

Dimensionless pressure and time are defined according to Agarwal et al[5] as follows*:

$$p_D = \frac{kh}{141.2q\mu B}\,\Delta p \quad \ldots \quad (1)$$

$$t_D = \frac{0.0002637\,k}{\phi\mu c_t r_w^2}\,t \quad \ldots \quad (2)$$

in a similar manner, the dimensionless wellbore storage parameter is given by:

$$c_D = \frac{0.8936\,C}{\phi c_t h r_w} \quad \ldots \quad (3)$$

where C is the wellbore storage constant.

Figure 5 and 6 show the match obtained by fitting field data obtained during the falloff period of an injection test performed on well PV_1. Fig. 5 correspond to a match on type-curves published by Agarwal et al[5] and Fig. 6 illustrates the match obtained by using type-curves presented by Gringarten et al[6]. Data for this test is shown in Table 1.

* Nomenclature at end of paper.

It was observed from the injection-fall off tests performed in this field that matching field data to the type curves of Gringarten et al was easier than when the match was made by means of Agarwal et al curves. Field data points measured during the infinite acting period of the test were well developed and relatively easy to adjust to one of the curves of Gringarten et al correlation, when plotted as Δp vs. Δt, as shown in Fig. 7. On the other hand, when Agarwal et al type-curve was used, it was observed that the match was not unique. In fact, field data points could have been fitted to curves having different values of C_D and s. This is because different curves on this correlation have similar shapes. However, once the wellbore storage constant was evaluated, a good and unique match was obtained, as shown in Fig. 6. The permeability-thickness product (kh) product was calculated from the pressure match, as illustrated in Appendix. Good agreement was obtained from both matches and results also agreed with those obtained from semi-log techniques. Table 2 summarizes these results for well PV_1.

Although fluid production from this field is most probably obtained from a combination of flow through fractures, fissures and interbedding planes of several lava flows, the high value of the skin factor obtained (s on the order of 20), was explained on the basis of several known factors.

Firstly, the injection-falloff test was carried out in well PV_1 shortly after a clean-up workover in this well was performed, and before any fluid production took place. This workover had to be undertaken because severe scaling in the well was detected, which had closed almost completely the wellbore after several short duration production periods[7]. Therefore, it seemed a reasonable assumption to consider that at least part of the scaling products removed from the wellbore during workover could have gone into the fracture

zones. In addition to this, surface chemical sampling provided a preliminary indication towards the possibility of some scaling deposition in the vicinity of the wellbore. A detailed geochemical sampling and additional well testing, was submited in order to properly define scaling mechanism and to indicate possible solutions to the problem[7].

After the start of the semi-log straight line has been determined, conventional well test interpretation techniques were used. This kind of analysis is well known and the basic equations are as follows[1,2]:

For a constant rate injection test, bottom-hole pressure is given as:

$$p_{wf} = p_{1hr} + m \log t \quad \ldots \quad (4)$$

The skin factor, s, is a follows:

$$s=1.1513\left[\frac{p_{1hr}-p_i}{m} - \log\left(\frac{k}{\phi\mu c_t r_w}\right)+ 3.2275\right]. \quad (5)$$

where:

$$p_{1hr}=p_i + m\left[\log\left(\frac{k}{\phi\mu c_t r_w^2}\right)-3.2275+0.86859s\right] \quad (6)$$

$$m = -\frac{162.6\, qB\mu}{kh} \quad \ldots \quad (7)$$

In a similar manner, bottom-hole pressure during falloff following a constant injection period is given by the following equation:

$$p_{ws} = p^* - m \log\left(\frac{t_p + \Delta t}{\Delta t}\right) \quad \ldots \quad (8)$$

From this equation it is evident that a plot of p_{ws} vs $\log\left(\frac{t_p + \Delta t}{\Delta t}\right)$, should produce a straight line whose slope is given by the following equation:

$$m = \frac{162.6\, qB\mu}{kh} \quad \ldots \quad (9)$$

The skin factor is as follows:

$$s=1.1513\left[\frac{p_{1hr}-p_{wf}(\,t=0)}{m} - \log\left(\frac{k}{\phi\mu c_t r_w^2}\right)+3.2275\right]$$

$$\ldots \quad (10)$$

Fig. 8 shows a semi-log plot of p_{ws} vs $\log\left(\frac{t + \Delta t}{\Delta t}\right)$.

The proper selection of the correct straight line is very important and is not always evident. Fig. 8 illustrates this point, where departure from the correct straight line is belived to be due mainly to thermal effects, without discarding the presence of some kind of outer boundary. The Appendix shows calculations by the semilog method and Table 2 summarizes results.

TWO-RATE AND MULTIPLE-RATE TESTING

To check kh values obtained from injection-falloff tests, two-rate and multiple-rate production tests were scheduled for wells in the Ribeira Grande Field. For a detailed description of the methodology involved, the reader is refered elsewhere[1,3].

Fig. 9 shows data from a two-rate flow test performed in well PV_1. This test was carried out following procedures previously described in reference 3. Before this test was conducted, the flashing point within the wellbore was properly located and the pressure bomb was set approximately 100 m below this point, so as to ensure the presence of only one-phase below the recording point during the duration of the test. Results were interpreted by using Russell[8], Selim[9] and Odeh and Jones[10] models, whose equations are listed below[3]:

a) Russell Model

$$p_{wf} = p_i - 527.4\frac{w_2 \nu_{sc} B\mu}{kh}\left(\log\frac{k}{\phi\mu c_t r_w^2}\right.$$

$$+ 0.891 + 0.87\ s)$$

$$- 527.4 \frac{w_1 \nu_{sc} B}{kh} \left(\log \frac{t+\Delta t'}{\Delta t'} + \frac{w_2}{w_1} \log \Delta t'\right) \quad \ldots (11)$$

From eq. (11) it is evident that by plotting p_{wf} vs $\left(\log \frac{t + \Delta t'}{\Delta t'}\right) + \frac{w_2}{w_1} \log \Delta t'$ a straight line is obtained. The slope of this line is given by:

$$m_R = 527.4 \frac{w_1 \nu_{sc} B\mu}{kh} \quad \ldots (12)$$

Figure 10 shows a graph prepared according to Russel's model.

b). Selim Model

Selim[9] suggested modification of the method proposed by Russell[8], by returning the well to the producing rate it had prior to the test once the well had reached stable conditions. The pressures and flow rates should be measured until new stabilized conditions are reached. The equation for this model is as follows:

$$p_{wf} = p_i - 527.4 \frac{w_1 \nu_{sc} B\mu}{kh} \left(\log \frac{k}{\phi \mu c_t r_w^2} + 0.891 + 0.87\ s\right) - 527.4 \frac{w_2\ sc B}{kh} \left(\log \frac{\left(\frac{w_1}{w_2}\right) t+\Delta t'+\Delta t''}{\Delta t''} + \frac{w_3}{w_2} \log \Delta t''\right) \quad \ldots (13)$$

From Eq. 13 it is evident that plotting p_{wf} vs. $\left(\log \left[\frac{\left(\frac{w_1}{w_2}\right) t+\Delta t'+\Delta t''}{\Delta t''}\right] + \frac{w_3}{w_2} \log \Delta t''\right)$ a straight line is obtained whose slope is

$$m_S = \frac{527.4 \nu w_2\ sc B\mu}{kh} \quad \ldots (14)$$

Figure 11 illustrates the graph obtained according to this model. There is an additional constraint that m_R and m_S should satisfy. This constraint is as follows:

$$\frac{m_R}{m_S} = \frac{w_1}{w_2} \quad \ldots (15)$$

Eq. (15) can be used to select the appropiate straight line portion in the event that several straight lines are present due to scatter of field data.

c) Odeh and Jones Variable Drawdown Model

The field data obtained during the transient conditions after the change in rate were analyzed as a variable drawdown case having w_1 and w_2 as the initial and final flow rates. The interpretation equation is as follows:

$$\frac{p_i - p_{wf}}{w_n} = 527.4 \frac{\nu_{sc} B\mu}{kh} \sum_{i=0}^{n-1} \frac{\Delta w_i}{w_n} \log(t_n - t_i) + 0.8926 + 0.87s + \log \frac{k}{\phi \mu c_t r_w^2} \quad \ldots (16)$$

Therefore, by graphing

$$(p_i - p_{wf}) \text{ vs } \sum_{i=0}^{n-1} \frac{\Delta w_i}{w_n} \log (t_n - t_i),$$

a straight line is obtained whose slope is given by the following equation:

$$m_{OJV} = 527.4 \frac{\nu_{sc} B\mu}{kh} \quad \ldots (17)$$

Fig. 12 shows the graph obtained when field data are plotted according to this model. Table 3 summarizes results obtained by applying the models mentioned above.

Equations (11) through (17) are expressed in metric geothermal units and flow rates are in terms of mass, rather than volume. For these equations the meaning of flow rates is as follows:

w_1 = Stabilized mass flow rate prior first rate change, ton/hr

w_2 = Stabilized mass flow rate after first rate change, ton/hr

w_3 = Stabilized mass flow rate after second rate change, ton/hr

All other variables are listed on the Nomenclature section.

INTERFERENCE TYPE TEST

It was considered of great importance to conduct a very rough interference test between wells PV_1, and PV_2 (see Fig. 2 for well locations). This attempt was carried out in spite of not disposing of adequate instrumentation such as high-precision bottom-hole pressure sensing and recording devices, such as the ones used in similar field applications[11].

It was decided to detect bottom-hole pressure changes in well PV_2, induced by fluid extraction from its neighbor well PV_1. Changes in pressure were detected, by means of the more precise Bourdon-type bottom-hole pressure recording device available, keeping in mind the range of resolution of this instrument. This attempt was encouraged also from evidences of interference of well PV_2 production on the productivity of well PV_1, when both were simultaneously under exploitation[12].

Fig. 13 shows the few meaningful data points obtained from this test after data filtration. An attempt to match this data with the exponential integral solution[13] is illustrated in Fig. 13. As it is evident, by using the few data available, three different matches could be made. Table 4 summarizes results obtained.

CONCLUSIONS

Based upon the results obtained from the well testing program carried out at the Ribeira Grande Geothermal Field and briefly described in this paper, the following conclusions can be drawn:

1. Reservoir characterization is a very important step in the adequate knowledge of the anisotropies and main features of a given geothermal field. This knowledge will definetely contribute towards a more precise definition of the electrical generation capacity of a reservoir.

2. Injection-falloff tests provide a useful tool for locating permeable zones in either igneous or sedimentary rocks and also to evaluate their capacity.

3. Two-rate flow testing can be applied to obtain basic reservoir parameters.

NOMENCLATURE

B = brine formation volume factor, (volume, reservoir conditions/volume, standard conditions).

C = wellbore storage constant, bbl/psi

C_D = dimensionless wellbore storage coefficient.

c_t = total compressibility, $(psi)^{-1}$

h = formation net thickness, ft.

k = permeability, md.

m = slope of a straight line

p = pressure, psi.

p_i = initial pressure, psi.

p_{wf} = flowing bottom-hole pressure, psi.

p_{1hr} = flowing bottom-hole pressure al 1hr,psi

p_{ws} = static bottom-hole pressure, psi.

p_D = dimensionless pressure.

p^* = false pressure, pressure obtained when linear portion of the plot of p_{ws} vs. $\log[(tp+\Delta t)/\Delta t]$ is extrapolated to $(tp+\Delta t)/\Delta t=1$, psi.

GREEK SYMBOLS

μ = viscosity, cp.
ν = specific volume, cm^3/gr
ϕ = porosity, fraction

For the two-rate flow test (equations (11) through (17), geothermal metric units were used. Therefore, for these equations, the following nomenclature was used.

B = brine formation volume factor, (volume, reservoir conditions / volume, standard conditions)
c = total fluid compressibility, $(kg/cm^2)^{-1}$
h = formation net thickness, m
k = permeability, md
m = slope of a straight line
n = constant rate intervals in Odeh and Jones model
p = pressure, kg/cm^2
p_i = initial pressure, kg/cm^2
p_{wf} = flowing bottom-hole pressure, kg/cm^2
p_{1hr} = flowing bottom-hole pressure 1 hr after the rate change, kg/cm^2
q = volumetric flow rate, bbl/day
r_w = wellbore radius, cm
s = skin factor, dimensionless
t = producing time to instant of rate change, hrs
t' = producing time measured from first rate change, hrs
t" = producing time measured from second rate change, hr
w = mass flow rate, ton/hr
y = correlation parameter in Odeh and Jones method

SUBSCRIPTS

1 = conditions prior to rate change
2 = conditions after first rate change
3 = conditions after second change
i = initial condition
OJV= refers to Odeh and Jones variable draw down model
R = refers to Russell's model
S = refers to Selim's model
sc = standard conditions
w = wellbore
wf = flowing conditions

ACKNOWLEDGEMENTS

The authors wish to thank Mr. Antonio M. Rodríguez-da Silva, Director do Programa Geotérmico dos Açores, Lab. Geo. e Tecnologia, for permission to publish the field data presented in this paper. The encouragment and support from the management of Aquater is also acknowledged. We also appreciate the assistance from Mr. A. Drei in processing field data.

REFERENCES

1. Earlougher, R.C., Jr.: Advances in Well Test Analysis, Society of Petroleum Engineers of AIME Monograph Volume 5, Dallas, Tex. (1977).

2. Rivera-R., J. and Saltuklaroglu, M.:"Well Testing at Los Azufres Geothermal Field", paper SPE 8348 presented at the 54th Annual Fall Technical Conference and Exhibition of the Society of Petroleum Engineers of AIME, Las Vegas, Nevada (Sep.23-26, 1979).

3. Rivera-R., J., and Ramey, H.J., Jr.: "Application of Two-Rate Flow Tests to the Determination of Geothermal Reservoir Parameters", Paper SPE 6887 presented at SPE-AIME 52nd Annual Technical Conference, Denver, Colorado (Oct.9-12, 1977).

4. Miller, C.W.: "Wellbore Storage Effects in Geothermal Wells", Soc. Pet. Eng. Jour., (Dec. 1980) 555-566.

5. Agarwal, R.G., Al-Hussainy, R., and Ramey, H.J., Jr.: "An Investigation of Wellbore Storage and Skin Effect in Unsteady-Liquid Flow, I Analytical Treatment", Soc. Pet. Eng. Jour. (Sept. 1970) 279-290.

6. Gringarten, A.C., Bourdet, D.P., P.A. and Kniazeff, V.J.: "A Comparison Between Different Skin and Wellbore Storage Type-Curves for Early-Time Transient Analysis", Paper SPE 8205 presented at 54th Annual Fall Technical Conference and Exhibition of the Society of Petroleum Engineers of AIME, Las Vegas, Nevada (Sep. 23-26,1979)

7. Aquater, S.p.A.: Feasibility Study of Geothermal Power Plant of Ribeira Grande-S. Miguel, FIRST-STEP REPORT,Annex D-Well Testing, San Lorenzo In Campo, Italy, June 1982.

8. Russell, D.G.: "Determination of Formation Characteristics by Two-Rate Flow Tests", J. Pet. Tech., December 1962, 1347-1355.

9. Selim, M.A.: "A Modification of the Two-Rate Flow Method for Determination of Reservoir Parameters", J. Institute of Petroleum, v. 53, No. 527, (Nov. 1967) 343-352.

10. Odeh, A.S., and Jones, L.G.:"Pressure Drawdown Analysis, Variable Rate Case", J. Pet. Tech., (Aug. 1965) 960-964.

11. Rivera-R., J., Samaniego-V., F. and Schroader, R.C.: "Pressure Transient Testing at Cerro Prieto Geothermal Field", Geothermics, Vol. 9 (1980) 189-196.

12. Rodrigues-da Silva, A., private communication.

13. Earlougher, R.C., Jr., and Ramey, H.J., Jr.: "Interference Analysis in Bounded Systems", Jour. Can. Pet. Tech. (Oct.-Dec. 1973) 33-45.

APPENDIX

A. Falloff test calculations

1. Type-curve procedures.

a) Agarwal et al

From the pressure match shown on Fig. 6, and from eq. (1), once the adequate transformation of units has been made, it follows:

Match point:

For $(t)_M = 10$ min., $t_D = 8.6 \times 10^5$

For $(\Delta p)_M = 10$ Kg/cm^2 (142 psi), $p_D = 20.5$, $s = 20$

From eq. (1) in the text:

$$kh = 141.2\, qB\mu_w \frac{(p_D)_M}{(\Delta p)_M} = 141.2(4604)(1.06)$$

$$(0.28)\frac{(20.5)}{142} = 8500 \text{ md-m}$$

b) Gringarten et al

From the pressure match shown on Fig. 7, and from eq. (1), the following results are obtained:

Match point:

For $(t)_M = 10$ min, $\frac{t_D}{C_D} = 10.5$

For $(p)_M = 10$ Kg/cm^2 (142 psi), $p_D = 26.5$,

$$C_D e^{2s} = 10^{30}$$

From eq. (1) in the text:

$$kh = 141.2\, qB\mu_w \frac{(p_D)_M}{(\Delta p)_M} = 141.2\ (4604)(1.06)$$

$$(0.28)\ (\frac{26.5}{142}) = 10987 \text{ md-m}$$

2. Semi-log methods.

From Fig. 8, the slope of the semi-log straight line during falloff is:

$$m = 0.50 \frac{Kg/cm^2}{cycle} \left(7.1 \frac{psi}{cycle}\right)$$

Then, from eq. (1) in the text:

$$kh = \frac{162.6\ qB\mu_w}{m} = \frac{162.5(4604)(1.06)(0.22)}{(7.1)\ (3.28)}$$

$$= 7496 \text{ md-m } (24588 \text{ md-ft})$$

B. Two-Rate flow test calculations

a) Russell's Model

From Fig. 10, $m_R = 1.66$.

Then:

$$(kh)_R = \frac{527.4\ W_1\ \nu_{sc} B\mu_w}{m_R}$$

$$= \frac{(527.4)(108.53)(1.043)(1.18)(0.145)}{1.66}$$

$$(kh)_R = 7002 \text{ mdm}$$

b) Selim's Model

From Fig. 11, $m_s = 0.68$.

Then:

$$(kh)_s = \frac{527.4\ w_2\ \nu_{sc} B\mu_w}{m_s}$$

$$= \frac{(527.4)(59.14)(1.043)(1.18)(0.165)}{0.68}$$

$$(kh)_S = 9315 \text{ mdm}$$

From Fig. 12, $m_{OJV} = 0.0115$

Then:

$$(kh)_{OJV} = \frac{527.4\ \nu_{sc} B\mu_w}{m_{OJV}}$$

$$= \frac{527.4)(1.043)(1.18)(0.165)}{0.0115}$$

$$(kh)_{OJV} = 9313 \text{ mdm}$$

Table 1. Data for falloff test in well PV_1. q_{inj}=4604 bbl/day.

Δt TIME (minutes)	BOTTOM-HOLE PRESSURE p_{ws} (Kg/cm^2)
0	39.53
0.5	37.95
1	36.25
2	33.45
3	31.35
4	30.01
5	28.72
6	27.85
7	27.31
8	26.85
9	26.51
10	27.27
15	25.64
20	25.52
30	25.52
40	25.61
50	25.65
60	25.70
70	25.75
80	25.76
90	25.77
98	25.77
CLOCK FAILURE	
206	25.80
226	25.72
246	25.59
266	25.44
286	25.25
306	25.09
326	24.92
346	24.76

Table 2.- Results obtained from falloff test performed in well PV_1

Interpretation Technique	Results	
	kh (md-m)	s
Type-curve matching (Agarwal et al.)	8500	20
Type-curve matching (Gringarten et al.)	10987	
Semi-log	7496	

Table 3.- Results obtained from two-rate flow test carried out in well PV_1

Interpretation Technique	kh (md-m)
Russell	7002
Selim	9315
Odeh & Jones	9313

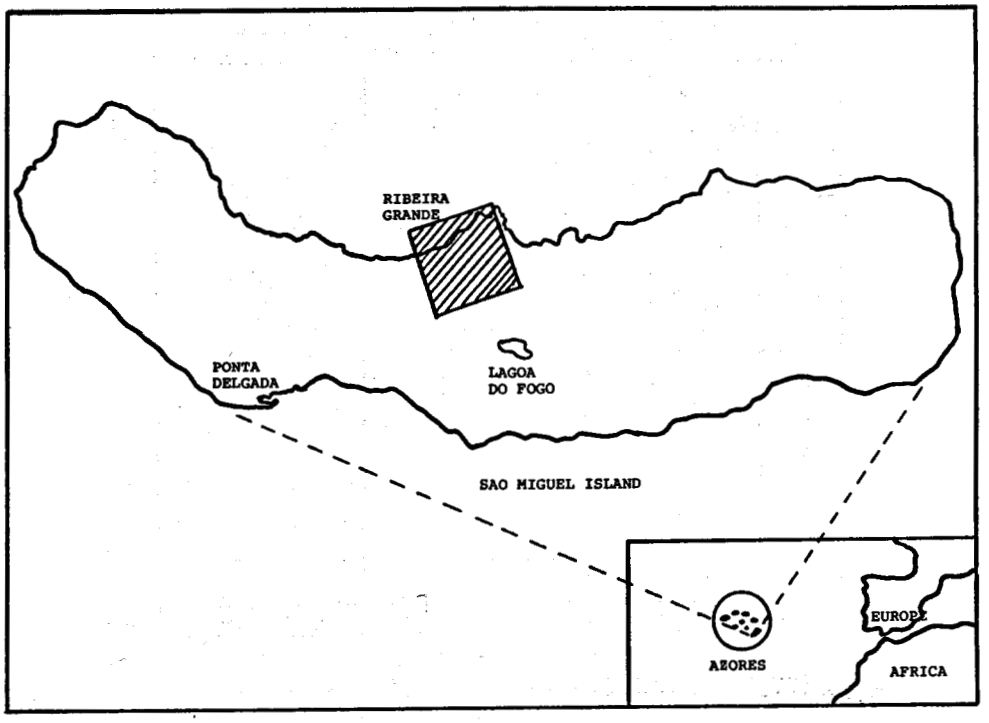

FIG. 1.-Location of the Ribeira Grande Geothermal Field

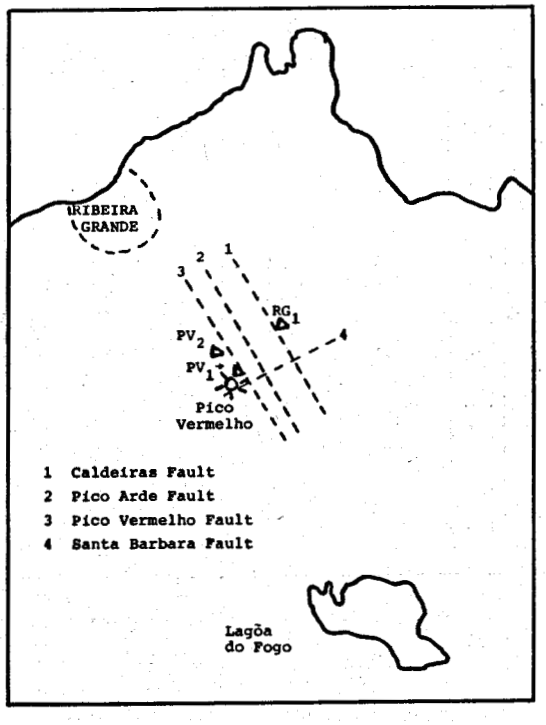

FIG. 2.-Main fault system associated with the Ribeira Grande Field

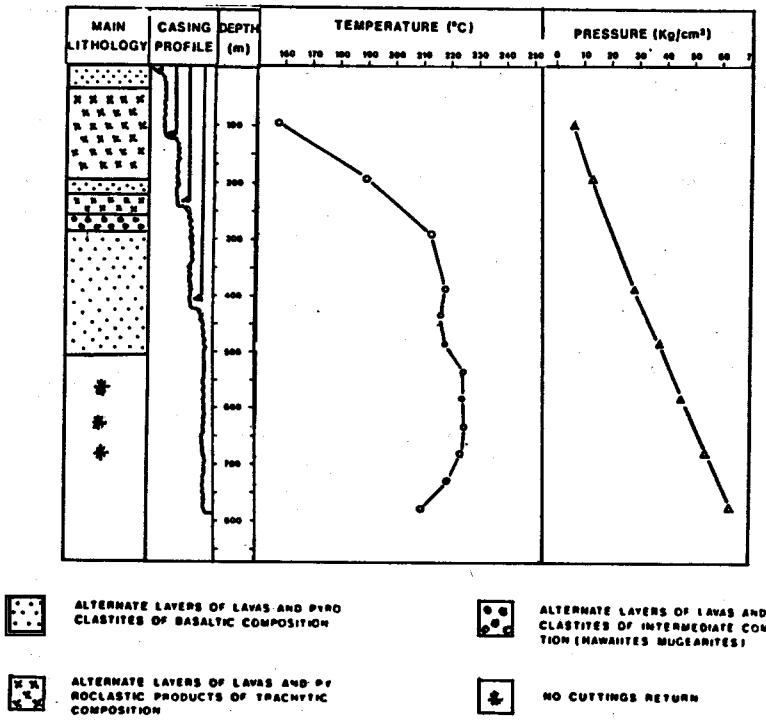

FIG. 3.-Well completion, lithology and pressure and temperature profiles for well PV_1

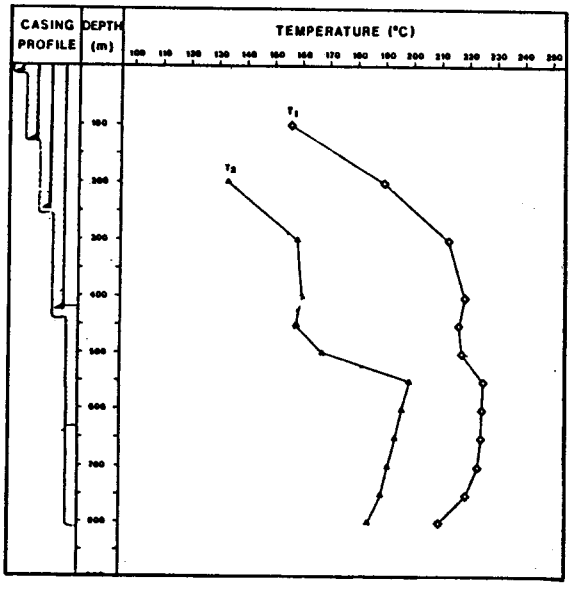

T_1 Static temperature profile

T_2 Temperature profile 6 hours after water injection stopped

FIG. 4.-Temperature profile before and after water injection in well PV_1

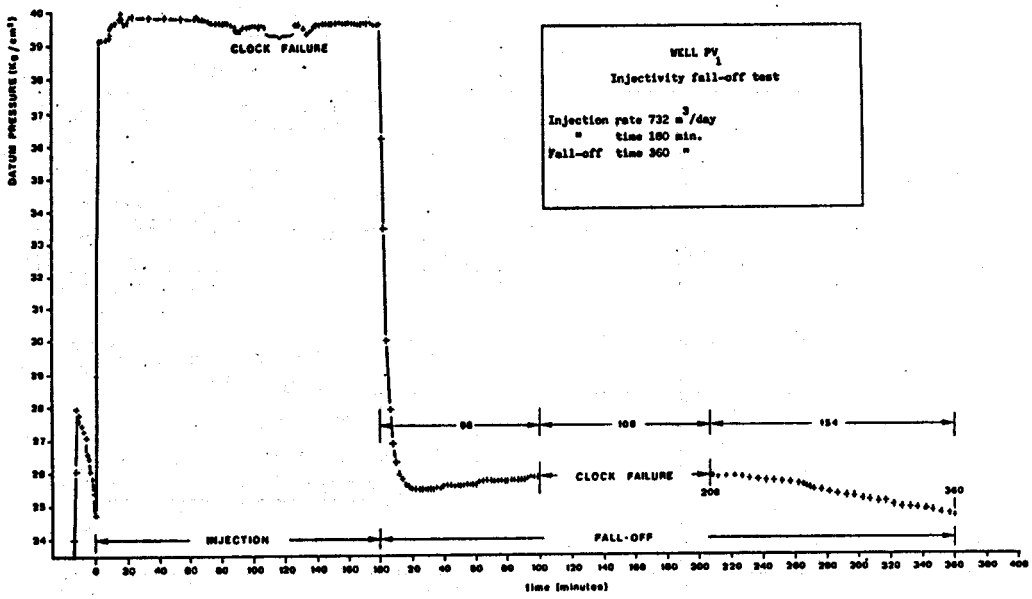

FIG. 5.-Datum pressure vs time - injectivity fall-off test

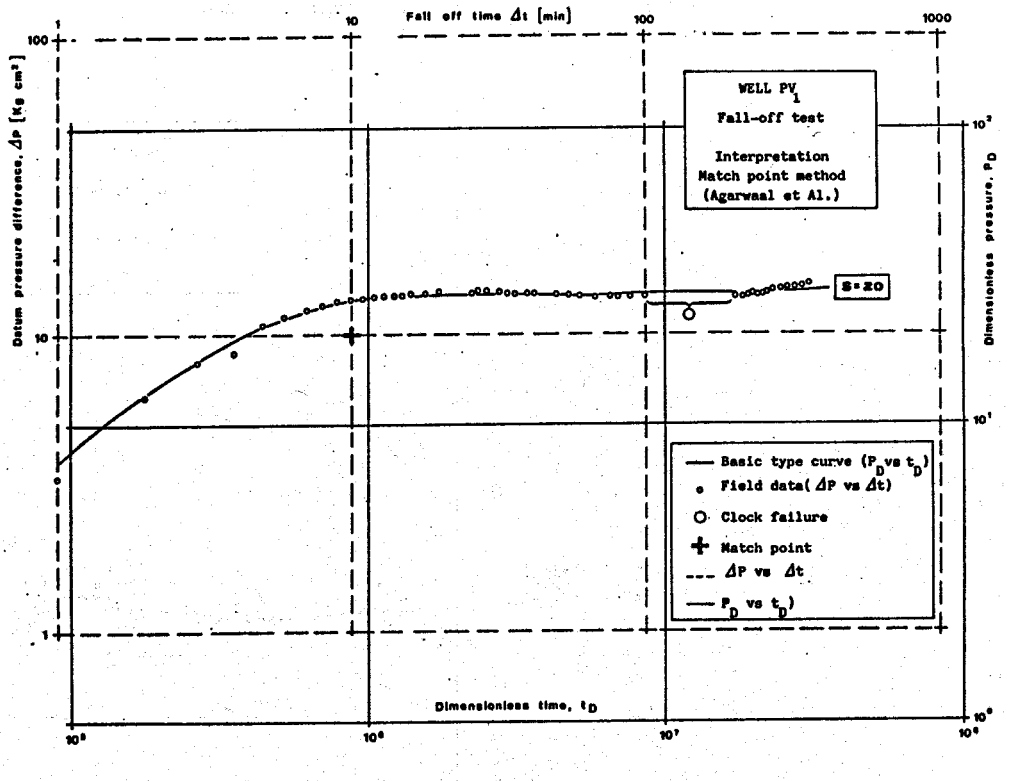

FIG. 6.-Datum pressure difference vs fall-off time; dimensionless pressure vs dimensionless time. log-log plots - fall-off test.

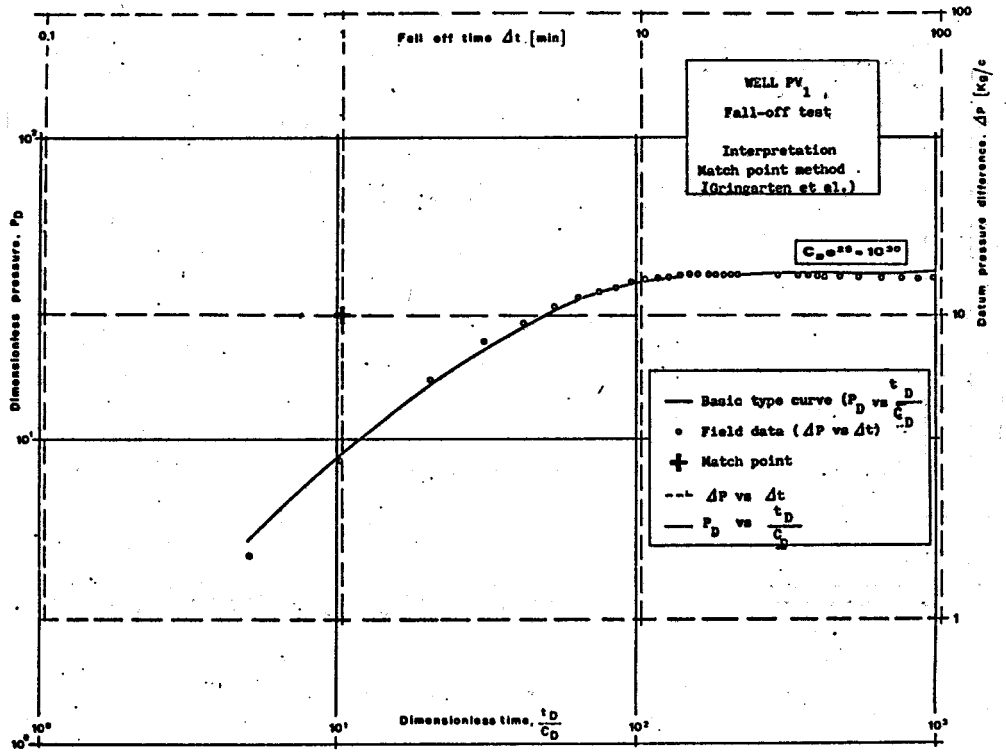

FIG. 7.-Datum pressure difference vs fall-off time; dimensionless pressure vs dimensionless time. log-log plots - fall-off test.

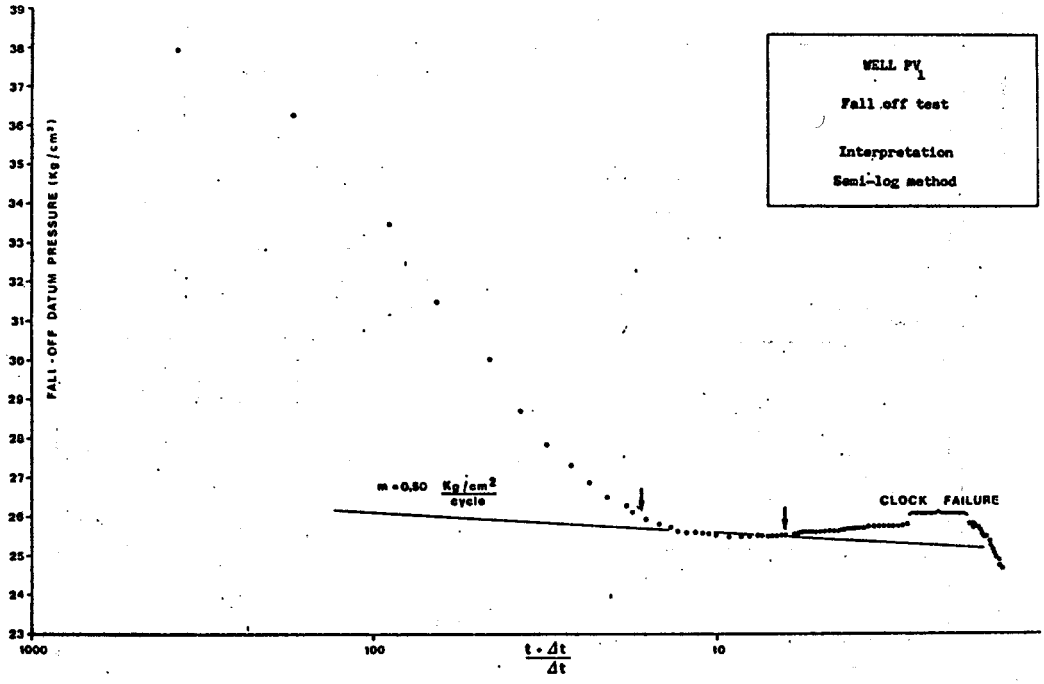

FIG. 8.-Datum pressure vs dimensionless time. Semi-log plot - fall-off test.

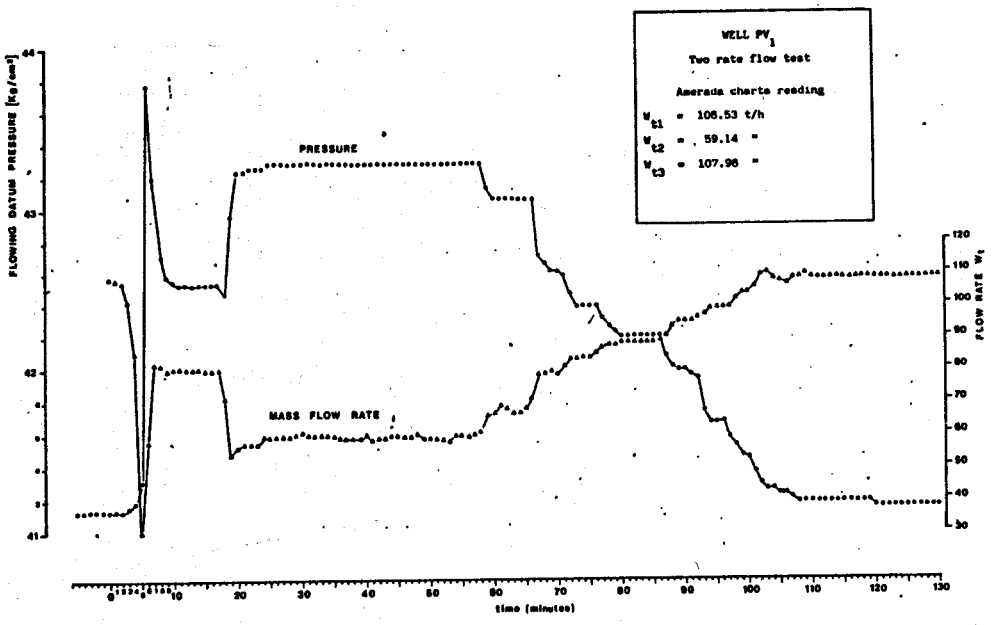

FIG. 9.-Flowing datum pressure vs time - two rate flow test

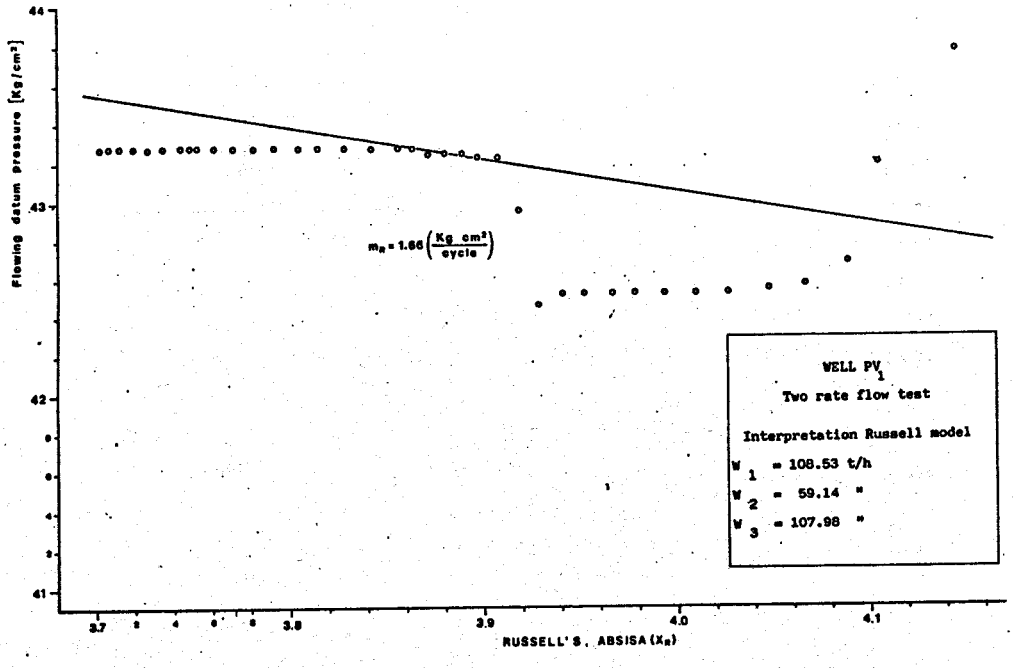

FIG. 10.-Flowing datum pressure P_{wf}, vs Russell's absisa (X_R) - two rate flow test

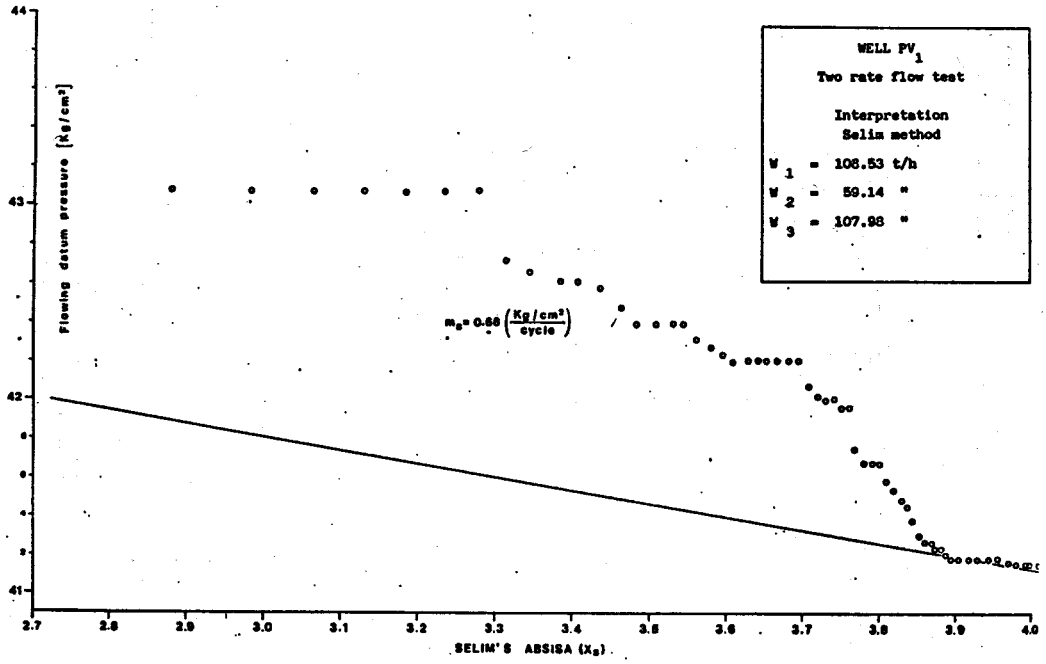

FIG. 11.-Flowing datum pressure P_{wf} vs time - Selim's absisa X_s - two rate flow test

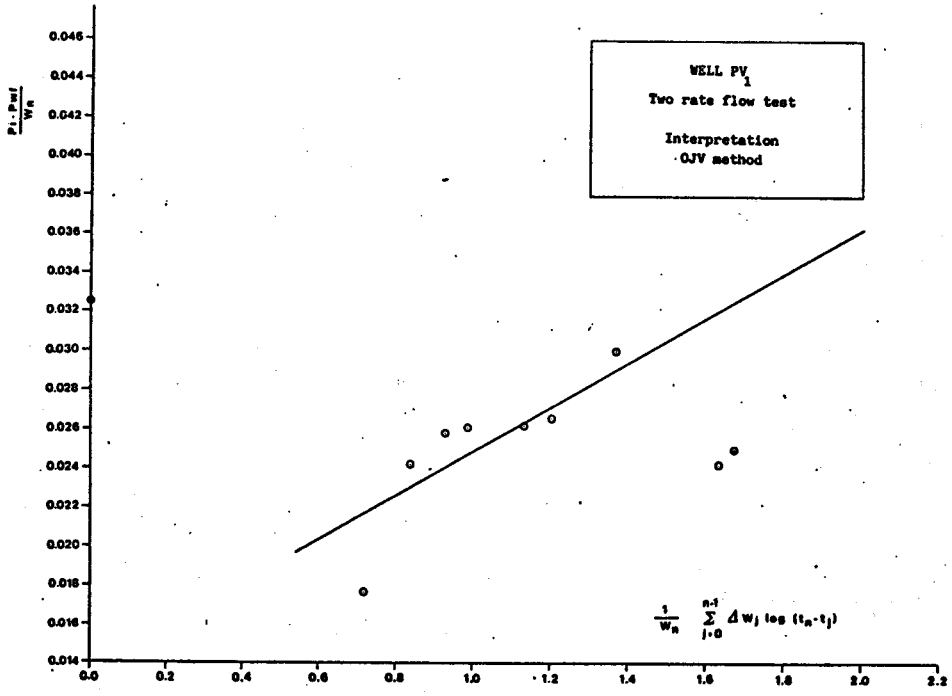

FIG. 12.-O.J.V. plot, two rate flow test.

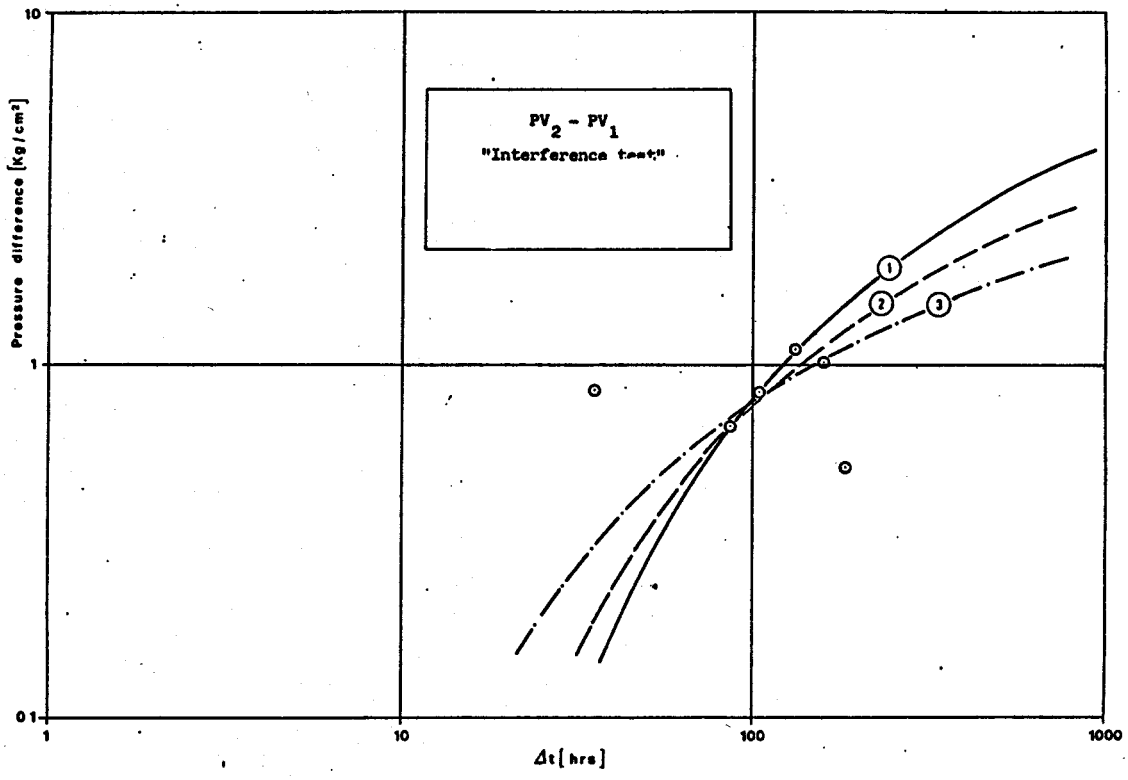

FIG. 13.-Pressure difference ΔP vs time - PV_1-PV_2 "Interference test".

Proceedings Eighth Workshop Geothermal Reservoir Engineering
Stanford University, Stanford, California, December 1982
SGP-TR-60

INTERPRETATION OF REDONDO CREEK FIELD PRESSURE BUILDUP TESTS

James B. Fallon

Union Oil Company of California
Santa Rosa, CA

Abstract

Recent pressure buildup analyses of Redondo Creek Field wells have been facilitated by identification of wellbore storage. The wellbore storage coefficient observed immediately after shut-in is controlled by the compressibility of the two-phase wellbore fluid, but the coefficient decreases when the wellbore storage is controlled by a rising liquid level. Identification of such phenomena aids in defining the correct radial flow regime of the pressure buildup response.

Introduction

The Redondo Creek Field is located within the Jemez Mountains in North Central New Mexico. The geothermal reservoir has been documented as containing a high temperature, low salinity water which is overlaid in a limited portion of the field by a steam-dominated zone (Union, 1978, and Atkinson, 1980). Union Oil Company of California has drilled nineteen wells in the field, four of which currently produce a two-phase mixture at commercial wellhead pressures; several others will produce at subcommercial wellhead pressures.

Figure 1 presents a wellbore schematic and pressure profile of a typical Redondo Creek well during production, shut-in, and transitional conditions. The flowing two-phase wellbore conditions change following shut-in to segregated liquid and vapor columns. These wellbore fluid behaviors have been associated with the wellbore storage regimes which dominate the early-time pressure response of all Redondo Creek pressure buildup tests. The initial wellbore storage coefficient is controlled by the compressibility of the initially two-phase wellbore fluid. Appendix A derives an approximate expression for the compressibility of a typical Redondo Creek two-phase wellbore fluid. This expression is dependent upon the volumetric heat content of the wellbore which in turn is dependent upon the volumetric steam fraction of the wellbore fluid and the assumed contributing heat content of the casing. A high volumetric heat content - large water fraction - results in a higher two-phase compressibility due to the increased energy available for phase change and hence a larger change in volume. The two-phase compressibility is up to an order of magnitude larger than the compressibility of steam.

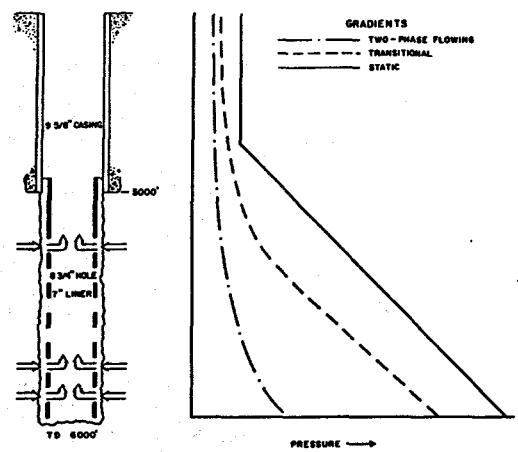

Figure 1 - Typical Redondo Creek Well; Casing Schematic and Pressure Profile During Production Shut-In and Transition.

Appendix B derives an expression for the total wellbore storage coefficient of a well which intersects a producing two-phase reservoir. Equation B-4 contains two factors which contribute to the total storage: a rising liquid level and wellbore fluid compressibility. The rising liquid level does not influence the observed wellbore storage until the wellbore liquid level rises above the pressure monitoring depth, at which time the magnitude of the wellbore storage factor will normally decrease. The duration of the compressibility storage will therefore be dependent upon the pressure monitoring depth and the steam quality of the fluid produced into the wellbore.

Identification of the different wellbore storage regimes has facilitated analysis of Redondo Creek buildup tests. Values of observed wellbore storage coefficients have been obtained from the unit slope of the log-log plot (Earlougher, 1977) where:

$$C = \frac{Wv\ \Delta t}{\Delta P}\ ft^3/psi \qquad (1)$$

W_v = volumetric production rate, $W_L v_L + W_g v_g$

Δt, ΔP = point on unit slope line

Comparison of the constant obtained from Equation 1 with the constant calculated from Equation B-4 has been used to classify wellbore storage regimes, identify wells which have intersected fractures, and obtain a qualitative estimate of the volumetric steam fraction produced from different zones in a well. While the intersection of fractures can be determined from the comparison, quantitative data concerning effective fracture volumes cannot be obtained because of the accompanying increase in two-phase compressibility due to increased effective heat content of the wellbore-fracture system.

Determination of the end of significant wellbore storage effects has helped to isolate reservoir characteristics. Once the wellbore storage effects have diminished, some Redondo Creek wells exhibit radial flow pressure fluctuations - an instability probably related to the reservoir equilibration of phases following a period of two-phase production. Whatever the physical mechanism, the instability appears to be aggravated by the withdrawal and reentry of wireline tools in and out of the wellbore.

The recent buildup tests conducted on four Redondo Creek wells will be used to illustrate this analytical tool. The Horner Analyses have assumed that all wells observed to have less than 30% wellhead mass steam fraction are dominated by a single-phase reservoir response. Wells with between 30% and 70% mass steam fraction have been considered as two-phase and analyzed in the manner proposed by Garg and Pritchett (1981). Analysis of wells with higher then 70% mass steam have combined this two-phase analysis with the ΔP^2 method commonly applied to a high compressibility, low pressure system.

Baca No. 15

Baca No. 15 produces from an upper steam-dominated zone and a lower liquid zone, with the well's high steam production originating almost entirely in the upper zone. The pressure response following the shut-in of Flow Test 3 (Figure 2) shows an initial wellbore storage dominated by the compressibility storage of the two-phase wellbore fluid. The contrast of the observed wellbore storage constant calculated from Equation 1 (167 ft^3/psi) with the calculated wellbore storage coefficient based upon the wellbore volume (28 ft^3/psi) suggests that the well intersects a large fracture network.

The abrupt decrease in wellbore storage observed in Figure 2 is a reflection of the wellbore liquid level reaching the pressure monitoring depth. The wellbore storage coefficient associated with the now dominant rising

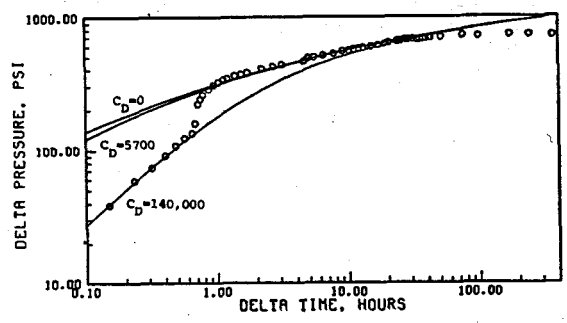

Figure 2 - Baca No. 15 Pressure Buildup Following Flow Test 3. P_{wf}=516 psig; s=-5.4; C_D=0, 5700, 140000.

liquid level is almost 25 times smaller than the earlier compressible storage coefficient.

Horner Analysis of the correct semilog straight line - reached almost immediately upon changing of dominant wellbore storage - results in an apparent kh of 3900 md-ft and a skin of -5.4 using a two-phase analysis (Figure 3). These values are consistent with the falloff testing results and the negative skin factor supports the wellbore storage indications of an intersected fracture network. The pressure stabilization at large shut-in times (Figures 2 and 3), characteristic of a constant pressure boundary, is attributed to the effect of the steam-dominating upper zone on the monitoring depth.

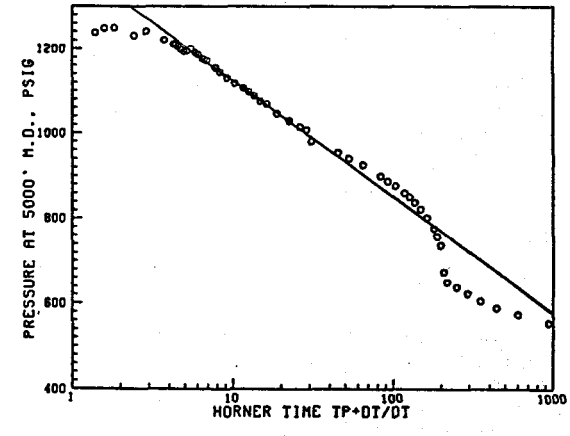

Figure 3 - Baca No. 15 Pressure Buildup Following Flow Test 3. t_p=140 hrs; m=275 psi/cycle; $P_{1\ HR}$=810 psig.

Baca No. 4

Baca No. 4 produces a limited amount of fluid from an upper steam-dominated zone, with the major production originating in a deeper zone producing a low steam-fraction fluid. The pressure responses following Flow Tests 4 and 5 are almost identical when displayed on a log-log plot (Figure 4). The early-time observed wellbore storage coefficient (28 ft^3/psi) compares favorably with the value calculated from Equation B-4 (25 ft^3/psi). This

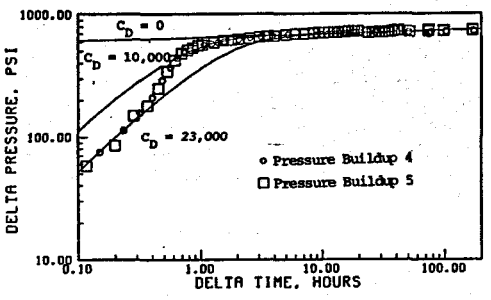

Figure 4 - Baca No. 4 Pressure Buildups Following Flow Tests 4 and 5. P_{wf}=500 and 470 psig; s=+10; C_D=0, 10000, 23000.

suggests that Baca No. 4 does not intersect significant reservoir fractures.

The decrease in wellbore storage coefficient observed in Figure 4 is not as abrupt as seen in Figure 2. The deep two-phase production of Baca No. 4 does not create as perfect a liquid interface as would be obtained from a well which produces nearly single-phase bottom zone fluid (Baca No. 15). The relatively small decrease in wellbore storage coefficient (2.3X) is due to the small effective wellbore volume contributing to the compressible storage and the small water fraction of the produced fluid.

Horner Analysis of the buildup data was complicated by reservoir pressure fluctuations (Figure 5). A single-phase analysis of the average pressure trend - designated by the straight line on Figure 5 - results in an apparent kh of 5200 md-ft and a skin of +10. These values are consistent with another Baca No. 4 pressure buildup analysis (Riney and Garg, 1981). The high skin factor is probably due to the reservoir flashing of fluid during production. The lack of fracture flow indications are consistent with the wellbore storage observations.

Baca No. 13

Baca No. 13 produces a moderate enthalpy fluid from at least two highly permeable zones in the deeper liquid reservoir. The well is completed with 9-5/8" casing from the surface to 3499' M.D. and a 7" liner hung from 3340' M.D. to 8200' M.D., the first 889 feet of which is blank with the remainder slotted. The pressure response following Flow Tests 7, 8 and 9 all had consistent, but unique, behaviors (Figure 6).

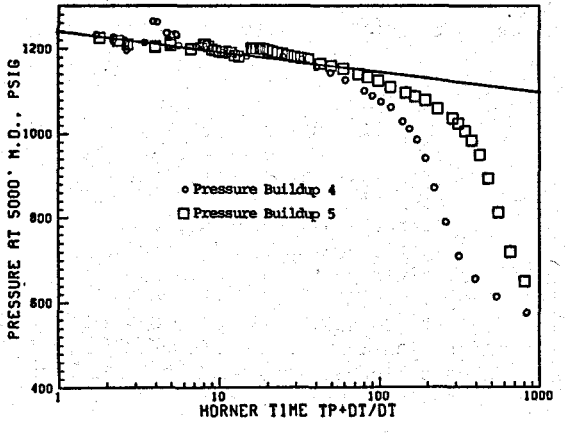

Figure 5 - Baca No. 4 Pressure Buildups Following Flow Tests 4 and 5. t_p=125 and 295 hrs; m=45 psi/cycle; $P_{1\ HR}$=1145 psig.

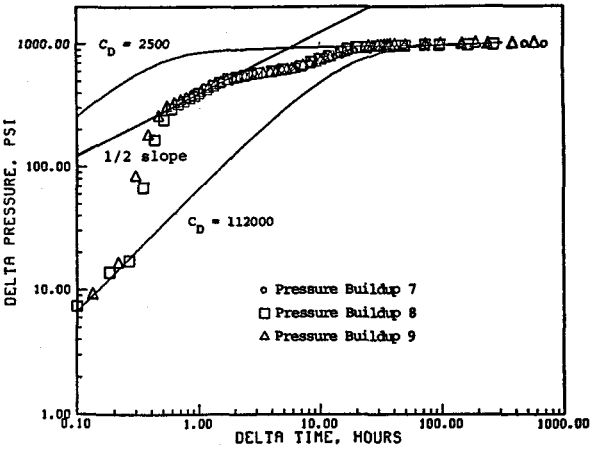

Figure 6 - Baca No. 13 Pressure Buildups Following Flow Tests 7, 8 and 9. P_{wf}=465 psig; s=+17; C_D=2500, 112000.

The initial pressure response is dominated by the compressibility of the two-phase wellbore fluid. The observed wellbore storage coefficient (135 ft^3/psi) differs from the theoretical value based upon the wellbore volume (48 ft^3/psi), suggesting the intersection of fractures. This is confirmed soon after the rising liquid level becomes the dominant wellbore storage factor. The associated decrease in wellbore storage coefficient creates the abrupt pressure rise observed in other wells, but before reaching the next wellbore storage regime or the semilog straight line (as observed in Baca Nos. 4 and 15) fracture flow begins to dominate the pressure response. This linear flow regime dominated the entire falloff pressure response following the Baca No. 13 injection test. The fracture must be located above the pressure monitoring depth and from temperature surveys has been tentatively identified near 4500' M.D..

The linear flow pressure response is interrupted by another wellbore storage phenomenon. When the wellbore liquid level reaches the 7" liner hanger, the water begins to spill over into the annulus of the blank liner section between the 7" liner and the 8-3/4" wellbore wall. Upon fill-up of this annulus the pressure response continues the transition to the semilog straight line, but not until the first 20 hours of the pressure buildup were dominated by either wellbore storage or fracture flow. Without identification of these wellbore storage regimes, the pressure buildup would have been interpreted as characteristic of a two-layer reservoir (Matthews and Russell, 1967).

The radial flow regimes of the three buildup tests are affected by the reservoir pressure fluctuations also observed in Baca No. 4. The Horner Analysis of the average pressure trend - designated by the straight line on Figure 7 - results in an apparent kh of 6400 md-ft and a skin of +17. The high skin factor is not consistent with the observed fracture phenomenon but is attributed to the extensive reservoir flashing of Baca No. 13.

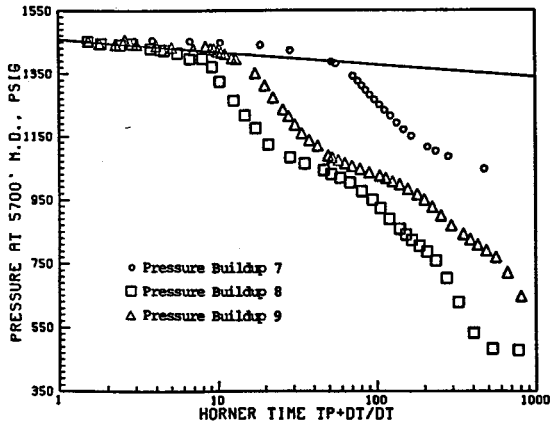

Figure 7 - Baca No. 13 Pressure Buildups Following Flow Tests 7, 8 and 9. t_p=1340, 130 and 309 hrs; m=43 psi/cycle; $P_{1\ HR}$=1352 psig.

Baca No. 21

Baca No. 21 is a shallow well (3000' M.D.) which produces a 95% steam fraction fluid. The anamolous pressure buildup behavior monitored following Flow Test 5 is a reflection of the anamolous behavior of the well in general. A static pressure gradient in Baca No. 21 reveals a high steam-fraction gradient without a liquid level, while a flowing gradient displays a liquid column below 2750'. Upon shut-in, the pressure response at 2750' is intially controlled by the wellbore storage of a rising liquid level as indicated in the close agreement between the observed storage coefficient (400 ft^3/psi) and the calculated storage coefficient (380 ft^3/psi). Depression of the liquid level to below the 2750' monitoring depth creates an increase in the effective wellbore storage coefficient. This depression is probably caused by several factors such as little water production combined with a quicker reservoir pressure recovery in the zone above 2750' than the zone below 2750'.

The magnitude of the second observed wellbore storage regime coefficient (2240 ft^3/psi) differs from the theoretical wellbore storage coefficient (50 ft^3/psi) based upon the wellbore volume suggesting that the wellbore has intersected a large fracture network. This appears to be confirmed by the excellent match of the log-log plot to the type-curve for a vertically fractured well with wellbore storage (Ramey, et al., 1975).

This match, shown on Figure 10, is clouded somewhat by reservoir pressure fluctuations and the failure of reaching the true radial flow regime. Analysis of the log-log type curve match indicates that Baca No. 21 has an apparent permeability of 2800 md-ft with an undetermined but negative skin factor.

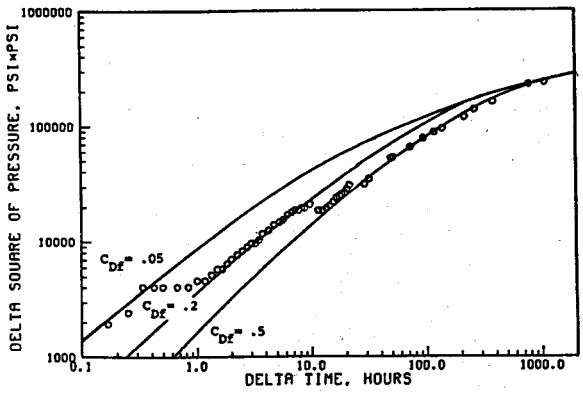

Figure 8 - Baca No. 21 Pressure Buildup Following Flow Test 5. Match With Type Curve for a Vertically-Fractured Well with Wellbore Storage (Finite-Difference Solution). C_{DF}=.05, .02, .5.

Summary

The results of the four pressure buildups discussed plus four other pressure buildup analyses are presented in Table 1. Derivation of an expression for the two-phase compressibility of a Redondo Creek wellbore fluid has been used in the calculation of the theoretical total wellbore storage coefficient. Comparison of this value with the observed wellbore storage coefficient has resulted in qualitative information which has been consistent with the results obtained from alternate methods of analysis. The correctly identified semilog straight lines have been analyzed and sometimes reveal significant reservoir pressure fluctuations which are probably associated with the equilibration of phases in the reservoir following a period of two-phase production.

Nomenclature

A = cross sectional area of the wellbore, ft^2
C = wellbore storage coefficient, ft^3/psi
C_c = specific heat of casing, Btu/lb°F
C_g = specific heat of steam, Btu/lb°F
C_h = specific heat of reservoir, Btu/lb°F
C_L = specific heat of liquid, Btu/lb°F
g ≅ gravitational constant, 32.2 ft/sec^2
g_c = units conversion, 32.2 lb-ft/lbf-sec^2
P = pressure, psia
V = volume, ft^3
V_f = wellbore fractional volume of fluid
V_g = volume of steam in the wellbore, ft^3
V_L = volume of liquid in the wellbore, ft^3

TABLE 1
SUMMARY OF REDONDO CREEK BUILDUP ANALYSES

WELL	TOTAL MASS FLOW RATE lb/hr	PRODUCED STEAM QUALITY OBSERVED WELLHEAD	ASSUMED BOTTOMHOLE	WELLBORE STORAGE COEFFICIENT OBSERVED	CALCULATED	kh md-ft	SKIN
Baca No. 4	161,100	30%	10%	28	25	5200	+10
Baca No. 13	187,200	25%	5%	135	48	6400	+17
Baca No. 15	282,700	34%	14%	167	28	3900	-5.4
Baca No. 19	158,600	20%	0%	1.2	1.1	3500	+1.4
Baca No. 20	56,100[1]	55.6%	35.6%	170	50	1850	-3.1
	46,700[2]	80%	60%	28	30	540	-6.7
Baca No. 21	35,300[3]	95%	85%	400	380	2800	—
	35,300[4]	95%	85%	2240	50		
Baca No. 24	281,300	20%	0%	7.4	2.6	9500	+2.4

1 - Before Stimulation
2 - After Stimulation
3 - First Storage Regime
4 - Second Storage Regime

$V_{2\phi}$ = volume of two-phase mixture in the wellbore, ft^3
β_t = total compressibility, psi^{-1}
β_g = compressibility of steam, psi^{-1}
β_L = compressibility of liquid, psi^{-1}
$\beta_{2\phi}$ = compressibility of two-phase flow, psi^{-1}
ρ = density, lb/ft^3
ρ_c = density of casing, lb/ft^3
ρ_g = density of steam, lb/ft^3
ρ_L = density of liquid, lb/ft^3

References

Atkinson, P.G. (1980), "Geothermal Reservoir Initial State; Baca Location No. 1 - New Mexico; Redondo Creek Field," Transactions Geothermal Resources Council, Vol. 4, pp. 435-438.

Earlougher, R.C., Jr. (1977), "Advances in Well Test Analysis," Monogram Series, Society of Petroleum Engineers of AIME, Vol. 5, pp. 10-13, 147-151.

Garg, S.K., and Pritchett, J.W. (1981), "Pressure Transient Analysis for Hot Water and Two-Phase Geothermal Wells: Some Numerical Results," Topical Report No. DOE/ET/27163-5, prepared by S^3 under Baca Geothermal Demonstration Project, October.

Grant, M.A., and Sorey, M.L. (1979), "The Compressibility and Hydraulic Diffusivity of a Steam Water Flow," Water Resources Research, Vol. 15, pp. 684-686.

Matthews, C.S., and Russell, D.G. (1967), "Pressure Buildup and Flow Tests in Wells," Monogram Series, Society of Petroleum Engineers of AIME, Vol. 1, pp. 97-105.

Ramey, H.J., Jr., and Gringarten, A.C. (1975), "Effect of High-Volume Vertical Fractures on Geothermal Steam Well Behavior," Proceedings of the Second Symposium on the Development and Use of Geothermal Resources, San Francisco, pp. 1759-1762.

Riney, T.D., and Garg, S.K. (1981), "Analysis of Flow Data from Several Baca Wells," Proceedings Seventh Geothermal Reservoir Engineering Workshop, Stanford, pp. 47-52.

Union Oil Company of California and Public Service Company of New Mexico (1978), "Technical and Management Proposal (Vol. II) for Geothermal Demonstration Power Plant," Submitted to DOE in response to program opportunity EG-77-N-03-1717.

Appendix A

Grant and Sorey (1979) obtained a simple formula for the total compressibility of two-phase reservoir which closely approximated the full expression. Expressed in simple engineering units, this formula is:

$$\phi\beta_t = (\rho C_h)(7.52)P^{-1.66},\ psi^{-1} \qquad (A\text{-}1)$$

The volumetric heat capacity of the reservoir, ρC_h, was a function of the rock heat capacity and the water heat capacity. If we consider a wellbore volume which contains volumes $V_f S_g$ of steam, $V_f(1-S_g)$ of water and $1 - V_f$ of casing, the heat capacity and the compressibility of the steam becomes significant. Equation A-1 can then be written as:

$$V_f\beta_t = \left(V_f S_g \rho_g C_g + V_f(1-S_g)\rho_L C_L + (1-V_f)\rho_c C_c\right)(7.52)P^{-1.66} + S_g\beta_g \qquad (A\text{-}2)$$

The contributing volumetric heat capacity of the casing for a typical Redondo Creek wellbore volume is assumed to only be dependent upon the innermost casing string depicted in Figure 1. With this assumption the average casing heat content contribution to the wellbore volume is:

$$\left(\frac{1-V_f}{V_f}\right) \rho_c C_c \cong 8.5 \text{ Btu/ft}^3\text{°F}$$

$$\beta_t = S_g\rho_g C_g + (1-S_g)\rho_L C_L + 8.5(7.52)P^{-1.66} + S_g\beta_g \quad \text{(A-3)}$$

Figure A1 displays the total wellbore compressibility factors obtained from Equation A-3 of a two-phase wellbore fluid as a function of pressure and volumetric fraction of steam. The discrepancy between the steam curve and the $S_g \cong 1.0$ curve is a reflection of the nonadiabatic conditions of the wellbore and the effect of an infitessimal amount of liquid present in the $S_g \cong 1.0$ condition. It is interesting to note that the compressibility increases with increasing liquid saturation in the wellbore. This is due to the increased heat content of the wellbore. An identical pressure change (and temperature change) will have a larger energy change and hence a larger mass will change phases in a high heat content system. The large associated volumetric change is the reason that a two-phase reservoir (high heat content) has a higher compressibility than a two-phase wellbore.

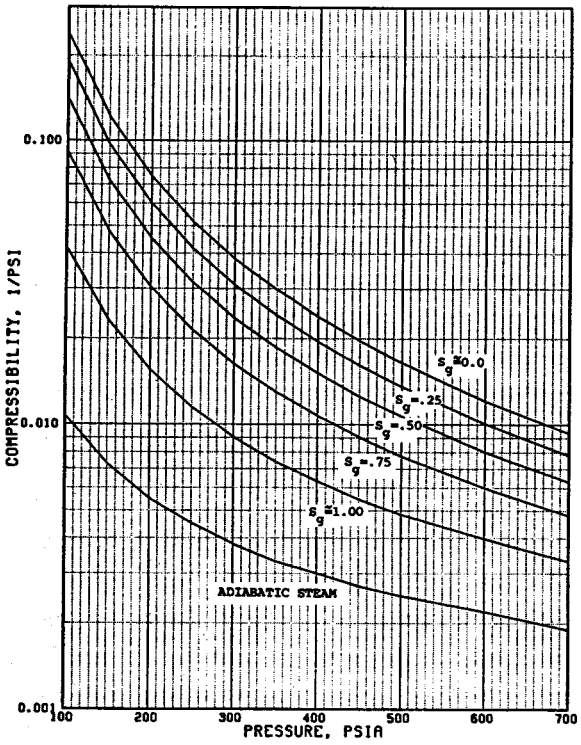

Figure A1 - Compressibility of a Two-Phase Wellbore Fluid; as a Function of Pressure and the Volumetric Fraction of Steam.

Appendix B

The wellbore storage (after-production) of a well is controlled by two effects: 1) the storage that results from the vertical movement of a gas-liquid interface and 2) the storage which results from the compression or expansion of the wellbore fluids (Earlougher, 1977). The wellbore storage coefficient is algebraically defined as:

$$C = \left(\frac{\Delta V}{\Delta P}\right)_{\text{Datum}} \quad \text{(B-1)}$$

Consider first the change in datum pressure due to water movement across the datum, ΔV_L. This volume will create a change in liquid interface elevation, $\Delta V_L/A$, which due to the hydrostatic gradient differences increases the datum pressure by:

$$\Delta P_1 = \frac{\Delta V_L}{A}\frac{(\rho_L - \rho_g)}{144}\frac{g}{g_c} \quad \text{(B-2)}$$

Next consider the pressure change due to the compressibility of the wellbore fluids. The effective wellbore volume change created by the total production of fluids, ΔV, compresses the wellbore fluids. The total compressibility of each phase times that phase's wellbore volume results in:

$$\Delta P_2 = \frac{\Delta V}{V_g\beta_g + V_L\beta_L + V_{2\phi}\beta_{2\phi}} \quad \text{(B-3)}$$

The total wellbore storage will be dependent upon the total pressure change, $\Delta P_1 + \Delta P_2$.

$$C = \frac{\Delta V}{\Delta P_1 + \Delta P_2}_{\text{Datum}} =$$

$$\frac{\Delta V}{\frac{\Delta V_L}{A}\frac{(\rho_L-\rho_g)}{144}\frac{g}{g_c} + \frac{\Delta V}{V_g\beta_g + V_L\beta_L + V_{2\phi}\beta_{2\phi}}}$$

or

$$C = \frac{1}{\frac{\Delta V_L}{\Delta V}\frac{(\rho_L-\rho_g)}{144\,A}\frac{g}{g_c} + \frac{1}{V_g\beta_g + V_L\beta_L + V_{2\phi}\beta_{2\phi}}} \quad \text{(B-4)}$$

Equation B-4 simplifies to the equations presented by Earlougher (1977) for a well with single-phase (liquid) production. If there is a water-gas interface:

$$C = \frac{A}{\frac{(\rho_L-\rho_g)}{144}\frac{g}{g_c}} \quad \text{if} \quad \frac{\rho_L-\rho_g}{144\,A} >> \frac{1}{V_g\beta_g + V_L\beta_L + V_{2\phi}\beta_{2\phi}}$$

and for a wellbore completely filled with a single-phase fluid:

$$C = V\beta$$

Proceedings Eighth Workshop Geothermal Reservoir Engineering
Stanford University, Stanford, California, December 1982
SGP-TR-60

EVALUATION OF INJECTION TEST DATA FROM A BACA WELL

T. D. Riney and S. K. Garg

S-CUBED
P. O. Box 1620
La Jolla, California 92038

ABSTRACT

Injection test data from Baca well B-20 show that half of the fluid enters a fractured zone below ~ 5000 ft whereas the primary production zone is at ~ 4000 ft. The fracture created during the subsequent stimulation of B-20 apparently intersects the lower fluid-accepting zone rather than a production zone. Fracture stimulation must provide a channel to a productive region of the natural fracture system to be effective.

INTRODUCTION

Non-productive wells in the Redondo Creek area of the Baca Geothermal Field have been used as injection wells. The ability of these wells to accept high injection rates implies that a well may penetrate a permeable zone which is a fluid acceptor but not a fluid producer. Interpretation of flow data from injection tests on wells in the Redondo Creek area, or other fractured geothermal systems, must consider this possibility.

As part of its evaluation of the geothermal reservoir in the Redondo Creek area, Union Oil Company performed both production and injection tests on several individual wells. S-CUBED independently analyzed available well test data under a contract funded by the U. S. Department of Energy. An earlier paper (Riney and Garg [1982]), described an analysis of the pressure build-up data for well B-20 subsequent to a 104-day production test (Flow Test No. 4). Data from an injection test performed on B-20 are analyzed here and the results compared with the results of the analysis of the production test data. This well is also one of two Baca wells (B-20 and B-23) which were hydraulically fractured by Republic Geothermal, Inc. The fracture stimulation of B-20 is discussed in view of the production and injection test analyses.

BACKGROUND

Well B-20 was drilled during the period June 26 - August 30, 1980 from ground level elevation (9065 ASL) to a total measured depth of 6374 ft (3026 ASL). Drilling terminated when 547 ft of tools stuck in the hole with the top of the fish located at 5827 ft. The well was completed with the bottom of a blank 9-5/8" casing set at 2505 ft; a 7" blank and perforated liner was hung from 2390 ft to 5812 ft.

The pressure and temperature profiles recorded above the fish before and after a 104-day production test indicated that production was primarily from a permeable zone located at ~ 4000 ft (Riney and Garg [1982]). The reservoir pressure and temperature in this zone were estimated to be P_o ~ 975 psig (p(a) = 67.9 bars) and T_o ~ 488°F (253°C), respectively. A second permeable zone located towards wellbottom was tentatively identified but production from this zone was minor. The values of the pressure and temperature estimated from recordings above the fish (at depth 5750 ft) are considered representative of the reservoir values in the lower permeable zone, i.e., P_o = 1443 psig (p(a) = 100.2 bars) and T_o = 549°F (287°C).

A CO_2 mass fraction of α_o = 0.0147 has been measured in the discharge fluid from well B-20. This is the high end of the range of values measured for the Redondo Creek wells. If we assume that the CO_2 content in the primary production zone is the measured value, then the initial thermodynamic state of the upper permeable zone may be determined from the equation-of-state for CO_2/water mixtures (Pritchett, et al. [1982]). The estimated condition (P_o = 67.9 bars, T_o = 253°C, α_o = 0.0147) implies that the permeable zone at 4000 ft is initially two-phase with an in situ gas saturation of S_g = 0.08. The initial condition of the lower permeable zone, represented by values at 5750 ft (P_o = 100.2 bars, T_o = 287°C, α_o = 0.0147), implies that the fluid there is single-phase liquid.

INJECTION TEST ANALYSIS (BEFORE STIMULATION)

Injection Test No. 1 was performed on B-20 during July, 1981. During the 129 hour injection period a cumulative volume of 1,793,000 gallons of water at 158-175°F was accepted at the wellhead under vacuum.

Spinner surveys and pressure/temperature surveys were run during injection; pressure/temperature surveys were also recorded downhole changes after injection stopped.

The spinner surveys indicate that approximately 20 percent of the injected fluid is lost into the formation just below the casing in the interval 2500–3000 ft, approximately 30 percent in the interval 4000–5000 ft, and approximately 50 percent below the bottom of the perforated liner located at 5812 ft. Figure 1 shows downhole temperature surveys made before, during and after the injection period. The depressed temperatures below 4500 ft apparently result from the penetration of the cold injection fluid into the formation at these depths.

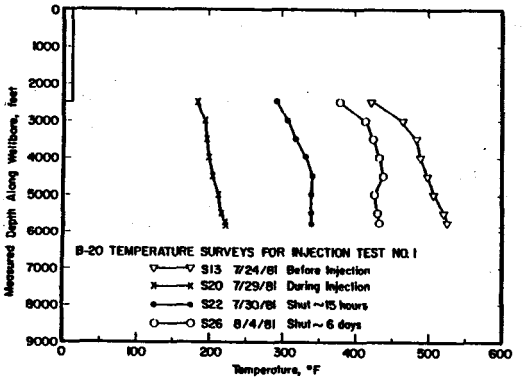

Figure 1. Temperature surveys for Injection Test No. 1.

It is noteworthy that the primary production zone at 4000 ft does not accept a significant portion of the injected fluid. Comparison of pressure profiles S13 and S20 (Figure 2) provides a partial explanation; the overpressure (pressure above reservoir pressure) during injection increases with depth.

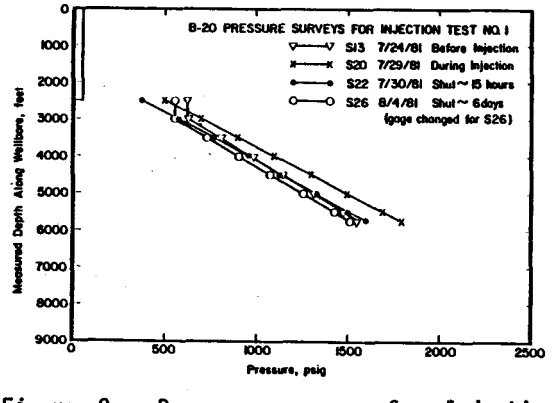

Figure 2. Pressure surveys for Injection Test No. 1.

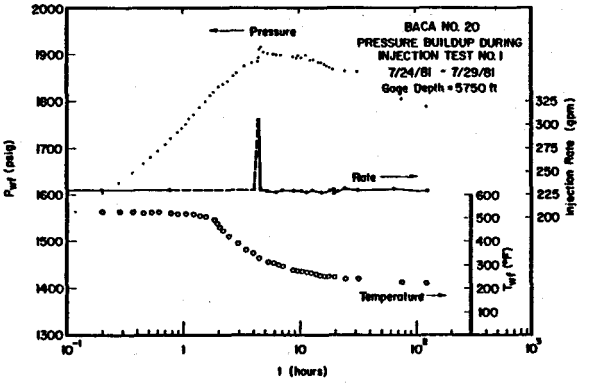

Figure 3. Bottomhole pressure and temperature and surface injection rate during Injection Test No. 1. Here t is time since injection started.

Figure 3 shows a semi-log plot of the pressure buildup and temperature data recorded by Union at a depth of 5750 ft during the injection period. The surface volumetric injection rate is also shown. A log-log plot of the pressure buildup data is given in Figure 4. The approximation of the data to the 1/2-slope line in this type curve indicates that the bulk of the injected fluid is entering a fracture. The fracture accepting the flow is towards wellbottom below the primary production zone. Both the injected fluid and the reservoir fluid are single-phase liquid at these depths; there is a nearly constant hydraulic head between the gage depth and the accepting horizon. Analysis of the pressure buildup data is complicated by the presence of the fracture flow and the temperature differences between the injected and reservoir fluids.

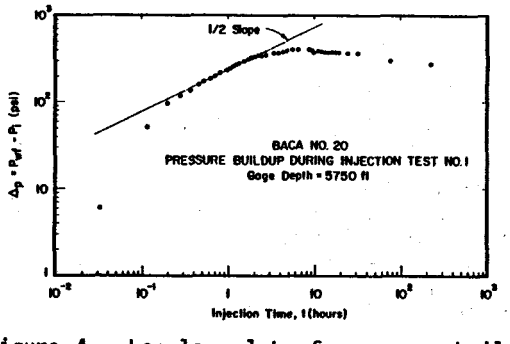

Figure 4. Log-log plot of pressure buildup during Injection Test No. 1. Here P_i = 1509 psig.

Except for the isolated spike in the injection rate at t = 4.5 hours, the surface volumetric injection rate is essentially constant. The downhole temperature of the

injected fluid starts to decrease rapidly at t ~ 2 hours from its initial value of ~ 520°F (271°C) to ~ 240°F (116°C). During the transition period the corresponding kinematic viscosity of the downhole injected fluid increases from $\nu \sim 1.3 \times 10^{-7}$ m^2/s to $\nu \sim 2.6 \times 10^{-7}$ m^2/s. Theoretical calculations by Pritchett and Garg [1980] have shown that the downhole viscosity of the injected fluid should be used when interpreting pressure buildup data.

The duration of the fit of the data to the 1/2-slope line in Figure 4 implies that pseudo-radial flow is not attained until the injection has been underway for at least t = 2 hours. The usual Horner methods of interpretation of the buildup data also fails in the temperature transition period (2 < t < 10 hours) because of the variation in the kinematic viscosity of the injected fluid. The reason for the rapid decrease in the downhole pressure required to sustain the injection rate at late times (t > 10 hours) is not known. Possible mechanisms include opening new injection fractures or increased mobility of the fluid in a two-phase entry (e.g., at 4000 ft) as the cold injection fluid decreases the steam saturation present earlier.

A log-log plot of the pressure falloff data recorded at 5750 ft is shown in Figure 5. The data are approximated by a 1/2-slope line for falloff at $\Delta t < 1$ hour subsequent to termination of injection. Figure 6 shows a Horner plot of the pressure falloff data; the temperatures recorded at depth 5750 ft are also shown.

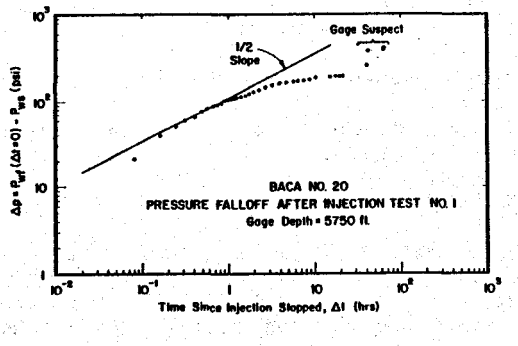

Figure 5. Log-log plot of pressure falloff subsequent to Injection Test No. 1. Here $P_{wf}(\Delta t = 0) = 1783$ psig.

The straight line of slope m = 68 psi/cycle (4.70×10^5 Pa/cycle) approximates data points at dimensionless times $(t + \Delta t)/\Delta t < 40$, corresponding to falloff times of $\Delta t > 3.3$ hours. The flow is assumed to be pseudo-radial at this point in time; the slope m can be used to estimate the kinematic mobility-thickness product for well B-20.

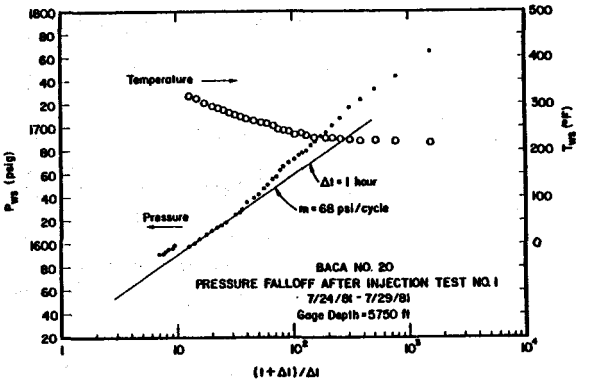

Figure 6. Pressure falloff and downhole temperature subsequent to Injection Test No. 1. Here the injection time is t = 129 hours.

The average mass rate corresponding to the injection of 1,793,000 gallons (6770 m^3) during the injection period of t = 129 hours is

$$\dot{M} = \frac{6770\ (975)}{129\ (3600)} = 14.2 \text{ kg/sec}$$

The kinematic mobility-thickness product is given by

$$\frac{kh}{\nu} = \frac{1.15\ \dot{M}}{2\pi m} = \frac{1.15\ (14.2)}{2\pi\ (4.7 \times 10^5)} = 5.53 \times 10^{-6} \text{ ms}$$

The theoretical calculations presented by Garg and Pritchett [1980] show that the kinematic viscosity of the reservoir fluid should be used when interpreting falloff data subsequent to reinjection. Since most of the injected fluid is assumed to enter the formation towards wellbottom, with representative initial reservoir conditions (287°C, 100.2 bars), the appropriate value is $\nu \sim 1.3 \times 10^{-7}$ m^2/s. The estimated formation kh product during falloff is

$$kh = (1.3 \times 10^{-7})\ (5.53 \times 10^{-6})$$

$$= 7.19 \times 10^{-13}\ m^2 = 2400 \text{ md-ft}$$

Although this value is of the same order of magnitude as the value kh = 3030 md-ft estimated from Flow Test No. 4 production data, comparison should be made with reservations. During production the flow is two-phase from a permeable zone at 4000 ft; during injection this zone accepts only a fraction of the injected liquid.

ANALYSIS OF DOWNHOLE DATA (AFTER STIMULATION)

During reworking well B-20 in preparation for fracture stimulation the 7" slotted liner was pulled, lost circulation zones plugged back to 3520 ft and then a 7" blank liner was cemented in place with the shoe at 4880 ft. Since the stimulation interval was designed to be from 4880 ft to 5120 ft, a sand plug was placed from the top of the fish at 5827 ft to 5400 ft and then capped with cement to 5120 ft (Morris and Bunyak [1981]).

Figure 7 presents temperature profiles recorded subsequent to the recompletion of B-20. Survey RGI, recorded by Republic Geothermal, Inc. just prior to the fracture stimulation, shows three zones that apparently accepted the cold workover fluids during recompletion; the zone at 4000 ft which was the primary production zone during Flow Test No. 4 prior to recompletion; the

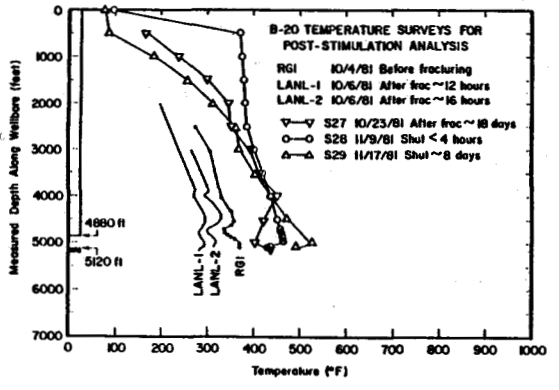

Figure 7. Temperature profiles before and after stimulation.

interval 4000-5000 ft which accepted approximately 30 percent of the injected fluid during Injection Test No. 1 prior to recompletion; a zone of less than 100 ft in height near the bottom of the open interval just above the top cement cap at 5120 ft.

The 240-foot interval (4880 ft - 5120 ft) stimulated was non-productive prior to fracture treatment, although there was a small rate of fluid loss during the well recompletion operation (Morris and Bunyak [1981]). This suggests that at least one lost circulation zone existed in the recompleted wellbore.

During the fracture treatment (October 5, 1981) approximately 9000 bbl of cold fluid was injected into the well. The first of several temperature surveys was made approximately 12 hours after the fracture stimulation. Surveys LANL-1 and LANL-2, shown in Figure 7, exhibit depressed temperatures at the same three zones as in survey RGI recorded prior to stimulation. The depression of the temperature near the bottom of the open interval, however, appears more pronounced.

The first post-stimulation temperature profile recorded by Union (S27) was eighteen days after the stimulation; the low temperature recorded at 5000 ft is noteworthy. Thereafter, a 14-day (October 26 - November 9, 1981) flow test (Flow Test No. 5) was performed to determine the wells productive capacity. Survey S28 was recorded by lowering the gage down the well immediately after shutin; the near-surface measurements were made several hours before the near-bottomhole measurements. The most noteworthy feature is the depressed temperature at the 5000 ft horizon. The survey taken 8-days after shutin (S29) verifies this characteristic which is attributed to cooling which accompanies the in-formation flashing of the fluid during Flow Test No. 5. The depressed temperatures presented earlier at the injection zones for the workover and injection fluids have disappeared.

In summary, the primary production zone in the stimulated well is at the center of the open interval, i.e., at 5000 ft. The initial reservoir temperature and pressure at this depth are estimated from S13 to be T_o = 507°F (264°C) and P_o = 1313 psig (p(a) = 91.2 bars). If we assume a CO_2 content of α = 0.0147, then the reservoir fluid would be initially single-phase but flash within the formation during Flow Test No. 5.

During the 14-day drawdown period of Flow Test No. 5, B-20 produced ~ 110,000 lbm/hr total mass flow initially, but declined rapidly to a final stabilized rate of ~50,000 lbm/hr (WHP = 25 psig). The steam fraction, based on mini-separator data, increased from ~50 percent to ~86 percent during drawdown. Since the well could not produce at commercial line pressures, build-up data sufficient for formation analysis were not obtained.

CONCLUSIONS

The stimulated zone (4880-5120 ft) was located in a region which was naturally fractured. Our analysis of the pre-stimulation production data (Flow Test No. 4) and injection data (Injection Test No. 1) indicates that the natural fractures at this depth were good acceptors but poor producers. The induced fracture apparently intersected the existing fractures but the inherent non-producibility of the natural fracture system remained.

ACKNOWLEDGEMENT

This work was performed under contract 4514510 with the Lawrence Berkeley Laboratory as part of the evaluation of the Baca reservoir conducted under a cooperative agreement between Union Oil Company and the U. S. Department of Energy.

REFERENCES

Garg, S. K. and J. W. Pritchett (1980), "Pressure Transient Analysis for Hot Water and Two-Phase Geothermal Wells: Some Numerical Results," Topical Report No. DOE/ET/27163-5, Prepared by S-CUBED under Baca Geothermal Demonstration Project, October.

Morris, C. W. and M. J. Bunyak (1981), "Fracture Stimulation Experiments at the Baca Project Area," Proceedings of Seventh Annual Workshop on Geothermal Reservoir Engineering, Stanford University, December 15-17.

Pritchett, J. W., M. H. Rice and T. D. Riney (1980), "Equation-of-State for Water-Carbon Dioxide Mixtures: Implications for Baca Reservoir," Topical Report No. DOE/ET/27163-8, Prepared by S-CUBED Under Baca Geothermal Demonstration Project, October.

Riney, T. D. and S. K. Garg (1981), "Analysis of Flow Data from Several Baca Wells," Proceedings Seventh Workshop on Geothermal Reservoir Engineering, Stanford University, December.

Proceedings Eighth Workshop Geothermal Reservoir Engineering
Stanford University, Stanford, California, December 1982
SGP-TR-60

Interpretation of Nonisothermal Step-Rate Injection Tests

Sally Benson
Earth Sciences Division
Lawrence Berkeley Laboratory
University of California
Berkeley, California 94720

INTRODUCTION

Injection tests are a common method of obtaining well and reservoir data in geothermal wells. Invariably the temperature of the injected fluid is different than that of the reservoir fluid. Because of the strong temperature dependence of fluid viscosity, and to a lesser extent, fluid density; nonisothermal related pressure transients must be considered to correctly interpret the data. Recent studies of single rate nonisothermal injection have shown that the pressure transients can be classified by one of two cases: 1) a moving thermal front dominated problem or 2) a composite reservoir problem. Analysis methods to determine the permeability thickness of a reservoir and the skin factor have been developed for both of these cases by Benson and Bodvarsson[1]. This paper discusses the extension of these methods to step-rate injection tests and proposes a new method for tracking thermal fronts in injection wells.

BACKGROUND

Several authors have discussed the interpretation of pressure transients during cold water injection into hot reservoirs. In particular, Bodvarsson and Tsang[2] and Mangold et al[3] demonstrated the behavior of nonisothermal pressure transients in geothermal reservoirs and illustrated the effect of the temperature dependent fluid properties, viscosity and density. Tsang and Tsang[4] developed a semi-analytic solution for pressure transients during moving front dominated injection tests. O'Sullivan and Pruess[5], and Garg[6] discussed the analysis of injection and falloff tests in two-phase geothermal reservoirs. These studies demonstrated that the pressure transients during injection tests can be used to determine the permeability thickness of the reservoir. Horne and Satman[7] proposed a method for estimating the distance to the thermal front from injection tests in two-phase reservoirs. The study by Benson and Bodvarsson[1] developed methods for calculating the skin factor from nonisothermal injection tests and discussed the conditions under which the pressure transients behaved like a composite reservoir or moving front dominated problem. The present study is an extension of this work.

SINGLE RATE ANALYSIS

The following analysis methods are applicable to a reservoir which is:

1) of uniform and constant porosity, compressibility, permeability, heat capacity and thermal conductivity;

2) horizontal, infinite, of constant thickness and bounded above and below by impermeable rock;

3) completely filled with slightly compressible liquid water; and

4) fully penetrated by a finite radius wellbore.

Under these conditions, single rate pressure transients are described by one of two cases; 1) a moving front dominated or 2) composite reservoir behavior. This is illustrated in Figure 1, where the pressure transients during 100°C injection into a 250°C reservoir are shown for four cases; injection into a hot reservoir and injection into a hot reservoir with pre-existing 1, 5 and 10 m cold spots.

Moving Front Dominated Problem

For injection with no pre-existing cold spot, pressure transients are initially identical to those of the hot (250°C) reservoir. After a period of time defined by

$$t_{oc} \approx \frac{\pi H r_w^2 e^{-2s}}{Q_c} ; \qquad (1)$$

the pressure data fall on a new curve that has a slope corresponding to the properties of the injected fluid. Pressure transient data that are controlled by a moving thermal front can be analyzed by the following procedure. The permeability-thickness is calculated:

$$kH = 0.183 \frac{q\mu_c}{\rho_c m_c} ; \qquad (2)$$

where m_c is the slope of the straight line on the P vs. log t plot that corresponds to the properties of the injected fluid. To determine P_{1s}, extrapolate m_c to 1 second. P_{1s} is then corrected to account for the offset between the isothermal and nonisothermal curves by

$$P^*_{1s} = P_{1s} + \Delta P_o \; ; \qquad (3)$$

where

$$\Delta P_o = \frac{q}{2\pi kH}\left[\frac{\mu_c}{\rho_c} P_D(t_{Doc})_c - \frac{\mu_h}{\rho_h} P_D(t_{Doc})_h\right] ; \qquad (4)$$

and

$$t_{Doc} = \frac{\pi H \rho_h}{q} \frac{k}{\phi \mu \beta_t} . \qquad (5)$$

The skin factor is then calculated

$$s = 1.151\left(\frac{P^*_{1s} - P_i}{m_c} - \log \frac{k}{\phi \mu_c \beta_t r_w^2} - .351\right) . \qquad (6)$$

Note that if P_{1s} is not corrected to account for the offset between the isothermal and non-isothermal pressure transients, the skin factor will be underestimated.

Composite Reservoir Behavior

The three other curves in Figure 1 are the pressure transients in response to injection with pre-existing cold spots of 1, 5, and 10 m radii. For each case, the data are initially identical to isothermal 100°C injection. When

$$t_{oh} > \frac{\phi \mu_c \beta_t}{4k} r_c^2 \qquad (7)$$

the data changes to a new slope that corresponds to the reservoir fluid properties. This two-slope behavior is referred to as the composite reservoir problem. At even longer times the data again change slope and become identical to the moving front-dominated problem, this last transition occurs at

$$t'_{oc} \approx \frac{\rho_w c_w}{\rho_a c_a} \frac{\pi H r_c^2}{Q_c} . \qquad (8)$$

Care must be taken in the analysis of pressure data near this region because the transition begins 1/4-log cycle before this point and lasts for 1/2-log cycle after it. Data from the final slope are analyzed according to the moving-front procedure.

Pressure fall-off data (when the well is completely shut in) are always analyzed with a composite reservoir model because once the well is shut in, the thermal front moves forward at a negligible rate.

The permeability-thickness of the reservoir and the skin factor can be evaluated by the following procedure. The permeability-thickness is calculated

$$kH = .183 \frac{q\mu_h}{\rho_h m_h} ; \qquad (9)$$

where m_h is the slope on the P vs. log t plot which corresponds to the properties of the reservoir fluid. P_{1s} is determined by extrapolating m_h to 1 second and correcting to account for the effect of the cold spot around the well:

$$P^*_{1s} = P_{1s} \pm .87 m_h s_c ; \quad \begin{matrix}(+ \text{ fall-off,} \\ - \text{ injection})\end{matrix} \qquad (10)$$

where

$$s_c = \left(\frac{\mu_c}{\mu_h}\frac{\rho_h}{\rho_c} - 1\right) \ln\left(\frac{r_c}{r_w}\right) . \qquad (11)$$

The skin factor for the well is calculated by:

$$s = 1.151\left(\frac{\mu_h \rho_c}{\mu_c \rho_h}\right)\left[\frac{P^*_{1s} - P_{i \text{ or } wf}}{m_h} - \log\left(\frac{k}{\phi \mu_h \beta_t r_w^2}\right) - .351\right] . \qquad (12)$$

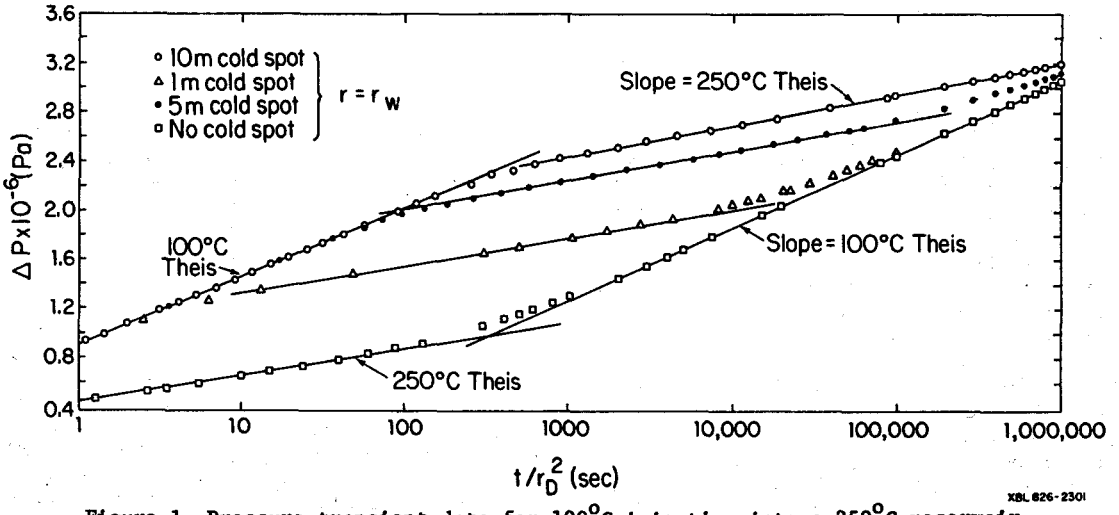

Figure 1. Pressure transient data for 100°C injection into a 250°C reservoir.

Relative to the hot reservoir, the effective skin factor is increased by a factor of $\mu_c\rho_h/\mu_h\rho_c$. If the skin value is calculated without considering the effect of the cold spot around the well, the skin factor will be grossly overestimated.

STEP RATE INJECTION TESTS

Typically, injection tests are not conducted at a single flow rate, but instead, conducted in a series of step rates followed or preceded by a complete shut in. Therefore, it is important to determine if the methods developed for single-rate tests can be adapted for the interpretation of step rate tests.

Approach

The computer code, PT, was used to simulate pressure transients during nonisothermal step-rate tests. PT employs the integrated finite-difference method to discretize the medium and formulate the mass and energy transport equations in a liquid-saturated porous medium[8,9]. The simulator allows both temperature and pressure-dependent fluid properties. These properties are computed internally to within 1% of their true values. A single-layer radial mesh with a realistic wellbore radius of 0.1 m radius was used. To accurately model the temperature changes during injection, very fine elements were used close to the well. Farther away, the spacing increased logarithmically. The outer boundary of the mesh was sufficiently distant to avoid any affect on the pressure transient data.

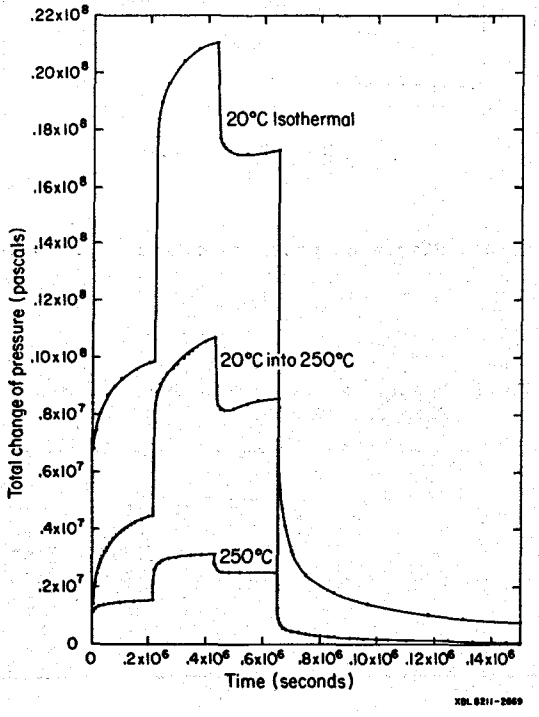

Fig. 2. Simulated pressure data from a step test with 20°C injection into a 250°C reservoir. Also shown are the simulated pressure data for isothermal 20°C and 250°C injection.

Simulated pressure data were then plotted in terms of

$$P \text{ vs. } \sum_{i=1}^{n} \frac{q_i}{q_n} \log \frac{t_i + \cdots + t_n + \Delta t}{t_{i+1} + \cdots + t_n + \Delta t}; \quad (14)$$

in accordance with conventional multirate theory[10]. From this plot, the permeability thickness can be calculated:

$$kH = .183 \frac{q_n \mu}{\rho m}; \quad (15)$$

where the appropriate μ, ρ and m are determined by procedures discussed in the following sections. For the moving front problem the skin factor is determined by

$$s = 1.151 \left[\left(\frac{q_n}{q_n - q_{n-1}} \right) \frac{P^*_{1s} - P_{wf}}{m_c} - \log \frac{k}{\phi \mu_c \beta_t r_w^2} - .351 \right]; \quad (16)$$

and for the composite reservoir problem:

$$s = 1.151 \frac{\mu_c \rho_h}{\mu_h \rho_c} \left[\left(\frac{q_n}{q_n - q_{n-1}} \right) \frac{P^*_{1s} - P_{wf}}{m_h} - \log \frac{k}{\phi \mu_h \beta_t r_w^2} - .351 \right]. \quad (17)$$

EXAMPLE

The following test was simulated to illustrate the key aspects of nonisothermal step rate injection tests. Three six-hour steps with injection rates of 0.1 kg/s/m, 0.2 kg/s/m and .15 kg/s/m of 20°C fluid into a 250°C reservoir were followed by a complete shut in. Table 1 summarizes the properties of the reservoir used for the simulation. The simulated pressure data are shown in Figure 2. For comparison, isothermal 20°C and 250°C injection are also plotted. Note that the magnitude of the non-isothermal pressure changes are intermediate between the two isothermal cases. For the first three steps, the shape of the curves are similar to the 20°C case, however, the fall-off data, except for the first few minutes, are identical to the 250°C case.

Pressure Transient Analysis

Step 1, a typical moving-front-dominated problem, is shown in Figure 3. Initially, the data are identical to the 250°C isothermal pressure transients (also shown in Figure 3). At approximately 300 seconds, the data depart from the initial curve and fall on a new slope which corresponds to the properties of the injected fluid. The data from 300 seconds to six hours can be analyzed to determine the permeability-thickness of the reservoir from Eq. 2 and the

skin factor from Eq. 6. Values of kH = 10^{-14} m^3 and s = 0.04 are calculated; both are in excellent agreement with the input values of 10^{-14} m^3 and 0.0, respectively. If P_{1s} is not corrected to account for the offset between the isothermal and nonisothermal curves, a skin value of -3.5 is calculated.

Step 2, shown in Figure 4, first displays the composite reservoir behavior and then, the moving front-dominated behavior. The early transients are governed by the 0.64 m cold spot generated by Step 1. At approximately 4 s the pressure data changes to a slope which corresponds to the properties of the reservoir fluid. At approximately 1.1 hours the data depart from the second slope and the moving thermal front controls the pressure response. The transition times are in good agreement with those calculated from Eq. 7 and Eq. 8, $t_{oh} \approx 3$ s and $t'_{oc} \approx$ 1.2 hours, respectively. It is apparent that superposition is an appropriate manner in which to treat this problem and that the equations developed for single-rate tests are valid if the effect of the growing cold spot is taken into consideration.

Data from step 2 may be difficult to analyze because wellbore storage may mask most of the data from the first and second slope. Also, the third slope will be clearly defined for less than one-half of a log cycle. If however, the second slope is apparent, the permeability thickness can be evaluated by Eq. 15 and the skin factor evaluated by Eq. 17. Values of 10^{-14} m^3 and -0.2 are obtained; these are in good agreement with the input values. The slight negative skin is calculated as a result of the approximation

$$r_c^2 \approx r_{tf}^2 = \frac{\rho_w c_w}{\rho_a c_a} \frac{Q}{\pi H} . \qquad (18)$$

An apparent skin value, the skin factor relative to the hot reservoir can be calculated:

$$s_a = 1.151 \left[\left(\frac{q_n}{q_n - q_{n-1}} \right) \frac{P_{1s} - P_{wf}}{m_h} - \log \frac{k}{\phi \mu_h \beta_t r_w^2} - .351 \right] . \qquad (19)$$

For step 2, the apparent skin factor is 14 (compared to a true skin value of 0.0), indicating that the cold spot around the well contributes a significant component to the pressure buildup.

Step 3 begins at 12 hours into the test. By this time the thermal front has advanced 1.75 m into the formation. Equation 7 indicates that the reservoir will behave as a composite system until 11.4 hours after the rate change. Therefore, the entire 6-hour step will only reflect the composite reservoir behavior. This is clearly shown in Figure 5 where only two slopes are apparent, the first corresponding to the fluid properties of the cold spot and the second, to the reservoir fluid. The second slope can be used in conjunction with Eq. 15 to calculate the permeability-thickness of the reservoir. The skin factor, calculated from Eq. 17, is equal to -0.04. The apparent skin factor, calculated from Eq. 19, is 18.9.

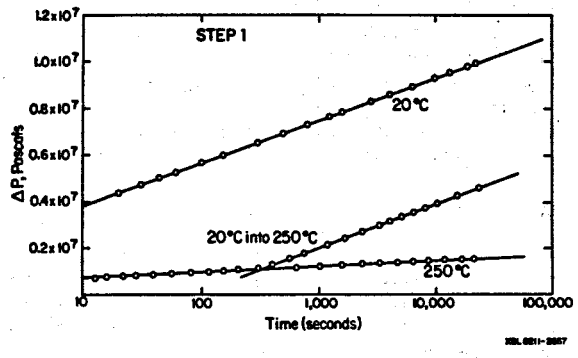

Fig. 3. Pressure vs. log t plot for step 1.

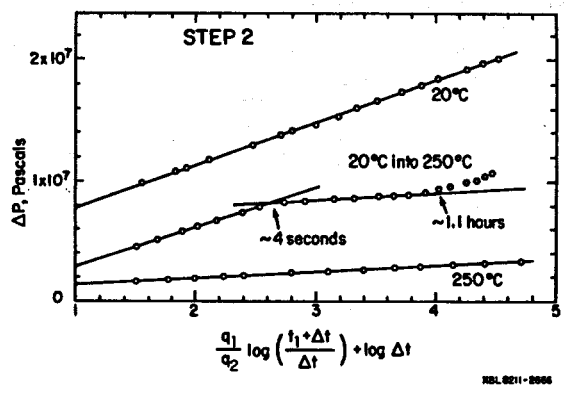

Fig. 4. Simulated pressure data from step 2.

Table 1 Reservoir Properties Used for Step Rate Simulation.

k	1.0 x 10^{-14} m^2
H	1.0 m
ϕ	0.2
c_r	1000.0 J/kg·°C
ρ_r	2200.0 kg/m^3
λ	2.0 J/m·°C·s
r_w	0.1 m
β_t	1.0 x 10^{-9} Pa^{-1}

Fall-off

The pressure falloff data following the step test are plotted in Figure 6. As expected, the data initially follow a slope corresponding to the properties of the cold spot and then become identical to the pressure fall-off data for 250°C isothermal injection. The data after 35 s can be used to calculate a kH of 10^{-14} m^3 and a skin value (from Eq. 17) of -0.2. The apparent skin factor (from Eq. 19) is 19.8.

Injectivity

It is interesting to note that the well injectivity, shown in Figure 7, is of little value for the inference of downhole well productivity. This results from the lack of an obvious relationship between the nonisothermal injectivity (middle curve) and the two isothermal cases (from which, theoretically, productivity could be inferred).

DISCUSSION

The previous analysis demonstrated the pressure transient response to nonisothermal step-rate tests. In the early steps, both the moving front-dominated and composite reservoir behavior were observed. During the last two steps, the pressure transient behaved like a composite reservoir. It is of importance to note that in this example the transmisivity (kH/μ) varied by a factor of ten during the step test, creating an apparent increase in the permeability-thickness, if misinterpreted.

It is possible to calculate the correct permeability-thickness of the formation from the pressure transient data if the fluid properties to which the slope corresponds can be determined. This can be determined by evaluating Eqs. 7 and 8. True skin factors can also be calculated from Eqs. 16 or 17. However, once the reservoir behaves as a composite system, it is important to have a reasonable estimate of the reservoir thickness and injection history from which the distance to the thermal front can be estimated. If these are not well known, it is not possible to calculate the skin factor with Eq. 17. On the other hand, it is possible to calculate the apparent skin factor from Eq. 19. Also, recall that the apparent skin factor increased from 14 to nearly 20 over the 18-hour step test discussed in the previous section. Since the apparent skin factor of the well is only a function of the true skin, the size of the cold spot and the contrast between the properties of the injected and in-situ fluid, and, if we assume that the true skin factor of the well does not change over the test period, then the growth in the apparent skin factor is a reflection of the growth of the cold spot. This relationship can be used as the basis of a procedure for estimating the true skin factor and size of the cold spot.

If the radius of the cold spot is less than 100 x r_w, then the cold spot around the well can be treated as the thermal skin where

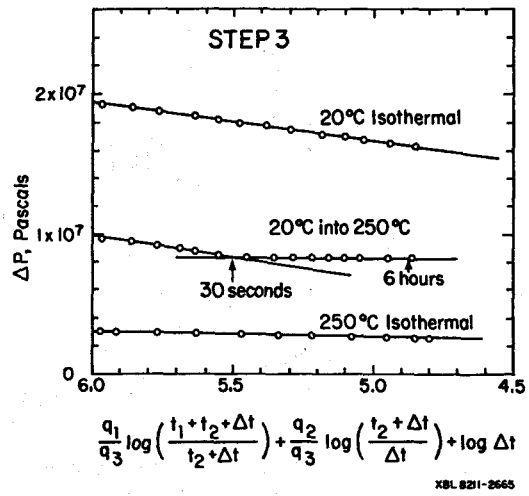

Fig. 5. Simulated pressure data from step 3.

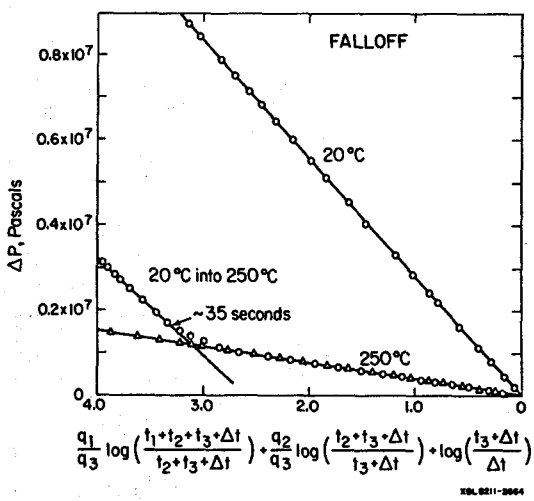

Fig. 6. Simulated pressure data from step 4 (falloff).

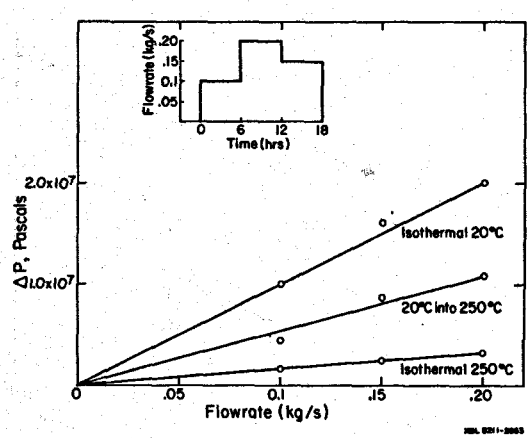

Fig. 7. Injectivity data from the simulated step test.

$$s_c = \left(\frac{\mu_c \rho_h}{\mu_h \rho_c} - 1\right) \ln\left(\frac{r_c}{r_w}\right); \quad (20)$$

as the cold spot grows, so does s_c. The size of the cold spot can be calculated from

$$r_c \approx r_{tf} = \sqrt{\frac{\rho_w c_w}{\rho_a c_a} \frac{C}{\pi H}}. \quad (21)$$

If this is substituted into Eq. 20, we find that

$$s_c = 1.151\left(\frac{\mu_c \rho_h}{\mu_h \rho_c} - 1\right)\left[\log C + \log \frac{\rho_w c_w}{\rho_a c_a} \frac{1}{\pi H r_w^2}\right]. \quad (22)$$

Therefore, on a plot of s_a vs. log C, the points should fall on a single straight line with a slope of

$$n = 1.151\left(\frac{\mu_c \rho_h}{\mu_h \rho_c} - 1\right). \quad (23)$$

Extrapolating n to a cumulative injection of $\pi r_w^2 H$, the point at which no cold fluid has been injected into the formation, s_{aw} can be evaluated. Recalling Eq. 12, one can determine that

$$s = s_{aw} \frac{\mu_h \rho_c}{\mu_c \rho_h}. \quad (24)$$

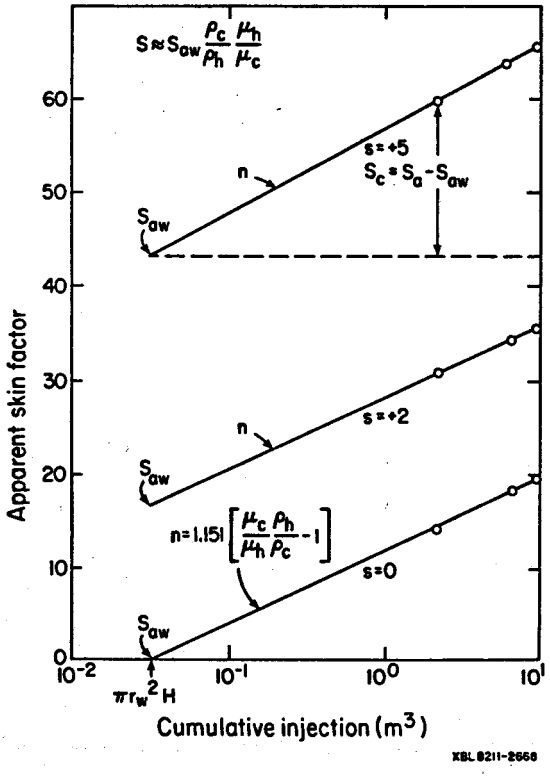

Fig. 8. Apparent skin vs. log C for three skin values, 0,2 and 5.

Knowing s_{aw}, the thermal skin effect s_c can be calculated

$$s_c = s_a - s_{aw}; \quad (25)$$

and the distance to the cold spot can be calculated

$$r_c = r_w e^{\left(\frac{1.151\, s_c}{n}\right)}. \quad (26)$$

The apparent skin factors calculated for the step-rate test discussed in the previous section are plotted in Figure 8, as a function of the cumulative injection. Also plotted, are data from similar step tests where the true skin values of the well are 2 and 5 respectively. Note that the slope of the line is identical in each case and is equal to $1.151(\mu_c \rho_h / \mu_h \rho_c - 1)$. The values of the skin factor calculated from Eq. 24 are, 0, 2.0, and 5.2, respectively. Similarly, using Eq. 26, the distance to the cold front can be estimated at each of the three values of s_a. The calculated values are 0.65 m, 1.20 m, and 1.55 m compared to the correct values of 0.7 m, 1.3 m, and 1.6 m, respectively. Both the calculated skin factors and distances to the thermal front are in excellent agreement with their true values.

The procedure described in the above section does not require a step-rate test but simply any pressure transient data (such as fall-off) after increasing quantities of injection. The procedure is useful not only in determining the effect of the growing cold spot around the well but also can be used to detect true damage or enhancement of a well. If the slope of the semilog line n, is greater or less than its expected value, then changes in the apparent skin factor must be caused by true damage to or enhancement of the near-wellbore region.

The analysis methods discussed and developed here are applicable to porous medium reservoirs where the movement of a thermal front can be described in terms of a t/r^2 relationship. Extension of these methods to fractured systems will require consideration of both the t/r^2 and t/r^4 dependence typical of fracture systems[2]. Also inherent to this analysis is the assumption that the compressibility of the fluid is nearly equal on both sides of the thermal front. In other words, these methods are not directly applicable to two-phase or dry steam reservoirs.

CONCLUSIONS

1) The methods developed for the interpretation of single-rate nonisothermal injection tests in conjunction with conventional multirate analysis methods are applicable to step-rate tests.

2) The generalization that pressure transients during injection are controlled by the properties of the injected fluid is not applicable to step rate tests.

3) Apparent skin factors (relative to the hot reservoir) can be used to calculate the true skin factor of the well and the distance to the thermal front.

4) Nonisothermal injection tests must be carefully designed to obtain data with clearly defined pressure transients which correspond to either the moving-thermal-front or composite-reservoir problem.

ACKNOWLEDGEMENTS

This work was supported by the Assistant Secretary for Conservation and Renewable Energy, Office of Renewable Energy, Division of Geothermal Energy and Hydropower Technologies, of the U.S. Department of Energy under Contract No. DE-AC03-76SF00098.

NOMENCLATURE

c	heat capacity (J/kg°C)
C	cumulative injection (m^3)
H	reservoir thickness (m)
k	permeability (m^2)
m	absolute value of the slope on a P vs. log t plot (Pa/cycle)
n	slope on an s_a vs. log C plot (m^{-3})
P	pressure (P_a)
P_{1s}	extrapolated pressure at 1s on a P vs. log t plot (Pa)
P^*_{1s}	corrected pressure at 1s (Pa)
P_D	dimensionless pressure
P_i	initial pressure (Pa)
P_{wf}	flowing pressure (Pa)
q	mass flow rate (kg/s)
Q	volumetric flow rate (m^3/s)
r	radius (m)
s	skin
s_a	apparent skin
s_c	thermal skin
s_{aw}	apparent skin evaluated at πrw^2H
t	time (s)
t_{oc}	time at which the hot and cold slopes intersect for injection with no initial cold spot.
t'_{oc}	time at which the hot and cold slope intersect for injection with a pre-existing cold spot.

Greek Letters

βt	total compressibility (Pa^{-1})
ϕ	porosity
μ	dynamic viscosity (Pa·s)
ρ	density (kg/m^3)

Subscripts

a	reservoir
c	cold
D	dimensionless
h	hot
n	index for flowrate step
tf	thermal front
w	water

REFERENCES

1. Benson, S.M. and Bodvarsson, G.S.: "Nonisothermal Effects During Injection and Falloff Tests," SPE paper 11137, presented at the 57th Annual Meeting of the Society of Petroleum Engineers, New Orleans, Louisiana, 1982.

2. Bodvarsson, G.S. and Tsang, C.F.: "Thermal Effects in the Analysis of Fractured Reservoirs" in 3rd Invitational Well Testing Symposium, Lawrence Berkeley Laboratory Report, LBL-12076, Berkeley, California, March, 1980.

3. Mangold, D.C., Tsang, C.F., Lippmann, M.J., and Witherspoon, P.A.: "A Study of Thermal Discontinuity in Well Test Analysis," Journal of Petroleum Technology (June, 1981), v. 33, No. 6.

4. Tsang, Y.W., and Tsang, C.F.: "An Analytic Study of Geothermal Reservoir Pressure Response to Cold Water Reinjection," in Proceedings 4th Workshop on Geothermal Reservoir Engineering, December, Stanford University, Stanford, California.

5. O'Sullivan, M.J., and Pruess, K.: "Analysis of Injection Testing of Geothermal Reservoirs," Geothermal Resources Council Transactions, vol. 4, 1980.

6. Garg, S.K.: "Pressure Transient Analysis for Two-phase (Liquid Water/Steam) Geothermal Reservoirs," SPE 7479, presented at the SPE 53rd Annual Meeting, Houston, Texas, (October 1-3, 1978).

7. Horne, R. N., and Satman, A.: "A Study of Drawdown and Buildup in Wells with Phase Boundaries," Geothermal Resources Council Transactions, vol. 4, 1980.

8. Edwards, A.L.: "TRUMP: A Computer Program for Transient and Steady State Temperature Distribution in Multidimensional Systems, Lawrence Livermore Laboratory, Livermore, California, UCRL-14754, Rev. 3, 1972.

9. Bodvarsson, G.S.: "Mathematical Modeling of the Behavior of Geothermal Systems Under Exploitation," Ph.D. dissertation, University of California, Berkeley, 1981.

10. Earlougher, Jr., R.C.: Advances in Well Test Analysis, Society of Petroleum Engineers, Monograph 5, 1977.

Proceedings Eighth Workshop Geothermal Reservoir Engineering
Stanford University, Stanford, California, December 1982
SGP-TR-60

THE MEASUREMENT OF PERMEABILITY BY INJECTION TESTS

Malcolm A. Grant

Applied Maths Division, DSIR, Wellington, New Zealand

ABSTRACT

In fractured geothermal reservoirs, injection tests should normally be interpreted by using formation fluid viscosity, not injected water viscosity. Some injection tests cannot be simply related to formation permeability because injection increases permeability.

INTRODUCTION

Injection of cold water is frequently used as a testing procedure for geothermal wells, as for example in a completion test at the end of drilling. The injectivity so measured is a fairly reliable indicator of the well's production. The precise evaluation of injection tests and pressure transients however poses some problems as to what fluid properties should be used. A test measures transmissivity kh/μ. As the viscosity of cold water is up to ten times greater than that of hot water, kh estimates are sensitive to the assumption used.

Using standard homogeneous porous medium models, injection testing has been analysed by Tsang & Tsang (1978), Bodvarsson & Tsang (1980), O'Sullivan & Pruess (1980), Mangold et al. (1981), Garg & Pritchett (1981) and Bodvarsson et al. (1981). These show a variety of results, with injected fluid properties being appropriate at some times - specifically during the buildup with injection - and not at other times.

Experience, in fractured reservoirs, shows a different conclusion. Formation fluid properties should be used. (Sigurdsson & Stefansson 1977, Ramey 1979, Grant et al. 1982). Although cold water is so much more viscous than hot water, the author at present knows of no case where injection of cold water required significantly greater back-pressure than the drawdown caused by discharging an equal mass flow from the same well.

Sometimes it is observed that a well accepts water for injection markedly more readily than it produces fluid for discharge. kh/μ for injection is several times greater than for production. To explain such observations it is neccesary to assume a genuine increase of permeability with injection, due either to hydraulic fracturing or to thermal contraction of rock and opening of fractures. Detailed tests in New Zealand have shown both mechanisms to occur, in different wells.

OBSERVATIONS

Given the many uncertainties remaining about geothermal reservoirs, and in particular the problems involved with the fractured nature of the permeability, theoretical conclusions are best checked against observations of actual practice as frequently as possible. It should be quite simple to determine the fluid properties controlling a well test: simply assemble a list of wells in which good-quality tests have been made of both injection and discharge transients, and compare. In practice there seem to be remarkably few such data available. There are some, and these are reviewed below.

NEW ZEALAND

It is standard practice in New Zealand to measure the injectivity of a well at completion. Thus a large number of injectivities and injection transients have been measured. There is a smaller library of discharge results. Table 1 lists the productivities and injectivities of the wells of Ngawha field. All the wells produce water at 210°-230°, from fractured greywacke.

TABLE 1. NGAWHA WELLS

Well no.	inj.	prod.
	--- t/h.b ---	
NG2	5	9
NG3	22	2
NG4	110	200
NG8	>8	12
NG11	42	25
NG18	10	1.5-4

If the injection results reflected the properties of injected fluid, the productivity should be about ten times greater than the injectivity. In fact it is about the same, or less. Had the

injection results been evaluated with cold water properties, a gross overestimate of the productivity would have been calculated.

Table 2 lists a similar set of comparisons for Broadlands wells. All measurements were made in 1970-71. In some cases productivity is taken not from a flowing profile but from an 'immediate shut' profile, ie 5-15 minutes shut, so that productivity is over-estimated. All wells were flowing with excess enthalpy, and produce from a reservoir of fractured volcanic rock at 245°-300°.

TABLE 2. BROADLANDS WELLS

Well no.	inj.	prod.
	---t/h.b---	
BR9	20	1-1.5
BR13	4-9	3.3
BR18	8	2.2
BR22	14	12
BR23	26	11
BR25	21	35
BR27	9	5.5
BR28	50	15

As with Ngawha, productivity is equal to or less than injectivity, not much greater.

A comparison of injection and discharge transients is reported by Grant (1980) for well KA28, Kawerau. As the well is two-phase, it is neccesary to make some assumption about relative permeabilities. Using fracture-flow permeabilities, consistency between injection and discharge results is obtained assuming that the injection test measures formation fluid properties. Use of cold water properties would give incompatible results. A series of tests at BR28 provide a similar result. Using the same method of calculation as KA28, two discharge tests give kh = 5.9 and 9.8 d-m. Four tests injecting water at 155°-160° give kh = 8.7 -15 d-m, using formation dynamic viscosity. Using the injected fluid viscosity would triple the kh estimates.

ICELANDIC OBSERVATIONS

Sigurdsson & Stefansson (1977) report tests on six early Krafla wells. In two, KG-8 and KJ-9, both injection and production transients were analysed. They are roughly consistent if the injection tests reflect formation fluid viscosity. If injected water properties are used, the injection test provides an overestimate of kh.

Bodvarsson et al (1981) report the analysis of injection tests in two Krafla wells. A theoretical analysis shows that cold water properties are appropriate. For well KG-12 values obtained for transmissivity kh/μ are in the range $1.2\text{-}2.4\times10^{-8}$ m^3/Pa.s, and a similar value for KG-13, which correspond to kh of about 15 d-m, using cold water viscosity. The old field of Krafla has generally poor permeability. The production history of KG-12 is shown by Stefansson & Steingrimsson (1980). Treating the mass flow decline as a flow at constant pressure, a kh of 0.1 d-m is found. The injection test did not predict the well performance. If hot fluid properties were used to evaluate the injection test, 1.5 d-m is found. It is still neccessary to assume some other effect - either stimulation during the injection test or a genuine decline in permeability under production.

VAPOUR SYSTEM

An extreme case of contrast between injected and reservoir fluid is provided by injection into a vapour-dominated reservoir. For four wells in the vapour-dominated reservoir of Kamojang, Indonesia, the following comparison was made: first, kh was evaluated from discharge measurement, usually from a decline analysis. (see, eg. Grant 1979, or Grant et al. 1982) Then, and injection test was evaluated to find kh/μ. Dividing the two gives the dynamic viscosity μ as found by the injection test. The values found lay in the range 200-500 μPa.s, ie corresponding to liquid water at temperatures of 55°-120°C. In this case the injection test reflected the properties of neither reservoir fluid nor injected fluid, but of water of intermediate temperature.

CONCLUSIONS

Permeability or injectivity as found by the injection of cold water into a geothermal reservoir in fractured rock reflects not the properties of the injected fluid, but usually something near the properties of reservoir fluid. Use of the injected fluid viscosity to evaluate injection tests results in a gross overestimate of permeability.

Given that theoretical calculations for a homogeneous medium indicate that injected fluid properties should apply, this conclusion is of great interest. For some reason the fractured medium acts, for injection, in a manner very different from a homogeneous one. One possible reason is that conductive heat transfer from block to fissure significantly changes the radius occupied by heated injected fluid (over that for a homogeneous medium) (Bodvarsson 1982). It is also possible that the formation permeability is effectively temperature-dependent. The normal result of long-term injection is that injectivity increases substantially, so that the cooling of the reservoir

may have opened fissures wider. Injection-production cycling at BR23 confirms this hypothesis (Grant et al. 1982), but this cannnot be the entire explanation since it would produce a random increase in permeability in injection wells, depending upon the local fracture geometry; whereas the injectivity/productivity comparisons show reasonable uniformity.

ACKNOWLEDGEMENTS

I thank Geothermal Energy NZ Ltd and the Governments of Indonesia and New Zealand for permission to reproduce the Kamojang results, and the Ministry of Works and Development, NZ, for the New Zealand data.

REFERENCES

Bodvarsson, G.S., S. Benson, O. Sigurdsson, G.K. Halldorsson & V. Stefansson, 1981 "Analysis of well data from the Krafla geothermal field in Iceland" Proc. 7th Workshop Geothermal Reservoir Engineering, SGP-TR-55, pp71-76.

Bodvarsson, G.S., 1982. Personal comm.

Bodvarsson, G.S. & C.F.Tsang, 1980 "Thermal effects in the analysis of fractured reservoirs", 3rd. Inv. well-testing symp., report LBL-12076, Lawrence Berkeley Laboratory.

Grant, M.A., 1979 "Mapping Kamojang reservoir" Trans. Geo. Res. Council, v3, pp271-274.

Grant, M.A., 1980 "The testing of KA28-pressure analysis in a two-phase reservoir" Proc. 6th Workshop Geothermal Reservoir Engineering, SGP-TR-50, pp170-177.

Grant, M.A., I.G. Donaldson & P.F. Bixley 1982 Geothermal reservoir engineering Academic Press.

Garg, S.K., & J.W.Pritchett, 1981, "Cold water injection into two-phase geothermal reservoirs", 7th Workshop, pp175-178

Mangold, D.C., C.F. Tsang, M.J. Lippmann & P.A. Witherspoon 1981 "A study of a thermal discontinuity in well test analysis" J. Pet. Tech., v33, no6, pp1095-1112.

O'Sullivan, M.J., & K.Pruess, 1980, "Analysis of injection testing in geothermal reservoirs" Trans. Geo. Res. Council, v4, pp401-404

Ramey, H.J.Jr., 1979 Personal comm.

Stefansson, V. & B. Steingrimsson, 1980 "Production characteristics of wells tapping two-phase reservoirs at Krafla and Namafjall" Proc. 6th. Workshop Geothermal Reservoir Engineering, SGP-TR-50, pp49-59.

Sigurdsson, O. & V. Stefansson 1977 "Permeability in Krafla wells" report OS JHD 7727, National Energy Authority, Iceland (in Icelandic).

Tsang, Y.W. & C.F. Tsang 1978 "An analytic study of geothermal reservoir response to cold water reinjection" Proc. 4th. Workshop Geothermal Reservoir Engineering, SGP-TR-30, pp322-342.

Proceedings Eighth Workshop Geothermal Reservoir Engineering
Stanford University, Stanford, California, December 1982
SGP-TR-60

TOWARD A TWO-EQUATION METHOD FOR GEOTHERMAL SIMULATION OF FRACTURED POROUS RESERVOIRS

D. E. Dougherty and G. F. Pinder

Princeton University
Princeton, N. J. 08544

ABSTRACT

In the "double-porosity" approach to the simulation of rigid geothermal reservoirs there are several options available in formulating the governing equations. The most basic method requires for each fluid phase the solution of four equations: the mass and energy balances for both the fractures and the porous matrix. It is customary to sum the equations for the fluid phases to eliminate condensation terms from the equations. When a double porosity approach is employed, fracture-matrix exchange terms arise; these terms require constitutive assertions to solve the resulting equations. Alternatively, one may add the fracture and porous matrix equations together. This procedure not only eliminates the troublesome fracture-matrix exchange terms from explicit consideration but also reduces the number of dependent variables and equations. The various summation procedures result in the transfer of information to terms which usually lead to a more diffuse solution.

INTRODUCTION

Equations of the motion for steam and water in a geothermal reservoir considered as a porous medium have been presented by many authors (e.g., Garg et al., 1978; Faust and Mercer, 1979). In this paper we examine the fractured porous medium case. The so-called double-porosity or double-continuum approach will be employed. Having presented the primitive equations we will examine the implications of summing certain of them. The paper extends the work of Kazemi et al. (1976), O'Neill and Pinder (1981), and Pinder and Shapiro (1982). We are particularly concerned about ways detailed information can be masked or lost through use of the summed equations.

CONCEPTUAL MODEL

In Figure 1, each of the six central blocks (1a-3a, 1b-3b) represents a set of balance equations for mass, momentum and energy. Each is associated with liquid, vapor, or solid in either fractures or matrix. There are thus 30 equations in this description of a fractured porous geothermal reservoir. Even at this level of complexity, the system has been simplified. Nevertheless let us take Figure 1 and the associated equations as our point of departure.

Although it is possible to consider the liquid, vapor, and rock phases of a porous medium separately, it is common to combine the balance equations for the 3 phases (1a-3a) to yield a single set of equations, Σa. Similarly, we combine (1b-3b) to form the set Σb. In summing across rows of the figure we have thus reduced from 30 to 10 the number of equations to be solved. The specification of fracture-matrix exchange terms is unfortunately an outstanding problem.

An alternative scheme for equation reduction is to sum columns, e.g., combine 1a and 1b to form $\Sigma 1$. In this case the condensation terms will appear in our equations although the fracture-matrix exchange terms will not.

Finally, all the exchange terms can be completely eliminated by adding all the equations together to form $\Sigma = \Sigma 1 + \Sigma 2 + \Sigma 3 = \Sigma a + \Sigma b$. This set of equations is generally used in current geothermal models.

One might actually wonder about the information costs paid for the equation simplifications achieved through this summation procedure. To determine this we must examine in more detail the strategy outlined above.

THE PRIMITIVE EQUATIONS

We begin with notation. Let the subscript α denote the alpha-th phase, and let the subscript λ denote the lambda-th topophase (fractures or porous blocks).

If λ is a property on the macroscopic, or measurable, scale then ψ_L^f and ψ_V^m are the values of ψ for the liquid (L) in the fractures (f) and for the vapor (V) in the matrix (m), respectively. This notation allows us to distinguish the type of rock comprising the porous matrix from the fill in the fractures.

The primitive equations corresponding to the entries of Figure 1 are:

(1) Mass

$$\partial_t(\rho_\alpha^\lambda) + \underline{\nabla}\cdot(\rho_\alpha^\lambda \underline{v}_\alpha^\lambda) = R_\alpha + R^\lambda$$

(2) Momentum

$$\partial_t(\rho_\alpha^\lambda \underline{v}_\alpha^\lambda) + \underline{\nabla}\cdot(\rho_\alpha^\lambda \underline{v}_\alpha^\lambda \underline{v}_\alpha^\lambda) - \underline{\nabla}\cdot\underline{\underline{t}}_\alpha^\lambda - \rho_\alpha^\lambda \underline{g} = \underline{P}_\alpha + \underline{P}^\lambda$$

(3) Energy

$$\partial_t(\rho_\alpha^\lambda e_\alpha^\lambda + \tfrac{1}{2}\rho_\alpha^\lambda|\underline{v}_\alpha^\lambda|^2) + \underline{\nabla}\cdot[(\rho_\alpha^\lambda e_\alpha^\lambda + \tfrac{1}{2}\rho_\alpha^\lambda|\underline{v}_\alpha^\lambda|^2)\underline{v}_\alpha^\lambda] - \underline{\nabla}\cdot\underline{q}_\alpha^\lambda - \underline{\nabla}\cdot\underline{\underline{t}}_\alpha^\lambda\cdot\underline{v}_\alpha^\lambda - \rho_\alpha^\lambda \underline{v}_\alpha^\lambda\cdot\underline{g} = T_\alpha + T^\lambda$$

subject to

(4) $$\sum_\alpha \sum_\lambda (R_\alpha + R^\lambda) = \sum_\alpha \sum_\lambda (\underline{P}_\alpha + \underline{P}^\lambda) = \sum_\alpha \sum_\lambda (T_\alpha + T^\lambda) = 0$$

where ρ_α^λ, $\underline{v}_\alpha^\lambda$, $\underline{\underline{t}}_\alpha^\lambda$, e_α^λ, $\underline{g}$, and $\underline{q}^\lambda$ are the partial mass density, velocity, partial stress, specific internal energy, body force, and partial heating. The right-hand side terms denote the exchange of mass energy and momentum between the phases and topophases. The subscripted term indicates exchange from all other phases in the λ topophase, while the superscripted term means exchange from all other topophases for all phases. Note that, for example,

(5) $$\sum_\alpha (R_\alpha + R^\lambda) = R^\lambda,$$

$$\sum_\lambda (R_\alpha + R^\lambda) = R_\alpha,$$

$$\sum_\alpha \sum_\lambda (R_\alpha + R^\lambda) = 0$$

The symbols ∂_t and $\underline{\nabla}\cdot$ are the partial derivative with respect to time and the divergence operator.

SUMMING OVER PHASES, DISTINCT TOPOPHASES

We now consider an approach for fractured media which echoes current methodology in simple porous medium analyses of geothermal systems. The procedure is to sum the balances (1)-(3) over the subscript α, i.e., we will obtain one equation for the fractures and another for the matrix, each of which embodies the three phases rock, liquid, and vapor. In the ensuing sections, we will only write the energy balance to conserve space and because the mass and momentum equations are similarly obtained.

We define the inner part of the stress and the heating by

(6a) $$\underline{\underline{t}}_I^\lambda := \sum_\alpha \underline{\underline{t}}_\alpha^\lambda$$

(6b) $$\underline{q}_I^\lambda := \sum_\alpha \underline{q}_\alpha^\lambda$$

The phase-summed energy equation can now be written

$$\begin{aligned}(7)\quad &\partial_t[\rho_R^\lambda(e_R^\lambda + \tfrac{1}{2}|\underline{v}_R^\lambda|^2) + \rho_L^\lambda(e_L^\lambda + \tfrac{1}{2}|\underline{v}_L^\lambda|^2) + \rho_v^\lambda(e_v^\lambda + \tfrac{1}{2}|\underline{v}_v^\lambda|)] + \underline{\nabla}\cdot[\rho_R^\lambda \underline{v}_R^\lambda(e_R^\lambda + \tfrac{1}{2}|\underline{v}_R^\lambda|^2) \\ &+ \rho_L^\lambda \underline{v}_L^\lambda(e_L^\lambda + \tfrac{1}{2}|\underline{v}_L^\lambda|^2) + \rho_v^\lambda \underline{v}_L^\lambda(e_v + \tfrac{1}{2}\underline{v}_v^\lambda|^2)] \\ &- \underline{\nabla}\cdot\underline{q}_I - \underline{\nabla}\cdot(\underline{\underline{t}}_R^\lambda\cdot\underline{v}_R^\lambda + \underline{\underline{t}}_L^\lambda\cdot\underline{v}_L^\lambda + \underline{\underline{t}}_v^\lambda\cdot\underline{v}_v^\lambda) \\ &- (\rho_R^\lambda \underline{v}_R^\lambda + \rho_L^\lambda \underline{v}_L^\lambda + \rho_v^\lambda \underline{v}_v^\lambda)\cdot\underline{g} = T^\lambda\end{aligned}$$

subject to

(8) $$\sum_\lambda T^\lambda = 0.$$

While these equations retain the basic formal structure of equations (1) - (3), they appear to be easier to treat. The reason is that the inter-phase exchange terms are summed leaving as residues only inter-topophase terms R^λ, $\underline{P}^\lambda$, and T^λ. Unfortunately, the constitutive expressions for these terms are not well understood.

Equation (7) can be written in terms of phase-averaged variables. To expedite this procedure we introduce new notation:

(9) $$\rho^\lambda := \sum_\alpha \rho_\alpha^\lambda$$

(10) $$\rho^\lambda \underline{v}^\lambda := \sum_\alpha \rho_\alpha^\lambda \underline{v}_\alpha^\lambda$$

(11) $$\underline{u}_\alpha^\lambda := \underline{v}_\alpha^\lambda - \underline{v}^\lambda$$

(12) $$\underline{\underline{t}}^\lambda := \underline{\underline{t}}_I^\lambda - \sum_\alpha (\rho_\alpha^\lambda \underline{u}_\alpha^\lambda \underline{u}_\alpha^\lambda)$$

(13) $$\rho^\lambda e^\lambda := \sum_\alpha (\rho_\alpha^\lambda e_\alpha^\lambda + \tfrac{1}{2}\rho_\alpha^\lambda|\underline{u}_\alpha^\lambda|^2)$$

(14) $$\underline{q}^\lambda := \underline{q}_I^\lambda + \sum_{\alpha_2} [\underline{\underline{t}}_\alpha^\lambda\cdot\underline{u}_\alpha^\lambda - (\rho_\alpha^\lambda e_\alpha^\lambda + \tfrac{1}{2}\rho_\alpha^\lambda|\underline{u}_\alpha^\lambda|^2)\underline{u}_\alpha^\lambda].$$

Note that

$$\sum_{\alpha} (\rho^{\lambda}_{\alpha} \underset{\sim}{u}^{\lambda}_{\alpha}) = \underset{\sim}{0}.$$

Summing equation (3) over α and using the above definitions we obtain

$$(15)\quad \partial_t(\rho^{\lambda}e^{\lambda} + \tfrac{1}{2}\rho^{\lambda}|\underset{\sim}{v}^{\lambda}|^2) + \underset{\sim}{\nabla}\cdot[(\rho^{\lambda}e^{\lambda} + \tfrac{1}{2}\rho^{\lambda}|\underset{\sim}{v}^{\lambda}|^2)\underset{\sim}{v}^{\lambda}] - \underset{\sim}{\nabla}\cdot\underset{\sim}{q}^{\lambda} - \underset{\sim}{\nabla}\cdot\underset{\approx}{t}^{\lambda}\cdot\underset{\sim}{v}^{\lambda} - \rho^{\lambda}\underset{\sim}{v}^{\lambda}\cdot\underset{\sim}{g} = T^{\lambda}$$

subject to equation (8).

SUMMING OVER TOPOPHASES, DISTINCT PHASES

We now present the second summing alternative designed to reduce the number of governing equations. In this case we will obtain balance statements for rock, liquid, and vapor. As before, we regretably begin the section with additional nomenclature:

$$(16)\quad \rho_{\alpha} := \sum_{\lambda} \rho^{\lambda}_{\alpha}$$

$$(17)\quad \rho_{\alpha}\underset{\sim}{v}_{\alpha} := \sum_{\lambda} \rho^{\lambda}_{\alpha}\underset{\sim}{v}^{\lambda}_{\alpha}$$

$$(18)\quad \underset{\sim}{\bar{u}}^{\lambda}_{\alpha} := \underset{\sim}{v}^{\lambda}_{\alpha} - \underset{\sim}{v}_{\alpha}$$

$$(19)\quad t_{\alpha} := \sum_{\lambda} (\underset{\approx}{t}^{\lambda}_{\alpha} - \rho^{\lambda-\lambda-\lambda}_{\alpha\,\alpha\,\alpha}\underset{\sim}{u}\,\underset{\sim}{u}\,\underset{\sim}{u})$$

$$(20)\quad \rho_{\alpha}e_{\alpha} := \sum_{\lambda} (\rho^{\lambda}_{\alpha}e^{\lambda}_{\alpha} + \tfrac{1}{2}\rho^{\lambda}_{\alpha}|\underset{\sim}{\bar{u}}^{\lambda}_{\alpha}|^2)$$

$$(21)\quad \underset{\sim}{q}_{\alpha} := \sum_{\lambda}[\underset{\sim}{q}^{\lambda}_{\alpha} + \underset{\approx}{t}^{\lambda}_{\alpha}\cdot\underset{\sim}{\bar{u}}^{\lambda}_{\alpha} - \rho^{\lambda}_{\alpha}(e^{\lambda}_{\alpha} + \tfrac{1}{2}|\underset{\sim}{\bar{u}}^{\lambda}_{\alpha}|^2)\underset{\sim}{\bar{u}}^{\lambda}_{\alpha}].$$

In addition we note that

$$\sum_{\lambda} (\rho^{\lambda-\lambda}_{\alpha\,\alpha}\underset{\sim}{u}) = \underset{\sim}{0}.$$

The governing energy equation becomes:

$$(22)\quad \partial_t(\rho_{\alpha}e_{\alpha} + \tfrac{1}{2}\rho_{\alpha}|\underset{\sim}{v}_{\alpha}|^2) + \underset{\sim}{\nabla}\cdot[\rho_{\alpha}\underset{\sim}{v}_{\alpha}(e_{\alpha} + \tfrac{1}{2}|\underset{\sim}{v}_{\alpha}|^2)] - \underset{\sim}{\nabla}\cdot\underset{\sim}{q}_{\alpha} - \underset{\sim}{\nabla}\cdot\underset{\approx}{t}_{\alpha}\cdot\underset{\sim}{v}_{\alpha} - \rho_{\alpha}\underset{\sim}{v}_{\alpha}\cdot\underset{\sim}{g} = T_{\alpha}$$

subject to

$$(23)\quad \sum_{\alpha} T_{\alpha} = 0.$$

SUMMING OVER PHASES AND TOPOPHASES

For those stubborn readers who have doggedly pursued the development to this point, we now combine balance equations (1) - (3) over all pseudophases; that is, over all phases (subscript α) and all topophases (superscript λ). The resulting lumped set of equations will have the form of a single-phase flow and energy transport equations of a porous medium continuum.

We begin again with new nomenclature:

$$(24)\quad \rho := \sum_{\alpha}\sum_{\lambda} (\rho^{\lambda}_{\alpha})$$

$$(25)\quad \underset{\sim}{v} := \frac{1}{\rho}\sum_{\alpha}\sum_{\lambda} \rho^{\lambda}_{\alpha}\underset{\sim}{v}^{\lambda}_{\alpha}$$

$$(26)\quad \underset{\sim}{\tilde{u}}^{\lambda}_{\alpha} := \underset{\sim}{v}^{\lambda}_{\alpha} - \underset{\sim}{v}$$

$$(27)\quad \underset{\approx}{t} := \sum_{\alpha}\sum_{\lambda} (\underset{\approx}{t}^{\lambda}_{\alpha} - \rho^{\lambda\tilde{\lambda}\tilde{\lambda}}_{\alpha\,\alpha\,\alpha}\underset{\sim}{u}\,\underset{\sim}{u}\,\underset{\sim}{u})$$

$$(28)\quad \rho e := \sum_{\alpha}\sum_{\lambda} (\rho^{\lambda}_{\alpha}e^{\lambda}_{\alpha} + \tfrac{1}{2}\rho^{\lambda}_{\alpha}|\underset{\sim}{\tilde{u}}^{\lambda}_{\alpha}|^2)$$

$$(29)\quad \underset{\sim}{q} := \sum_{\alpha}\sum_{\lambda} [\underset{\sim}{q}^{\lambda}_{\alpha} + \underset{\approx}{t}^{\lambda}_{\alpha}\cdot\underset{\sim}{\tilde{u}}^{\lambda}_{\alpha} - (\rho^{\lambda}_{\alpha}e^{\lambda}_{\alpha} + \tfrac{1}{2}\rho^{\lambda}_{\alpha}|\underset{\sim}{\tilde{u}}^{\lambda}_{\alpha}|^2)\underset{\sim}{\tilde{u}}^{\lambda}_{\alpha}].$$

Moreover it follows that

$$\sum_{\alpha}\sum_{\lambda} (\rho^{\lambda\tilde{\lambda}}_{\alpha\,\alpha}\underset{\sim}{u}) = \underset{\sim}{0}.$$

The governing energy equation is then

$$(30)\quad \partial_t(\rho e + \tfrac{1}{2}\rho|\underset{\sim}{v}|^2) + \underset{\sim}{\nabla}\cdot[(\rho e + \tfrac{1}{2}\rho|\underset{\sim}{v}|^2)\underset{\sim}{v}] - \underset{\sim}{\nabla}\cdot\underset{\sim}{q} - \underset{\sim}{\nabla}\cdot\underset{\approx}{t}\cdot\underset{\sim}{v} - \rho\underset{\sim}{v}\cdot\underset{\sim}{g} = 0.$$

DISCUSSION

Each set of equations has its advantages and disadvantages. The first set (1-3) is unattractive due to the number of equations which must be solved and the large number of exchange terms which must be specified.

The second set of equations represented by (7) or (15) offers a reasonable model. The topophase characteristics are kept clearly separate, so that in the absence of fractures the system of equations easily reduces to the standard geothermal equations. However, one is left with the problem of defining the exchange terms between the topophases.

The third set of equations has great initial appeal because the dependent variables are written for each phase, which coincides with field data (e.g., quality of produced fluid is

obtained, not quality of fluid produced from fractures). On the otherhand, a number of conceptual difficulties arise because the distinctive production mechanisms of fractures and matrix may be obscured. Moreover, there remains the difficulty of determining the exchange term between the phases.

The final set of equations corresponds to the most widespread technology for studying geothermal reservoirs -- fractured or not. The fractured reservoir is considered, in this scheme, to be a porous medium, and fractures or fracture zones are incorporated by adjustments to material properties.

Let us consider now the question of information transfer within the equations. Each equation summation has generated a new set of dependent variables which are related to the primitive variables through their defining equations. Each summed balance equation contains terms which describes the contributions of the primitive variables. Of particular interest are the heat flux terms $\underset{\sim}{q}^{\lambda}$(14), $\underset{\sim}{q}_{\alpha}$(21), and q(29) which must be expressed in terms of the averaged variables to solve the resulting system of equations. The functional form of these constitutive relationships is generally diffusive (behaves like Fick's first law), i.e., the information lost in defining the new summed variables is imbedded in a diffusion-generating term. Consequently, the summed equations are inherently more diffusive than the primitive equations and their solutions will therefore be more smeared. We note that in current practice equation (7) rather than (15) is used (in the absence of fractures), avoiding the transfer of information to the heat flux terms. The outstanding issue now is the significance of this phenomenon for practical applications.

ACKNOWLEDGEMENTS

We thank our colleagues W. Gray, M. Allen, and I. Kinnmark for discussions on related issues. U. S. Department of Energy grant DE-AC03-80SF11489 provided partial support for this work.

REFERENCES

Garg, S.K., J.W. Pritchett, D.H. Brownell, and T.D. Riney (1978). Science, Systems, and Software, Inc., Report SSS-R-78-3639.

Faust, C.F. and J.W. Mercer (1979). Water Resources Research, 15:1:23-46.

Kamemi, H., L. Merrill, K. Porterfield, and P. Zeman (1976). SPE Journal, 16:6:317-326.

Pinder, G.F. and A. Shapiro (1982). Geol. Soc. Amer., Spec. Paper 189, pp. 25-30.

O'Neill, K. and G.F. Pinder (1981). Adv. Wat. Resources, 4:4:150-164.

	Liquid	Vapor	Solid	Combined Equations
Porous Blocks	Water in Pores [1a]	Steam in Pores [2a]	Solids in Blocks [3a]	Steam, Water, and Rock Porous Medium [Σa]
Fractures	Water in Fractures [1b]	Steam in Fractures [2b]	Solids in Fractures [3b]	Steam, Water, and Rock Fractured Medium [Σb]
"Effective" Single Porosity Model	Water in Pores and Fractures [Σ1]	Steam in Pores and Fractures [Σ2]	Solids in Blocks and Fractures [Σ3]	Steam, Water and Rock in Fractures Plus Porous Blocks [Σ]

Figure 1.

Proceedings Eighth Workshop Geothermal Reservoir Engineering
Stanford University, Stanford, California, December 1982
SGP-TR-60

WELL TEST ANALYSIS FOR NATURALLY FRACTURED RESERVOIRS

Giovanni Da Prat

INTEVEP,S.A.
Apartado 76343
CARACAS VENEZUELA 1070

ABSTRACT

Pressure transient solutions for constant rate production and transient rate analysis for constant pressure production are presented for a naturally fractured reservoir. The results obtained for a finite no-flow outer boundary -- are surprising. Initially, the flow rate shows a rapid decline, then it becomes nearly constant for a certain period, and finally it falls to zero. Ignoring the presence of a constant flowrate period in a type-curve match can lead to erroneous estimates of the dimensionless matrix pressure and fracture pressure distributions are presented for both the constant rate and constant pressure production cases. Interference test for-constant rate production can be interpreted for long times by means of the line-source solution. For the constant pressure production case, the pressure away from the wellbore does not correlate well with the line source solution.

INTRODUCTION

Naturally fractured reservoirs or reservoirs with double porosity behavior as they are commonly referred consist of heterogeneous porous media where the opening (fissures and fractures) vary considerably in size. Fractures and openings of large size form vugs and interconnected channels, whereas the fine cracks form block systems which are the main body of the reservoir. The porous blocks store most of the fluid in the reservoir and are often of low permeability, whereas the fractures have a low storage capacity and high permeability. Most of the fluid flow will occur through the fissures with the blocks acting as fluid sources.

These systems have been studied extensively in the petroleum literature. One of the first such studies was published by Pirson(1.953). In 1959 Pollard presented one of the first pressure transient models available for interpretation of well test data from two-porosity systems. The most complete analysis of transient flow in two-porosity systems was presented by Barenblatt and Zheltov (1960) - The Warren avad Root (1963) study is widely considered to be the forerunner of modern interpretation of two-porosity systems. The behavior of fractured systems has long been a topic of controversy. Warren and Root and Kazemi (1969) have indicated that the graphical technique proposed by Pollard is susceptible to error caused by approximations in the mathematical model-nevertheless, the Pollard method is still used. The most complete study of two-porosity systems appears to be the Mavor and Cinco- Ley Study in 1979. This study considers wellbore storage and skin effect, and also considers production, both at constant rate and at constant pressure. However, little information is presented concerning the effect of the size of the system on pressure build-up behavior.
In this paper a literature review is presented on the basic solutions which can be applied in dealing with pressure transient analysis naturally fractured reservoirs.

PARTIAL DIFFERENTIAL EQUATIONS

The basic partial differential equations for fluid flow in a two-porosity system were presented by Warren and Root in 1963. The model has been extended by Mavor and Cinco Ley (1979) to include wellbore storage and skin effect. Da Prat (1981) extended the model and developed a method to determine the permeability thicknes product.Kh. Deruyck et all(1982) applied with success the Warren and Root model to study interference data from a geothermal field.
The basic partial differential equations are: Da Prat (1981).

$$\frac{\partial^2 p_{Df}}{\partial r_D^2} + \frac{1}{r_D}\frac{\partial p_{Df}}{\partial r_D} = (1-\omega)\frac{\partial p_{DM}}{\partial t_D} + \omega\frac{\partial p_{Df}}{\partial t_D} \quad (1)$$

and

$$(1-\omega)\frac{\partial p_{Dm}}{\partial t_D} = \lambda(p_{Df} - p_{Dm}) \quad (2)$$

p_{fD} and t_D are defined in the nomenclature.

where ω is the dimensionaless fracture storage parameter:

$$\omega = \frac{(\phi c)_f}{\{(\phi c)_f + (\phi c)_m\}} \quad (3)$$

and λ controls the interporosity flow and is given by

$$\lambda = \alpha \frac{km}{k_f} r_w^2 \quad (4)$$

A complete mathematical definition requires additional equations which represent the appropiate initial and boundary conditions.

The initial boundary conditions is:

$$p_{mD} = p_{fD}(r_D, 0) = 0 \quad (5)$$

For a well producing at a constant pressure the inner boundary condition is:

$$p_{fD} - S\left(\frac{\partial p_{fD}}{\partial t_D}\right)_{r_D=1} = 1 \quad (6)$$

Where S is the skin factor

For a well producing at a constant flow rate the condition is:

$$C_D \frac{\partial p_{fwD}}{\partial t_D} - \left(\frac{\partial p_{fD}}{\partial r_D}\right)_{r_D} = 1 \quad (7)$$

where:

$$C_D = \frac{c}{2\pi h \{(\phi c)_f + (\phi c)_m\} \cdot r_w^2} \quad (8)$$

The skin effect condition is:

$$p_{fwD} = p_{fD} - S\left(\frac{\partial p_{fD}}{\partial r_D}\right)_{r_D=1} \quad (9)$$

Two outer boundary conditions are considerated in this study: an infinitely large reservoir and a closed outer boundary. For an infinitely large reservoir, we have:

$$\lim_{r_D \to \infty} p_{fD}(r_D, t_D) = 0 \quad (10)$$

For the closed outer boundary, the condition is:

$$\frac{\partial p_D}{\partial r_D}\Big|_{r_D = r_{eD}} = 0 \quad (11)$$

The dimensionless flow-rate into the wellbore is given by:

$$q_D(t_D) = -\left(\frac{\partial p_D}{\partial r_D}\right)_{r_D=1} \quad (12)$$

where:

$$q_D = \frac{141.2\, q \mu B}{k_f h (pi - p_{wf})} \quad (13)$$

METHOD OF SOLUTION

A common method for solving Eqs. 1 and 2 is to use the Laplace transformation. The equations are transformed into a system of ordinary differential equations which can be solved analytically. The resulting solution in the transformed space is a function of the Laplace variable s, and the space variable, r_D. To obtain the solution in real time and space the inverse Laplace tranform is used. In the present work, the inverse was found by using an algorithm for approximate numerical inversion of the Laplace space solution. This algorithm was presented by Stehfest (1970).

TRANSIENT PRESSURE SOLUTIONS-CONSTANT FLOWRATE PRODUCTION

The solutions for the dimensionless wellbore pressure from either an infinite or a closed outer boundary system have appeared in several places in the literature (see Mavor and Cinco-Ley (1979) and Da Prat (1981). Fig. 1 shows the solution for p_{fwD} for an infinite system for two values of ω and several values of λ (C_D= o and skin effect = o). At early times, p_{fwD} depends on t_D and ω. For a given value of λ, as time increases a period is reached where in the pressure tries to stabilize due to flow from the matrix. After this transition period, the solution becomes the same as that for a homogeneous system. Fig. 2 shows the solution for the dimensionless wellbore pressure for a well located in a closed outer boundary system. At early times the solution depends on t_D and ω (assuming skin effect = o and C_D= o) for any value of λ. Then the solution goes to a transition period to finally meet the solution for a homogeneous system. Fig. 3 shows the wellbore storage effect on the Horner plot for a two porosity system where ω= 0.01 and $\lambda = 5.10^{-7}$. It is seen that low values of C_D have a large impact on the initial straight line making impossible the evaluation of ω. For large values of C_D, not only the initial straight line, but also the transition zone is obscured by wellbore - storage.

The analysis of interference tests in two porosity - systems has been the subject of study for many years. These tests can be used to provide information such as mobility thickness product, $\frac{k h}{\mu}$, and the porosity-compressibility - thickness product, $\Phi c_t h$. Kazemi (1969), based on the two-porosity model of Warren and Root, presented results for the fracture-pressure distribution in the reservoir. In Kazemi's work, the wellbore response to an interference test is dependent on the pressure variations in the fractures, rather than in the matrix. Hence, - this study is limited to the case where the wells used in the tests are completed in the fractures. Streltsova-Adams (1976) considered both fracture and matrix pressure distribution and pointed out the importance of differencing matrix flow and fracture flow in the analysis of test made on fractured formations. Recently Deruyck et al (1982) presented a systematic approach for analyzing interference tests in reservoir with double porosity behavior and field tests conducted in a geothermal reser - voir are discussed to illustrate the method. Fig. 4 shows the solution for the dimensionless fracture pressure us t_D/r_D^2 for several values of ω and θ. The parameter θ is equal to λr_D^2. It was found to be a correlating group. Fig. 5 shows the solution for the dimensionless matrix pressure for several values of the parameters $\theta (= \lambda r_{D2})$ and ω.

TRANSIENT RATE SOLUTIONS-CONSTANT PRESSURE PRODUCTION

Although decline curve analysis is widely used, methods specific to naturally fractured reservoirs do not appear to be available. Fig. 6 shows the dimensionless flowrate functions for a well produced at a constant pressure from a two-porosity system where ω= 0.01 and $\lambda = 10^{-5}$.

Fetkovich (1980) observed that for homogeneous systems at the onset of depletion (a type of pseudosteady state) all solutions for various values of r_{eD} develop exponential rate decline, and converge to a single curve. This statement is not true for two-porosity systems as a shown in Fig. 6. It can be seen that the solutions do not converge to a single line. Log-log type - curve matching to analize rate-time data can be applied to naturally fractured systems. Howe - ver, the relationship between q_D and t_D is controlled by ω and λ, as well as by other parameters. Thus more than one type-curve may be necessary. Figs. 7 to 20 show the solutions for different values of ω and λ.

In the case of homogeneous systems, interferen ce tests have been used with success in many cases, Earlougher (1977). For wells producing at constant inner pressure, Ehlig-Economides (1979) observed that, unlike the constant rate solution, the pressure distribution for cons - tant inner pressure does not correlate with the line-source solution. A different solution results for each value of r_D. Considering the ho mogeneous reservoir solution, a particular case of the naturally fractured reservoir solu - tion, it can be expected that the same depen - dence on r_D applies for two-porosity systems. Fig. 21 shows p_{fD} vs t_D/r_{D^2} for the case of r_D = 1000, and several values of ω and λ. Fig. 22 shows the solution for the dimensionless ma trix pressure p_{mD} vs t_D/r_{D^2}, for a well produced at a constant inner pressure.

INTERFERENCE EXAMPLE

The use of type-curve matching will be illus - trated with a simulated injection test. During an interference test, water was injected into a well for 400 hours. The pressure response in a well 250 ft away was observed during the injection process. Reservoir properties and the observed pressure data are given in table 1. - The pressure change was graphed as a function of time on tracing paper and then placed over Fig. 4 (see Fig. 23). From the match, ω and θ can be obtained as parameters. From Fig. 23, - θ= 1 and ω= 0.01. The fracture permeability is given by:

$$k_f = \frac{141.2\, qB\, \mu}{h} \left(\frac{p_{fD}}{\Delta p}\right)_M = \frac{141.2(-100)(1)(1)}{480} \frac{0.4}{(-10)}$$

$$= 1.2 \text{ md}$$

From the time - t_D/r_D^2 match, the total storativity is obtained:

$$\{(\phi c)_f + (\phi c)_m\} = \frac{0.000264\, k_f}{r^2} \left(\frac{t}{t_D/r^2_D}\right)$$

$$= \frac{0.000264\,(1.2)}{(250)^2} \left(\frac{100}{1.5}\right)$$

$$= 3.38\ 10^{-7} \text{ psi}^{-1}$$

From ω= 1 and the total storativity, the fracture storativity is:

$$(\phi c)_f = \{(\phi c)_f + (\phi c)_m\}$$

$$= (0.01)\{3.38\text{x}10^{-7}\} = 3.38\ 10^{-9} \text{ psi}^{-1}$$

as $\theta = \lambda r^2_D = 1$:

$$\lambda = \frac{\theta}{r^2} \quad \frac{1}{(1000)^2} = 10^{-6}$$

also from the relation $\theta = \alpha \frac{k_m}{k_f} r^2 =$

$$\alpha\, k_m = \frac{\theta\, k_f}{r^2} =$$

$$= \frac{(1)\ (1.2)}{(250)^2} = 1.9\text{x}10^{-5} \text{ md/ft}^2$$

Thus, if km can be obtained from core analysis, then the shape factor α is equal to:

$$\alpha = \frac{1.9\text{x}10^{-5}}{k_m} \text{ md - ft}^{-2}$$

The shape factor α can provide information - about the effective block size in the system.

DISCUSSION AND CONCLUSIONS

This work presents basic solutions that can be used to analyse pressure or flowrate transient data from a naturally fractured reservoir. The model used assumes pseudo steady state flow - from matrix to fractures. According to the literature the solutions assuming transient flow have been presented by many authors: Raghavan and Ohaeri (1981) presented declining rate type curves for a constant producing pressure De - ruyck et al (1982) presented solutions for the pressure distribution throughout a reservoir with double porosity behavior considering boths pseudo-steady state flow and transient interporosity flow. The authors concluded based on field examples that the pseudo-steady state and the transient interporosity flow models are shown to yield consistent interpretations.

From the solution presented in this work the following conclusions can be derived:

1) The initial decline in flowrate is often not representative of the final state of depletion.

2) The fracture permeability k_f; total storativity, $\{(\phi c)_m + (\phi c)_f\}$; and the shape factor "$\alpha$" can be obtained from type curve matching.

3) Both dimensionless matrix pressure and fracture pressure are necessary for proper analysis of interference tests.

4) For constant-rate production interference

tests can be analized at long times using the line-source solution.

5) In analyzing interference tests for cons - tant-inner-pressure production, a different solution for the pressure distribution re - sults for each value of radial distance, r_D. The pressure function does not correlate with the line-source solution.

NOMENCLATURE

A= Drainage area, ft^2
B= formation volume factor, RB/STB
c= compressibility, psi^{-1}
h= formation thickness, ft
k= permeability, md
p_{ws}= wellbore pressure during the build-up period, psi
$\bar{p}$= average reservoir pressure, psi
p_D= dimensionless wellbore pressure

$$\frac{k_f h}{141.2\ qB\mu}(p_i - p_w)$$

p_{fD}= dimensionless fracture pressure
p_{mD}= dimensionless matrix pressure
q= volumetric rate, B/D
q_D= dimensionless flowrate

$$\frac{141.2\ qB\mu}{k_{fh}(p_i - p_w)}$$

r= radius, ft
r_w= wellbore radius, ft
r_D= dimensionless radius, r/r_w
r_e= reservoir outer boundary radius, ft
r_{eD}= dimensionless outer boundary radius, r_e/r_w
S= skin effect
t= time, hours
t_D= dimensionless time

$$\frac{2.637\ 10^{-4}\ k_f\ t}{\{(\phi c)_m + (\phi c)_f\}\ \mu\ r_w^2}$$

$t_{AD} = \frac{t_D\ r_w^2}{A}$, dimensionless

Δt= shut-in time, hr

Subscripts

f= fracture
m= matrix
D= dimensionless

Greek

μ= viscosity, cp
ϕ= porosity, fraction
α= interporosity, flow shape factor, ft^{-2}

$\lambda = \frac{\alpha km\ r_w^2}{k_f}$, dimensionless

$\omega = \frac{(\phi c)_f}{\{(\phi c)_f + (\phi c)_m\}}$, dimensionless

$\theta = \lambda r_D^2$, correlating group, dimensionless.

ACKNOWLEDMENT

My sincere thanks to Henry Ramey Jr. of Stan - ford University for his guidance during this study and INTEVEP, S.A. for permission to publish this paper.

REFERENCES

Barenblatt, G.I. and Zheltov, Iu. P.: (1960) - "On the Basic Flow Equations of Homogeneous Liquids in Fissured Rocks" (in Russian), Dokl. Akad. Nauk SSSR.

Da Prat, G.: (1981) "Well Test Analysis for Naturally Fractured Reservoirs", Ph.D Disserta - tion, Stanford University.

Deruyck, B., Bourdet, D., Da Prat, G., Ramey,- H. (1982) "Interpretation of interference tests in reservoirs with double porosity Behavior - Theory and field examples", paper SPE 11025 presented at the 1982 annual fall meeting, SPE of Aime, New Orleans, LA, Sept. 26-29.

Earlougher, R.C., Jr. (1977) "Advances in Well Test Analysis, Monograph Series, SPE of AIME, Dallas, 5.

Fetkovich, M.J.: (1980) "Decline Curve Analy - sis Using Type-Curves", J. Pet. Tech. 1065.

Kazemi, H.: (1969) "Pressure Transient Analy - sis of Naturally Fractured Reservoirs", Trans., AIME. 256, 451-461.

Mavor, M.J., and Cinco-Ley, H.: (1979) "Tran - sient Pressure Behavior of Naturally Fractured Reservoirs", Paper SPE 7977, presented at the 1979 California Regional Meeting, SPE of AIME, Ventura, California, Apr. 18-20.

Pirson, J. Silvan: (1953) "Performance of Fractured Oil Reservoirs", Bull. Amer. Assn. Petrol. Geol. 37 (2), 232-244.

Pollard, P.: (1959) "Evaluation of Acid Trat - ments from Pressure Build-Up Analysis", Trans., AIME, 216, 38.

Raghavan, R., and Ohaeri, C.U.: (1981) "Unsteady Flow to a Well Produced at constant Pressure in a Fractured Reservoir", paper SPE 9902 presented at the SPE 1981 California Regional Meeting, Bakersfield, California, March 25-26.

Streltsova-Adams, T.D.: (1976) "Hydrodynamics of Groundwater Flow in a Fractured Formation", Water Resources Research, 12, No. 13, 405.

Stehfest, H.: (1970) "Algorithm 368, Numerical Inversion of Laplace Transforms", D-5, Communications of the ACM, 13, No. 1, 47-49.

Warren, J.E., and Root, P.J.: (1963) "The Behavior of Naturally Fractured Reservoirs", SPE J. 245-255.

Ehlig-Economides, C.A.: (1979) "Well Test Analysis for Wells Produced at a Constant Pressure", Ph.D. Dissertation, Stanford University.

TABLE I

q = —100 B/D		r = 250 ft
h = 480 ft		B_w = 1,0 RB/STB
p_i = 0		μ_w = 1 cp
t_{iny} = 400 hr		
t hours	P_w (psig)	$\Delta p = p_i - p_w$ (psi)
0	0	—
4,7	11	—11
6.7	11	—11
11.5	12	—12
16.5	12,5	—12,5
26.5	13.5	—13,5
46	15.5	—15.5.
65	17	—17
98	19,5	—19.5
135	22	—22
200	26	—26
265	29	—29
400	33,5	—33,5

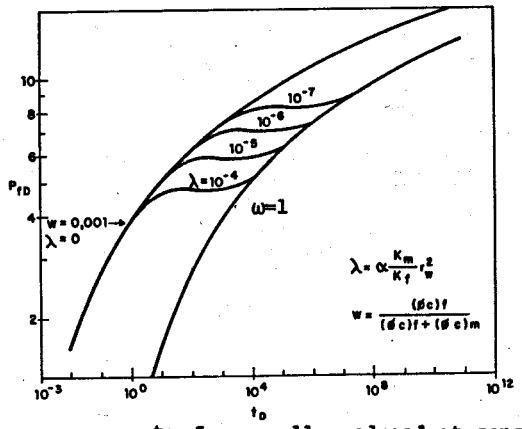

Fig. 1. p_{fD} vs t_D for a well produced at constant flowrate from an infinitely large system (c_D =0, S = 0)

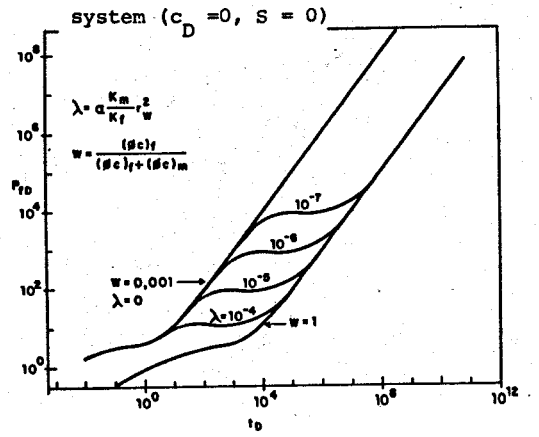

Fig. 2. p_{fD} vs t_D for a well produced at constant flowrate from a bounded, two-porosity system (r_{eD} = 50)

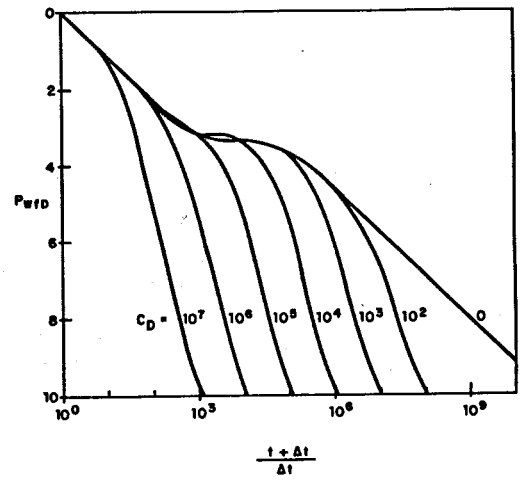

Fig. 3. Wellbore storage effect in horner build-up, infinite two porosity system (ω= 0.01, $\lambda = 5.10^{-7}$, S = 0)

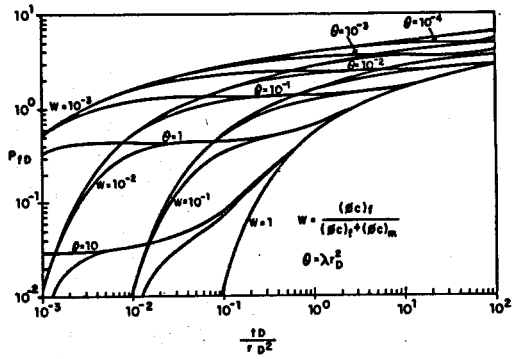

Fig. 4. p_{tD} vs t_D/r_D^2 for a well producing at constant flowrate from an infinitely large two-porosity system.

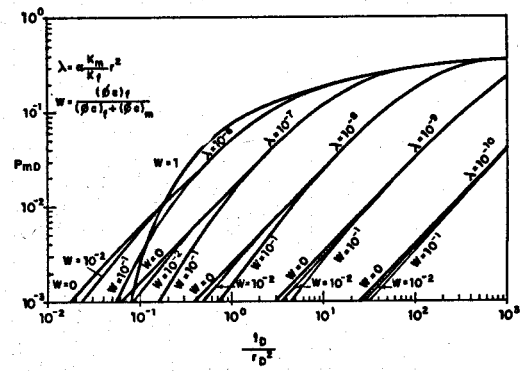

Fig. 5. p_{mD} vs t_D/r_D^2 for a well producing at a constant flowrate from a naturally fractured reservoir.

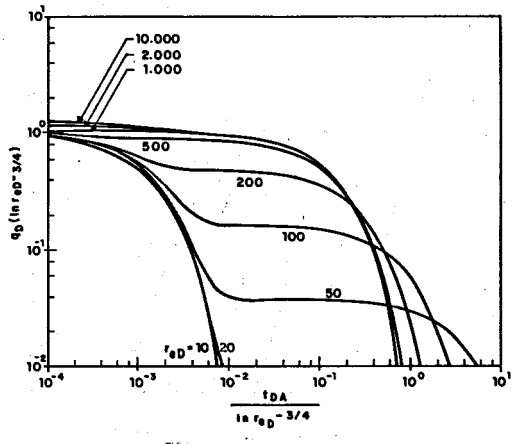

Fig. 6. Dimensionless flowrate functions for a well produced at a constant pressure from a two-porosity system (ω= 0.01, λ= 10^{-5}).

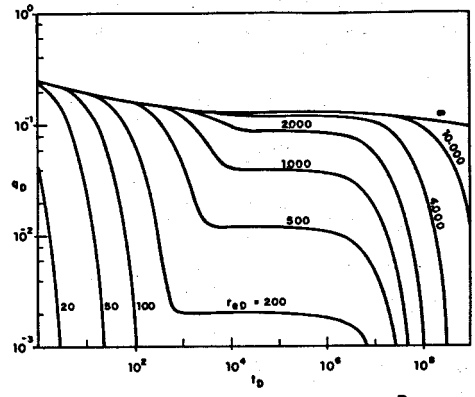

Fig. 9. q_D vs t_D ω = 0.001, λ = 10^{-7}

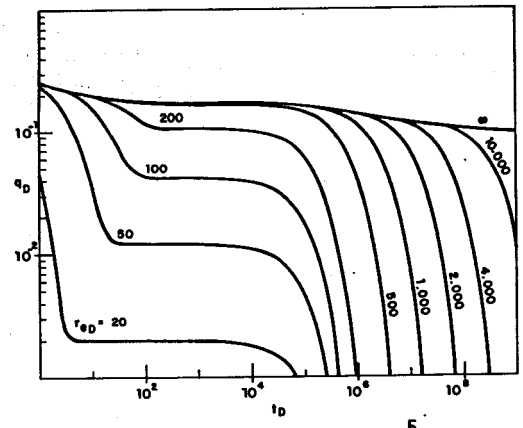

Fig. 7. q_D vs t_D ω = 0.001, λ = 10^{-5}

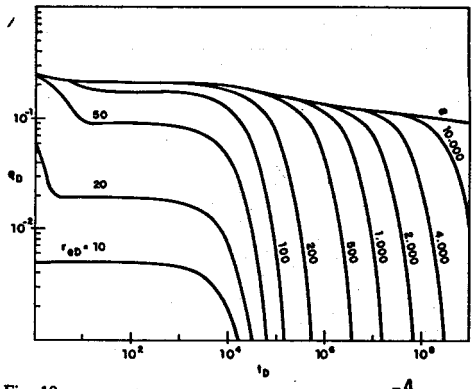

Fig. 10. q_D vs t_D ω = 0.001, λ = 10^{-4}

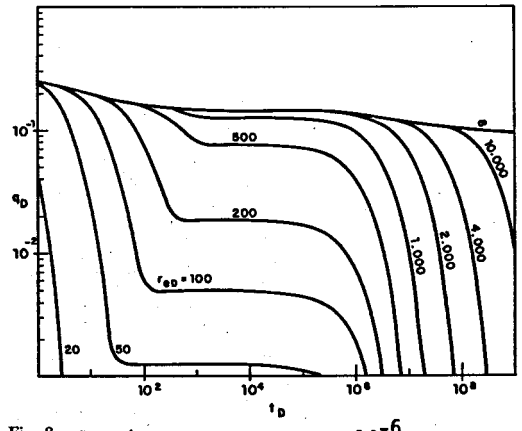

Fig. 8. q_D vs t_D ω = 0.001, λ = 10^{-6}

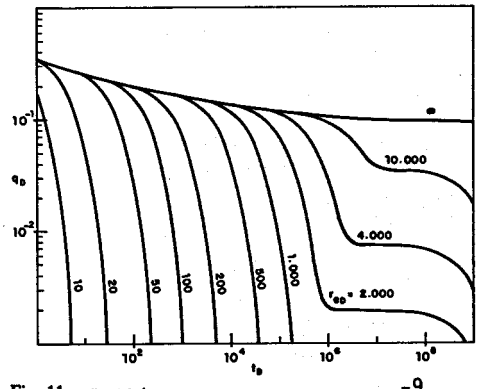

Fig. 11. q_D vs t_D ω = 0.01, λ = 10^{-9}

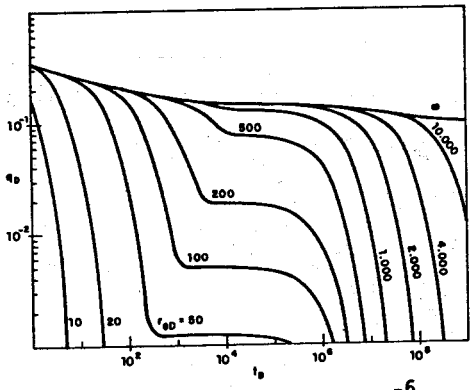

Fig. 12. q_D vs t_D $\omega = 0.01$, $\lambda = 10^{-6}$

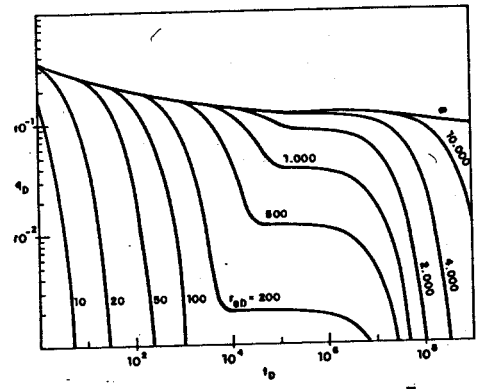

Fig. 13. q_D vs t_D $\omega = 0.01$, $\lambda = 10^{-7}$

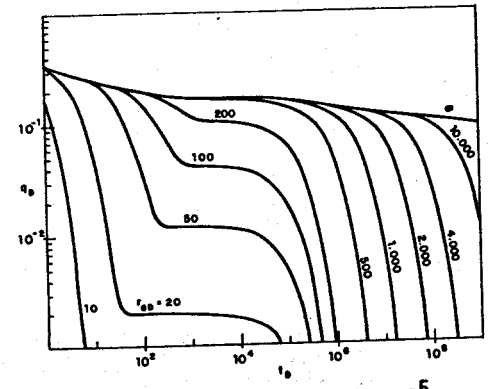

Fig. 14. q_D vs t_D . $\omega = 0.01$, $\lambda = 10^{-5}$

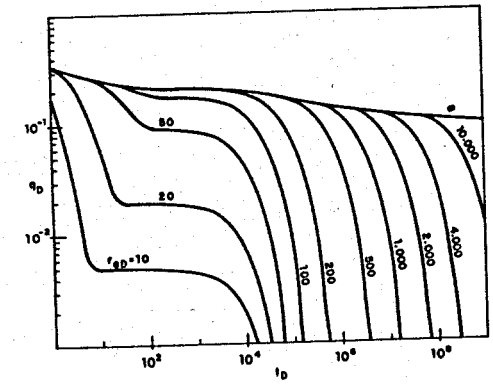

Fig. 15. q_D vs t_D $\omega = 0.01$, $\lambda = 10^{-4}$

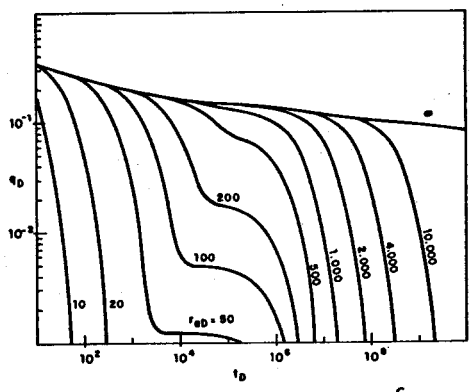

Fig. 16. q_D vs t_D $\omega = 0.1$, $\lambda = 10^{-6}$

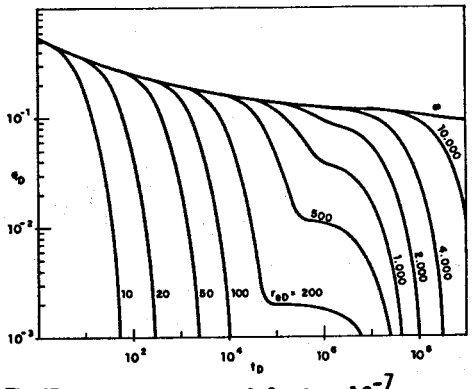

Fig. 17. q_D vs t_D $\omega = 0.1$, $\lambda = 10^{-7}$

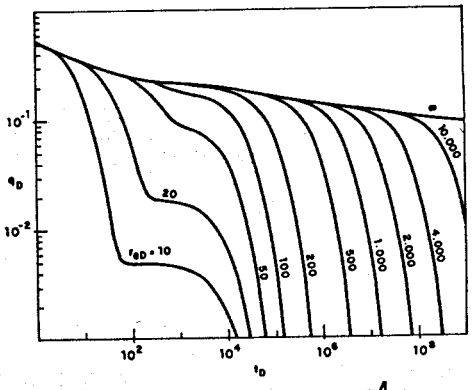

Fig. 18. q_D vs t_D $\omega = 0.1$, $\lambda = 10^{-4}$

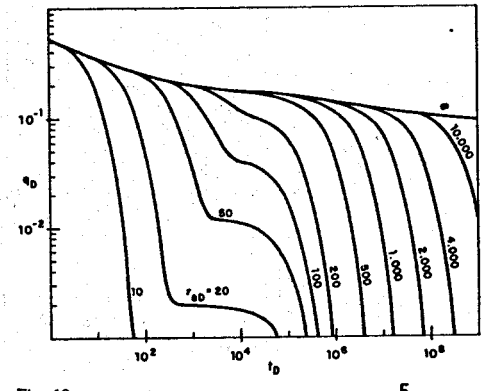

Fig. 19. q_D vs t_D $\omega = 0.1$, $\lambda = 10^{-5}$

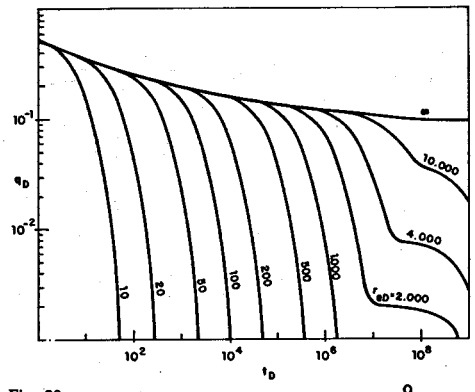

Fig. 20. q_D vs t_D $\omega = 0.1, \lambda = 10^{-9}$

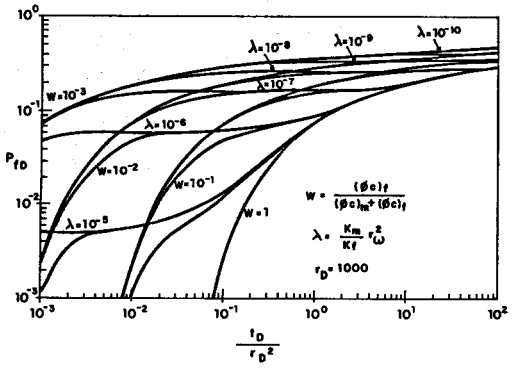

Fig. 21. P_{fD} vs t_D/r_D^2 for a well produced at constant inner pressure from an infinitely large, two porosity system.

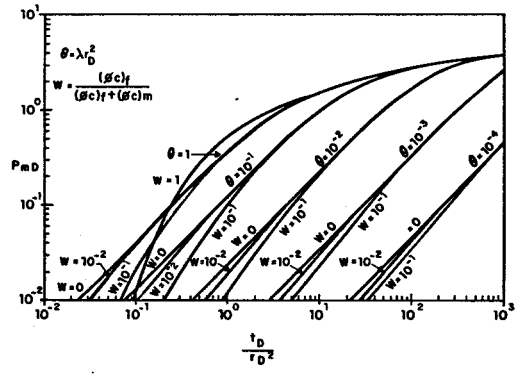

Fig. 22. P_{mD} vs t_D/r_D^2 for a well producing at at constant flowrate from a naturally fractured reservoir.

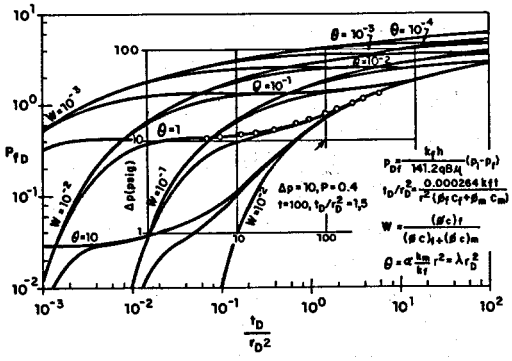

Fig. 23. Type-curve matching for interference example.

Proceedings Eighth Workshop Geothermal Reservoir Engineering
Stanford University, Stanford, California, December 1982
SGP-TR-60

AN EXPERIMENT IN RELATIVE PERMEABILITIES AND TWO-PHASE TRANSIENT THEORY

Malcolm A. Grant
Applied Maths Division, DSIR, Wellington, New Zealand
Richard B. Glover
Chemistry Division, DSIR, Taupo, New Zealand
Mark W. Killup
Ministry of Works & Development, Taupo, New Zealand

ABSTRACT

A series of pressure transients were observed at BR21, a high-enthalpy well. The variation in transient behaviour with enthalpy gives some indication of the form of relative permeability functions for fractured media. The consistent form of the observed transients indicates that two-phase transient observations can be used to determine reservoir parameters.

INTRODUCTION

BR21 is a high-enthalpy well in Broadlands geothermal field, New Zealand. The recent theoretical work (Sorey et al. 1980; Bodvarsson et al. 1980; Garg & Pritchett 1981) on the transient changes occurring in two-phase flow to geothermal wells requires good experimental data to check model predictions. For this purpose a test discharge was carried out at BR21, in which the transient changes in pressure, mass flow, enthalpy and gas and water chemistry were monitored with high frequency during a period of discharge with changes in flow rate and brief shutins. The test history is shown in Figure 1.

THE WELL

BR21 was drilled in 1970 to a depth of 1120m. There were circulation losses around 500m, and the casing is set at 425m. Figures 2a&b show some profiles measured at various times and under various conditions. Permeability is indicated at 500m and around 800-900m; which permeable zones were confirmed by a spinner survey during injection after the flow test. Comparison of pressures with the well cold (P1) with profiles after warmup (P2&4) indicates that the upper zone is dominant (Hitchcock 1971). During most injection tests, the upper zone is discharging and the lower injecting (T1,T19) and flowmeter or temperature profiles can be used to determine that the productivity of the upper zone is about 5 t/h.b; and the injectivity of the lower zone about the same.

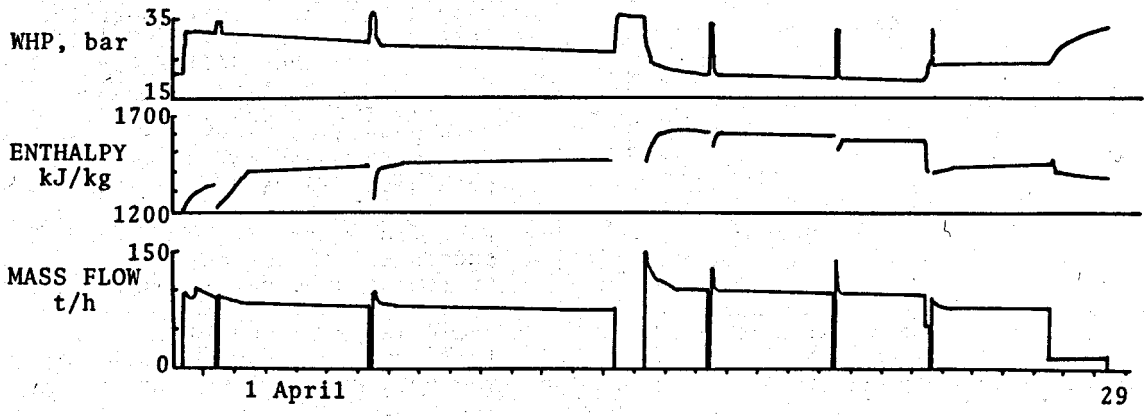

FIGURE 1. FLOW TEST HISTORY, BR21, 30 March - 29 April 1982.

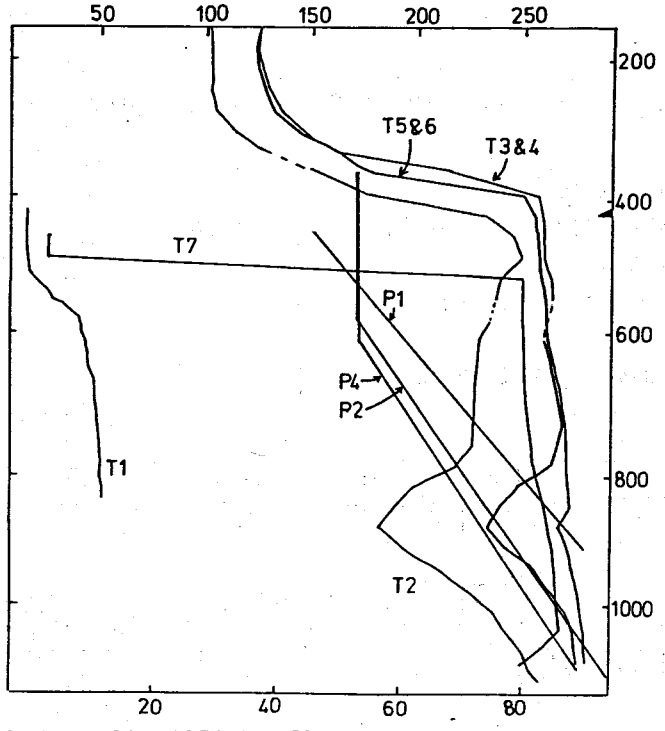

FIGURE 2A. 1970 Profiles.
P1 12/6, immediately after injection.
T2 16-17/6; T3,P2 3/7; T4 6/7; T5 3/9;
P4 21/10; T6 22/10. T7 injecting 1971.

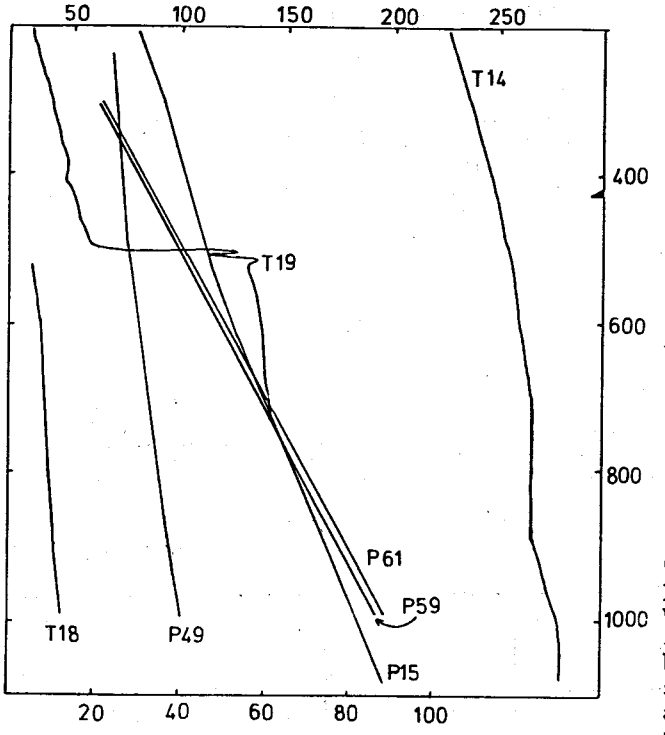

FIGURE 2B 1982 Profiles.
T14,P15 17/3 bleeding; P49 26/4 flowing 90 t/h; P59 21/5 injecting 6.7 1/s;
T18,P61 21/5 injecting 21.4 1/s;
T19 21/5 injecting (continuous log).

It is not possible to make an immediate comparison between the two zones from this result, because one cannot immediately compare injection and discharge results. The injectivity of a permeable zone in fractured rock is commonly about equal to its productivity, or considerably greater. (See, eg., Baca - Garg & Riney 1982.) In the case of BR21 there is fortunately one injection period (T18, P61) when the upper zone was accepting water. Comparing this with the profile P59, there is an incremental injectivity of over 50 t/h.b. The much higher injectivity must result from the upper zone beginning to accept water, and its injectivity must be at least ten times that of the lower zone.

The upper zone at 500m is thus the dominant producing zone, and its parameters are used for the interpretation of the transients. Stable pressure is 46-47 bar. Temperature is unobservable because there is a permanent upflow in the well (eg T14 showing 270° water entering at 900m). Chemical geothermometers indicate 255-258°, which is saturated with the 1-2 bar gas partial pressure present. T3&4 show 263° in 1970, when pressure was higher. A reservoir temperature of 255° is now assumed.

TRANSIENT OBSERVATIONS

BR21 was opened on 30/3, and flowed at a slowly declining rate until 13/4, was shut for a day, flowed again until 23/4, then throttled slightly, throttled again on 27/4, and finally shut on 29/4. Each flow period was interrupted by brief shutins. The available data thus covers:

two openings, one from one day shut
two throttlings
a number of closures and reopenings
in addition a long buildup in 1971

All measurements were made with Kuster gauges using three-hour clocks. The same gauge was used through the 1982 test to minimise error. The transient results are thus defined by one or several consecutive runs showing a transient record within each run, and then possibly a number of later runs from which only one datum point is obtained. Figure 3 shows the downhole pressure history during the first two-week flow period. There are four successive three-hour runs, followed by ten later observations. There is some calibration problem present. To avoid jumps in the record, the second to fourth runs have been decreased by one bar, and all subsequent runs increased by three bars. The latter lies outside the normal range of calibration error. Figure 4 shows the pressure buildup recorded in 1971 when the well was shut after 8 months' flow.

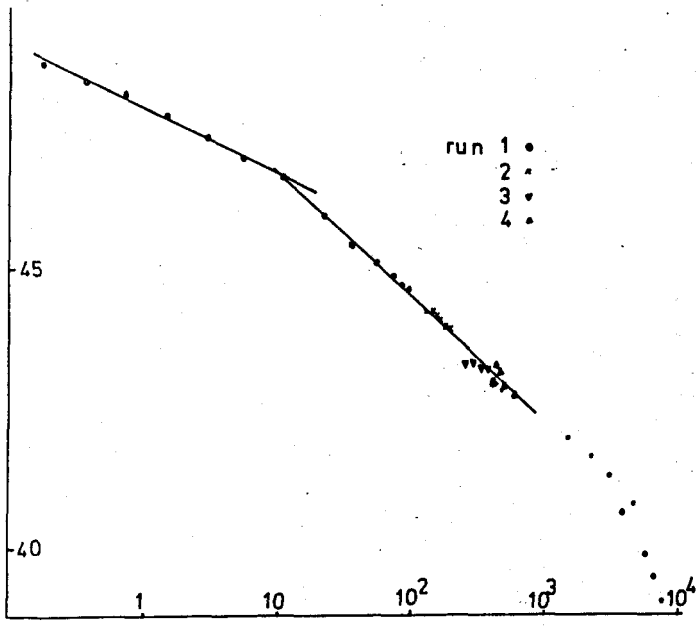

FIGURE 3. Pressure drawdown during first flow period. Pressure in bars, time in minutes.

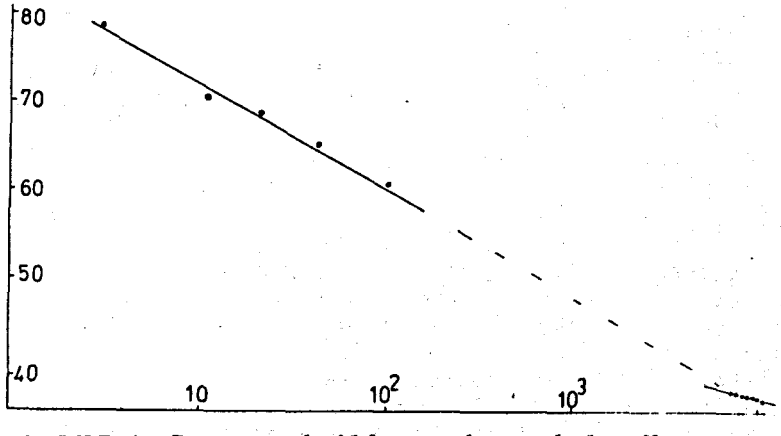

FIGURE 4. Pressure buildup at bottomhole, Horner plot. Pressure in bars.

The two results shown in Figures 3 and 4 are the longest records which are not affected by previous changes in flow rate. All other transients were recorded during the flow test, with a history of prior flow changes, and so only a short period after each flow rate can be simply interpreted. For this reason most other transients rely upon a single 3-hour record.

Figures 3 and 4 show what is a persistent feature of the results: two straight lines. The first begins a few seconds after the flow change, and is replaced by the second line at a fraction of an hour. Sometimes only one line is present, as is shown in Figure 5. These two straight lines gave considerable problems in interpretation. Type-curve matches were tried, which showed that

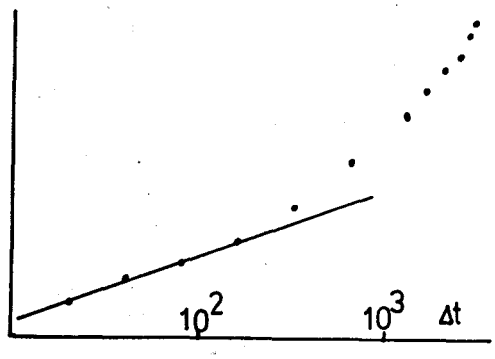

FIGURE 5. Pressure buildup after shutin, 20/4/82.

the early slope is not an artifact of storage and/or skin. Because a straight line develops so quickly, no useful purpose was served by such matching. The reservoir is of course fractured, so there is the possibility that the early slope is in fact the transition period of a fractured medium. The full transient would show two parallel lines joined by a flatter transition, but the first line can be easily obscured by storage effects. However, for this interpretation the ratio of the two slopes must be less than 2:1, and it is in fact about 3:1. Also, the enthalpy transient is interpreted as due to a fractured medium, and the relaxation time of the blocks is 400 hours (Grant & Glover, in prep.).

As the two lines are not always present, it was decided in the end to ignore the problem of their significance, and proceed to the object of the test, the variation of the transient behaviour with discharge enthalpy of the well. Table 1 lists the results of the pressure buildups during the 1982 tests, the 1971 buildup and the two drawdowns. The mass flow and enthalpy given is that just before shut, for the buildups, or midway through the straight-line period, for the drawdowns. Where two straight lines are present, both are given. From the enthalpy, k_{rw}/k_{rs} is computed. Then, assuming the fracture-flow relative permeabilities ($k_{rw}+k_{rs}=1$), kh_{ff} is computed. See the Appendix for details. Figure 6 shows the values of kh_{ff} plotted against k_{rw}/k_{rs}. Unfortunately there are no transients in which the discharge enthalpy is equal to downhole water, from which an unambiguous interpretation of kh can be made. According to the results of Sorey et al. (1980), there should be a marked overrecovery

TABLE 1 SHUTINS AND OPENINGS

Date	W t/h	H_t kJ/kg	m bar/cy.	kh_{ff} d-m
	---- openings ------			
30/3	96	1200	1.2	7.2
		1300	2.2	4.1
14/4	131	1500	8.5	2.3
	------shutins-------			
31/3	89	1333	1.3	8.1
			3.0	3.4
5/4	74	1413	.80	12.6
			2.7	3.8
13/4	73	1440	1.1	9.1
			3.8	2.6
16/4	100	1620	2.2	7.8
			5.4	3.2
20/4	97	1590	1.8	9.3
1971	55	1975	2.7*	10.4
			7.2*	3.9

*Bottomhole data corrected to 500m

in saturation at wellface during shutin. It was hoped that this would produce a discharge of liquid water on reopening. Although discharge enthalpy was markedly lower at each reopening than at the preceeding shut, it was never as low as liquid water.

The variation of kh_{ff} is equivalent to the variation of $k_{rw}+k_{rs}$, since

$$kh_{ff} = (k_{rw}+k_{rs}).kh$$

If the fracture-flow relative permeabilities do apply, kh_{ff} should be constant over variations in enthalpy, and will in fact be equal to kh. If some other form of relative permeability applies, kh_{ff} varies proportionately to $k_{rw}+k_{rs}$.

Both early and late slopes show no well-defined trend, within the considerable scatter of ±30%. Within this scatter, the results are consistent with the fracture flow permeabilities, but the data are few and this result correspondingly tentative. The kh value indicated for BR21 is 3 d-m from the late slopes and 9 d-m from the early.

At the top of Figure 6 is shown the form of variation that would be given by a porous medium obeying the Corey relative permeabilities. It is not consistent with either the early or late slope data. Over the range of observation, the Corey relative permeabilities attain a maximum value of $(k_{rw}+k_{rs})$ of about 0.4. The greatest variation in relative permeability is then in the range of single-phase and nearly single-phase flow, which unfortunately the BR21 results do not span. Rather than data covering a range of two-phase flow conditions, the most important test of relative permeability forms would be provided by a comparison of single-phase and two-phase results.

There does not seem to be any major inconsistency between the results of the buildups and the two drawdown tests.

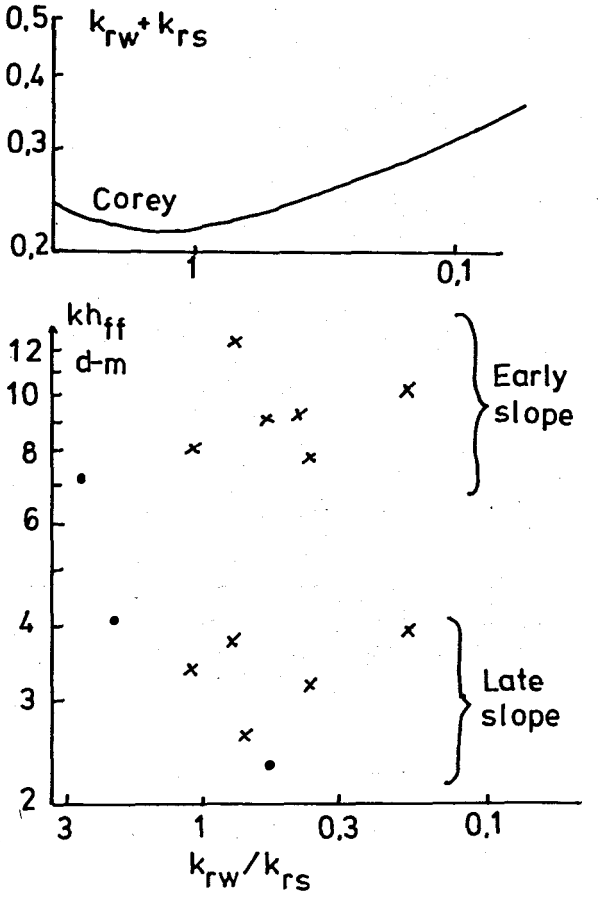

FIGURE 6. Above: variation of $k_{rw}+k_{rs}$ with k_{rw}/k_{rs}, for Corey relative permeabilities. Below: variation of kh_{ff} for BR21 with k_{rw}/k_{rs}.

The drawdowns (denoted by dots) fit into Figure 6 consistently. As the pressure buildup data are easier to interpret - they generally give better straight lines and there is a single unique value of mass flow and enthalpy to use - it is normally easier to use buildup data for well test analysis.

The pressure falloff when the well was reopened after each brief shutin was more difficult to interpret. The brief closure produces sharp radial gradients in saturation around the well, so that the pressure transient on reopening propagates outward into a radially inhomogeneous medium. It is also difficult to allow for the effect of the preceeding closure, by a simple Horner plot or two-rate analysis, because of the different viscosities created by the differing enthalpies. This applies also to the two throttlings. No attempt was made to allow for the effect of the preceeding closure, and all the falloffs were plotted as MDH plots. The effect of the preceeding flow change should then appear

as a flattening of the curve. Table 2 lists the results of these falloffs. They appear to vary more strongly with enthalpy than those of Table 1, although this result is strongly dependent on one result (20/4).

TABLE 2 REOPENINGS.

Date	W t/h	H_t kJ/kg	m bar/cy.	kh_{ff} d-m
31/3	94	1225	1.4	6.2
5/4	100	1280	.95	11.0
		1400	2.3	5.7
16/4	55	1560	6.9	1.3*
20/4	51	1550	11.9	.69

*Result dubious - plot erratic.

The well was twice throttled, and transient changes measured. This was done primarily to observe the expected fall in discharge enthalpy, analagous to that expected after shutin. The pressure transient suffers from difficulty in analysis because of the change in enthalpy and hence in viscosity. It was decided to compute kh proportionally to the change in the product $(W\nu_t)$, not just to the change in mass flow W. This gave results reasonably consistent with those of Table 1, and are shown in Table 3.

TABLE 3 THROTTLINGS

Date	W_1 t/h	W_2	H_{t1} kJ/kg	H_{t2}	m b/cy	kh_{ff} d-m
23/4	93	51	1562	1404	1.5	5.5
					3.3	2.5
27/4	72	12	1406	1380	.99	8.0

SATURATION

From observations of pressures and enthalpy, it is possible to determine the relative permeabilities as functions of each other, but not their dependence on saturation. The saturation is unobservable from these data. It can in theory be determined from chemical transient data, as the transient changes in chemical composition of the discahrge involve a balance between the fluxes of fluid flowing and the amounts in storage in the porous medium. A major object of the chemical analysis was to obtain such estimates of saturation. Six were obtained, one for each shutin period and one for the first period of flow. Two results were discarded, and the remainder give saturations of 12-40%, surprisingly low. These apply only to the fracture medium, not to the entire fracture-block medium. It is not known what to make of these saturation estimates. For further discussion see Grant & Glover (in prep.).

MEASUREMENT AT BR2

Because of the importance of a comparison between single-phase and two-phase transients on the same well, a test was made (9-10 Nov 82) on well BR2. This well is very well documented (see Grant et al. 1982) and has in the past flowed at high enthalpy. At present it produces liquid water at 245°-248°C from its primary feedpoint at 450m. A buildup after one day's flow at 240 t/h gave kh = 20 d-m.

A pressure buildup in 1968 at discharge enthalpy 1480 kJ/kg gave

$$kh/\nu_t = 2.6\times10^{-5}\text{m.s},\ kh_{ff} = 8\text{d-m}.$$

By contrast using the Corey permeabilities gave kh = 34d-m, so this comparison implies that the actual result lies between the fracture and Corey relations. In fact

$$k_{rw} + k_{rs} = 0.4$$

at the observed value of k_{rw}/k_{rs} = 0.4.

The constancy of the BR21 results with varying enthalpy implies that this value of $k_{rw}+k_{rs}$ applies over most of the range of the BR21 test, ie k_{rw}/k_{rs} between 0.2 and 3.

CONCLUSIONS

Observations of pressure transients at different discharge entahlpies has shown some systematic variation of kh estimates with enthalpy, consistent with relative permeability functions lying between the 'fracture-flow' and Corey expressions. This conclusion is sensitive to the small amount of data.

When a well discharges at high and variable enthalpy, the pressure buildup after a flow period provides the simplest data to interpret, as drawdown data is often affected by changes of flow rate or enthalpy. The form of the transients observed at BR21, with early and late slopes, was surprisingly stable over 11 years, indicating that such form relfects real propoerties of the reservoir rather than artifacts of the well or high enthalpy.

ACKNOWLEDGEMENTS

We are very appreciative of the time and trouble taken by the measurements team of the Ministry of Works and Development, Wairakei to collect the data used.

REFERENCES

Bodvarsson, G.S., M.J.O'Sullivan & C.F. Tsang, 1980 "The sensitivity of geothermal reservoir behaviour to relative permeability parameters" 6th Workshop, pp224-237

Garg,S.K. & J.W.Pritchett, 1981 "Buildup analysis for two-phase geothermal reservoirs" GRC Trans v5 pp287-290.

Garg,S.K. & T.D.Riney, 1982, "Reservoir definition and conceptual model" in report LBL-14132, Lawrence Berkeley Lab

Grant,M.A. & R.B.Glover, in prep. "Two-phase heat and mass transfer experiment at well BR21, Broadlands".
Grant,M.A. & M.L.Sorey, 1979, "The compressibility and hydraulic diffusivity of a water-steam flow" Wat. Resour. Res. v15 pp684-686.
Grant,M.A., I.G.Donaldson & P.F.Bixley, 1982, "Geothermal Reservoir Engineering" Academic Press.
Hitchcock,G.W. 1971, Internal report.

NOTATION

kh	permeability-thickness
k_r	relative permeability
H	enthalpy
k_r	$= k_{rw}+k_{rs}$
W	mass flow
m	log slope of pressure transient
ν	kinematic viscosity

Subscripts

w	water
s	steam
ff	assuming fracture-flow relative permeabilities

APPENDIX

Transients are calculated following the formulation of Grant & Sorey (1979) or Grant et al. (1982). Given enthalpies of discharge, water and steam (the latter at reservoir temperature), the reservoir dryness is $X = (H_t-H_w)/H_{sw}$.

$$\frac{k_{rw}}{k_{rs}} = \frac{\nu_w}{\nu_s} \cdot \frac{H_s-H_t}{H_t-H_w}$$

$$= \frac{\nu_w}{\nu_s} \left(\frac{1}{X} - 1 \right)$$

If fracture relative permeabilities are valid

$$k_{rw}+k_{rs} = |k_r| = 1$$

and $$\nu_t = \nu_{tff} = X\nu_s+(1-X)\nu_w$$

For any other relative permeability

$$\nu_t = \nu_{tff}/|k_r|$$

Given log slope m

$$kh_{ff} = |k_r| . kh = 2.303W\nu_{tff}/4\ m.$$

For the calculation of the throttling transients

$$kh_{ff} = (2.303/4\ m)((W\nu_{tff})_1 - (W\nu_{tff})_2)$$

At 255°C H_w=1110, H_s=2798 kJ/kg
ν_w= .812 ν_s= .137 x10^{-6}m^2/s

Proceedings Eighth Workshop Geothermal Reservoir Engineering
Stanford University, Stanford, California, December 1982
SGP-TR-60

A MODIFIED GAS CORRECTION FOR THE LIP-PRESSURE METHOD

Malcolm A. Grant
Applied Maths Division, DSIR, Wellington, New Zealand
Russell James
Chemistry Division, DSIR, Taupo, New Zealand
Paul F. Bixley
Ministry of Works & Development, Taupo, New Zealand

ABSTRACT

The lip-pressure method is the most convenient means of measuring the flow of many geothermal wells. The technique used is empirical and is based upon measurements made on wells with low content of noncondensible gas or dissolved solids. A correction was suggested by James (1970) for gas content. Recent results from wells of high gas content show that this correction must be revised. A theoretical derivation from Fauske's critical flow model partly supports the revision.

INTRODUCTION

Geothermal reservoirs containing significant amounts of noncondensible gas or dissolved solids occur in many parts of the world. The most extensively used method of flow measurement is the lip-pressure method suggested by James (1962). A correction for gas content of discharge was suggested by James (1970):

$$P'_{lip} = P_{lip}(1-y/3.2) \qquad (1)$$

where y is the ratio of gas to steam by mass at the lip. This has apparently been satisfactory in practice although careful checks of its validity were never made.

From 1978 onwards wells have been drilled at Ngawha geothermal field, finding a reservoir of water at 220°-250°C and with gas content of 1-3% (wt) in deep fluid. Flow measurement by lip pressure and weir consistently gave discharge enthalpies up to 100 kJ/kg above liquid water enthalpy at feed-point temperature, although downhole profiles showed liquid water entering the wellbore. Careful checking of all instruments and apparatus left only the gas correction itself as the possible source of error.

We suggest a revised equation

$$P'_{lip} = P_{lip}(1-f_s) \qquad (2)$$

correcting by the mass fraction f_s of gas in the vapor phase at the lip.

For the purposes of computation, rather than actually correcting the lip pressure, it is more convenient to directly correct the enthalpy by ΔH_t:

$$\Delta H_t = H_2(H_t).f_s \qquad (3)$$

where H_2 is defined in the Appendix and shown in figure A1. Equation (3) is simply a reformulation of Eq.(2), and permits the evaluation of the gas correction in one step.

NOTE

To avoid confusion, we will use "vapor" to refer to the gaseous phase containing both steam and noncondensible gas, and "steamwater" to refer to the combined amount of steam and water, exclusive of noncondensible gas. The enthalpy as found by the corrected lip pressure method is the enthalpy of the steamwater flow, not the total flow of steam, water and gas.

NGAWHA RESULTS

Table 1 lists the results of flow measurements by lip-pressure and weir at some Ngawha wells, and compares the results with discharge enthalpy as measured by discharging profiles showing feedwater temperature. The measurements used are those at the time of the chemical sampling. The flowing profiles are measured at other times. Experience elsewhere indicates that wells feeding from liquid water are very stable in performance, and in particular in feedwater temperature. There are many more discharge measurements, at times when a chemical sample was not taken. These show considerable scatter in the (uncorrected) enthalpy, and this scatter is not removed by a gas correction if the gas content does not vary. This scatter is unusual and its source is not yet known. The uncorrected enthalpy of each well may vary over a range of 40 kJ/kg, so that only differences beyond this range are significant for testing the gas correction.

Of the Ngawha wells, NG18 gives the results of greatest significance, because it has the greatest gas content and hence correction. In all cases the new correction gives an enthalpy that lies within 40 kJ/kg of the correct value, and the old correction gives some values that differ by more than this; but the scatter is such that alternative forms

Well	Date	WHP	P_{lip}	W''_w	P_{sample}	x_s^{sample}	H_t kJ/kg			
		bar	bar	t/h	bar	mM/M	actual	uncorr.	old	revised
NG8	22.6.82*	10.1	2.30	205	3.9	28.3	900	914	902	884
	22.6.82	9.0	2.40	205	3.9	28.3	900	936	924	906
	29.6.82	18.7	1.97	89	4.7	49.5	900	982	957	925
NG2	12.8.82	18.8	1.42	55	3.8	35.2	1000	1080	1064	1043
NG9**	6.9.81	6.8	2.25	89	6.6	38	980	1057	1042	1022
NG18	24.8.82	6.8	2.5	102	6.1	113	940	1039	985	917
	24.8.82	6.8	2.5	102	5.4	113	940	1039	989	928

TABLE 1. Ngawha well measurements.
Notes. *taken 20 minutes after opening, enthalpy probably depressed by drilling fluid. **deep zone of dual completion. All pressures absolute. All gas measurements by courtesy of D. Sheppard, DSIR. Lip pressure pipe 154mm dia except for NG9 (204mm).

might be suggested instead.

The Ngawha results are limited in that they cover only a small range of discharge enthalpies, and so do not test for any systematic variation with enthalpy.

DNG-2 RESULT

An example at very different enthalpy is provided by DNG-2. This is the second well at Dieng, a high-temperature field in Indonesia. James (1980) describes the measurement of this well. At a wellhead pressure of 11.2 bar the flow was measured by separator and orifice meters as 24.4 t/h of steam, 20.0 t/h of water and 8.6 t/h of gas, giving for the steamwater flow a mass of 44.4 t/h and an enthalpy of 1880 kJ/kg.

At the same wellhead pressure, the lip pressure was 2.2 bar. The flow of water at atmospheric pressure can be computed from the separator results as 16.8 t/h. With no gas correction the enthalpy would be estimated as 2055 kJ/kg. At the lip pressure, the steam contains 24% (wt) of gas. The old correction gives an enthalpy of 2000 kJ/kg and the new 1920 kJ/kg.

Alternatively, we can compute that the steamwater flow alone would give a lip pressure of 1.53 bar, or 70% of the actual 2.2 bar. A correction of 30% is required, and Eq.(2) gives a 24% value.

CONCLUSION

The lip pressure correction suggested by James (1970) does not allow for the full effect of gas. A revised correction is suggested that is supported by a small amount of data. This interim revision will be checked against better data in the near future.

REFERENCES

Grant,M.A., I.G.Donaldson & P.F. Bixley, 1982, "Geothermal reservoir engineering" Academic Press.

James,C.R., 1962 "Steam-water critical flow through pipes" Proc. Inst. Mech, Engrs., 741.

James,C.R., 1970, "Factors controlling borehole performance" 1st UN Symposium, Spec. Issue, Geothermics, v2, pp1502-1515.

James,C.R., 1980, "Test on geothermal well Dieng no.2", unpub report to Pertamina.

Karamarakar, M. & P.Cheng, 1980, "A theoretical assessment of James' method for the determination of geothermal wellbore characteristic", report LBL-11498 (GREMP-12), Lawrence Berkeley Laboratory.

ACKNOWLEDGEMENTS

We thank Doug Sheppard for the Ngawha chemical analyses and MWD for the Ngawha physical results. We thank Pertamina for the DNG-2 results. One author (PFB) acknowledges the permission of the Comissioner of Works to publish.

NOTATION

This follows Grant et al. (1982). Symbols defined in text are not repeated.

- C specific heat
- f mass fraction of gas or solid
- H specific enthalpy, kJ/kg
- P pressure
- T temperature
- v specific volume
- W''_w weir water flow
- x_w mole fraction of gas
- $X = (H_t - H_w)/H_{sw}$ dryness

Subscripts

- g gas
- s steam
- t total flow
- w water

APPENDIX 1. CALCULATING A GAS CORRECTION

Given the lip pressure P_{lip} and weir water flow W''_w, the discharge enthalpy H_t is given by (James 1970, Grant et al. 1982)

$$H_t = f(Y, P_{atm}) \qquad \text{(A1.1)}$$

$$Y = W''_w/(AP_{lip}^{0.96}) \qquad \text{(A1.2)}$$

A correction to lip pressure results in a correction to the enthalpy. Let F be the fractional correction in Y (ie $\Delta Y/Y$).

Then

$$\Delta H_t = - H_1 \cdot F \quad \text{(A1.3)}$$

where $$H_1 = -Y \frac{\partial H}{\partial Y} t \quad \text{(A1.4)}$$

The relation between H_t and Y is

$$W''_w/(AP_{lip}^{0.96}) = Y = C(H''_s - H_t)/H_t^{1.102} \quad \text{(A1.5)}$$

where H''_s is steam enthalpy at atmospheric separation pressure. Then

$$H_1 = H_t(H''_s - H_t)/(1.102H''_s - 0.102H_t) \quad \text{(A1.6)}$$

It incurs little error to take steam enthalpy as the sea level value, 2675 kJ/kg, for any elevation. Then if the lip pressure is corrected by Eq.(2), $F = 0.96f_s$, and eq.(3) is found, with $H_2 = 0.96H_1$, or

$$H_2 = H_t(2675 - H_t)/(3070 - 0.11H_t) \quad \text{(A1.7)}$$

The function H_2 is shown in figure A1.

For example, consider NG2 in table 1. The uncorrected enthalpy is 1080, so H_2 = 584. Assuming $T_{lip} = T_s(P_{lip})$, the gas sample gives $f_s \leq 7\%$, using the uncorrected enthalpy to calculate the additional flashed steam between the sample and lip pressures. Then

$$\Delta H_t = 585 \times 0.07 = 40 \text{ kJ/kg.}$$

APPENDIX 2. THEORETICAL DERIVATION

Karamarakar and Cheng (1980) use three models of critical flow to make estimates of lip-pressure conditions and the critical mass flux density G_M. The simplest of these is Fauske's model. Under practical conditions, where

$$k_M = (v_s/v_w)^{0.5} \gg 1$$

and $$k_M X \gg 1$$

their expression can be greatly simplified to

$$G_M^{-2} = - \frac{d}{dP}(X^2 v_s) \quad \text{(A2.1)}$$

$$= \frac{X^2 v_s}{P}(1 + 2R) \quad \text{(A2.2)}$$

where $$R = \frac{H_s - H_t}{H_t - H_w} \frac{C_w}{H_{sw}} P \frac{dT}{dP} \quad \text{(A2.3)}$$

The derivation of G_M is not specific to water substance. The results for a gassy fluid can be obtained by substituting the thermodynamics of a water-carbon dioxide mixture. We now redefine G_M and X as the flux density and dryness of the steamwater flow. Then the enthalpies of water and steam, and the dryness, remain unchanged as functions of temperature or saturation pressure, ignoring the heat of solution of CO_2. Then with f_t the mass fraction of gas in the total flow, and assuming sufficient flashing that all gas is in the vapor phase at the lip, the dryness of the total flow is $X + f_t$, and the total mass flux density is $G_M^t/(1 - f_t)$.

$$P_g = 18 f_t P_s/(44X) \quad \text{(A2.4)}$$

which gives $$\frac{dP}{dT} = \frac{dP_s}{dT}\left(1 + \frac{18Rf_t}{44X}\right) \quad \text{(A2.5)}$$

Then $$G_M = \sqrt{\frac{PX^2}{v_s(1+2R)}}\,(1 - R_1 f_t) \quad \text{(A2.6)}$$

$$R_1 = 1 + \frac{1+R}{X(1+2R)} - \frac{9R}{44X} \quad \text{(A2.7)}$$

The fractional correction F to mass flow is $R_1 f_t$, or a correction of $R_1 f_t/0.96$ to the lip pressure. This lies between the old correction and the new correction in most cases, and is closer to the new correction.

A dissolved solid has negligible effect on the P-T relation, but does affect dryness and mass flux, as the liquid phase contains more mass. With f_t as the fraction of dissolved solid in the total flow, and it is not neccessarily true that this fraction is negigibly small,

$$(1 - f_t)^2 G_M^{-2} = - \frac{d}{dP}(v_s(1 - f_t)^2 X^2) \quad \text{(A2.8)}$$

since $1 - f_t$ is the fraction of water substance in the total flow and $X(1 - f_t)$ is the dryness. Eq.(A2.8) indicates that the lip pressure is unaffected by dissolved solid, provided that the lip pressure is regarded as measuring the flow of water substance, and the dissolved solid is just an inert contaminant. We have no experimental data to check this conclusion.

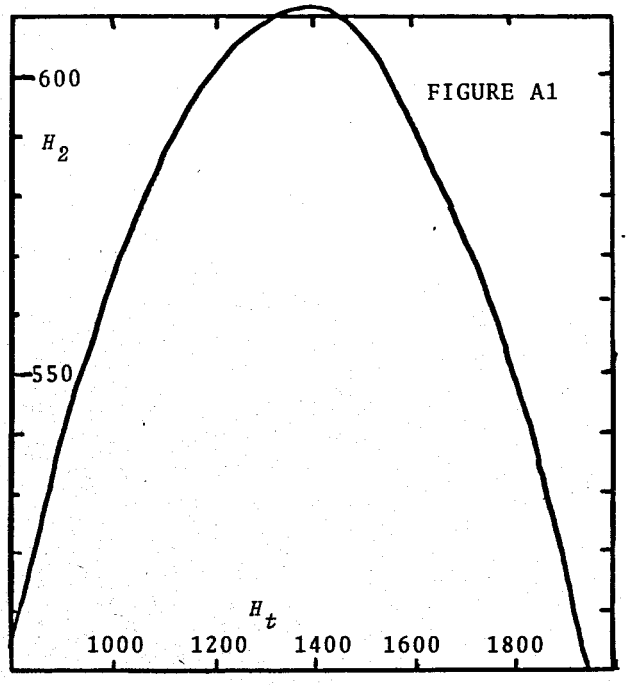

FIGURE A1

Proceedings Eighth Workshop Geothermal Reservoir Engineering
Stanford University, Stanford, California, December 1982
SGP-TR-60

ESTIMATING RESERVOIR PROPERTIES AND WELL PERFORMANCE USING SURFACE PRODUCTION DATA

Dr. Viet T. Hoang

Chevron Resources Company

ABSTRACT

Reliable and sufficient welltest data is necessary for the evaluation of reservoir properties and well performance. Best results are usually obtained by monitoring downhole pressure and flow rate continuously during a transient test. However, a recurring problem for geothermal welltests has been the failure of the downhole pressure instrument in the high temperatures and hostile environments, typical of these wells. Usually an incomplete set of data or data without downhole pressure is used for analysis which provides only limited or erroneous results.

This paper presents a technique of applying a wellbore simulator and a reservoir simulator sequentially to the surface data in order to simulate the downhole condition during a flowtest, thus allowing estimation of the reservoir properties and well performance.

Comparisons of the estimated results and the results obtained from the conventional welltest analysis indicate that this technique can provide a good estimate of the reservoir properties and well performance when downhole data is lacking.

INTRODUCTION

Pressure transient tests performed in wells during field evaluation and development constitutes one of the reservoir engineer's most important source of data. Analysis of these data can provide information about reservoir characteristics, well performance, well condition, etc. During the past few decades considerable interest has been generated in well test analysis. Several analytical and graphical techniques have been derived to provide solutions for the pressure transient data. All of these techniques require reliable and sufficient data from the well test, and downhole pressure monitored continuously during a transient test is preferred (1,2). However, a recurring problem for geothermal well tests has been the failure of the downhole pressure instruments to withstand the high temperature and high salinity environments to which they are subjected. In many cases an incomplete data set or data without downhole pressure will be used for analysis, which provides only very limited or erroneous results. Converting wellhead pressures to downhole values in geothermal wells, where flashing usually occurs, then applying conventional analysis techniques is a difficult if not impossible, task. Chevron uses a technique of sequentially applying a wellbore simulator and a reservoir simulator to the surface data during a well test to simulte the downhole condition and to estimate reservoir properties and well performance.

APPROACH

The basic idea is dividing the problem into two parts: (1) the wellbore through which single or two-phase fluid flows upwards and (2) the reservoir which feeds a single phase fluid to the well. First, the wellbore simulator is used to estimate a few bottomhole flowing pressure (BHFP) values corresponding to the measured wellhead temperatures, pressures and surface flow rates. Usually the BHFP at shut-in and at a few points during the flow period, when the flow was stabilized, are preferred. Then from these estimated bottomhole flowing pressures and the production history of the flow test, a simple radial flow reservoir simulator is used to simulate a complete set of downhole flowing pressures. The reservoir simulator also provides the estimate of reservoir parameters, and well performance, through the recursive estimation techniques.

WELLBORE SIMULATOR

The Chevron wellbore simulator is a highly generalized steady state pressure flow simulator for single or multi-phase fluid flow piping systems. It is a computerized mathematical description of the fluid flow laws within a producing or injection system consisting of well tubing and/or annulus and surface facilities. Pressure losses, flow rates and temperature of the system can be calculated at any point in the network for any combination of reservoir deliverability, fluid types, etc., by applying the mass, momentum, and energy conseration principles. In a steam/water system as the program proceeds through a traverse, the change in pressure is determined by a pressure drop correlation:

$$\underset{\text{total}}{\frac{\partial p}{\partial z}} = \underset{\text{elevation}}{\frac{\partial p}{\partial z}} + \underset{\text{friction}}{\frac{\partial p}{\partial z}} + \underset{\text{acceleration}}{\frac{\partial p}{\partial z}}$$

where p = pressure
z = distance

The change in temperature is determined by a complete energy balance of the system including heat loss, heat of vaporation, and specific heat calculation, then related to pressure by the thermodynamic properties of the fluid.

RESERVOIR SIMULATOR

Chevron has developed a computer program designed for estimating reservoir parameters using pressure - production data from well tests. It does not require constant production rates and even if flow measurements are not available during certain phases of the test, the program can still be used to recover some estimates from the data on the remainder of the producing period.

The simulator is built around a series of idealized models for various reservoir configurations and a series of models for wellbore dynamics. The simplest model assumes a slightly compressible single fluid flowing radially into a well in an infinite system:

$$\frac{1}{r}\frac{\partial}{\partial r}\left[k(r)r\ \frac{\partial p}{\partial r}\right] = \phi\mu CB\frac{\partial p}{\partial t}$$

where ϕ is the porosity, μ the viscosity, C the total compressibility in the formation, and B the formation volume factor. k (r) is the permeability distribution function:

$$k(r)=\begin{cases} k_1, & r_w \leq r \leq r_I \\ k_2, & r_I \leq r \leq r_e \end{cases}$$

where r_I is the interface or the radius of damage. The boundary conditions are: no flow at r_e, as $r_e \to \infty$ and given $p(t, r_w) = p_w(t)$. The initial condition is a given pressure p_i, uniform throughout the field.

The transient behavior is to be simulated using the given production history q(t) and calculating the downhole pressure p using the pressure drawdown at the sand face as the boundary condition:

$$q(t)=-2\pi\frac{k_1 h r_w}{\mu}\frac{\partial p}{\partial t}(t, r_w)$$

If there is wellbore storage, the rate of fluid accumulation in the wellbore is subtracted from the above equation to provide the surface production rate. Long term tests where boundary effects are felt can be analyzed using either finite reservoir models or infinite reservoir models with one or two intersecting faults. These models can be modified for gas reservoirs to account for the real gas behavior.

The basic method used to determine reservoir parameters is to history match a numerical model to the observed data. The history matching part of the program is based on the algorithm known as Recursive Estimation which was described in detail by Padmanabhan and Woo(3).

CALCULATION PROCEDURE

The objective is to find a set of bottomhole flowing temperature, pressure and reservoir parameters to satisfy the wellhead conditions and production data. The following assumptions are normally made in the calculations:

1. Steady state flow in the wellbore.
2. Single phase, radial flow in the reservoir.
3. k and ϕ are uniform anywhere in the reservoir or at most exhibit one radial discontinuity.

Following is the iteration sequence for calculating the reservoir parameters and well performance.

1. Bottomhole flowing temperature and pressure are assumed for the well based on the static condition and wellhead condition.
2. The flowing single stream pressures and temperatures are calculated by the wellbore flow simulator in a forward traverse from the assumed bottomhhole flowing temperature and pressure - resulting in a set of wellhead pressures and temperatures.
3. The calculated wellhead temperatures and pressures are compared with measured values. If tolerances are not met, new bottomhole flowing pressure and/or temperature are assumed.
4. Steps 1 through 3 are repeated until the tolerances are met.
5. The calculated bottomhole pressures, the production and buildup data, the fluid properties and the range of expected k, ϕ, Pi values are entered into the reservoir simulator. Here, prior knowledge of the reservoir is useful for the estimation of the range of k, ϕ, Pi values and in selecting the reservoir model.
6. The Reservoir simulator will simulate the transient behavior of the reservoir using the given production history q(t) and estimates the downhole flowing pressure p(t).

Once the reservoir parameters and bottomhole flowing pressures are known the well performance can be easily obtained. The estimation procedure is summarized in Figure 1.

EXAMPLES

A few field examples will be utilized to demonstrate the validity of the method to analyze the production data. In every case, bottomhole pressures estimated from the surface data will be compared with the measured values to show the quality of the estimations.

1. Production Test on Well A.

Well A was produced for 3 days and during the flow test its flowrate was kept relatively constant between 280,000 lb/hr. and 290,000 lb./hr. Using the wellhead temperature, wellhead pressure and flowrate at shut-in, the wellbore simulator estimated that the flowing pressure at 5000' was 1841.6 psig compared to the measured value of 1842.7 psig. The estimated flowing temperature also compared very well with the measured value. These estimated temperatures and pressures provide a base for the determination of fluid properties such as viscosity, density, etc. The estimated flowing pressure, along with the fluid properties, were incorporated with the measured flow rates during the test, at four hour intervals, and input into the reservoir simulator to simulate the flowing pressures at 5000' and to estimate reservoir parameters. Figure 2 shows the comparison of the simulated and measured pressures. The measured flowrates are also plotted on the same figure. The simulated pressures correlated very well with the measured pressures, and they are very sensitive to the flow rates. The simulated values responded to every change in the flowrate while in some cases the measured values didn't. The estimated transmissivity (kh/μ) and the flow efficiency (FE) are $1.73 \times 10^6 \pm 0.25 \times 10^6$ md-ft/cp and 0.34 respectively. Using the build-up data, Horner analysis gave $kh/\mu = 1.65 \times 10^6$ md-ft/cp and FE = 0.48. It would be more appropriate to compare the estimated results with the Horner analysis of the drawdown data, however in this case the drawdown data are not sufficient for analytical or graphical analyses.

2. Production Test on well B

During this test well B was flowed for 300 hours at three different rates. Bottomhole flowing pressure was monitored throughout the test. Figure 3 presents the measured flowrate and bottomhole pressure history. The wellhead conditions and flowrates were used to estimate the downhole flowing pressures and temperature at shut-in and at three different points during the early parts of flowing period. These estimated values in conjunction with the production data were used to simulate the downhole pressure during the flowtest and to estimate reservoir parameters. For comparison the simulated pressures were also plotted on Figure 3. Generally the simulated pressures agreed very well with the measured pressures. As pointed out before, the simulated flowing pressures are very sensitive to the values of flowrate, and validity of the estimated results is strongly dependent on the accuracy of measured flowrates. Some discrepancies between the two pressures are most likely due to the inaccuracy of the measured flowrates. The estimated formation kh/μ is 247,000 $\pm$ 33,000 md. ft/cp and the estimated F.E. is 0.74. The multirate analysis of the buildup data gave kh/μ = 306,000 md-ft/cp and FE = 0.63.

3. Production test on well C

Well C produced for 60 hours with varying flowrates between 29,000 B/D and 27,000 B/D. Using the estimated bottomhole pressure at shut in and a few flow rates during the flow test the reservoir simulator gave kh/μ = 229,400 $\pm$ 58,800 md ft/cp and FE = 0.92. The Horner analysis of the buildup data gave kh/μ = 223,500 md. ft/cp and FE = 0.99. In this case, the estimated results are in good agreement with the Horner analysis results, although the variance increases because of the lack of production data. Since the first downhole measurement was not made until 2 hours prior to shut-in, only the simulated and measured pressures can be compared (Figure 4). During the first 10 minutes of shut-in, which was effected by the wellbore storage, there are discrepances in the measured and the simulated pressures. However, as the shut-in time increased, these two pressures converged and approached the same value.

Table 1 summarizes the results of these examples. Other sets of field data have also been compared to their estimated values, with results as satisfactory as was obtained in the above examples. In every case the technique provides not only the estimates of the parameters but also their confidence limits so that one can gauge the quality of the estimates. It is important to point out that applying this technique to analyze well test data is not an automatic process. Engineering judgement and prior knowledge of the reservoir always play an important role in selecting data, reservoir model, and interpreting the results obtained.

Conclusion

Comparisons of simulated and measured downhole pressures, and estimated reservoir parameters with those calculated by the conventional techniques indicate good agreement. This demonstrates that the sequential use of wellbore and reservoir simulators can provide a good estimation of the reservoir parameters and well performance in case of lack of downhole pressures.

Acknowledgement

The author would like to thank Chevron Resources for permission to publish this paper and I. J. Epperson for a critical review of the manuscript.

References

1. Earlougher, R.C., "Advances in Well Test Analysis," Society of Petroleum Engineers, Monograph 5, Dallas, 1977.

2. Matthews, C.S., Russell, D.G., "Pressure Build-up and Flow Tests in Wells", Society of Petroleum Engineers, Monograph 1, Dallas, 1957.

3. Padmanabhan, L., Woo, P.T., "A New Approach to Parameter Estimation in Well Testing," SPE 5741, Fourth SPE Symposium on Numerical Simulation, LA, February 1976.

Table 1
Comparison of Different Analysis Methods

Well	Horner/Multirate Analysis kh/μ (md-ft/c.p.)	F.E.	Estimation kh/μ (md-ft/c.p.)	F.E.
A	1.65×10^6	0.48	$1.73 \pm 0.25 \times 10^6$	0.34
B	3.06×10^5	0.63	$2.47 \pm 0.33 \times 10^5$	0.74
C	2.23×10^5	0.99	$2.29 \pm 0.59 \times 10^5$	0.92

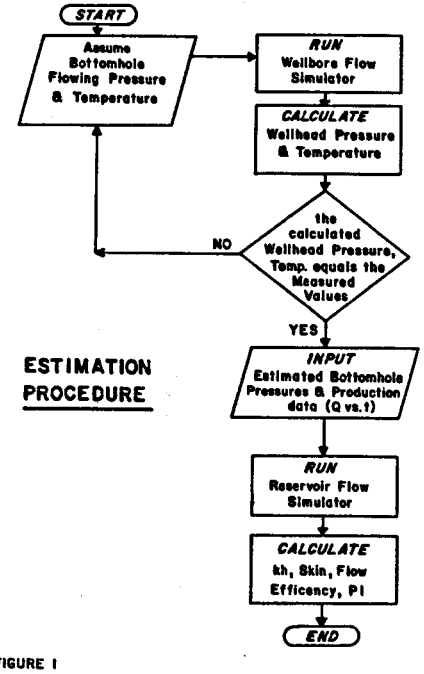

FIGURE 1

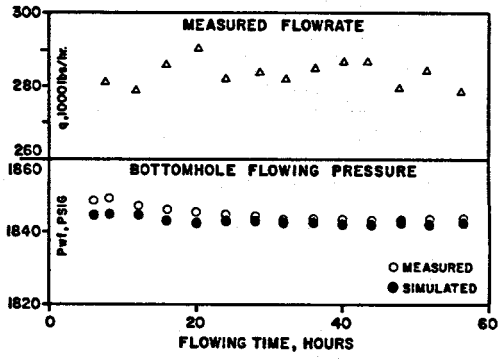

FIG. 2 - COMPARISON OF MEASURED AND SIMULATED PRESSURES OF WELL 'A'

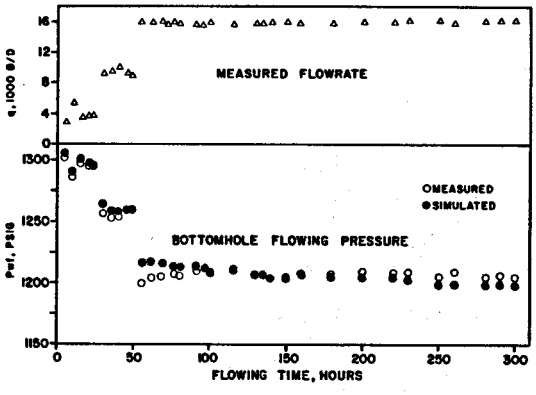

FIG. 3 - COMPARISON OF MEASURED AND SIMULATED PRESSURES OF WELL 'B'

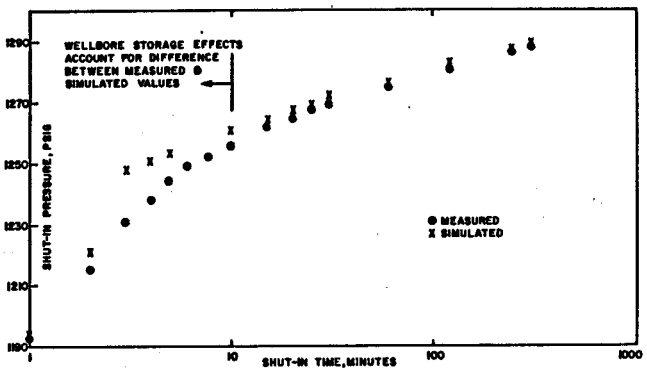

FIG. 4 – COMPARISON OF MEASURED AND SIMULATED PRESSURES OF WELL 'C'

Proceedings Eighth Workshop Geothermal Reservoir Engineering
Stanford University, Stanford, California, December 1982
SGP-TR-60

FLASHING FLOW IN FRACTURED GEOTHERMAL RESERVOIRS

A. J. Menzies*
J. S. Gudmundsson
R. N. Horne

Petroleum Engineering Department
Stanford University

ABSTRACT

Flashing two-phase flow can occur in fractured geothermal reservoirs when water flows toward the wellbore. The mass flow and enthalpy characteristics of wells with two-phase flow feedzones have been investigated by using a modified critical flow slip model. The model includes the effect of heat transfer from the reservoir rock to the two-phase flowing mixture. It was possible to estimate the effective fracture width of geothermal reservoir-well systems and to demonstrate under what conditions choking may occur in feedzone fractures.

INTRODUCTION

Flashing can occur when liquid water flows rapidly into a region where the pressure is below the saturation pressure corresponding to the liquid temperature. In geothermal energy production this situation arises in the transmission of two-phase mixtures up wellbores and along pipelines to steam-water separations. However flashing flow may also occur in the reservoir when liquid water flows toward the wellbore with a strong pressure gradient. In geothermal reservoirs this flow will more likely than not be along fractures.

The purpose of this paper is to report the use of a developed two-phase flow model to flashing steam-water flow in fractured reservoirs. The streamtube model of Wallis & Richter (1978) is applied to an idealized reservoir-well system where the steam-water mixture enters the well through a single fracture. It is an attempt to understand the complex flow of two-phase mixtures in geothermal fractures using a simple model. More details of this work are discussed by Menzies (1982).

FLOWING WELLS

Geothermal wells can be characterized by the massflow and enthalpy of the steam-water mixture produced at various wellhead pressures. Simultaneous massflow and enthalpy measurements are still rare worldwide but data on massflow against wellhead pressure are more readily available. The fluid entering a flowing well in a liquid dominated reservoir is commonly pressurized water or brine. The water flashes as it rises in the wellbore and for most practical purposes the enthalpy of the steam-water mixture is that of the pressurized water. The enthalpy is usually taken to be independent of wellhead pressure, although that need not be the case.

The fluid entering a flowing well in a liquid dominated reservoir is not always pressurized water. It can also be a two-phase mixture of steam and liquid water that results from flashing outside the wellbore. These two-phase feedzone wells are the subject of the current paper. The task at hand is to find a model that can describe the flashing process near the wellbore. Many assumptions have to be made about the reservoir-well system for this to be possible. The two main assumptions of concern to reservoir engineers are that the well has only one two-phase feedzone through a fracture and, the steam-water flashing occurs as it would in pipes and nozzles. The validity of these and other assumptions must then be gauged against the results.

As an example, the flowrate and enthalpy of the steam-water mixture produced by well 403 in Tongonan is shown in Fig. 1 at various wellhead pressures (P.N.O.C. 1981). The characteristic features of these data are the near constant flowrate (massflow) and the increasing enthalpy with decreasing pressure. The measurements show that the enthalpy of the fluid entering the well at low wellhead pressures is higher than at high pressures. There are at least two ways to explain this behavior. The well may have two or more feedzones (which produce different enthalpy fluids in proportions dependent on the wellhead pressure) or, the well may have a two-phase feedzone and flashing in the reservoir.

In addition to the flowrate and enthalpy measurements shown in Fig. 1, there are

* Now, KRTA, Auckland, New Zealand

available flowing temperature and pressure surveys for well 403. All these measurements were conducted between August 1980 and February 1981. Field analysis of the data shows that well 403 has a major feedzone at 2000-2200 m depth and a minor feedzone at a shallow depth which may contribute to the total flow at high wellhead pressures. The flowing surveys show that well 403 has two-phase flow in the wellbore at least down to the major feedzone at 2000-2200 m depth. This indicates that the fluid entering the well is two-phase and probably results from flashing in the reservoir. When liquid water flashes in fractures the fluid temperature decreases and causes a temperature difference between the rock and the two-phase mixture. This in turn can result in heat transfer from the reservoir rock to the flashing water such that the mixture enthalpy rises. It may be that the enthalpy increase measured in well 403 results from such reservoir heat transfer.

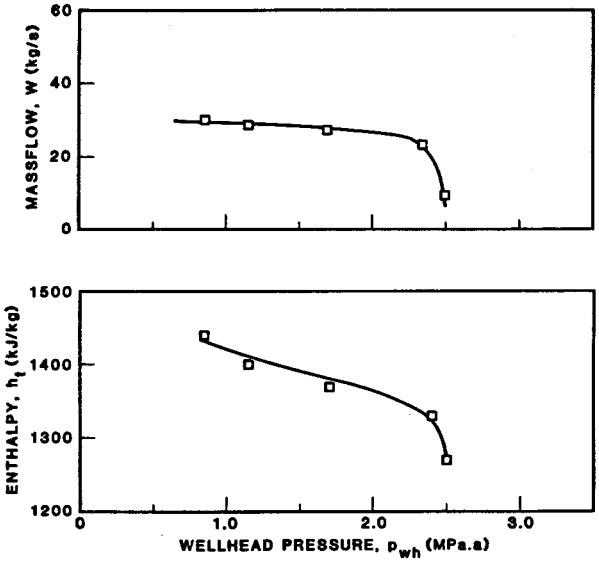

Fig. 1 Measured flowrate and enthalpy of well 403, Tongonan

The flowrate characteristic of well 403 in Tongonan is rather flat, except at high wellhead pressures. Fig. 1 shows that the flowrate does not increase much when the wellhead pressure decreases below about 2 MPa. This behavior indicates that the wellflow has reached some maximum value which depends on the nature of the reservoir-well system. The wellflow is choked because a lower receiver pressure (wellhead pressure) does not result in a larger massflow. The well has a similar casing design as other Tongonan wells which are capable of massflows 3-4 times greater than that of well 403. The choking is therefore likely to occur in or close to the major well feedzone at 2000-2200 m depth. Although the details of this two-phase choking are not well defined, it can be useful to analyze the situation by using a simple model. It is suggested here that the choking steam-water flow in well 403 can be analyzed by assuming two-phase flashing flow in a fracture.

STREAMTUBE MODEL

Various analytical approaches have been taken to two-phase critical flow (Wallis 1980). There are three main types of models that have been developed and these can be classified as homogeneous, slip and separated flow models. A two-phase slip model that predicts critical flow in nozzles, at least as accurately as any other model, is the streamtube model of Wallis & Richter (1978). This model is based on isentropic expansion of individual streamtubes that originate at the vapor-liquid interface as flashing progresses. The velocity field and thermodynamic state vary normal to the main flow direction. In this paper the streamtube model will not be derived and explained in detail. Interested readers are referred to Wallis & Richter (1978) and Menzies (1982). However, the model will be discussed briefly here to provide some background for its application in fractured geothermal systems.

In the streamtube model, discrete pressure steps are used to approximate the flashing process. At each pressure step a new streamtube is created in which initially only saturated steam flows. The steam in streamtubes that already exist is assumed to expand isentropically. A small amount of steam condenses during expansion and within each streamtube the homogeneous flow model applies. There is assumed to be no interaction between the streamtubes and thus no transfer of energy, mass and momentum occurs. Each streamtube has a different velocity, the first vapor streamtube the highest and the liquid streamtube the lowest. In the Wallis & Richter (1978) model only enthalpy and velocity changes were considered in the energy balance and the assumption of isentropic expansion requires the overall process to be reversible. The system is frictionless and an enthalpy decrease results in a velocity increase. These assumptions have been found to be valid in the study of two-phase flow in pipes and nozzles. The streamtube model provides an ideal reference process that can be useful in the study of real systems.

In geothermal reservoir systems, the transfer of heat from the formation rock to the flashing two-phase fluid can be important. This energy gain Q can be expressed by the

basic thermodynamic relationship

$$Q = C_p \Delta T (1-\eta_s) \qquad (1)$$

where C_p is the fluid heat capacity, ΔT the temperature difference between the reservoir rock and the flowing fluid and η_s, the effective isentropic efficiency of the flashing process. The efficiency term η_s attempts to relate the ideal model and the real process. The above heat transfer step was added to the basic streamtube model of Wallis & Richter (1978) to make it more applicable to flashing in or near feedzones of geothermal wells. After each discrete pressure step in the model, a heat transfer step was added to allow the two-phase mixture to approach the rock temperature to a degree determined by the effective isentropic efficiency. For example, if $\eta_s = 1$ the flashing process is said to be ideal and no heat transfer occurs. In a real system, however, some heat may transfer and $\eta_s < 1$. The basic steps of the modified streamtube model are illustrated in Fig. 2 which shows the enthalpy-entropy diagram of the process. The energy gain Q is easily related to enthalpy and entropy. In the modified model the mixture velocity field is assumed to remain constant during the added heat transfer step.

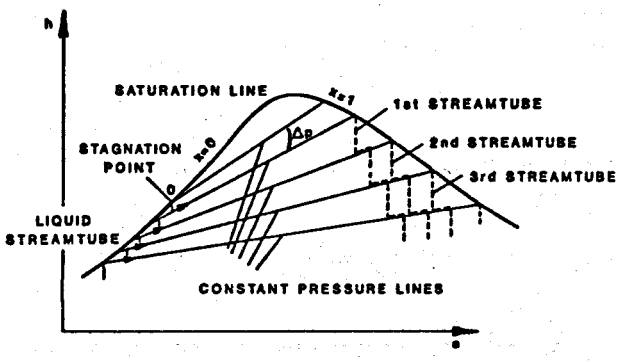

Fig. 2 Enthalpy-entropy diagram of the modified streamtube model

In the streamtube model the flashing two-phase massflux G can be calculated for each discrete pressure step. In the calculations reported here the pressure was decreased from the saturation pressure p_{sat} of the reservoir fluid in 50 kPa steps to the feedzone pressure of the well p_{wf} (downhole pressure, flowing well). The massflux was calculated for increasing $\Delta p = p_{sat} - p_{wf}$ values until two-phase critical flow was reached at:

$$\frac{dG}{dp} = 0$$

Typical results from the modified streamtube model are illustrated in Fig. 3. They show the two-phase massflux G increasing with increasing pressure drop Δp as more liquid flashes and the mixture velocity becomes greater. Fig. 3 shows the massflux for several values of the effective isentropic efficiency η_s for a reservoir temperature of 280°C. It also shows the total two-phase mixture enthalpy h_t. When the isentropic efficiency η_s is close to unity (= 0.995 say) there is no heat transfer from the formation rock to the flowing fluid. The mixture enthalpy remains constant as flashing progresses and the massflux attains a maximum value. However, when the efficiency η_s is lower (= 0.92 say) the enthalpy increases as the fluid flashes and the critical (choking) massflux is about 25% lower compared to the no heat transfer situation.

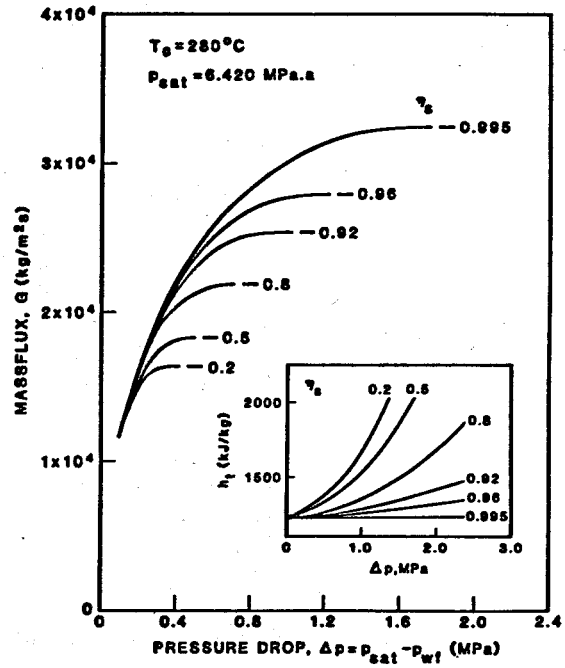

Fig. 3 Typical results from the modified streamtube model, reservoir temperature 280°C

MODEL TESTING

The modified streamtube model can be used to estimate the massflux and enthalpy of a two-phase flow mixture entering a geothermal well through a major fracture on feedzone. Field data can be used to test the model provided downhole pressure (and temperature) measurements are available in addition to wellhead massflow and enthalpy (and pressure) determinations. Such data are available for well 403 in the Tongonan geothermal field, the Philippines (P.N.O.C. 1981, Menzies 1982).

The massflow G entering a geothermal well through a major fracture needs to be related to the massflow W (flowrate) when model

calculations and field data are compared. This calls for an assumption about the geometry of the fracture-feedzone where the two-phase mixture enters the well. A single horizontal fracture was assumed and is shown in Fig. 4. The two-phase flow was assumed to enter the wellbore uniformly around the circumference. The effective fracture width w_f was taken to be constant in the feedzone so the smallest flow area becomes $A = \pi d w_f$ where d is the wellbore diameter. The orientation of the fracture may affect the flow entering a well. This effect can be taken to be included in the effective isentropic efficiency η_s for the overall flashing process.

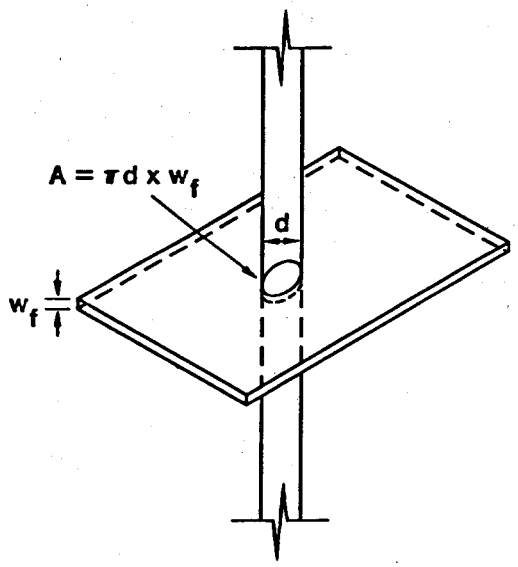

Fig. 4 Geometry of fracture feedzone of well

Well 403 in Tongonan is 2470 m deep and has a major feedzone at 2000-2200 m depth. The wellbore diameter at depth is 8 5/8" or 0.22 m. The reservoir temperature near the feedzone has been estimated at 295°C, which corresponds to a water saturation pressure of 8 MPa. The reservoir pressure near the feedzone has been measured at 12 MPa. The measured flow characteristics of well 403 in Fig. 1, illustrate the massflow W and enthalpy h_t against wellhead pressure p_{wh}. These data and three flowing survey feedzone pressures p_{wf} are shown in Table 1.

In the streamtube model the massflux G and enthalpy h_t are calculated in discrete steps from the liquid saturation pressure p_{sat} to the measured feedzone flowing pressure p_{wf}. This can be done for several effective isentropic efficiencies η_s until the calculated and measured enthalpy are the same. The isentropic efficiency found by this trial-and-error method can then be used to calculate the corresponding massflux and also the effective fracture width w_f. Using the relevant data for well 403 it was determined that $\eta_s = 0.987$ gave a reasonable match between model calculations and field data. Table 2 shows the results. The effective fracture width w_f was found to be about the same for the two data sets, 1.1 mm and 1.2 mm. Using the average effective fracture width of $w_f = 1.15$ mm, the flow characteristics (massflow and enthalpy) of well 403 were calculated at various feedzone pressures p_{wf}, and are shown as solid lines in Fig. 5 along with the two data sets. The effective isentropic efficiency $\eta_s = 0.987$ was used in the model calculations. Choking was estimated to occur when the feedzone pressure becomes less than 6.15 MPa, indicating that the maximum reservoir-well system massflow would be limited to 28 kg/s.

Table 1. Measured Flow Characteristics of Well 403, Tongonan (P.N.O.C. 1981)

Wellhead Pressure P_{wh} (MPa.a)	Feedzone Pressure P_{wf} (MPa.a)	Massflow W (kg/s)	Enthalpy h_t (kJ/kg)
0.95	—	30.2	1440
1.26	3.73*	28.8	1400
1.80	—	26.6	1370
2.46	7.20	22.8	1330
2.58	11.33	9.0	1270

* Estimated from flowing temperature survey.

Table 2. Modified Streamtube Model Calculations for Well 403

Feedzone Pressure P_{wf} (MPa.a)	Flowrate W (kg/s)	Massflux G (kg/m²s)	Area A (m²)	Fracture Width w_f (mm)
3.73	28.8	34,088	0.00084	1.2
7.20	22.8	29,063	0.00078	1.1

Model calculations have also been compared to field data from Roosevelt Hot Springs in Utah (Butz & Plooster 1979) and Krafla in Iceland (Stefansson & Steingrimsson 1980). For well 12 in Krafla, which has a choking flowrate of 6.7 kg/s, the effective fracture width was estimated at 0.3 mm when using an effective isentropic efficiency of 0.950. The reservoir-well system was estimated to be choked below a feedzone pressure of about 10 MPa. Well 14-2 in Roosevelt Hot Springs was calculated to become choked below a feedzone pressure of 3.44 MPa at a production rate of 75 kg/s. The effective fracture width was estimated at 3.8 mm and 4.1 mm for two data sets. The effective isentropic efficiency used in the calculations was 0.995. At high

wellhead pressures well 14-2 flashes in the wellbore. Bodvarsson (1981) has derived an expression that relates pressure drop and massflow in fractures under conditions of liquid flow. When this expression is applied to well 14-2 the effective fracture width is estimated as 4.1 mm and 4.5 mm for the two data sets which are available for when flashing occurs in the wellbore. The agreement with the two-phase flow estimates is more than reasonable.

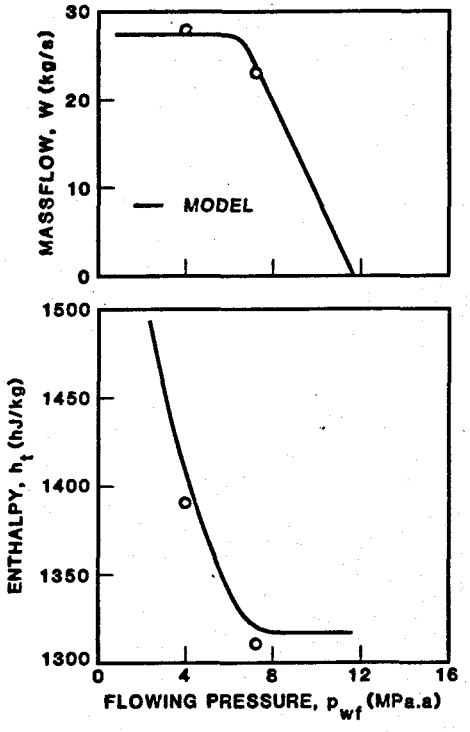

Fig. 5 Calculated massflow and enthalpy of well 403, Tongonan

CLOSURE

In this paper a new approach to two-phase flow in geothermal reservoir-well systems is reported. The approach concerns the gross assumptions that are made about the nature of flashing flow in fractures and how two-phase mixtures can enter a well. The work is based on a critical two-phase flow model which was developed for pipes and nozzles. By using the modified streamtube model it is possible to study flashing flow processes and make comparisons with field data. When this was done for wells with two-phase feedzones the results were found to be encouraging.

The notion that flashing in two-phase feedzone wells may in general occur close to the wellbore seems to be supported by the results of this study: the streamtube model appears to apply and; the flashing mixture approaches the reservoir rock temperature only to a limited extent.

It seems that critical two-phase flow can occur in fractures in geothermal reservoir-well systems. The choking behavior of some two-phase feedzone wells may be due to critical flow in fractures near the wellbore. Heat transfer from reservoir rock to a flowing two-phase mixture will lower the maximum flowrate a fracture can feed into a well.

The fracture width in geothermal reservoirs seems to be a few mm or less when estimated for two-feedzone wells. The streamtube model assumes frictionless two-phase flow which may not be true in narrow fractures. Although heat transfer from the rock formation to the flashing fluid would tend to counteract frictional effects, the effective fracture width would be larger if friction was indicated in the modified streamtube model.

ACKNOWLEDGEMENT

This work was in part supported by the Geothermal and Hydropower Technologies Division of the U.S. Department of Energy through contract DE-AT03-80SF11459.

REFERENCES

Bodvarsson, G. (1981): "Interstitial Fluid Pressure Signal Propagation Along Fracture Ladders," Proceedings, Seventh Workshop on Reservoir Engineering, Stanford University, SGP-TR-55, 139-141.

Butz, J. and Plooster, M. (1979): "Subsurface Investigations at the Roosevelt KGRA, Utah," Denver Research Institute, University of Denver, Report DOE/ET 28389-1.

Menzies, A. J. (1982): "Flow Characteristics and Relative Permeability Functions for Two-Phase Geothermal Reservoirs From A One Dimensional Thermodynamic Model," Stanford Geothermal Program, Stanford University, Report SGP-TR-59.

Philippine National Oil Company (1981): Unpublished data.

Stefansson, V. and Steingrimsson, B. (1980): "Production Characteristics of Wells Tapping Two-Phase Reservoirs at Krafla and Namafjall," Proceedings, Sixth Workshop on Geothermal Reservoir Engineering, Stanford University, SGP-TR-50, 49-59.

Wallis, G. B. (1980): "Critical Two-Phase Flow," Int. J. Multiphase Flow, 6, 97-112.

Wallis, G. B. and Richter, H. J. (1978): "An Isentropic Streamtube Model for Flashing Two-Phase Vapor-Liquid Flow," J. Heat Transfer, 100, 595-600.

Proceedings Eighth Workshop Geothermal Reservoir Engineering
Stanford University, Stanford, CAlifornia, December 1982
SGP-TR-60

DESCRIPTION OF GEOTHERMAL RESERVOIR SIMULATOR "NSCGREATS" AND A PRELIMINARY SIMULATION OF THE KIRISHIMA FIELD

Masaharu Tachimori

Process Technology R&D Laboratories,
Nippon Steel Corporation
Kitakyushu City, Japan 805

Abstract

Anumerical simulator for geothermal reservoirs (NSCGREATS) is presented, that includes sub-simulator for flow in geothermal wells. The flow in reservoir is expressed on the basis of mass and energy transport in porous media. The flow toward the well in the wellblock are treated as a steady horizontal radial flow. The vertical flow in geothermal wells is expressed by a new set of correlations. Its details are presented in another paper by the author in these proceedings.

NSCGREATS has been applied to a preliminary simulation of the Kirishima geothermal field. The simulation revealed several mechanisms at work in the transition of the reservoir. The important mechanisms are: (1) steam/water counterflow which forms a steam cap in shallow levels but remains liquid water at deep levels, and (2) recharging from outside of the reservoir which compensates for production to a considerable extent. It has been predicted by the simulation that an enthalpy of 1500 GJ/h may be produced by wells drilled at intervals of 200m in a main fault zone having a length of 1.2Km. However, further investigations into the deep levels in the field are necessary to make more accurate prediction, since production depends strongly on recharging from the fluid source deep below the reservoir.

Introduction

A computer simulator for geothermal reservoirs called NSCGREATS has been developed by the author. It is a three-dimensional and distributed parameter model, applicable to compressed water, superheated steam and two-phase steam-water reservoirs. Compaired to the other simulators that have been presented in previously published literature, the main distinctive feature of NSCGREATS is that it includes the simulation of flow in wells and makes it possible to perform simulations under the practical conditions prescribed at well heads. The numerical model for the flow in qeothermal wells used in NSCGREATS has also been developed by the author and its details are reported in another paper presented at these proceedings.

NSCGREATS is now in practical use for preestimating the characteristics and the performance of the reservoirs and wells at the Kirishima geothermal field in Japan that is currently under development now. The results of a preliminary simulation of the Kirishima geothermal field is presented in this paper.

1. Description of simulator

Equations

Basic equations of fluid and energy transport in geothermal reservoirs, used in this simulator, are mass and energy conservation equations and Darcy's flow equation, using the assumptions given below.

Assumptions:
1) All rock properties are independent of temperature, pressure, and vapor saturation.
2) Liquid, vapor, and rock are in local thermodynamic equilibrium.
3) Capillary pressure is ignored.
4) Kinetic energy and potential energy are ignored.
5) Momentum balance is not considered.

Coupled equations for the conservation of mass and energy are solved in terms of fluid specific internal energy u and density ρ. Advantages of this formulation are that variables u and ρ are continuous and single-valued beyond phase changes, and that u and ρ are directly related to the conserved quantities of mass and energy.

The numerical method used for space discretization of equations of mass and energy is an integrated finite difference method. This method maintains conservative properties of the original differential equations in the numerical equations for the discretized system, so that abnormal phenomena caused by cumulative errors are eliminated. Besides that this method makes it easy to deal with boundary conditions. Time is discretized fully-implicitly as a first-order finite difference. The weighted upstream method is used to calculate the mass and energy fluxes between grid blocks. It uses the fluid properties of the upstream grid block. Nonlinear finite difference equations are solved using the Newton/Raphson method and the SSOR method.

The basic equations and the finite difference equations are similar to those used by Pruess et al. [1], [2], their descriptions are not presented here.

Production condition

This simulator is available for the production conditions that prescribe the pressure or discharge rate at well heads, as well as that prescribe sinks/sources at wellblocks, because it is provided with the sub-simulator for the flow in geothermal wells. At the beginning of each time step, the production rates and the pressure drops in the well and in the formation around the well are calculated on the basis of the last calculated state of the wellblocks. The calculated production rates are assigned to the blocks as explicit sink/source terms for the calculation of mass and energy transport between blocks in the new time step. The correlation of wellbore pressure P_W and block pressure P_B is expressed as follows using the assumptions below.

$$P_W - P_B = \frac{W \ln (r_e/r_w)}{2\pi kH\left(\frac{K_g}{\nu_g}+\frac{K_\ell}{\nu_\ell}\right)} \quad (1)$$

$$r_e = \gamma(\Delta x\ \Delta y)^{\frac{1}{2}} \quad (2)$$

where W is mass flow rate, H open interval in a well, r_W wellbore radius, Δx, Δy well block spacing.

Assumptions:
1) Flow toward the wellbore in the wellblock is steady, horizontal radial flow.
2) Steam and water flow rates are proportional to the ratios of the relative permeability k_g, k_ℓ and the kinematic viscosity ν_g, ν_ℓ or each phase [3].
3) Relative permeabilities are uniform along the radial direction and take the values calculated from the state of the wellblock.
4) The absolute permeability k in Eq.2 is evaluated as the arithmetic average of its directional components.

Factor γ of effective radius r_e takes the value proposed by van poollen [4] in most cases and those by Pritchett [5] in special cases of two dimensional simulations.

Boundary condition

The following boundary conditions, allowing any overlaps, satisfy various boundary conditions encountered in reservoir simulations.
1) Prescribed mass or energy fluxes through the boundary.
2) Prescribed fluid and rock properties at prescribed distances outside the boundary.

2. Preliminary simulation

Outline of the Kirishima field

The Kirishima geothermal field that Nippon Steel Corporation and Nittetsu Mining Company have been developing is located 2km west of the Kirishima group of volcanoes in the southern part of Kyushu island, Japan. The area of our field is about 15km². Geological, geophysical, and geochemical surveys have been carried out to locate wide regions of hydrothermal alteration, low electric resistivity, and several faults. The prominent faults run from SW to NE and along them on the surface are found hydrothermal alteration zones, hot springs and fumaroles. They could be considered to penatrate into the basement. To date, three test wells have been drilled by NSC and NMC in the northern quarter of the area. These have been tested to examine subsurface structures and reservoirs. Figure 1 shows a cross section of the area, including some speculations on deep layers. The area is one of andesitic volcanism, and lavas are in layers with a thin layer of tuff breccias and sediments between them. Underlying the lavas are the Kirishima welded tuffs, which are of very poor permeability, and the Shimanto Group of sediments, which is considered the basement. The hydrothermal alteration of andesites has several zones with increasing depth. At shallow levels the alteration mineral assemblage is Montmorillonite-Crystobalite-Tridymite-Pyrite. Below a depth of about 400m it is Chlorite-Quartz-Calcite-Sericite-Wairakite-Laumontite-Epidote. Table 1 shows the results of well test analysis. The major permeable formations are associated with faults and the second permeable formations are tuff breccias and sediments. The andesitic lavas have some fractures in them, but they are generally of poor permeability. The pressures and temperatures at the main feed zones and the fluid enthalpies indicates that fluids in the prominent fault are saturated water or steam-water mixtures and in other formations are compressed water. It is estimated that permeable formations of faults, tuff breccias, and sediments from a depth about 400m to the top of the welded tuffs form reservoirs in this area, and that promi-

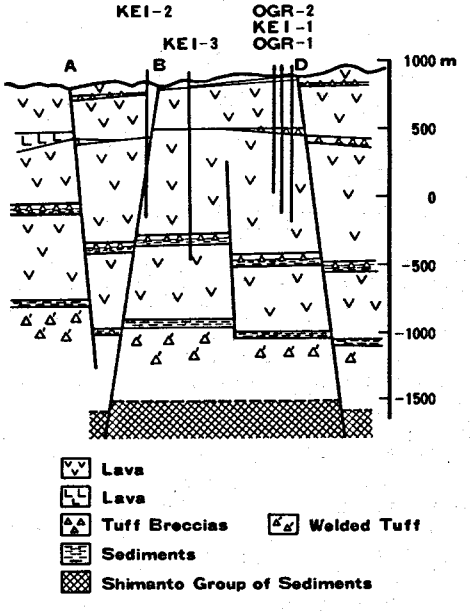

Figure 1. Cross section of the northern part in the Kirishima field, showing the positions of wells. OGR-1, 2 are the MITI's wells.

Table 1. Results of Well Test Analysys

MAIN FEED ZONE

WELL	FORMATION	DEPTH m	TEMPERATURE °C	PRESSURE MPa	FLOW-CAPACITY Darcy.m	FLUID ENTHALPY kJ/kg
KE1-1	LAVA	820	190	3.5-3.8	0.07	170
KE1-2	FAULT	560	225	2.8	5-10	440
KE1-3	T.B.S.*	1170	230	5.0	0.5	220

* T.B.S. is indicates formations of tuff breccias and sediments.

Table 2. Rock Properties for Simulation

FORMATION	PERMEABILITY md	POROSITY	DENSITY kg/m³	SPECIFIC HEAT kJ/kg	THERMAL CONDUCTIVITY J/sm°C
FAULT	100	.20	2200	1.	1.75
T.B.S	10	.15	2200	1.	1.75
LAVA	1	.10	2200	1.	1.75

nent faults form the main passages for geothermal fluids rising from deep sources.

Before going to the next stage of development, a preliminary simulation was performed in order to evaluate energy production rate tapped by a well located at a prominent fault (indicated as 'B' in the Figure 1), and to study transition of the reservoir.

Reservoir modeling and rock properties

A vertical cross section of the reservoir was chosen which extends from SE to NW across the main fault. Figure 2 shows the finite-difference grids and the simplified subsurface structure. The region has a width of 200m, a length of 1100m, and a height of 1400m (i.e. from 400 to 1800m in depth). The structure is assumed to be symmetrical on both sides of the main fault. Table 2 presents the rock properties of the formations, which were obtained from well tests and drilled-core investigations.

Initial state

Since the temperature and pressure data from test wells were not enouth to cover the distribution of temperature and pressure of the whole area concerned, several simulations were tried to reproduce the pressures and temperatures observed in the test wells and the natural leakage of fluid and enthalpy on the ground surface. This procedure is similar to that used by Mercer et al. [6]. To maintain the ground surface leakage in the steady state, a fluid and energy source had to be considered to supply geothermal fluids to the reservoir through the bottom boundary of the main fault. The initial pressure distribution is shown in Figure 3, and the initial temperature distribution in Figure 4. Slow circulation of flow is characteristic of the natural steady state. Fluids flow upward along the main fault, and downward along the subfaults.

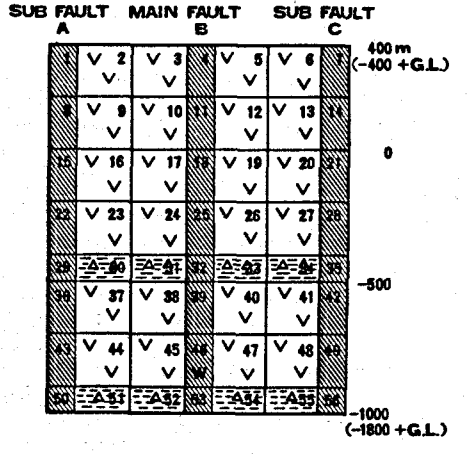

Figure 2. Simplified geological structure and finite difference grids used in the simulation. W indicates well position, and numbers in grids are sequential block numbers.

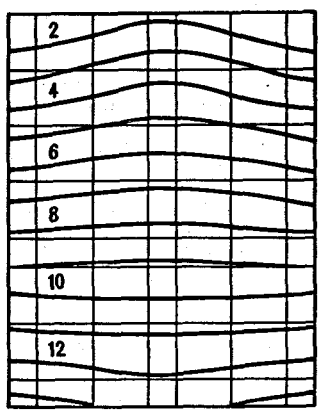

Figure 3. Initial pressure (MPa) distribution.

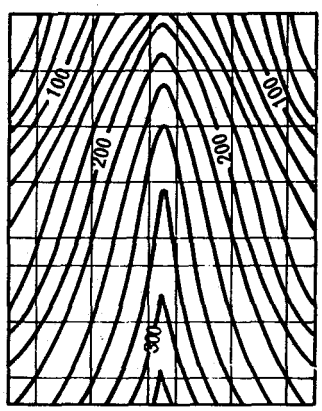

Figure 4. Initial temperature (°C) distribution.

Boundary condition

All boundaries of lava layers are assumed to be in the no-flow condition. Leakage only through the bounderies of permeable formations are considered. At 75m above the top boundaries of the faults the ground-water surface is prescribed, which is balanced against the initial pressure at the top blocks in the subfaults. At 1500m below the bottom boundary of the main fault a geothermal source almost in the critical state is prescribed. At 1000m outside the side boundaries of the tuff breccia formations, pressures, temperatures and vapor saturations are prescribed to keep constant values equal to the initial values at the blocks just inside the boundaries.

Production condition

One well is located in the main fault zone at a depth of 1600m, that is, in the No.46 block. The inner diameter of the well is chosen at 240mm. The well-head pressure is prescribed to keep a constant value of 1 MPa.

Results and discussion

The transitions of the total fluid (i.e. steam + water) and steam production rates are shown in Figure 5, that of the enthalpy produced in Figure 6. Production is large at first, but decreases rapidly and becomes steady because of pressure drops. In steady state an enthalpy of 250 GJ/h is produced. Since the main fault is known to extend for 1.2Km, an enthalpy of 1500 GJ/h may be expected in the whole fault. The recharge increases with time, and compensates for production to a considerable extent. About 70% of the recharge comes in through the bottom boundary of the main fault.

The pressure transitions in the main fault are shown in Figure 7. As a consequence of production, pressure drops in the wellblock, so that flow toward the well is initiated. The pressure decline spreads rapidly through the whole reservoir region. In shallow blocks pressure drops continue for a long term because of boiling. As shown in Figure 10, pressure drops are large in the main fault, which is the production zone.

Temperature behaviors in the main fault are similar to that of pressure, as seen in Figure 8. The temperature in the well field is maintained by hot fluid recharge through the botom boundary of the main fault. As shown in Figure 11, temperature drops are prominent in the main fault above the wellblock, in the subfaults, and in the holizontal permearble formations. They are cooled by the cool water initially stored in the shallow region, and by recharge of cold water through the top boundaries of the faults.

Figure 9 shows the transition in vapor saturation in the main fault. Pressure drop causes phase transitions to two-phase conditions and subsequent steam/water counterflow in the main fault zone. Steam rises along the fault and temporally accumulates in the top region of the main fault, whereas water flows downward toward the well field. Continual downflow promotes pressure drops, boiling, and increase of vapor saturation in shallow two-phase regoins that spread consequently to horizontally adjacent blocks,as seen in Figure 12.

The results indicate that the significant changes in the reservoir conditions progresses downward from the top zone, and that the recharge of fluids and energy, especially those supplied through the bottom boundary of the main fault, are very important in maintaining the productive potential of the reservoir. Deeper production wells are less affected by the reservoir transition and recharge themselves readily from the source, thus extending the life of the reservoir.

Conclusion

NSCGREATS made it possible to simulate the coupled systems of the geothermal reservoir and well. The method used in NSCGREATS, which assumes steady horizontal flow around wells, is a practical method. A preliminary simula-

Page missing from original document

Page missing from original document

Proceedings Eighth Workshop Geothermal Reservoir Engineering
Stanford University, Stanford, California, December 1982
SGP-TR-60

A NUMERICAL SIMULATION MODEL FOR VERTICAL FLOW IN GEOTHERMAL WELLS

Masaharu Tachimori

Process Technology R&D Laboratories,
Nippon Steel Corporation
Kitakyushyu-City, Japan 805

Abstract

This paper presents a numerical simulation model for vertical flow in geothermal wells. The model consists of equations for the conservation of mass, momentum, and energy, for thermodynamic state of water, for friction losses, for slip velocity relations, and of the criteria for various flow regimes. A new set of correlations and criteria is presented for two-phase flow to improve the accuracy of predictions; bubbly flow - Griffith and Wallis correlation, slug flow - Nicklin et al. one, annular-mist flow - Inoue and Aoki and modified by the author. The simulation method was verified by data from actual wells.

Introduction

Numerical simulation of flow in geothermal wells are useful for evaluating downhole pressures, temperatures, enthalpies, and steam qualities from those at well heads, for predicting producible steam and water flow rates by production wells on the basis of data about the reservoir characteristics obtained from wildcat wells, and for designing proper casing programs for wells.

Simulation methods for flow in oil wells have been applied to flow in geothermal wells with a heat transfer equation by several authors [1]-[3]. However, we found that they are not accurate enough for two-phase flow especially in a well with a small diameter of 3 or 4 inches.

A number of correlations for two-phase flow discussed in existing literature have been examined and a set of correlations has been selected to improve the accuracy of calculated values. A new relationship has been developed to deal with the annular-mist flow regime.

Flow equations

Flow in geothermal wells has a variety of configurations, such as subcooled water flow, water-steam mixture flow, and superheated steam flow. In the description of flow equations, subcooled water flow and superheated steam flow are regarded as particular cases of two-phase flow with steam fraction 0 and 1 respectively. Two-phase vertical flow is expressed by the separate and slipping flow model (Figure 1). Water and steam phases are assumed to be in local thermodynamic equilibrium. The steady flow equations are given as follows.

Mass conservation equation

$$\rho_g v_g f_g + \rho_\ell v_\ell (1 - f_g) = W_s \qquad (1)$$

Momentum conservation equation

$$[\rho_g v_g^2 f_g + \rho_\ell v_\ell^2 (1 - f_g) - P + \{\tau + (\rho_g f_g + \rho_\ell (1 - f_g))g\} dz] A = [\rho_g^\circ v_g^{\circ 2} f_g^\circ + \rho_\ell^\circ v_\ell^{\circ 2} (1 - f_g^\circ) - P^\circ] A^\circ \qquad (2)$$

Energy conservation equation

$$[\rho_g v_g f_g (\tfrac{1}{2} v_g^2 + h_g) + \rho_\ell v_\ell (1 - f_g)(\tfrac{1}{2} v_\ell^2 + h_\ell) + (W_s g + Q) dz] A = [\rho_g^\circ v_g^\circ f_g^\circ (\tfrac{1}{2} v_g^{\circ 2} + h_g^\circ) + \rho_\ell^\circ v_\ell^{\circ 2} (1 - f_g^\circ)(\tfrac{1}{2} v_\ell^{\circ 2} + h_\ell^\circ)] A^\circ \qquad (3)$$

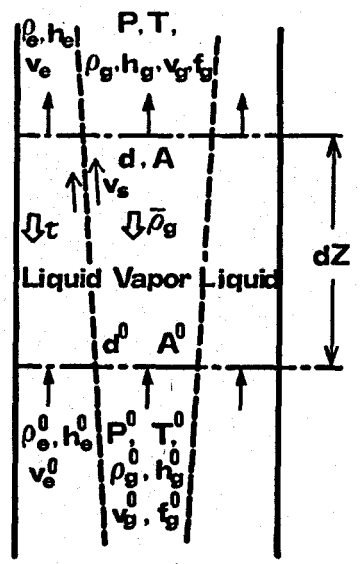

Figure 1. Separate and slipping two-phase flow model.

The acceleration term in Eq.2 has often been neglected by other authors [1]-[3], except in the annular-mist flow regime, however, in case of geothermal wells acceleration is important for slag flow, as well.

Dependent unknown variables of the equations are temperature T, depth increment dz, and velocity v_g or v_ℓ for single-phase flow, steam fraction f_g, depth increment dz, velocities v_g and v_ℓ for two-phase flow.

In addition to the above three conservation equations, equations of the friction loss gradient, of the slip velocity relationships, and of the fluid state, are required.

Flow regimes

The configuration of steam-water two-phase flow is complicated and usually divided into three or four flow regimes [1]-[3]. In the present work, three flow regimes are defined: bubbly flow, slug flow, and annular-mist flow. The correlations employed for each regime are as follows.

Bubbly flow	Griffith and Wallis
Slug flow	Nicklin et al.
Annular-mist flow	Inoue and Aoki as modified by the author

The boundary of bubbly and slug flow regimes is determined by the criteria proposed by Duns and Ros [6], and that of slug and annular-mist by the criteria presented by the author. The experimental results on flashing flow [9] have shown that the slug-annular transition occurrs in the steam fraction range of 0.7-0.8. When steam quality is less than 0.3, a steam fraction of 0.6 is chosen as the criterion for the slug-annular boundary to obtain a smooth transition between the regimes when using the present correlations.

Bubbly flow

$$(q_g/q_t) \le L_B \qquad (4)$$

Slug flow

$$(q_g/q_t) > L_B, \quad \begin{matrix} f_g<0.6 & (\text{when } x<0.3) \\ f_g<0.75 & (\text{when } x\ge 0.3) \end{matrix} \qquad (5)$$

Annular-mist

$$(q_g/q_t) > L_B, \quad \begin{matrix} f_g\ge 0.6 & (\text{when } x<0.3) \\ f_g\ge 0.75 & (\text{when } x\ge 0.3) \end{matrix} \qquad (6)$$

where

$$L_B = 1.071 - 7.14 v_t^2/gD, \quad L_B \ge 0.13$$

Friction loss gradient

The friction loss gradient is basically calculated by a Fanning type of friction law.

$$\tau = \lambda \rho v^2/2D \qquad (8)$$

where the friction factor λ is obtained by entering the Moody diagram with the appropriate Reynolds number N_{Re} and relative roughness of tube ε/D.

Single phase flow

The density, velocity and viscosity values of the phase must be entered in Eq.8 and in the Reynolds number $N_{Re} = vD/\nu$.

Bubbly flow

As the gas bubbles are dispersed inside the liquid and rise with small slip velocities, they have little effect on the friction losses.

$$\tau = \lambda \rho_\ell v_\ell^2/2D \qquad (9)$$

where λ is determined as a function of $N_{Re} = v_\ell D/\nu_\ell$.

Slug flow

The friction losses are mainly caused by liquid slugs, at the center of which liquid velocities are nearly equal to the mean fluid velocity.

$$\tau = \lambda \rho_\ell (1-f_g) v_t^2/2D \qquad (10)$$

where λ is determined as a function of $N_{Re} = v_\ell D/\nu_\ell$.

Annular-mist flow

According to Inoue and Aoki [7], the friction loss gradient is calculated by multiplying the friction loss gradient associated with the specific liquid velocity by the factor R, as shown in Eq.11 and 12.

$$\tau = R\lambda W_s^2/\rho_\ell/2D \qquad (11)$$

$$R = 1 + 250[x/(1-x)] \qquad (12)$$

Their equations give rather large values for friction losses compared to observed pressure drops in geothermal wells. Instaed of them the following equations are used in the present work.

$$\tau_\ell = \lambda_\ell \rho_\ell v_\ell^2 (1-f_g)^2/2D \qquad (13)$$

$$\tau_g = \lambda_g \rho_g v_g^2 f_g^2/2D \qquad (14)$$

$$\tau = \gamma \tau_g x + \tau_\ell (1-x) \qquad (15)$$

where λ_ℓ and λ_g are determined as a function of $N_{Re\ell} = v_\ell (1-f_g) D/\nu_\ell$ and $N_{Reg} = v_g f_g D/\nu_g$ respectively. γ is about 0.7.

Slip velosity

Bubbly flow

Experimental results [9] indicate that the slip velocities, $v_g - v_\ell$, are independent of the tube size and are approximately constantsat 20-30 cm/s when tube diameters are greater than five times the effective diameter of the bubbles. In the present work a constant slip velocity of 24cm/s suggested by Griffith and Wallis [4] is used.

Slug flow

Gas slug velocity has been given by Nicklin et al. [5]. Its relationship is rewritten as follows.

$$v_s = [v_g + 1.75\ (gD)^{\frac{1}{2}}]/6(1-f_g) \qquad (16)$$

Annular-mist flow

Inoue and Aoki [7] have proposed a slip velocity relationship that is valid from the slug flow regime to the annular. It is given as follows.

$$v_s = \alpha[v_\ell(1-f_g)]^\beta x \qquad (17)$$

where

$$\alpha \approx \rho_\ell/\rho_g$$
$$\beta \approx 1 \qquad (18)$$

Eq. 17 can be rewritten as follows.

$$v_s = (W_s/\rho_g)x(1-x) \qquad (19)$$

Thermodynamic properties of the fluids

The densities ρ_g, ρ_ℓ, the enthalpies h_g, h_ℓ, the kinematic viscosities ν_g, ν_ℓ are obtained from the equations prepared by the International Formulation Committee of the Sixth International Conference on the Properties of steam.

Computational procedure

The flow chart of the numerical simulator is presented in Figure 2. The outline of the computational procedure follows.

1. Input the casing geometries and the flow conditions either at the well head or at the well bottom: pressure, temperature, steam flow rate and water flow rate.

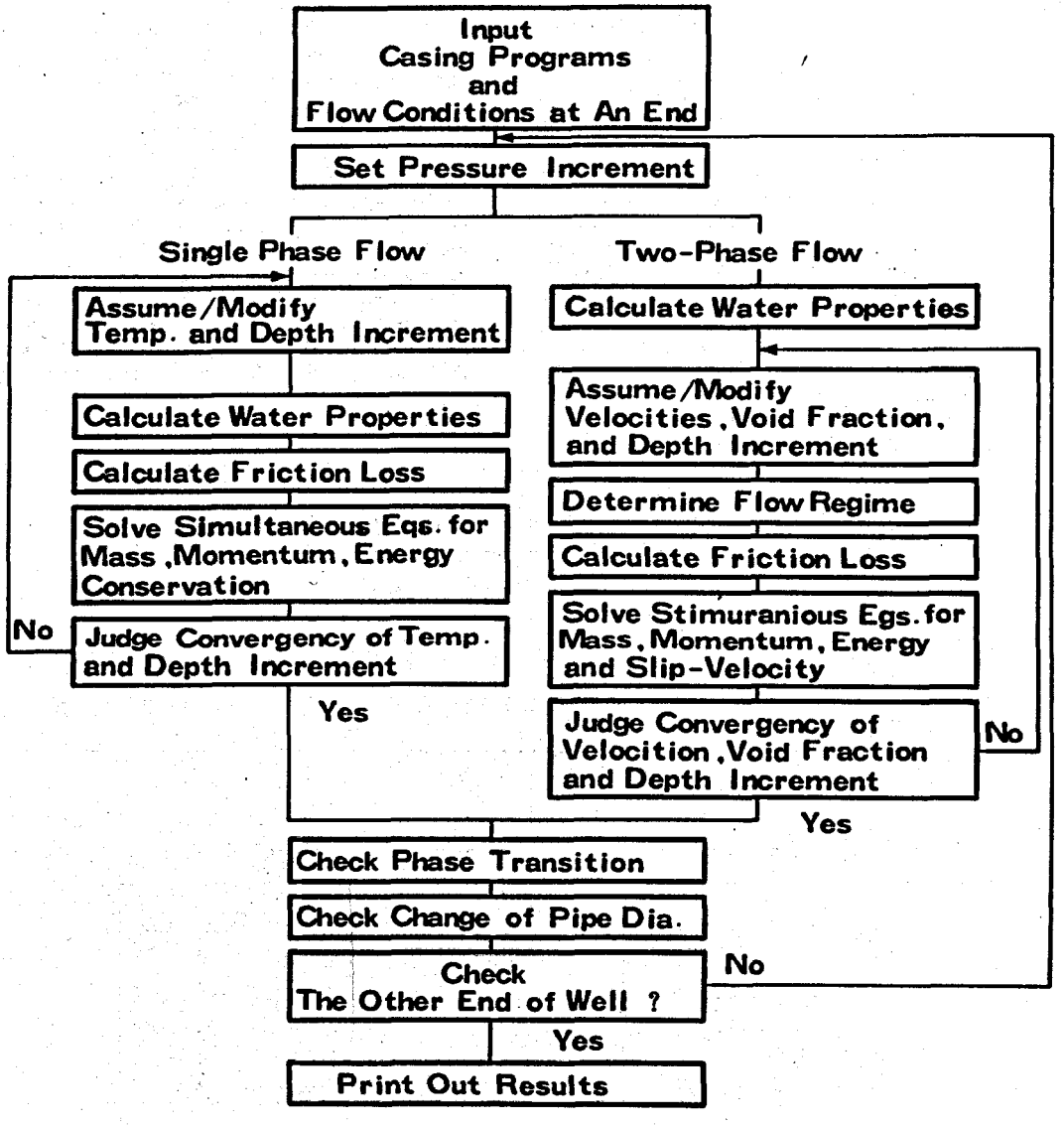

Figure 2. Flow chart of simulation for flow in geothermal wells.

2. Set the pressure increment and determine thermodynamic properties of the fluids.
3. Assume a flow regime, calculate the friction loss gradient and chose the appropriate slip velocity relationship.
4. Solve the coupled equations for mass, momentum, energy conservation and slip velocity by means of the Newton-Raphson method.
5. Check whether the flow regime determined from the calculated values of steam and water flow rates, and of steam fraction, is the same as the assumed one. When they differ, repeat the procedures 3 - 5. When they agree, return to 2 and go to the next pressure increment.
6. Repeat the procedures 2 - 5 until reaching the other end of the well.

Verification of model

To test the validity of the model, the numerical simulator developed was applied to well KE1-3 which was drilled in the Kirishima geothermal field by Nippon Steel Corp. and Nittetsu Mining Co., and to HGP-A in Hawaii.

Table 1 presents the completion characteristics of the KE1-3, and Table 2 the well head conditions of KE1-3 during the well tests. During discharge a Kuster pressure instrument was put down into the well and remained for a few minutes at every one hundred meters to measure pressure. Figure 3 shows the predicted and measured pressures at KE1-3. The calculated results indicate that the subcooled water flow is at deep levels and above it apper the slug and annular flow. Although the predicted pressures near the well head are slightly lower than measured ones, as a whole they agree well.

The other test was performed using the data published on HGP-A in Hawaii [8]. Since HGP-A has high steam quality, it was interesting to test the validity of the correlation for the annular-mist regime which had never been examined in the high quality ranges. The well head conditions of HGP-A during flashing are referenced and shown in Table 3. HGP-A is cased by a pipe (9×5/8 in.) to a depth of 2500 ft and below it is liner pipe (7×5/8 in.). Its bottom is at a depth of 6450 ft. Figure 4 shows the predicted and actual pressures on HGP-A. The agreement is fairly good.

Conclusion

1. A numerical simulation model has been presented for vertical flow in geothermal wells. The algorism is based on the coupled equations for mass, momentum, and energy conservation. Friction losses and slip velocities are calculated to the phase and the flow regime at each point in a well.
2. A new set of correlations has been proposed to improve the accuracy of the predicted values for two-phase flow. The Griffih and Wallis correlation is used for bubbly flow regime, the Nicklin et al. correlation for slug flow regime, and the Inoue and Aoki correlation, which has been modified by the author, for annular-mist flow regime. A new criteria on the boundary of the slug and annular-mist flow regimes has also been presented.
3. The method has been tested for validity on three cases of a water-dominated actual well, and on four cases of a vapor-dominated well. Although in all cases the heat losses to the formation were not considered, good agreement between the predicted and observed values was obtained.

Table 1. Completion characteristics of KE1-3.

Cased Depth m	Liner Length m	Casing Pipe I.D. mm	Slotted Liner I.D. mm	Feed zone Depth m
885	316	102.3	67	1170

Table 2. Well head conditions of KE1-3 during well test.

Test	Pressure (kg/cm^2G)	Steam Flow RATE (tonne/hr)	Water Flow RATE (tonne/hr)	Enthalpy (kcal/kg)
1	1.40	3.96	17.14	223
2	4.20	1.75	13.47	211
3	2.74	3.11	16.56	222

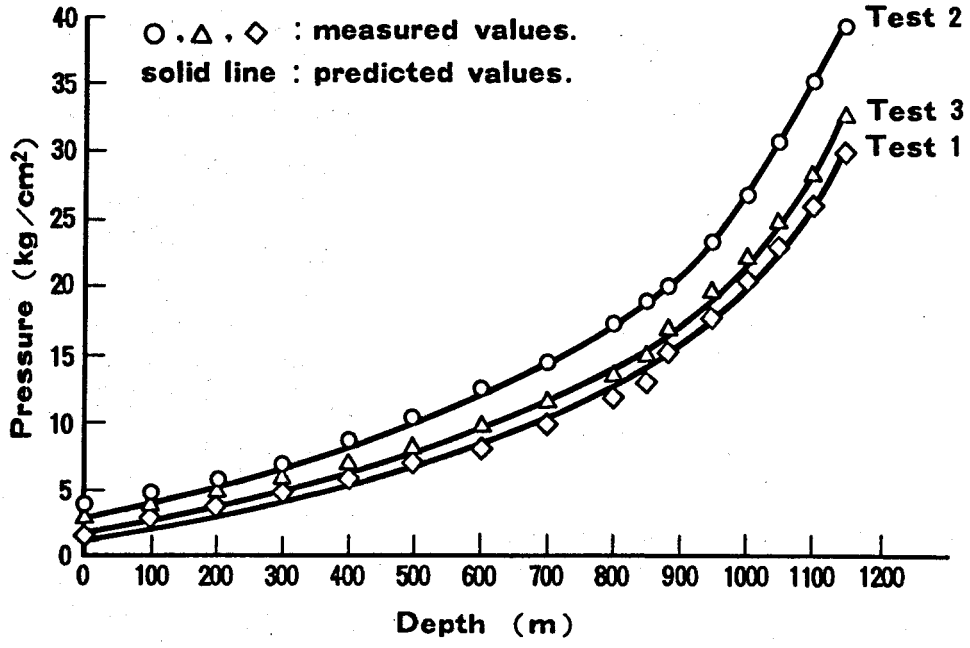

Figure 3. Comparison of measured pressures and predicted pressures on KE1-3 in the Kirishima field.

Table 3. Well head conditions of HGP-A during flashing.

Total Mass Flow Rate (tonne/hr)	Steam Flow Rate (tonner/hr)	Pressure (kg/cm²G)	Temp. (°C)
44.9	31.8	3.8	149
42.2	29.9	7.0	170
38.1	26.3	16.7	205
34.5	22.7	26.4	226

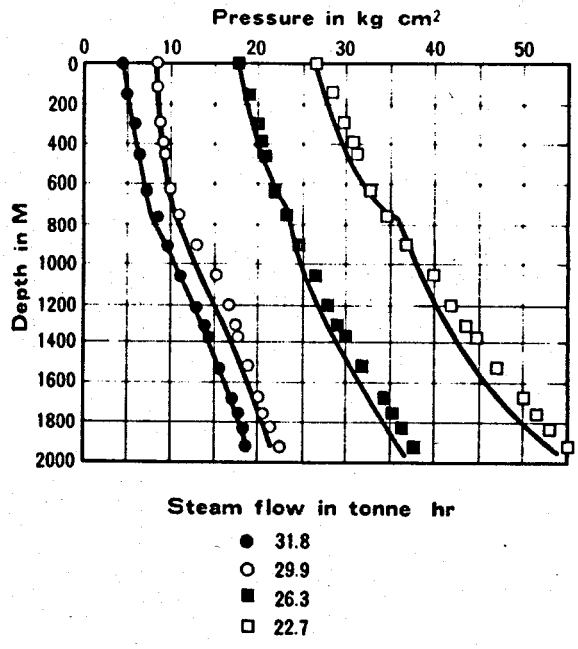

Figure 4. Comparison of measured pressures (symbols) and predicted pressures on HGP-A in Hawaii.

Nomenclature

A = flow area of pipe, m^2
D = pipe diameter, m
dz = depth increment, m
f_g = void fraction, volumetric gas fraction, -
g = acceleration of gravity, m/s^2
h_g = specific enthalpy of gas, J/kg
h_ℓ = specific enthalpy of liquid, J/kg
N_{Re} = Reynolds number, -
P = pressure, Pa
Q = heat loss to surroundings, J/sm
q_g = volumetric flow rate of gas, m^3/s
q_ℓ = volumetric flow rate of liquid, m^3/s
q_t = volumetric flow rate of fluid, m^3/s
T = temperature, °C
v_g = velocity of gas, m/s
v_ℓ = velocity of liquid, m/s
v_s = slip velocity, m/s
v_t = mean velocity of two-phase flow, m/s
W_t = mass flux of fluid, kg/m^2s
x = quality, -
ε = pipe wall roughness, m
λ = Moody friction factor,
μ_g = dynamic viscosity of gas, Ns/m
μ_ℓ = dynamic viscosity of liquid, Ns/m
ν_g = kinematic viscosity of gas, m^2/s
ν_ℓ = kinematic viscosity of liquid, m^2/s
ρ_g = density of gas, kg/m^3
ρ_ℓ = density of liquid, kg/m^3
τ = friction loss gradient, N/m

Ackowledgment

I express my appreciation to the management of Nippon Steel Corporation for the permission to publish this paper. I thank M. Fujiura, Dr. I. Yoshida, and Y. Monden for their encouragement and suggestions regarding this work. I am also indebted to Dr. S. Sugawara and the members of the Geothermal Resources Development Office of NSC for their field data and consultations.

References

1. Gould, T. L.: Vertical Two-phase Steam-Water Flow in Geothermal Wells, J. Pet. Tech., (Aug. 1974) 833-842
2. Sugiura, T. : A Comprehensive Wellbore Steam-Water Flow Model For Steam Injection and Geothermal Application, Paper SPE 7966 AIME (1979)
3. Fandariana, L., Sanyal, S. K. and Ramey, H. J. Jr.: A numerical Simulator for Heat and Fluid Flow in a Geothermal Well, Department of Petroleum Engineering Scool of Earth Science, Stanfod Univ. Stanford, California, (Oct. 1981)
4. Griffith, P. and Wallis, G. B.: Two-Phase slug Flow, J. Heat Transfer, Trans, AIME (Aug. 1961) 307-320
5. Nicklin, D. J., Wilkes, J. O. and Davison, J. F.: Two-Phase Flow in Vertical Tubes, Trans., Chem Eng., (1962) 40, 61-68
6. Duns, H. Jr. and Ros, N. C. J.: Vertical Flow of Gas and Liquid Mixtures in Wells, Proc. Sixth World Pet. Congress, Frankfurt (1963) Sec. paper 22-PD6, 451-465
7. Inoue, A. and Aoki, N.: Kannai Nisoryu no Atsuryoku Sonshitsu ni kansuru Kisoteki Kenkyu (II), Trans. Japan Soc. Mech. Eng. (Part 2), (1966), 32, (238), 940-94
8. Univ. of Hawaii: Hawaii Geothermal Project, Phase III - Well Testing and Analysis, DOE-ET-28302-T-11, 1977
9. Sekoguchi, K.: Kieki Nisoryu, Den Netsu Kogaku no Sinten, Yokendo, Tokyo 1973

Proceedings Eighth Workshop Geothermal Reservoir Engineering
Stanford University, Stanford, California, December 1982
SGP-TR-60

RESISTIVITY MONITORING OF FLUID MIGRATION AT THE CERRO PRIETO GEOTHERMAL FIELD

N.E. Goldstein, K. Pruess, M.J. Wilt, and G.S. Bodvarsson

Earth Sciences Division
Lawrence Berkeley Laboratory, University of California
Berkeley, California 94720

ABSTRACT

Apparent resistivities, measured by means of repetitive, dipole-dipole dc resistivity surveys since 1979, show significant and somewhat systematic changes over the area of the Cerro Prieto "α" reservoir. These changes are attributed to temperature and salinity changes, consequences of production, and natural recharge. To better understand the observed geophysical phenomena, we performed a series of simple reservoir simulation studies combined with the appropriate dc resistivity calculations to determine the magnitude and form of resistivity change. We considered production from a liquid-dominated reservoir with dimensions and parameters of the Cerro Prieto α reservoir and assumed lateral and vertical recharge of colder, less saline waters. The associated apparent resistivities increase 10 to 20% over the production area during a 3 year period at the current rate of production. These calculated changes agree in magnitude with the observed changes for the same production period. However, displayed in conventional pseudosection form, the patterns of calculated resistivity change only partially resemble the observed data. This is explained by the fact that natural recharge into the α reservoir is more complicated than our simple two-dimensional schematic recharge model. It is concluded that if properly conducted, dc resistivity monitoring appears capable of providing indirect information on fluid flow processes, including reinjection in a producing reservoir. Such information is extremely valuable for the development of quantitative predictions of reservoir performance.

INTRODUCTION

Since the inception of the joint U.S. Department of Energy (DOE) - Comisión Federal de Electricidad (CFE) reservoir engineering project to study the Cerro Prieto Geothermal Field, LBL and CFE have conducted numerous dc resistivity surveys to help define the reservoir and map subsurface structures and thermal conditions. Beginning in 1978, we have undertaken repetitive resistivity measurements along one long line that passes directly over the producing reservoir on the assumption that reservoir parameters altered by production might be indirectly monitored from the surface. This technique was suggested by Risk's studies at the Broadlands Geothermal Field (Risk, 1975). Recently, similar investigations have also been extended to monitoring formation resistivity changes accompanying tertiary oil recovery (Bartel and Wayland, 1981).

Since 1979, when we were satisfied our field technique produced high quality data, we have observed rather systematic changes in apparent resistivities that could be caused by several possible hydrological, thermophysical and thermochemical mechanisms (Wilt and Goldstein, 1981a, 1981b). (i) natural recharge of less saline ground waters, (ii) coalescence of two-phase zones near the wells into a more extensive two-phase region, (iii) gradual cooling, and (iv) porosity reduction due to the precipitation of zeolites and carbonates as cooler waters react with the hotter rocks near the reservoir boundaries.

When the apparent resistivity changes were first noticed, we attempted to explain them using simple conjectured resistivity models (Wilt and Goldstein, 1981a). The results were unconvincing, and we therefore studied the problem in a more rigorous fashion. First we applied numerical modeling techniques to map the migration of waters of different temperature and salinity in response to production. Next we used computed changes of temperature and salinity within volume elements of the numerical model to estimate changes in apparent resistivity that would be observed at the surface. Although our studies employ rather schematic and simplified reservoir models, they demonstrate the technique of combining reservoir engineering and geophysical methods for reservoir monitoring.

RESISTIVITY CHANGES OVER THE RESERVOIR

Figure 1 shows in pseudosection form the magnitude and pattern of resistivity change relative to baseline data collected in the Fall of 1979. The field data were collected using the dipole-dipole array with a dipole length of 1.0 km and dipole separations n from 1 to 8 (n = integer multiples of the dipole length). Results are plotted at the intersection of the 45° diagonals subtended from the mid-points of the

transmitter and receiver dipoles. In these pseudosections the n-spacing bears a rough relationship to depth of exploration. For example, at n=1 most of the information comes from the upper 600 m, whereas at n=8 most of the information is a volume averaged composite of the upper 2 km. The α production zone lies approximately between resistivity electrodes 10 and 12 at a depth of 1.1 to 1.4 km. However, as lateral discontinuities in resistivity manifest themselves as diagonal stripes on a pseudosection, data points having a high information content of resistivity change within the reservoir would occur along diagonals centered at station 11 and particularly at n-spacings of 5, 6, and 7. The dipole-dipole electrode array was used in this study because it is sensitive to lateral discontinuities in subsurface resistivity, even when these occur beneath a conductive overburden layer (Beyer, 1977).

It may be observed in Figure 1 how resistivity changes have evolved with time and how by the Fall 1981, 2.5 years after the baseline data set was collected, a definite resistivity increase developed along the western part of the reservoir region, and a broad resistivity decrease developed along the eastern margin of the reservoir.

Near-surface resistivities are seen to be increasing on both ends of the line. The increase on the west (stations 1 through 6) is believed due to an increased level of irrigation. The increase on the east may be related to increased underflow of Colorado River waters because of high runoff last year.

SIMULATION OF A RESERVOIR WITH TWO WATERS OF DIFFERENT SALINITY

To simulate the resistivity changes we begin by considering production of liquid water from a porous α reservoir with an initial temperature of T = 300°C. The vertical pressure profile is assumed hydrostatic, with an average pressure P_{av} = 120 bars. The reservoir communicates with recharge waters of T = 100°C above and at the margins. The mass fraction of recharge water is denoted by x; initially x = 0 in the reservoir. The recharge waters are assumed to have different (lower) salinity than the water initially in place in the reservoir. For purposes of numerical modeling, however, we ignore all differences in thermophysical properties arising from different salinity, such as differences in viscosity, density, boiling curve, etc. We write separate mass balances for "water 1" (x = 0) and "water 2" (x = 1), which makes it possible to keep track of the individual waters as they start flowing and mixing in response to production. A similar approach was presented by Geshelin et al. (1981) for tracing fluid migration during steam assisted oil recovery.

The reservoir simulations were carried out with LBL's compositional simulator MULKOM, which is similar to the geothermal reservoir simulator SHAFT79 (Pruess and Schroeder, 1980), except that two water components are included. In this paper we will describe only one of the models for which calculations were made. Other results were previously presented by Pruess et al. (1982). The model shown in Figure 2 is a two-dimensional reservoir with recharge from above (vertical recharge) and the sides (horizontal recharge); the bottom is assumed to be an impermeable boundary. The vertical recharge zone begins 600 m beneath the surface and extends to the reservoir top at 800 m depth. The vertical extent of the reservoir is 400 m and its lateral width is 1600 m.

Due to symmetry, only one half of the system needs to be modeled. Laterally, the reservoir is connected to a recharge zone of 1000 m length with boundary conditions of T = 100°C, x = 1 on the outer boundary. The initial distributions in temperature and fluid composition between reservoir and vertical and lateral recharge boundaries are assumed to vary smoothly as follows:

(i) composition:

$$x_{in} = \begin{cases} 0 \text{ in reservoir;} \\ f(\ell) \text{ between reservoir and recharge boundary;} \\ 1 \text{ at recharge boundary;} \end{cases}$$

(ii) temperature:

$$T_{in} = \begin{cases} 300°C \text{ in reservoir;} \\ 300 - f(\ell) \times (300-100)°C \text{ between reservoir and recharge boundary;} \\ 100°C \text{ at recharge boundary.} \end{cases}$$

Here ℓ is the distance from the vertical or horizontal reservoir boundary, and

$$f(\ell) = \begin{cases} \frac{2}{L^2}\ell^2 & \text{for } \ell < L/2 \\ 1 - \frac{2}{L^2}(\ell-L)^2 & \text{for } \ell > L/2, \end{cases}$$

L is the vertical or horizontal distance between reservoir and recharge boundaries ($L_{vertical}$ = 200 m; $L_{horizontal}$ = 1000 m).

The computational mesh employs 100 m horizontal and 50 m vertical spacing, for a total of (18 x 8) + (8 x 4) = 176 elements, plus elements for representing the boundaries. The problem is initialized with approximate gravitational equilibrium relative to a reference pressure of p = 120 bars at 1000 m depth. (Due to the temperature differences between reservoir and recharge waters no rigorous gravitational equilibrium is possible). Production rate was taken as 600 kg/s (~2,160 tonnes/hr), approximately the actual average production rate at Cerro Prieto. Fluid sources of equal size are

placed in elements D1, E3, D5, and E7 of the model (Figure 2).

Horizontal permeability is taken to be 100 x 10^{-15} m^2, corresponding to a kH = 40 x 10^{-12} m^3. This agrees closely with the "field value" 36 x 10^{-12} m^3, which can be derived from an average transmissivity kH/μ = 0.4 x 10^{-6} m^3/Pa.s (Liguori, 1979) and μ (300°C) = 9.01 x 10^{-5} Pa.s. Vertical permeability was assumed one tenth of horizontal permeability. For these permeabilities, the reservoir can easily sustain the applied production rate. The largest observed pressure decline after 5 years is approximately 1 MPa, so that pressures remain well above saturation pressure and no two-phase zones evolve.

Temperature profiles for layers C, E, and G after 3 years of simulation are presented in Figure 3. The initial temperature distribution (t = 0) is also plotted for comparison. The figure shows a significant cooling in the lateral recharge zone (850 to 1600 m from the line of symmetry) due to the massive exploitation. Lateral migration of the recharge waters is evident in Figure 3 from a comparison of temperature profiles for layers C and G to the initial temperature distribution (t = 0). The temperatures in layer G are everywhere higher than the temperatures in layers C and E in the outside region (> 800 m away from the symmetry line) because of buoyancy effects. The migration of the colder recharge waters from above is evident from the lower temperatures in the G layer in comparison with the temperature profile in the C layer in the production region.

The composition profiles for layers C, E, and G after 3 years of simulation are shown in Figure 4. Again, the initial composition profile (t = 0) is included for reference. The compositional change within the reservoir and lateral recharge zones, as well as buoyancy effects, are clearly evident and are more pronounced than the temperature changes. Compositional change within the production region is dominated by vertical recharge. Accordingly, the mass fraction of recharge water is greatest in layer G, and smallest in layer C near the bottom of the reservoir. A different picture is observed at the reservoir margins at a distance of 800 m from the symmetry line. There lateral recharge is dominant, which, due to buoyancy effects, tends to be stronger in the lower portions of the reservoir, so that x (layer C) > x (layer E) > x (layer G). The buoyancy effects cause x (layer G) to decrease more rapidly away from the lateral recharge boundary (at 1800 m distance from the symmetry line) than is observed for layer E or C. Notice that in layer G vertical recharge causes minimum in x near the reservoir margin (800 m). A complex interplay of vertical and lateral recharge is also observed for layer E.

RESISTIVITY MODELING OF A RESERVOIR WITH WATER MIXING

A two-dimensional finite difference computer code was used in numerical calculations for resistivity models in this study. The code RESIS2D solves finite difference equations for the electric potentials in or on the surface of a two-dimensional half space with an arbitrary conductivity distribution (Dey and Morrison, 1976; Dey, 1976).

The code utilizes a mesh of 113 x 16 nodes of which 58 x 13 can be used for arbitrary resistivity distributions. Because of the limited mesh size, only 32 elements were used to describe resistivity within the production zone, and thus resistivity variations due to temperature and salinity changes were averaged over fairly large cross-sectional areas. This should produce some inaccuracies but these are not considered significant for the purposes of this demonstration. A larger source of error lies in the fact that we use a simple, schematic reservoir model as the sole basis for creating an initial subsurface resistivity distribution. This distribution, described in the next section, is different from the one developed by Wilt and Goldstein (1981a) from the field data. As a result, the percent changes in calculated resistivity from the baseline resistivities will contain an error that is a function of the volume averaged difference between model and true subsurface resistivities.

CALCULATION OF RESISTIVITY VARIATIONS

A study of the variations in resistivity due to changes in fluid properties in geothermal systems has recently been published (Ershagi et al., 1981). In the present paper we use those results to calculate resistivity as a function of salinity and temperature.

Figure 5 indicates the effect of salinity and temperature on resistivity for "typical" sediments in a geothermal environment. For our study we assume that recharge waters have .3% dissolved solids by weight and are at a temperature of 100°C. In the production zone the parameters are 1.5% and 300°C, respectively. These values are based on observed water chemistry at Cerro Prieto (Grant et al., 1981). Figure 5 shows that resistivity variations due to salinity and temperature changes can be quite large. In the recharge zone, initial resistivity is 50 percent larger than in the production zone due to temperature variation and more than 300 percent larger due to salinity differences.

The initial subsurface resistivity distribution assumed in this study is shown in Figure 6. The 5 ohm-m surface layer corresponds to a caprock. The 15.6 ohm-m background is sedimentary rock with 15 percent porosity and saturated

with 100°C water at .3 weight percent NaCl. The 15.6 ohm-m resistivity value for the background was calculated from Archie's law. The geothermal reservoir is represented by a 1600 m x 400 m zone buried at a depth of 800 m. Within the reservoir region the resistivity is initially 2.15 ohm-m. This number was derived by adjusting the background of 15.6 ohm-m for increased salinity and temperature in the reservoir region. Note that the center of the model (Station 6) would correspond to Station 11 in the field data (Figure 1).

RESULTS AND DISCUSSION

Resistivity calculations for the two-dimensional resistivity model were made for a dipole-dipole array centered over the reservoir. In the calculations a dipole length of 800 m was used because of convenience, rather than 1000 m as used in the field survey. Therefore, calculated and field results are not geometrically identical but the differences should not deter simple comparisons. Resistivity pseudosections were calculated for various points in the production history; prior to production and then at times of 0.5, 1, 3, and 5 years after the onset of production. Apparent resistivity changes for each time relative to preproduction are then calculated and presented in pseudosection form in Figure 7.

Despite the large rate of production the apparent resistivity changes are small after one year of production. During such early times, production - related resistivity changes might be obscured by seasonal variations in rainfall, runoff, or irrigation or obscured by measurement errors if sufficient accuracy cannot be achieved (Wilt and Goldstein, 1982). However, it is clear from this example that the hydraulic (salinity) front moves relatively rapidly, and that significant changes in apparent resistivity appear between one and three years after the start of production.

A comparison of the simulated resistivity changes to the actual changes for times of 1, 1.5, and 2.5 years after the 1979 baseline data (Figure 1) reveals that the field data show a far more complex pattern of change, but there are also similarities in pattern and magnitude that deserve mention. Notice that only the western limb of the resistivity increase emerges after 2.5 years (Fall 1981). The asymmetry in the resistivity change indicates an asymmetry in the physical processes, in distinction from the symmetrical recharge of our schematic model. There is no unique solution to the problem, but a fluid flow model that might produce the observed changes is one proposed by Halfman et al. (1982); i.e., (a) cooler, less saline recharge from the west and above, and (b) hot, saline recharge from below and from the east.

Second, because the initial resistivity model is not an accurate facsimile of what we believe the true resistivity distribution was in 1979, there is little chance that the model results would match the observed field changes. That they match as well as they do in places, suggests that we are on the right track toward understanding the reservoir processes.

CONCLUSIONS

A methodology has been presented for indirect study of a geothermal reservoir which combines numerical reservoir simulation with modeling of apparent resistivities as measured with the dipole-dipole technique. For a Cerro Prieto-type reservoir, temporal changes in apparent resistivity due to production and recharge of colder and less saline waters are both calculated and are observed to be substantial over time intervals of several years. It therefore appears feasible to use resistivity for monitoring reservoir processes. Our schematic models predict resistivity changes which are only approximately comparable to field observations, and thus more refined numerical models will be required.

For most geothermal reservoirs, the patterns of fluid flow and resistivity change will be three-dimensional. Therefore, accurate resistivity monitoring requires measurements along several intersecting profiles.

The proposed methodology should also be applicable for monitoring the migration of reinjected fluids.

ACKNOWLEDGEMENT

We thank Drs. M. Lippmann and C.F. Tsang for a critical review of the manuscript. This work was supported by the Assistant Secretary for Conservation and Renewable Energy, Office of Renewable Technology, Division of Geothermal and Hydropower Technologies of the U.S. Department of Energy under Contract No. DE-AC03-76SF00098.

TABLE 1

Parameters for Production Simulation

rock density	2600 kg/m^3
porosity	15%
horizontal permeability	100 x 10^{-15} m^2
vertical permeability	10 x 10^{-15} m^2
heat conductivity	2.1 W/m°C
rock specific heat	900 J/kg°C
vertical extent of reservoir	400 m
volumetric rate of production	9.74 x 10^{-7} kg/s.m^3
initial reservoir temperature	300°C
average initial reservoir pressure	12 MPa (120 bars)

REFERENCES

Bartel, L.C., and Wayland, J.R. (1981), "Results from Using the CSAMT Geophysical Technique to Map Oil Recovery Processes," Paper SPE 10230, presented at the 56th Annual Fall Technical Conference and Exhibition of the SPE, San Antonio, Texas, October 5-7, 1981.

Beyer, J.H. (1977), "Telluric and D.C. Resistivity Techniques Applied to the Geophysical Investigation of Basin and Range Geothermal Systems, Part II: A Numerical Model Study of the Dipole-Dipole and Schlumberger Resistivity Methods," Lawrence Berkeley Laboratory, Report LBL-6325 2/3.

Dey, A. (1976), "Resistivity Modeling for Arbitrarily Shaped Two Dimensional Structures, Part II: Guide to the FORTRAN Algorithm RESIS2D," Lawrence Berkeley Laboratory Report LBL-5283.

Dey, A., and Morrison, H.F. (1976), "Resistivity Modeling for Arbitrarily Shaped Two-Dimensional Structures, Part I: Theoretical Formulation," Lawrence Berkeley Laboratory Report LBL-5233.

Ershaghi, I., Dougherty, E.E., and Hardy, L. (1981), "Formation Evaluation in Liquid Dominated Geothermal Reservoirs," Report for Department of Energy No. DOE/ET/28384-T1.

Geshelin, B.M., Grabowski, J.W., and Pease, E.C. (1981), "Numerical Study of Transport of Injected and Reservoir Water in Fractured Reservoirs During Steam Stimulation," Paper SPE 10322, presented at 56th Annual Fall Technical Conference and Exhibition of the SPE, San Antonio, Texas, October 5-7, 1981.

Grant, M.A., Truesdell, A.H., and A. Mañón M. (1981), "Production induced Boiling and Cold Water Entry in the Cerro Prieto Geothermal Reservoir Indicated by Chemical and Physical Measurements," In Proceedings, Third Symposium on the Cerro Prieto Geothermal Field, Baja California, Mexico, Lawrence Berkeley Laboratory Report LBL-11967, pp 221-237.

Halfman, S.E., Lippmann, M.J., Zelwer, R., and Howard, J.H. (1982), "Fluid Flow Model of the Cerro Prieto Geothermal Field Based on Well Log Interpretation," Lawrence Berkeley Laboratory, LBL-14898, 13 p.

Liguori, P.E. (1979), "Simulation of the Cerro Prieto Geothermal Field Using a Mathematical Model," In Proceedings, Second Symposium on the Cerro Prieto Geothermal Field, Mexicali, Baja California, October 17-19, 1979, p. 521-524.

Pruess, K., and Schroeder, R.C. (1980), "SHAFT79 User's Manual," Lawrence Berkeley Laboratory Report LBL-10861, Berkeley, California.

Risk, G.F. (1975), "Monitoring the Boundary of the Broadland Geothermal Field, New Zealand," Proceedings, Second United Nations Symposium on the Development and Use of Geothermal Resources, San Francisco, California, May 20-29, 1975, v. 2, p. 1185-1189.

Wilt, M.J., and Goldstein, N.E. (1981a), "Resistivity Monitoring at Cerro Prieto," Geothermics, v. 10, n. 3/4, p. 183-194.

Wilt, M.J., and Goldstein, N.E. (1981b), "Results from Two Years of Resistivity Monitoring at Cerro Prieto," In Proceedings, Third Symposium on the Cerro Prieto Geothermal Field, Baja California, Mexico, Lawrence Berkeley Laboratory Report LBL-11967, p. 372-379.

Wilt, M.J., and Goldstein, N.E. (1982), "Interpretation of Dipole-Dipole Resistivity Monitoring Data at Cerro Prieto," In Proceedings, Fourth Symposium on the Cerro Prieto Geothermal Field, Guadalajara, Mexico, August 10-12, 1982, in preparation.

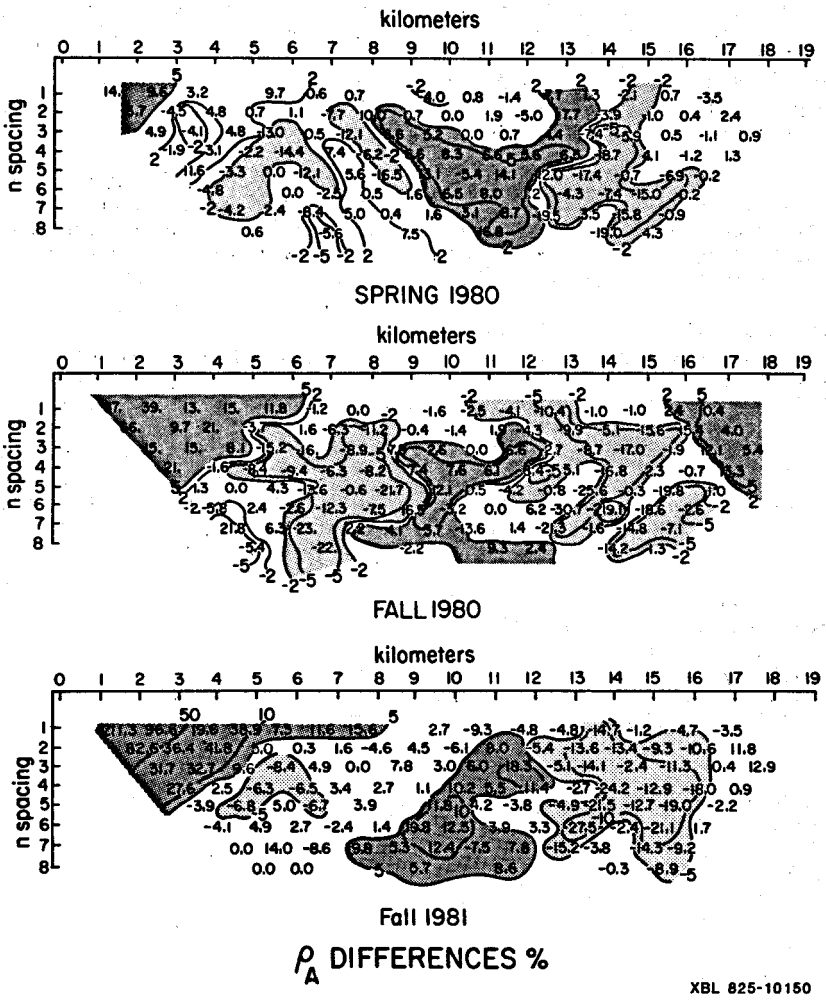

Figure 1. Resistivity pseudosections measured over the Cerro Prieto Geothermal Field shown as percent changes from the 1979 baseline data set.

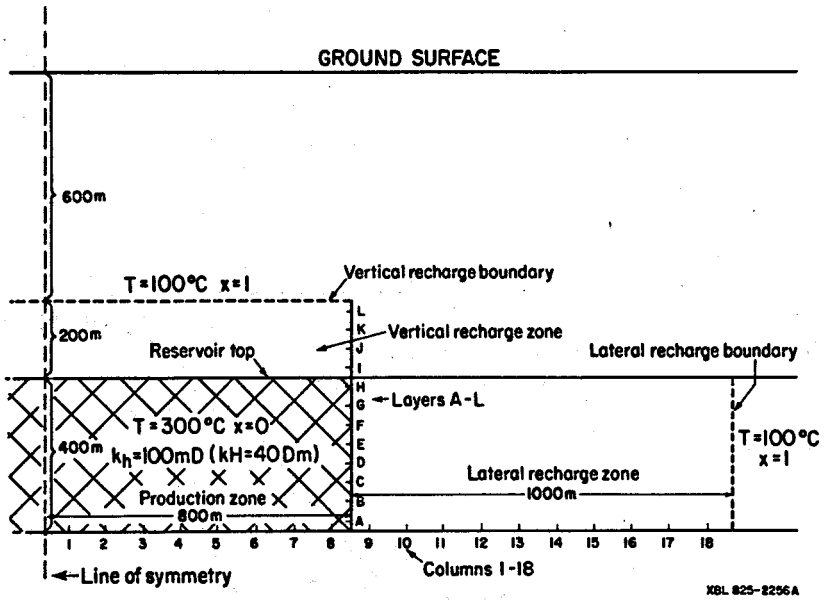

Figure 2. Two-dimensional reservoir model for vertical and lateral recharge.

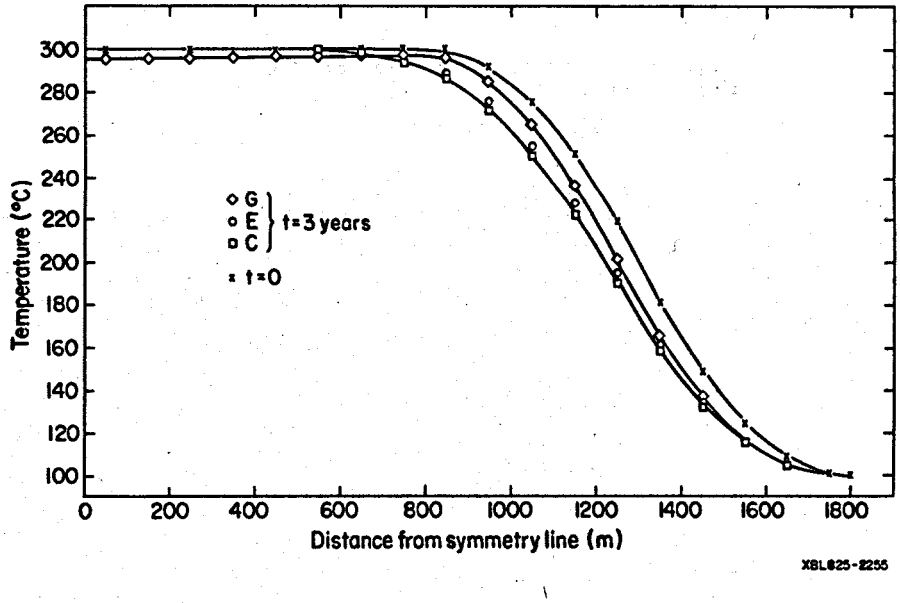

Figure 3. Temperature profiles for two-dimensional model.

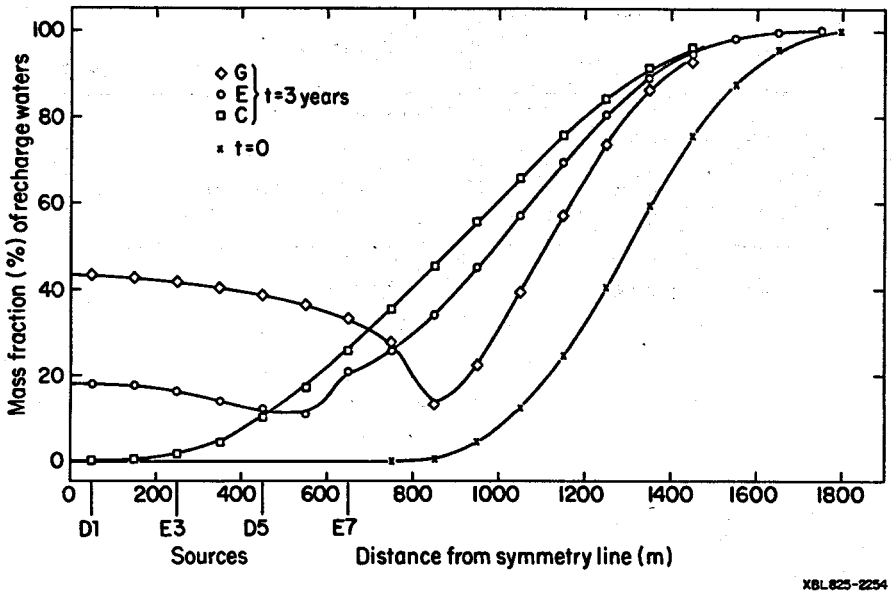

Figure 4. Composition profiles for two-dimensional model.

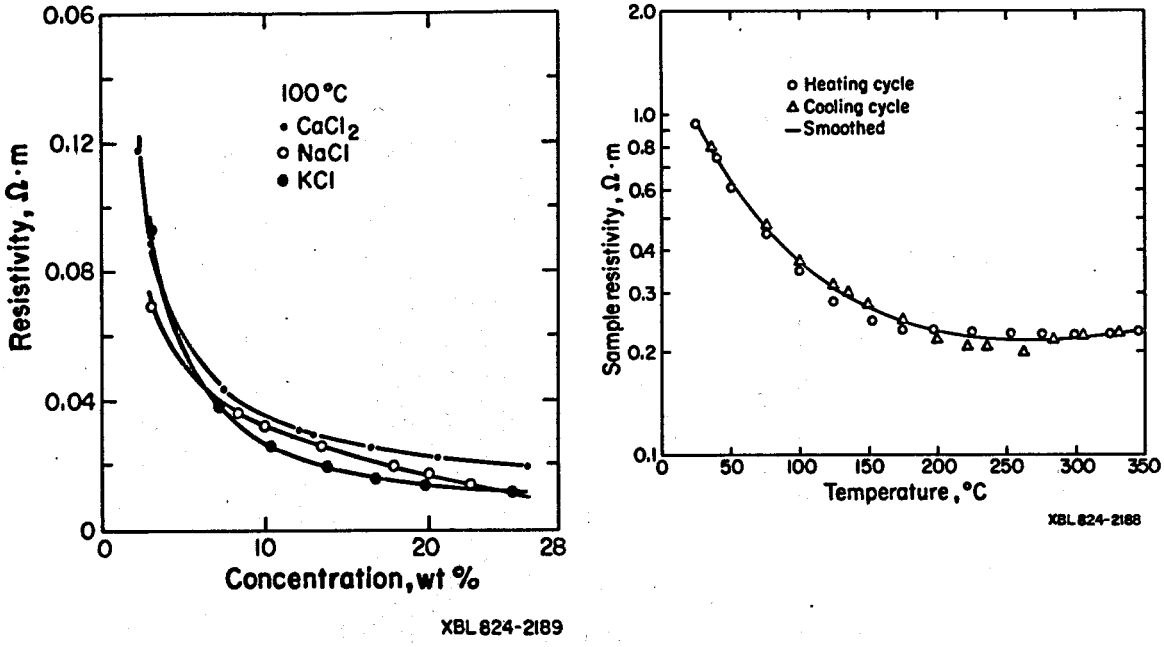

Figure 5. Dependence of resistivity on (a) salinity and (b) temperature for sedimentary rocks.

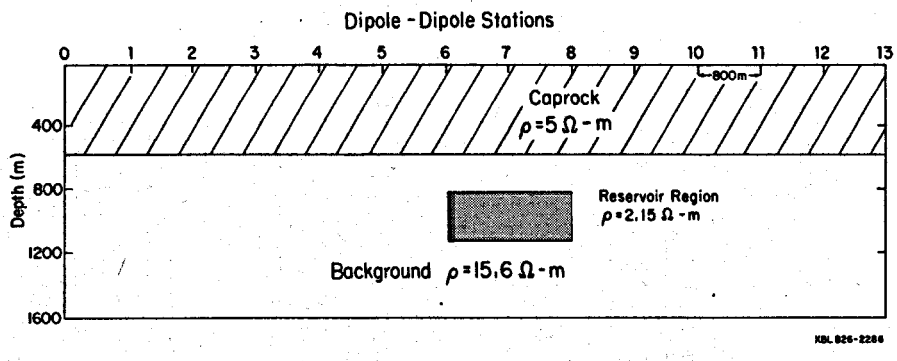

Figure 6. Undisturbed resistivity distribution.

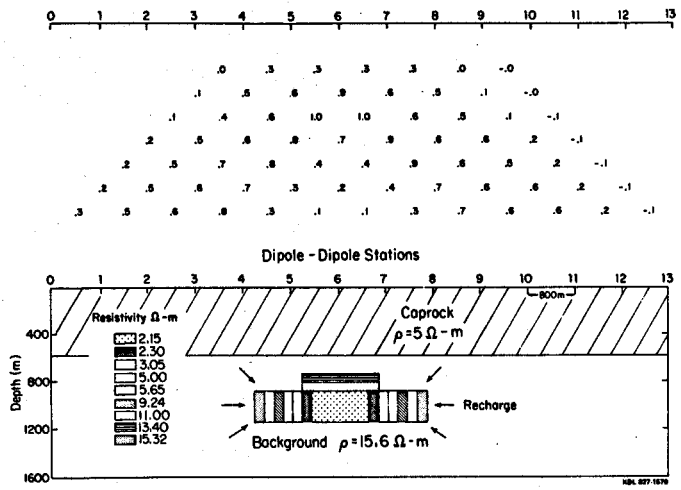

(A)

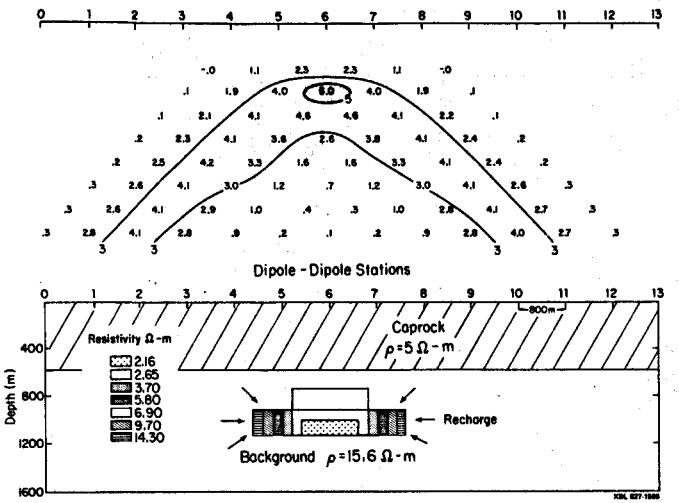

(B)

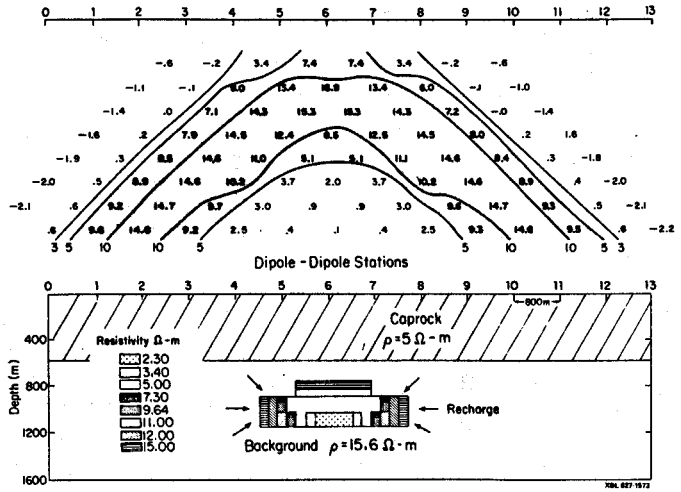

(C)

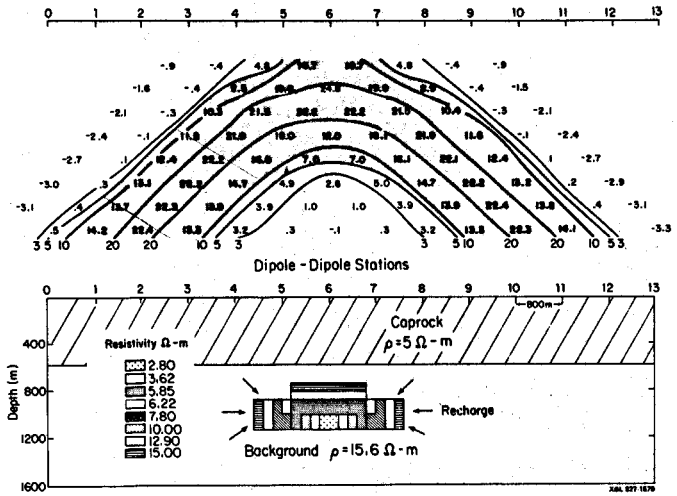

(D)

Figure 7. Resistivity pseudosections for reservoir with vertical and lateral recharge (percent changes) at (A) Six months, (B) One year, (C) Three years, and (D) Five years after the beginning of production at rate of 600 kg/s.

Proceedings Eighth Workshop Geothermal Reservoir Engineering
Stanford University, Stanford, California, December 1982
SGP-TR-60

THE MOVEMENT OF GEOTHERMAL FLUID IN THE CERRO PRIETO FIELD AS DETERMINED FROM WELL LOG AND RESERVOIR ENGINEERING DATA

S. E. Halfman, M. J. Lippmann, and R. Zelwer

Earth Sciences Division
Lawrence Berkeley Laboratory, University of California
Berkeley, California 94720

ABSTRACT

A hydrogeologic model of the Cerro Prieto geothermal field in its undisturbed state, developed on the basis of well log and reservoir engineering data, is discussed.

According to this model, geothermal fluid enters the field from the east through a deep (>10,000 ft) sandstone aquifer which is overlain by a thick shale unit which locally prevents the upward migration of the fluid. As it flows westward, the fluid gradually rises through faults and sandy gaps in the shale unit. Eventually, some of the fluid leaks to the surface in the western part of the field, while the rest mixes with surrounding colder waters.

INTRODUCTION

The Cerro Prieto liquid-dominated geothermal field is located in Baja California, Mexico, about 20 miles south of the US-Mexico border (Figure 1). A vast amount of subsurface geologic and reservoir enginnering data have been gathered from over 100 wells (some as deep as 11,600 ft) completed in this field (Figure 2).

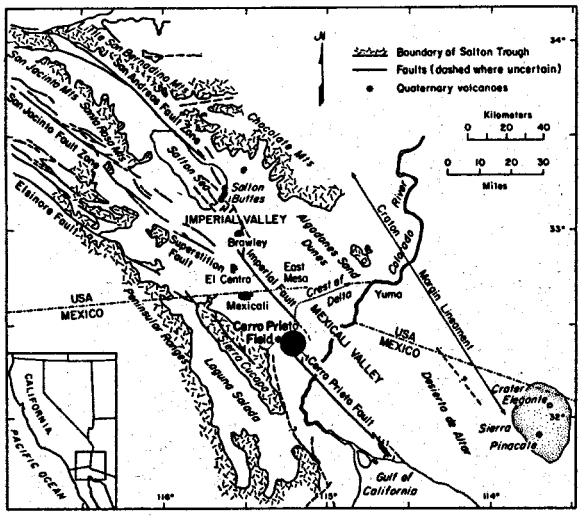

Figure 1. Regional geology of the Salton Trough (i.e., Imperial and Mexicali Valleys) and location of the Cerro Prieto area.

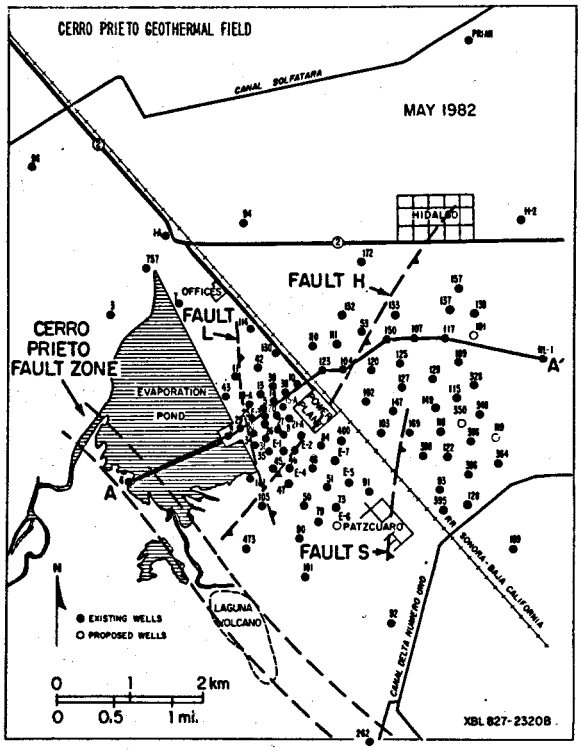

Figure 2. Location of wells, principal faults, and cross section A-A' at Cerro Prieto.

Jased on geochemical, mineralogical, and downhole temperature logs, it has been shown that the geothermal fluid enters the field from the east, gradually flowing to the west as it ascends to shallower depths (Mercado, 1968 and 1976; Bermejo et al., 1979; Elders et al., 1981). However, in the models developed by these authors, the movement of hot fluids in the subsurface is shown only schematically. We will discuss a hydrogeologic model for the Cerro Prieto reservoir in its natural (pre-production) state (Halfman et al., 1982). The model provides details on the westward and upward flow of geothermal fluids in the field and the geologic features controlling this movement.

METHODOLOGY

First, a geologic model of the Cerro Prieto field was constructed based on geophysical and

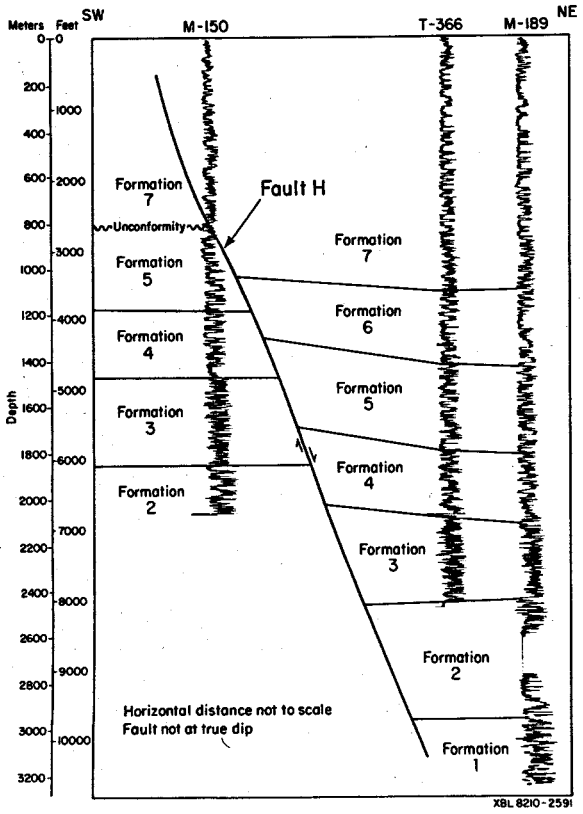

Figure 3. Simplified stratigraphy of the Cerro Prieto field. The traces correspond to gamma-ray (GR) logs.

lithological well logs. Downhole temperature profiles and well production interval data were then incorporated into the geologic model to develop a geothermal fluid flow model that would show the actual fluid flow paths. This model was then used to identify the lithologic and structural features that control the movement of the geothermal fluid.

From the geologic model, we were able to identify faults on the basis of significant vertical displacements of formations and by recognizing that sections or entire formations were missing in some wells (Figure 3). Seven distinct formations were defined, based mainly on the interpretation of gamma-ray (GR), spontaneous potential (SP), deep induction (ILD), and formation density gamma-gamma (RHOB) logs (Halfman et al., 1982).

Using a different approach, the beds were categorized into three lithofacies groups (sandstone, sandy-shale, and shale) on the basis of the well log analysis criteria followed by Lyons and van de Kamp (1980). Basically, the sandstone group is comprised of thick, permeable, and well defined sandstone beds (with some interbedded shales); the sandstone beds in the sandy-shale group are thinner and less permeable (with a higher percentage of intercalated shales), and are yet thinner (<10 ft) in the shale group. After assigning the beds to the different lithofacies groups, lithofacies cross sections were constructed incorporating the faults previously defined.

The method used to group the different beds, based mainly on the GR log, is illustrated in Figure 4. This figure (well M-150, a typical

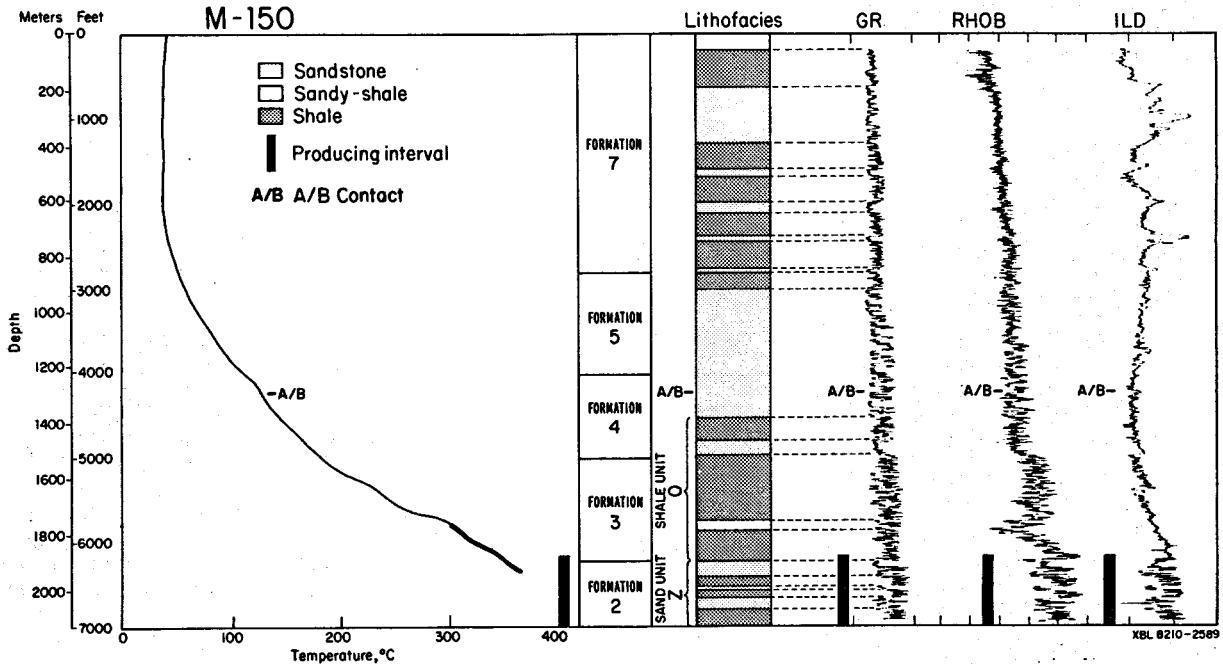

Figure 4. Well M-150, showing temperature profile; interpreted formation and lithofacies columns; and gamma-ray (GR), formation density gamma-gamma (RHOB), and deep induction (ILD) logs.

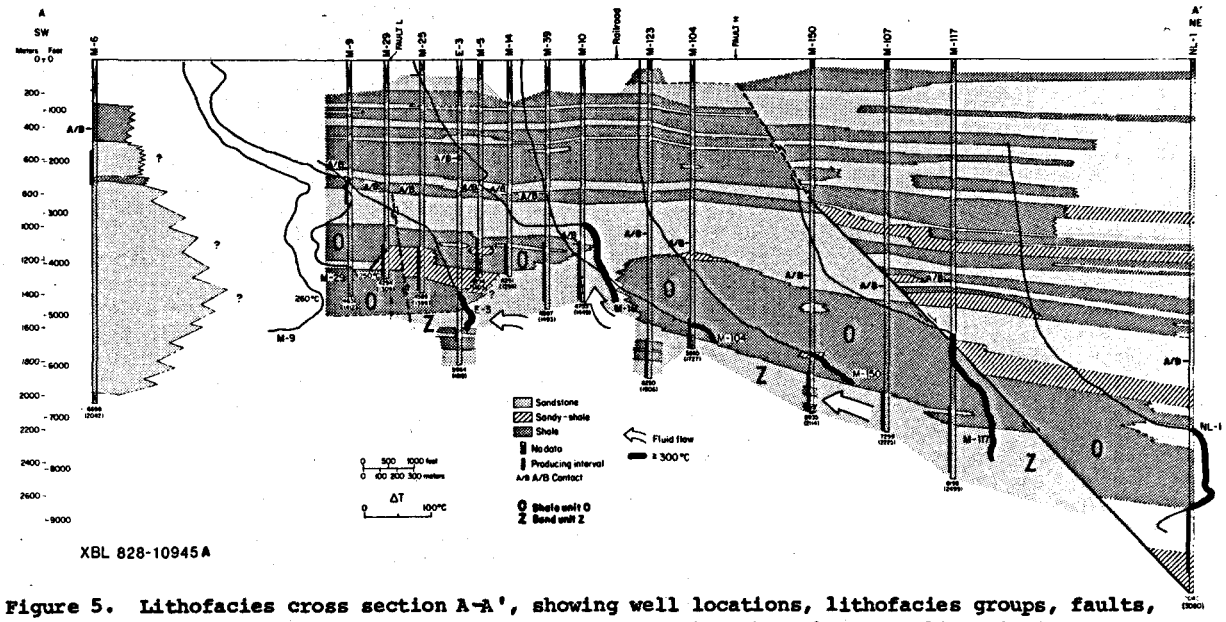

Figure 5. Lithofacies cross section A-A', showing well locations, lithofacies groups, faults, temperature profiles (the parts of the temperature profiles shown by heavy lines indicate temperatures 300°C or greater), producing intervals, A/B contacts, Shale Unit 0, Sand Unit Z, and arrows indicating direction of geothermal fluid flow.

Cerro Prieto well) shows the GR, RHOB, ILD and temperature logs, as well as the interpreted formation column, A/B contact, Shale Unit 0 and Sand Unit Z, which will be discussed below.

RESULTS

Geologic Model

Three concealed normal faults (Faults H, L, and S), believed to have an important impact on the natural (pre-exploitation) circulation of geothermal fluid in the system, were identified (Figure 2). All three faults have a northeast-southwest strike, dipping to the southeast. Fault H has displacements as great as 1650 ft in the northeastern areas and as small as 1000 ft in the southwest. Faults L and S have displacements of about 200 and 400 ft, respectively (Halfman et al., 1982). The existence of these faults have also been inferred from geophysical and mineralogical data (Majer and McEvilly, 1982; Williams, 1982).

In Figure 5, the three types of lithofacies distinguished in this study are shown correlated across section A-A'. Two main sedimentary units, one comprised mostly of the shale group (Shale Unit 0), and another comprised of mostly the sandstone group (Sand Unit Z) were identified. These two units, along with the faults, will be shown to play an important role in controlling the flow of the geothermal fluid.

The well log readings indicate that some of the sediments in the Cerro Prieto field have been hydrothermally altered. The sandstones and shales above Shale Unit 0 show fairly normal log readings for a sedimentary environment (Figures 4 and 5). The high ILD readings in the upper 3,000 feet, which may look unusual, are actually only due to fresh water sandstones (Lyons and van de Kamp, 1980; Seamount and Elders, 1981). Shale Unit 0 and the underlying Sand Unit Z, however, show some anomalous log values because they have been affected by the heat and fluid moving through the subsurface.

Shale Unit 0, especially its lower part, acts as a barrier to the upward migration of geothermal fluid and convective heat flow. This is substantiated by the lithology, temperature and low porosity readings obtained from the logs (Figure 4). The lower portion of Shale Unit 0 consists mainly of thinly bedded sandstones and shales and lacks any thick permeable sandstone beds that would permit fluid flow. This is confirmed by the general sharp rise in temperature gradient observed near the top of Shale Unit 0 (Figure 5), indicative of strata through which heat is transferred by conduction rather than convection. Furthermore, the unusually high RHOB (shales generally >2.6 gm/cm^3) and ILD (shales generally >6.5 ohm-m) values commonly found near the base of Shale Unit 0 indicate low porosity, especially in wells southeast of Fault H. The density values have been shown by Seamount and Elders (1981) to be much higher than expected from normal compaction of sediments at these depths. Ershaghi and Ghaemian (1980) explain that the unusual high resistivity readings may be due to porosity loss resulting from chemical reactions and also to drastic reduction in clay conductivity. Thus Shale Unit 0 is a thick, relatively impermeable, low-porosity body that acts as a local cap rock, as will be shown below. By a local cap rock, we

mean a geologic unit of lower permeability which overlies the reservoir, locally preventing the upward migration of fluid.

Sand Unit Z, below Shale Unit 0, permits the flow of geothermal fluids. This is confirmed by its lithology, temperature profile, high porosity indicated by the logs, and the depths of the producing intervals. The upper portion of this unit consists of thick sandstone beds interbedded with some shales. The vertical temperature profiles in Sand Unit Z usually show a fairly constant temperature of about 300°C or slightly greater (Halfman et al, 1982). This constant temperature is indicative of circulating fluids; i.e., a region where heat is transferred by convection rather than conduction. Most of the producing intervals in wells east of the railroad tracks and deeper ones west of them (Figures 2 and 5) are located in Sand Unit Z. The low ILD and RHOB values of the sandstone beds of this unit indicate high porosity, possibly due to secondary (dissolution) porosity (Lyons and van de Kamp, 1980). Thus Sand Unit Z has thick, permeable, high-porosity sandstone beds that act as conduits for the geothermal fluid.

Also shown in cross section A-A' (Figure 5) are the A/B contacts, and the producing intervals. The A/B contact separates the unconsolidated (Unit A) from the underlying indurated (Unit B) sediments (Puente and de la Peña, 1978). The induration of the sediments is believed to be due to post-depositional thermal effects which modified the deeper materials (Unit B) leaving the shallower ones (Unit A) relatively unaffected (Elders et al., 1978).

Based on the depths of the producing layers, the Comisión Federal de Electricidad has identified two liquid-dominated reservoirs at Cerro Prieto. The shallower one, designated A by Prian (1979) and α by Sánchez and de la Peña (1981), is restricted to the area west of the railroad tracks and corresponds to the sandier layers of the upper part of Shale Unit 0 (Figure 5). The deeper and hotter reservoir, designated B or β by the same authors, is found in Sand Unit Z throughout the field.

Geothermal Fluid Flow Paths

Using an approach suggested by Howard (1981), it was found that the actual fluid flow paths become readily apparent when downhole temperature profiles and well production intervals (Bermejo et al., 1979; personal communication, 1982) were superimposed on the lithofacies cross section A-A' (Figure 5). In this section, the portions of the temperature profiles shown by heavy lines indicate temperatures of 300°C or greater. The maximum temperatures of cooler wells are indicated next to the corresponding curve.

From Figure 5, it can be seen that the temperature profiles show sharp increases in gradient near the A/B contact, and that the depth of the A/B contact (Cobo, 1981), producing intervals, and increases in temperature gradient are observed at progressively greater depths towards the east. Well M-117 does not conform to this trend, however, and will be discussed below.

Comparison of the temperature profiles with the lithology of wells M-104, M-150, and NL-1 (Figure 5) indicates that the sharp increases in temperature gradient occur near the boundary between Shale Unit 0 and the overlying sandstone group. In wells E-3, M-29, and M-9, this increase is observed near a shallower shale, which is found in well M-29 at the same depth as the A/B contact. The increase in temperature gradient, therefore, suggests that the shale units must be barriers to convective heat transport; i.e., they are essentially acting as local cap rocks.

According to Elders et al. (1982) and Goldstein et al. (1982), the heat source for the Cerro Prieto system is in an area of current mafic rock intrusion beneath the eastern regions of the field. The invaded rocks heat the circulating fluid, which is thought to enter the field from the east through Sand Unit Z (Reservoir β) after which it moves westward toward Fault H (the arrows in Figure 5 indicate the flow of geothermal fluid). The fluid then moves up Fault H until it encounters Sand Unit Z once again. A small portion of the fluid continues up Fault H, resulting in a temperature of 300°C at a relatively shallow depth in well M-117. Most of the fluid, however, moves westward through Sand Unit Z in the upthrown block, west of Fault H. This essentially horizontal flow continues to the area near well M-10, where there exists a sandy gap in Shale Unit 0 which permits the communication between the reservoirs α and β. In this area, the geothermal fluid flows upward, resulting in high temperatures at shallow depths in well M-10. Some of the fluid enters the southwestern part of Shale Unit 0, which is sandier here than in the east, and constitutes the Reservoir α. Then the fluid moves westward until encountering Fault L near well M-29. There, the fluid flows upward through the fault and then westward through the sands above Shale Unit 0. Fluid that does not enter Shale Unit 0 continues to flow westward through the underlying Sand Unit Z (Reservoir β). Eventually, some fluid leaks to the surface through the Cerro Prieto Fault Zone, which bounds the field to the west (see Figure 2), and the rest mixes with the colder waters that surround the geothermal anomaly.

Based on cross section A-A' and other sections given by Halfman et al. (1982), it is inferred that most of the geothermal fluid flows through high porosity, permeable sandstone beds in Sand Unit Z (Reservoir β), underlying the low-porosity, impermeable Shale Unit 0, which acts as a local cap rock. Figure 6 shows a contour map of the top of the β reservoir; the postulated direction of geothermal fluid flow through these sandstone beds is indicated by the arrows. As shown in this figure, the fluid is generally believed to enter the field (at great depth)

from the east, gradually moving westward (and rising to shallower depth), and finally reaching the surface in the western regions of the field. Several wells to the southeast are cooler (i.e., M-189). This suggests that these wells are bypassed by the hot fluids entering the field.

SUMMARY AND CONCLUSIONS

By integrating the geologic model of Cerro Prieto with downhole temperature profiles and well production intervals, we have identified the geothermal fluid flow paths in the field. It has been shown that the movement of hot fluids in the subsurface is strongly controlled by stratigraphic and structural features. Our model indicates that a continuous cap rock does not exist at Cerro Prieto which would prevent the upward migration of geothermal fluids to the surface. This supports the conclusion of Grant et al. (1981) and Grant and O'Sullivan (1982) that the reservoir, especially its western part, is a leaky aquifer.

The results of our model are consistent with mineralogical observations and interpretations (Elders et al., 1981), and with reservoir engineering and geochemical studies (Mercado, 1976; Grant et al., 1981) carried out on this geothermal system, and was used to simulate the behavior of the Cerro Prieto field in its natural state and under exploitation (Lippmann and Bodvarsson, 1982; Tsang et al., 1982).

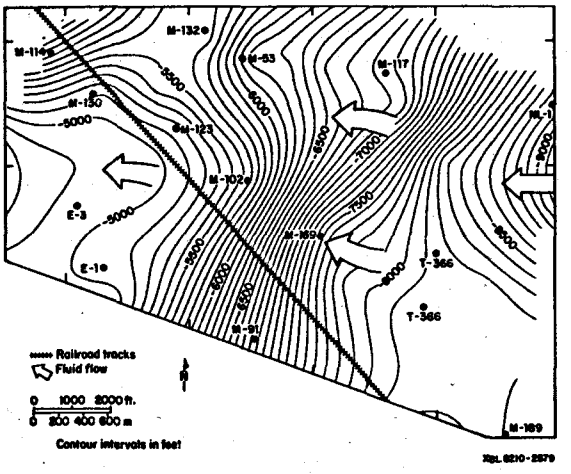

Figure 6. Contour lines indicate the top of Reservoir β. Arrows indicate the direction of geothermal fluid flow through this unit.

ACKNOWLEDGMENTS

We would like to thank Norman Goldstein and Harold Wollenberg of Lawrence Berkeley Laboratory for their helpful comments and suggestions.

This work was supported by the Assistant Secretary for Conservation and Renewable Energy, Office of Renewable Technology, Division of Geothermal and Hydropower Technologies of the U. S. Department of Energy under Contract Number DE-AC03-76SF00098.

REFERENCES

Bermejo M., F. J., Navarro O., F. X., Castillo B., F., Esquer P., C. A., and Cortez A., C., 1979. Pressure variations at the Cerro Prieto reservior during production, in Proceedings, Second Symposium on the Cerro Prieto geothermal field, October 17-19, 1979. Mexicali, Comisión Federal de Electricidad, pp. 473-493.

Cobo R., J. M., 1981. Configuration of mudstones, gray- and coffee-colored shale lithoglogic units, zones of silica and epidote, and their relationship to the tectonics of the Cerro Prieto geothermal field, in Proceedings, Third Symposium on the Cerro Prieto geothermal field, September 20-22, 1981. Berkeley, Lawrence Berkeley Laboratory report LBL-11967, pp. 29-45.

Elders, W. A., Hoagland, J. R., McDowell, S. D., and Cobo R., J. M., 1978. Hydrothermal mineral zones in the geothermal reservoir of Cerro Prieto, in Proceedings, First Symposium on the Cerro Prieto geothermal field, September 20-22, 1978. Berkeley, Lawrence Berkeley Laboratory report LBL-7098, pp. 68-75.

Elders, W. A., Williams, A. E., and Hoagland, J. R., 1981. An integrated model for the natural flow regime in the Cerro Prieto hydrothermal system based upon petrological and isotope geochemical data, in Proceedings, Third Symposium on the Cerro Prieto Geothermal Field, March 24-26, 1981. Berkeley, Lawrence Berkeley Laboratory report LBL-11967, pp. 102-109.

Elders, W. A., Bird, A. E., Williams, A. E., and Schifman, 1982. Model for a heat source of the Cerro Prieto magma-hydrothermal system, in Proceedings, Fourth Symposium on the Cerro Prieto Geothermal Field, August 10-12, 1982, Mexicali, Mexico, Comisión Federal de Electricidad, (in preparation).

Ershaghi, I., and Ghaemian, S., 1980. Detection of hydrothermal alteration in a sedimentary type geothermal system using well logs, presented at the 55th Annual Fall Technical Conference and Exhibition of the Society of Petroleum Engineers of AIME, September 21-24, 1980. Dallas, Texas, SPE 9499.

Goldstein, N. E., Wilt, M. J., and Corrigan, D. J., 1982. Analysis of the Nuevo León magmatic anomaly and its possible relation

to the Cerro Prieto magmatic-hydrothermal system, in Proceedings, Fourth Symposium on the Cerro Prieto Geothermal Field, August 10-12, 1982, Mexicali, Mexico, Comisión Federal de Electricidad (in preparation).

Grant, M. A. and O'Sullivan, M. J., 1982. The old field at Cerro Prieto considered as a leaky aquifer, in Proceedings, Fourth Symposium on the Cerro Prieto geothermal field, August 10-12, 1982. Mexicali, Mexico, Comisión Federal de Electricidad (in preparation).

Grant, M. A., Truesdell, A. H., and Mañón M., A., 1981. Production induced boiling and cold water entry in the Cerro Prieto geothermal reservoir indicated by chemical and physical measurements, in Proceedings, Third Symposium on the Cerro Prieto geothermal field, March 24-26, 1981. Berkeley, Lawrence Berkeley Laboratory report LBL-11967, pp. 221-237.

Halfman, S. E., Lippmann, M. J., Zelwer, R. and Howard, J. H., 1982. Fluid flow model of the Cerro Preito geothermal field based on well log interpretation, in Proceedings, Fourth Symposium on the Cerro Prieto geothermal field, August 10-12, 1982. Mexicali, Mexico, Comisión Federal de Electricidad (in preparation).

Howard, J. H., 1981. Comments on the geology of the Cerro Prieto geothermal field as of the AAPG meeting 1981, Berkeley, Lawrence Berkeley Laboratory Internal Memorandum.

Lippmann, M. J., and Bodvarsson, G. S., 1982. Modeling studies on Cerro Prieto, in Proceedings, Fourth Symposium on the Cerro Prieto geothermal field, August 10-12, 1982. Mexicali, Mexico, Comisión Federal de Electricidad (in preparation).

Lyons, D. J., and van de Kamp, P. C., 1980. Subsurface geological and geophysical study of the Cerro Prieto geothermal field, Baja, California, Mexico. Berkeley, Lawrence Berkeley Laboratory report LBL-10540.

Majer, E. L., and T. V. McEvilly, 1982. Seismological studies at the Cerro Prieto Field: 1978-1982, in Proceedings, Fourth Symposium on the Cerro Prieto geothermal field, August 10-12, 1982. Mexicali, Mexico, Comisión Federal de Electricidad (in preparation).

Mercado G., S., 1968. Localización de zonas de máxima actividad hidrotermal por medio de proporciones químicas, campo geotérmico de Cerro Prieto, B.C. Presented at the III Congreso Mexicano de Química Pura y Aplicada, March 21-23, 1968. Guadalajara, México, Sociedad Química de México.

Mercado G., S., 1976. Movement of geothermal fluids and temperature distribution in the Cerro Prieto geothermal field, in Proceedings, Second United Nations Symposium on the Development and Use of Geothermal Resources, San Francisco, California, May 20-29, 1975, pp. 489-494.

Prian, C., R., 1981. Drilling rate for the Cerro Prieto stratigraphic sequence, in Proceedings, Third Symposium on the Cerro Prieto geothermal field, March 24-26, 1981. Berkeley, Lawrence Berkeley Laboratory report LBL-11967, pp. 77-87.

Puente C., I., and de la Peña L., A., 1978. Geology of the Cerro Prieto geothermal field, in Proceedings, First Symposium on the Cerro Prieto geothermal field, September 20-22, 1978. Berkeley, Lawrence Berkeley Laboratory report LBL-7098, pp. 17-37.

Sánchez R., J., and de la Peña L., A., 1981. Geohydrology of the Cerro Prieto geothermal aquifer, in Proceedings, Third Symposium on the Cerro Prieto geothermal field, March 24-26, 1981. Berkeley, Lawrence Berkeley Laboratory report LBL-11967, pp. 309-323.

Seamount, D. T., and Elders, W. A., 1981. Use of wireline logs at Cerro Prieto in the identification of the distribution of hydrothermally altered zones and dike locations, and their correlation with reservoir temperatures, in Proceedings, Third Symposium on the Cerro Prieto geothermal field, March 24-26, 1981. Berkeley, Lawrence Berkeley Laboratory report LBL-11967, pp. 123-133.

Tsang, C. F., Mangold, D. C., Doughty, C., and Lippmann, M. J., 1982. Prediction of reinjection effects in the Cerro Prieto geothermal system, in Proceedings, Fourth Symposium on the Cerro Prieto geothermal field, August 10-12, 1982, Mexicali, Mexico, Comisión Federal de Electricidad (in preparation).

Williams, A. E., 1982. Stable isotope systematics of oxygen and carbon in and around the Cerro Prieto geothermal anomaly, Baja California, Mexico, in Proceedings, Fourth Symposium on the Cerro Prieto geothermal field, August 10-12, 1982. Mexicali, Mexico, Comisión Federal de Electricidad (in preparation).

Proceedings Eighth Workshop Geothermal Reservoir Engineering
Stanford University, Stanford, California, December 1982
SGP-TR-60

MONITORING FLUID DEPLETION AT THE GEYSERS BY THE GRAVITY CHANGE/SUBSIDENCE RATIO

R.G. Allis

Geophysics Division, D.S.I.R.,
Wairakei, New Zealand.

Abstract The ratio of gravity change to subsidence may be a useful indicator of the rate of fluid depletion in vapour-dominated reservoirs. For an average reservoir porosity less than about 10%, this ratio is close to -40 μgals/cm if there is no recharge or reinjection to the reservoir. The ratio is independent of reservoir thickness, pressure drop and porosity. If R is the fractional recharge mass (assumed to be <100°C), the ratio is reduced by a factor $\frac{1 - R}{1 + 0.4\ R}$. The rate of injection of condensate into The Geysers reservoir would reduce this ratio to between -24 to -28 μgals/cm. Analysis of the available data at The Geysers (1974-1977) shows the most heavily produced part of the reservoir to have a ratio of -14 μgals/cm. This discrepancy may be significant, and could be due to a component of natural liquid recharge, or to decompression effects at the boundaries of the vapour-dominated zone. A much more negative value for the ratio is implied by the few data points in the smaller pressure sink around power plants 9-10, suggesting little recharge or reinjection is occurring in this area. The very small value of the ratio in the unproduced part of the reservoir could be caused by tectonic subsidence, or could be due to decompression of a predominantly liquid-dominated reservoir.

Introduction During the mid-1970's, monitoring of gravity, and both vertical and horizontal movement at The Geysers, showed significant changes due to fluid withdrawal from the reservoir (Isherwood, 1977, 1981; Lofgren, 1981). More recently Denlinger, et al., (1981) modelled these changes, showing they yield reasonable estimates of the volume of the reservoir.

In this paper the relationship between gravity changes and subsidence is examined more closely to see whether variations within the reservoir may provide useful constraints for monitoring the effects production and reinjection.

Theory *Liquid Depletion Caused by a Pressure Drop.* In a vapour-dominated production zone, steam is the continuous, pressure-controlling phase, but trapped water is usually the dominant phase by mass. As pressure decreases, water boils, and the excess steam volume flows towards the source of the pressure drop. The heat of vapourization extracted from the rock and residual water causes a temperature decline. While water still remains in the rock, temperature and pressure follow the saturation curve. In most vapour-dominated zones (especially at The Geysers and Lardarello) temperature and pressure are in the range 220-250°C and 20-40 bars. Temperature changes (ΔT) and pressure changes (ΔP) are approximately linearly related by (error <10%):

$$\Delta T(^{\circ}C) = 1.8\ \Delta P\ (\text{bars}) \qquad (1)$$

Let x be the fractional volume of water in the rock which boils to steam during a small pressure drop ΔP and a temperature drop ΔT. If S is the fractional saturation of the pore volume before the pressure drop, then heat balance considerations yield:

$$x = [(1 - \phi)\rho_r C_r + \phi S\ \rho_w C_w]\Delta T/\rho_w L \qquad (2)$$

where ϕ = porosity
$\rho_{r,w}$ = density of rock, water
$C_{r,w}$ = specific heat of rock, water
and L = heat of vapourization

For the temperature range considered here, ρ, C, and L can be considered as constant, with ρ_w = 800 kg/m^3; C_r = 1 kJ/kg°C; C_w = 4.8 kJ/kg°C; and L = 1800 kJ/kg. If the porosity is less than about 10% (as at The Geysers) equation 2 simplifies to:

$$x = \rho_r C_r \Delta T/\rho_w L \qquad (3)$$

Inserting the appropriate values, with ρ_r = 2650 kg/m^3, gives:

$$x = 0.0018\ \Delta T(^{\circ}C), \text{ or}$$
$$x = 0.0032\ \Delta P(\text{bars}) \qquad (4)$$

That is, x is 1% if a pressure drop of 3 bars, and a temperature drop of 5-6°C occurs.

Gravity Change Caused by Liquid Depletion. The average reservoir density change caused by a fractional volume, x, of water being replaced by steam is $x(\rho_s - \rho_w)$, where ρ_s is the density of steam (15 kg/m^3). The one-dimensional gravity change, Δg, due to this density change is therefore:

$$\Delta g = 2\pi G H x(\rho_s - \rho_w) \qquad (5)$$

where G = gravitational constant
$(6.7 \times 10^{-11}\ \text{Nm}^2\ \text{kg}^{-2})$,

and H = average production zone thickness. Inserting the appropriate values and substituting for x using equations 1 and 4 gives:

$$\Delta g(\mu gals) = -110H\Delta P \quad (6)$$

where H is in km and ΔP is in bars. Because of the one-dimensional assumption, this equation is only valid where the sides of the production zone are a much greater distance from the observation point than the depth of the production zone. When used on its own, the equation may only be a reasonable approximation near the centre of the production zone. A one-dimensional expression for subsidence is also used in this papaer. The one-dimensional assumptions are not as restrictive as first appears, because the ratio of gravity change to subsidence is used in the interpretation.

Equation 6 gives the gravity change for a production-induced pressure drop in a vapour-dominated reservoir. Reinjection of excess condensate will cause an additional pressure drop as the water is heated to reservoir temperature. The reinjection will also decrease the size of the gravity change. If R is the mass fraction of the produced steam which returns to the reservoir, the gravity change will be reduced by a factor (1 - R). The temperature and pressure decline in the reservoir as the reinjected water comes to thermal equilibrium can be estimated if the initial enthalpy of water is known. Assuming the temperature of the water to be 70 ± 30°C (i.e. specific enthalpy of 300 ± 120 kJ/kg), the change in enthalpy after it has reached thermal equilibrium with a 230 ± 10°C reservoir, is 700 ± 160 kJ/kg. However the change in enthalpy caused by boiling trapped pore water to steam for production is 1800 kJ/kg. Therefore the reservoir heat loss, and also ΔT and ΔP, will be increased by a factor of (1+0.4R) due to reinjection. That is, the observed pressure drop, ΔP', is:

$$\Delta P' = \Delta P(1 + 0.4R) \quad (7)$$

where ΔP is the original pressure drop due to production alone. Since R is small at The Geysers (0.2 - 0.3), the uncertainty in the enthalpy change of the reinjected water becomes relatively small when considered in equation 7. Substituting for the original ΔP and Δg in equation 6, the simplified equation relating gravity change and average reservoir pressure drop becomes (superscript on ΔP' is also dropped):

$$\Delta g(\mu gals) = -110H\Delta P(1 - R)/(1 + 0.4R) \quad (8)$$

where H is in km and ΔP is in bars.

A check that equation 8 is reasonable can be made by substituting published values for The Geysers. The gravity change in the heavily produced part of the reservoir ranged between -150 and -200 μgals between 1974 and 1977 (Isherwood, 1977; corrected for elevation change). Assuming the production zone to be 2 km thick, this implies a pressure decline of 1.2 ± 0.3 bars. Lipman, et al. (1977) show the pressure decline at Cobb Mountain No. 1 well to have been 24 psi, or 1.7 bars, between 1974 and 1977. Considering the uncertainty in production zone thickness, the difference between the two figures is remarkably small.

Equation 8 emphasizes the value of repeat gravity surveys for monitoring depletion of The Geysers reservoir. With modern gravimeters, the standard error for surveys should be around ± 10 μgals. Since changes in production zone thickness should be negligible once the field has been on production for a few years, the theoretical resolution of repeat gravity surveys is equivalent to ± 0.1 bars reservoir pressure. The main factor limiting this resolution is varying near-surface groundwater level. This becomes significant if water level changes are in excess of several metres.

Subsidence The one-dimensional relationship between subsidence, Δh, and reservoir consolidation at depth is (after Geertsma, 1973):

$$\Delta h = 2(1 - \nu).\ [\text{consolidation}] \quad (9)$$

where ν = Poisson's ratio (0.25 ± 0.15 usually). Reservoir consolidation can occur from both a temperature decline and a pressure decline. Equation 9 therefore becomes:

$$\Delta h = 1.5\ (\alpha H\Delta T + aH\Delta P) \quad (10)$$

where α is the coefficient of linear expansion, and a is the uniaxial compaction coefficient ($a \simeq 0.5$ (bulk compressibility) $\simeq 0.5$ (bulk modulus)$^{-1}$). For most rocks $\alpha \simeq 10 \pm 2 \times 10^{-6}$ °C^{-1} (Skinner, 1966) and $a \simeq 1 \times 10^{-6}$ bars^{-1} for rocks with low porosity (Birch, 1966). This value for a is also consistent with the elastic properties of The Geysers reservoir inferred from seismic velocities (Majer and McEvilly, 1978). Inserting these values in equation 10, and substituting for ΔT using equation 1 gives:

$$\Delta h(cm) = 2.9\ H\ \Delta P; \quad (11)$$

where H is in km and ΔP is in bars. It is also evident that the thermal contraction component is an order of magnitude larger than the fluid decompression component. This is a characteristic of a low-porosity reservoir. For high-porosity reservoirs (e.g. $\phi > 20\%$; these are usually liquid dominated) subsidence is mostly due to fluid decompression.

The heavily produced part of the production borefield at The Geysers subsided by 10 ± 2 cm between 1974 and 1977 (Lofgren, 1981). Using H = 2 km again, equation 11 implies a pressure drop of 1.7 ± 0.3 bars. This is also very close to the pressure drop observed in Cobb Mountain No. 1 well during that time.

Ratio of Gravity Change/Subsidence. Combining equations 8 and 12 gives the ratio of gravity change to subsidence as:

$$\Delta g/\Delta h \simeq -38\ \frac{1 - R}{1 + 0.4\ R}\ \mu gal/cm \quad (13)$$

The accuracy of the ratio is difficult to estimate, as it depends on the accuracy of the values chosen for the various physical parameters. The value of Poissons ratio and the uniaxial compaction coefficient have the greatest uncertainty. As a result, the uncertainty in the ratio in equation 13 is probably ±20%. The ratio should be less sensitive to boundary effects than either of the one-dimensional expressions for Δg and Δh, because the two parameters are independent physical properties of the same anomaly. Boundary effects will therefore tend to cancel. The advantage of the ratio is its independence of the actual reservoir thickness or the pressure drop in the reservoir. It is also insensitive to variations in porosity as long as the porosity is less than about 10%, and 2-phase, vapour-dominated conditions exist.

With no reinjection, the ratio of gravity change/ subsidence should be around 38 μgals/cm.

Analysis of the Data Fortunately an overlapping set of gravity and subsidence data has been published for The Geysers reservoir. Gravity changes were measured between 1974 and 1977 over a large portion of the produced part of the reservoir (Isherwood, 1977). Levelling surveys were made in 1973, 1975 and 1977 (Lofgren, 1981). A profile of gravity change and subsidence across the reservoir is shown in Fig. 1. This extends from the produced part of the reservoir onto the unproduced part (Fig. 2). Both the gravity and the subsidence profiles are referred to assumed stable benchmarks 20 km from the reservoir. Fig. 1 shows the main area of subsidence and gravity change coinciding with the produced area of the reservoir.

To ensure that the subsidence corresponds to the same period as the gravity changes, the subsidence between 1974 and 1975 is assumed to be half that between 1973 and 1975. In addition, the gravity changes discussed by Isherwood (1977) are not corrected for subsidence of the benchmarks (pers. comm., W.F. Isherwood, 1982), so the free-air correction of 3 μgals/cm has been applied. Thirty four benchmarks at The Geysers have both gravity change and subsidence measurements for the period 1974-1977. The distribution of the benchmarks is shown in Fig. 2, and the data is plotted in Fig. 3. All 34 points show a weak trend of increasing gravity change with increasing subsidence. However, a much clearer pattern emerges when the points are split-up according to their location in Fig. 2. The data can be divided into 4 groups:

A: Points within the most heavily produced part of the reservoir (near power plants 1-8, 11) having both a large gravity change and a large subsidence value (black circles);

B: Points close to power plants 9, 10, having a large gravity change with only moderate subsidence values (black squares);

C: Points between groups B and D with moderate gravity changeand moderate subsidence (downward triangles) and

D: Points in the unproduced part of the reservoir having little gravity change with moderate subsidence (upward triangles).

Group A, with 15 points, defines a regression line of slope -14 μgals/cm, and intercept -17 μgals, with a regression coefficient of 0.85. This line is compared with 4 theoretical lines in Fig. 3. The horizontal line for R = 1 corresponds to no mass loss from the reservoir; R = 0 corresponds to no reinjection; and the two intervening lines correspond to varying amounts of reinjection.

Despite the scatter in group A data points (each gravity change has an accuracy of about ± 30 μgals, Isherwood, 1977), the fact the regression line passes close to the origin suggests the data may be behaving according to the theory outlined above. A systematic error in the amount of subsidence, such as that caused by the base-station benchmark being unstable, or tectonic tilt occurring, would have caused the line to pass wide of the origin. The slope of the line is equivalent to R = 0.55, which is significantly greater than the R = 0.2 - 0.3 normally cited for The Geysers (Reed and Campbell, 1976; Bufe and Shearer, 1980). This discrepancy is reduced if the reservoir rock is more compressible than originally assumed. However even with an order of magnitude larger compressibility, R is only reduced to 0.4. Assuming the discrepancy to be real, it could be caused by a component of natural recharge to the production zone. If present, this would most likely take the form of water draining down from shallow depth. An alternative explanation is that boundary effects, where the rock is liquid dominated and pressure is greatly in excess of saturation pressure, are biasing the ratio. Appendix I shows that decompression of a single-phase liquid zone

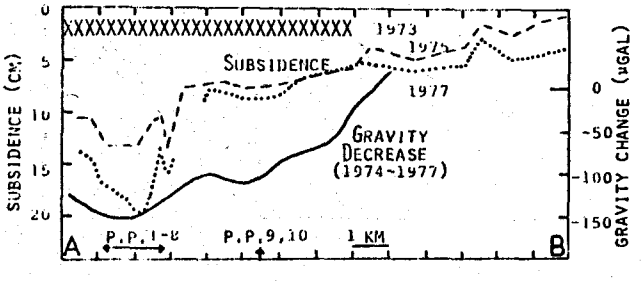

Fig. 1: Profiles of gravity change (Isherwood, 1977) and subsidence (Lofgren, 1981) along a NW-SE line across The Geysers reservoir. The row of crosses denotes the area of production, which also coincides with the area of induced seismicity.

should have a gravity change/subsidence ratio of -1 to -2 μgals/cm. An interesting feature in Fig. 2 is the spread of group A points to the west of the main pressure sink shown by Lipman, et al.(1977). This suggests that drawdown in the reservoir extended further toward Mt Cobb than was recognised at that time.

In contrast to group A points, the average of the four group B points (-155 μgals; 4.5 cm) lies on a line equivalent to R = 0.1. These points are influenced by production from power plants 9 and 10. The reinjection well for these plants is 1-2 km north of the four benchmarks. Possibly very little fluid is returning to the vicinity of the production wells. The fact these four points lie so close to the R = 0 line also suggests that the values assumed for the elastic constants in equations 9 and 10 may be reasonably accurate. This in turn, confirms that the slope of the group A regression is significantly less than the lines for R = 0.2 or 0.3.

Group C benchmarks lie in a transition zone between the produced and unproduced parts of the reservoir. Their gravity changes and subsidence reflect this, being intermediate between groups A, B, and group D points (Fig. 3).

Subsidence of the Unproduced Reservoir Group D points in the unproduced part of the reservoir have negligible average gravity change, and an average subsidence of 4 cm. One explanation for this could simply be that the subsidence here has a tectonic origin. However if true, it is surprising that tectonic subsidence of this magnitude has not also

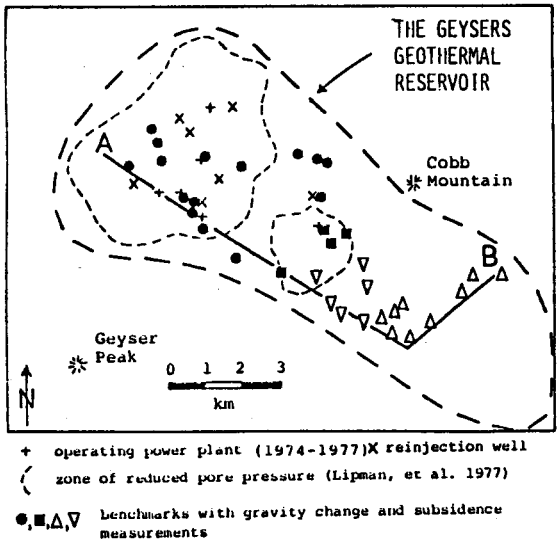

Fig. 2: Location of benchmarks which were monitored for gravity change and subsidence between 1974 and 1977. The benchmarks are divided into four groups according to location in the reservoir.

affected group A points in the produced part of the reservoir. An alternative explanation is that the unproduced part of the reservoir is mostly liquid dominated, with average reservoir pressure greatly in excess of steam saturation (e.g. vertical pressure gradient near to hydrostatic). Decompression of an all-liquid zone with low porosity would cause the ratio of gravity change to subsidence to be between -1 and -2 μgal/cm. (Appendix 1). Subsidence of 4 cm would therefore be associated with a gravity decrease of -4 to -8 μgals, which is too small to have been measured in the 1974-1977 gravity surveys. If the subsidence was due to liquid decompression then the 4 cm of subsidence could have been caused by a liquid pressure drop of 13 bars (equation 4). At this rate, the pressure at production depth would take many years to fall to 30-40 bars saturation pressure (for 230-250°C water).

Allis (1982) has suggested that the induced seismicity in the exploited part of The Geysers reservoir could be partly due to a large fluid pressure drop caused by production. This explanation implies that the initial fluid state of the reservoir was liquid-dominated but that it rapidly became vapour-dominated with production. The presence of subsidence without a significant gravity change in the unproduced part of the reservoir could be additional supporting evidence.

The obvious difficulty with this explanation is the fact that investigation wells in the unproduced reservoir apparently discharged steam after a short period of 2-phase discharge immediately after drilling. Down-hole pressure therefore indicates that an extensive vapour-dominated zone may already exist. The only way this contradiction can be reconciled is if the pressure measured in a well which has been discharged is not representative of average reservoir conditions. This could conceivably occur if the large fractures which represent the primary permeability are finite in volume and, in general don't form an intersecting network through the entire reservoir. For example, the major features could be arranged in an en echelon pattern, which would be consistent with the right-lateral shear at The Geysers. Each fracture must be large enough so that steam wells have a high transmissivity, but also small enough so that on first opening, the pressure drops to steam saturation within the first few hours, or at most, days. Such behaviour is feasible because the hydraulic diffusivity of single phase, 250°C water is 1000 times higher than that of 2-phase, 250°C fluid (derived from Grant and Sorey, 1979). Once depleted of excess water, such fractures may take many years to become liquid-dominated again, because of both the lower, secondary permeability of the surrounding rock, and the 'insulating effects of 2-phase fluid.

Conclusions Combined use of gravity change and subsidence monitoring at The Geysers is

capable of providing valuable constraints on reservoir modelling. Both parameters are linearly dependent on the fluid pressure drop. However they are also dependent on assumptions of the size and shape of the reservoir, and the amount of reinjection. By forming a ratio of the gravity change to subsidence, several of the dependent variables cancel. Systematic variations in the ratio are best analysed by plotting the gravity change against subsidence for all benchmarks. Examination of the graph for 1974-1977 data at The Geysers shows lateral variations in the extent of production and reinjection can be identified by this method. However a full understanding of these variations will probably only come when the data is used in conjunction with other reservoir information (such as downhole pressure or discharge enthalpy changes). The additional information would help clarify whether the anomalously low gravity change/ subsidence ratio in the heavily produced part of the reservoir is due to a component of recharge, or some other factor. The accuracy that can be attained with both gravity and precise levelling surveys is such that repeat surveys should be carried out each year.

Acknowledgements Bill Isherwood kindly forwarded a table of the gravity changes measured at benchmarks around The Geysers field. I also thank Trevor Hunt for commenting on an earlier version of the manuscript.

References

Allis, R.G.: Mechanism of induced seismicity at The Geysers geothermal reservoir, California. Geophysical Research Letters, v. 9, p 629-632, 1982.

Birch, F.: Compressibility; elastic constants, in *Handbook of Physical Constants*, ed. S.P. Clark, Geological Society of America memoir, 97, p 97-174, 1966.

Bufe, C.G. and Shearer, P.M.: Geothermal induced seismicity - bane or blessing? proceedings, 2nd DOE-ENEL Workshop for cooperative research in geothermal energy, LBL, Berkeley, p 86-97, 1980.

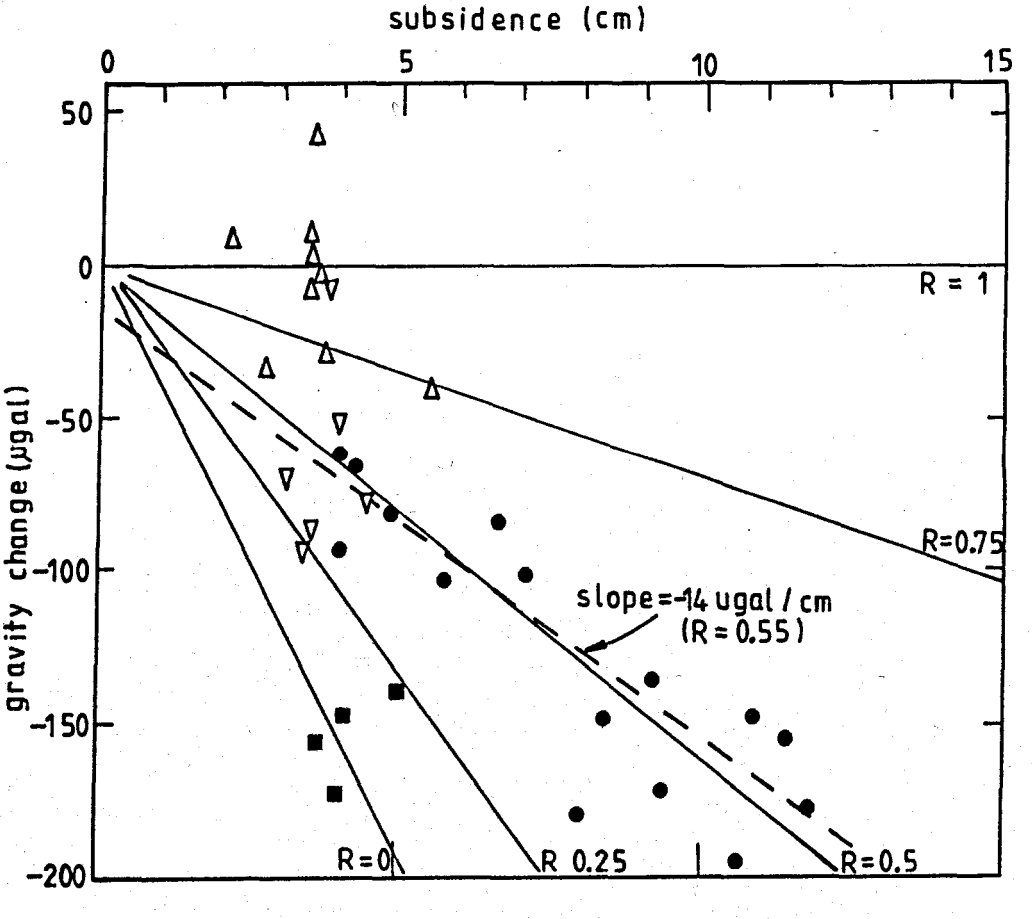

Fig. 3: Plot of gravity change (corrected for elevation change) against subsidence for the period 1974-1977 at The Geysers (from Isherwood, 1977; Lofgren, 1981). The different symbols denote location with the reservoir (Fig. 2). Solid lines are theoretical relationships for varying amounts of reinjection (refer to text). Dashed line is the regression line for the 15 black circles.

Denlinger, R.P., Isherwood, W.F. and Kovach, R.L.: Geodetic analysis of reservoir depletion at The Geysers steam field in northern California. Journal of Geophysical Research, v. 86, p 6091-6096, 1981.

Geertsma, J.: Land subsidence above compacting oil and gas reservoirs, Journal of Petroleum Technology, v. 25, p 734-744, 1973.

Grant, M.A. and Sorey, M.L.: The compressibility and hydraulic diffusivity of a water-steam flow, Water Resources Research, v. 15, p 684-686, 1979.

Isherwood, W.F.: Geothermal reservoir interpretations from changes in gravity, in, proceedings of, Geothermal Reservoir Engineering Workshop - 1977, Stanford California, p 18-23, 1977.

Isherwood, W.F.: Geophysical overview of The Geysers, in, Research in The Geysers - Clear Lake geothermal area, northern California, eds. McLaughlin, R.J. and Donnelly-Nolan, J.M., U.S.G.S. prof. paper 1141, p 83-95, 1981.

Lipman, S.C., Strobal, C.J. and Gulati, M.S.: Reservoir performance of The Geysers field, Geothermics, v. 7, p 209-218, 1978.

Lofgren, B.E.: Monitoring crustal deformation in The Geysers - Clear Lake region, in, Research in The Geysers - Clear Lake geothermal area, northern California, eds. McLaughlin, R.J. and Donnelly-Nolan, J.M., U.S.G.S. prof. paper 1141, p 139-148, 1981.

Majer, E.L. and McEvilly, T.V.: Seismological investigations at The Geysers geothermal field, Geothermics, v. 44, p 246-268, 1978.

Reed, M.J. and Campbell, G.E.: Environmental impact of development at The Geysers geothermal field U.S.A., in, proceedings, Second United Nations Symposium on the Development and Use of Geothermal Resources, p 1399-1410, 1976.

Skinner, B.J.: Thermal expansion, in, Handbook of Physical Constants, ed. Clark, S.P., Geological Society of America, memoir 97, p 75-96, 1966.

Appendix 1: *Decompression of a single-phase liquid zone.* Consider a reservoir in which the water is under a pressure greatly in excess of steam saturation. When a drop in fluid pressure occurs, the increase in effective pressure on the rock causes a decrease in pore volume, and the pore water also becomes less dense. The fractional volume of water expelled from the rock due to these two effects will be $\Delta P(A + b\phi)$, where A is the bulk compressibility of the rock, and b is the fluid compressibility ($\simeq 1 \times 10^{-4}$ bars^{-1} for 250°C liquid). The one-dimensional expression for the gravity change during a pressure drop is therefore:

$$\Delta g = -2\pi G H \rho_w \Delta P(A + b\phi) \qquad (1A)$$

where all symbols are the same as in the main body of the paper. Inserting a bulk compressiblity value appropriate for the low porosity rock at The Geysers (assumed to be 2×10^{-6} bars^{-1}), and assuming the porosity to be between 0.03 and 0.07,

$$\Delta g = -(0.24 \pm 0.06) H \Delta P \qquad (2A)$$

where H is in km and ΔP is in bars. As before, the subsidence will be:

$$\Delta h = 2(1 - \nu) H a \Delta P \qquad (3A)$$

where a is the uniaxial compaction coefficient ($\simeq 1 \times 10^{-6}$ bars^{-1}). Therefore Δh(cm) $\simeq 0.15 H \Delta P$, and the ratio of gravity change to subsidence is:

$$\Delta g/\Delta h \simeq -1 \text{ to } -2 \text{ } \mu\text{gals/cm} \qquad (4A)$$

Proceedings Eighth Workshop Geothermal Reservoir Engineering
Stanford University, Stanford, California, December 1982
SGP-TR-60

COMPARISON OF SUBSIDENCE AT WAIRAKEI, BROADLANDS AND KAWERAU FIELDS, NEW ZEALAND

R.G. Allis

Geophysics Divn, D.S.I.R., Wairakei, New Zealand

Abstract. Exploitation has caused over 9 m of subsidence at Wairakei since 1950, up to 30 cm at Broadlands between 1968 and 1974, and up to 25 cm at Kawerau since 1970. Despite these differences and large differences in the rate and amount of mass withdrawal, there are similarities in the pattern of subsidence at all 3 fields. In each field, pressure drawdown in the production zone can be identified as a nearly circular area of consolidation centred on the production borefield. The circular shape suggests that the predominant fault direction may not be the main factor controlling horizontal permeability. In addition to production zone consolidation, each field has a small area of relatively intense subsidence originating from shallow depth. The area of shallow consolidation is near to the natural outflow zone where geothermal water originally rose to near-surface and dispersed in highly compressible formations. Early identification of such areas in other fields is important because the high rate of consolidation at shallow depth can cause large horizontal strain and tilt of the ground surface. There is also evidence of cool groundwater inflow near the area of shallow consolidation in all three fields. Shallow reinjection into these areas may mitigate the effects of subsidence and groundwater invasion.

Introduction. Wairakei field has become renowned for the amount of subsidence which has been caused by production (Hatton, 1971; Stilwell, et al., 1976; Allis and Barker, 1982). An unusual feature of the subsidence is the area of maximum subsidence being displaced from the production borefield. The explanation for this has been controversial (Pritchett, et al., 1980; Narasimhan and Goyal, 1979). However, recent study has shown that the subsidence can be readily explained by conventional consolidation behaviour of the reservoir with most of the consolidation occurring in the steam zone (Allis and Barker, 1982). The purpose of this paper is to show that although the magnitude of the subsidence at Wairakei may be unique, there are broad similarities between the subsidence at Wairakei, Broadlands and Kawerau geothermal fields. All three fields lie within the active volcanic zone of the North Island, New Zealand, and their production zones (generally 500-1000 m depth) comprise Quarternary rhyolitic-andesitic volcanics and sediments. Because of space limitations, only a brief summary of the subsidence history and modelling of each field is given here. More detailed descriptions can be found in the references cited.

Wairakei field. The total amount of subsidence at Wairakei has now exceeded 9 m, with the area of maximum subsidence still subsiding at >0.4 m/y (Allis and Barker, 1982). This exceeds all known cases of subsidence caused by any form of fluid withdrawal. A map of the subsidence since exploitation of the field began in 1950 is shown in Fig. 1. The area of intense subsidence covers less than 1 km^2 and this is centred close to the northern boundary of the field, about 0.5 km from the eastern production borefield. Subsidence ranges between 1 and 2 m across most of the production borefield, and over the rest of the field, it is mostly within 0.5 ± 0.1 m. Fig. 2 shows an E-W cross-section which summarizes the relationship between subsidence, the geology and temperature variations within the field, and the pressure and gravity changes caused by exploitation. Modelling of the area of maximum subsidence, using the analytical solutions for consolidating circular disks (after Geertsma, 1973), suggests the top of the consolidating zone is at about 150 m depth. This places the consolidation zone in Huka pumice breccia, a relatively permeable unit deposited between the upper and lower lacustrine mudstone units of the Huka formation (Grindley, 1965). The modelling suggests about 15 m of consolidation has caused the 8.5 m of surface subidence up to December

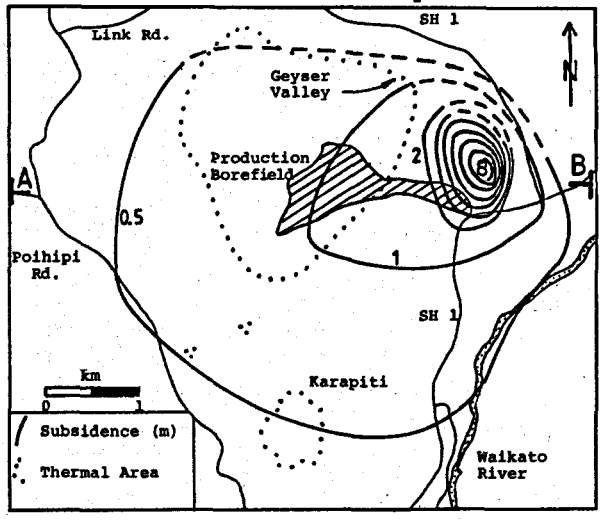

Fig. 1: Subsidence at Wairakei field between 1950 and December 1980. Contour interval is 1 m apart from 0.5 m contour.

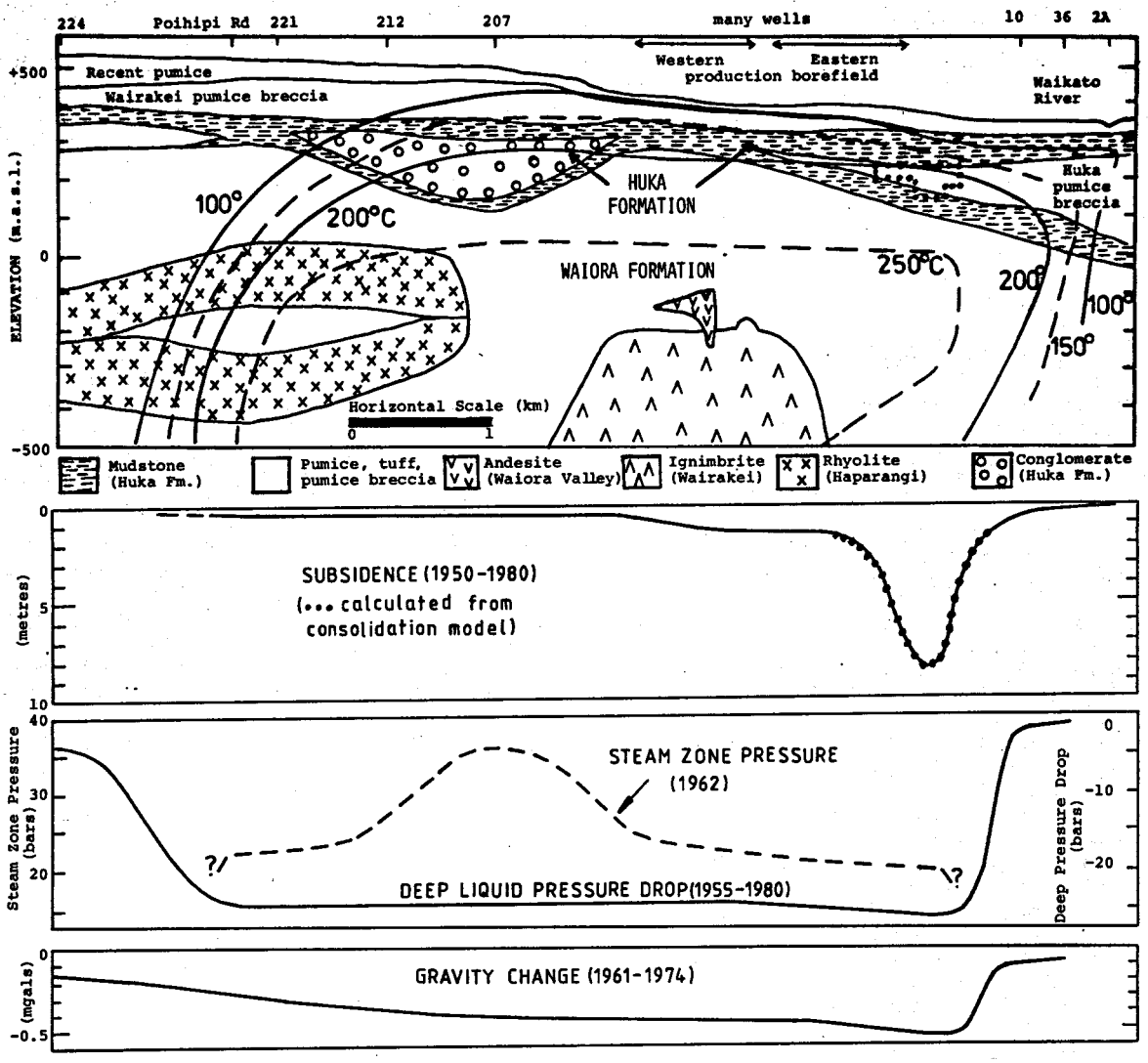

Fig. 2: Cross-section of Wairakei field showing relationship between geology and temperature, and the subsidence, pressure changes and gravity change caused by exploitation. The 1962 steam pressure is from Grant (1982); the gravity change is from Hunt (1977). Dotted area on cross-section is the consolidation model that fits the area of maximum subsidence, 1980 (Poisson's ratio assumed to be 0.25).

Assuming the pumice breccia unit is 220 m thick beneath the area of maximum subsidence, and fluid pressure has dropped by 10 bars, the compressibility of the unit must be around 8 kbars^{-1}. Laboratory compressibility measurements on cores of pumice breccia confirm this, with compressibility ranging between 8 and 17 k bars^{-1} for an effective pressure increase of 5-15 bars (Allis and Barker, 1982). The high compressibility of near-surface pumice breccia is due to its high porosity (50-80% typically). The deeper Waiora pumice breccia generally has a porosity of <30% and a compressibility 2 to 3 orders of magnitude less than near surface pumice breccias. The 0.5 m of subsidence across a large area of Wairakei field can be accounted for if the consolidation occurs in a 500 m-thick zone with an average compressibility of 0.02-0.03 kbars^{-1} (pressure drop of 25 bars). However, much of this consolidation may be occurring in a thinner zone of more compressible material near the top of the Waiora formation. This is because subsidence linearly correlates with pressure decline in the steam zone, rather than pressure decline in the deeper liquid zone (Allis and Barker, 1982). Steam zone pressure has steadily fallen by 10-15 bars since the steam zone formed around 1960. The pressure continues to fall at 0.2-0.5 bars/y despite deeper liquid pressure being almost constant since the early 1970's.

Broadlands field. Extraction of fluid from Broadlands began in 1967, and rapidly rose to a peak equivalent to 100 MW (electrical) in 1971. Subsequent discharge of production wells has been intermittent, with the annual average being less than one tenth of the peak in 1971. This discharge history caused pressure to fall by 15 bars between 1967 and 1971, and pressure has subsequently recovered by about 8 bars (Hitchcock and Bixley, 1976). In contrast, benchmarks in the centre of the production borefield subsided

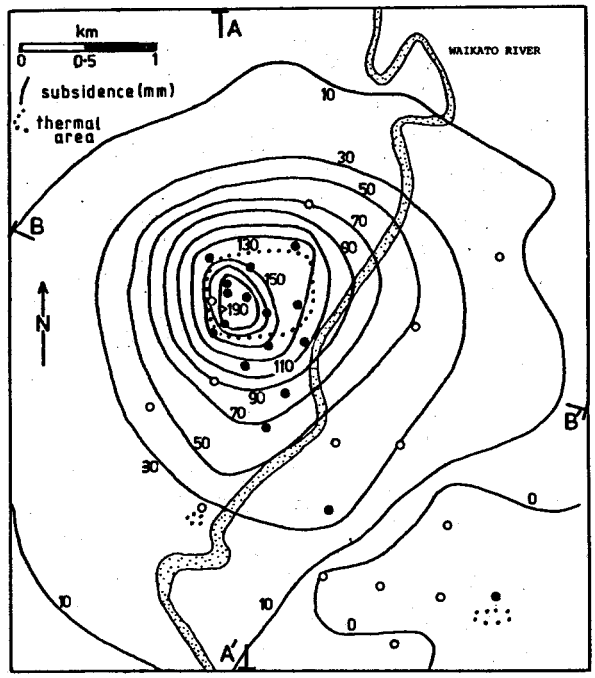

Fig. 3: Subsidence at Broadlands field between 1968 and 1974 (in mm). The black circles are wells discharged during this time. Open circles are other production wells

by 15-30 cm between 1968 and 1971, and there has been relatively little subsidence since then. The lack of rebound of benchmarks, despite a 50% recovery in reservoir pressure, indicates that consolidation is occurring as permanent pore collapse rather than elastic compression (Allis, 1982a). This behaviour was also observed in the laboratory compression measurements on pumice breccia from Wairakei. The amount of subsidence between 1968 and 1974 is shown in Fig. 3. Most of the subsidence had occurred by 1971, the time of the maximum pressure decline. A model for the subsidence is shown in Fig. 4. This assumes a uniform compressibility of 0.025 kbars^{-1}. Pressure drawdown in the production zone (500-1000 m depth) is incapable of explaining the relatively small area of maximum subsidence in the centre of the borefield. Part of the discrepancy can be accounted for by modelling drawdown above the production zone (100-500 m depth). However, even this cannot fit the entire subsidence profile, and an area of relatively high compressibility at shallow depth (probably <100 m depth) is required in the centre of the borefield. The 0.8 km^2 area of drawdown above the production zone coincides with an area of low resistivity at <100 m depth, and with an area of relatively high surface heat flow and chloride outflow prior to 1968. Since 1968 this area has become notable for decreased groundwater levels, increased gravity (up to 0.3 mgal) and decreased downhole temperature and chloride concentration in production wells (Allis, 1982a). These changes are consistent with a downflow of cool groundwater into the production zone. The area of shallow consolidation at Broadlands was originally the main area of geothermal fluid outflow prior to exploitation, and this has changed to an area of groundwater downflow with production.

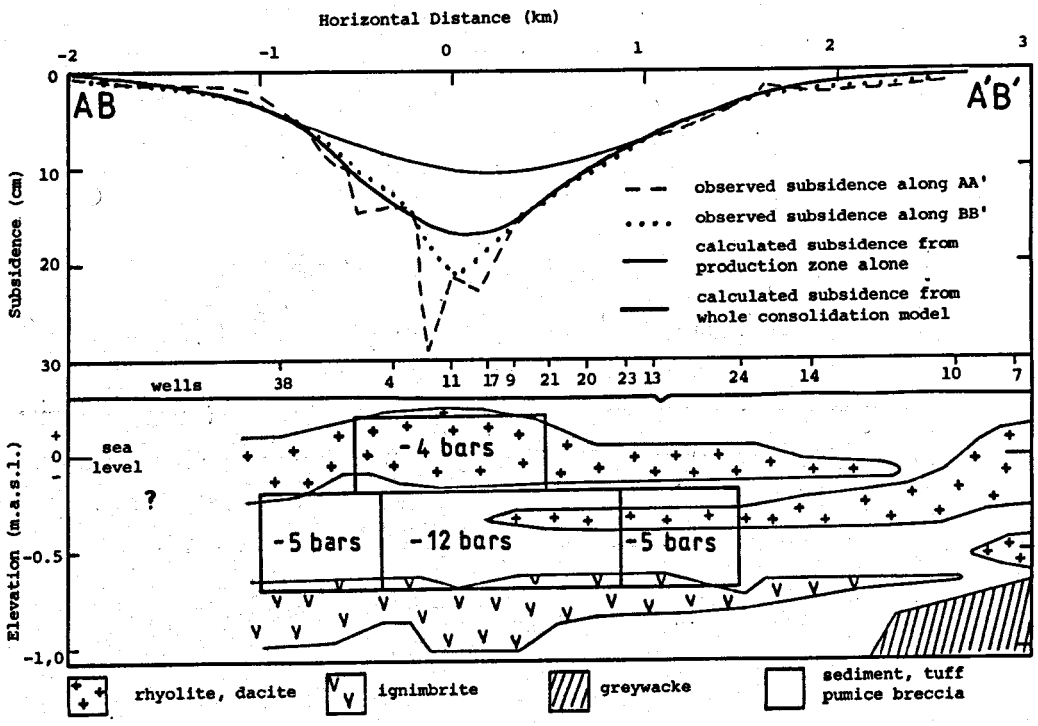

Fig. 4: Consolidation model for the Broadlands field. Production zone compaction is modelled as a central disk with 12 bars of pressure drawdown, and an annular zone surrounding this with 5 bars of drawdown. A circular area of consolidation above the production zone with a drawdown of 4 bars is included in the model.

Kawerau field. Although the first wells at Kawerau were discharged during the 1950's, the field was not levelled until 1970. Since this time, the rate of mass withdrawal has been almost constant at 7×10^9 kg/y and the maximum rate of subsidence has also not varied greatly, ranging between 15-20 mm/y. There has been no measurable drawdown in the production zone (600-1200 m depth; pressures to ±1 bar). The subsidence pattern is asymmetric, with maximum subsidence occurring on the NE side of the field (Fig. 5). An E-W cross-section (Fig. 6) shows clearly that the subsidence is composed of two components: a broad zone of consolidation probably occurring in the production zone, and a small area of consolidation from shallow depth (Allis, 1982b). Modelling of the subsidence profile confirms this, with the top of the production zone anomaly occurring at about 50 m depth, and the shallow anomaly occuring at about 200 m depth. The shallow anomaly could have been modelled at <200 m depth, but consideration of the geology suggests it may originate in an explosion breccia unit at that depth. According to the model, production zone consolidation is occurring at 8 mm/y, while the shallow zone is consolidating at 17 mm/y. The depth extent of the two consolidation zones shown in Fig. 6 is inferred from the geology because of uncertainty in both the compressibility and the rate of pressure decline. Many of the Kawerau production well discharges have suffered declines in the enthalpy and chloirde content, indicating invasion by cooler water. The possibility that the subsidence is being caused by thermal contraction has been investigated and found to be untenable (Allis, 1982b). The observed cooling rates of several °C/y means that the cool water is entering the field along restricted paths, such as faults or down the outside of well casing, and the bulk of the reservoir rock remains close to its original

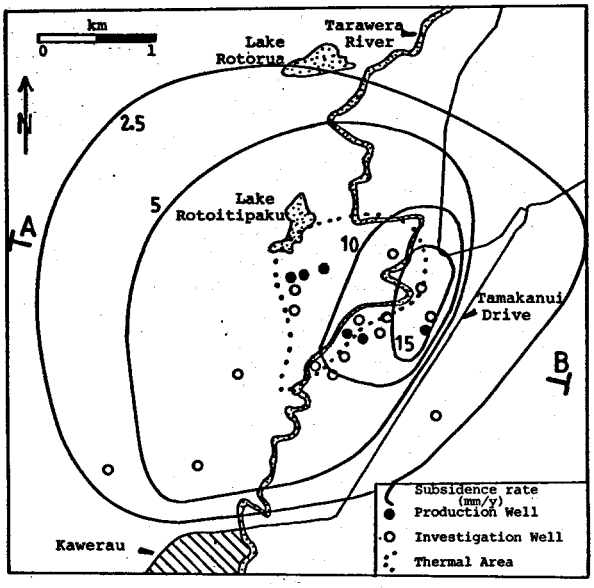

Fig. 5: Rate of subsidence at Kawerau field between 1978 and 1982 (in mm/y).

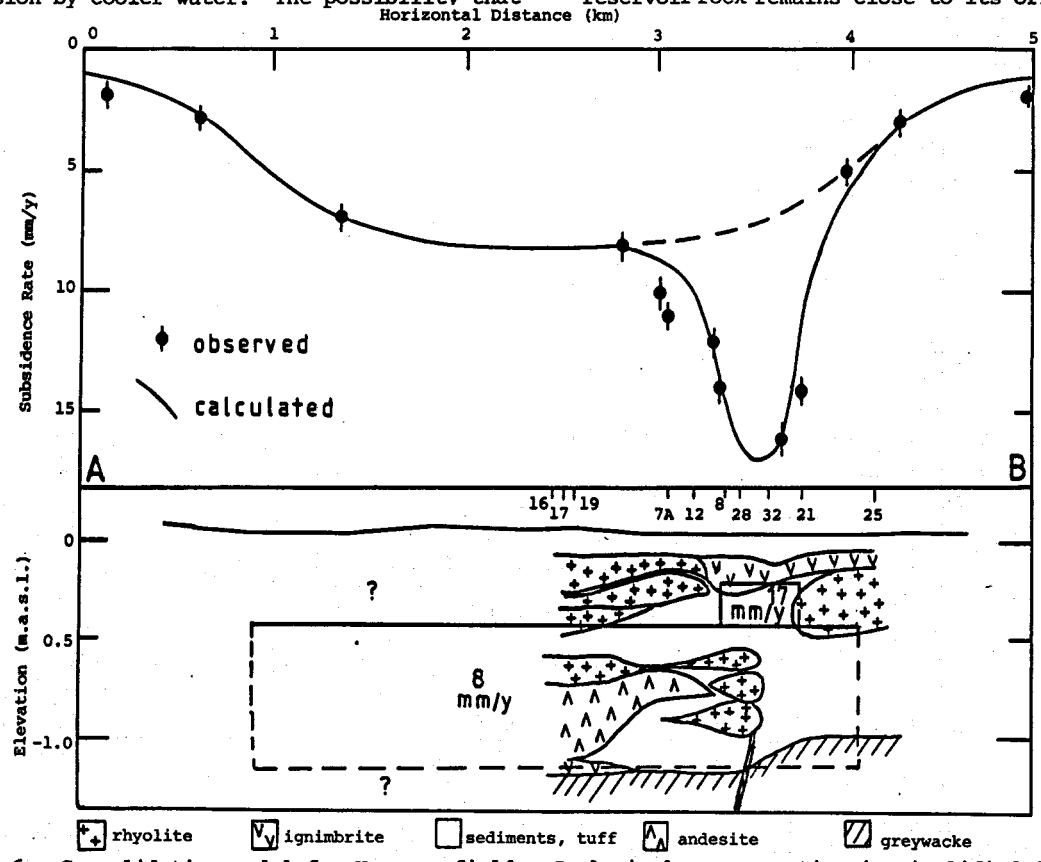

Fig. 6: Consolidation model for Kawerau field. Geological cross-section is simplified from Nairn (1982).

temperature. Although the pressure drop at production depths has been less than 1 bar, the cooling feed-zone temperatures could mean a larger pressure drop has occurred at shallow depth. This would be the case if the water is being drawn down from shallow depth. In the area of maximum subsidence, there has been a small but systematic variation in the rate of subsidence since 1970 which relates to the amount of production from nearby wells. This implies that near-surface water is being drawn down to production depths, because the subsidence in this area is dominated by consolidation at shallow depth. A cooling of 30-40°C in the feed zones, with no pressure change at production depths, would cause near-surface pressure to fall by about 3 bars. Pivoting of the pressure depth curve with time implies that production zone consolidation may be restricted to the upper part of the production zone.

Discussion and Conclusions. An unexpected feature of the subsidence at the 3 fields is the roughly circular shape of the outer subsidence contours. These contours are concentric about the region of maximum mass withdrawal, and they reflect the lateral extent of drawdown in the production zone. The predominant faults in each field are normal faults trending NE-SW. If these faults were controlling permeability, elliptical contours with NE-trending major axes would have occurred. The circularity of the contours suggests that the production zones have uniform horizontal permeability and that they are behaving as homogeneous (horizontally), porous-permeable media. Possibly it is only the deep (>1 km) upflow parts of these fields where permeability is strongly fault controlled. At these depths compressibility is relatively small, and there is little contribution to the subsidence.

Modelling of the subsidence in all 3 fields has shown that there are 2 components: a zone of consolidation associated with the production zone which is comparable in the area to the area of the field; and a relatively small area of more intense consolidation at shallower depth. The depth of these two consolidation zones cannot be determined uniquely from the modelling, but it appears likely that the shallow component is occurring at less than 300 m depth, whereas the production zone component may be at about 500 m depth. The characteristics of the 2 consolidation zones in each field are summarised in Table 1. The consolidation potential in the right hand column of Table 1 is a measure of sensitivity to drawdown. It is equal to the product of the average compressibility and the average thickness of the consolidation zone.

The characteristics of the shallow consolidation zones make them very important when considering the environmental or engineering consequences of subsidence. In all 3 fields, the maximum horizontal strain and tilt occur around the boundaries of these zones. The extreme examples of this are at Wairakei, where horizontal strain reaches 5×10^{-4}/y, the maximum ratio of horizontal to vertical movement is 0.7, and maximum tilt is around 1 mrad/y (0.05°/y) (Allis and Barker, 1982). Clearly, the prediction or identification of similar zones in other fields is essential during the initial stages of field development. A common feature appears to be their proximity to chloride-bearing springs and seeps. In addition, these areas have low resistivity at shallow depth. This is probably caused by the presence of chloride water in the sediments rather than acid-sulphate waters or a clay-rich steam zone. The chloride water means that the consolidation zone is in a natural outflow part of the field, and therefore it may have a direct, liquid connection to the reservoir at depth. Once the reservoir is under production, such areas may experience the full effects of drawdown. A second feature is the presence of material with a high compressibility. At both Wairakei and Kawerau the shallow consolidation appears to be occurring in a pumice breccia or explosion breccia which may have been rapidly deposited and poorly consolidated. Early dectection of potential areas of high consolidation may be possible if compressiblity measurements are made on core

	Period of Data	Mass Discharged	Maximum Subsidence	Amount of Consolidation	Area of Consolidation	Pressure Decline	Consolidation Potential
Production zone WAIRAKEI shallow anomaly	1950-80	1400×10^9 kg	8.6 m	500 mm 15000	10 km^2 0.5	25 bars 10-15	20 mm/bar 1000-1500
production zone BROADLANDS shallow anomaly	1968-74	30×10^9 kg	0.3 m	100 mm 150	5 km^2 0.8	12 bars 1-5?	8 mm/bar 30-150?
production zone KAWERAU shallow anomaly	1978-82	7×10^9 kg/y	0.25 m	8 mm/y 17	9 km^2 0.4	0.1-0.2? bars/y 0.1-0.5?	40-80? mm/bar 34-170?

Table 1: Summary of subsidence characteristics. Production zone and shallow anomaly refer to the 2 consolidation zones causing the subsidence in each field.

from all formations, with particular emphasis on core from <300 m depth.

There is evidence in all 3 fields of cold water inflow near the shallow consolidation zone. At Wairakei, cold water may be flowing down the faults which originally channelled the hot water towards Geyser Valley (Allis, 1981). In addition, a cold intrusion at shallow depth has been identified in a well just outside the area of maximum subsidence (Allis, 1982c). The evidence at Broadlands has already been discussed. At Kawerau the cold intrusions may by more widespread. However, wells near the area of maximum subsidence originally had the hottest temperatures at shallow depth, but their shallow feed zone had suffered significant temperature declines by 1960, and the wells have had to be deepened (Grant, 1977). The only way of mitigating the effects of cold intrusions may be reinjected of waste borefield water into the inflow region. Reinjection into the shallow consolidation zone has the added advantage of possible repressuring of this zone, and reducing the maximum rate of subsidence in the field.

Acknowledgement. I am grateful for access to the survey data of Ministry of Works and Development, Wairakei, who carried out the repeat levelling surveys in all 3 fields.

References

Allis, R.G. 1981: Changes in heat flow associated with exploitation of Wairakei geothermal field, New Zealand. N.Z. Journal of Geology and Geophysics, v. 24, p 1-19.

Allis, R.G. 1982a: Reassessment of the physical changes caused by exploitation of Broadlands goethermal field. Geophysics Division Report, in prep., D.S.I.R., Wellington, N.Z.

Allis, R.G. 1982b: Interpretation of the subsidence at Kawerau. Unpublished Geothermal Circular RGA-5, Geophysics Division, D.S.I.R., Wellington, N.Z.

Allis, R.G. 1982c: Geologic controls on shallow hydrologic changes at Wairakei field. proceedings, Pacific Geothermal Conference and 4th N.Z. Geothermal Workshop 1982, University of Auckland, N.Z.

Allis, R.G. and Barker, P. 1982: Update on subsidence at Wairakei. proceedings, Pacific Geothermal Conference and 4th N.Z. Geothermal Workshop 1982, University of Auckland, N.Z.

Geertsma, J. 1973: Land subsidence above compacting oil and gas reservoirs. Journal of Petroleum Technology, v. 25, p 734-744.

Grant, M.A. 1977: Temperature patterns and changes at Kawerau. Unpublished Geothermal Circular, MAG-16. Applied Maths Division, D.S.I.R., Wellington, N.Z.

Grant, M.Z. 1982: Recharge to Wairakei field. proceedings, Pacific Geothermal Conference and 4th N.Z. Geothermal Workshop 1982, University of Auckland, N.Z.

Grindley, G.W. 1965: The geology, structure and exploitation of the Wairakei geothermal field, Taupo, New Zealand. N.Z. Geological Survey Bulletin, n.s. 75, D.S.I.R.

Hatton, J.W. 1970: Ground subsidence of a geothermal field during exploitation: proc. U.N. Symposium on the Development and Untilisation of geothermal resources, Pisa, Geothermics, Spec. Issue 2, p. 1294-1296.

Hitchcock, G.W. and Bixley, P.F. 1976: Observations of a 3-year shutdown at Broadlands geothermal field, New Zealand. 2nd U.N. Symposium on the development and use of geothermal resources, San Francisco, v. 3, p 1657-1661.

Hunt, T.M. 1977: Recharge of water in Wairakei geothermal field determined from repeat gravity measurements. N.Z. Journal of Geology and Geophysics, v. 20, p 303-317.

Nairn, I.A. 1982: Geology of Kawerau field (MKII). Results of drilling, 1977-1982. Unpublished Geothermal Circular, IAN-4, N.Z. Geological Survey, Rotorua.

Narasimhan, T.N. and Goyal, K.P. 1979: A preliminary simulation of land subsidence at Wairakei geothermal field in New Zealand. Summaries of the fifth Workshop Geothermal Reservoir Engineering, Stanford University, Stanford.

Pritchett, J.W., Rice, L.F. and Garg, S.K. 1980: Reservoir simulation studies: Wairakei geothermal field, New Zealand: LBL-11494, GREMP-11, SS-R-80-4313.

Stilwell, W.B., Hall, W.K. and Tawhai, J. 1976: Ground movement in New Zealand geothermal fields. proceedings, 2nd U.N. Symposium on Development and use of geothermal resources, San Francisco. p 1427-1434.

Proceedings Eighth Workshop Geothermal Reservoir Engineering
Stanford University, Stanford, California, December 1982
SGP-TR-60

RESISTIVITY LOGGING OF FRACTURED BASALT

V. Stefansson, G. Axelsson and O. Sigurdsson

Orkustofnun
Grensásvegi 9
Reykjavik, Iceland

INTRODUCTION

The electric log has been used for about half a century as a tool for studying the formations penetrated by a borehole. At early stage, comprehensive studies of sedimentary rock established the dependence of formation resistivity factor upon porosity. Archie (1942) pioneered this effort by suggesting his well-known empirical formula correlating the formation factor and porosity. Ever since, Archie's law has been a central point in interpretation methods for electrical logs.

Despite the simple empirical dependance of rock conductivity on porosity as expressed by Archie's law, there does not exist a simple theoretical explanation for this phenomenon. Mathematical modeling to prove the validity of an Archie type relationship has been carried out by Greenberg and Brace (1969), Shankland and Waff (1974) and Madden (1976). However, all models depend on simplistic geometrical assumptions of pore space distributions and the degree of realism can be disputed.

During the last decade, investigations on geothermal reservoirs have accentuated the role of fractures in reservoir physics. Various types of geophysical logs have been applied in order to distinguish between fractured and intergranular reservoirs. One of the strong candidates for that is the electric log (Towle 1962, Aguilera 1974 and 1976). The main reason for that is the fact that the exponent <m> in Archie's law seem to be 1.0 in the case of fractured rock (Brace and Orange 1968), where as a value of 2.0 seems to be valid for non-fractured rock (Brace et.al. 1965).

In this paper a simple lumped double porosity model is studied in order to estimate the effects of fractures on the resistivity-porosity relationship. Further, the results of resistivity and porosity logging in Icelandic basalt is presented, and it is shown that the distribution of porosity in these rocks are dominated by fractures.

LUMPED DOUBLE POROSITY MODEL

Consider an idealized model for fractured rock in order to estimate the effects of fractures on resistivity-porosity relations. This model is presented in figure 1 and consists of cubes representing the rock and the spacing between the parallelepipeds representing waterfilled fractures. Similar models have been presented before (Towle 1962, Aguilera 1974 and 1976, Hirakawa and Yamaguchi 1981), but the present approach is somewhat different.

The following parameters are used in the model:

- ρ_w = resistivity of water in pores and fractures
- ρ_b = resistivity of rock matrix
- ϕ_b = porosity of rock matrix (relative to matrix volume only)
- x = length of each matrix cube, fraction
- $1-x$ = width of fractures, fraction

It is convenient to introduce lumped resistances in approximating the resistivity of the model as is shown in figure 1. Thus the resistance of an unit cube is approximately given by

$$\frac{1}{R} = \frac{1}{R_1 + R_2} + \frac{1}{R_3} \qquad (1)$$

and the resistivity of the model is

$$\rho = R \qquad (2)$$

Referring to figure 1

$$R_1 = \frac{x}{x^2}\,\rho_b \qquad (3)$$

$$R_2 = \frac{1-x}{x^2}\,\rho_w \qquad (4)$$

$$R_3 = \frac{1}{1-x^2}\,\rho_w \qquad (5)$$

JHD-BM-9000 G Ax
82.09 1060 Sy.J

Figure 1

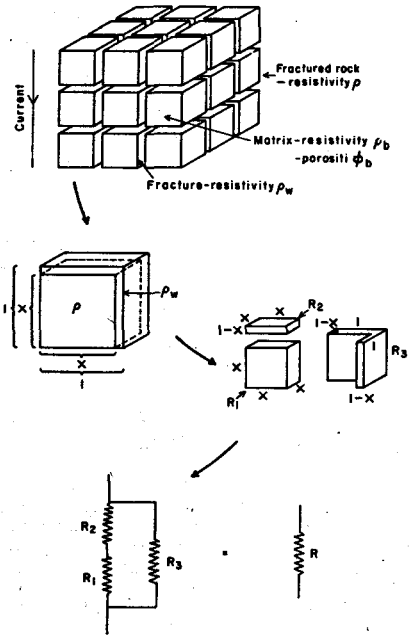

Figure 1 Schematic figure of the double porosity model and the equvalent resistivity calculated for each unit cube.

and the resistivity of the fractured rock is according to equation 1

$$\frac{1}{\rho} = \frac{1-x^2}{\rho_w} + \frac{x^2}{(1-x)\rho_w + x\rho_b} \qquad (6)$$

Introducing the fracture porosity

$$\phi_f = 1 - x^3 \qquad (7)$$

an approximation for the formation resistivity factor for the double porosity model is obtained as:

$$\frac{1}{F} = 1 - (1-\phi_f)^{2/3} + \frac{(1-\phi_f)^{2/3}}{\left[1-(1-\phi_f)^{1/3}\right] + (1-\phi_f)^{1/3}\rho_b/\rho_w} \qquad (8)$$

where

$$F = \rho/\rho_w \qquad (9)$$

Equation 8 is somewhat simpler than the one presented by Hirakawa and Yamaguchi (1981), but gives similar results.

The same approach can be used to estimate the formation factor for models with either vertical fractures only or horizontal fractures only. Omitting the details of the derivation one obtains for vertical fractures only:

$$F = \frac{1}{\phi_f + (1-\phi_f)\rho_w/\rho_b} \qquad (10)$$

and for horizontal fractures only

$$F = \phi_f + (1-\phi_f)\rho_b/\rho_w \qquad (11)$$

Equation 8 is used to estimate the formation resistivity factor for the double porosity model. Here it is assumed that

$$\rho_b = \rho_w/\phi_b^2 \qquad (12)$$

The use of an exponent of 2 is supported by the results of Brace and Orange (1968b). From their experiments with different rock samples, saturated with brine and measured at 4 kbar to close up most of the crack porosity, an exponent of 2 dependence of resistivity upon residual porosity was obtained. These results were confirmed by the simulation studies of Shankland and Waff (1975). Equation (12) has been recognized as an empirical law in the petroleum industry and is valid for normally cemented sandstone.

The relationship between the porosity and the formation factor according to equation 8 is presented in figures 2 and 3. The results for horizontal fracture only (equation 11) are presented in figure 4.

JHD-BM-9000 G Ax.
82.09. 1061. Sy.J.

Figure 2

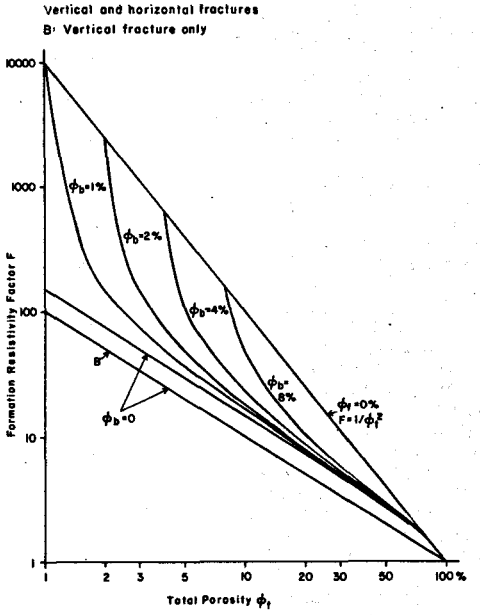

Figure 2 Relation between formation resistivity factor and total porosity as calculated from the double porosity model. Curve B represents vertical fracture only with matrix porosity equal to zero. Other curves are for cases where both vertical and horizontal fractures are present.

JHD-BM-9000. G.As 82.09. 1062. SyJ

Figure 3

Vertical and horizontal fractures

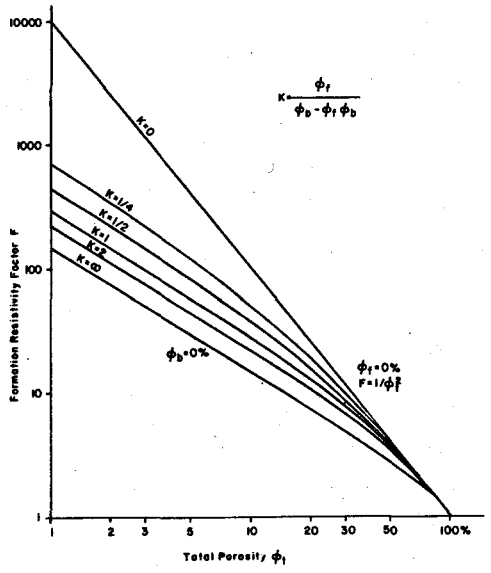

Figure 3 Relation between formation resistivity factor and total porosity for vertical and horizontal fractures, given various values of the ratio between fracture porosity and matrix porosity.

JHD-BM-9000. G.As 82.09. 1063. SyJ

Figure 4

Horizontal fracture only

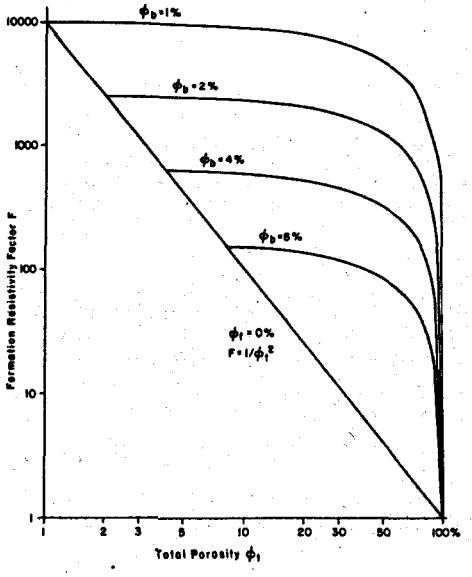

Figure 4 Relation between formation resistivity factor and total porosity for horizontal fracture only.

Equations 8, 10 and 11 can be combined with Archie's law (Archie 1942)

$$F = a/\phi_t^m \tag{13}$$

where

$$\phi_t = \phi_f + \phi_b - \phi_f\phi_b \tag{14}$$

is the total porosity. The double porosity model in the presence of vertical and horizontal fractures, when $\phi_b = 0$ and ϕ_t <30% then yields, a = 1.4 and m = 1.0. This compares favorably with the values a = 1.5 and m = 1.0 obtained by Towle (1962) for his plane model, but it is identical to the model used here. Similarly for vertical fracture only, a = 1.0 and m = 1.0 when $\phi_b = 0$. A m = 1.0 dependence upon total porosity is also seen to be valid when the ratio

$$k = \frac{\phi_f}{\phi_b - \phi_f\phi_b} \tag{15}$$

is constant and total porosity is small (figure 3), but the values for <a> increase with decreasing k-values.

These results are different from the relationships commonly used in the petroleum industry. An exponent of 1.0 is however in an agreement with the results of Brace and Orange (1968a), who observed that stressing rock samples into the dilant region of new crack formation produced an esponent of 1.0 dependence upon crack porosity.

It can be seen from the different values for <a> estimated above, for vertical and horizontal fractures, and for vertical fracture only, that resistivity-porosity relations, for fractured rock, are highly dependent on the ratio of vertical to horizontal fractures, i.e. fracture orientation. Different ratios of vertical to horizontal fractures can be modeled using the simple lumped approach used above. Space does not permit a detailed discussion, but results indicate a rapid increase in resistivity, at near constant total porosity, with decreasing importance of vertical fractures (figure 4).

The results from the above discussion can be summarized as follows.

1) Even though the present results are only a first order approximation it can be seen that the empirical relation $F = \phi^{-2}$ is not valid for fractured rock. An exponent of 1.0 is probably more correct.

2) The relationship between resistivity and porosity for fractured rock is in general not simple (figures 2, 3 and 4), but depends on the amount of matrix porosity as well as the fracture orientation.

3) Results indicate that porosity of fractured rock should not be determined form resistivity data based on a $F = a\phi^{-m}$ relation alone.

4) Assuming that the ratio of vertical to horizontal fractures is as in the model of figure 1 with total porosity and formation factor known from geophysical logging data, one can estimate roughly the relative importance of fracture- and matrix porosity by the use of the approximate model presented above.

RESISTIVITY-POROSITY RELATIONS FOR BASALT

Extensive geophysical logging has been performed in several deep (2 km) boreholes in Iceland. Among the parameters observed were resistivity (16" and 64" normal) and porosity (neutron-neutron). Examples of resistivity (formation resistivity factor)-porosity crossplots from two boreholes in basaltic environment are presented in figures 5 to 7. These figures show only few, but representative examples.

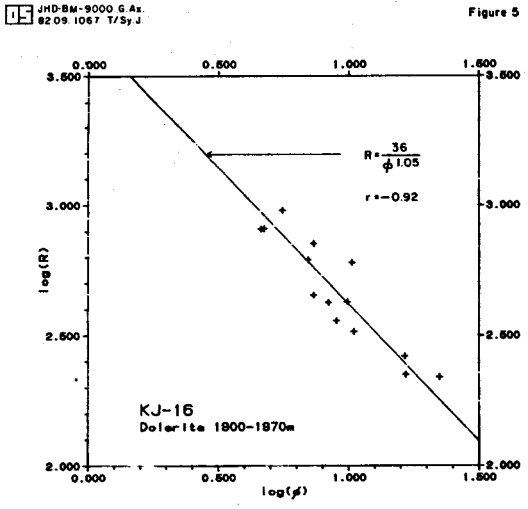

Figure 5 Resistivity - porosity cross plot for Dolerite at 1900 - 1970 m depth in well KJ-16 in the Krafla high temperature geothermal field. The best linear fit to the data points is shown along with its correlation coefficient.

Well KJ-16 is a production hole drilled inside the Krafla geothermal area (Stefánsson 1981) in the neovolcanic zone of Iceland. The IRDP-hole (Fridleifsson et.al 1982, Robinson et.al. 1982) is drilled in approximately 10 My old basalt pile in Eastern Iceland. The pore water resistivity (ρ_w) is fairly well known, as a function of depth, for the IRDP-hole, which enables the estimation of the formation resistivity factor (figures 6 and 7).

A rather good correlation between resistivity and porosity is seen for the examples in figures 5 to 7. A relationship of the form $\rho = a \rho_w \phi^{-m}$ has been fitted to these data and the results are presented in the

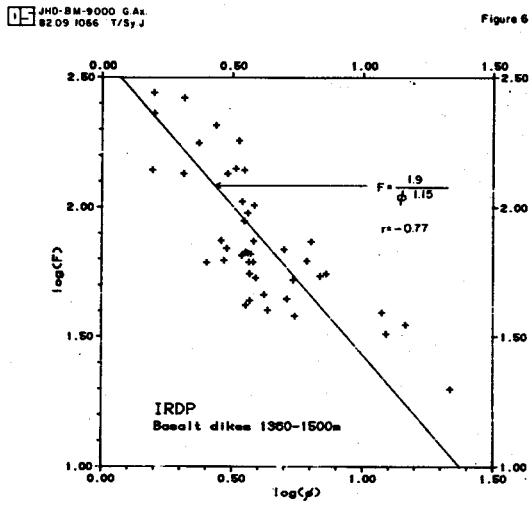

Figure 6 Formation resistivity factor - porosity cross plot for Basalt dikes in the depth interval 1360-1500 m in the IRDP hole in Eastern Iceland.

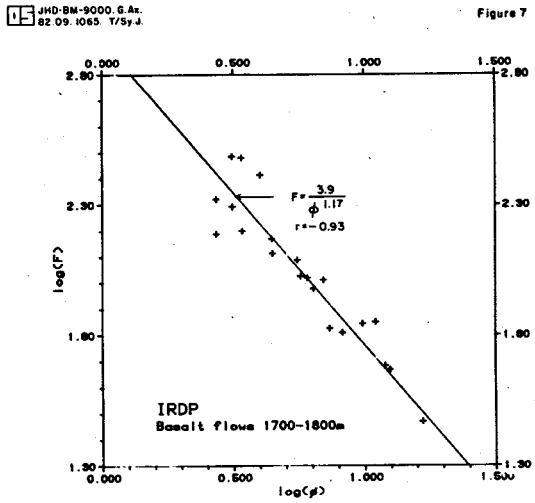

Figure 7 Formation resistivity factor - porosity cross plot for Basalt flows in the depth interval 1700-1800 m in the IRDP hole in Eastern Iceland.

figures. An equation of this form has also been fitted to data from other intervals, not presented here, and weighted average for the exponent <m> calculated for the two different areas. The results are presented in table I.

Table I

Location	<m> Weighted Average	Data based on
Krafla (0-1 My)	1.02 ± 0.07	205 m out of 2 x 1300 m
IRDP (~10 My)	1.10 ± 0.04	430 m out of 1100 m

These results are in good agreement with results for basalt from Hawaii (Keller et.al. 1974) and results from the Atlantic Ridge at 23°N (Kirkpatrick 1979).

How do we interpret an exponent <m> close to 1.0 ? This indicates, according to the double porosity model presented before and the results of Brace and Orange (1968a), that fractures constitute an important part of the porosity for the basalts studied. However, we can not determine, on the basis of the values for <m> alone, how important fractures are in the overall porosity. According to the double porosity model an exponent of 1.0 is possible, even though matrix porosity is considerable.

A more complete interpretation of formation resistivity factor-porosity cross-plots can be attempted on the basis of the double porosity model. The model can be used to estimate the relative importance of fracture- and matrix porosity when the pore water resistivity is known. We will take as examples three cross-plots from the IRDP-hole presented in figures 8 to 10. The two extremum cases ($\phi_b = 0$ and $\phi_f = 0$), for vertical and horizontal fractures, as well as one or two lines for constant k-ratios are superimposed on these cross-plots. We see from the figures that these data can be interpreted on the basis of the double porosity model. An interpretation of that kind is of course approximate, requires an exact knowledge of the value for and is limited by the underlying assumption of fracture orientation.

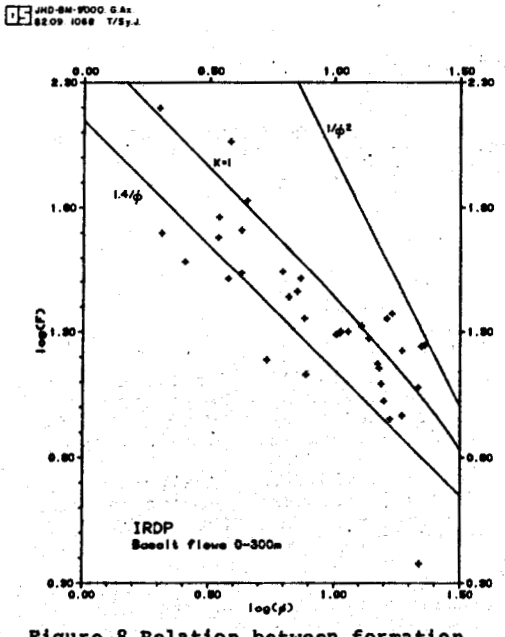

Figure 8 Relation between formation resistivity factor and total porosity for Basalt flows in the depth interval 0-300 m in the IRDP hole in Eastern Iceland. superimposed are lines for the two extremum cases $\phi_b = 0$ and $\phi_f = 0$ and one line for constant ratio between fracture porosity and matrix porosity.

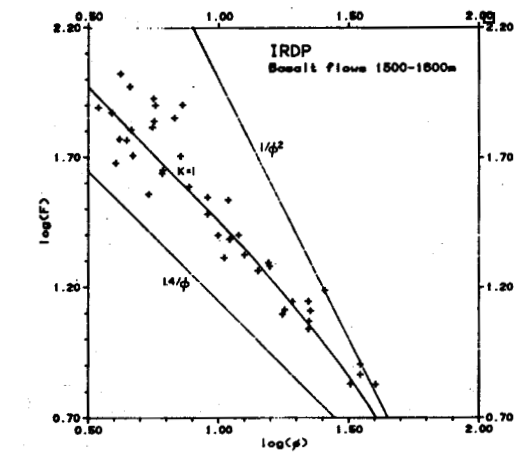

Figure 9 Relation between formation resistivity factor and total porosity for Basalt flows in the depth interval 1500-1600 m in the IRDP hole in Eastern Iceland. Superimposed are lines for the two extremum cases $\phi_b = 0$ and $\phi_f = 0$ along with a line for constant ratio between fracture porosity and matrix porosity.

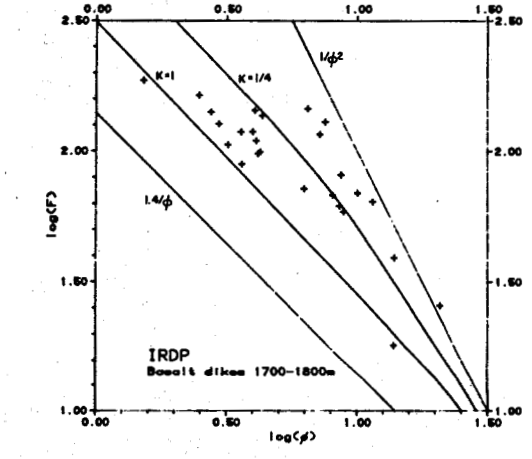

Figure 10 Relation between formation resistivity factor and total porosity for Basalt dikes in the depth interval 1700 - 1800 m in the IRDP hole in Eastern Iceland. Superimposed are lines for the two extremum cases $\phi_b = 0$ and $\phi_f = 0$ along with lines for constant ratio between fracture porosity and matrix porosity.

Using figure 3 we can estimate roughly the ratio of fracture- to matrix porosity. For the cases from the IRDP-hole presented in figures 8 to 10 the following results are obtained (table II):

Table II

Interval	ϕ_f/ϕ_t
0-300 m Basalt flows	≈0.7
1500-1600 m Basalt flows	≈0.5
1700-1800 m Basalt dikes	≈0.2-0.3

The apparent decrease in fracture porosity with depth is noteworthy, but the underlying assumptions mentioned above should be kept in mind. A decrease in fracture porosity could be the result of increasing pressure with depth closing up some fractures. This effect could on the other hand also result from changes in fracture orientation with depth.

To conclude this discussion we present one example for a non-basaltic unit in figure 11, where formation resistivity factor - porosity crossplot for a diorite (55% SiO_2) unit from the IRDP-hole is shown. Here we see a relationship which is quite different from the relationships for the basalt presented above. Interpreting the data in figure 11 according to the double porosity model we find that fracture porosity should be insignificant in this diorite unit.

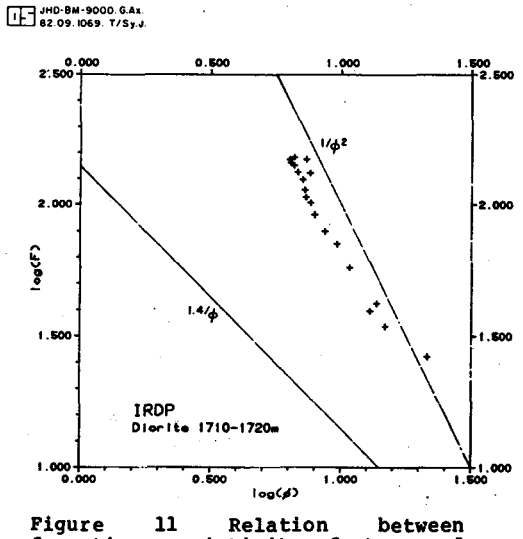

Figure 11 Relation between formation resistivity factor and total porosity for 10 m thick Diorite formation at 1710 m depth in the IRDP hole in Eastern Iceland. Superimposed are lines for the two extremum cases $\phi_b = 0$ and $\phi_f = 0$. The data points fall close to and parallel with the line $\phi_f = 0$ indicating that fracture porosity is negligible.

CONCLUSION

A lumped double porosity model has been studied in order to estimate the effect of fractures on resistivity - porosity relations. It is found that the relationship between resistivity and porosity for fractured rock is in general not simple and depends both on the amount of matrix porosity as well as the fracture orientation. However, when fractures dominate over matrix porosity the exponent <m> is close to 1.0.

Resistivity-porosity relations have been determined for large amount of basaltic formations in Iceland. An exponent close to 1.0 is found in all cases investigated. This is interpreted as fractures constitute a considerable part of the porosity of the basalts. In the IRDP-hole in Eastern Iceland it is found that the ratio of fracture porosity to total porosity decreases with depth.

In contrast to the exponent of 1.0 found for basaltic formations in Iceland, many interbedded formations in the basaltic pile reveal an exponent of approximately 2.0. This is interpreted as matrix porosity dominates fracture porosity in these cases.

The study of resistivity-porosity relationship presented demonstrates that common geophysical logs can distinguish between fractured and porous reservoirs.

Aknowledgements

We thank Rafmagnsveitur Ríkisins-Kröfluvirkjun for permission to use data from the Krafla field.

REFERENCES

Aguilera, R. (1974), "Analysis of Naturally Fractured Reservoirs From Sonic and Resistivity Logs", J. Pet. Tech., 26, p. 1233-1238.

Aguilera, R. (1976), "Analysis of Naturally Fractured Reservoirs From Conventional Well Logs", J. Pet. Tech., 28, p. 764-772.

Archie, G.E. (1942), "The Electrical Resistivity Log as an Aid in Determining Some Reservoir Characteristics", Tran. AIME, 146, p. 54-67.

Brace, W.F., Orange, A.S. and Madden, T.R. (1965), "The Effect of Pressure on the Electrical Resistivity of Water-Saturated Crystalline Rocks", J. Geophys. Res., 70, p. 5669-5678.

Brace, W.F. and Orange, A.S. (1968a), "Electrical Resistivity Changes in Saturated Rocks during Fracture and Frictional Sliding", J. Geophys. Res., 73, p. 1433-1445.

Brace, W.F. and Orange, A.S. (1968b), "Further Studies of the Effects of Pressure on Electrical Resistivity of Rocks", J. Geophys. Res., 73, p. 5407-5420.

Fridleifsson, I.B., Gibson, I.L., Hall, J.M., Johnson, H.P., Christensen, N.I., Schmincke, H.U. and Schonharting, G. (1982), "The Iceland Research Drilling Project", J. Geophys. Res., 74, p. 6359-6362.

Greenberg, R.J. and Brace, W.F. (1969), "Archie's Law for Rocks Modeled by Simple Networks", J. Geophys. Res., 74, p. 2099-2102.

Hirakawa, S. and Yamaguchi, S. (1981), "Geothermal Well Logging and Its Interpretation", Proceedings Seventh Workshop Geothermal Reservoir Engineering, Stanford, p. 115-119.

Keller, G.V., Murray, J.C. and Towle, G.H. (1974), "Geophysical Logs From the Kilauea Geothermal Research Drill Hole", paper presented at Fifteenth Annual Meeting of SPWLA, McAllen, L.

Kirkpatrick, R.J. (1979), "The Physical State of the Oceanic Crust: Results of Downhole Geophysical Logging in the Mid-Atlantic Ridge at 23°N", J. Geophys. Res., 84, p. 178-188.

Madden, T.R. (1976), "Random Networks and Mixing Laws", Geophysics, 41, p. 1104-1125.

Robinson, P.T., Hall, J.M., Christensen, N.I., Gibson, I.L., Fridleifsson, I.B., Schmincke, H.U. and Schonharting, G. (1982), "The Iceland Research Drilling Project: Synthesis of Results and Implications for the Nature of Icelandic and Oceanic Crust", J. Geophys. Res. 87, p. 6657-6667.

Shankland, T.J. and Waff, H.S. (1974), "Conductivity in Fluid-Bearing Rocks", J. Geophys. Res., 79, p. 4863-4868.

Stefansson, V. (1981), "The Krafla Geothermal Field, Northeast Iceland", in Geothermal Systems: Principles and Case Histories, L. Ryback and L.J.P. Muffler (Editors), p. 273-294. John Wiley & Sons Ltd.

Towle, G. (1962), "An Analysis of the Formation Resistivity Factor porosity Relationship of Some Assumed Pore Geometries", paper presented at Third Annual Meeting of SPWLA, Houston.

Proceedings Eighth Workshop Geothermal Reservoir Engineering
Stanford University, Stanford, California, December 1982
SGP-TR-60

EFFECTS OF TEMPERATURE AND STRESS ON THE COMPRESSIBILITIES, THERMAL EXPANSIVITIES, AND POROSITIES OF CERRO PRIETO AND BEREA SANDSTONES TO 9000 PSI AND 280°C

Enrique Contreras and Eduardo Iglesias

Instituto de Investigaciones Eléctricas
Apartado Postal 475, Cuernavaca, Mor. Mexico

Francisco Bermejo

Comisión Federal de Electricidad
Apartado Postal 3-636, Mexicali, B.C., Mexico

ABSTRACT

We measured matrix and bulk compressibilities and thermal expansion coefficients of Berea sandstone and of a sandstone from Cerro Prieto well M-94. Furthermore, we developed and demonstrated a novel technique for computing porosities as functions of effective stress or temperature from uniaxial compression and thermal expansion measurements respectively. Unlike previous results, which are limited to temperatures below 200°C, our measurements cover the range from ambient temperature to 280°C. Our data for Berea sandstone generally agree with previous results. The matrix and bulk compressibilities of the Cerro Prieto sandstone are considerably greater than those of two Imperial Valley sandstones, reported in the literature, indicating significantly greater subsidence potential for Cerro Prieto. The porosities of the rocks studied decrease with increasing effective stress; our results indicate that porosity reductions due to pore pressure drawdown in sandstone dominated geothermal reservoirs are probably small. Porosities decrease also with increasing temperatures because the grains expand at the expense of the pore volume. Porosity increases due to thermal drawdown are likely to be small in sandstone geothermal reservoirs, but greater porosity relative changes are expected for tighter sandstones.

INTRODUCTION

Most physical properties of rocks vary with temperature and stress. Knowledge of the corresponding dependences and of their magnitudes is important for geothermal reservoir assesment and interpretation. Among the petrophysical properties of major interest for the geothermal industry are porosity, compressibilities and thermal expansivities. Sandstones constitute the main producing horizons in the extense Mexicali/Imperial Valley geothermal region. Understanding the behavior of these sedimentary rocks at reservoir conditions is therefore economically important. However, the information available about the stress and temperature dependences of porosities, compressibilities and thermal expansivities of these rocks is scarse. This information is briefly reviewed in the next paragraph.

Compressibilities of several sandstones to high pressures (~16,000 psi) and to medium temperature (~200°C) were measured by Lobree (1968), Von Gonten and Choudhary (1969), and Somerton et al (1974); they found that bulk matrix compressibilities generally increased with increasing temperature, despite some erratic behavior of matrix compressibilities. Thermal expansivities of Berea, Boise, and Bandera sandstones to 160°C were presented recently by Somerton et al (1981); these results indicate that thermal expansivities are nearly independent of stress and of the amount of fluid saturation. Porosity variations with stress in sandstones to ~10,000 psi were investigated by Somerton (1978) who drew on data by Fatt (1953), Somerton et al (1974), and Von Gonten and Choudhary (1969); it was found that porosity reductions with stress are greater at higher temperatures. Variations of pore volume versus temperature to 170°C for three sandstones were reported by Somerton et al (1981); these authors showed that pore volumes of liquid saturated sandstones under stress decrease with increasing temperature, and that the pore volume thermal contraction is a function of porosity, values decreasing with increased porosities.

This paper focuses on the magnitudes and on the temperature and stress dependences of the compressibilities, thermal expansivities and porosities of Cerro Prieto and Berea sandstones. Berea is a well-known rock used extensively in laboratory investigations, and as such, valuable for comparison purpouses. Apart from its obvious importance for characterization of the Cerro Prieto reservoir itself, knowledge of the properties of Cerro Prieto sandstones provides valuable information concerning the whole Mexicali/Imperial Valley geothermal area. We have measured bulk and matrix compressibilities and thermal expansivities as functions of stress and temperature. From these measurements we computed porosities as functions of stress and temperature by means of a novel technique devised by us for this purpouse. Unlike previously published data, which are limited to temperatures below 200°C, our measurements cover the range from ambient temperature to 280°C.

EXPERIMENTAL METHODS

From each of the samples studied in this work (Berea sandstone and a sandstone from Cerro Prieto well M-94) four specimens were obtained. Two of them were dry jacketed for bulk compressibility and thermal expansion measurements; the rest were used unjacketed for matrix compressibility and thermal expansion measurements. The specimens were cilindrical, 2.54 cm in diameter by 5.08 in length; their ends were ground flat and parallel to within 2.54 x 10^{-3} cm.

Linear thermal expansion and linear compaction were measured along the specimens axis by means of high resolution LVDT's (linearly variable diferencial transformers) attached to the top of the test specimens by quartz rods. Thermal and mechanical induced deformations of up to 2.5 x 10^{-2} cm can be measured in our equipment with an accuracy of ± 6.2 x 10^{-5} cm. Averaging the outputs of the two LVDT's removes any false strain due to tilting. More details on the test configuration used are given by Ennis et al (1979).

During the compressibility tests, confining pressure was changed at a uniform rate of 785 psi/min (5MPa/min). The specimen was subjected to loading-unloading cycles, until no permanent strain was detected, to insure reproducibility. Compressibilities were computed from the loading portion of the cycle. Temperature was kept constant at the test value with an accuracy of ± 1°C.

When running thermal expansion tests, the sample temperature was increased at a uniform rate of about 1.5°C/min. The heating rate chosen, according to our own experience, is low enough to prevent large irrecoverable microestructural damage in the rock sample. Confining pressure was kept constant with an accuracy of ± 1 psi.

A computer based data aquisition system which allows sampling of the channel transducers involved in the test with a frequency of up to 180/minute was used. In the compressibility tests data were collected every 10 seconds; while in the thermal expansion tests the frequency was once every minute.

The initial porosity ϕ_o of each sample, used in our computations of porosity as a function of effective stress or of temperature, was determined by averaging the porosities of the corresponding four specimens. These porosities were measured using the liquid vacuum saturation method.

RESULTS AND DISCUSSION

Matrix compressibilities

These were computed assuming isotropy from uniaxial compression measurements on unjacketed samples at constant temperature with hydrostatic confining pressures ranging from o to 9000 psi. The corresponding results are shown in Table 1. The linearity of the uniaxial compression data with hydrostatic stress

TABLE 1. Matrix compressibilities

Temp. (°C)	BEREA Compress. (psi^{-1})	BEREA Corr. coeff.	CERRO PRIETO Compress. (psi^{-1})	CERRO PRIETO Corr. coeff.
20	1.46×10^{-7}	0.9975	1.59×10^{-7}	0.9999
280	2.39×10^{-7}	0.9997	3.06×10^{-7}	0.9991

is excellent, as indicated by the magnitudes of the corresponding correlation coefficients.

Our results for Berea sandstone are in good agreement with those by Somerton et al. (1974) as shown in Fig. 1. Pooling together our results with Somerton et al's we find that the matrix compressibility of Berea sandstone increases with temperature at a constant rate equal to 3.26 x 10^{-10} psi^{-1} $°C^{-1}$. The corresponding correlation coefficient equals 0.9477.

Comparison of our results for Cerro Prieto sandstone from well M-94 at a depth of 6900 feet with Somerton et al's results for an Imperial Valley sandstone denominated W823, from a depth of 5073 feet (Fig. 1) shows that the corresponding matrix compressibilities differ significantly from each other, and that the matrix compressibilities of both rocks increase with temperature at nearly the same

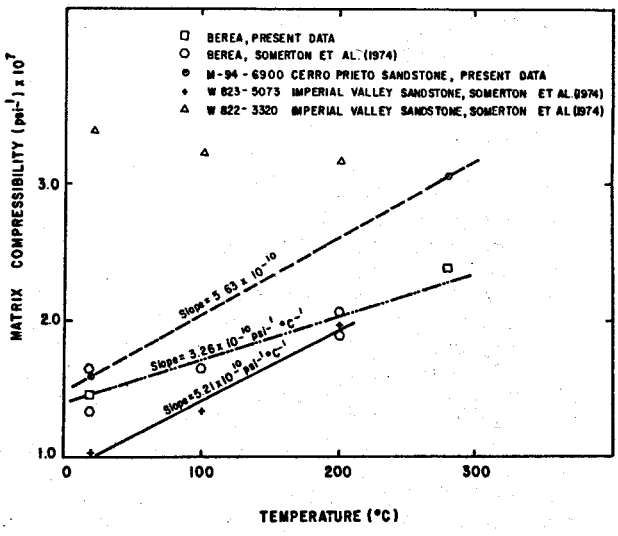

FIGURE 1. Effect of temperature on matrix compressibility

rate which is significantly greater than that of Berea. This temperature dependence lends credibility to the data corresponding to sample W823-5073, which were deemed doubtful by Somerton et al (1974) due to the large change of matrix compressibility with temperature. Compared with the evidence accumulated for Berea, Cerro Prieto and Imperial Valley W823-5073 sandstones, the trend of matrix compressibility decreasing with increasing temperature depicted by Somerton et al's data (Fig.1) on Imperial Valley sample W822-3320 seems anomalous.

Bulk compressibilities

These were computed assuming isotropy from uniaxial compression measurements on dry jacketed samples at constant temperature. The confining hydrostatic pressure was assumed to equal the effective (confining minus pore) stress. Our results for Berea sandstone at 20°C and 280°C are shown in Fig. 2. Observe that bulk compressibilities increase with increasing temperature. At 20°C these data agree well with the corresponding data from Somerton et al (1974); our 280°C data are consistent with Somerton et al's high temperature (≤ 200°C) data.

Our results for M-94-6900 Cerro Prieto sandstone at 20°C and 280°C are shown in Fig. 3. These compressibilities are significantly higher (about +90% at 2000 psi, 20°C and 280°C) than our results for Berea sandstone. They are also significantly higher than the bulk compressibilities reported for Imperial Valley sandstones by Somerton et al (1974): about + 50% at 20°C, 2000 psi for W823-5073, and about +120% at 20°C, 2000 psi for W822-3320. Subsidence computations should reflect these differences in bulk compressibilities.

Matrix thermal expansivities

We measured uniaxial thermal expansions to 280°C on unjacketed samples at constant hydrostatic pressure. The corresponding strain-temperature plots for Berea and Cerro Prieto sandstones are shown in Figs. 4 and 5 respectively. From the slopes of these curves it is seen that the linear thermal expansion coefficients of both rocks are functions of temperature. The thermal expansion coefficients increase with increasing temperature until a nearly constant value is achieved. Furthermore, for temperatures exceeding about 150°C for Berea sandstone, and greater than about 100°C for Cerro Prieto sandstone, linear thermal expansivities depend on stress. Note that for Berea sandstone thermal expansivity increases with decreasing confining pressure. For the Cerro Prieto sample the effect is more complex: at lower temperatures (100-150°C) the thermal expansivity increases with increasing confining pressure, and at higher temperatures (>200°C) the thermal expansivity decreases with increasing confining pressure. Representative values of linear thermal expansion coefficients are presented in Table 2.

TABLE 2. Matrix linear thermal expansion coefficients

Temp. Int. (°C)	Rock	Conf. Press (psi)	Coeff. ($°C^{-1}$)
20-100	Berea	435 and 3000	12.5×10^{-6}
150-280	"	435	21.2×10^{-6}
150-280	"	3000	19.4×10^{-6}
20-100	Cerro Prieto	435	11.5×10^{-6}
20-100	" "	3000	12.5×10^{-6}
200-280	" "	435	22.0×10^{-6}
200-280	" "	3000	20.0×10^{-6}

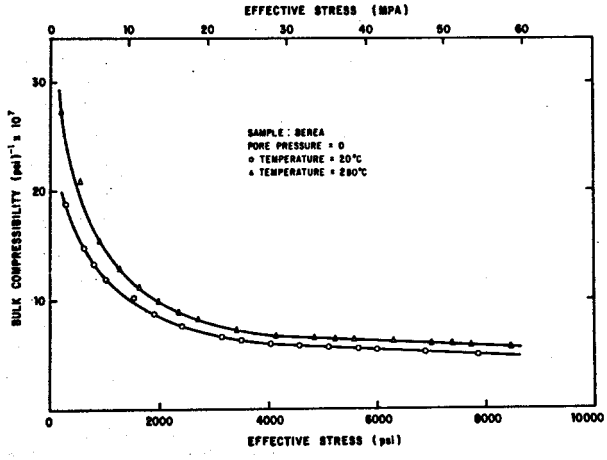

FIGURE 2. Effect of stress at constant temperature on the bulk compressibility of Berea sandstone.

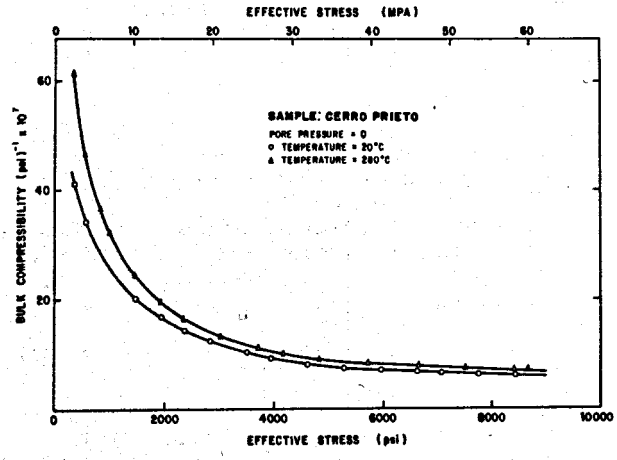

FIGURE 3. Effect of stress at constant temperature on the bulk compressibility of the Cerro Prieto sandstone.

Bulk thermal expansivities

We measured uniaxial thermal expansions on dry jacketed samples at constant hydrostatic confining pressure to 280°C. The corresponding strain-temperature plots for the rocks studied are shown in Figs. 4 and 5. It will be noticed that linear bulk thermal expansion coefficients depend both on temperature and pressure, as is the case for matrix thermal expansivities. Representative values of linear bulk thermal expansion coefficients computed from Figs. 4 and 5 are given in Table 3. Our values for Berea sandstone closely bracket the value of 13.0 x 10^{-6} $°C^{-1}$ for 100-200°C found by Somerton et al (1981).

TABLE 3. Linear bulk thermal expansion coefficients

Temp. Int. (°C)	Rock	Conf. Press. (psi)	Coeff. ($°C^{-1}$)
20-100	Berea	435 and 3000	10.0 x 10^{-6}
150-280	"	435	14.7 x 10^{-6}
150-280	"	3000	14.0 x 10^{-6}
20-100	Cerro Prieto	435 and 3000	8.3 x 10^{-6}
120-180	"	435	13.8 x 10^{-6}
120-200	"	3000	11.8 x 10^{-6}
200-280	"	435	13.8 x 10^{-6}
200-280	"	3000	13.8 x 10^{-6}

For Berea sandstone our results indicate that for T >150°C the linear bulk thermal expansion coefficient decreases with increasing effective stress. This is consistent with the results of Somerton et al (1981), and with theoretical estimates by Sweet (1978). Our results for the Cerro Prieto sandstone studied indicate however that increasing the effective stress does not necessarily result in a decrease of the bulk thermal expansion coefficient.

Porosity vs. stress

Combining our uniaxial compression measurements on jacketed and unjacketed samples, we computed the effects of stress at constant temperature on the porosities of the samples studied. From the definitions of porosity and of matrix and bulk linear compressibilities, and assuming isotropy, it is easy to show that

$$\phi/\phi_o = \left\{1 - (1-\phi_o)\ (1+3\,\frac{\Delta L'}{L'_o})/(1+3\,\frac{\Delta L}{L_o})\right\}/\phi_o \quad (1)$$

were ϕ is the porosity at a given effective stress; ϕ_o, L'_o and L_o the porosity and the lengths of the unjacketed and jacketed samples respectively at the initial stress of the test; $\Delta L'$ and ΔL the uniaxial compressions for the unjacketed and jacketed samples respectively; and all these quantities correspond to the (constant) temperature of the test. The validity of expression (1) hinges on the usual

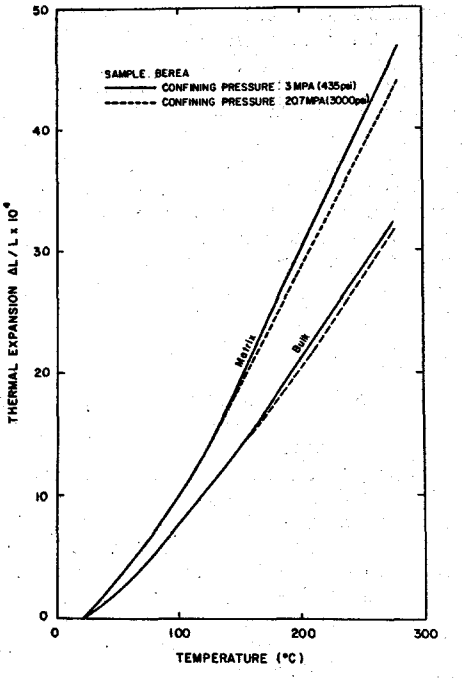

FIGURE 4. Linear matrix and bulk thermal expansion at constant effective stress for Berea sandstone.

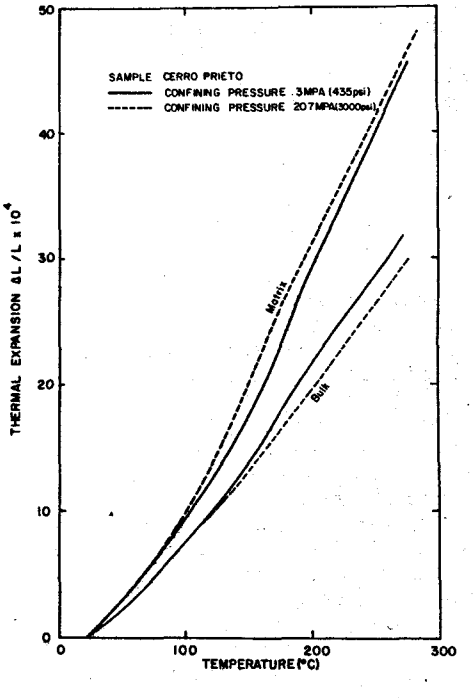

FIGURE 5. Linear matrix and bulk thermal expansion at constant effective stress for the Cerro Prieto sandstone.

assumption that the deformation of the matrix is the same for both unjacketed and jacketed samples. In actual computations with expression (1) we used the values of ϕ_o corresponding to 20°C and 14.7 psi. This is strictly correct for the data at 20°C, and introduces a small error in the data corresponding to 280°C: about 0.1 percent for a 3 percent error in ϕ_o.

Expression (1) was used to compute the results shown in Fig. 6. Clearly, increasing the effective stress reduces the porosity. This effect is more pronounced for the Cerro Prieto sandstone than for the Berea sandstone, due to the higher compressibilities of the former.

Increasing the temperature results in increased porosity reductions, which is consistent with bulk compressibilities being greater at higher temperatures. Again, this effect is more pronounced for the Cerro Prieto sandstone than for Berea.

The relative porosity reductions $\Delta\phi/\phi_o$ computed by Somerton (1978) for Berea sandstone at 20°C are much higher (about 134 percent at 9000 psi) than our results for the same rock. These calculations by Somerton were based on heterogeneous data: bulk compressibilities from Somerton et al. (1974), and pore compressibilities from Von Gonteu and Choudhary (1969). Using expression (1) and matrix and bulk compressibilities from Somerton et al. (1974) we computed values of $\Delta\phi/\phi_o$ much closer to our own results: at 9000 psi about 18 percent higher than the results of Fig. 6 using one set (El-Shaarani, 1973) of data, and about 10 percent lower than our results for the set of data corresponding to Lobree (1968). This close agreement lends credibility to the computed porosities shown in Fig. 6.

These results indicate that in sandstone-dominated geothermal reservoirs, such as most found in the Mexicali/Imperial area, changes of porosity due to pressure drawdown are probably small. For example our data shows that the Cerro Prieto sandstone from well M-94 at a depth of 7000 feet, with an initial pore fluid pressure equal to 3000 psi, and a temperature of 280°C would undergo a reduction in porosity of only about 0.4% upon a pore pressure reduction of 1000 psi.

Porosity vs. temperature

Combining our uniaxial thermal expansion measurements on jacketed and unjacketed samples, and using an expression analogous to (1), where the uniaxial compressions were replaced by uniaxial thermal expansions, we computed the effects of temperature, at constant stress, on porosity. The validity of this method of computation hinges on the usual assumption that the matrix thermal expansion is independent of the samples being jacketed or unjacketed. As before, in actual computations of relative porosities ϕ/ϕ_o versus temperature we used the values of ϕ_o corresponding to 20°C and 14.7 psi, because the errors introduced in this way are small.

Porosities vs. temperature for Berea and Cerro Prieto sandstones are shown in Fig. 7. It will be noticed that porosities decrease with increasing temperature. We interpret this effect as demonstrating that in confined rocks the thermal expansion of the grains is partly at the expense of the pore volume, because the measured bulk thermal expansion coefficients are smaller than the matrix thermal expansion coefficients (Tables 2 and 3).

The effects of the (constant) confining stress seem to depend on the type of rock. For temperatures exceeding about 120°C the porosity of the Cerro Prieto sandstone studied decreases faster for greater confining pressure. However the effect of the confining pressure on Berea sandstone seems to be opposite: for T > 160°C its porosity decreases more rapidly for smaller confining pressures. This opposite dependence of the porosities of Cerro Prieto and Berea sandstones is traceable to the behavior of the corresponding matrix strain-temperature curves (Figs. 4 and 5), which show opposite dependences with stress.

The curves in Fig. 7 show that at the lower temperatures porosities decrease relatively slowly; then at intermediate temperatures the absolute value of the rate of change increases; and finally, at higher temperatures, the absolute value of the rate of change decreases again and becomes nearly constant. From pore volume thermal contraction measurements Somerton et al (1981) made similar observations. These authors concluded that both the temperature at which the nearly constant rates of

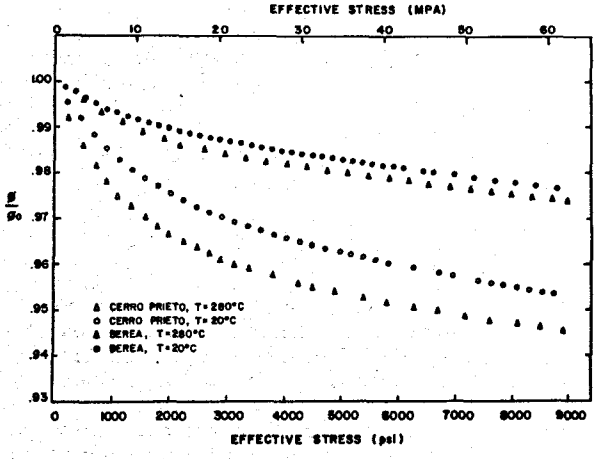

FIGURE 6. Effect of stress at constant temperature on the porosities of Berea and Cerro Prieto sandstones.

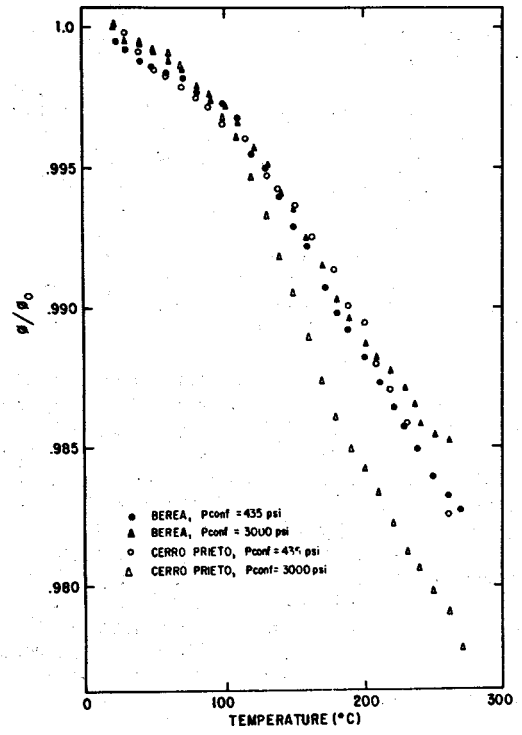

FIGURE 7. Effect of temperature at constant effective stress on the porosities of Berea and Cerro Prieto sandstones.

change begin, and the corresponding slopes are related to the porosity of the sandstone: (a) for lower porosity sandstone the absolute value of $(\partial\phi/\partial T)_p$ is greater; and (b) for lower porosity sandstone the onset of the constant slope takes place at lower temperature. Conclusions (a) and (b) are consistent with the data presented in Fig. 7. To understand the physical reasons underlying observations (a) and (b) it is helpful to consider the thermal expansion analogue of expression (1). Noting that $\varepsilon' = 3\Delta L'/L'_o << 1$ and that $\varepsilon = 3\Delta L/L_o << 1$, equation (1) can be approximated by

$$\varepsilon = 1 - (1 - \phi_o)\ (1 + \varepsilon' - \varepsilon), \quad (2)$$

and

$$\left(\frac{\partial\phi}{\partial T}\right)_p = -(1-\phi_o)\ \left(\frac{\partial\varepsilon'}{\partial T} - \frac{\partial\varepsilon}{\partial T}\right)_p \quad (3)$$

Thus it is seen that the absolute value of $(\partial\phi/\partial T)_p$ increases with decreasing values of ϕ_o, as observed. This can also ve verified pluging the values of ϕ_o for Berea and Cerro Prieto sandstones (0.185 and 0.178 respectively) and the high temperature thermal expansion coefficients from Tables 2 and 3 in expression (3).

Regarding point (b), we approximated each of the bulk and matrix strain-temperature curves (Figs. 4 and 5) by two straight lines: One with the slope corresponding to the lower temperature intervals in Tables 2 and 3, and the other with the slope corresponding to the high temperature intervals of those tables. With these approximations and equation (2) it is easy to show that (i) the curves (ϕ/ϕ_o) vs. T should show three different slopes, as observed; and (ii) the temperatures at which these slopes change values are given by

$$T_* = \frac{(\Delta L'/L')_i}{\alpha_{i-1} - \alpha_i} \quad (4)$$

where $(\Delta L'/L')_i$ is the intercept of the straight line representing the matrix strain-temperature curve to the high temperature side of T_*, α_i the matrix linear thermal expansion coefficient for $T > T_*$, and α_{i-1} the coefficient corresponding to the low temperature side of T_*. The important point here is that T_* does not depend explicitly on ϕ. Therefore Somerton et al's conclusion (b) seems to be either fortuitous or arising from some correlation between porosity and the matrix thermal expansion coefficient. Such correlation is not apparent from our data (see Figs. 5 and 6 and Table 2), perhaps because the porosity contrast between the Berea and Cerro Prieto sandstones studied is small.

SUMMARY AND CONCLUSIONS

We have measured matrix and bulk compressibilities and thermal expansion coefficient of Berea sandstone and of a sandstone from Cerro Prieto well M-94 to 280°C. Furthermore, we have developed and demonstrated a novel technique for computing porosities as functions of effective stress or temperature, from uniaxial compression and thermal expansion measurements respectively. Finally, we compared our results with published data on Berea sandstone and on two Imperial Valley sandstones. The following conclusions may be reached from this work.

1. The measured matrix and bulk compressibilities of the Cerro Prieto sandstone from M-94 are significantly higher than those found for Berea sandstone and for two Imperial Valley sandstones (W822-3320 and W823-5073). If the trend indicated by the samples from Cerro Prieto and Imperial Valley is representative of these locations, our results indicate significantly greater subsidence potential for Cerro Prieto.

2. The porosities of Berea and Cerro Prieto sandstone M-94-6900 decrease slightly with increasing effective pressure at constant temperature: about 2.5% for Berea sandstone and about 4.5% for Cerro Prieto sandstone at 9000 psi. The greater sensitivity shown by the Cerro Prieto sandstone is due to its higher compressibility. These porosity changes are smaller at lower temperatures, reflecting the temperature dependence of the matrix and bulk compressibilities. Our results indicate that in sandstone dominated geothermal reservoirs. changes of porosity due to pressure drawdown are probably small.

3. The porosities of Berea sandstone and of the Cerro Prieto sandstone M94-6900 decrease with increasing temperature at constant effective stress. This effect is due to the grains expanding partly at the expense of the pore volume (because the bulk thermal expansion coefficients are smaller than the corresponding matrix thermal expansion coefficients). Our results indicate that in sandstone dominated geothermal reservoirs changes of porosity due to thermal drawdown are, very likely, small.

4. At intermediate to high temperatures (>150°C) porosity decreases with temperature more rapidly for rocks of smaller porosities because the absolute value of $(\partial\phi/\phi T)_p$ is proportional to $(1-\phi_o)$. Thus, greater increases in porosity are expected for tighter sandstones upon thermal drawdown in geothermal reservoirs.

5. Comparison of our results with others found in the literature shows that significant differences in the magnitudes and in the thermal behavior of the compressibilities, thermal expansivities, and porosities of different sandstones exist which warrant further studies at high temperatures.

ACKNOWLEDGEMENTS

We thank Ing. Alfredo Mañon M. at Comisión Federal de Electricidad, Coordinadora Ejecutiva de Cerro Prieto, for his interest in this work and for permission to publish its results. Martín Uribe F. collaborated in the experimental work, and Adrián Patiño M. and Juan Flores F. drafted the figures. This work forms part of the Cooperative Geothermal Program between Instituto de Investigaciones Eléctricas and Stanford University.

REFERENCES

• Ennis D.O., Butters S.W., Lingle R., Van Buskirk R.G., and Prater F.R. (1979), "Capabilities to Measure Geothermal Material Properties at Simulated In-Situ Conditions", Terratek Report TR79-49.

• Lobree D.T., (1968), "Measurement of Compressibilities of Reservoir Type Rocks at Elevated Temperatures", MS thesis, University of California, Berkeley.

• Somerton W. H., El-Shaarani A.H., and Mobarak S.M., (1974), "High Temperature Behavior of Rocks Associated with Geothermal Type Reservoirs", Soc. Petrol. Engrs. preprint No. 4897.

• Somerton W. H., (1978), "Some Physical Properties of Cerro Prieto Cores", Proceedings 1st. Symp. on the Cerro Prieto Geothermal Field, pp. 333-338, Lawrence Berkeley Laboratory Report LBL-7098.

• Somerton W.H., Janah A.H., and Ashquar P.I., (1981), "Thermal Expansion of Fluid Saturated Rocks Under Stress", SPWLA Twenty-Second Annual Logging Symp., Mexico City, June 23-26 1981.

• Sweet J.N., (1978), "Pressure Effects on Thermal Conductivity and Expansion of Geologic Material", D.O.E. Report # SAND 78-1991.

• Von Gonten W.D., and Choudhary B.K., (1969), "Effect of Pressure and Temperature on Pore Volume Compressibility", Soc. Petrol. Engrs. preprint No. 2526.

Proceedings Eighth Workshop Geothermal Reservoir Engineering
Stanford University, Stanford, California, December 1982
SGP-TR-60

EFFECTS OF CONTAMINATION BY GEOTHERMAL DRILLING MUD ON LABORATORY DETERMINATIONS OF SANDSTONE PORE PROPERTIES: AN EVALUATION

A. Arenas, E. Iglesias, G. Izquierdo, M. Guevara,
R. Oliver, and S. Santoyo

Instituto de Investigaciones Eléctricas
Apartado Postal 475, Cuernavaca, Mor., México

INTRODUCTION.

Numerous studies have been presented, mainly in the petroleum literature, about permeability impairment of reservoir formations due to rock/drilling fluid interactions. For example, Glenn et al;(1957) showed that mud particles can invade to an appreciable depth into the pores of a porous medium, form a "filter cake" in the pores, and cause a substantial reduction in the permeability of the invaded zone. Drilling muds contain water and dissolved salts that can cause reductions in permeability attributed to clay minerals which expand or disperse upon contact with water (Alexander and Johnson, 1949) that is less saline than the connate water (Jones, 1964; Atwood, 1964, Monaghan et al; 1959). Other studies showed that permeability reduction due to salinity changes, can also occur in formations containing only nonexpandable clays, such as illite or kaolinite, and that permeability impairement can be caused by changes in PH (Mungan, 1965). Experiments designed for geothermal conditions indicated that formation damage depends on the composition of the drilling mud, temperature and stagnation time (Ennis et al; 1979). These and other studies (e.g. Abrams, 1977; Nicholson, 1978) demostrated that permeability reduction is site-specific, in the sense that it depends strongly on the compatibility of the rock/drilling fluid system.

We are initiating research to evaluate formation damage related to drilling fluids used in Mexican geothermal fields. The initial work, reported in this paper, has been done on Berea sand stone for two reasons: a) to save valuable reservoir drill cores while developing and turning experimental techniques, and b) for comparison with results from other investigations, since Berea sandstone has been extensively studied and used in permeability impairment research This paper focuses on the magnitudes of permeability reductions associated with high-temperature rock/geothermal drilling fluid interactions, and on the possibility of restoring the unperturbed permeability to reservoir drill cores for its measurment in the laboratory.

EXPERIMENTAL METHOD.

Two sets (A and B) of experiments were conducted. In both of them the permeabilities of specimens extracted from two samples, one corresponding to each set, were measured before and after contamination with drilling fluid at simulated geothermal borehole conditions. The specimens of set A were then subjected to a washing process widely used in the petroleum industry, and their permeabilities remeasured. In this way the fraction of the initial permeability restored by washing was evaluated.

With set B the depth of invasion by mud particles, and permeability restoration by mechanical treatment were investigated. One end of each (cilindrical) specimen was wire-brushed, and then the permeability of the specimen was remeasured. This sequence was then repeated for the other end. Next, a thin slice was cut from one end, and the permeability of the shortened specimen was measured again. This process was repeated, alternating the ends of the specimen, several times.

The use of several specimens in each set of experiments was intended to statistically compensate for inhomogeneities in the samples.

Permeabilities to nitrogen were determined at room temperature by means of a Core Lab gas permeater. These measurements were then corrected for Klinkenberger slippage to obtain absolute permeabilities. Before the permeability measurements the specimens were ovendried at 100°C for 24 hours. Porosities were measured by the liquid vacuum saturation method.

Interaction of the rock specimens with drilling fluid at simulated geothermal borehole conditions was achieved with the experimental set up illustrated in Fig. 1. The specimens were loaded into a stainless steel pressure cell. Subsequently the drilling fluid was added at ambient temperature, and the cell was sealed. The pressure was then raised (by means of pressurized nitrogen) before heating to avoid flashing the drilling fluid. Once the temperature and pressure planned for the experiment were achieved, their values were achieved, their values were kept constant for fixed periods. The conditions chosen for both sets of experiments are shown in Table 1.

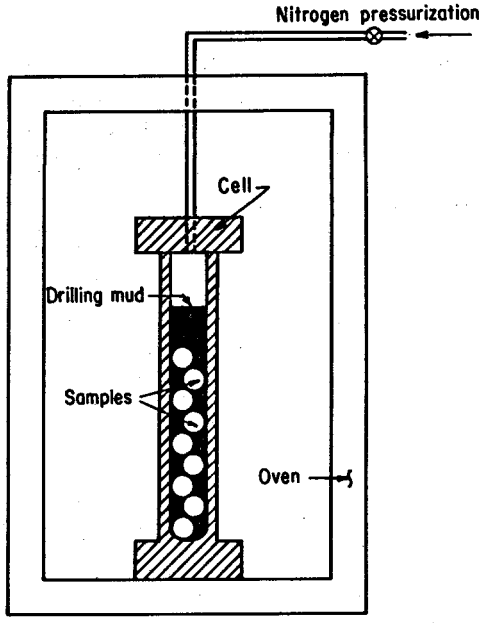

FIGURE 1- EXPERIMENTAL SETUP FOR ROCK/DRILLING FLUID.

The selected drilling fluid is commonly used in the geothermal field of Cerro Prieto for the depth range 300-2000 m. (Domínguez, 1982; A. Fernández and M. Flores, 1982). Its composition is given in Table 2. Other properties of the fluid (API norm RP 13B) are given in Table 3. After contamination the excess mud adhered to the specimens was removed by means of a wet rag.

Table 1. Experimental Parameters.

Parameter	Set A	Set B
Pressure (psi)	1600	400
Temperature (°C)	200	150
Stagnation time (hs)	6	20

Table 2. Composition of the drilling fluid.

Component	Weight (%)
Tap water	76
Rock cuttings	13
Bentonite	7
Diesel oil	3
Lignite	1
NaOH	<0.1 to adjust pH to 9.0

Table 3. Rheological Characteristics of the Drilling Fluid.

Density	1.14 g cm^{-3}
Marsh viscosity	47 s/l
Plastic viscosity	13 cps
Yield point	5 lb/100 ft^2
Initial gel strength	0' = lb/100 ft^2
Final gel strength	10' = 2 lb/100 ft^2
API filtration	13 ml/30 min,
Mud cake thickness	3 mm

Washing was done with methanol in a Core Lab centrifuque operating at 1000 rpm during 12 hs.

Petrological studies by X-Ray diffraction and thin sections were conducted on specimens reserved for this purpouse. For X-Ray diffraction samples were prepared by grinding the material into a very fine powder in an agate mortar. The powdered sample was pressed on a glass holder, ready to be X-Rayed. Crystalline phases were identified by powder X-Ray diffraction with a Siemens diffractometer (D 500) with Ni, filtered Cu kα1 α2 radiation. The scanning speed of the goniometer was 2°2θ/min. Phase identification was carried out from the ASTM powder diffraction file.

Thin sections were prepared using the standard lamination technique. Petrographic analysis were conducted with a petrographic microscope (Carl Zeiss) with polarized light capability and up to 1250 X magnification.

RESULTS AND DISCUSSION.

The initial permeabilities measured in clean specimens from core sample A are shown in Fig. 2 as a function of the specimen's position in the core. It will be noticed that there is a marked change of permeability along the core sample. The regression line shown has an associated correlation coefficient equal to 0.9285; its slope is 0.462 md/cm. The standard deviation of the data points (circles) with respect to the regression line equals 5.18 md, or about 4 percent. The data points illustrated with triangles were not included in the correlation. These points correspond to specimens which under/went saturation with distilled water and then a drying cycle before their permeability to nitrogen was measured. We attribute the observed permeability impairment in these specimens to clay swelling, which could not be removed by the 24 hours, 100°C drying cycle.

The permeabilities measured after the rock specimens interacted with the drilling fluid at simulated borehole conditions are presented in Table 4. The specimens appearing in Fig. 1 but missing in this table were used for experiments no reported in this paper. Table 4 also shows the permeabilities recorded after the washing process. The results are presented as fractions of k_{regr}, the permeabilities of the clean specimens as obtained from the regression line of Fig. 2. From Table 4 the average fractional permeability of the contaminated samples is 0.704, with a standard deviation equal to 0.054, or 7.7 percent. It will be noticed that the washing process seems to have impaired the permeabilities even further: the mean fractional permeability of the washed specimens is 0.656, with a standard deviation equal to 0.056, or about 8.5 percent. With only ten cases, the observed differential between both mean fractional permeabilities is not statistically compelling. Therefore the differential is taken only as indicative that the washing process could actually reduce the permeability. What is certain though, is that washing with methanol did not improve the permeabilities.

Table 4. Permeabilities after contamination and washing for core sample A.

Sample #	Position (cm)	regr (md)	cont / regr	wash / regr
1	1.85	112.35	.751	.689
2	5.65	114.10	.835	.779
3	13.02	117.51	.700	.654
4	20.53	120.98	.662	.608
5	24.17	122.66	.661	.589
6	31.70	126.14	.719	.703
11	57.67	138.13	.677	.618
12	65.16	141.59	.679	.626
13	68.85	143.30	.687	.652
14	76.38	146.78	.670	.642

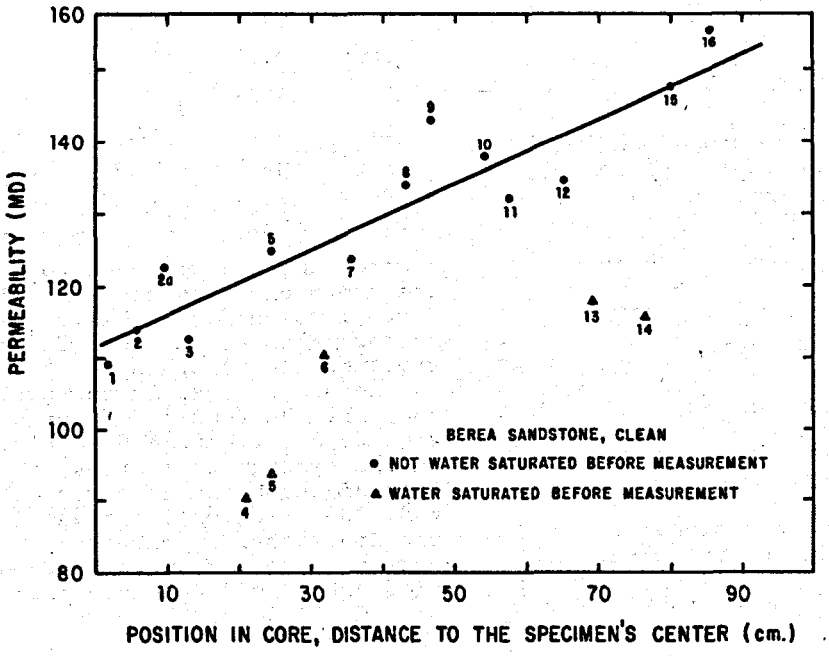

FIGURE 2.- PERMEABILITY vs. POSITION IN CLEAN CORE SAMPLE A.

Having evaluated the amount of permeability reduction associated with the rock/drilling-fluid interaction at geothermal borehole conditions, and the effectiveness of the washing process, the question remains as to what actually caused the observed permeability impairement. We investigated the penetration of drilling fluid particles by means of petrological thin sections studies and by X-Ray diffraction. Samples for these studies were taken from the flat ends of cilindrical specimens (identified by the letter a after their label numbers) which were subjected to contamination and washing simultaneously with the specimens used for permeability measurements. The results of our semiquantitative analysis are shown in Table 5. The minerals in this Table are arranged in order of decreasing abundance. We were unable to find evidence of invasion of the porous medium by particles from the drilling fluid. Electron scanning micrographs are planned for future work.

Table 5. Results of semiquantitative petrological analysis for core sample A.

SAMPLES	MAINS COMPONENTS
	CLEAN SAMPLES
2a,5a,15a	Quartz, feldspars, chlorite, dolomite, mica, calcite*
3a	Quartz, feldspars, dolomite, chlorite, mica, plagioclase? calcite*
7a, 13a	Quartz, feldspars, chlorite, dolomite, mica (illite T), calcite*
9a, 11a	Quartz, feldspars, chlorite (clinochlore), dolomite, mica, calcite*
	CONTAMINED SAMPLES
2a,3a,13a	Quartz, feldspar, dolomite, chlorite (clinochlore), mica, calcite*
5a, 11a	Quartz, chlorite, feldspar, dolomite, mica, calcite*
	WASHED SAMPLES
5a	Quartz, feldspar, chlorite (clinochlore), dolomite, mica, calcite*
13a	Quartz, chlorite (clinochlore), feldspar, dolomite, mica, calcite*

*Low concentration.

As complement to this study we measured the porosities of the clean and washed specimens. Turbidity was observed in the water used for these measurements. The corresponding results are shown in Table 6. Unlike the results reported for permeability, no sistematic variation of porosity with position along the core was found to exist. The average porosity and standard deviation for the clean specimens are 18.11% and 0.45% respectively; the corresponding values for the washed specimens are 17.7% and 0.40% respectively. Although the evidence is not statistically compelling due to the relatively modest number of cases considered, a slight decrease of porosity is indicated for the washed samples. This indication taken together with the results of our petrological studies sugest clay swelling as a possible explanation for the porosity reduction.

Table 6. Porosities of clean and washed specimens from core sample A.

Sample #	Porosity (%) ϕclean	ϕwash
1	19.1	17.6
2	17.6	17.8
2a	17.5	16.7
3	18.0	17.8
3a	17.5	17.5
4	18.3	17.7
5	18.2	17.9
5a	18.3	17.4
6	18.1	18.0
11	17.8	17.6
11a	17.7	17.8
12	18.3	18.4
13	18.4	17.9
13a	18.1	17.3
14	18.7	18.2

Core sample B was used to investigate the depth of invasion by drilling fluid particles, and permeability restoration by mechanical treatment. The mechanical treatment (wire-brushing and slicing) has been described in the preceeding section. The results of set B of experiments are summarized in Fig. 3. Whith in the experimental error, the permeability of the blank specimen was unaffected. The fractional permeabilities of the four other specimens decreased in average to 0.735, with a standard deviation equal to 0.068 upon contamination with drilling mud. The agreement of these values with those found for set A is excellent. Therefore, we deduce that

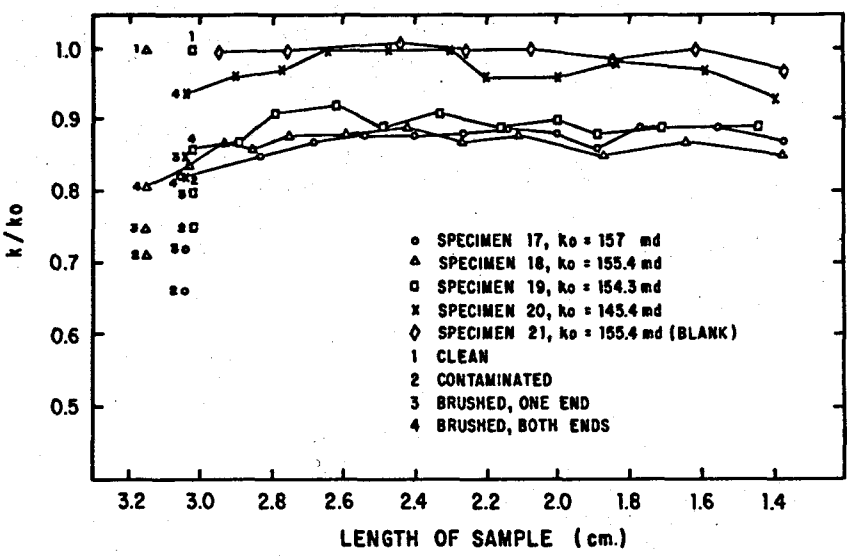

FIGURE 3.- EFFECTS OF WIRE-BRUSHING AND SLICING ON THE PERMEABILITIES OF SPECIMENS FROM CORE SAMPLE B.

possible permeability impairment effects associated with the different pressures, temperatures and stagnation times corresponding to sets A and B must be small for the conditions of our experiments.

The effect of brushing the ends of the specimens is important: in every case it accounts for most of the permeability restoration. Slicing the ends of the specimens increases the permeability slightly at first, but very rapidly a stabilized permeability value is reached. The average stabilized fractional permeability, about 0.91, is significantly higher than 0.656, the value corresponding to the washing process.

For the conditions of the experiments reported in this paper, our results of set B indicate that permeability impairement is due to two distinct phenomena. Surface blocking accounts for about two thirds of the permeability reduction. And some other mechanism, operating in the whole rock, not just in the surface, acounts for the rest of the permeability impairement. Based on the presence of mica, and expandable clay, in any samples (Table 5), and on the turbidity of the water observed during our porosity determinations, we suggest clay swelling and dispersion as responsible for the later mechanism.

CONCLUSIONS.

The following conclusions may be reached from our work with Berea sandstone and a drilling fluid used in the Cerro Prieto geothermal field for the depth range 300-2000 m.

1) Permeability reduction due to rock/drilling fluid interaction at geothermal borehole conditions is of the order of 30 percent for the system studied. This result in insensitive to pressure, temperature, and stagnation time within the range of parametrs explored.

2) Two mechanisms are responsible for permeability impairment. One acting on a thin surface layer, accounts for approximately two thirds of the total effect. The other is distributed in the bulk of the rock, and accounts for about one third of the total permeability impairment.

3) About 90 percent of the original permeability can be restored by mechanical means (wire-brushing and cutting). This removes the permeability damage associated with the "surface mechanisms", but does not affect that due to the "bulk mechanism".

4) Washing contaminated specimens with methanol does not restore their permeability in any discernible way, and may actually cause further permeability impairement.

AKNOWLEDGEMENTS.

We thank Ing. Guillermo Barroso at IIE for providing the Berea cores and some of the equipment and materials used in this work. Juan Flores F., drafted the figures. We also aknowledge the collaboration of Ing. Antonio Rodríguez G. at Instituto Mexicano del Petróleo for washing the samples. The present investigation forms part of the Cooperative Geothermal Program between Instituto de Investigaciones Eléctricas and Stanford University.

REFERENCES.

Abrams, A. "Mud Design to Minimize Rock Impairment Due to Particle Invasion", Jour. Pet. Tech. May 1977, pp 586-592

A.E. Alexander and P. Johnson (1949), "Colloid Science", Oxford AT the Claredon Press, Volume II, pp 704-721

Atwood, D.K. "Restoration of Permeability to Water-Damaged Cores", Jour. Pet Tech., April 1964, pp 1405

B. Domínguez, "Geothermal Drilling at Cerro Prieto Geothermal Field, Baja California, México; Agosto 1982, Guadalajara, Jalisco, México, Vol. I, pp 217-232

Ennis, D.O., Bergosh, J.L. Butters, S. W., and Jones, A.H., 1979 "Drilling Fluid/Formation Interaction at Simulated In Situ Geothermal Conditions", Terratek Report TR 79-85

A. Fernández and M. Flores, "Geothermal Well Drilling Manual at Cerro Prieto" Fourth Symposium on the Cerro Prieto Geothermal Field, Baja California, México; Agosto 1982 Guadalajara, Jalisco, México, Vol. I, pp 245-249

Glenn, E.E. and Slusser, M.L. (1957) "Factors Affecting Well Productivity. II. Drilling Fluid Particle Invasion into Porous Media", Petrol. Trans. AIME, pp 132-139

Jones, F.O., "Influence of Chemical Composition of Water on Clay Blocking of Permeability", Jour. Pet. Tech., April 1964, pp 441-446

Monaghan, P.H. Salathiel, R.A., Morgan, B.E. and Kaiser, A.D., (1959) "Laboratory Studies of Formation Damage in Sands Containing Clays", Trans. AIME, Vol. 216, pp 209.

Mungan, N., "Permeability Reduction Through Changes in PH and Salinity", Jour. Pet. Tech. December 1965, pp 1449-1453

Nicholson, R.W., (1978) "Drilling Fluid Formation Damage in Geothermal Wells", Geoth. Reservoir Council Trans, Vol. 2, pp 503-505

Proceedings Eighth Workshop Geothermal Reservoir Engineering
Stanford University, Stanford, California, December 1982
SGP-TR-60

Modeling Studies of the Natural State of the Krafla Geothermal Field, Iceland

Gudmundur S. Bodvarsson*, Karsten Pruess*,
Valgardur Stefansson+, and Einar T. Eliasson[x]

Earth Sciences Division
Lawrence Berkeley Laboratory, University of California
Berkeley, California 94720

Introduction

The Krafla geothermal field is located on the neovolcanic zone in north-eastern Iceland. To date, over 20 wells have been drilled at the site (Figure 1), revealing the presence of high temperature (up to 350°C) geothermal reservoirs. The subsurface rocks are mostly basaltic, with tuffs dominating in the uppermost 800 meters, and subareal lavas and intrusions dominating below 800 m. In the "old" wellfield (west of the gully Hveragil) there are two reservoirs. Below a 200 m thick caprock, there is a compressed liquid reservoir extending to a depth of approximately 1000 m. This reservoir (upper reservoir) contains fluids with temperatures of 200 - 220°C (Figure 2). Below the upper reservoir there is a confining layer at depths of 1000 - 1500 m; the confining layer increases in thickness to the west. The lower reservoir underlies the confining layer and extends to a depth in excess of 2200 m (the depth of the deepest well). It contains a gas-rich steam-water mixture.

In the new wellfield (to the east) the two-phase zone extends practically to the surface, and the temperatures follow the boiling curve with depth.

Prior to the exploitation of a geothermal system, the mass and heat flows in the reservoir are controlled by natural driving forces. The mass transfer is generally dominated by upflow zones, where hot fluids emerge from depth, and by lateral flows that result from the regional groundwater pressure gradients. Geochemical evidence has indicated the presence of three major upflow zones at Krafla, the first one in the Leirhnjukur area (west of the old wellfield), the second one in the "old" wellfield close to Hveragil, and the third one in the "new" wellfield (Armannsson, Gislason and Hauksson, 1982). The latter two upflow zones control the natural flows as conceptualized in the model shown in Figure 2 (Stefansson, 1982).

A gas-rich steam-water mixture flows from the west in the lower reservoir in the old wellfield, and rises through a fracture zone near Hveragil, where it mixes with fluids from the reservoir in the new wellfield. Most of the noncondensible gases and some of the fluids discharge at surface manifestation in Hveragil, but the rest recharge the upper reservoir in the old wellfield. In the new wellfield a steam-water mixture rises through an upflow zone, moves laterally to the west towards Hveragil and mixes with fluids from the lower reservoir in the old wellfield. Some of the fluids in the reservoir in the new wellfield are discharged to the surface as evidenced by surface manifestations there.

In modeling the Krafla reservoir in its natural state, all of the major physical processes that take place in the reservoir must be considered. These include mass transport, conductive and convective heat transfer, and boiling and condensation. The major objectives of the present work are:

1) To verify a conceptual model of the field.

2) To resolve the mechanism that controls the low temperatures in the upper reservoir, which is recharged by fluids of much higher temperatures.

3) To quantify natural mass and heat flows in the reservoir.

4) To verify permeability values obtained from the analysis of injection test data.

5) To obtain a better understanding of the dynamic nature of the reservoir; i.e., set the background for further reservoir modeling studies.

* Lawrence Berkeley Laboratory, Berkeley, California
+ National Energy Authority of Iceland
x State Electric Power Works of Iceland, Krafla Division

Approach

It should be emphasized that the modeling of a two-phase reservoir in its natural state is not a simple task. Simulations must be carried out for tens or hundreds of thousand years before steady state conditions are reached. Thus, these studies are very time consuming and incur substantial conputational expenses.

The Krafla field in its natural state is a dynamic system. However, the changes in thermodynamic conditions with time are probably very slow, so that a steady state approximation for the modeled reservoir system is reasonable.

The simulations reported below were carried out with Lawrence Berkeley Laboratory's general purpose simulator MULKOM (Pruess, 1982). Effects of non-condensible gases were neglected. A trial-and-error procedure is used, in which parameters of the reservoir model are initially fixed according to field data or estimates. Then the model is run until steady state is reached, and the resulting thermodynamic conditions and flows are compared with field observations. Model parameters are then modified until a satisfactory agreement with all relevant field information is obtained.

One question that arises in this procedure is, which of the field data should be used as model input, and which field data can be employed to check and confirm hypothetical assumptions and predictions of the model. We selected a small set of the most reliable field data as input, thereby avoiding to constrain the model by parameters of questionable accuracy. Most of the field data, which are known with less accuracy or confidence, can then be used as a check on calculated results.

Our reservoir model is a 1 m thick vertical section from west to east, which is based on the conceptual model in Figure 2. It extends from wells 5 and 7 in the west all the way to the impermeable fault zone between wells 17 and 18 in the east. The mesh design shown in Figure 3 is somewhat schematic, but preserves the main features and dimensions of the conceptual model. Surface discharge of steam in Hveragil and in the new wellfield is represented by appropriate sinks in elements 34, 44, 40 and 50. Influx areas and pressure boundary conditions are represented by boundary nodes B1 through B16 (Figure 3). Simulations were initialized with arbitrary thermodynamic conditions, but a possible dependence of the steady state on assumed initial conditions was investigated (see below).

Relative permeabilities were assumed to depend linearly on saturation, with immobile liquid and steam saturations of 0.30 and 0.05, respectively. While certainly not unique, this parametrization was shown to be consistent with individual well performance in Krafla (Pruess and Bodvarsson, to be published).

Best Model

After a lengthy process of trial and error we have obtained a model that represents very well the observed data on the natural state of the Krafla field. In the model we use 8 different regions that represent rocks with different material properties. The different regions are shown in Figure 4 and their material properties are given in Table 1. All of the regions are assumed to have the same values of rock density, heat capacity, and porosity. These parameters do not affect the results presented here, as steady state conditions do not depend upon storage-type parameters.

Regions 1 and 2 have low permeability, and represent a caprock and a confining layer, respectively. Region 3 is the average fracture/matrix material, the permeability of which was chosen according to the average value obtained from injection tests (Bodvarsson et. al., to be published). Regions 4 through 8 represent highly fractured zones, for whose existence and location there is direct evidence in the field.

The results for the steady state pressure distribution in the reservoir are shown in Figure 5. The figure shows that pressures are fairly uniform in the lower two-phase part of the reservoir. However, in the upper zone there are significant pressure differences at a given depth between the new and old wellfields. The 5-10 bar pressure difference compares well with field data. A comparison between observed and calculated pressure profiles for a typical well in the old wellfield is shown in Figure 6. The agreement is good, with slight differences most likely due to inaccurate measurements. The agreement between calculated and observed pressure profiles in the new field is similarly good.

The calculated temperature distribution in the system is shown in Figure 7. The figure shows that temperatures of 300°C are found at a depth of about 1000 m, and of over 340°C at a depth of 2000 m. At shallower depths the temperatures in the new wellfield are considerably higher than those in the upper reservoir in the old wellfield. This is due to boiling in the Hveragil fracture and the discharge of high enthalpy fluid to surface springs at Hveragil. The model shows that 0.00842 kg/s·m of high enthalpy vapor escapes to the surface at Hveragil. This compares very well with the value of 0.008 kg/s·m estimated by Armannsson and Gislason (personal communication, 1982). Similarly, the model indicates that 0.0023 kg/s·m of vapor feeds surface manifestations in the new wellfield, which

closely agrees with the estimated value of 0.003 kg/m·s.

The model shows excellent agreement with observed temperature profiles in the new wellfield. The comparison between observed and calculated temperature profiles in the old wellfield is not as good. Figure 8 shows temperature profiles for all wells in the old wellfield east of wells 5 and 7, as well as the calculated temperature profile in the old wellfield (broken line). The temperature gradients are highest in the low permeability caprock and the confining layer, where conduction dominates the heat transfer. There are two major discrepancies between the observed and calculated data. Firstly, the coarse mesh used in the simulations makes it impossible to accurately model the sharp break in the temperature profiles at a depth of 200 meters. The second difference is evident in the lower elements in the upper reservoir in the old wellfield. Field data indicate virtually isothermal conditions in the upper reservoir, whereas the calculated results show a 5-15°C difference in temperature between depths of 400 and 800 m. It is quite possible that the temperatures observed in wells do not accurately reflect formation temperatures. Our results are in agreement with hydrothermal alteration data, which indicate that the temperature in the upper reservoir should increase with depth (Stefansson, Kristmannsdottir, and Gislason, 1977). Furthermore, silica thermometer analysis of fluids from the upper reservoir shows temperatures of up to 240°C. It is also possible that the differences between observed and calculated temperatures may be due to the two-dimensional approximation employed in our model.

The steady state vapor saturation contours are shown in Figure 9. It should be emphasized that vapor saturations depend greatly on poorly known parameters such as relative permeabilities, so that the values shown in Figure 9 should be considered approximate. Also, the vapor saturations represent average values in the fracture system; vapor saturations in the rock matrix may be much lower. The figure shows that both the lower reservoir in the old wellfield and the reservoir in the new wellfield are under two-phase conditions. On the other hand the upper reservoir in the old wellfield is a compressed liquid reservoir. These observations agree with current notions about the reservoir. In general, most of the two-phase reservoir contains 10-20% of vapor by volume. The vapor saturation is higher in the upper part of both the lower reservoir in the old wellfield and the reservoir in the new wellfield. This is a result of upflow of steam from depth due to the nearly hydrostatic pressure gradient. It should be noted that infiltration of surface water (rainfall), which we have neglected, will tend to reduce vapor saturations in the upper parts of the reservoirs.

The steady state flow field in the reservoir system is shown in Figure 10. The arrows represent the total mass flow, i.e., the sum of the flows of the liquid and the vapor phase. Fluids enter the system from the west in the lower reservoir, and flow towards the east until they reach the high permeability upflow zone that intersects the surface at Hveragil. Most of the fluids from the upflow zone in the new wellfield rise until they reach the high permeability horizontal zone at a depth of 1000 m. The fluids then flow laterally along this fracture zone until they reach the Hveragil fracture, where the fluids from the old and the new wellfield mix. Some of the fluid mixture flows up the fault zone, and feeds surface manifestation at Hveragil, whereas the major portion recharges the upper reservoir at a rate of 0.013 kg/s·m. The results of the present model indicate that about 60% of the fluids come from the lower reservoir in the old wellfield and 40% from the upflow zone in the new wellfield. Geochemical data indicate that these mixing ratios are reasonable based on the chemical composition of the fluids from the different reservoirs (Gislason, personal communication, 1982).

It is of interest to note that fluid fluxes are largest (0.015 kg/s·m) in the Hveragil fault zone. This may indicate that wells intersecting this fault zone could be productive. Flow velocities are lowest in regions of low permeability and/or high vapor saturations, due to low mobilities of the fluids.

Sensitivity Studies

In order to check our natural state model of the Krafla reservoir, we have conducted sensitivity studies of many of the key model parameters. As mentioned earlier the steady state results obtained are not at all sensitive to storage-type parameters, such as porosity, rock density, and heat capacity. We will discuss the results only briefly due to the limited space available.

Permeability distribution

As a first example we consider the case of a homogeneous reservoir with a permeability of 2.0×10^{-15} m^2 (2mD), which is the average permeability inferred from analysis of injection tests of Krafla wells. The steady-state results showed too low pressures in the upper parts of the reservoirs when realistic pressures are applied at boundary nodes in the lower parts of the reservoirs. Using an anisotropy ratio of 5 (i.e., the vertical permeability is 5 times the horizontal permeability), reasonable pressures were obtained throughout the reservoir system. This seems to indicate that vertical fractures are very important fluid conduits in the Krafla reservoirs, and suggests that directional drilling may be more successful than conventional "straight-down" drilling. The steady-state flow field for the case of an anisotropy of 5 is shown in Figure 11.

Thermal Conductivities

For the reservoir model considered we find that convection is the dominant heat transfer mechanism. The convective heat loss to the surface springs is approximately 28700 W for the 1 m thick vertical section modeled. In comparison, the total heat loss through the caprock is only 1300 W, or only 5% of the convective heat losses. As a result, varying the thermal conductivity has relatively little effect on the steady-state thermodynamic conditions and fluid flows within the reservoir system, except in the upper reservoir in the old wellfield. Using a more detailed representation of the heat loss to the caprock we find that the best comparison with observed data is achieved when a thermal conductivity of 1.15 J/m·s·°C is used. The thermal conductivity of the confining layer is too insensitive a parameter to be determined with any accuracy.

Heat fluxes from below

The heat flux from below has a significant effect on steady state vapor saturations and pressures in the upper parts of the reservoir system. When the heat flux from below is neglected, a zone of single phase liquid results in the lower parts of the reservoir system. Similarly, when the heat flux is doubled from what we use in the best model (2.0 W/m^2), the pressures in the upper parts become too high due to higher vapor saturations and consequently greater upflow of steam.

Flow at surface springs

The fluid flow to the surface springs in Hveragil, extracted from elements 34 and 44, has major impact upon the temperature distribution in the upper reservoir. Consequently, the appropriate values were determined with good accuracy by the simulation. The flow to the surface springs in the new wellfield cannot be as accurately determined, but is within the range of 0.002 - 0.0027 kg/s·m.

Relative permeabilities

In the base case (best model) we used linear relative permeability functions with immobile liquid and steam saturations of 0.30 and 0.05, respectively. An attempt was made to match the field data using the Corey relative permeability curves, with the same irreducible saturations. We found that the field data could not be matched using the Corey curves.

Uniqueness of steady-state solution

In the case of highly non-linear problems such as two-phase porous flow, there is always the question of uniqueness of the steady-state solution. In the simulations reported above we used initial conditions that resembled the observed data from the field (hot reservoir). In order to check on the uniqueness of the solution for the best model, we initialized a simulation with a "cold" reservoir, i.e. the temperatures of each layer were assigned values corresponding to a normal geothermal gradient (30°C/km). The results showed that after a lengthy transient heating period an identical steady-state solution was obtained. This provides evidence that the steady-state solutions using the best model may be unique.

Summary

The modeling of the natural state of the Krafla system has yielded results that closely match all available field data, and agree with a conceptual model developed from geochemical observations. Furthermore, studies of the sensitivity of various parameters give valuable insight into the permeabilities of different reservoir zones, thermal conductivity of the caprock, rates and enthalpies of natural recharge and discharge, and various other important reservoir parameters. The model presented here is two-dimensional, and only considers a part of the old wellfield. In the future, we hope to develop a natural-state model for the entire Krafla system, taking into account the three-dimensional nature of fluid flows.

Acknowledgement

The authors thank Sally Benson for a critical review of the manuscript. This research was performed as a part of a cooperative scientific investigation of the Krafla geothermal field between NEA, SEPW, ERI and SI of Iceland and LBL of U.S.A. This work was supported by SEPW of Iceland and the Assistant Secretary for Conservation and Renewable Energy, Office of Renewable Technology, Division of Geothermal and Hydropower Technologies of the U.S. Department of Energy under Contract No. DE-AC03-76SF00098.

References

Armannsson, H., Gislason, G. and T. Hauksson, Magmatic gases in wellfluids aid the mapping of the flow pattern in a geothermal system, Geochemica et Cosmochimica Acta, Vol. 46, pp. 167-177, 1982.

Pruess, K., Development of the general purpose simulator MULKOM, Annual Report 1982, Earth Sciences Division, Lawrence Berkeley Laboratory, Berkeley, Ca., 1982.

Stefansson, V., personal letter to G. S. Bodvarsson, April 1982.

Stefansson, V., Kristmannsdottir, H., and G. Gislason, Holubref 7, Orkustofnun, 1977.

Table 1: Material Properties of Reservoir Zones.

Zone	Density (kg/m^3)	Heat Capacity ($J/kg°C$)	Thermal Cond. ($J/m.s.°C$)	Porosity	Hor. Perm. (m^2)	Vert. Perm (m^2)
1	2650.	1000.	1.5	0.05	2×10^{-18}	2×10^{-18}
2	2650.	1000.	1.7	0.05	2×10^{-18}	2×10^{-18}
3	2650.	1000.	1.7	0.05	2×10^{-15}	2×10^{-15}
4	2650.	1000.	1.7	0.05	2×10^{-15}	3×10^{-14}
5	2650.	1000.	1.7	0.05	2×10^{-14}	2×10^{-15}
6	2650.	1000.	1.7	0.05	1×10^{-14}	2×10^{-15}
7	2650.	1000.	1.7	0.05	1×10^{-14}	3×10^{-14}
8	2650.	1000.	1.7	0.05	1×10^{-14}	2×10^{-14}

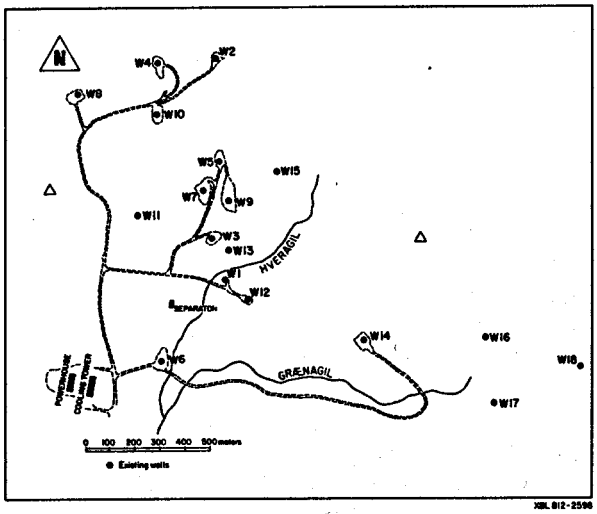

Figure 1: Well locations in Krafla field.

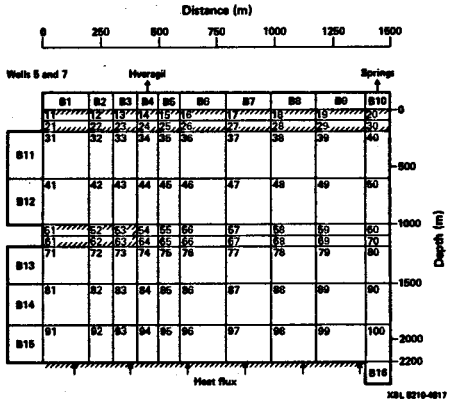

Figure 3: Simplified reservoir model and mesh used in the study of the natural state.

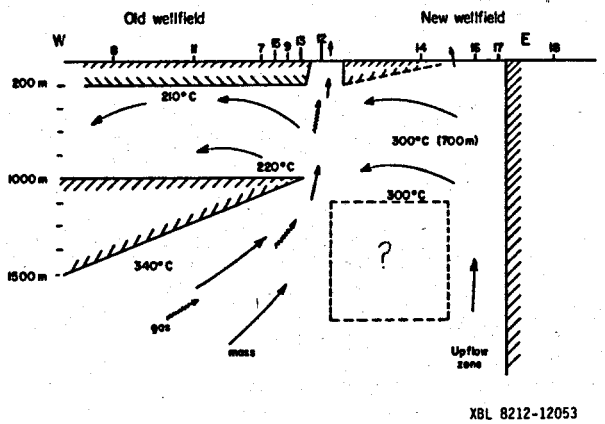

Figure 2: Conceptual model of the Krafla field.

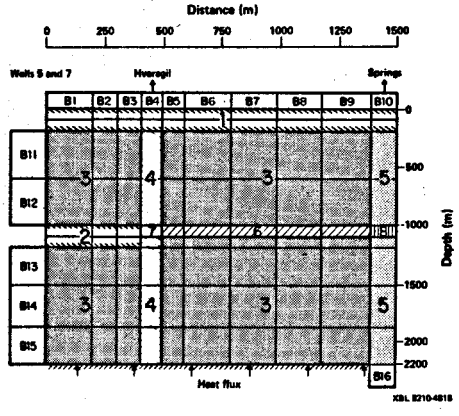

Figure 4: Different reservoir zones used in the best model.

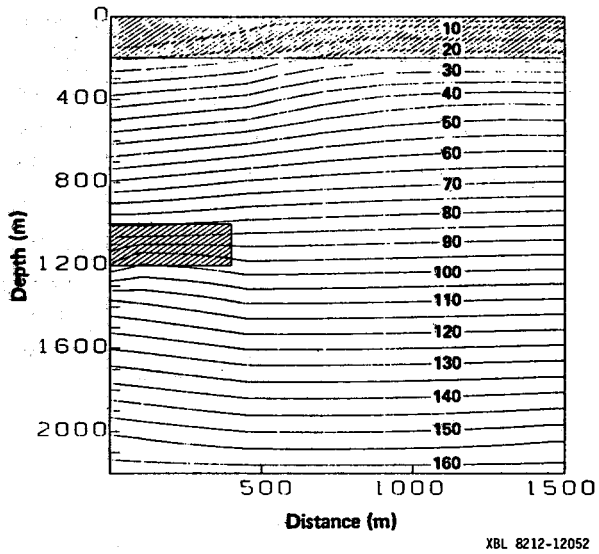

Figure 5: Steady-state pressure distribution in the natural state.

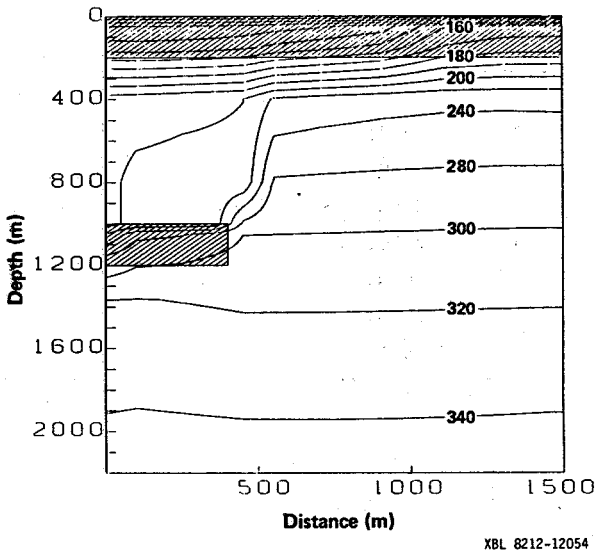

Figure 7: Steady-state temperature distribution in the natural state.

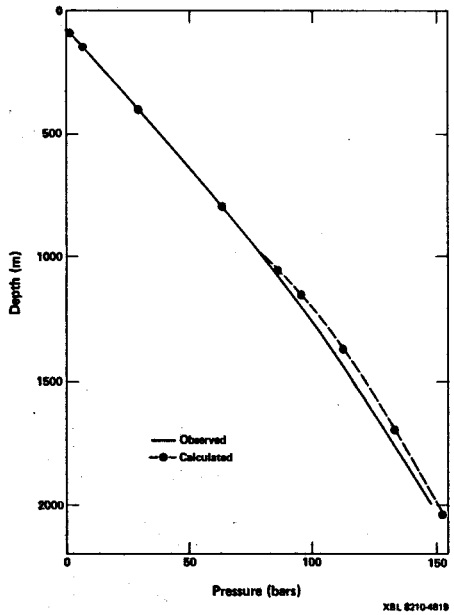

Figure 6: Comparison between observed and calculated pressure profiles in the old wellfield.

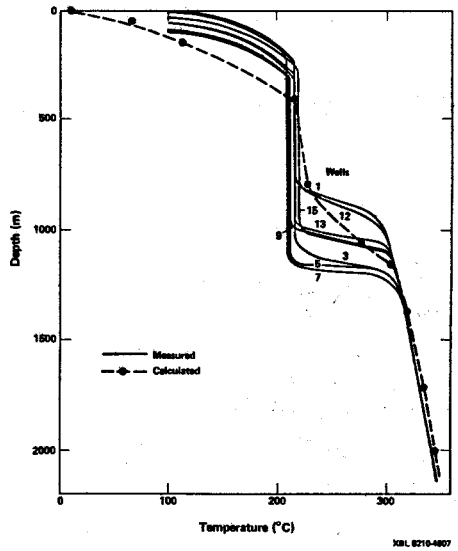

Figure 8: Comparison between observed and calculated temperature profiles in the old wellfield.

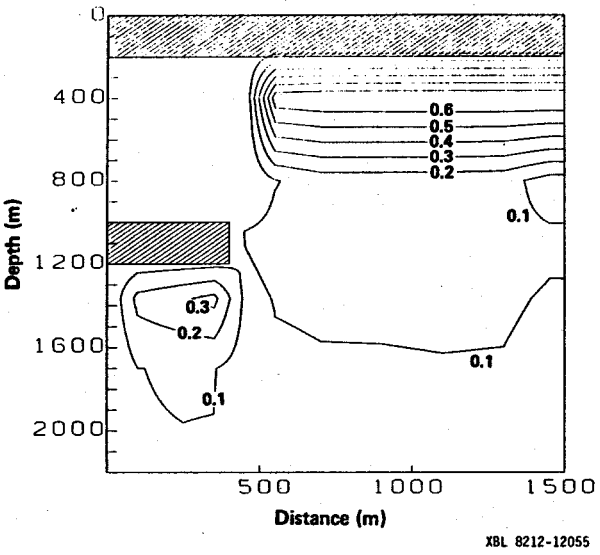

Figure 9: Steady-state vapor saturations in the natural state.

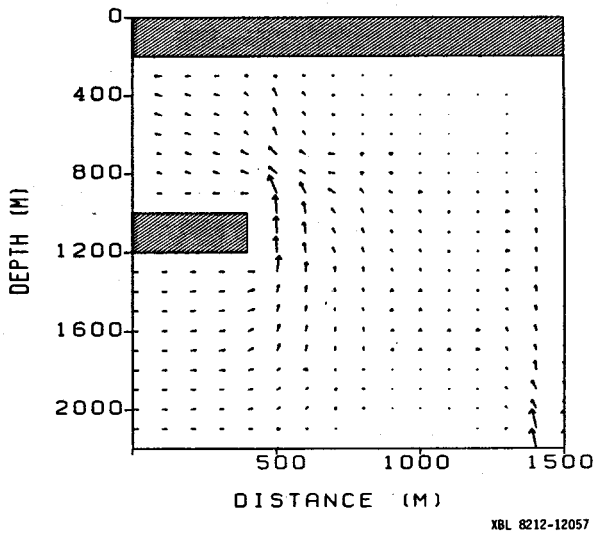

Figure 11: Steady-state flow field for the case of an anisotropy of 5.

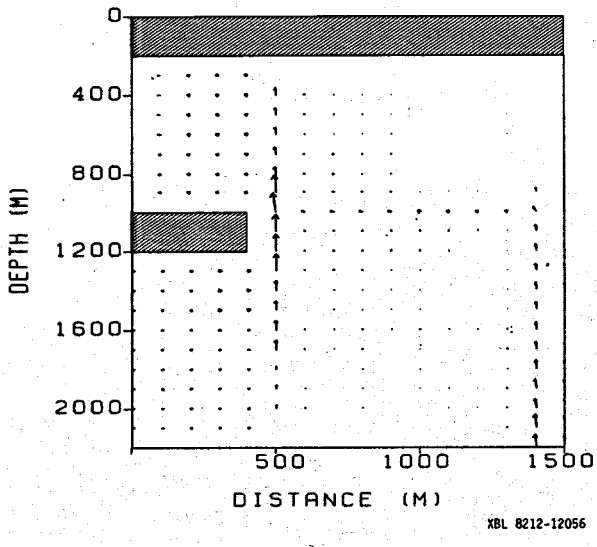

Figure 10: Steady-state flow field in the natural state (best case).

Proceedings Eighth Workshop Geothermal Reservoir Engineering
Stanford University, Stanford, California, December 1982
SGP-TR-60

Proximity Functions for Modeling Fluid and Heat Flow in Reservoirs with Stochastic Fracture Distributions

Karsten Pruess and Kenzi Karasaki

Earth Sciences Division
Lawrence Berkeley Laboratory
Berkeley, California 94720

1. Introduction

It is well established that most high-temperature geothermal reservoirs are extensively fractured. The fractures provide the principal conduits for fluid and heat flow. The rock matrix contains most of the fluid and heat reserves, but it usually has a very low permeability, perhaps in the microdarcy-range.

Conventional approaches to geothermal reservoir modeling have employed a porous medium approximation, although the validity of this approximation for naturally fractured reservoirs has never been demonstrated in detail. It appears that most researchers expected a porous medium approximation to work in cases with "not too large" fracture spacing. Recently it was shown by Pruess and Narasimhan (1982a), that in two-phase geothermal reservoirs strong discontinuities in vapor saturation can arise at matrix/fracture interfaces, due to an interplay between fluid convection and heat conduction. This suggests that fractured systems with two-phase fluid may behave quite differently than porous medium systems even in cases where fracture spacing is small in comparison to characteristic dimensions of the problem (e.g., reservoir size, well spacings, completion intervals).

In order to quantitatively model fractured reservoir behavior, Pruess and Narasimhan (1982b) developed a "multiple interacting continua" method ("MINC"), which is a generalization of the double porosity model of Barenblatt et al. (1960) and Warren and Root (1963). The classical double-porosity work employed a quasi-steady approximation for "interporosity" flow between rock matrix and fractures, which severely limits the range of systems and processes to which it is applicable. The MINC-method on the other hand, treats interporosity flow entirely by numerical methods. This makes possible a fully transient representation of interporosity flow, which is applicable to problems with coupled fluid and heat flow, and to multiphase fluids with large and varying compressibility, such as steam-water mixtures.

The work of Pruess and Narasimhan employed highly idealized regular fracture distributions, but the authors pointed out that the MINC-method can be extended to realistic (stochastic) fracture distributions as well. It is the purpose of the present paper to carry out the generalization to arbitrary irregular fracture distributions. After briefly reviewing the main assumptions of the MINC-method, we shall introduce the concept of a "proximity function" as the central geometrical quantity which defines the matrix-fracture interaction. Subsequently we shall consider proximity functions for regular or irregular fracture distributions, using Monte Carlo integration techniques.

2. Summary of the MINC - Method

The MINC-method follows the double-porosity approach in adopting a continuum treatment for both the fracture network and for the porous rock matrix. Global flow in the reservoir is assumed to occur only through the network of interconnected fractures, whereas fractures and rock matrix can exchange fluid and heat locally. In order to obtain a numerical description for interporosity flow, it is necessary to partition the flow domain into discrete volume elements, or grid blocks. The crucial point of the MINC-method is the partitioning (or discretization) procedure adopted for interporosity flow. It should be noted that the customary equations for mass- and energy-conservation, when written in integral form, hold for arbitrary reservoir subdomains (Narasimhan, 1982). However, discretized equations are only useful (solvable), when the flow terms between volume elements can be related to the accumulation of mass and heat within volume elements. Fluid and heat flow are driven by gradients of pressure and temperature, respectively, and these can be expressed in terms of average values of thermodynamic variables if (and only if) there is approximate thermodynamic equilibrium within each volume element at all times. In porous media, this requirement will usually be satisfied for any suitably "small" simply-connected subregion, as thermodynamic conditions generally vary continuously and smoothly with position.

The situation can be quite different in fractured media, where changes in thermodynamic conditions as a consequence of boiling or cold water injection may propagate rapidly in the fracture network, while migrating only slowly into the rock matrix. Thus, thermodynamic conditions may show strong variations as a function of position in the vicinity of the fractures. Because of the different response times, thermodynamic changes in the rock matrix will locally depend mainly upon the distance from the nearest fracture. Then, interporosity flow will be perpendicular to the fracture faces. This suggests partitioning (discretizing) of the rock matrix into sequences of nested volume elements, which are defined on the basis of distance from the fractures. Figure 1 illustrates this concept for the case of an idealized two-dimensional fracture distribution. In this case the geometric quantities governing the interporosity flow (element volumes, interface areas, and nodal distances) can be easily obtained in explicit analytical form (Pruess and Narasimhan, 1982b).

The mesh design concept as shown in Figure 1 can be generalized, to make it more suitable for applications of practical interest. In reservoir regions where thermodynamic conditions vary slowly as a function of position, it is not necessary to have separate volume elements within each of the elementary units depicted in Figure 1. Instead, corresponding nested volumes in neighboring units, which are identified by an index number in Figure 1, can be lumped together into one computational volume element. Element volumes and interface areas scale proportional to the number of elementary units which are lumped together, whereas nodal distances remain unchanged. The scaling procedure can be further generalized by applying the same scaling law to grid blocks of arbitrary size or shape. Thus we arrive at a two-step procedure for defining a computational mesh for a fractured reservoir. The first step is to construct a mesh just as would be done for a porous-medium type system with small grid blocks near wells, etc. ("primary mesh"). The second step is to sub-partition each grid block into several continua, the respective volumes, interface areas, and nodal distances of which are obtained by appropriate scaling from the quantities pertaining to the basic fractured unit ("secondary mesh").

The concept of partitioning based on distance from the fractures can be readily extended to arbitrary irregular fracture distributions. Figure 2 illustrates this for a set of fractures of finite length. First it is necessary to eliminate the dead-end portions of the fractures, which do not participate in global flow within the fracture system (Figure 2b). The rock matrix can then be readily partitioned into several continua with increasing distance from the fractures (Figure 2c). While the general case of irregular fractures is straightforward from the conceptual point of view, it is not possible to obtain the geometrical parameters for the sub-continua in an explicit fashion. To accomplish this we introduce an auxiliary function, termed a "proximity function", which can be calculated for any given facture distribution, and which allows to completely define all geometric parameters for interporosity flow.

3. The Concept of Proximity Functions

For any given reservoir subdomain with known fracture distribution a function V(x) can be defined, which represents total matrix volume V within a distance x from the fracture faces. Note that the volume V will generally consist of a finite number of disjoint multiply-connected regions, representing a quite complex topological structure (see Figure 2c). If V_0 is the volume of the subdomain, and ϕ_1 is the volume fraction (average porosity) of the fracture system, the volume of the fracture continuum within V_0 is $V_1 = \phi_1 \cdot V_0$. It is convenient to introduce a "proximity function" PROX(x), which expresses, for a given reservoir subdomain V_0, the total fraction of matrix volume within a distance x from the fractures. Noting that the total matrix volume in domain V_0 is

$$V_m = (1-\phi_1)\, V_0 \tag{1}$$

we have

$$\mathrm{PROX}(x) = \frac{V(x)}{V_m} = \frac{V(x)}{(1-\phi_1)\, V_0} \tag{2}$$

In the MINC-method, a discretization is adopted for the rock matrix (see Figure 3) whereby all matrix volume within a distance x_2 from the fracture faces will be lumped into one computational volume element (or subcontinuum) V_2; matrix volume within a distance larger than x_2 but less than x_3 will be lumped into V_3, etc. This is illustrated in Figure 3 for a regular fracture network, but it is evident that the same procedure can be applied to arbitrary irregular fracture distributions, see Figure 2c. To define flow towards or away from the fractures, it is necessary to specify interface areas and nodal distances between the matrix sub-continua. From the definition of the proximity function as given above, the interface area for flow at distance x is simply

$$A(x) = \frac{dV}{dx} = (1-\phi_1)\, V_0 \frac{d\ \mathrm{PROX}(x)}{dx} \tag{3}$$

In conventional porous medium-type simulation methods with simply-connected grid blocks, the computational nodes are points, usually located at the center of a volume element. For the multiply connected volume elements of the MINC-method, the

element nodes become nodal surfaces, which are located half-way between the inner and the outer surface of an element. The discretization procedure adopted in the MINC-method can now be described as follows. First, a "primary" mesh is specified in integral finite difference form by means of a set of volume elements $\{V_n;\ n=1, \ldots, N\}$, interface areas A_{nm}, and nodal distances d_{nm}. All primary "connections" (A_{nm}, d_{nm}) between volume elements are assigned to the fracture continuum. Each grid block V_n of the primary mesh is then partitioned into a sequence of interacting continua V_{nj} $(j=1, \ldots, J)$. The continua are specified by means of a set of volume fractions ϕ_j $(j=1, \ldots, J)$, where ϕ_1 is the average fracture porosity, and the $\phi_2, \ldots, \phi_J$ denote volume fractions in the matrix at increasing distance from the fractures. Obviously we must have

$$\sum_{j=1}^{J} \phi_j = 1 \tag{4}$$

Apart from this constraint, the ϕ_j $(j=2, \ldots, J)$ are arbitrary, but for best accuracy the volume fractions near the fractures $(\phi_2, \phi_3, \ldots)$ should be chosen not "too" large. The volumes of the sub-partitioning are simply

$$V_{nj} = \phi_j \cdot V_n \tag{5}$$

so that

$$\sum_{j=1}^{J} V_{nj} = V_n \tag{6}$$

In the "secondary" mesh $\{V_{nj};\ n=1, \ldots, N;\ j=1, \ldots, J\}$ each of the primary grid blocks V_{n1} (representing fractures) interacts with its neighbors through the fracture continuum, and with a one-dimensional string $V_{n2}, V_{n3}, \ldots, V_{nJ}$ of nested grid "blocks" in the matrix. The distances x_j to which the V_{nj} extend can be simply obtained by inverting the proximity function. We have

$$\mathrm{PROX}(x_j) = \sum_{j'=2}^{j} \frac{\phi_{j'}}{1-\phi_1} \tag{7}$$

The interface area between elements V_{nj} and V_{nj+1} is simply $A(x_j)$ as given by equation (3). Nodal distances are given by $(j=2, \ldots, J-2)$

$$d_{nj,\ nj+1} = \frac{x_{j+1} - x_j}{2} + \frac{x_j - x_{j-1}}{2} = \frac{1}{2}\,(x_{j+1} - x_{j-1}) \tag{8}$$

The fracture nodes are placed at the fracture-matrix interface, so that

$$d_{n1,\ n2} = \frac{x_2}{2} \tag{9}$$

The innermost nodal distance requires special consideration. Writing

$$d_{nJ-1,\ J} = \frac{x_{J-1} - x_{J-2}}{2} + D_J \tag{10}$$

we introduce the distance D_J of the nodal surface with index J from the innermost interface area, $A_{nJ-1,\ nJ}$. D_J should be chosen in such a way that the finite difference approximation for pressure - and temperature - gradients gives the most accurate estimate for the actual gradients at the interface $A_{nJ-1,\ nJ}$. In general, D_J may be taken in quasi-steady flow approximation. A good approximation for the quasi-steady nodal distance in many cases is (Warren and Root, 1963)

$$D_J = \frac{\left(V_{nJ}\right)^{1/3}}{10} \tag{11}$$

4. Examples of Proximity Functions

In the case of regularly shaped matrix blocks, analytical expressions can be written down for proximity functions. For example, for two-dimensional square matrix blocks with side length a the matrix volume within a distance x from the block faces is (per unit thickness)

$$V(x) = a^2 - (a-2x)^2 \tag{12}$$

so that, according to equation (2)

$$\mathrm{PROX}(x) = \frac{V(x)}{a^2} = 4\,\frac{x}{a} - 4\left(\frac{x}{a}\right)^2 \tag{13}$$

An interesting application of the methods presented here is for the Stanford large reservoir model, which has a loading of regularly shaped rocks. There are six layers, each of which has five parallelepiped blocks and four triangular blocks with side lengths a, b, c. The proximity function for a rectangular block is

$$P_r(x) = 8\,\frac{x^3}{ab^2} - \left(\frac{8}{ab} + \frac{4}{b^2}\right)x^2 + \left(\frac{4}{b} + \frac{2}{a}\right)x \tag{14}$$

and for a triangular block we have

$$P_t(x) = \left(3+2\sqrt{2}\right)\frac{4x^3}{ab^2} - \left[\frac{6+4\sqrt{2}}{b^2} + \frac{4\ 2+\sqrt{2}}{ab}\right]x^2 + \left(\frac{4+2\sqrt{2}}{b} + \frac{2}{a}\right)x \tag{15}$$

The averaged proximity function in each layer is

$$P_{rt}(x) = \frac{5}{7} P_r(x) + \frac{2}{7} P_t(x) \qquad (16)$$

These functions are illustrated in Figure 4. Fluid and heat flow calculations using these functions are reported in another paper presented at this workshop (Hunsbedt et al., 1982).

In the general case of arbitrary irregular fracture distributions, proximity functions can be computed by means of Monte Carlo - integration. A computer program was written which generates random points within a region V_0 with known fracture distribution. The minimum distance of each point from the fractures is computed, and all points are sorted in order of increasing distance. The fraction of points falling below a certain distance x is the value of the proximity function at x. This procedure, which is applicable to arbitrary fracture distributions, defines the proximity function at discrete points, subject to statistical fluctuations from the Monte Carlo - integration process. In order to be able to numerically compute derivatives of the proximity function, a smoothed curve is computed by fitting the discrete function with a succession of cubic splines. The accuracy of the Monte Carlo procedure was tested by computing proximity functions and their derivatives for cases where the results are known in analytical form.

Figures 5 and 6 show proximity functions and their derivatives for square matrix blocks. Note that the results of the Monte Carlo - integration give a close approximation to the analytical solution as given by equation (13) already for 5,000 integration points. However, small deviations are magnified when interface areas are computed by differentiation. When 50,000 integration points are used, a good approximation is obtained for interface areas, see Figure 6b.

Figure 7 shows a two-dimensional stochastic fracture pattern. This was generated with a computer program developed at LBL, according to a given distribution of orientations and lengths, with random locations (Long et al., 1982). The proximity function for this system, obtained by Monte Carlo - integration with 100,000 integration points, is shown in Figure 8, while Figure 9 gives the interface areas as obtained by numerical differentiation.

5. Summary

The proximity function quantifies, for a given fractured rock mass, the volume of rock matrix present in dependence upon the distance from the fractures. This function and its first derivative are sufficient to completely define the geometric parameters for interporosity flow between rock matrix and fractures, as required by the method of "multiple interacting continua" (MINC; Pruess and Narasimhan, 1982b). For regularly shaped matrix blocks, proximity functions can be written down in analytical form, while for stochastic fracture distributions they are obtained by means of Monte Carlo-integration. We are currently studying the dependence of proximity functions upon the parameters of fracture distributions, and upon sample size and specific realization of a stochastic distribution. Also, we have begun simulations of fluid and heat flow in geothermal reservoirs with realistic fracture distributions.

It should be emphasized that for modeling of flow in fractured rock masses, the proximity function of the flow system can be computed once and for all, ahead of actual flow simulations. A pre-processor program has been written (Pruess, 1982), which generates all geometric parameters for interporosity flow in a format compatible with Lawrence Berkeley Laboratory's geothermal simulators SHAFT79 and MULKOM. The preprocessor can also interface with other integral finite difference simulators, such as TRUST (saturated-unsaturated flow), PT (single-phase non-isothermal flow), and TRUMP (advective-diffusive heat and chemical transport). With the methods outlined in this paper, modeling of fluid and heat flow in naturally fractured reservoirs is no more difficult than simulations for porous media.

Acknowledgement

The authors thank Drs. T. N. Narasimhan, C. R. Wilson, and Jane Long for reviewing the manuscript. This work was supported by the Assistant Secretary for Conservation and Renewable Energy, Office of Renewable Technology, Division of Geothermal and Hydropower Technologies of the U.S. Department of Energy under Contract No. DE-AC03-76SF00098.

References

Barenblatt, G.E., Zheltov, I.P., and Kochina, I.N., 1960. Basic Concepts in the Theory of Homogeneous Liquids in Fissured Rocks, J. Appl. Math., (USSR), 24(5), 1286-1303.

Hunsbedt, A., Lam, S.T., Kruger, P., and Pruess, K., 1982. Heat Extraction Modeling of the Stanford Hydrothermal Reservoir Model, paper presented at the Eighth Workshop on Geothermal Reservoir Engineering, Stanford University, Stanford, CA.

Long, J.C.S., Remer, J.S., Wilson, C.R., and Witherspoon, P.A., 1982. Porous Media Equivalents for Networks of Discontinuous Fractures, Water Resources Research, 18(3), 645-658.

Narasimhan, T.N., 1982. Multidimensional Numerical Simulation of Fluid Flow in Fractured Porous Media, Water Resources Research, 18(4), 1235-1247.

Pruess, K., and Narasimhan, T.N., 1982a. On Fluid Reserves and the Production of Superheated Steam from Fractured, Vapor-Dominated Geothermal Reservoirs, Jour. Geophys. Res., in press.

Pruess, K., and Narasimhan, T.N., 1982b. A Practical Method for Modeling Fluid and Heat Flow in Fractured Porous Media, Proc. Sixth SPE-Symposium on Reservoir Simulation (paper SPE-10509), New Orleans, LA.

Pruess, K., 1982. GMINC - A Mesh Generator for Flow Simulations in Fractured Reservoirs, Lawrence Berkeley Laboratory Report LBL-15227, Berkeley, CA.

Warren, J.E., and Root, P.J., 1963. The Behavior of Naturally Fractured Reservoirs, Soc. Pet. Eng. J., 245-255.

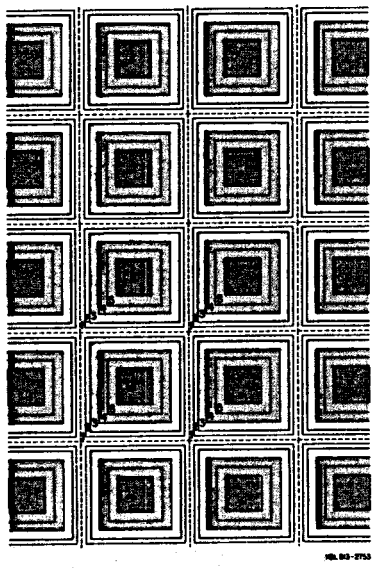

Figure 1. Basic computational mesh for fractured porous medium, shown here for a 2-D case. The fractures enclose matrix blocks of low permeability, which are subdivided into sequences of nested volume elements.

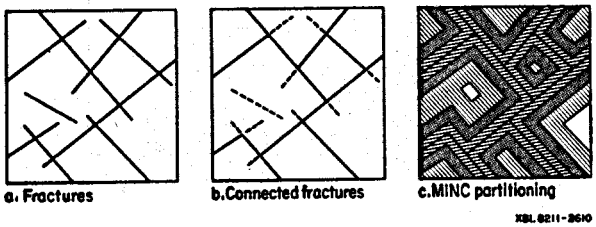

Figure 2. Illustration of the MINC-concept for an arbitrary two-dimensional fracture distribution.

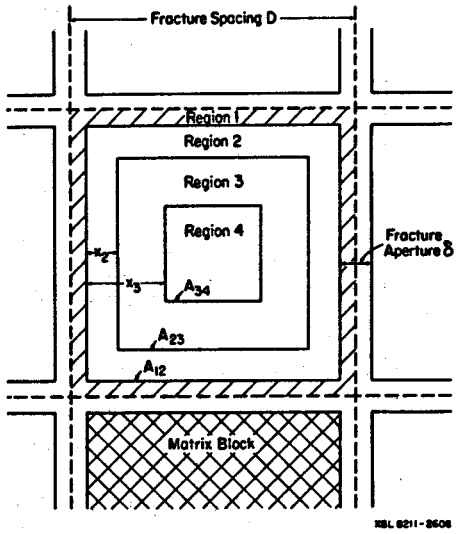

Figure 3. MINC-partitioning for an idealized fracture system.

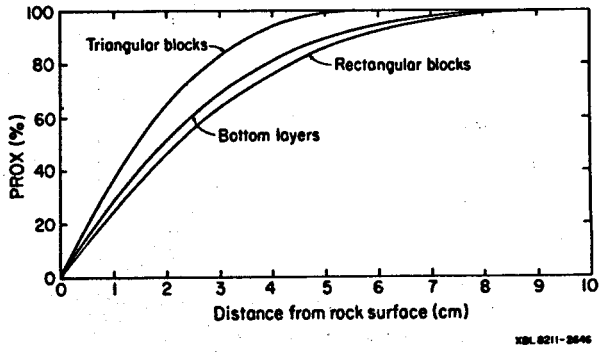

Figure 4. Proximity functions for Stanford large reservoir model.

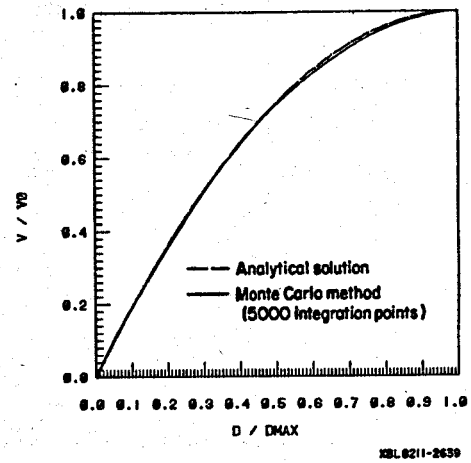

Figure 5. Proximity function for 2-D square matrix blocks (maximum distance from fractures is DMAX = a/2). (a) 5,000 integration points.

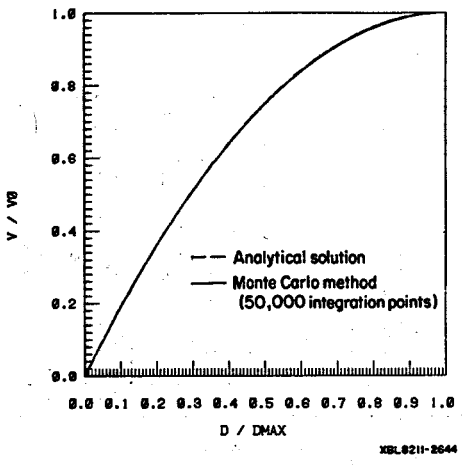

Figure 5. (b) 50,000 integration points.

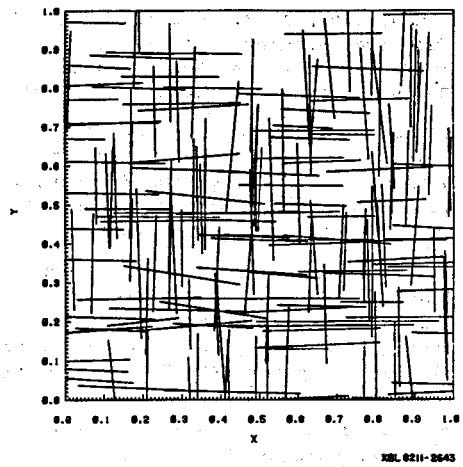

Figure 7. Two-dimensional stochastic fracture distribution.

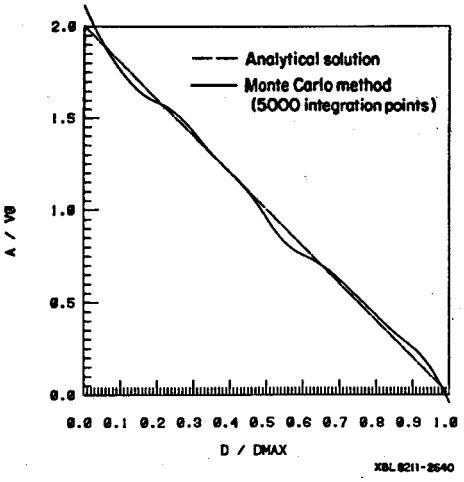

Figure 6. Derivative of proximity function for two-dimensional square matrix blocks (DMAX = 1). (a) 5,000 integration points.

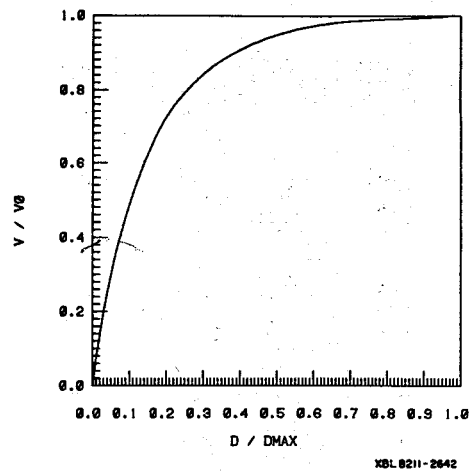

Figure 8. Proximity function for stochastic fracture distribution.

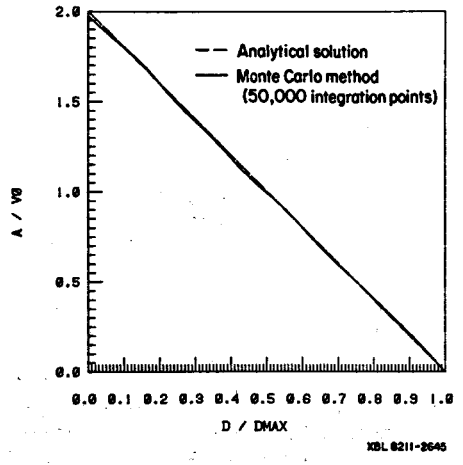

Figure 6. (b) 50,000 integration points.

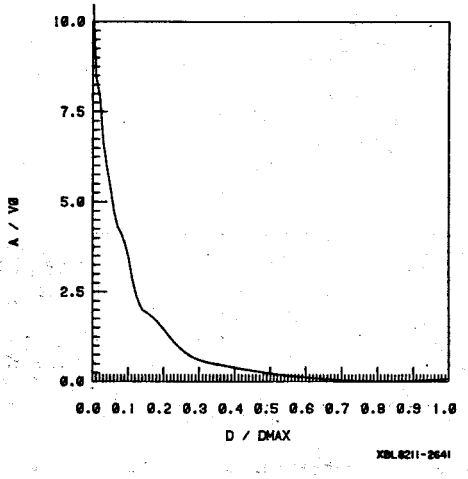

Figure 9. Derivative of proximity function for stochastic fracture distribution.

Proceedings Eighth Workshop Geothermal Reservoir Engineering
Stanford University, Stanford, California, December 1982
SGP-TR-60

QUASI-THREE-DIMENSIONAL MODEL APPLIED TO GEOTHERMAL RESERVOIR SYSTEM WITH HEAT FLOW FROM DEEPER ZONES

Seiichi Hirakawa and Makoto Ichikawa

The University of Tokyo, Faculty of Engineering
Bunkyo-ku, Tokyo 113, JAPAN

ABSTRACT

It is important to grasp the reservoir fluid behavior under operations in the geothermal reservoir development. The authors clarify the calculation procedure of quasi-three-dimensional model and present a flow chart of the model. As example calculations, the developed simulator is applied to simplified geothermal reservoirs which contain heat flow from the deeper zones.

INTRODUCTION

In the geothermal reservoir development, it is important to grasp the reservoir fluid behavior under operations. Generally in mathematic model, fluid behavior in the reservoir is expressed by the three dimensional finite difference equations of mass and energy.[1)-3)] Three dimensional calculations require large data preparation, computing time and storage. Considering these defects of three-dimensional model, Faust and Mercer[4)] presented quasi-three-dimensional model. The equations of the mathematical model are derived by vertical integration of three-dimensional equations. Although the vertical equilibrium in the reservoir is assumed to be achieved in order to obtain the alternative equations, the calculation procedure and the flow chart are not published in their paper. So, the authors clarify the calculation procedure of quasi-three-dimensional model and present a flow chart of the model in this paper. As example calculations, the developed simulator is applied to simplified geothermal reservoirs which contain heat flow from the deeper zones. And, the calculated results on no heat flow case are compared with those of three dimensional calculation.[5)]

THEORY

The behavior of three dimensional two phase flow in a geothermal reservoir is described by conservation equations for mass and energy. Assuming potential and kinetic energy terms and capillary pressure terms are negligible, the equations are written as,[4)]

$$\frac{\partial(\phi\rho)}{\partial t} + \nabla\cdot(\rho_w V_w + \rho_s V_s) - q'_m = 0 \qquad \text{------- (1)}$$

$$\frac{\partial\left[\phi\rho h + (1-\phi)\rho_r h_r\right]}{\partial t} + \nabla\cdot(\rho_w h_w V_w + \rho_s h_s V_s) - \nabla\cdot(K_m \nabla T) - q'_h = 0 \qquad \text{------- (2)}$$

where

$$V_w = -\frac{Kk_{rw}}{\mu_w}(\nabla p_w - \rho_w g \nabla D)$$

$$V_s = -\frac{Kk_{rs}}{\mu_s}(\nabla p_s - \rho_s g \nabla D)$$

$$\rho = S_w\rho_w + S_s\rho_s$$

$$h = (S_w\rho_w h_w + S_s\rho_s h_s)/\rho$$

The equations describing quasi-three-dimensional (areal) two phase flow are obtained by partial integration of Eq.1 and Eq.2 in the vertical direction.

The equations of areal model are written as,

$$b\frac{\partial}{\partial t}(\langle\phi\rho\rangle) - \frac{\partial}{\partial x}\left[b\langle w_x\rangle\left(\frac{\partial}{\partial x}\langle p\rangle - \langle\rho g\rangle\frac{\partial\langle D\rangle}{\partial x}\right)\right] - \frac{\partial}{\partial y}\left[b\langle w_y\rangle\left(\frac{\partial}{\partial y}\langle p\rangle - \langle\rho g\rangle\frac{\partial\langle D\rangle}{\partial y}\right)\right] - b\langle q'_m\rangle - \left(w_x\frac{\partial p}{\partial x}\right)\Big|_{z_1}\frac{\partial z_1}{\partial x} - \left(w_y\frac{\partial p}{\partial y}\right)\Big|_{z_1}\frac{\partial z_1}{\partial y} + \left(w_z\frac{\partial p}{\partial z} + w_{gz}\right)\Big|_{z_1} + \left(w_x\frac{\partial p}{\partial x}\right)\Big|_{z_2}\frac{\partial z_2}{\partial x} + \left(w_y\frac{\partial p}{\partial y}\right)\Big|_{z_2}\frac{\partial z_2}{\partial y} - \left(w_z\frac{\partial p}{\partial z} + w_{gz}\right)\Big|_{z_2} = 0 \qquad \text{------- (3)}$$

$$b\frac{\partial}{\partial t}\left[(<\phi\rho h>+<\rho_r h_r>-<\phi\rho_r h_r>)\right]$$

$$-\frac{\partial}{\partial x}\left[b<w_{hx}>(\frac{\partial}{\partial x}<p> - <\rho g>\frac{\partial <D>}{\partial x})\right]$$

$$-\frac{\partial}{\partial y}\left[b<w_{hy}>(\frac{\partial}{\partial y}<p> - <\rho g>\frac{\partial <D>}{\partial y})\right]$$

$$-\frac{\partial}{\partial x}\left[b<w_{cp}>(\frac{\partial}{\partial x}<p> - <\rho g>\frac{\partial <D>}{\partial x})\right]$$

$$-\frac{\partial}{\partial y}\left[b<w_{cp}>(\frac{\partial}{\partial y}<p> - <\rho g>\frac{\partial <D>}{\partial y})\right]$$

$$-\frac{\partial}{\partial x}(b<w_{ch}>\frac{\partial}{\partial x}<h>) - \frac{\partial}{\partial y}(b<w_{ch}>\frac{\partial}{\partial y}<h>)$$

$$- b<q'_h> - (w_{hx}\frac{\partial p}{\partial x})\Big|_{z_1}\frac{\partial z_1}{\partial x}$$

$$- (w_{hy}\frac{\partial p}{\partial y})\Big|_{z_1}\frac{\partial z_1}{\partial y} + (w_{hz}\frac{\partial p}{\partial z} + w_{hgz})\Big|_{z_1}$$

$$+ (w_{hx}\frac{\partial p}{\partial x})\Big|_{z_2}\frac{\partial z_2}{\partial x} + (w_{hy}\frac{\partial p}{\partial y})\Big|_{z_2}\frac{\partial z_2}{\partial y}$$

$$- (w_{hz}\frac{\partial p}{\partial z} + w_{hgz})\Big|_{z_2}$$

$$- (w_{cp}\frac{\partial p}{\partial x} + w_{ch}\frac{\partial h}{\partial x})\Big|_{z_1}\frac{\partial z_1}{\partial x}$$

$$- (w_{cp}\frac{\partial p}{\partial y} + w_{ch}\frac{\partial h}{\partial y})\Big|_{z_1}\frac{\partial z_1}{\partial y}$$

$$+ (w_{cp}\frac{\partial p}{\partial z} + w_{ch}\frac{\partial h}{\partial z})\Big|_{z_1}$$

$$+ (w_{cp}\frac{\partial p}{\partial x} + w_{ch}\frac{\partial h}{\partial x})\Big|_{z_2}\frac{\partial z_2}{\partial x}$$

$$- (w_{cp}\frac{\partial p}{\partial y} + w_{ch}\frac{\partial h}{\partial y})\Big|_{z_2}\frac{\partial z_2}{\partial y}$$

$$- (w_{cp}\frac{\partial p}{\partial z} + w_{ch}\frac{\partial h}{\partial z})\Big|_{z_2} = 0 \qquad \text{-------- (4)}$$

where

$$w_x = \frac{K_x k_{rw}\rho_w}{\mu_w} + \frac{K_x k_{rs}\rho_s}{\mu_s}$$

$$w_{hx} = \frac{K_x k_{rw}\rho_w h_w}{\mu_w} + \frac{K_x k_{rs}\rho_s h_s}{\mu_s}$$

$$w_{cp} = K_m\left(\frac{\partial T}{\partial p}\right)_h$$

$$w_{ch} = K_m\left(\frac{\partial T}{\partial h}\right)_p$$

$$w_{gz} = \frac{K_z k_{rw}\rho_w^2 g}{\mu_w} + \frac{K_z k_{rs}\rho_s^2 g}{\mu_s}$$

$$w_{hgz} = \frac{K_z k_{rw}\rho_w^2 g h_w}{\mu_w} + \frac{K_z k_{rs}\rho_s^2 g h_s}{\mu_s}$$

In the above integration, Faust and Mercer's technique[4] detailed in Appendix is used.

BOUNDARY CONDITIONS

Boundary conditions are required for pressure and enthalpy. For this simulater, no flow boundary condition is applied except for top and bottom boundaries. Convective and conductive fluxes at the reservoir top and bottom are considered in Eq.3 and Eq.4. These terms include the derivatives $\partial p/\partial z$ and $\partial h/\partial z$, which are evaluated by pressure and enthalpy gradients in each grid. In addition to this, as a source term, heat flow rate q_b is specified across the reservoir bottom. Eq.4 is rewritten as,

$$b\frac{\partial}{\partial t}\left[(<\phi\rho h>+<\rho_r h_r>-<\phi\rho_r h_r>)\right]$$

$$-\frac{\partial}{\partial x}\left[b<w_{hx}>(\frac{\partial}{\partial x}<p> - <\rho g>\frac{\partial <D>}{\partial x})\right]$$

$$-\frac{\partial}{\partial y}\left[b<w_{hy}>(\frac{\partial}{\partial y}<p> - <\rho g>\frac{\partial <D>}{\partial y})\right]$$

$$-\frac{\partial}{\partial x}\left[b<w_{cp}>(\frac{\partial}{\partial x}<p> - <\rho g>\frac{\partial <D>}{\partial x})\right]$$

$$-\frac{\partial}{\partial y}\left[b<w_{cp}>(\frac{\partial}{\partial y}<p> - <\rho g>\frac{\partial <D>}{\partial y})\right]$$

$$-\frac{\partial}{\partial x}(b<w_{ch}>\frac{\partial}{\partial x}<h>) - \frac{\partial}{\partial y}(b<w_{ch}>\frac{\partial}{\partial y}<h>)$$

$$- b<q_i> - q_b - (w_{hx}\frac{\partial p}{\partial x})\Big|_{z_1}\frac{\partial z_1}{\partial x}$$

$$- (w_{hy}\frac{\partial p}{\partial y})\Big|_{z_1}\frac{\partial z_1}{\partial y} + (w_{hz}\frac{\partial p}{\partial z} + w_{hgz})\Big|_{z_1}$$

$$+ (w_{hx}\frac{\partial p}{\partial x})\Big|_{z_2}\frac{\partial z_2}{\partial x} + (w_{hy}\frac{\partial p}{\partial y})\Big|_{z_2}\frac{\partial z_2}{\partial y}$$

$$- (w_{hz}\frac{\partial p}{\partial z} + w_{hgz})\Big|_{z_2}$$

$$- (w_{cp}\frac{\partial p}{\partial x} + w_{ch}\frac{\partial h}{\partial x})\Big|_{z_1}\frac{\partial z_1}{\partial x}$$

$$- \left(w_{cp}\frac{\partial p}{\partial y} + w_{ch}\frac{\partial h}{\partial y}\right)\Big|_{z_1}\frac{\partial z_1}{\partial y}$$

$$+ \left(w_{cp}\frac{\partial p}{\partial z} + w_{ch}\frac{\partial h}{\partial z}\right)\Big|_{z_1}$$

$$+ \left(w_{cp}\frac{\partial p}{\partial x} + w_{ch}\frac{\partial h}{\partial x}\right)\Big|_{z_2}\frac{\partial z_2}{\partial x}$$

$$- \left(w_{cp}\frac{\partial p}{\partial y} + w_{ch}\frac{\partial h}{\partial y}\right)\Big|_{z_2}\frac{\partial z_2}{\partial y}$$

$$- \left(w_{cp}\frac{\partial p}{\partial z} + w_{ch}\frac{\partial h}{\partial z}\right)\Big|_{z_2} = 0 \qquad \text{-------- (5)}$$

In Eqs.3 and 5, independent variables are pressure and enthalpy of the steam-water mixture. Saturated values of h_w, h_s, ρ_w, ρ_s are calculated directly from steam tables as functions of pressure and enthalpy. The density of the steam-water mixture and water saturation can be treated as functions of pressure and enthalpy. Several additional assumption are necessary to describe behavior of geothermal fluid. First, it is assumed that thermal equilibrium exist among all phases. With this assumption, temperature is treated as a function of pressure and enthalpy. The other assumptions are as follows. Viscosities are functions of pressure and temperature given from steam tables. Porosity is a function[4] of pressure, given by $\phi = \phi_i + \beta(p - p_i)$. Relative permeabilities are linear functions[6] of water saturation, given by $k_{rw} = (S_w - S_{wr})/(1.0 - S_{wr})$.

CALCULATION PROCEDURE

Eqs.3 and 5 for the areal model are expanded in finite difference formulas, and solved by the Newton-Raphson iteration. Using a direct method,[6),7)] the equations are solved for pressure and enthalpy at each iteration.

Flow chart of calculation procedure is shown in Fig.1. The followings are detail of this procedure.

Step 1. Read parameters required for the difference calculation (time step, block number, block size and convergence criterion) and reservoir data (permeability, elevations on the base and top of the reservoir, thermal conductivity, specific heat of reservoir rock and specific gravity of reservoir rock).

Step 2. Read initial condition of reservoir for each block (pressure, enthalpy, production rate and injection rate).

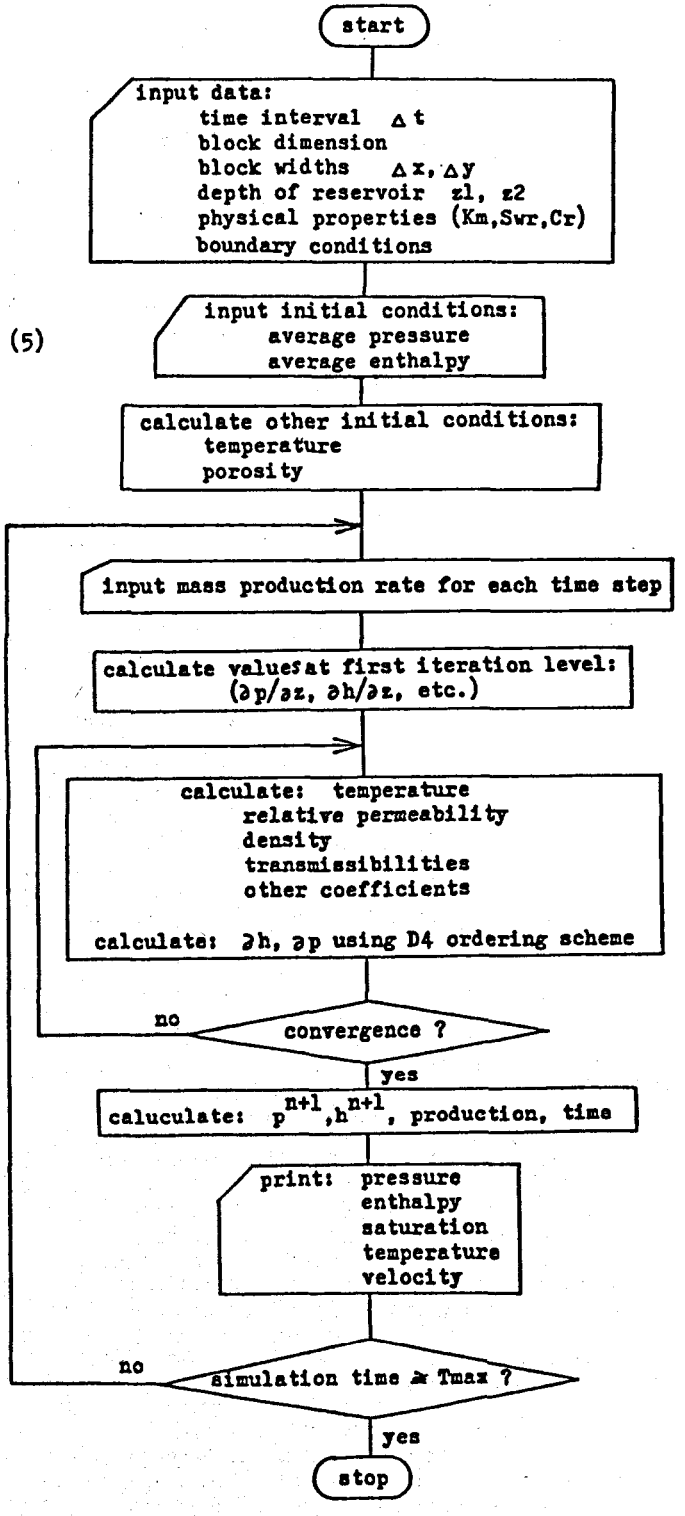

Fig. 1 Flow chart of quasi-three-dimensional model

Step 3. Calculate the other initial conditions[8),9)] (temperature and porosity).
Step 4. As precondition of iteration, calculate variables required for the first iteration level.
Step 5. Calculate variables (relative permeabilities, fluid densities, transmissibilities and so on) required for solving Eqs.3 and 5, and obtain δp and δh using D4 ordering.[6)]
Step 6. Check convergence for pressure and enthalpy.
Step 7. Calculate values of pressure and enthalpy.
Step 8. Print calculated values (pressure, enthalpy, saturation, temperature and velocity).
Step 9. Check computing period.

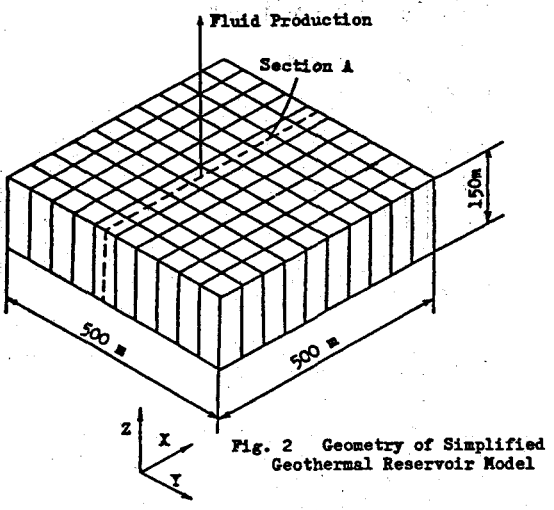

Fig. 2 Geometry of Simplified Geothermal Reservoir Model

Table 1 Initial Condition for Example Calculation

Length of reservoir, (cm)	50000
Width of reservoir, (cm)	50000
Thickness of reservoir, (cm)	15000
Grid size: Δx, Δy, (cm)	5000
Porosity	0.380
Horizontal permeability, (darcy)	0.100
Vertical permeability, (darcy)	0.0100
Thermal conductivity, (cal/cm-sec-°C)	0.450×10^{-2}
Specific heat of reservoir rock, (cal/g-°C)	0.170
Specific gravity of reservoir rock, ($g\text{-}cm^{-3}$)	2.65
Formation compressibility, (atm^{-1})	1.67×10^{-5}
Vertical averaged pressure, (atm)	40.0
Vertical averaged enthalpy, (cal/g)	260
Vertical averaged temperature, (°C)	248
Residual water saturation	0.200

SAMPLE CALCULATION

This sample calculation illustrate the application of the quasi-three-dimensional model to a simplified geothermal reservoir. The grid for the reservoir model is shown in Fig. 2. The quasi-three-dimensional calculation is performed over 10x10 grids. The reservoir fluid is assumed to be pure water and to be initially in the two phase zone. Parameters and initial conditions used in this sample calculation are given in Table 1. For this calculation, location of assumed production well is the grid point (5,5). Initial production rate is 0.683×10^{4} g/sec. Time step is 1.44×10^{5}s. After comfirming the stability and the convergence of the model, the simulater is applied to the geothermal systems. Assuming heat flow of 4.0×10^{-5} cal/sec-cm^2 and no mass flow from bottom of the reservoir, simulations of the thermal conduction and dispersion are carried out. Fig.3 shows the assumed heat flow is not large enough to maintain the isoenthalpy production.

Shown in Figs.4 and 5, the calculated results in the author's another paper [10)] are

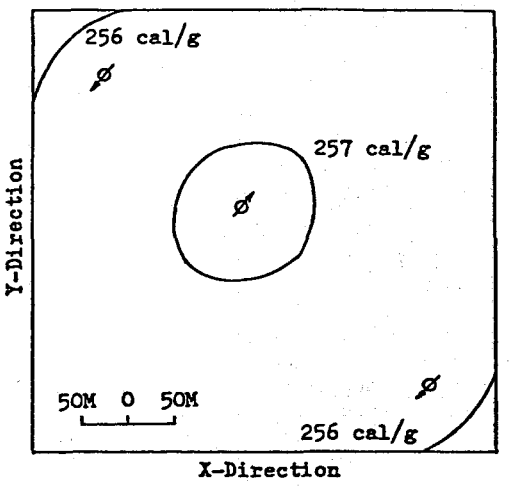

Fig. 3 Depth-averaged enthalpy map for a two-phase geothermal reservoir after 300days. This geothermal system involves heat flow (4.0×10^{-5} cal/sec·cm^2) from exterior of the reservoir.

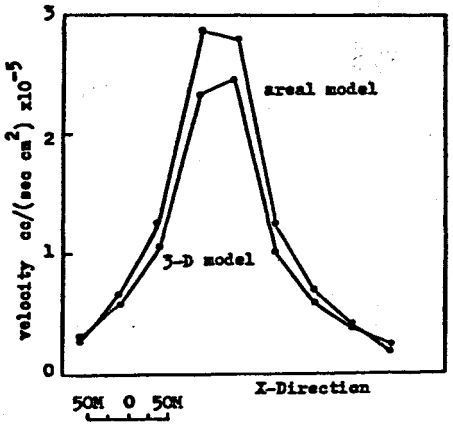

Fig. 4 Depth-averaged fluid velocity along section A (Fig.2) after 100days areal and 3-D model.

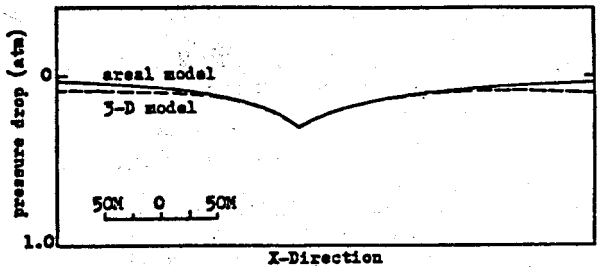

Fig. 5 Depth averaged pressure drop along section A (Fig.2) after 100days for areal and 3-D model.

compared with those of three dimensional calculation in case of no heat flow at the boundaries. HITAC M200-H was used for this computation. As to computing time, quasi-three-dimensional calculation required 1.57s per iteration step and three-dimensional calculation required 10.38s per iteration step. This indicates that reduction of computing time is performed by the quasi-three-dimensional model. These values mainly depend on the grid number, so that, if the grid number become increase, the reduction of computing time will become larger. If the convergence conditions are equal, whole computing time will be more small for the quasi-three-dimensional model, which needs less iteration steps because of its smaller grid number.

NOMENCLATURE

b = reservoir thickness, cm
C_r = specific heat of reservoir rock, cal/g-°C
D = depth, cm
g = gravitational acceleration, cm/sec^2
h = specific enthalpy, cal/g
K = absolute permeability, darcy
k_{rl} = relative permeability of the phase 1, fraction
K_m = reservoir thermal conductivity, cal/cm-sec-°C
p = reservoir pressure, atm
p_i = initial reservoir pressure, atm
q_b = heat flow rate across boundary, cal/sec-cm^2
q'_h = heat source term, cal/sec-cm^3
q'_m = mass source term, g/sec-cm^3
S = saturation, fraction
S_{wr} = residual water saturation, fraction
T = reservoir temperature, °C
T_{max} = period of simulation, sec
t = time, sec
Δt = time step size, sec
v = averaged phase velocity, cm/sec
z_1 = elevation of the bottom of the reservoir, cm
z_2 = elevation of the top of the reservoir, cm
β = formation compressibility, atm^{-1}
μ = viscosity, cp
ϕ = porosity, fraction
ϕ_i = initial porosity, fraction
ρ = density, g/cm^3

Subscripts

h = enthalpy, m = mass,
n = iteration level, r = reservoir,
s = steam, w = water,
x,y,z = directions in the Cartesian co-ordinate system

Operators

∇ = divergence operator

ACKNOWLEDGEMENT

This study has been carried out by a Grant-in-Aid for Particular Project Research on Energy from the Ministry of Education, Science and Culture of Japan.

REFERENCE

1) Whiting, R. L. and Ramey, H. J., Jr. (1969) Application of Material and Energy Balances to Geothermal Steam Production, Journal of Petroleum Technology, 21, 7, 893-900.
2) van Poollen, H. K., Bixel, H. C. and Jargon, J. R. (1971) Reservoir Modeling, The Petroleum Publishing Company.
3) Thomas, L. K. and Pierson, R. G. (1978) Three Dimensional Geothermal Reservoir Simulation, Society of Petroleum Engineers Journal, 18, 2, 151-161.
4) Faust, C. R. and Mercer, J. W. (1979) Mathematical Models for Liquid and Vapor Dominated Hydrothermal Systems, Water Resources Research, 15, 1, 23-46.
5) Hirakawa, S., Fujinaga, Y. and Miyoshi,M.: Three-Dimensional Model and Its Sample Calculation for the Simulation of Geothermal Reservoirs, J. Geothermal Research Society of Japan, (under contribution).

6) Aziz, K. and Settari, A. (1979) Petroleum Reservoir Simulation, Applied Science Publishers Ltd.
7) Crichlow, H. B. (1977) Modern Reservoir Engineering-A Simulation Approach, Prentice-Hall, Inc.
8) Craft, B. C. and Hawkins, M. F. (1959) Applied Petroleum Reservoir Engineering, Prentice-Hall, Inc.
9) Kruger, P. and Otte, C. (1973) Geothermal Energy, Stanford University Press.
10) Hirakawa, S. and Ichikawa: Quasi-Three-Dimensional Simulation Study of Simplified Geothermal Reservoir, J. Geothermal Research Society of Japan, (under contribution).

APPENDIX

Derivation of quasi-three-dimensional equation by Faust and Mercer's technique.
In the equations of the areal model, parameters are expressed as depth averaged value given by

$$\langle\psi\rangle = \frac{1}{b}\int_{z_1}^{z_2}\psi\,dz$$

where z_1, z_2 and b are function of x-y space and time. For the following equation should hold.

$$\int_{z_1}^{z_2}\frac{\partial\psi}{\partial x}\,dz = \frac{\partial}{\partial x}\int_{z_1}^{z_2}\psi\,dz$$

$$+\psi(x, y, z_1, t)\frac{\partial z_1}{\partial x}$$

$$-\psi(x, y, z_2, t)\frac{\partial z_2}{\partial x}$$

The diviation of ψ from $\langle\psi\rangle$ is defined as

$$\hat{\psi} = \psi - \langle\psi\rangle$$

The above two equations are applied in the integration of Eq.1 and Eq.2. In the areal equations, the deviation terms higher than second order can be omitted, and the discontinuities in the quantities on the water-steam interface are negligible. With those assumptions and assuming gravity segregation, the equations of quasi-three-dimensional are derived.

Proceedings Eighth Workshop Geothermal Reservoir Engineering
Stanford University, Stanford, California, December 1982
SGP-TR-60

RESERVOIR SIMULATION STUDIES ON THE CERRO PRIETO GEOTHERMAL FIELD: PRELIMINARY RESULTS.

M. Castaneda*, A. Abril**, V. Arellano*, R. Marquez**

* Instituto de Investigaciones Electricas
** Coordinadora Ejecutiva de Cerro Prieto
Mexicali B.C. Mexico

ABSTRACT

A reservoir engineering and simulation study is being carried out on the Cerro Prieto geothermal field. A preliminary material balance has been applied to the old part of this field. A single block with constant properties in the horizontal direction was used for this preliminary material balance. The vertical block column was subdivided in several levels in order to take into account the known lithologic column. From existing pressure and enthalpy field histories, a single phase (liquid) reservoir assumption was selected. Under this assumption, a lateral radial recharge was considered in obtaining the pressure and enthalpy history match. These preliminary results indicate that another type of recharge is probably taking place in this part of the field, rather than lateral radial.

INTRODUCTION. The Cerro Prieto geothermal field is a liquid dominated geothermal system located 30 Km south of Mexicali B.C., Mexico. This field is situated at the southern end of the Salton-Mexicali trough, which includes other geothermal anomalies as Heber and East Mesa. In april 1973, Comision Federal de Electricidad (CFE) started operating a geothermal power plant which present installed capacity is 150 MW. This amount is expected to increase as further field development continues. Such activity will require more trainned people on the reservoir engineering area. That concern nas led to a joint project where CFE, Instituto de Investigaciones Electricas (IIE) and INTERCOMP of Houston Tx are presently involved in performing reservoir engineering and simulation studies on the Cerro Prieto geothermal field.

The project objectives are first, the gathering and analysis of field data. Such data would be used in performing a preliminary material balance on this field with a simplified geological model. Some general understanding of the behavior of this field under explotation period would be obtained with this simplified model. Then, a coarse grid model would be elaborated to furtner investigate such field behavior in a more detailed way. This study presents the results obtained from that preliminary material balance.

GEOLOGICAL MODEL. The preliminary material balance was applied to the field area denominated Cerro Prieto I (see figure 1). This represents an area of 2.045 Km^2. This was done mainly because this area has been under production since 1973 and consequently, most field data comes from here. Only after 1979, wells from other field areas started to produce.

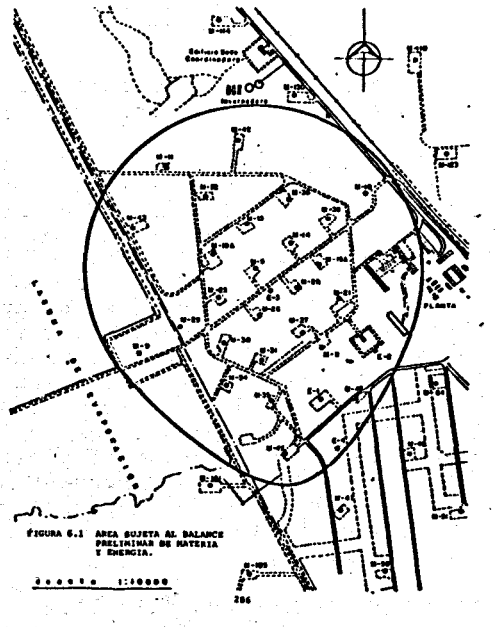

Figure 1. Area of study (Cerro Prieto I, units 1 and 2).

The geological structure in this part of the field was presented by Abril and No-

ble[3] in 1978. The formation is of sedimentary type with alternating shale and sandstone layers, resting on a highly fracture granitic basement. The litholo gic column was subdivided into three u- nits: the upper unit (unit A) consist-- ing of unconsolidated sediments, the middle one (unit B) consisting of conso lidated material and the lower unit (u- nit C) of granodioritic and metamorphic rocks. Unit A is considered to act as a cap rock while unit C constitutes an im permeable bed rock. Unit B contains in- terval L_2 (rock with high content of carbonate cement) and the reservoirs A and B (considered to be the main geo- thermal reservoirs). Figure 2 presents a squematic description of this litholo gic column.

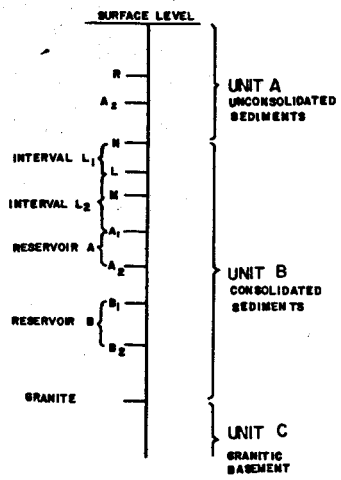

Figure 2. Lithologic column for Cerro Prieto I area (from Abril and Noble).

Some facts have to be pointed out. First there has been no agreement among seve- ral authors on the existance of a uni- form cap rock. Grant[8] et al., (1981), based on geochemical data mantained that the whole system was open on the top and the sides (ie., there was no such cap rock). That idea was suggested earlier by Mañon[11] et al. (1978). Later, Grant[9] et al. (1982), based on a simplified chloride balance on some wells of that area, stated that the producing aquifer of Cerro Prieto I could be best consider ed as a leaky aquifer. They suggested that one quarter to one half of its re- charge derived from cooler fluids coming from above unit B.

On the other hand, Prian[12] (1981), based on a significant change of the drilling rate in going from unconsolidated to con solidated sediments, stated the existan- ce of such cap rock.

Second, the question about the intercon- nection between reservoir A and B in the Cerro Prieto I area has not been solved. A shale layer 150 m thick be - tween these two reservoirs reported by Prian[12] (1981), could be indicative of hydraulic isolation. In addition, che- mical analysis of brines from wells dri lled deeper in the same Cerro Prieto I area (reaching reservoir B) showed that they are different from those coming from reservoir A wells. No appropiated interference tests have been carried out to answer the question of interconnection.

Based on these facts, our simplified geological model included mainly the in terval L_2 and reservoir A because, as explained, all Cerro Prieto I wells are completed in one or both intervals and consequently, all reservoir data (befo- re 1979), such as production and well test data, come from these zones. A small shale layer was interposed be - tween both intervals as suggested by A- bril and Noble[1] (1978). A set of iso- pach maps were developed for both inter vals (Castañeda[6] et al., 1982).

Porosity values for both intervals were determined by means of geophysical well log analysis (Castañeda[5] et al., 1981). These data were modified according to:

$$\Phi_g = \frac{h_n}{h_g} \Phi_n$$

where:

Φ_g = modified porosity value

h_g = gross thickness

Φ_n = average porosity/interval

h_n = net thickness

With this modified porosity value the reservoir gross thickness can be used for both reservoir mass/heat content and transmissibility calculations. The resulting porosity values were consis- tent for both intervals. Thus, an arith metic average was used to obtain a re- presentative porosity value for each in terval.

A permeability value was obtained from analysis of several two-rate tests con- ducted in wells of the Cerro Prieto I a rea (Castañeda[6] et al., 1982). An avera ge value of 30 md was obtained from that analysis. Because all wells tested were completed in both intervals, the same permeability value was assigned to L_2 and reservoir A intervals. We should point out that permeability values as high as 100 md have been reported and a ssigned to this area by other authors

ducing from interval L_2 and reservoir A only after 1976.

The following stabilized shut-in temperature profile of well M-5 was used as a representative initial temperature distribution for these intervals:

Depth (m)	Temp. (°C)
950	246
1000	267
1150	288
1200	298
1335	312

These initial conditions (pressure, temperature and enthalpy) neglect any changes occured before 1973. Although some wells were completed and tested in the late 60's, full production started in 1973.

SIMULATION RUNS. Based on the isobaric and isoenthalpic map configurations, a radial system was used in the simulation work, resulting in a circular reservoir with an equivalent area of 2.045 Km^2 and a radius of 807 m. The vertical representation was considered as follows: L_2 interval was subdivided into two homogeneous layers (layers 1 and 2) to take into account partial completion of some wells in this interval. A shale layer (layer 3) was interposed between interval L_2 and reservoir A as explained before. Reservoir A was represented by one layer (layer 4). A well completed from layer 2 to 4 was placed at the center of this circular reservoir. A production representing the summation of the production of all wells included in the area of study was assigned to this well.

INTERCOMP's geothermal reservoir simulator (GEOTHERM) was used in this study. The finite difference formulation of this simulator is explained in reference 7.

The prime objective was to match the observed field pressure and enthalpy history under two assumptions: first, considering no mass/heat recharge, i e., assuming a closed boundary reservoir, and second, allowing fluid and heat recharge. Only the most representative simulation runs are presented here for each case.

Figure 4 also presents the simulated pressure and enthalpy histories when no recharge is considered. As can be seen, reservoir pressure can not be sustained in this case. Reservoir enthalpy increases as the reservoir falls into two phase conditions. These results do not reflect the observed field pressure and enthalpy histories. Although not shown here, a sensitivity study was made with a reasonable change in values of parameters affecting the above behavior (such as porosity, thickness) and the same conclusion was obtained.

In considering recharge, is necessary to make a distinction between the terms reservoir and aquifer in a geothermal system. A good representation in this case is that the portion of the geothermal system outside of the circular reservoir model is an "aquifer", although the total system is actually an aquifer and the circular reservoir model simply encloses a region of anomalous temperature. Two factors are important when recharge from an aquifer is considered: the amount of recharge and its temperature. In a lateral radial recharge scenario, this required placing outer elements to the circular model.

The pressure support supplied by the aquifer to the reservoir was calculated according to the Carter and Tracy's method. In this case, an infinite single phase (liquid) aquifer was considered. Aquifer porosity was assumed equal to reservoir porosity. The aquifer permeability-thickness product (kh_{aq}) was varied in proportion to reservoir permeability-thickness value (kh_{res}). Figure 6 presents the obtained pressure and enthalpy histories for different kh_{aq}/kh_{res} values, when aquifer temperature was considered to be the same as reservoir temperature. Although a pressure match is obtained with a ratio of 100, the enthalpy could not be matched. Lower recharge temperature is needed to obtain a decrease later with time in the simulated reservoir enthalpy as observed for field reservoir enthalpy. Figure 6 also presents the simulated pressure and enthalpy histories when lower recharge temperature values were used. The best match was obtained with a kh_{aq}/kh_{res} ratio of 100 and a recharge temperature of 235 °C. This rather high ratio was reduced to 25 when reservoir permeability was increased to 100 md, as suggested by other authors. Figure 7 presents these results. If we assume equal aquifer and reservoir thickness, this ratio yields an aquifer permeability value of 2500 md. Although no aquifer permeability data exists to compare this result, it is generally believed that zones surrounding Cerro Prieto I area, are zones of higher permeability.

At this point, we have only considered lateral radial recharge into this model An additional source of fluid could be obtained if recharge from permeable la-

(Abril[2] et al., 1981 and Lippmann[10] et al., 1978). Figure 3 presents a summary of values of thickness, porosity and permeability for each interval as well as other parameter values used in the simulation process.

	interval M_2	shale layer	reserv. A
porosity	0.18	0.04	0.13
k_h (md)	30.0	3.0	30.0
k_v (md)	3.0	0.3	3.0
thermal cond. (BTU/ft-day °F)	35.0	35.0	35.0
rock heat cap. (BTU/ft^3-°F)	39.5	39.5	39.5
rock comp. (psi^{-1})	$4x10^{-6}$	$4x10^{-6}$	$4x10^{-6}$
thickness (m)	252.0	20.0	137.0
top (m)	944.0	1196.0	1216.0
bottom (m)	1196.0	1216.0	1353.0

Figure 3. Formation parameter values used in the simulation work.

FIELD HISTORY. Average reservoir pressure and enthalpy histories for Cerro Prieto I zone were obtained from a set of isobaric and isoenthalpic maps presented in reference 6. The isobaric maps were generated with the same information presented by Bermejo[3] et al., 1978 for years 1973, 1975, 1977 and 1979, but the map configurations were changed to what it was believed to be a better field pressure distribution. Figure 4 presents pressure and enthalpy histories, respectively. Both set of values are representative of a 1200 m depth zone.

Figure 5 compares the average pressure and enthalpy history values to that of the steam-water saturation curve. As can be observed, this area has remained single phase (liquid) during the production period 1973-1979. However, these histories represent overall averaged values for this zone and do not exclude the possibility of "local boiling zones". Grant[8] et al.,1981, have shown that, although local near-well boiling is a common phenomenon in Cerro Prieto I (due to local pressure decrease and intergranular flow to wells), a more extensive steam zone has not been formed in this part of the field, under natural or exploitation conditions.

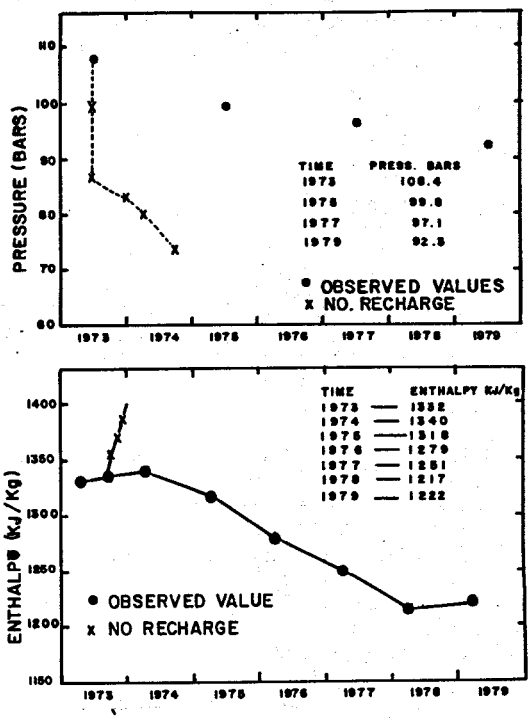

Figure 4. Observed and simulated field history: no recharge case.

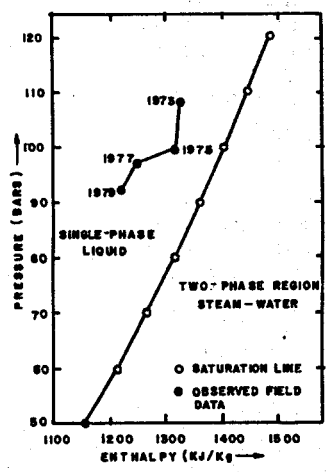

Figure 5. Comparision of average field pressure and enthalpy values with steam-water saturation curve values.

Production history of all wells contained in the area of study was presented in reference 6. The production from well M-9 was not taken into account. This well was producing from above unit B. In addition, well M-29 started pro-

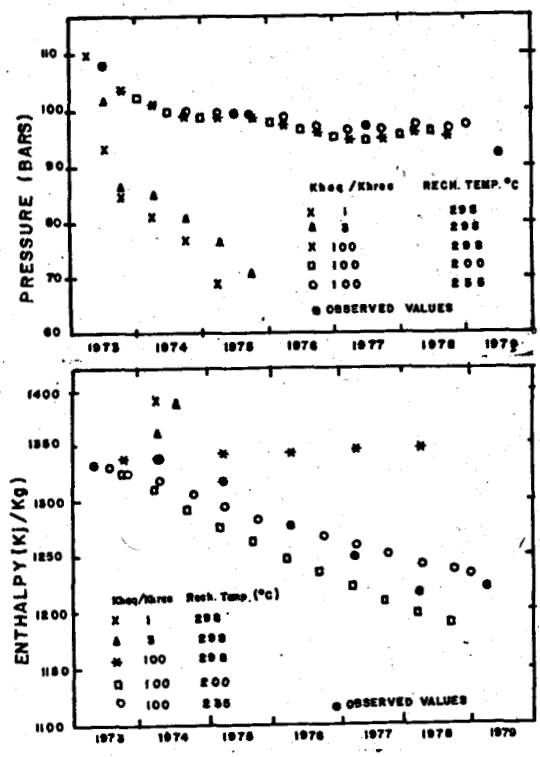

Figure 6. Simulated pressure and enthalpy histories when recharge is considered.

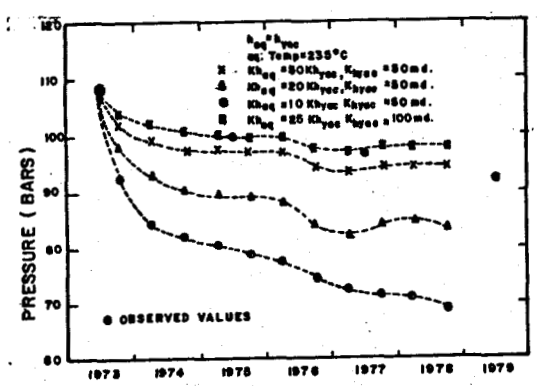

Figure 7. Sensitivity to reservoir permeability.

yers above unit B is considered (i e., assuming that no perfect cap rock exists). This possibility could further reduce the kh_{aq}/kh_{res} ratio. Actually, no field data from that part of the geothermal system (formation properties pressures, etc) nave been generated but the use of a reasonable value for such parameters would be of help in testing this later possibility.

CONCLUSIONS.

1.- Average pressure and enthalpy histories were obtained for the Cerro Prieto I area for 1973-1979 production period.

2.- From comparision of these histories with the steam-water saturation curve, it was concluded that this part of the field was initially in single-phase conditions and it has remained in that way during explotation period 1973-1979.

3.- A strong recharge (kh_{aq}/kh_{res} =25) was needed to match the observed field pressure. Recharge water with lower temperature (235 °C) than existing reservoir temperature was needed to match the observed field entnalpy history.

4.- The above ratio could be further reduce in order to have a physically more realistic aquifer description. This could be done if additional recharge from permeable layers above unit B strtum is considered.

ACKNOWLEDGMENTS.

The authors would like to thank Coordinadora Ejecutiva de Cerro Prieto and also Instituto de Investigaciones Electricas for the opportunity given to them in presenting this paper.

REFERENCES.

1.- Abril, A.G. and Noble, J.E. (1978): "Geophysical Well-Log Correlations Along Various Cross-sections Of The Cerro Prieto Geothermal Field", Proceedings of the First Symposium On The Cerro Prieto Geothermal Field, Baja California, Mexico, Sept. 20-22, San Diego Ca., pp41-46.

2.- Abril, A.G. and Vargas, C.G. (1981) "Results Of The Latest Transient Well Pressure Tests At Cerro Prieto", Procc. Of The Third Symposium On The Cerro Prieto Geothermal Field, Baja CAlifornia, Mexico, March 24-26, San Francisco Ca. pp 504-509.

3.- Bermejo, F.J., Cortez, C.A., Aragon, A.A. (1978):"Physical And Thermodinamic Changes Observed In the Cerro Prieto Geothermal Reservoir", Proccidings Of The First Symposium On THe Cerro Prieto Geothermal Field, Baja CAlifornia, Mexico, Sept. 20-22, San Diego CA., pp 300-329.

4.- Carter, R.D., and Tracy, G.W.(1960) "An Improved Method For Calculating Water Influx", J. Pet. Tech., Dec., pp 58-60.

5.- Castañeda,M., Abril, A.G., Arellano V., McCoy, R.L. (1981):"Well log Analysis Applied To The Cerro Prieto Geothermal Field", Procc. Of The 7th Workshop On Geothermal Reservoir Engineering, Stanford University, Stanford Ca., Dec. 15-17.

6.- Castañeda, M., Abril,A.G., Arellano V., Marquez, R.M., Sanchez, J.R. (1982):"Entrenamiento Para El Desarrollo Sistematico De La Ingenieria De Yacimientos En El Campo Geotermico De Cerro Prieto", Instituto de Investigaciones Electricas, Internal Report IIE/FE-G30/1678/1, Sept.

7.- Coats, K.H., George, W.D., Chu, Chieh and Marcum, B.E. (1974):" Three Dimensional Simulation Of Steam Flooding", Trans. AIME, 257, 573.

8.- Grant, M.A., Truesdall, A.H., Mañon A.M. (1981):"Production Induced Boiling And Cold Water Entry In The Cerro Prieto Geothermal Reservoir Indicated By Chemical And Physical Measurements",Procc. Of The Third Symposium on The Cerro Prieto Geothermal Field, Baja California, Mexico, March 24-26, San Francisco Ca., pp 221-237.

9.- Grant, M.A., O'sullivan, M.J.(1982) "The Old Field At Cerro Prieto Considered As A Leaky Aquifer", Procc. Of The Fourth Symposium On The Cerro Prieto Geothermal Field, Baja California, Mexico, August 10-12, Guadalajara Jal., Mexico, pp123-132

10.-Lippmann, M.J., Bodvarsson, G.S., et al. (1978):"Preliminary simulation Studies Related o The Cerro Prieto Field", Procc. Of The First Symposium On THe Cerro Prieto Geo-Thermal Field, Baja California, Mexico,Sept. 20-22, San Diego CA. pp 375-383.

11.-Mañon, A.M., Sanchez, A.A., Esquer, I.P., et al. (1978):"Preliminary Geochemical Model Of The Cerro Prieto Geothermal Field", Procc. Of The First Symposium On THe Cerro Prieto Geothermal Field, Baja California, Mexico, Sept. 20-22, San Diego Ca., pp 83-90.

12.-Prian, R.C. (1981):"Drilling rate for the Cerro Prieto Stratigraphic Sequence", Procc. Of The Third Symposium On THe Cerro Prieto Geothermal Field, Baja California, Mexico, March 24-26, San Francisco Ca., pp 77-85.

Proceedings Eighth Workshop Geothermal Reservoir Engineering
Stanford University, Stanford, CAlifornia, December 1982
SGP-TR-60

THE STIMULATION OF A HOT DRY ROCK GEOTHERMAL RESERVOIR IN THE CORNUBIAN GRANITE, ENGLAND

A S BATCHELOR

CAMBORNE SCHOOL OF MINES GEOTHERMAL ENERGY PROJECT
PENRYN, CORNWALL, TR10 9DU
ENGLAND

ABSTRACT

A Hot Dry Rock geothermal reservoir has been created at a depth of 2000 m in granite. The stimulation was carried out using 40 000 m^3 (10 million US gal) from a 350 m open hole section that had been treated with a purpose-designed explosive tool. On-line seismic mapping has shown that the reservoir has developed in the direction of the maximum principal stress despite the fact that the joint directions are not orientated in that direction. Photographic and television inspection has been used to correlate acoustic seisviewer and conventional wire logging results including observations of fracture width at the wellbore during pressurisation.

Downward growth of the reservoir has been observed despite the fact that the stimulation fluid was fresh water. This has been explained tentatively as predominantly shear growth because the shear stress gradient is sub-hydrostatic due to the highly anisotropic stress field. Preliminary calculations have shown that the reservoir structure has a volume of 100-200 million m^3 but there is no direct, low resistance flow path between the wells and the residence time is in excess of 5 days.

INTRODUCTION

Hot Dry Rock geothermal exploitation has a well established literature (eg, Smith (1975), Smith (1978), Parsons (1919), Batchelor (1978), Armstead (1979), Milora et al (1976), etc, and there is active research in a number of countries. However, only two, USA and Great Britain, have substantial field programmes and only the USA has reached potential production temperatures. The work in the UK by the author has concentrated on developing stimulation techniques to create HDR reservoirs in a jointed, highly stressed granite body heated by natural radioactivity. Figure 1 shows a panoramic view of the site during pumping operations.

A massive hydraulic stimulation commenced on 4 November this year in Cornwall, England, and more than 40 000 m^3 (10 million US gal) has been used to interlink two wells at a depth of 2000 m. The results presented in this paper are from the start of the stimulation to the onset of steady circulation at noon on 21 November 1982. Full interpretation of the data will not be completed for some time but the results form a useful case study for evaluating the potential application of HDR systems in this area of the UK.

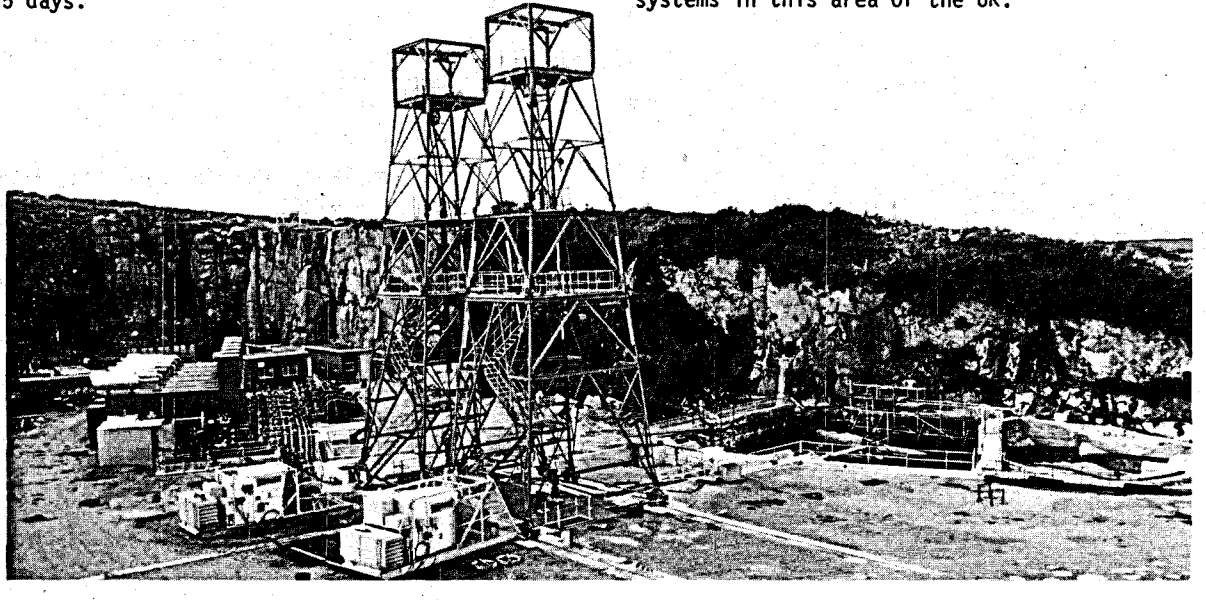

Figure 1: View of site showing tool handling towers and enclosed pump units at the wells

REGIONAL GEOLOGICAL AND THERMAL SETTING

South West England is a peninsula comprising the counties of Devon, Cornwall and part of Somerset, which is bounded by the Atlantic Ocean, the Bristol Channel and the English Channel. The majority of the rocks in the area are shales and mudstones with subordinate bands of grit and conglomerate which have been subjected to varying degrees of metamorphism. These rocks are usually referred to by the local name 'Killas' and they are primarily of Devonian age together with slightly younger Carboniferous rocks to the north east of the area. Towards the end of the Carboniferous period, the thick sedimentary beds were folded along an east-north-east trend by movements of the Armorican orogeny; the intrusions of the granite into this rock mass occurred in the late Carboniferous or early Permian period and formed large cupolas and bosses above a batholith some 200 km in length.

Figure 2 is a sketch plan showing the location and idealised granite structure of the region. The area has been mapped extensively by innumerable authors during the last 200 years because of the interest in the intense mineralisation associated with the granite. Hosking (1949 and 1964) proposed a conjectural mega-structure for the batholith from surface and underground mappings. Bott et al (1958, 1964 and 1970) have confirmed the detailed shape using gravity, magnetic and seismic data. Exley and Stone (1964) have presented the largely definitive survey of its petrography and geochemistry. Bromley (1976) postulated that the whole batholith is the product of crustal thickening providing a uniform melt during intrusion.

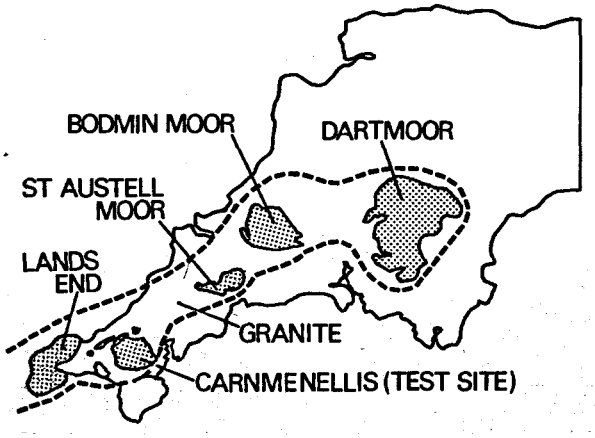

Figure 2: Sketch map of SW England and the Cornubian batholith

The larger plutons are now exposed as elevated moorlands between 200 m and 300 m above sea level and they are circular or elliptical in shape with evidence of multiple intrusion. There is some strong geophysical evidence that the plutons rise on a more or less continuous ridge from Dartmoor to the Isles of Scilly and possibly as far as the rocks of Haig Fras. The model proposed by Bott et al (1970) envisages that granitic material with a seismic velocity of 5850 m/s extends to 12 km depth, although a recent re-interpretation adds 6 km to this figure. It is believed that an intermediate composite lower crust with an average velocity of 6500 m/s continues to the well-defined Moho at 27 km. The bulk of the constituent rocks of the batholith are coarse to fine grained, biotite muscovite granites with and without megacrysts of potash feldspar.

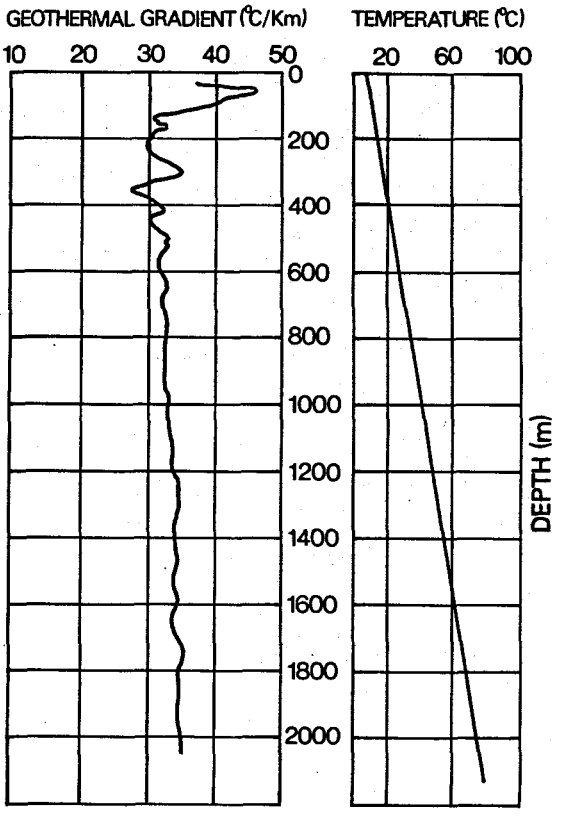

Figure 3: An equilibrium temperature log. Note the increasing gradient.

The HDR research site is located in the centre of the Carnmenellis pluton away from any known mineralisations. The surface area of the Carnmenellis pluton is approximately 300 km^2 and is comprised of a coarse grained porphyritic biotite muscovite granite except in two small areas where the biotite granite is a fine grained porphyry. The south eastern part of the pluton has shown itself to be particularly suitable for hot dry rock experiments because of the massive nature of the granite exposed to the surface. It exhibits well defined vertical jointing which has been

extensively mapped at an earlier phase in the Project. The principal rock constituents are:

Quartz	30%
Potash feldspar	30%
Plagioclase feldspar	26%
Biotite	6%
Muscovite	6%
Other minerals	2%

The radioactive element distribution is consistent throughout the batholith:

Uranium	13 ppm (2.5 ppm)
Thorium	8 ppm (2.5 ppm)
Potassium	4.6% (.7%)

Numbers in parentheses are standard deviations.

Wheildon et al (1977) have mapped the heat flow regime in detail and have shown that there is a persistent regional heat flow of 120 mW/m^2 with a surface thermal gradient of 31°C/km. The temperature gradient was observed to increase with depth to 36°C/km at 2000 m, Figure 3.

STRESS FIELD AND JOINT STRUCTURE

The geometry and extent of the heat transfer zone created by massive hydraulic stimulation is controlled by the prevailing stress field and its interaction with the natural joint structure, Batchelor et al (1980) and Smith et al (1982).

The surface joint structure within 5 km of the site was mapped by Bergin et al (1980) and the simple, bi-modal distribution of both dip and direction was assumed to persist to depth because of the consistent surface patterns. Limited confirmation of this assumption was possible from observations in the nearest deep mine 10 km away at a depth of 800 m.

The majority of the joints are held shut by the stress field and are thought to be have residual widths of 10 μm to 100 μm. The surfaces have varying thicknesses of hydrothermal alteration and none are completely free of alteration products showing that groundwater circulation has occurred within the granite mass since its emplacement.

The stress field has been measured by both hydraulic fracturing (Pine et al, 1982a) and overcoring (Pine et al, 1982b) and the results are shown in Figure 4. The excellent agreement between the two types of measurement at sites over 9 km apart gave considerable confidence in the results.

Figure 5 shows a stereo plot of the joint strikes with the measured stress field at 2000 m depth superimposed. It can be seen that there is an offset between the joints and the stress field, producing high shear stresses across the joint faces.

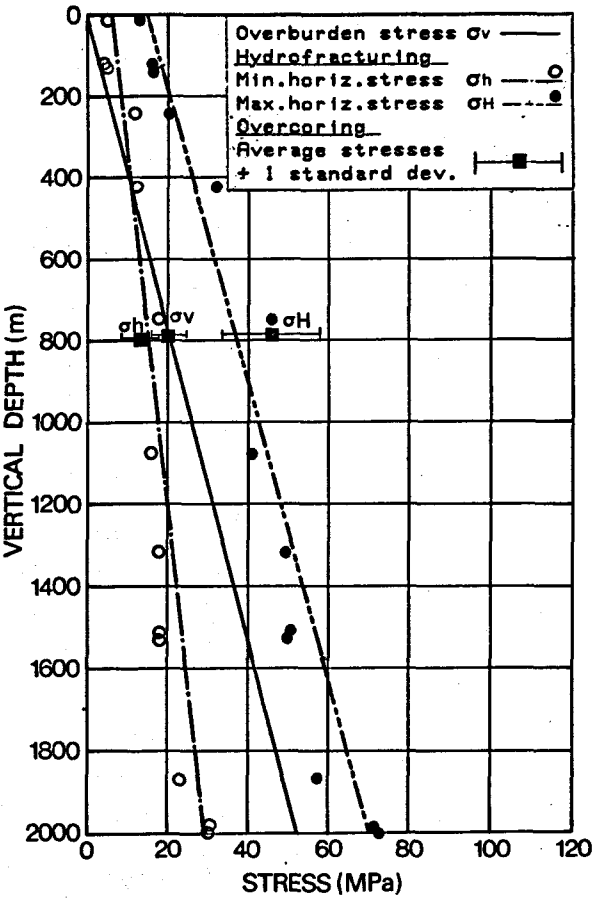

Figure 4: The stress measurement results from hydraulic fracturing and overcoring

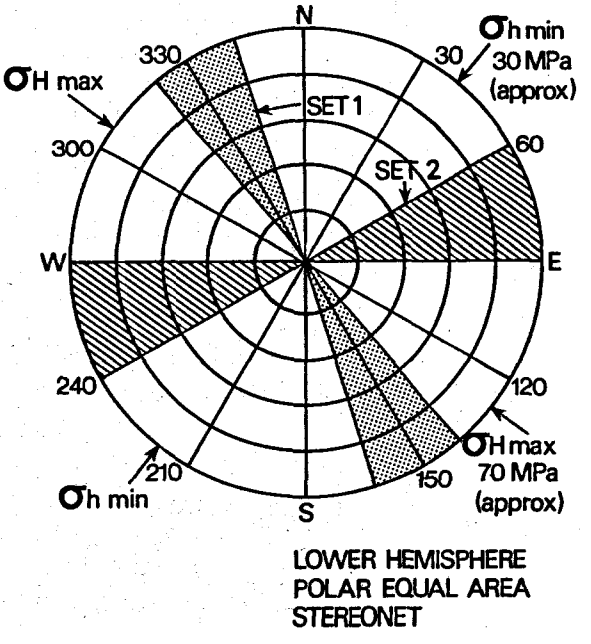

Figure 5: The observed joint strike directions in relation to the measured stresses

THE WELL DIRECTIONS

The boreholes were drilled to give an inclined access to the joint sets within the reservoir. The majority of the joints have dips steeper than 70° to the horizontal so an inclination of 30° was chosen to give as good an access as possible without excessively high torque requirements during drilling. Both wells were completed within a total of 125 days, an average of 32 m/day. The drilling programme has been described by Beswick (1982) and Beswick et al (1982).

Figure 6 & 7 show the projections of the wells and the two casing points can be seen to be vertically aligned. The production well, RH11, was extended to a similar vertical depth as the injection well, RH12, to ensure that the maximum opportunity existed for the interwell connection during fracturing.

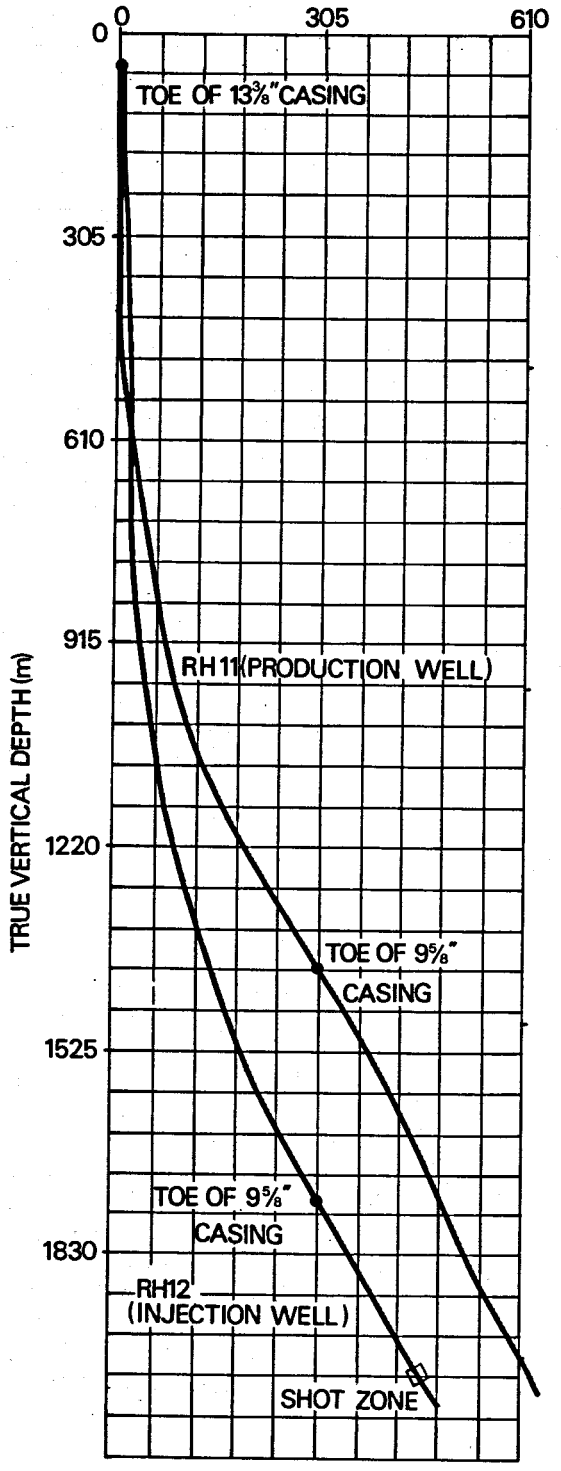

Figure 6: Vertical projection of the wells.

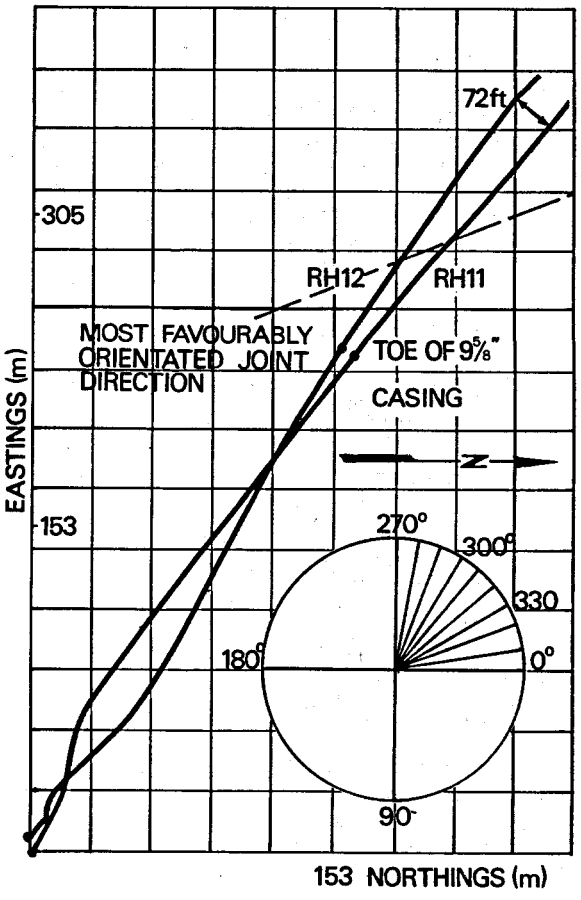

Figure 7: Plan projection of the wells

The stress directions were not known before drilling commenced, so the borehole directions were chosen to be at approximately 40° to both joint directions. This would maximise the chance of interconnection from either set of joints depending on the confinement in each case. However, it was not expected that the plane of the boreholes would be aligned virtually normal to the minimum principal stress.

These were the first two deep wells in this area and were treated as "wildcats" from the point of view of stresses. Intuitively, it

would have been better to orient the wells at 90° to their actual trajectory to give more planar connections along the axis of the well but the early reservoir results indicate that the stimulated zone is sufficiently large for adequate heat extraction.

LOGGING RESULTS

An extensive suite of geophysical logs was run at the end of drilling and before the hole was cased. Figure 8 shows the coverage of the logs versus depth. The principal objective of the logging was to determine the pre-stimulation joint characteristics at the wellbore. Joint aperture, intersection length and orientation are all relevant to any HDR stimulation procedure and it was hoped to identify likely flow connections from the wells. The data is virtually impossible to reproduce for a paper such as this but it did show that the natural fracturing did persist to depth and was orientated in similar directions to the joints at the surface. There were zones of extensive fracturing (spacing 100-500 mm) with long intact zones (30 m), irregularly spaced in the open hole section.

However, it was not possible to identify any particular characteristics that were associated with the joints that eventually accepted the water during injection. Low flow rate injections (3 l/s) were used in conjunction with continuous temperature logs to find the naturally flowing joints at pressures very much lower than the eventual fracturing pressures and these were used to select the explosively stimulated zone.

A television and photographic survey was eventually completed after all the logs had been run and work is still continuing to correlate the logs and the TV results.

The flowing temperature logs showed five exit points from the open hole section with one major connection (30% of the flow) and the four others reasonably uniformly distributed. Figure 9 shows two flow meter logs taken during stimulation and the early one shows a very similar flow distribution to the logs derived from the temperature surveys.

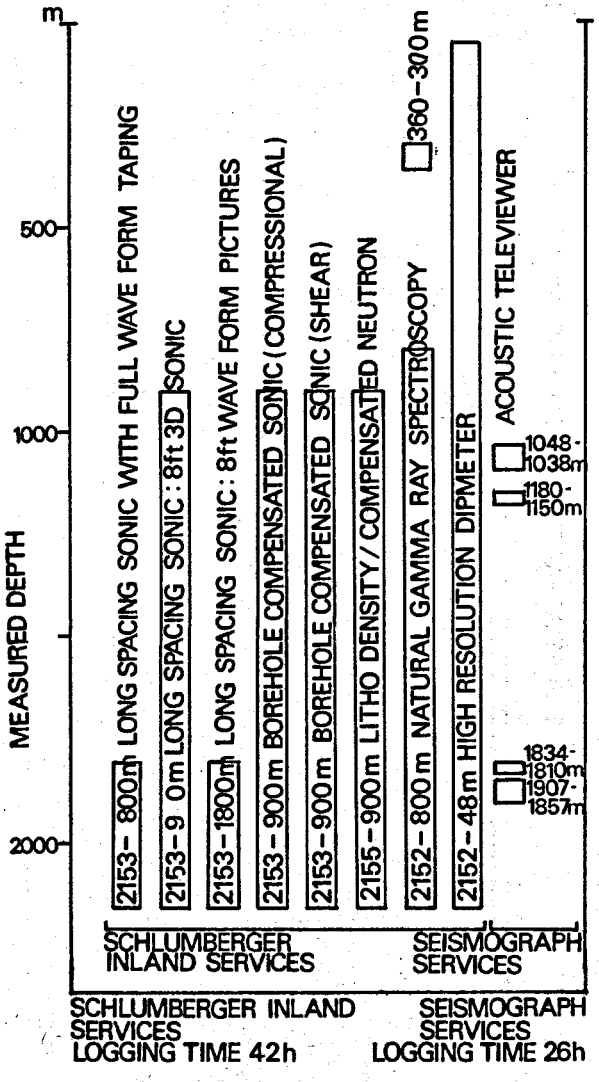

Figure 8: The logging coverage on the injection well

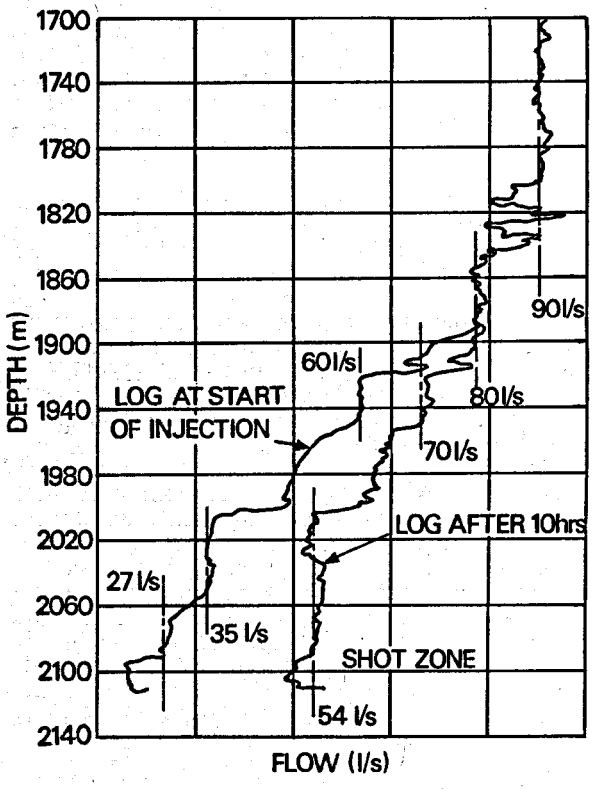

Figure 9: Flow meter logs during stimulation showing the shot zone developing

THE EXPLOSIVE STIMULATION

A depth of 2125 m was chosen for the top of the charge, which was 5 m long. The purpose of the explosive shot is described in detail by Batchelor (1982) but, briefly, it is designed to open self-propped fractures at the wellbore to provide low impedance connections to the natural fracture system prior to hydraulic stimulation.

The complete success of the process is evident in Figure 9, where the second flow meter log, approximately 10 hr after the first, shows more than 60% of the flow is leaving the well in that region. The explosive tool ensures that the minimum pressure loss occurs at the well bore/fracture connection and full pressure can then be applied within the formation.

THE MICROSEISMIC EVENT LOCATION SYSTEM

The only method which can be used to define the extent of a hydraulically stimulated region is microseismic event location mapping. This technique has been used with great success at LANL (for example, Smith et al, 1982) using single sonde, multiaxes geophones. At the site in Cornwall, however, the granite was exposed at the surface and tests had showed that the attenuation factor, Q, was greater than 150 at frequencies up to 1 kHz. This meant that a surface sensor network in shallow boreholes (up to 200 m deep) could be used in conjunction with a downhole system. Vertical axis accelerometers were used in the surface net with three hydrophones deployed on a standard logging cable forming the sub-surface system.

All of the data was collected on the site VAX 11/780 computer via a multi-channel transient digitiser. The signals were then processed via a purpose-written code 'METAL' (Microseismic Event Timing and Location) which used a variety of location algorithms, HYPO (Ref Lee et al (1975)), SPAM (Ref Dechman et al (1977)), and EMI (Ref Thorn-Emi (1981)), to derive locations and rms errors. The system is described more fully in the Project progress reports (1982a and 1982b).

Many thousands of events were detected with one calculated maximum local magnitude of 0.6. Several hundred of the events were large enough to be seen on a surface seismometer network consisting of eight stations at radii of 1 km to 6 km. This surface network was operated by the Global Seismology Unit of the Institute of Geological Sciences.

The event maps are shown in Figures 11 & 12 in the section of the hydraulic stimulation.

THE HYDRAULIC STIMULATION

The purpose of the hydraulic stimulation was to interlink the two wells that were 350 m apart vertically and 200 m horizontally. See Figures 6 and 7. The minimum earth stress was estimated to be 30 MPa at 2000 m, meaning an effective surface pressure of 10 MPa or more would be required to open a favourably orientated joint.

The offset between the joints and the stress direction is shown in Figure 5, meaning that a pressure in excess of the minimum earth stress would be required to open the most favourably orientated set. This pressure was calculated to be 16-18 MPa. Any one joint forming a direct connection between the wells would need 400 m^3 of fluid if it was dilated to a width of 1 mm over a circular area centred on the injection point. There were between 5-10 such joints within the open hole section and a minimum volume of 4000 m^3 was thought necessary to achieve connection with this simple mechanism.

Figure 10 shows the pressure history on the injection well. The pressure peak was reached after 3 hrs but the initial response on the production well, RH11, was a fall in water level and this continued until the point indicated on the figure. The level fell by approximately 150 m in 14 hrs before turning. The water level then began to rise at an ever

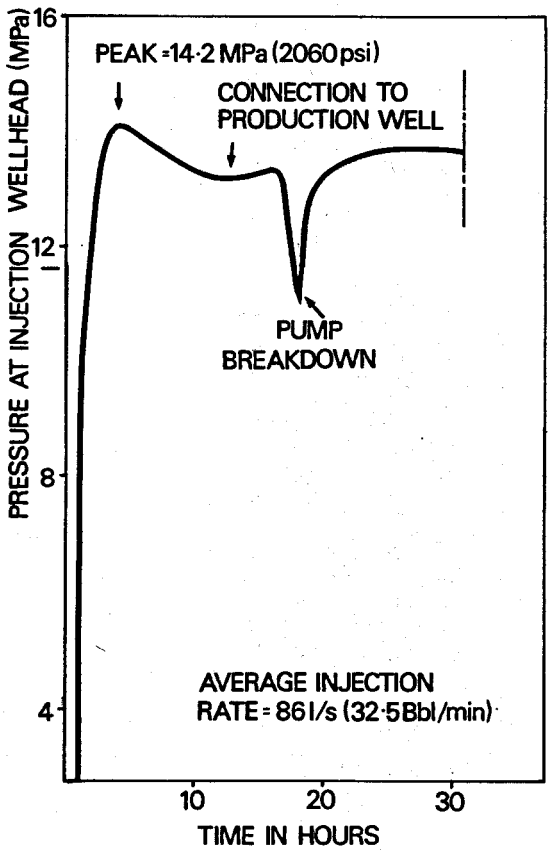

Figure 10: Pressure history on the injection well during stimulation

accelerating rate and the well was filled after the pressure rise was seen to be sustained for 4 hrs.

After 22 hrs of pumping, the production well commenced flowing and the surface pressure control equipment was fitted to enable the pressure to rise on the well. The high injection flow rate was continued until a total of 9000 m^3 (56 600 Bbl) had been injected.

The surface pressure in RH11 rose steadily and production was commenced when it had reached 2.8 MPa (400 psi). The flow declined rapidly and 8 cycles of production and shut-in were used to determine if the connection was improving. Eventually, a sustained 2 l/s was produced for 24 hrs and no further improvement was observed using this procedure. This period lasted 80 hrs and consumed a further 9000 m^3 to maintain a wellhead pressure of 10.5 MPa. There were no significant perturbations in the injection well pressure as the production flow from RH11 was cycled.

It was concluded that there was no direct connection between the two wells and that production was controlled by a diffusive zone fed by a "constant pressure" boundary within the main structure.

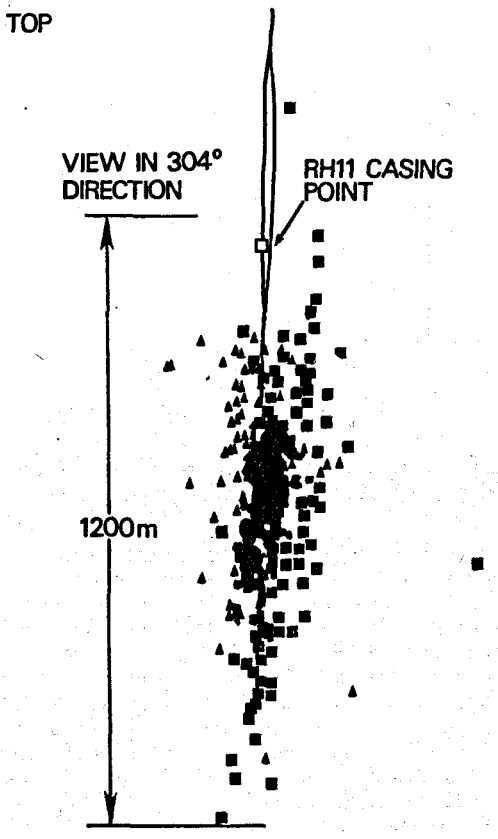

Figure 11: A vertical section through the seismic events at the reservoir

During this period it had been established (see Figure 9) that the majority of the water in the injection well had left the borehole at the shot zone despite the presence of natural fractures elsewhere that had accepted flow at low pressures. The conclusion was that the lower impedance outlet at the shot had enabled a more satisfactory widening of a natural joint set in that vicinity.

The seismic events (see Figures 11 and 12) had been triggering the automatic acquisition system at a rate of one every 5-10 secs and continuous interpretation proved impossible. The two maps were not produced during the fracturing but plan and borehole section plots were used which gave the false impression of an unstructured sphere of events about 350 m in radius. However, it was clear that both wells were completely enveloped by the seismic events and that two thirds of them were from below the reservoir by as much as 600 m.

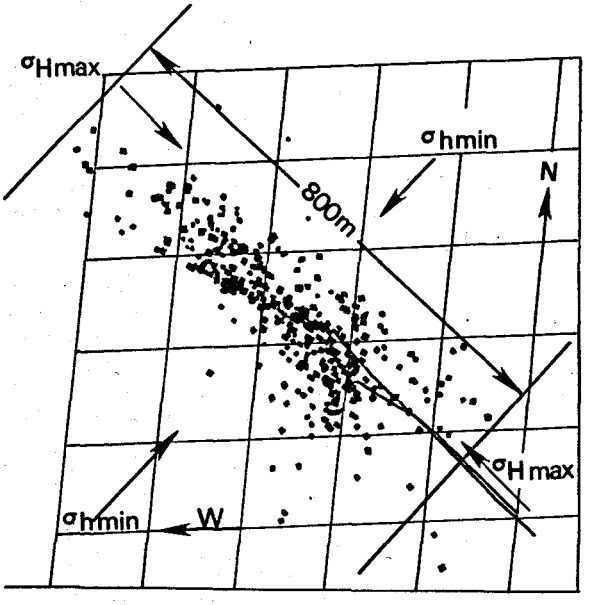

Figure 12: A projection of the seismic events normal to the main structure

When the downward growth was identified, a study of the shear stress gradient showed that shearing would indeed produce downward growth because the gradient was subhydrostatic. The first circulation results showed that water in excess of the TD temperature of the production well was being produced, thus demonstrating that heat transfer was occurring in the deep sections of the region.

The flowing connections to RH11 under injection conditions were know but it was not possible to log in RH11 under initial production because the hydrophone string was positioned in the well. It was decided to try a short (2 hr) high flow rate injection into RH11 in an attempt to form a direct connection

to the reservoir and risk the creation of a separate system from RH11.

This injection was completed successfully and the well was put on immediate production flow at 78 l/s (29 Bbl/min) to flush the joints in and around the well. However, it was observed that RH12's shut-in pressure dropped rapidly during the 2 hr pump into RH11 but stabilised immediately the injection to RH11 ceased. This was taken to indicate that no direct connection was formed and, indeed, eventually, a flow of 3.7 l/s could be sustained for 48 hrs, an increase of only 1.7 l/s.

The production well, RH11, was then shut in and a pressure of 2.5 MPa was reached over a 16 hr period with steady pumping into the injection well at 25 l/s. The injection flow rate was then increased rapidly but the rate of pressure increase on RH11 decreased, showing that the perverse influence had not been eradicated. The implication was clear; much more energy was required to break down the final high impedance barrier.

It was decided to pump a nominal 100 l/s into RH11 until a significant change was observed in RH12 or the microseismic data indicated excessive upward growth from RH11.

Figure 13 shows dP/dt of the shut-in pressure on RH12. The ever decreasing fall of dP/dt during the day is evident but, as the injection into RH11 ceased, the pressure started to rise. A total of 3200 m^3 (20 100 Bbl) was injected but the pressure just rose steadily (maximum 11 MPa, 1600 psi) and showed no signs of a breakdown. The injection was terminated because a cluster of microseismic events were received within a few metres of the casing shoe.

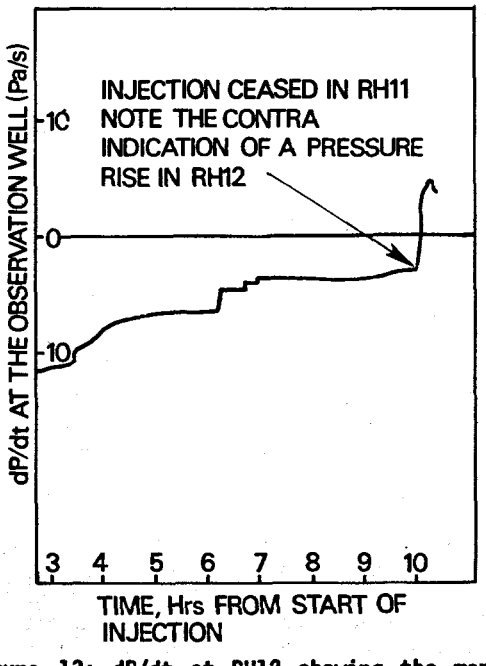

Figure 13: dP/dt at RH12 showing the marked rise when pumping ceased on the other well

RH11 was left shut-in and then pumping commenced again on RH12 at 100 l/s. Figure 14 shows the wellhead pressure in RH11 and note that the pressure falls more slowly from 7.8 MPa. This was just at the point when pumping ceased on the other well because of a weld failure.

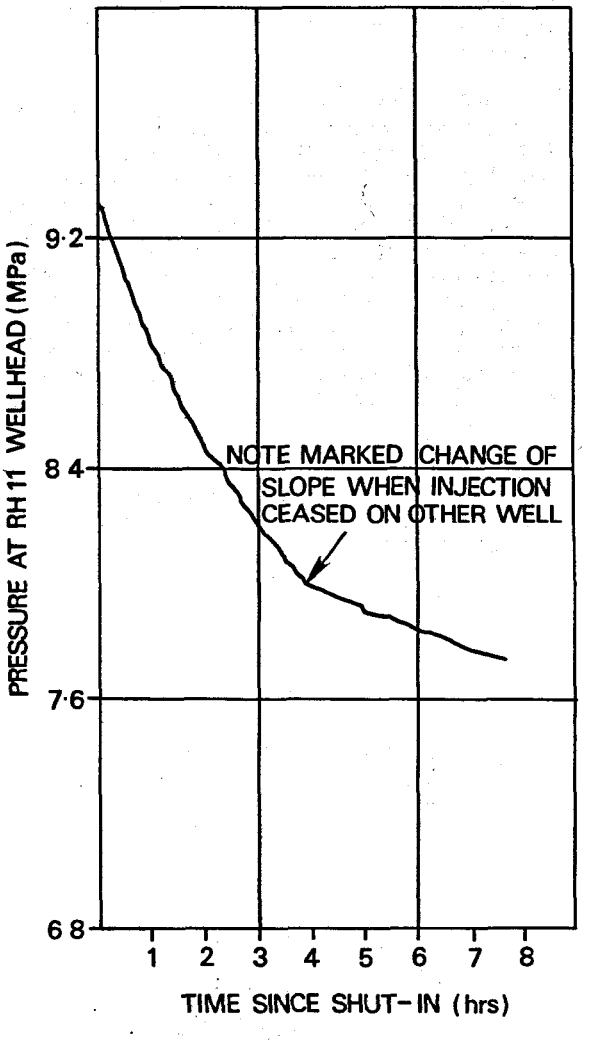

Figure 14: RH11 wellhead pressure after the 3200 m^3 injection and before production

Despite the massive injection into RH11 it was thought that no direct connection could exist because of the perverse nature of the pressure responses and it was decided to commence production on RH11 in an attempt to understand the mechanics of the connection to the well. Figure 15 shows the wellhead pressure during this period; production drew the well pressure down significantly until a pressure of approximately 3.8 MPa was reached. At this point, it proved possible to hold the pressure reasonably steady by increasing the injection flowrate on RH12 and raising its pressure. This was the first time that there was an indication of a flowing connection between the wells that was able to sustain a reasonable

and increasing flow rate. The pressure did decline initially during the increase in RH12's pressure but, thereafter, it remained steady.

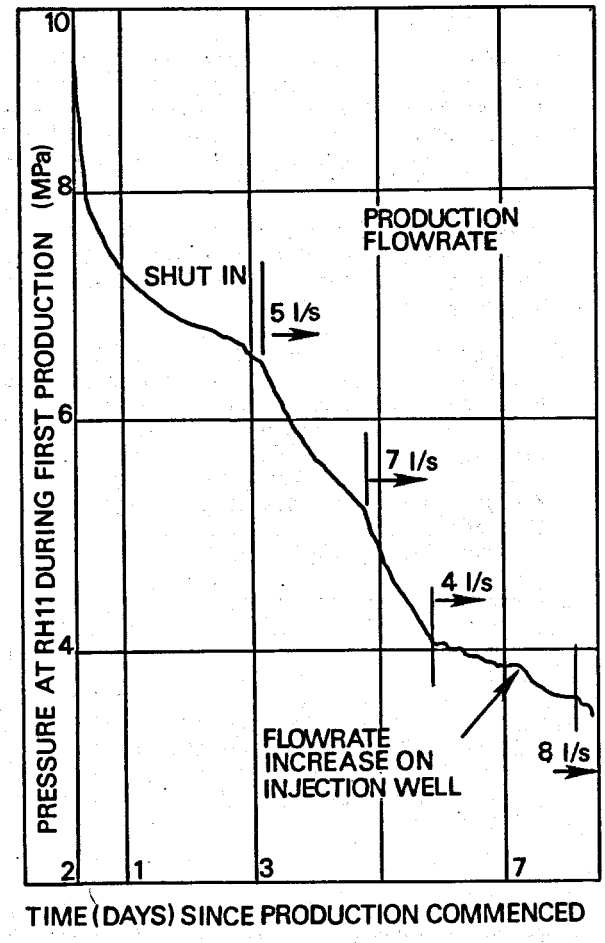

Figure 15: RH11 wellhead pressure during initial production

PRELIMINARY ANALYSIS

a The stored volume

The reservoir region delineated by the microseismic events is 1200 m high, 800 m wide and 100 m thick, a volume of 96 x 10^6 m^3. The stored water volume was of the order of 40 000 m^3 which, therefore, would only require a 0.04% porosity change to accommodate it within such a rock volume. This is the equivalent of a 0.4 mm dilation/m, which appears to be a realistic value.

b The seismicity

Microseismic activity after massive stimulation has generally declined but the system is apparently pressure-sensitive because the event rate increases rapidly when the injection wellhead pressure on RH12 exceeds 10.5 MPa. It is not clear whether or not the seismicity is related to the absolute pressure value or the differential pressure across the wells.

Figure 11 shows that the majority of the reservoir has been developed to the North East of RH11, although there is considerable microseismicity at the base of the well. This is in good agreement to the hydraulic data which indicates that the connection has been made by a tortuous path.

c Geochemistry

The return water has been sampled for a suite of ions and its radon content has also been monitored. The data is influenced by the cement and drilling additives, but it would appear to imply that the residence time was of the order of 5 days and could be reducing. No tracer tests have yet been run because of the lack of hydraulic equilibrium.

d Hydraulic data

The most important observation to explain is the perverse, repeatable and reversible effect that increasing pressure on either well causes the pressure to reduce on the observation well.

There is only one mechanism that can cause a reduction in pressure and that is that an increase in available storage volume occurred that could not be fed by the injection zone.

Figure 16 is a graphical output from a fully explicit computer code, FRIP, (Ref Cundall, 1981), that models the rock mass as discrete blocks that can shear, deform and translate in space. It supports the hypothesis that dilation zones can form within a jointed,

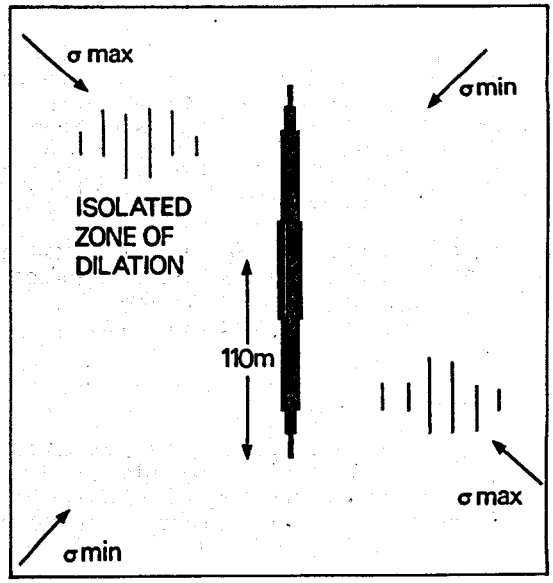

Figure 16: The results of the reservoir simulator code showing isolated dilation zones

discontinuous rock mass simply because the confining stresses are disturbed by the pressurised zone.

The position of RH11 is such that the majority of the openhole section is aligned in this manner with respect to the growing structure from RH12.

The implication of this modelling is that seismicity can be generated in regions not associated with flow from the main structure. However, there is no evidence to support the converse argument that flow could occur without seismicity.

Hydraulic access to these zones is dependent on generating flow normal to the main structure and it will be essentially diffusive through tightly shut joints.

During the circulation trials, it was tentatively concluded that the production well should be kept at sufficient pressure to cause reasonable joint dilation and, hence, a reduction in inlet impedance but not so high that the dilation zones were affected adversely by causing a low differential pressure. It appeared possible to increase the flow rate from the production well with a much smaller decrease in pressure than had been observed at higher total pressures. This confirms an observation of Tester (1981) that the impedance reduction caused by high back pressures was associated with excessively restricted flow and that there was an optimum, but low, back pressure to be found.

e **The logging data**

The injection well flow distribution changed markedly during the first few hours of operation but it has remained stable since that time.

The return flow pattern has changed both in temperature and flow rate. One of the most interesting observations was that water was entering the well at temperatures in excess of the highest temperature observed in the well (+81°C). Circulation must be occurring below the wells and sweeping through hotter rock.

All the return points are at positions that are known to have accepted water on injection but the reverse is not true; some of the low pressure injection zones did not produce fluid.

CONCLUSIONS

At the time of writing this paper, most of the results are only seven days old and so it follows that any conclusions must be of a tentative nature. However, some of the observations are irrefutable.

- Reservoir growth has proceeded normal to the minimum horizontal stress and not along a known joint direction. This confirms that the stress directions measured 10 km away in a local mine were of regional significance.
- The marked stress anisotropy has been confirmed by the restricted width of the seismically active zone.
- Seismic events were recorded with wellhead pressures as low as 4.5 MPa, although there is a marked increase in events when wellhead pressures in excess of 10.8 MPa are reached. The latter figure corresponds to the measured minimum horizontal stress.
- Two-thirds of the reservoir growth has been downwards and water is circulating through rock that is hotter than the TD temperatures of the wells.
- A mechanism of induced, isolated joint dilation has been observed which caused pressure reductions in the return well when the reservoir structure is pressurized; the reverse effect was also seen when it was depressurized. It takes between 2 and 14 hrs for the effect to diminish, implying that the zones are totally isolated from the reservoir away from the wells.
- Reservoir growth has been contained within a structure 1200 m x 800 m x 100 m and insignificant far field losses have been identified.
- Explosive stimulation provides sufficient self-propped fractures at the wellbore to allow hydraulic stimulation to activate joints more effectively than those which are not treated in this fashion.
- It is essential to predict accurately, or measure, the in situ stress field at any potential HDR site. The stress effects override the actual joint structure in controlling the reservoir zone.
- Seismic event rate is associated with the absolute value of the pressure and its rate of change. Adequate stimulation flow rates appear to be in excess of 90 l/s at this site.
- The majority of the events originate from shear, strike-slip motions within the reservoir and are obviously associated with natural joint activation rather than any fracturing.

Although the reservoir system is supporting a continuing return flow rate (8 l/s on 24 November 1982), with an equally increasing downhole temperature, it may not be possible to achieve the designed 50 l/s because of the suspected unfavourable borehole positions. However, the system will be hydraulically tested to its limits in the programme to understand the heat transfer aspects of the reservoir.

ACKNOWLEDGEMENTS

This work was funded by the UK Secretary of State for Energy, Contract No E/5A/CON/115/173/017, and the Commission of the European Community, Contract No EG-D-2-003-UK(N). The support and encouragement of the two programme managers has ensured that the operation has run smoothly.

The results reported here are the product of a research team. This paper would not have been possible without the dedication and commitment of all concerned, and the author gratefully acknowledges the contributions of the entire staff.

Much of the strategic planning for the programme was based on detailed discussions with the present and past staff at the Los Alamos National Laboratory and the author expresses his thanks for their support.

All the ideas expressed in this paper are personal opinions and are not necessarily endorsed by the UK Secretary of State or the Commission of the European Communities.

REFERENCES

Armstead H C (1979), "Geothermal Energy" London: Spon, 1979, 356 pp.

Batchelor A S (1978), "The granites of South West England and their engineering properties related to possible dry rock geothermal exploitation", Nordic Symposium on Geothermal Energy, Gothenburg, Sweden, 1978, pp 15-31.

Batchelor A S, Pearson C M, Halladay N P, (1980), "The enhancement of the permeability of granite by explosive and hydraulic fracturing", paper presented at the 2nd International Seminar on the results of the EEC Geothermal Energy Research (EUR 6862), Dordrecht, Holland, 1980, 28 pp.

Batchelor A S (1982), "The creation of hot dry rock systems by combined explosive and hydraulic fracturing". In International Conference on Geothermal Energy, Florence, May 1982. Papers BHRA Fluid Engineering, Cranfield, Beds, Vol 2, 1982, pp 321-342.

Bergin N K, Tovey N P (1980), "A survey of joint orientations in the Rosemanowes area of the Carnmenellis granite". Camborne School of Mines Geothermal Energy Project, 1980, 53 pp.

Beswick A J (1982), "Well Drilling and Casing Volume 1 Summary Report", CSM Geothermal Energy Project, 1982, 31 pp, (Rep 2-15).

Beswick A J, Forrest J (1982), "New low-speed high-torque motor experience in Europe", Society of Petroleum Engineers of AIME, 1982, 16 pp, (SPE-11168).

Bott M, Day A, Masson-Smith D (1958), "The geological interpretation of gravity and magnetic surveys in Devon and Cornwall". Phil Trans Roy Soc, V251A, pp 161-191.

Bott M, Scott P (1964), "Recent geophysical studies in South West England". In Present views of some aspects of the geology of Devon and Cornwall, Hosking/Shrimpton, Eds, Pub Roy Geol Soc Cornwall, 1964, pp 25-43.

Bott M, Holder A, Long R, Lucas A (1970), "Crustal structure beneath the granites of South West England". In Mechanism of Igneous Intrusion, Liverpool, pp 93-102.

Bromley A (1976), "Granites in mobile belts, the tectonic setting of the Cornubian batholith". Journal of Camborne School of Mines, Vol 76, 1976, pf 40.

Camborne School of Mines Geothermal Energy Project (1982a), "Bi-monthly information circular: Report of Activities Dec 81-Jan 82 (8)".

Camborne School of Mines Geothermal Energy Project (1982b), "Bi-monthly information circular: Report of Activities Jun 82-Jul 82 (11)."

Cundall P (1981), "FRIP - Users Manual", Internal Report, Camborne School of Mines, Cornwall, England, Oct 1981, 24 pp.

Dechman G H, Sun M C (1977), "Iterative approximation techniques for microseismic source location", US Bureau of Mines, RI8254, 23 pp.

Exley C, Stone M (1964), "The granitic rocks of South West England". In Present views of the geology of Devon and Cornwall, Hosking/Shrimpton, Eds, Pub Roy Geol Soc Cornwall, pf 131.

Hosking K (1949), "Fissure systems and mineralisation in Cornwall". Trans Roy Geol Soc Cornwall, V18, pp 949.

Hosking K (1964), "Permo-carboniferous and later primary mineralisation." In Present views of the geology of Devon and Cornwall, Hosking/Shrimpton, Eds, Pub Roy Geol Soc Cornwall, pp 201-244.

Lee W H K, Lahr J C (1975), "HYPO 71 (revised): A computer program for determining hypocentre, magnitude and first motion pattern of local earthquakes", US Geological Survey, Open-File Report 75-311, Menlo Park, Calif, 114 pp.

Milora S J, Tester J W (1976), "Geothermal energy as a source of electric power", the MIT Press, 1976, Cambridge, Mass.

Parsons C (1919), "Presidential Address to the British Association for the Advancement of Science", Annual Report for 1919 of the Brit Assoc for Advmt of Sci, pp 3-23.

Pine R J, Tunbridge L W, Kwakwa K A (1982a), "In situ stress measurement in the Carnmenellis granite: 1 - Overcoring tests at South Crofty mine at a depth of 790 m." Internation Journal of Rock Mechanics and Mining Sciences. Submitted Sept 1982.

Pine R J, Merrifield C M, Ledingham P (1982b), "In situ stress measurement in the Carnmenellis granite: 2 - Hydrofracture tests at Rosemanowes Quarry to depths of 2000 m." International Journal of Rock Mechanics and Mining Sciences. Submitted Sept 1982.

Smith M C (1975), "The potential for the production of power from geothermal resources", Los Alamos Scientific Laboratory Report, LA-UR-73-926, 1975.

Smith M C (1978), "Initial results from the first Los Alamos hot dry rock energy system". In Nordic Symposium on Geothermal Energy, Gothenburg, Sweden, 1978, pp 151-158.

Smith M C, Ponder G M, editors, (1982), "Hot Dry Rock Geothermal Energy Development Program Annual Report Fiscal Year 1981", Los Alamos National Laboratory, NM, (LA-9287-HDR).

Tester J (1981), Priv. Com.

Thorn-EMI Electronics Ltd (1981), "A general algorithm for sensor point observers", Doc Ref MS/G/113, Iss 1, Camberley Division, Surrey, UK, 18 pp.

Wheildon J, Francis M, Thomas-Betts A (1977), "Investigation of the South West England thermal anomaly zone", Seminar on Geothermal Energy, Brussels, Dec 1977, Pub EEC, EURO 5920, pp 175.

Proceedings Eighth Workshop Geothermal Reservoir Engineering
Stanford University, Stanford, California, December 1982
SGP-TR-60

RECENT RESULTS: LOS ALAMOS HOT-DRY-ROCK PROJECT

Donald W. Brown

ESS-DOT, Los Alamos National Laboratory
Los Alamos, New Mexico 87545

ABSTRACT

A new deeper reservoir is presently being investigated at the Laboratory's Fenton Hill Hot Dry Rock (HDR) site. The region surrounding the lower of two inclined boreholes, directionally-drilled to about 4 km in hot crystalline rock, has been pressurized in a sequence of injection tests. Based primarily on the measurements made by two close-in microseismic detectors, two similar volumetric reservoir regions have been developed by massive hydraulic fracturing, but with no significant hydraulic communication with the upper borehole as yet.

INTRODUCTION

Since June of 1982 -- including a 10-week furlough period -- the Los Alamos National Laboratory has been attempting to connect two deep inclined boreholes in hot granitic rock by means of massive hydraulic fracturing. As of this writing (November 1982), we have yet to be successful in making a connection, although close-in microseismic data have revealed the probable causes of our difficulties. Renewed fracturing operations early next year, guided by a careful assessment of recent pumping and seismic data, hopefully will result in a significant number of fracture connections, and a very large thermal reservoir.

The setting for these experiments, beneath the Jemez Mountains of northern New Mexico, is depicted in the sectional view of Figure 1. The Fenton Hill Hot Dry Rock (HDR) Geothermal Site is located several kilometers west of the Valles Caldera, in a region of low apparent structural complexity, but of high volcanic-associated heat flow. The trajectories of our two new wellbores -- EE-2 and EE-3 -- are shown in the plan and sectional views of Figures 2 and 3. The lower openhole portions of these two near-parallel directionally-drilled boreholes are inclined 35° from the vertical, and were drilled to the east, approximately parallel to the direction of the least principal earth stress.

BRIEF DESCRIPTION OF FRACTURING EXPERIMENTS

A series of three large-scale pumping experiments have been performed in the lower portion of the new -- Phase II -- reservoir region, at injection rates up to about 90 ℓ/s. After cementing in a scab liner about 150 m above the bottom of EE-2 for wellbore isolation, the openhole interval (at a mean depth of 4310 m) was pressurized in three successively larger injection tests of 500, 3000 and 4900 m^3 respectively. Despite these relatively large volumes of injected water, we failed to achieve hydraulic communication with the upper borehole (EE-3) for reasons discussed below.

Following these tests, the EE-2 wellbore was sanded up to within about 150 m of the casing shoe, providing an isolated openhole interval in the upper portion of the Phase II reservoir region. Two injection tests of 900 and 3200 m^3 have recently been performed in this upper region, with only a slight indication of hydraulic communication so far. Because of the nature of the fractured reservoir being developed, it now appears that significantly larger volumes of injected water will be required to achieve the desired level of communication.

FRACTURE GEOMETRY INFERRED FROM CLOSE-IN MICROSEISMIC DATA

Extensive downhole measurements of the locations of microseismic events generated by the hydraulic fracturing process have been made during all of the injection tests. The microseismic event locations were primarily determined from signals received by a three-axis oriented high-temperature geophone sonde at a depth of 2950 m in EE-1 (the injection borehole for the previous shallower Phase I HDR reservoir at Fenton Hill). Also, for the more recent injection experiments, a series of detonator shots were made deep in EE-3 prior to pumping. This was done to provide both a redundant geophone package orientation, and a relative sensitivity calibration of the geophones (the sensitivity of the vertical geophone as compared to that of the two horizontal geophones, which is needed for accurate particle motion determinations). For most of the injection tests, a newly-developed

three-axis oriented high-temperature accelerometer sonde was also positioned in the EE-3 borehole adjacent to the pressurized interval in EE-2 (following the detonator shots). Although the accelerometer tool is still under development, it has generally provided accurate $V_s - V_p$ time differences for the microseismic events, significantly reducing location errors associated with the analysis of the geophone-measured signals.

The microseismic event locations associated with the pumping experiments performed in the lower part of the Phase II reservoir suggest that three distinct -- but parallel -- fracture zones, inclined about 45° from the vertical, were opened (hydraulically fractured). These fracture zones strike roughly north-south, dip towards the west, and appear to extend upwards and to the east away from EE-3. Thus, these upward-extending fracture zones may have all missed -- passed below -- the bottom of EE-3, explaining the lack of hydraulic communication. Figure 4 shows, in both plan and elevation views, the seismic data for one 50-minute time interval during the last (4900 m^3) injection test. The steeply-dipping seismic feature apparent in the elevation view of Figure 4, which persisted for about 5 hours, is one of three roughly parallel zones that were developed during this sequence of pumping tests in the deeper part of the Phase II reservoir.

The microseismic event locations associated with the pressurization of the upper part of the Phase II reservoir exhibit a more volumetric character than those associated with the lower part of the reservoir. Figure 5 shows the microseismic pattern for the last two hours of EE-2 pressurization during the second (3200 m^3) injection test in the upper part of the reservoir.* In both the plan and elevation views, the microseismic event locations appear to be fairly uniformly distributed around the openhole section of EE-2, having not yet reached EE-3 as shown in the elevation view. A rough ($\sim R^2$) scaling based on the microseismic event location data shown in the elevation view of Figure 5 suggests that a total injected volume of about 13,000 m^3 (3.4×10^6 gallons) would be required to extend the active seismic boundary -- growing radially outwards from EE-2 -- to the vicinity of the EE-3 wellbore.

If the volumetric interpretation of the seismically-active region surrounding EE-2 is correct, this would imply that we have already hydraulically activated 37 million cubic meters of hot crystalline rock in the upper part of the Phase II reservoir. A statistical analysis of the microseismic data from the first pumping test indicates that this fractured volume is formed by the intersections of two -- and probably three -- joint sets. The major set strikes N10W and dips about 60° to the west, while the sub-major set strikes N35E and dips very steeply ($\sim$80°) to the west. The minor set (at least seismically) is vertical and strikes somewhat east of north.

*In Figure 5, the smaller letters "T" and "B" represent the top and bottom of the openhole interval.

DIFFERENCES BETWEEN THE TWO FENTON HILL HDR RESERVOIRS

The Phase II reservoir appears to differ from the previous -- and somewhat shallower -- Phase I reservoir in two distinct ways. First, the Phase I reservoir was formed mainly by a parallel set of near-vertical fractures, whereas the Phase II reservoir appears to be much more volumetric in nature, and is controlled by the principal set of 60° west-dipping fractures. Second, the Phase II reservoir exhibits a very marked volcanic association when compared with the Phase I reservoir. We have been surprised by both the large amounts of dissolved CO_2 encountered in the connate pore -- or fracture (?) -- fluids in the Phase II reservoir, and the lesser amounts of associated H_2S. This dominant inclined fracture system that appears to truncate the older near-vertical joint sets, in combination with typical volcanically-derived dissolved gasses, strongly suggests that the Phase II reservoir has a significant volcanic association that was not exhibited by the Phase I reservoir.

In a sense, our Fenton Hill site has allowed us to investigate two significantly different HDR regimes: one of relatively simple structure typical of the Basin-and-Range Province, and the other more typical of volcanically active regions.

PRESSURE/FLOW DATA AND EARTH STRESS IMPLICATIONS

The most significant feature of the Phase II reservoir, from the pressure/flow standpoint, has been the much higher fracture opening stress levels when compared to the Phase I reservoir. However, if one accepts that we are primarily opening inclined joints in the Phase II reservoir as compared to vertical joints in the overlying Phase I reservoir, then the significant increase in fracture closure stress as inferred from fluid injection pressure levels is more easily explained.

For the lower part of the Phase II reservoir at a mean depth of 4300 m, the effective fracture closure stress obtained from four instantaneous shutin pressure (ISIP) measurements during the final (4900 m^3) injection test was 805 bars (11,680 psi), corresponding to a 376 bar (5450 psi) surface pressure. If one linearly extrapolates the measured Phase I value for the least principal earth stress* to the lower part of the Phase II reservoir and

*S_3 = 358.5 bars (5200 psi) at 2700 m in the Phase I reservoir.

uses the overburden stress as the maximum principal stress (S_1), the measured fracture closure stress of 805 bars would correspond to an inclined fracture zone dipping 49° to the west, in good agreement with the seismic data shown in Figure 4.

The pressure/flow behavior of the upper part of the Phase II reservoir is much more anomalous, as shown by the ISIP data of Table I.

The shutin pressure data for the upper part of the reservoir during the second injection test (Expt. 2020) show a steady rise in the ISIP with time, and therefore with total injected volume. Surprisingly, about half way through Expt. 2020, the ISIP (surface) had exceeded the average measured ISIP value for the lower part of the Phase II reservoir. Even more anomalous is the very significant 70 bar (1000 psi) increase in the ISIP between the end of the first injection test (after a total injection of 905 m^3), and early during the second injection test (after having injected only 114 m^3).

Although our understanding of these ISIP data is still not complete, one fact is clear. We have produced a bounded volumetric reservoir in the upper region. It would appear that we are inflating a contained region with limited outflow, and activating progressively higher-closure-stress joints within the pressurized region as the static inflation pressure slowly rises: a very foreign concept among the experts on hydraulic fracturing in the petroleum industry.

Table I

ISIP Summary for Upper Phase II Reservoir

Experiment Number	ISIP, Surface bars (psi)	Flow Rate ℓ/s (BPM)	Cumulative Flow m^3 (gallons)
2018	293 (4250)	33.4 (12.6)	905 (239,000)
	[EE-2 vented between experiments]		
2020	339 (4910)	5.0 (1.9)	117 (31,000)
2020	363 (5270)	12.5 (4.7)	114 (30,000)
2020	371 (5380)	25.1 (9.5)	170 (45,000)
2020	367 (5330)	42.1 (15.9)	254 (67,000)
2020	395 (5730)	90 (34)	1840 (486,000)
2020	401 (5820)	82 (31)	3200 (844,000)

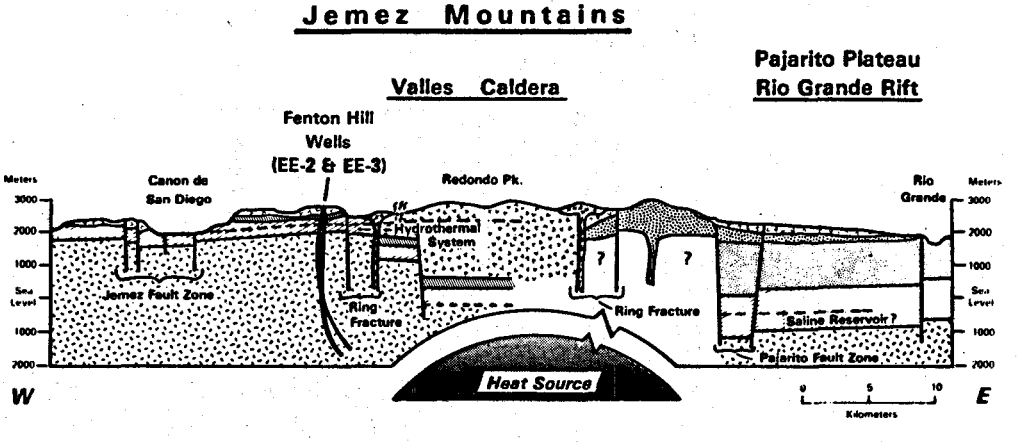

Figure 1. Setting for the Fenton Hill Hot Dry Rock Project.

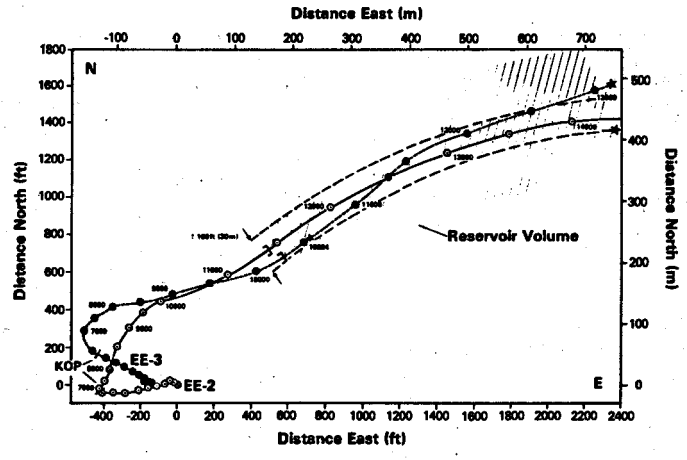

Figure 2. Plan view of Holes EE-2 and EE-3.

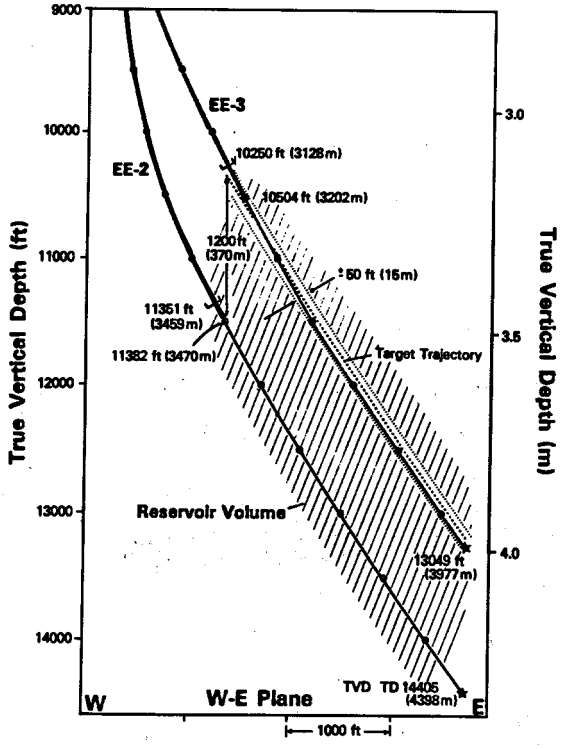

Figure 3. Section view of the openhole portions of EE-2 and EE-3.

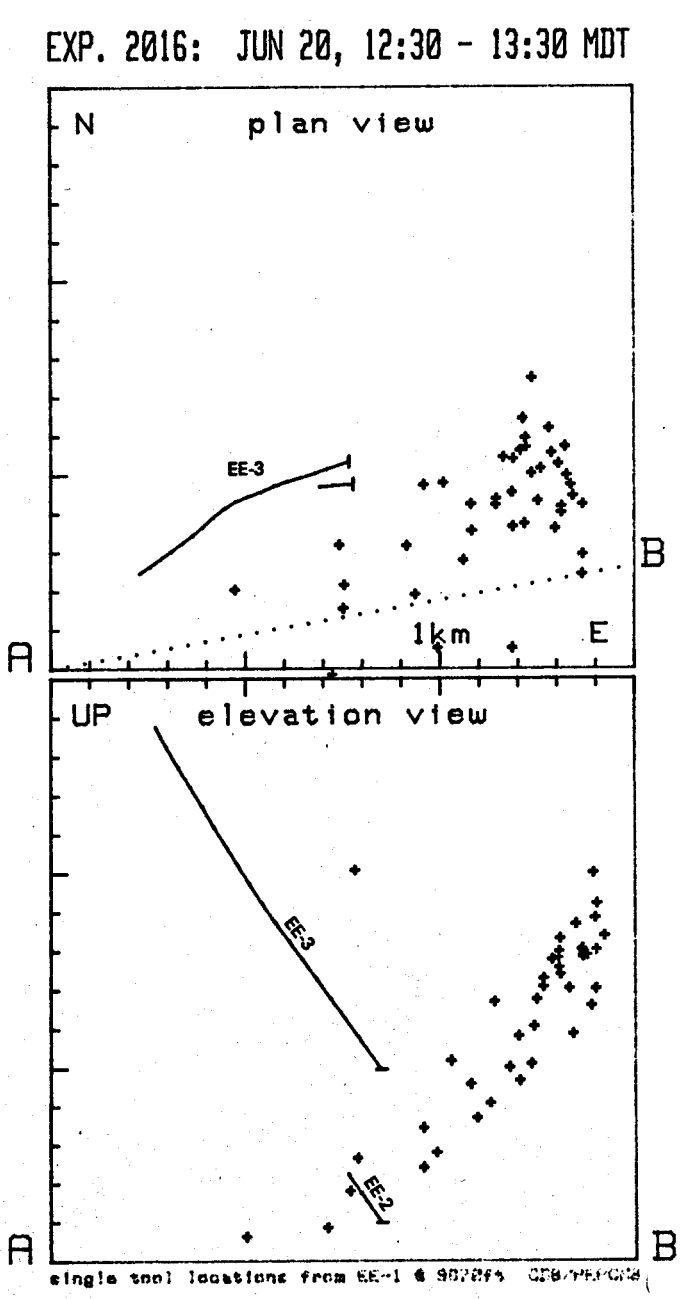

Figure 4. Hypocenters of microseismic events typical of the time between 10:00 and 15:00 when seismicity occurred along a narrow inclined region in the deeper part of the Phase II reservoir.

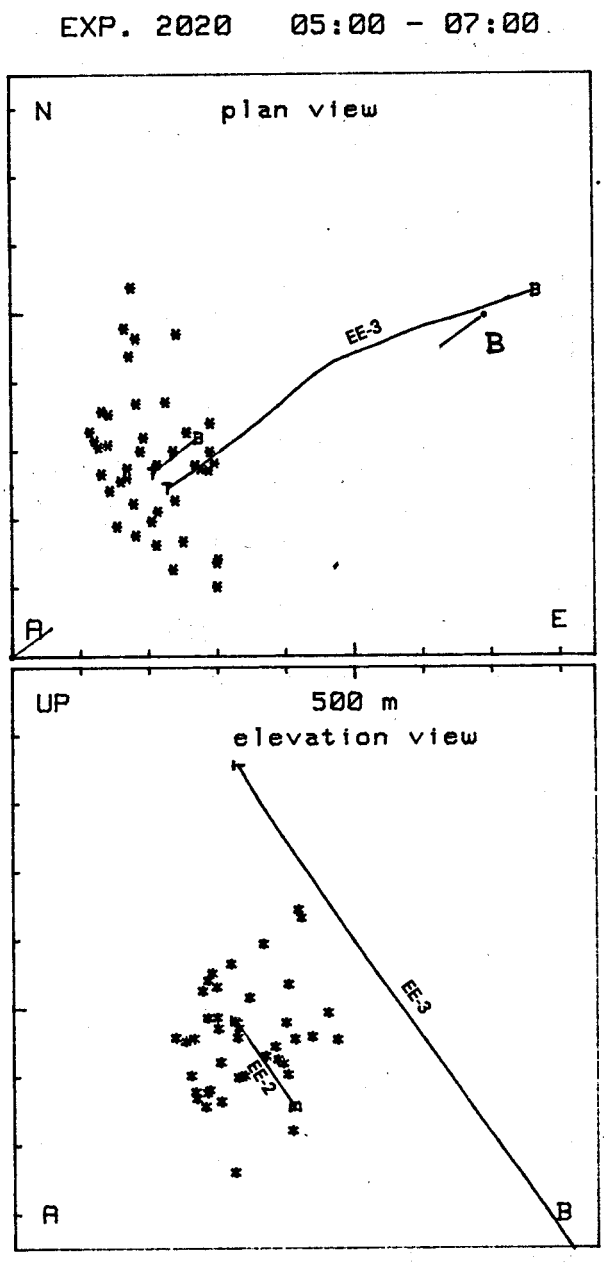

Figure 5. Microseismic event locations during the last two hours of injection into the upper part of the Phase II reservoir.

Proceedings Eighth Workshop Geothermal Reservoir Engineering
Stanford University, Stanford, California, December 1982
SGP-TR-60

HEAT EXTRACTION MODELING OF THE STANFORD HYDROTHERMAL RESERVOIR MODEL

A. Hunsbedt, S. T. Lam, and P. Kruger
Stanford Geothermal Program
Stanford University
and
K. Pruess
Earth Sciences Division
Lawrence Berkeley Laboratory

INTRODUCTION

Long-term commercial development of geothermal resources for electric power production will depend on significant heat extraction from hydrothermal reservoir rock as well as production of hot water. The study of heat extraction in the Stanford Geothermal Program has concentrated on developing a useful model for estimating the potential for heat extraction from fractured hydrothermal reservoirs. The project encompasses a physical model for data acquisition and mathematical models for interpretation of the results.

The physical model consists of a pressure vessel containing a rock matrix simulating a fractured hydrothermal reservoir. Early rock loadings consisted of irregular shape rock fragments of various sizes (Hunsbedt, Kruger, and London 1977, 1978) to develop the production characteristics and a one-dimensional cold-water sweep model. The current rock loading consists of granite rock blocks having regular shape, closer packing of the rocks, and a larger average rock size. Flow conditions in this rock configuration can be varied to obtain a large range of rock-to-water temperature differences. These conditions were designed to test the equivalent rock radius approach used in the one-dimensional sweep model. The experimental data are also used to assist in the development of more sophisticated numerical models of thermal production from hydrothermal reservoirs.

A major parameter in the one-dimensional sweep model is the effective number of heat transfer units, N_{tu}, which indicates the extent of heat extraction from the reservoir rock. Results of the first experiment with the current rock loading at $N_{tu} = 7$ were presented by Swenson and Hunsbedt (1981). Subsequently, two additional heat extraction experiments were performed. One of these was at a higher flowrate to reduce the N_{tu} parameter to 2 and the other was at a lower flowrate to yield a N_{tu} parameter of 15. A fourth experiment was performed to calibrate the heat loss calculation in the mathematical model without fluid injection and production.

This paper summarizes the experimental results and the current mathematical modeling efforts using the one-dimensional sweep model and the LBL numerical reservoir simulator.

HEAT EXTRACTION EXPERIMENTS

The SGP physical model has been described in several reports, e.g., Hunsbedt, Kruger, and London (1977, 1978). The reservoir is a 1.52 m (5 ft) high by 0.61 m (2 ft) diameter insulated pressure vessel. The rock matrix used in these experiments consists of 30 granite rock blocks of 0.19 x 0.19 m (7.5 x 7.5 inches) rectangular cross section and 24 triangular blocks as shown in Figure 1. The blocks are 0.26 m (10.4 inches) high. The average porosity of the matrix is 17.5 percent.

Vertical channels between blocks are spaced at 0.0064 m (0.25 inch) and horizontal channels between layers are spaced at 0.0043 m (0.17 inch). Significant vertical flow can also occur in the relatively large edge channels between the outer rock blocks and the pressure vessel.

Cold water is injected at the bottom of the vessel by a high pressure pump through a flow distribution baffle at the inlet to the rock matrix. System pressure is maintained above saturation by a flow control valve downstream of the vessel outlet. Most of the system pressure drop is in this valve while the rock matrix has essentially infinite permeability.

The water temperature is measured at the several locations shown in Figure 1: the inlet to the vessel, the I-plane just below the baffle, the B-plane half-way up the first rock layer, the M-plane half-way up the third rock layer, the T-plane near the top of the rock matrix, and the vessel outlet. Temperatures are also measured at the center of four rock blocks. The bottom central rock, to be used to examine effects of repeated thermal stressing on heat transfer properties, has two additional thermocouples.

For the three N_{tu} parameter experiments, the rock-water-vessel system was heated to the uniform initial temperatures indicted in Table 1 by electric strap heaters outside the vessel. Heat extraction was initiated by starting the injection pump and opening the flow control valve. The injection rate was constant during the experiments. Data for

the reservoir conditions and parameter values for these experiments are summarized in Table 1.

For the heat loss calibration experiment, the system was heated to a uniform temperature of about 242°C. The vessel isolation valves in the inlet and outlet lines of the vessel were closed during this experiment. Temperature and pressure data were recorded as the system cooled down as a result of heat loss through the vessel insulation and through metal objects protruding from the vessel.

EXPERIMENTAL RESULTS

Measured water and rock temperature data for the three heat extraction experiments are given in Figures 2 to 4. The locations of the measurement planes are indicated in Figure 1. The temperature of the water entering from the distribution baffle below the rock matrix, indicated by thermocouples IW1 and IW2, decreases approximately exponentially from temperature levels near the initial matrix temperature to the injection water temperature indicated by thermocouple 109. The inlet water temperature appears to be relatively uniform in all experiments except for experiment 5-2 (Figure 3). The maximum temperature difference between water entering the rock matrix at the bottom is about 38°C (100°F). This large nonuniformity in entering water temperature is probably caused by the higher heating rate from the steel vessel lower head and flanges when cooled more rapidly by the higher water flowrate.

The water temperature distribution in the other three measurement planes were observed to be quite uniform. The maximum temperature difference or range of water temperature data was usually less than 5°C (9°F). The water temperatures given in the figures for the B-, M-, and T-planes are the averages of all thermocouples in each plane. Since the uncertainty interval of the temperature measurements is estimated to be 3°C (5°F), it is concluded that water temperatures in the various flow channels appears to be virtually uniform, indicating good cross mixing between flow channels.

The effect of water flowrate on rock-to-water temperature differences is also indicated in Figures 2 through 4. The maximum temperature difference developed was about 150°C (270°F) for experiment 5-2 with the highest water flowrate to 28°C (50°F) for experiment 5-3 with the lowest flowrate. The maximum temperature difference occurred in the bottom plane that experiences the highest cooldown.

Although high rock-to-water temperature differences result in higher rates of heat extraction from the rock, insufficient heating of the water may result in premature drop in produced water temperatures for high water flowrates. In that case much of the energy stored in the rock is not utilized. The premature drop in produced water temperature as a function of water flowrate is not clearly illustrated in the experimental results because of the effects of total heat losses from the vessel which are much larger for experiment 5-3, lasting for about 10.5 hr as compared to experiment 5-2, lasting only 1.5 hr. The steady drop in produced water temperature in Figure 4 is caused by greater vessel insulation heat losses to the environment because of the longer time period involved.

Mathematical modeling of the experimental system requires accurate data of this heat loss term as a function of production time. The low flowrate experiments last for longer time periods, and the heat loss term becomes a more important factor in the heat balance equation relative to the rock heat extraction term. Data from the calibration cooldown experiments are expected to reduce the uncertainty in the net heat extraction from the rock matrix. Average water and rock temperatures inside the vessel for the calibration experiment are given in Figure 5. The data are compared to the average water temperature data obtained from an earlier experiment. The agreement between these two experiments is very good, and the difference is probably caused by different volumetric heat capacitances of the two test systems.

Table 1
EXPERIMENTAL DATA AND PARAMETERS

	Heat Extraction Experiment		
	5-1	5-2	5-3
Average Reservoir Pressure (MPa)	3.8	3.8	3.6
Initial Reservoir Temperature (°C)	239	220	220
Final Water Temperature at Top (°C)	156	125	141
Final Water Temperature at Bottom (°C)	19	20	28
Injection Water Temperature (°C)	15	15.6	18.3
Injected Water Mass (kg)	340	341	330
Water Injection Rate (kg/hr)	68	227	31.4
Production Time (hr)	5	1.5	10.5

NUMERICAL MODELING

The results of these heat extraction experiments are being examined with a distributed parameter model (Pruess and Schroeder, 1980). All important processes involved in the thermal sweep model are represented: (1) upflow of water through the void spaces in the vessel, (2) heat conduction in the rocks, (3) heat transfer from the rock blocks to the water, (4) heat transfer between water and the walls of the vessel, (5) heat conduction in the walls, and (6) heat transfer between the walls and the surroundings.

The basic computational mesh is shown in Figure 6, which also indicates the major subdomains to be treated in the modeling effort. The main portion of the mesh is a two-dimensional r-z system, with additional irregularly shaped grid blocks employed to represent the zones at the top and bottom of the vessel, respectively. The interior of the vessel (rock loading and water in the voids) is represented by a one-dimensional column of 30 disk-shaped elements (5 per layer). This column is surrounded by two columns of concentric rings, which represent the vessel wall and the (ambient) boundary conditions, respectively. Each interior element is further sub-partitioned into a one-dimensional string of 4-8 elements, so that heat conduction from the interior of the rock blocks to the surfaces, and subsequent heat transfer to the invading cold water, can be modeled in quantitative detail. The sub-partitioning is based on the method of "multiple interacting continua", or MINC, as developed by Pruess and Narasimhan (1982). Specific details on the mesh generation methodology are described by Pruess and Karasaki (1982).

Calculations were carried out with Lawrence Berkeley Laboratory's geothermal simulators SHAFT79 and MULKOM (Pruess and Schroeder, 1980). These simulators feature an accurate representation of the thermophysical properties of water substance (International Formulation Committee, 1967). Handbook values were used for the thermal parameters of the steel vessel and the rock loading. Figure 2 shows the comparison of the simulated temperature transients with the experimental measurements for run 5-1. The overall agreement is rather good, considering that no adjustments were made in the parameters employed in the simulation. The largest discrepancies occur for the bottom layer (B-plane in Figure 2), and are probably due to too coarse discretization near the cold water inlet. Temperatures in the M-plane agree better, with the simulation predicting a somewhat too broad distribution. The best comparison is obtained near the top (T-plane).

These results are certainly encouraging, and improvements in various details of the model to obtain a better match of the experiments are in progress. These efforts focus on: (1) improving the computational mesh to more faithfully represent the physical model, and (2) checking on the thermal parameters of the system components. The simulation shows that heat transfer from the steel vessel to the injected water is of the same order of magnitude as heat transfer from the rocks. Therefore, heat conduction in the vessel walls and heat loss to the surroundings must be modeled with a high degree of accuracy. Work is in progress to adjust the heat loss term in the numerical model. It is evident from the predictions given in Figure 5 for the cooldown experiment using the present numerical model that model heat losses are greater than actual physical system heat losses. Once the heat loss term has been adjusted the calculations should be sufficiently sensitive to the rock-water heat transfer to allow quantitative testing of the approximations made in the MINC-method.

The heat extraction experiments were also modeled using the one-dimensional cold-water sweep model. The rock geometry in this model is represented by uniform size spheres with an equivalent diameter resulting in heat transfer characteristics that are similar to those of the actual rock configurations (Iregui et al. 1978).

The predicted water temperatures in the three planes are compared to measured temperatures in Figures 2 through 4 for experiments 5-1 through 5-3, respectively. The comparisons show that the predicted temperatures are generally higher than the experimental temperatures during early times but tend to drop more rapidly at later times. In contrast, the distributed numerical model predicted a cooldown which was generally slower than the experimental results during later times.

CONCLUSIONS

Three heat extraction experiments using a known-geometry rock loading and a calibration cooldown experiment for this rock loading yielded a set of useful hydrothermal reservoir production data covering a range of cooldown rates. The one-dimensional sweep model being developed for early use in hydrothermal reservoirs shows good agreement with the experimental data. A numerical model of the experimental system is under development and early predictions indicate reasonable agreement between numerical model output and experimental results. Future efforts will concentrate on improving details of the model particularly those related to experimental system heat loss characteristics. Once completed, a more detailed evaluation of the rock heat transfer process and appropriate simplified modeling approaches for use in the one-dimensional sweep model can be made.

REFERENCES

Hunsbedt, A., P. Kruger, and A. L. London, "Recovery of Energy from Fracture-Stimulated Geothermal Reservoirs," Journal of Petroleum Technology, August 1977.

Hunsbedt, A. , P. Kruger, and A. L. London, "Laboratory Studies of Fluid Production from Artificially Fractured Geothermal Reservoirs," Journal of Petroleum Technology, May 1978.

International Formulation Committee, "A Formulation of the Thermodynamic Properties of Ordinary Water Substance", IFC Secretariat, Dusseldorf, Germany, 1967.

Iregui, R., A. Hunsbedt, P. Kruger, and A. L. London, "Analysis of Heat Transfer and Energy Recovery in Fractured Geothermal Reservoirs", Stanford Geothermal Report SGP-TR-31, June 1978.

Pruess, K. and Karasaki, K., "Proximity Functions for Modeling Fluid and Heat Flow in Reservoirs with Stochastic Fracture Distributions", Proceedings, Eighth Workshop on Geothermal Reservoir Engineering, Stanford University, Stanford, December 1982.

Pruess, K. and Narasimhan, T. N., "A Practical Method for Modeling Fluid and Heat Flow in Fractured Porous Media", Proc. Sixth SPE-Symposium on Reservoir Simulation (paper SPE-10509), New Orleans, 1982.

Pruess, K. and Schroeder, R. D., SHAFT79 User's Manual, LBL-10861, Lawrence Berkeley Laboratory, Berkeley, 1980.

Swenson, Jr., L. W. and A. Hunsbedt, "Experimental and Finite Element Analysis of the Stanford Hydrothermal Reservoir Model", Proceedings, Seventh Workshop Geothermal Engineering, Stanford, December 1981.

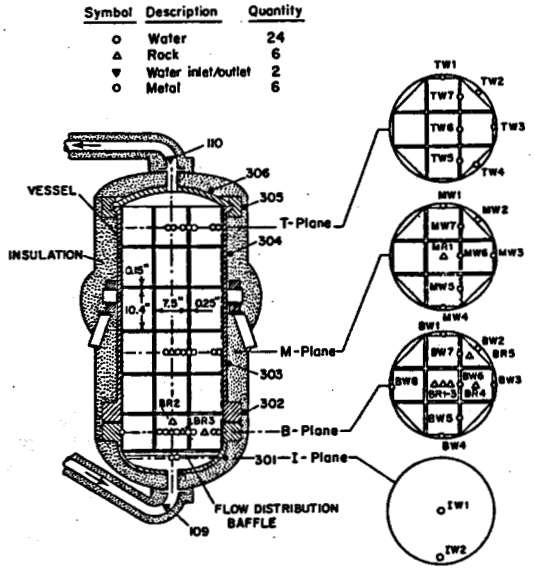

Figure 1. Experimental Rock Matrix Configuration and Thermocouple Locations.

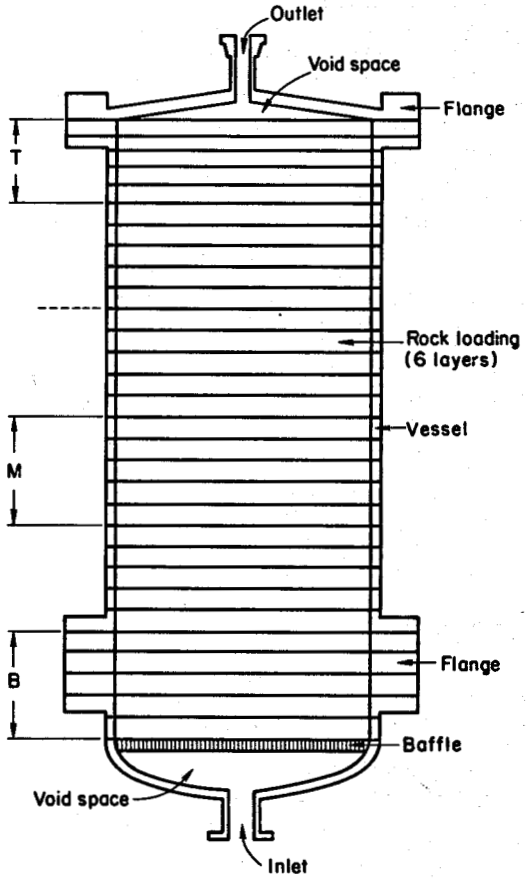

Figure 6. Basic Computational Mesh of the of Experimental System.

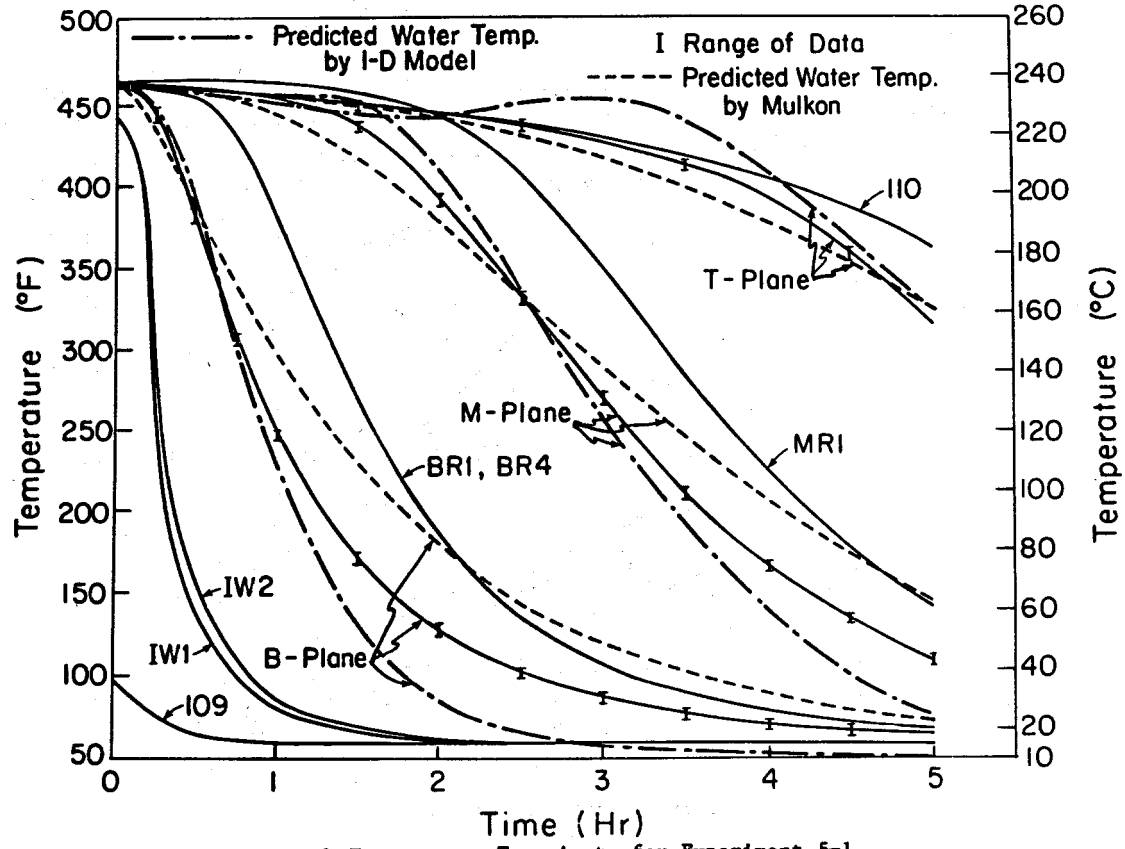

Figure 2. Water and Rock Temperature Transients for Experiment 5-1.

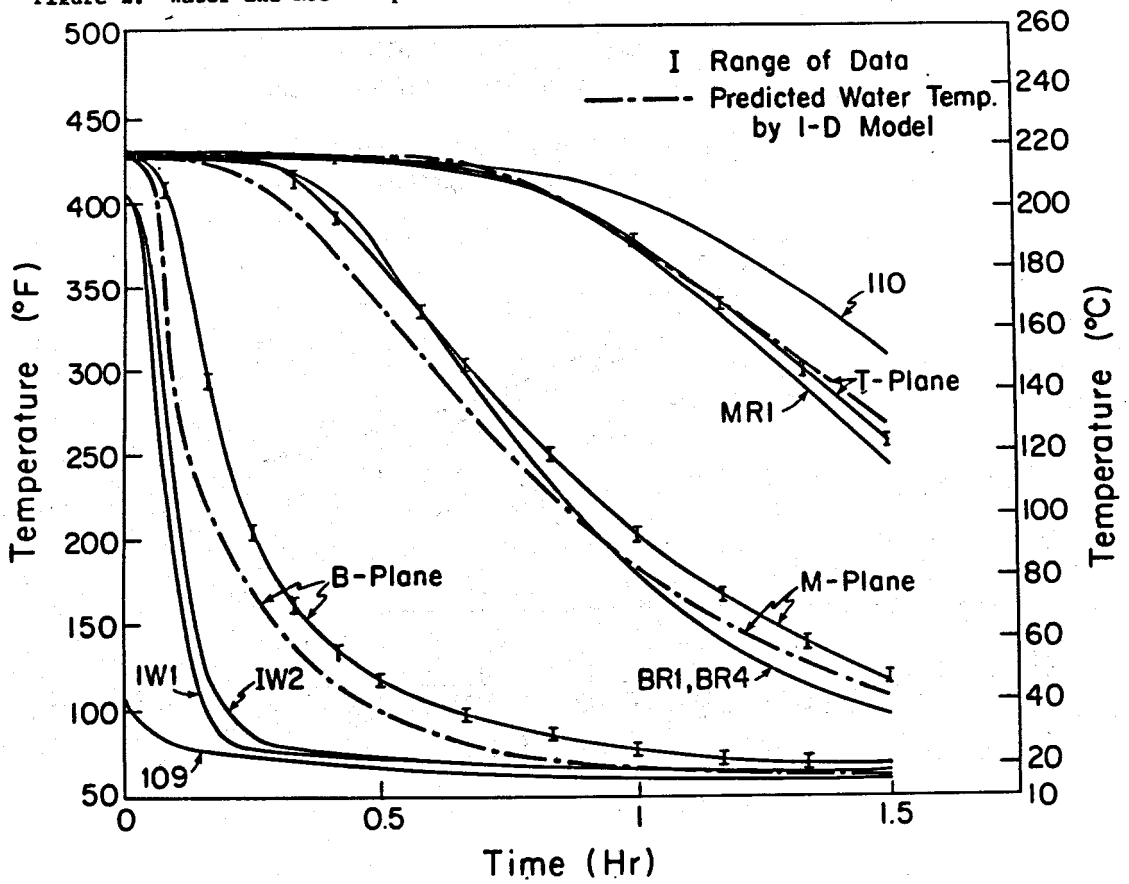

Figure 3. Water and Rock Temperature Transients for Experiment 5-2.

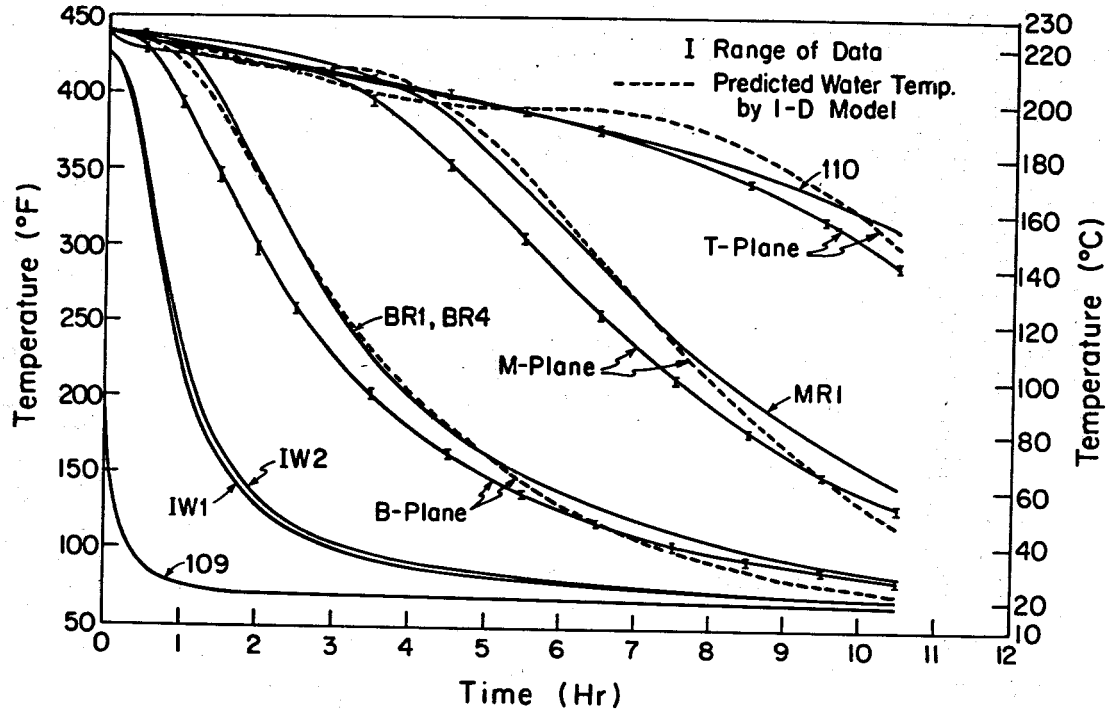

Figure 4. Water and Rock Temperature Transients for Experiment 5-3.

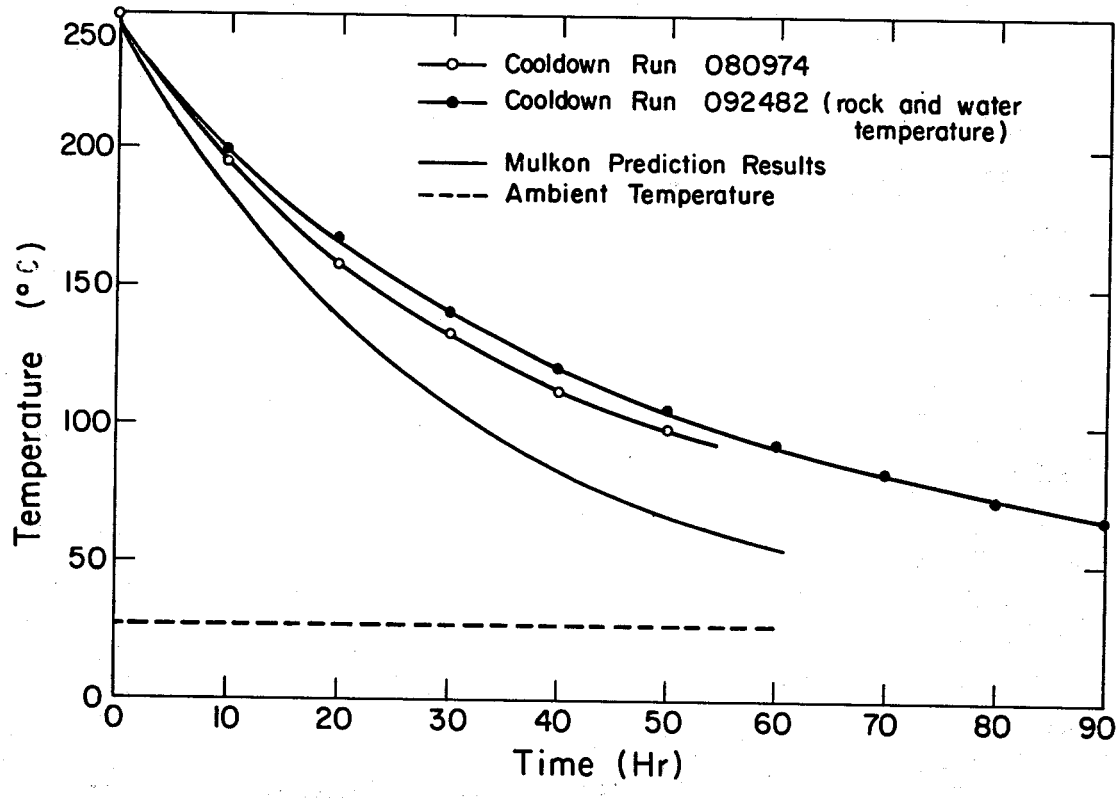

Figure 5. Average Vessel Temperature Transients for Calibration Experiment.

Proceedings Eighth Workshop Geothermal Reservoir Engineering
Stanford University, Stanford, California, December 1982
SGP-TR-60

ANALYSIS OF SWEET LAKE GEOPRESSURED-GEOTHERMAL AQUIFER

M. Andrade, F. Rago, H. Ohkuma
K. Sepehrnoori, E. Peters and M. Dorfman

Department of Petroleum Engineering
The University of Texas
Austin, Texas 78712

ABSTRACT

Geopressured-geothermal aquifers are presumed to contain a large resource of natural gas in solution with the native brine. Whether this resource can be produced economically at the present time depends upon the ability of these reservoirs to produce at high rates for extended periods of time.

The Sweet Lake geopressured-geothermal aquifer, located southeast of Lake Charles, Louisiana, is one such aquifer modeled by a two-dimensional geopressured-geothermal simulator. This aquifer is a sandstone within the Frio formation at depths between 15,000 to 15,640 ft with a net porous thickness of 250 ft, a calculated in-situ permeability (from drawdown data) of 17 md, an estimated porosity of 24 per cent, a uniaxial compaction coefficient of 4.5×10^{-7} psi^{-1} and a solution gas-water ratio of 11 SCF/STB all at the initial reservoir pressure of 12,060 psi. These parameters are typically pressure sensitive in geopressured-geothermal aquifers and are critically important to aquifer performance. Several simulation experiments are conducted which investigate the effects of varying initial values for these parameters with the experimentally determined values as means. The simulations give both optimistic and pessimistic expectations for aquifer performance. The expected life of the geopressured-geothermal well is reported for each simulation.

INTRODUCTION

The Sweet Lake geopressured-geothermal energy prospect is located approximately 25 miles southeast of Lake Charles, Louisiana. The prospective zone is the Miogypsinoides ("Miogyp") sand of the Frio Formation, which is found at depths between 15,000 and 15,640 ft in the test well, MG-T/DOE AMOCO Fee No. 1.

The prospect is a sedimentary basin developed on the north flank of a salt ridge of east-west trend. The south side of the basin is bounded by a major fault down-thrown to the north. This fault converges eastward with another major east-west fault down-thrown to the south to form a graben. There is a small fault in the west, but it is not known whether this fault extends northeastward and bounds the sands. If this fault is considered as the boundary to the west, the reservoir in this graben has an areal dimension of approximately 9 miles by 3.5 miles. Extension of good quality sand is uncertain at this stage. The dip on the top of the sand sequence is about 20° to the northwest.

Eight sand members were recognized in the 640 foot interval, with 250 ft of net sand thickness. A single zone, fifth from the top, was completed for testing with perforation between 15,387 and 15,414 ft (Durrett and Durham, 1981). The initial reservoir pressure was 12,060 psia at the center of perforation at a depth of 15,400 ft, which is about 4,870 psi above a normal reservoir pressure at this depth. The reservoir temperature at the same depth was 299 °F. Core analysis of the sand yielded air permeability of 3.6 darcys, from which permeability to water is estimated as about 400 md, and porosity of 24 percent. The measured salinity of the brine from the zone was 140,000 ppm. The gas-water ratio observed during the production tests averaged 11 SCF/STB. Compared with solution gas of 34.5 SCF/STB estimated for a saturated brine at the afore-mentioned reservoir condition, this sand had a very undersaturated reservoir fluid. The bubble point pressure for 11 SCF/STB at 299 °F is expected to be about 2,600 psia (Gould et al., 1981).

The first part of this report presents the results of an analysis of the well test data observed over a ten month period. Using the reservoir permeability obtained from this analysis together with the other data acquired at the well, reservoir simulation was conducted and the results are presented.

WELL TEST ANALYSIS

The flow test of the MG-T/DOE AMOCO Fee No. 1 well began on July 1, 1981 and continued more than ten months. During this period, the flow rates were varied step-wise, and also the well was intermittently shut-in to observe pressure build-up. More than 300 chronological data points of bottom hole pressures and flow rates acquired from the test were treated by the multirate test analysis technique (Earlougher, 1977). The result is shown in Figure 1. The slope of the straight line, m, of this figure is 0.147 psi/(STB/day cycle). At the initial reservoir condition, the water formation volume factor, B_w, is estimated to be 1.0575 BBL/STB and the viscosity, μ_w, 0.395 cp (Gould et al., 1981). Employing these data and the net sand thickness, H, of 27 ft, the reservoir permeability is

$$K = \frac{162.6\, B_w \mu_w}{m H} = \frac{(162.6)(1.0575)(0.395)}{(0.147)(27)} = 17.1 \text{ md}$$

The laboratory measurements on the cores by Jogi

et al., (1980) showed the uniaxial compaction coefficient of about 4.5×10^{-7} psi^{-1} for the sand at the in-situ stress, which implies the pore compressibility of 1.5×10^{-6} psi^{-1} for 24 percent porosity. Adding these to the water compressibility, the total compressibility, c_t, is estimated as 5.0×10^{-6} psi^{-1}. The well radius, r_w, is 0.229 ft (the well diameter is 5½ inches). With the intercept value of b = 0.17, the skin factor is calculated as

$$s = 1.1513\left\{\frac{b}{m} - \log\left(\frac{K}{\phi\mu_w c_t r_w^2}\right) + 3.2275\right\}$$

$$= 1.1513\left\{\frac{(0.17)}{(0.147)} - \log\left[\frac{(17.1)}{(0.24)(0.395(5\times10^{-6})(0.229)^2}\right] + 3.2275\right\} = -5.13$$

It is suspected that the tested sand zone has communication with other sand layers. The negative skin factor seems to be ascribed to the layer communication and the formation dip (Earlougher, 1977).

No changes in the line slope are apparent in Figure 1, indicating that no permeability barriers exist in the vicinity of the well. Earlier Gould et al., (1981) reported two barriers, one at a distance of 452 ft from the well and the other at 1,753 ft, based on a preliminary three-day drawdown test. The same authors, however, stated that no such barriers were recognized on pressures measured during the second flow test which followed the three-day test and lasted for 17 days. If these permeability barriers exist, the influence of the nearest barrier may have escaped from detection in our analysis, since approximately one data point per day was used, and with 17.1 md the influence is estimated to appear within 2 days. However, the second barrier should have been reflected in Figure 1.

Gould et al., further postulated that the observed barriers would coincide with the major faults, and hence assumed that only a triangular area of 25° to 48° with the well at its apex would contribute to production. Based on the original geologic interpretation, the two major faults are considered to lie about 1 mile away from the well. With the low permeability resulted from our analysis, the radius of investigation will encompass these faults if the well is flowed for more than 40 days. Furthermore, in order for the boundary effects of the faults to be felt as a slope change of a well pressure drawdown curve, it is necessary to continue the drawdown test for over 6 months. None of the intermediate pressure drawdown tests were as long as these numbers suggest. We, therefore, believe that the original fault locations (Hoffman and Durham, 1981) do not need to be altered.

The large discrepancy of the permeability, 343 md and 17.1 md, is evidently due to the above difference of the assumption on drainage area. The air permeability of 3.6 darcys, from which the water permeability of 400 md has been estimated, is likely to be the results from measurements on unstressed cores. According to the experiments on the Sweet Lake sand cores by Jogi et al., (1981), the permeabilities at the in-situ stress fall in the range between 20 and 110 md. Their measurements were conducted at room temperatures. It is known that sandstone permeability to water substantially decreases when temperature increases (Weinbrandt et al., 1975; Casse and Ramey, 1976). Consequently, 17.1 md appears to be a reasonable estimate for the Sweet Lake reservoir permeability. The observed steep pressure drawdown is considered to have been caused by this low permeability rather than a restricted drainage area.

PARAMETRIC RESERVOIR STUDY

A parametric sensitivity study was initiated in order to define both pessimistic and optimistic aquifer behavior. Our perspective is that the aquifer extends over an area of 17,280 acres (27 mi^2) and is bounded as originally interpreted via seismic and geologic control and that the uncertainties in aquifer behavior result from sparse aquifer data. The present knowledge of this aquifer consists of that data gathered at the location of the MG-T/DOE AMOCO Fee No. 1 well. The initial aquifer pressure (12,060 psia) and initial aquifer temperature (299 °F) at this location when coupled with the geologic structure are sufficient to accurately predict these parameters at other locations in the aquifer, however, measured values for salinity (140,000 ppm), solution gas-water ratio (11 SCF/STB), uniaxial compaction (4.5×10^{-7} psi^{-1}), porosity (24 percent) and absolute permeability (17.1 md) at the well site are not sufficient to predict these parameters at other aquifer locations. Via a parametric study one can obtain the sensitivity of expected well performance to changes in these parameters and thus determine the economic viability of the prospect when faced with a very limited data base.

The focus of the study is the effect that uncertainties in gas-water ratios, porosity, uniaxial compaction and permeability have on the gas production rate at the wellhead. The criteria for comparison is the time that it takes for the gas production rate to decline to 200 MCF/day, which is assumed to be the economic limit for the well completed in the Sweet Lake geopressured aquifer. Here we make the very simplified assumption that if a well will payout before the economic limit is reached then the well may be profitable to drill.

The Aquifer Model. The simulator which was used in this study is a 2-D finite difference simulator specifically designed to solve the mass balance equations for 2-phase, isothermal flow in compacting porous media. Fluid properties (B_w, R_s, μ_w, B_g, μ_g), where the subscripts w and g indicate water phase and gas phase, are treated as functions of pressure at the initial aquifer temperature (Table 1). The water formation volume factor and viscosity in Table 1, both after Gould et al., (1981), are those for the undersaturated water. The gas properties are estimated assuming pure methane. Rock properties (K and ϕ) are likewise treated as functions of pressure. Relative permeability data and capillary

pressure data were not available for the MG-T/DOE AMOCO Fee No. 1 well and experimental data from another geopressured prospect, the Pleasant Bayou field in Brazoria County, Texas, was used (Table 2).

The aquifer was discretized into a 13 x 13 areal point-distributed grid containing 169 blocks each 140 acres in size. The aquifer geometry was duplicated by placing faults in the blocks as indicated by the geological interpretation. The entire Miogyp sand sequence was perforated containing 250 ft of porous sand. In effect we assume that the data obtained from the fifth sand member would be representative of all sand members in the sequence. Each simulation was continued for a period of 10 years. The initial water flow rate, Q_w, is 40,000 STB/day. The aquifer is presumed able to maintain the constant flow rate well condition until the BHP reaches 7,000 psia. At such time the simulator maintains a constant BHP well condition with corresponding declining flow rates.

Effect of Solution Gas on Aquifer Performance. The first study was to determine the effect of variable solution gas-water ratio on the economic life of the well. In these runs the aquifer was presumed homogeneous with K = 17.1 md, ϕ = .24 and $c_m = 4.5 \times 10^{-7}$ psi^{-1}. The data for B_w and μ_w were not altered from those for the undersaturated water shown in Table 1. The solution gas-water ratio was the only variable in these runs.

Log analyses reveal that not all members of the Myogyp sequence yield the same calculated salinity. As was the case in the Pleasant Bayou prospect (Kharaka et al., 1979), water salinity may greatly alter over the areal extent of the Sweet Lake reservoir. Since water can dissolve more gas as its salinity decreases, the suggested salinity variation implies heterogeneity in gas solubility, both vertically and areally. Moreover, gas availability over the geological time span might have varied from place to place, depending on local geologic environments. Therefore, although the brine of the fifth sand at the MG-T/DOE AMOCO Fee No. 1 well is very undersaturated, brines of other sand members and/or those at other locations may contain more hydrocarbon gas. For these reasons, this parameter was included in the investigation.

The available measured data yields 11 SCF/STB for the fifth Miogyp sand member. A saturated brine at the initial conditions would contain dissolved gas in the ratio of 34.5 SCF/STB. We assume that the cummulative effect of production from the Miogyp sequence will display a R_s between these limits. Figure 2 depicts the relative importance of R_s on well performance. The top curve is the case for R_s = 34.5 SCF/STB and the bottom curve is that for R_s = 11 SCF/STB. The reservoir, whether it is saturated or undersaturated, can sustain the desired water rate no more than a month. The well, therefore, produces at declining rates with the bottom hole pressure maintained at 7,000 psi. Figure 2 illustrates this feature. The results are obvious: if R_s approaches 34.5 SCF/STB the well will have an economic life of over 50 years, however with R_s = 11 SCF/STB the economic life of the well will only slightly exceed 10 years.

Viewing the results of these runs as bounds of expected performance, it is clear that the economic life of the well is a strong function of the solution gas-water ratio. This result is not unexpected but does serve to define the minimal life of the well (10 years) when considering R_s as the only variable. We choose the value R_s = 11 SCF/STB as the base case for subsequent simulations and examine the effect that uncertainties in ϕ, c_m, and K will have on the now established minimal time scale of production.

Effects of Porosity Changes. A set of 4 simulations were run to examine the effect that porosity changes have on the established 10 year life of the well. For these simulations R_s = 11 SCF/STB, K = 17.1 md and ϕ took on values of .15, .20, .24 and .30. Porosity was the only variable in these runs. The results are presented in Figure 3. These indicate that if the aquifer behaves as if the effective porosity were .15 the economic limit would be reached in 9 years whereas if the aquifer responds as if the effective porosity were .30 the economic life would extend to 11.25 years. We conclude that the economic life of the well is very slightly affected by large changes in porosity and do not believe that uncertainties in porosity distributions will be critical to the Sweet Lake prospect. It is also pointed out that these simulations reveal that as the economic limit is raised the effect of porosity uncertainty becomes less on the economic life of the well.

Effects of Changes in Uniaxial Compaction. Three simulations were run to examine the effect that uncertainty in uniaxial compaction will have on aquifer performance. Since sedimentary rocks are generally more elastic at higher temperatures, the reported value of c_m resulted from the measurements at room temperatures was regarded as the minimum. For these runs R_s = 11 SCF/STB, K = 17.1 md, ϕ = .24 and c_m was given values of 4.5×10^{-7} psi^{-1}, 9.0×10^{-7} psi^{-1} and 18×10^{-7} psi^{-1}. c_m was the only variable in these runs. The results are presented in Figure 4. For $c_m = 9 \times 10^{-7}$ psi^{-1} the economic limit is reached in 14 years while for $c_m = 18 \times 10^{-7}$ psi^{-1} the limit is reached in 18 years. The base case of $c_m = 4.5 \times 10^{-7}$ psi^{-1} yields a life of 10 years. At the economic limit of 200 MCF/day uncertainties in c_m of 1×10^{-7} psi^{-1} yield changes in the life of the well of 1.6 years. These deviations become less significant as the economic limit is raised.

Effects of Changes in Permeability. With the exception of the solution gas-water ratio, this study indicates that permeability is the most important parameter which influences the economic viability of the well. Five simulations were conducted to examine the effect of changes in this parameter. For these runs R_s = 11 SCF/STB, ϕ = .24, $c_m = 4.5 \times 10^{-7}$ psi^{-1} and K varied as 17.1 md, 30 md, 50 md, 100 md and 200 md. Permeability was the only variable in these simulations.

Figure 5 is a plot of BHP vs. Time for these runs.

The bottom curve of this figure is the case for K = 17.1 md and corresponds to the Gas Rate vs. Time curves that are presented in Figures 2, 3 and 4. It is obvious from Figures 2, 3 and 4 that the gas rate begins an almost immediate decline. With K = 17.1 md and H = 250 ft, 40,000 STB/day is above the well's capacity to produce so the well always produces with a constant BHP well condition as observed by inspection of the bottom curve in Figure 5.

Figure 6 shows Gas Production Rate vs. Time for these simulations. Comparing Figures 5 and 6 it is observed that as the well produces at a constant Q_w the pressure at the well declines and when the well produces at a constant BHP condition the flow rate declines. These results are also not unexpected and are only presented for continuity.

Figure 6, Gas Rate vs. Time, demonstates the effect that changes in K have on the economic life of the well. As before the base case with K = 17.1 md gives a life of 10 years. For K = 30 md the life of the well is increased to 12 years and when K = 50 md the life is 13 years. We conclude that uncertainties in the permeability do not significantly alter the time scale of production from 10 years established earlier for the base case. The significance of the permeability is in the prolonged period of constant water rate production, which greatly improves cumulative gas recovery.

To investigate the impact on the saturated reservoir, similar runs were repeated with the R_s data shown in Table 1. Figure 7 presents Water Production Rate vs. Time for these simulations. The corresponding gas production behaviors are exhibited in Figure 8. Figure 8 demonstrates that production below the bubble point results in increasing free gas saturation with resulting increased relative gas permeability which gives rise to the positive slope as observed. Comparing Figures 7 and 8, the point at which the slope breaks can be seen to coincide with the well production strategy change from a constant flow rate well condition to a constant BHP well condition. (We assumed zero critical gas saturation.) For the saturated aquifer the effects of uncertainties in absolute permeability are more profound due to the free gas phase flow.

Figure 9 presents the results of a simulation designed to investigate the effects of locating a well in a "high permeability spot". For this run we again consider the undersaturated aquifer with R_s = 11 SCF/STB, ϕ = .24 and c_m = 4.5×10^{-7} psi^{-1}. We plot 3 cases; the first is the homogeneous aquifer with K = 17.1 md (our usual base case), the second is a homogeneous aquifer with K = 200 md, and the third is a heterogeneous aquifer in which the well has been placed in a 140 acre section of 200 md permeability while the remaining field acreage has a permeability of only 17.1 md. The effect on economic life is not significant. What is significant, however, is that for high initial rates of recovery (short payout time) a well in a high permeability region of an otherwise low permeability aquifer is economically equivalent to a well in a homogeneous aquifer of the same high permeability. This result suggests that the artificial fracturing of a reservoir, whereby a narrow lenticular permeability "high spot" is created in a low permeability reservoir, will increase the initial rate of recovery to bring the sub-marginal reserves into the marginal category. Alternatively, though the present well may not be productive enough, economical production from the Sweet Lake prospect will be possible from another well located in a high permeability spot, if such spots can be delineated.

Effects of Permeability Barriers. As a final consideration of the parametric sensitivity analysis a study was conducted to determine the influence of faulting on aquifer behavior. For threse runs R_s = SCF/STB, ϕ = .24, c_m = 4.5×10^{-7} psi^{-1} and K = 17.1 md. We considered 3 cases: the first is our base case with no faulting, the second assumed a continuous fault (K_F = 10^{-3} md) located to the west of the well so as to bisect the aquifer, and the third assumes a similar fault except it has a narrow opening (about 1,500 ft long) that communicates the divided two regions. The results are presented in Figure 10.

We also ran the continuous fault cases in which the leakiness of a fault, K_F, was further reduced. The results were identical to the second case. Therefore, the distant region separated by the fault remained undisturbed in these cases, and the effective drainage area available to the well was decreased to one-half of the base case of no faults. The influence of such faults is very critical, as the well life of 10 years of the base case is shortened to merely 5.5 years. As seen in Figure 10, the narrow communication opening improves the well behavior only slightly.

Recall that if economical, the well will produce at declining rates maintaining the minimum pressure. Therefore, distant faults are detectable only from steeper declines of the gas (or water) rates. If faults are as far as assumed in this study, Figure 10 dipicts that it would take more than half-a-year for their influence to be observed at a well.

CONCLUSION

The results of this study indicate that permeability-thickness and solution gas-water ratio are critical parameters when estimating the economic viability of a geopressured aquifer. The solution gas-water ratio appears to control the economic life of the well and the permeability-thickness controls the rate of recovery.

The permeability of the fifth member of the Miogyp sand sequence is determined to be on the order of 17 md. This value differs significantly from the expected permeability of 400 md but it is supported by the excessive pressure drawdown observed in testing of the MG-T/DOE AMOCO Fee No. 1 well. Further, the measured solution gas-water ratio is 11 SCF/STB and is less than anticipated. This ratio establishes the economic life of the well at close to 10 years. The low permeability limits the capacity of the well to water rates below the design of 40,000 STB/day if this permeability is representative of the entire interval. The rate of recovery may not be

sufficient to payout this well before the economic limit is reached and thus these reserves are believed to be sub-marginal at present gas values.

However, gas production from the Sweet Lake geopressured aquifer may be upgraded to a marginal category, if an extensive fracture system can be created at the existing well or if another well is drilled by delineating a high permeability spot.

ACKNOWLEDGEMENT

The authors gratefully acknowledge support of this work by the Department of Energy, Contract DE-AC08-79ET27112.

REFERENCES

Casse, F. J, and Ramey, H. J., Jr. (1976) "The Effect of Temperature and Confining Pressure on Single Phase Flow in Consolidated Rocks," presented at the 46th Annual California Regional Meeting of SPE-AIME, Long Beach, California, SPE Paper No. 5877.

Durrett, L. R., and Durham, C. O., Jr. (1981) "Geopressured-Geothermal Testing Plan: MG-T/DOE AMOCO Fee No. 1 Well, Sweet Lake Prospect, Cameron Parish, Louisiana," MAGMA Gulf-Technadril/Department of Energy.

Earlougher, R. C., Jr. (1977) "Advances in Well Test Analysis," SPE of AIME.

Gould, T. L., Kenner, C. B., and Clark, J. D. (1981) "Reservoir Engineering and Computer Model Analysis of Flow Tests on the Miogypsinoides Sandstone: Sweet Lake Geothermal-Geopressured Prospect," Proc. of the 5-th Conference on Geopressured-Geothermal Energy in U. S. Gulf Coast, October 13-15, 1981, LSU, Baton Rouge.

Hoffman, K. S., and Durham, C. O. Jr. (1981) "Geology of the Sweet Lake Prospect, Cameron Parish, Louisiana - An Update," Proc. of the 5-th Conference on Geopressured-Geothermal Energy in U. S. Gulf Coast, October 13-15, 1981, LSU, Baton Rouge.

Jogi, P. N., Kalra, S., Gray, K. E., and Thompson, T. W. (1981) "Compaction Measurements on the Sweet Lake Test Well," Proc. of the 5-th Conference on Geopressured-Geothermal Energy in U. S. Gulf Coast, October 13-15, 1981, LSU, Baton Rouge.

Kharaka, Y. K., Lico, M. S., Wright, V. A., and Carothers, W. W. (1979) "Geochemistry of Formation Waters from Pleasant Bayou No. 2 Well and Adjacent Areas in Coastal Texas," Proc. of the 4-th United States Gulf Coast Geopressured-Geothermal Energy Conference, October 29-31, 1979, The University of Texas, Austin.

Weinbrandt, R. M., Ramey, H. J., Jr., and Casse, F. J. (1975) "The Effect of Temperature on Relative and Absolute Permeability of Sandstones," SPEJ, 376-384.

Table 1

Fluid Properties

P psia	B_w BBL/STB	R_s SCF/STB	μ_w cp	B_g BBL/mcf	μ_g cp
5000.	1.0700	18.500	.3700	.819	.02170
5500.	1.0698	21.000	.3710	.765	.02250
6000.	1.0695	21.500	.3720	.717	.02300
6500.	1.0685	23.500	.3725	.674	.02400
7000.	1.0680	24.000	.3750	.637	.02550
7500.	1.0670	25.000	.3765	.615	.02650
8000.	1.0660	26.500	.3780	.588	.02730
8500.	1.0650	27.000	.3800	.567	.02820
9000.	1.0630	29.000	.3835	.548	.02900
9500.	1.0625	30.500	.3850	.532	.03000
10000.	1.0618	31.500	.3860	.517	.03100
10500.	1.0600	33.000	.3880	.500	.03300
11000.	1.0590	34.000	.3900	.494	.03520
11500.	1.0580	35.500	.3920	.482	.03600
12000.	1.0575	37.000	.3950	.475	.03750
12500.	1.0570	38.000	.3970	.467	.03880
13000.	1.0560	39.500	.3990	.456	.03900
13500.	1.0555	40.500	.4050	.451	.03910
14000.	1.0470	41.500	.4200	.443	.03920

Table 2

Capillary Pressure and Relative Permeabilities

S_w	P_c	k_{rw}	k_{rg}
frac	psi	frac	frac
1.0	3.20	1.00000	0.0000
0.959	9.25	0.56400	0.0360
0.935	12.27	0.41500	0.0630
0.911	15.20	0.32200	0.1220
0.880	17.72	0.24900	0.2280
0.848	21.35	0.16400	0.3300
0.820	24.98	0.10600	0.4420
0.802	27.39	0.08400	0.5590
0.788	29.82	0.07800	0.6870
0.764	31.76	0.06100	0.8170
0.719	37.21	0.03500	0.9150

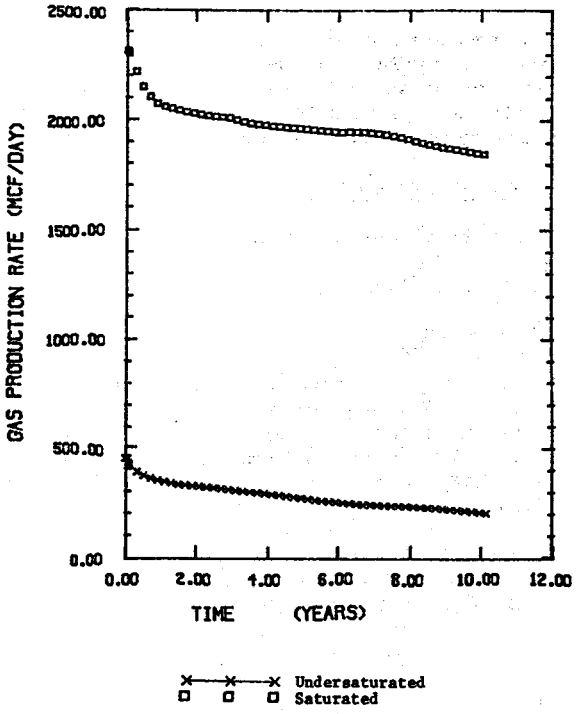

Figure 2. Gas production from reservoirs containing brines saturated and undersaturated with gas.

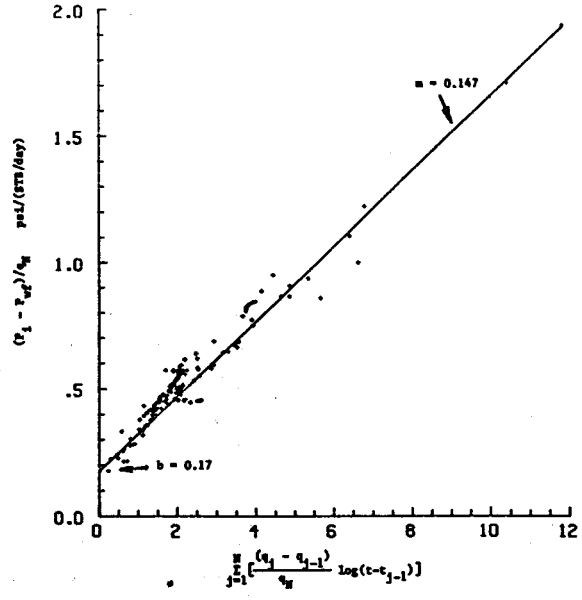

Figure 1. Multirate drawdown test analysis.

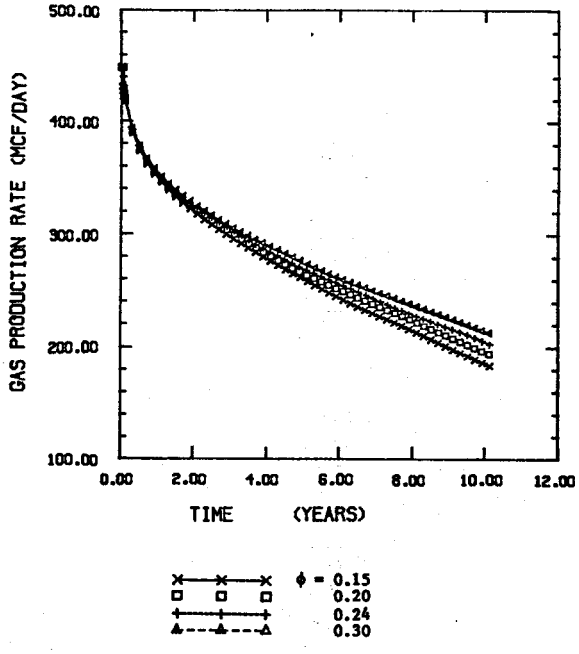

Figure 3. Effects of porosity level on gas production.

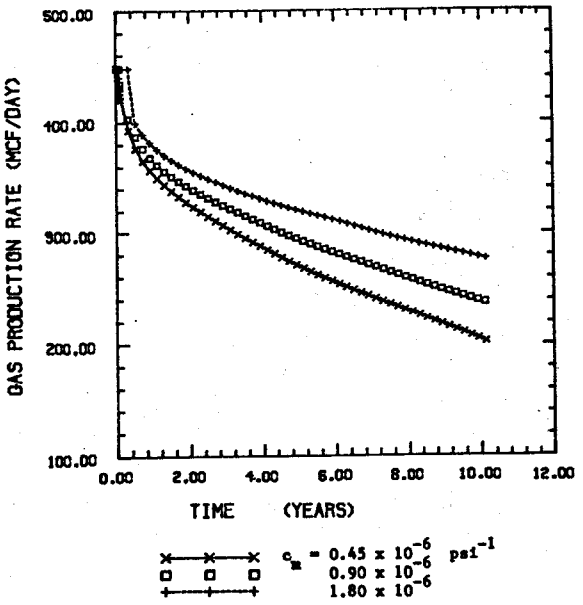

Figure 4. Effects of compaction coefficient on gas production.

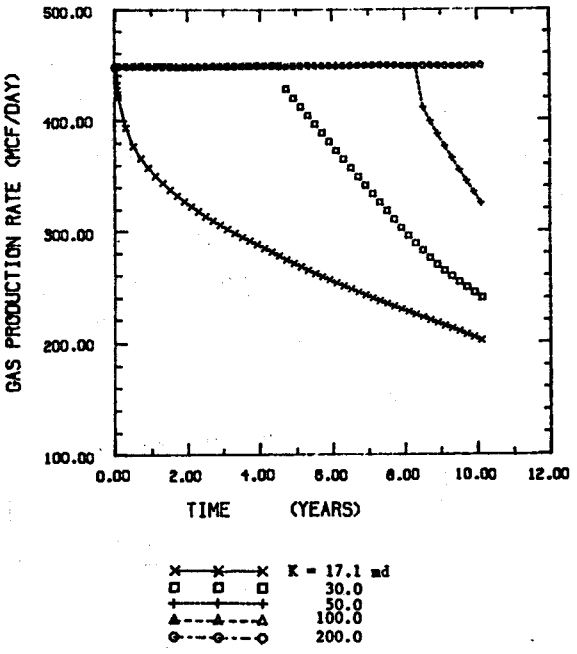

Figure 6. Influence of reservoir permeability on gas production from undersaturated reservoirs.

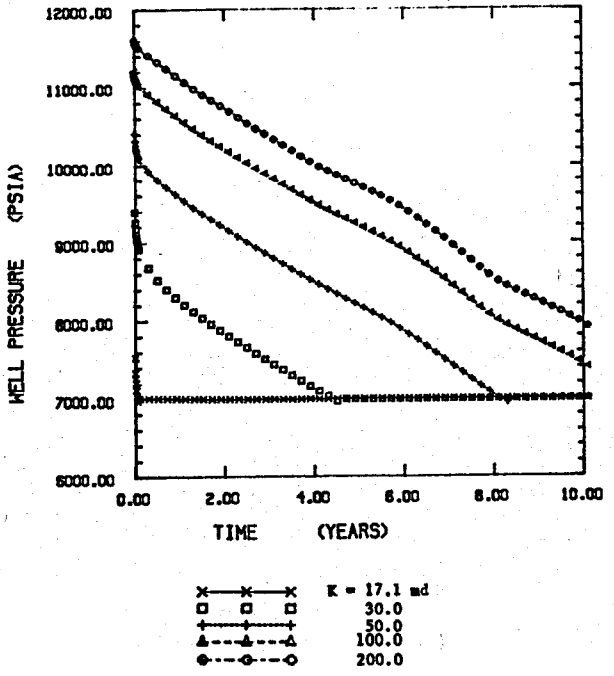

Figure 5. Influence of reservoir permeability level on well pressure performance.

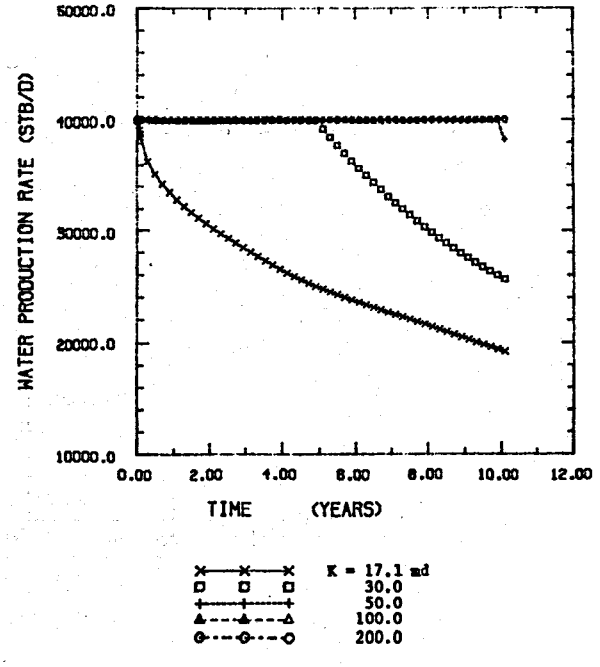

Figure 7. Influence of reservoir permeability level on water production from saturated reservoirs.

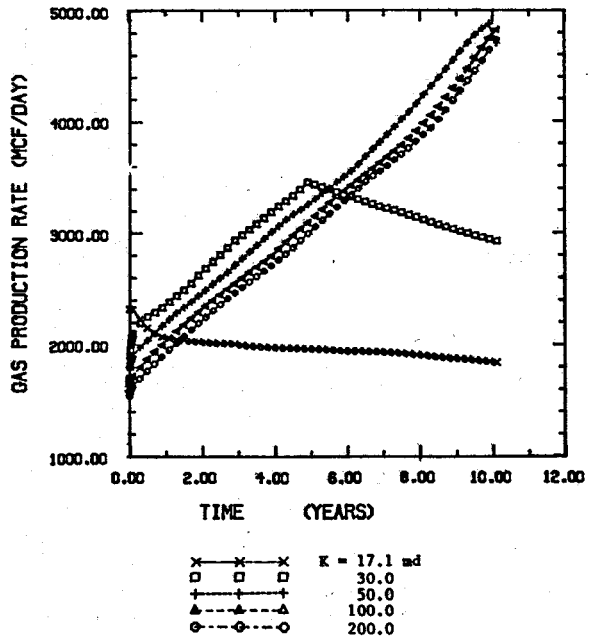

Figure 8. Influence of reservoir permeability level on gas production from saturated reservoirs.

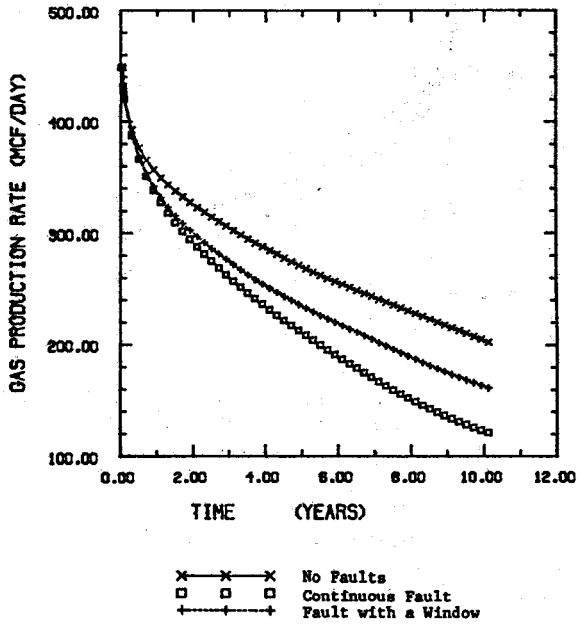

Figure 10. Effects of minor faults on gas production.

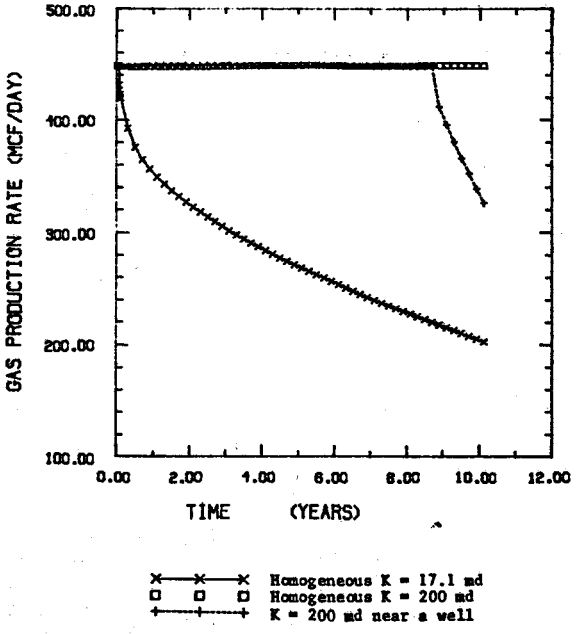

Figure 9. Improvement of gas production due to high permeability near a well.

Proceedings Eighth Workshop Geothermal Reservoir Engineering
Stanford University, Stanford, California, December 1982
SGP-TR-60

PROBLEMS ASSOCIATED WITH APPLICATION OF A WELLBORE HEAT TRANSMISSION COMPUTER CODE

Zora V. Dash and George A. Zyvoloski

ESS-4, Los Alamos National Laboratory
Los Alamos, New Mexico 87545

ABSTRACT

An analysis of the discrepancies between actual temperature surveys and results obtained from a wellbore heat transmission computer code are presented for recent workover operations in well EE-2 at the Fenton Hill Hot Dry Rock Geothermal site. Several sources of error in modeling the thermal behavior of wellbores are considered. These are errors in the estimation of in-situ properties, particularly thermal conductivity, the failure to include frictional heating effects when high flow rates are involved, and error in reporting the flow rate history. These errors were also found to have a cumulative effect. A sensitivity analysis of the computed results to each error type is presented for countercurrent flow. It is concluded that all the errors considered can cause temperature discrepancies between measured and computed temperature. Wellbore codes should have provisions for variable thermal properties and frictional heating. In addition, modeling efforts should be coordinated with periodic temperature surveys so cumulative errors can be minimized.

INTRODUCTION

During recent workover operation in the EE-2 wellbore at the Fenton Hill Hot Dry Rock site a wellbore heat transmission computer code (WBHT) was used to simulate downhole temperatures. Downhole temperature predictions were desired for planning of operations involving temperature limited equipment. Such operations included commercial logging for wellbore characterization, use of packers with temperature sensitive elements in fracturing attempts and the cementing of liners.

Operations over approximately a one month period, April 21 to May 15, 1982 were modeled. Figures 1 and 2 show the flow rate schedule (half hour averages) and the computed bottom hole (≈15150 ft) and casing shoe (≈11580 ft) temperatures. Periodic temperature logs showed a deteriorating match with time between the measured and computed values. The maximum temperature difference was about 15°C after 25 days. This caused some concern on the codes ability to model the operation and prompted the investigation of possible sources of error. Figures 3 and 4 show computed and measured wellbore temperatures for April 27 and May 3. An additional log from May 10 is used in the section on error analysis.

DESCRIPTION OF THE COMPUTER CODE

The Los Alamos wellbore heat transfer modeling code, WBHT, was designed for modeling the flow of compressed liquid in either uniaxial or countercurrent flow conditions. The equations which are solved describe the convective heat transport in the wellbore and annulus and the heat conduction in the rock matrix. These equations may be written for the wellbore:

$$\frac{\partial(\rho_w u_w)}{\partial t} + \dot{q}\frac{\partial(\rho_w h_w)}{\partial z} + Q_{r-w} = 0$$

and for the rock:

$$\rho_r C_r \frac{\partial T}{\partial t} + \frac{\partial}{\partial z}\left(k\frac{\partial T}{\partial z}\right) + \frac{1}{r}\frac{\partial}{\partial r}\left(k_r\frac{\partial T}{\partial r}\right) + Q_{w-r} = 0$$

Here T is the temperature, h is the enthalphy, k is the thermal conductivity, m is the mass flow rate, ρ is the density and w and r refer to the water and rock respectively. These equations are augmented by appropriate initial and boundary conditions. The equations are discretized using finite differences then a block iterative method is used to solve the resulting algebraic equations.

The code has been verified against published radial heat flow solutions (Carslaw and Jaeger, 1957) and very good numerical accuracy was achieved with a 400 node grid. Table 1 shows the input data used in the computer program.

SOURCES OF ERROR

In this study three sources of possible error are considered. The inaccurate reporting of wellhead data, failure to account for temperature dependent physical properties, and heating effects due to pressure drop in the pipe. These effects will be discussed and WBHT code runs with and without corrections will be compared to the temperature survey of

TABLE 1
Parameters for Wellbore Model

Parameter	Value
Rock Density (ρ_r)	2500 kg/m^3
Rock Specific Heat (C_r)	1000 J/kg°C
Radial Extent	40 m
Depth Along Wellbore	4660 m
True Vertical Depth	4396m
Nodes in r direction	10
Nodes in z direction	40
Flow rate	variable
Initial Temperature Distribution [T(°C), z - Depth along wellbore (m)]	$T = 15.3 + .093\ z$ for $z \leq 747$ m $T = 60.7 + .0289\ z + 5.67\ (10^{-6})\ z^2$ for $z > 747$ m

May 10. The effects of spatial differencing will not be discussed.

In the complicated workover operations modeled in this study, there were several instances where inaccurate wellhead information made a significant difference in the calculated downhole temperature. In the case at hand, it was estimated that flow rates may have been as low as 80% of the previously reported values. Figure 5 shows the effect of modeling operations with a reduced flow rate. The computed results are improved a little.

The physical properties which affect the transient thermal behavior of the wellbore and rock system are the density of water and the thermal conductivitity of the rock. The effects of rock permeability and porosity are negligible because the wellbores are located in granite which has extremely small values of these properties. The importance of correctly accounting for changes in water density with temperature and pressure had been recognized from the codes' inception and an appropriate density function was obtained from steam table data. The thermal conductivity of granite varies about 25% from 40°C to 300°C (Sibbet et al, 1978). Originally the code provided for spacially dependent thermal conductivity but was later programmed to account for the temperature dependence given below:

$$K = 2.9\ (1. - \frac{T}{900}) \quad \frac{W}{m°C}$$

The effect of the temperature dependent thermal conductivity on modeling is seen in Figure 6. It is disappointing that the match is poorer with the temperature dependent thermal conductivity included, though it does follow the measured flat temperature trend at the bottom of the well better than the other model.

The effects of pressure heating are usually negligible. However for circulating flow rates of 10-15 BPM though a drillpipe and wellbore can cause significant wellbore heating effects. In the original version of the computer code, the pressure heating effects were ignored; after adding the enthalpy transport terms which include the effects of pressure drop, calculated downhole temperatures during flow periods increased 20°C.

Figure 7 shows a match to the May 10th temperature log with and without the effects of frictional heating included. It is evident that the inclusion of the frictional heating produces a better match (except very near the bottom of the hole). Finally, Figure 8, shows a match of the May 10th temperature survey when the WBHT code was run including both temperature dependent thermal conductivity and frictional effects. As can be seen this improves the match and reduces the overheating effect near the bottom.

CONCLUSIONS

Errors caused in wellbore modeling by improper input data, temperature dependent thermal conductivity and frictional heating accounted for only a portion of the differences observed between temperature surveys and computed values. Other sources of errors could include the presence of fractures around the wellbore which would negate the assumption of radial flow. Overall, however, the WBHT code proves to be a useful tool, predicting temperature within ± 12°C. This could be improved by using the periodic temperature surveys to update input data and minimize cumulative effects.

REFERENCES

Carslaw, H.S. and Jaeger, J.C. (1957), Conduction of Heat in Solids, Oxford University Press, pp. 342-344.

Sibbet, J.G., Dodson, J.G. and Tester, J.W. (1978), "Thermal Conductivity of Rocks Associated with Energy Extraction from Hot Dry Rock Geothermal Systems", Thermal Conductivity, v. 15, pp 399-421.

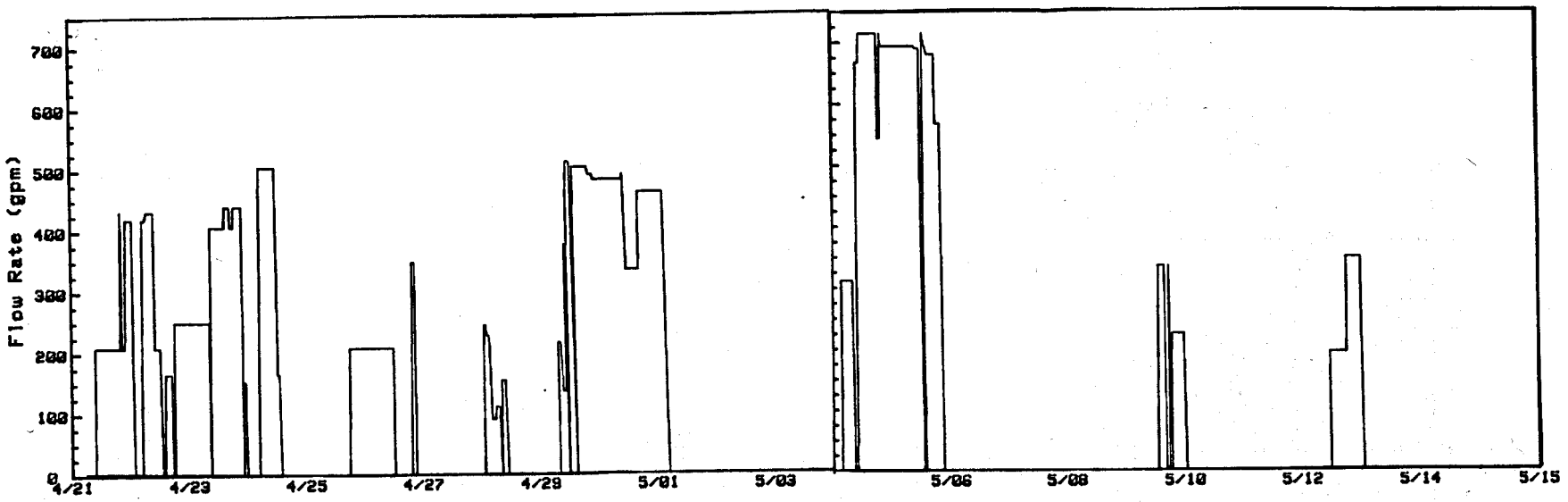

Figure 1. Flow rate history for April 21 through May 15, 1982.

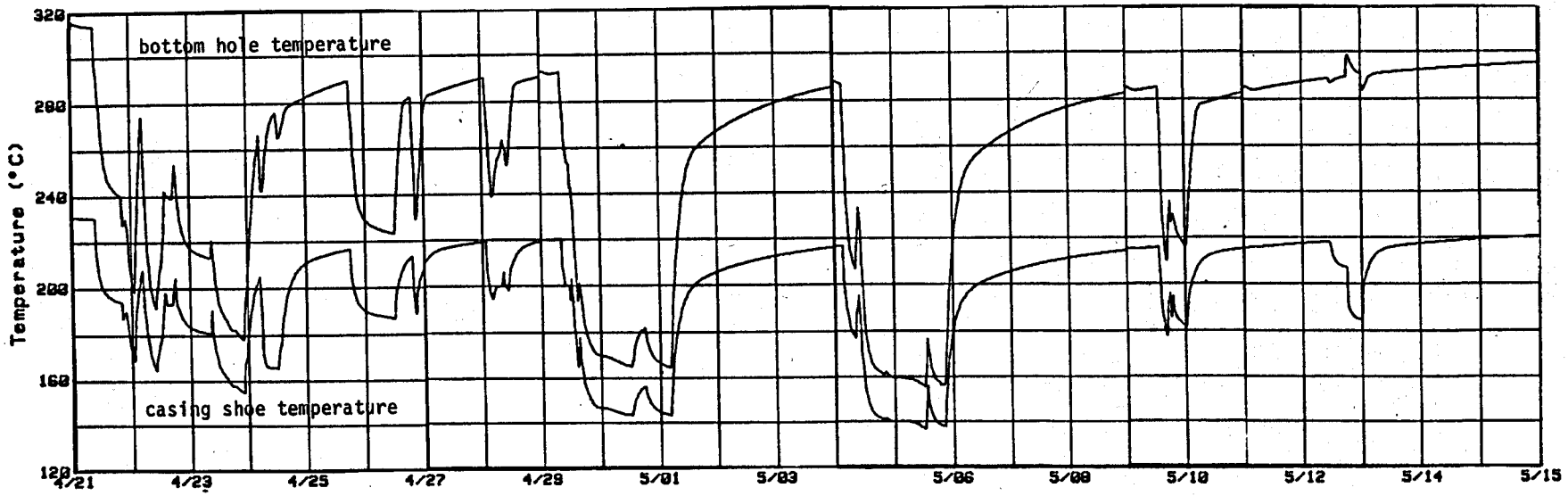

Figure 2. Computed bottom hole and casing shoe temperatures for April 21 through May 15, 1982.

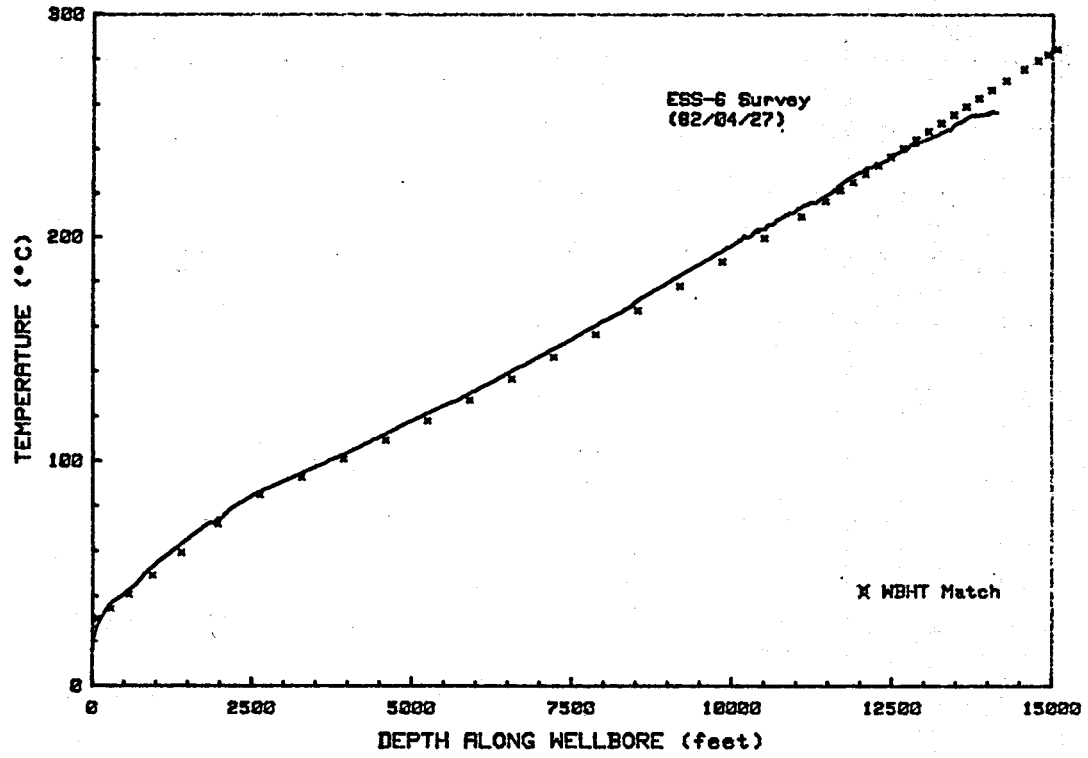

Figure 3. Temperature Survey in EE-2 wellbore, April 27, 1982, with WBHT code match.

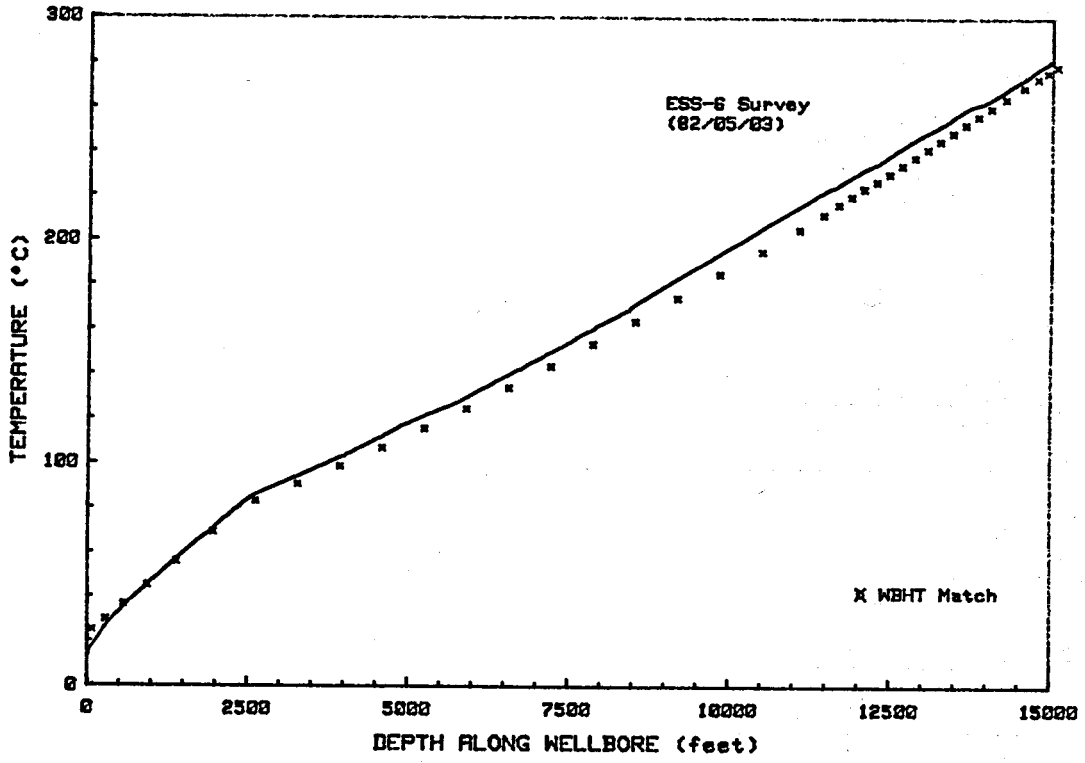

Figure 4. Temperature Survey in EE-2 wellbore, May 3, 1982, with WBHT code match.

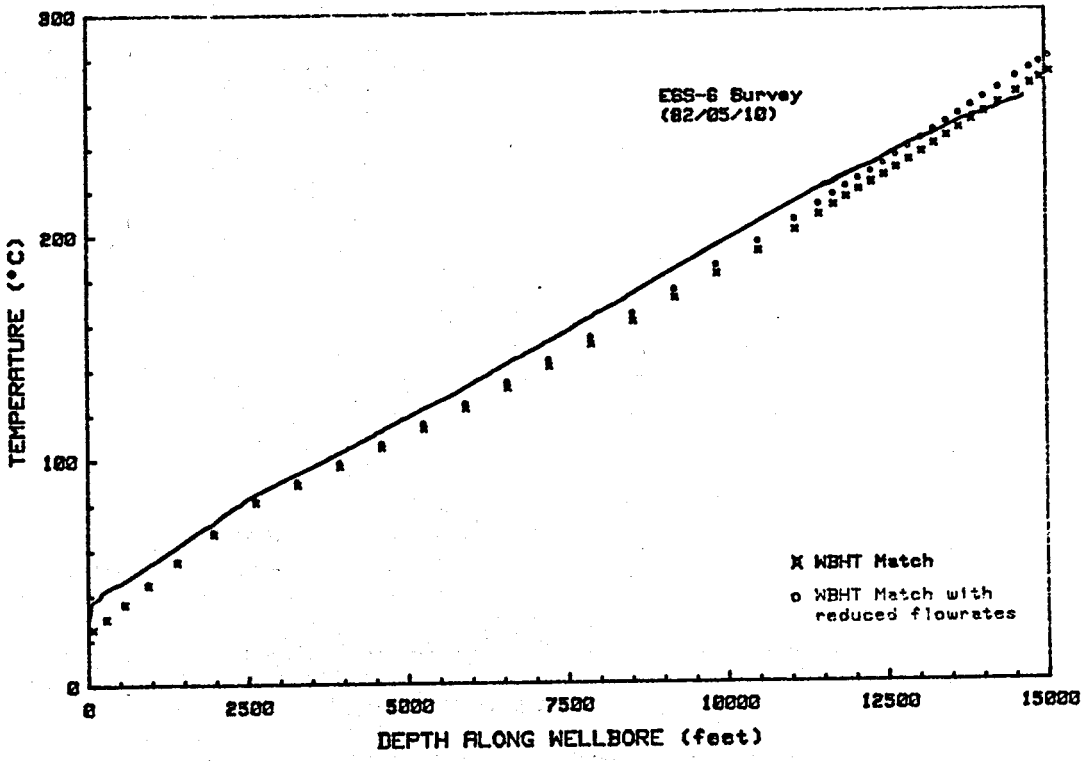

Figure 5. May 10, 1982 Temperature survey in EE-2 with WBHT code matches with and without reduced flow rates.

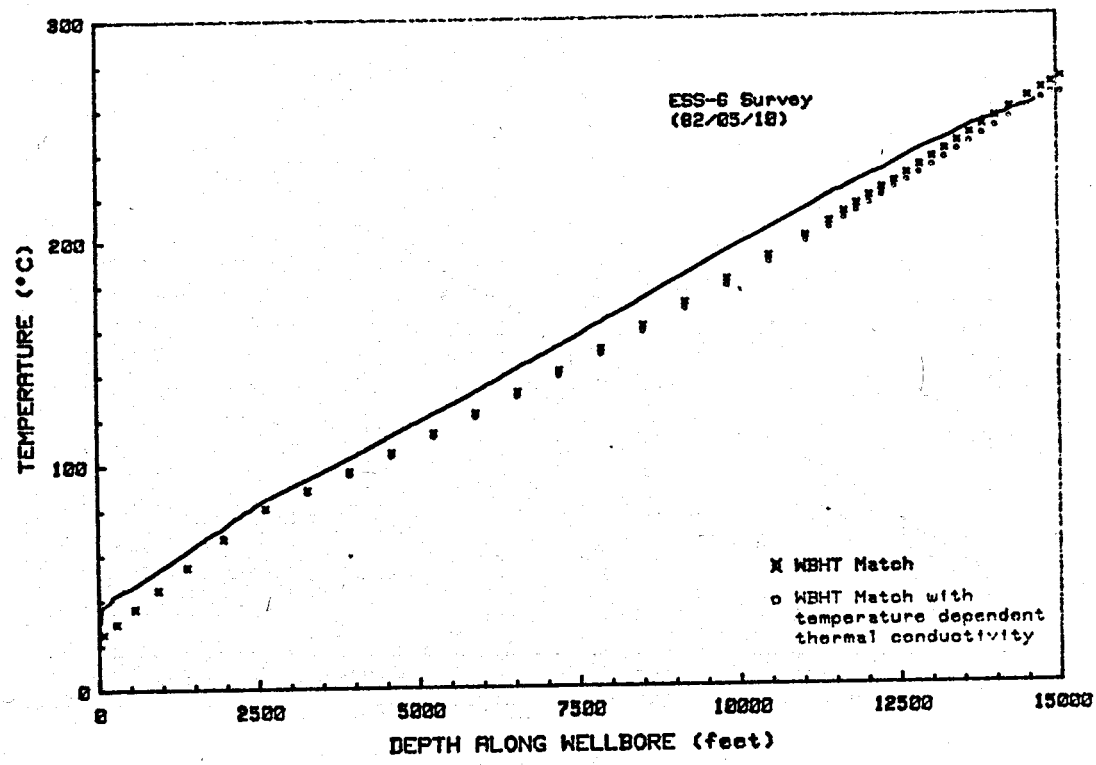

Figure 6. May 10, 1982 Temperature survey in EE-2 with WBHT code matches with and without temperature dependent thermal conductivities.

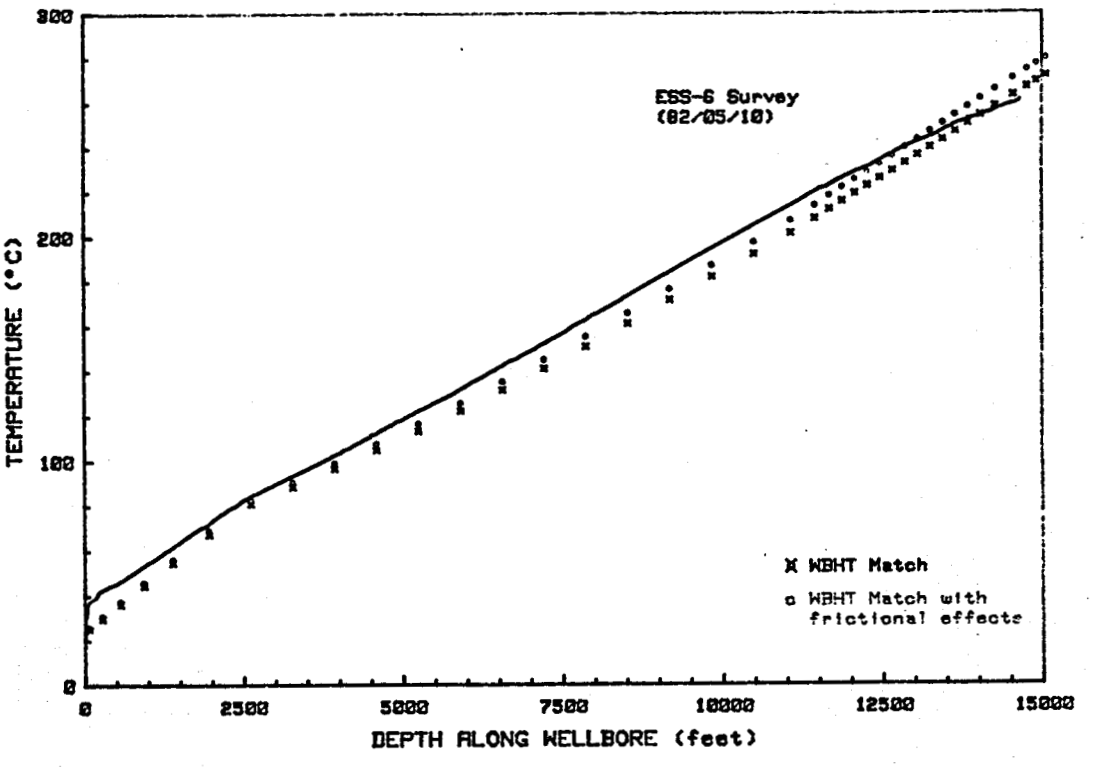

Figure 7. May 10, 1982 Temperature survey in EE-2 with WBHT code matches with and without frictional heating effects.

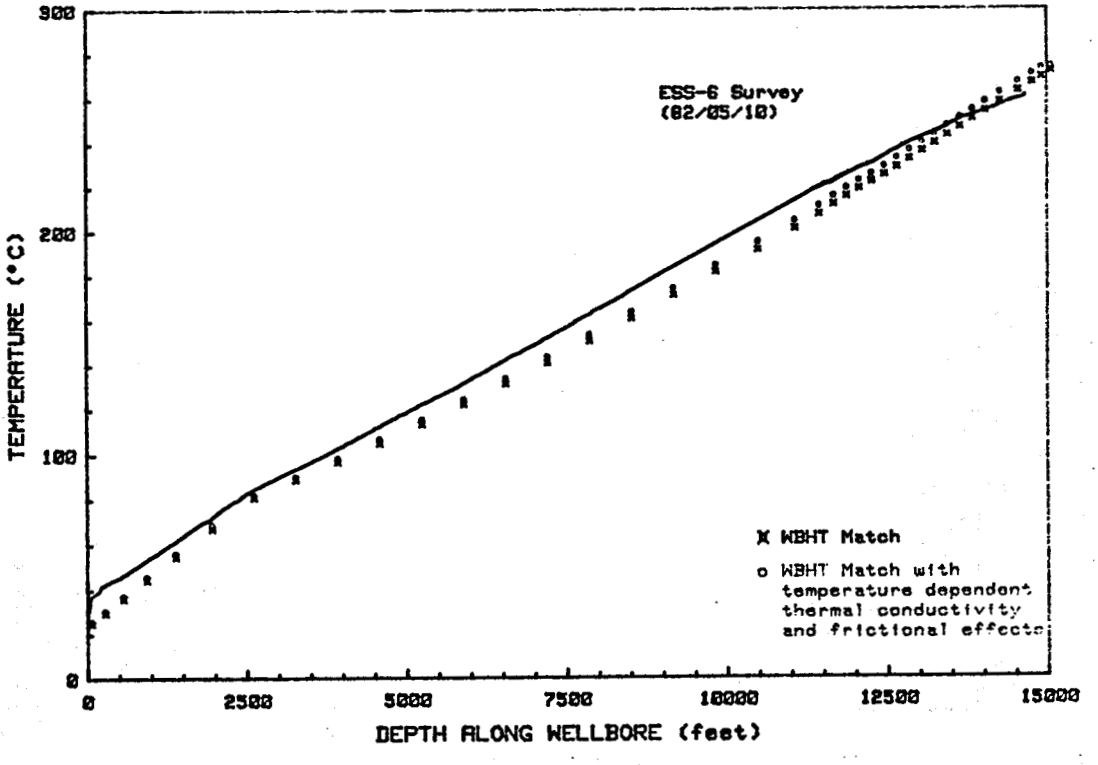

Figure 8. Temperature survey of May 10, 1982 in EE-2 with WBHT match including temperature dependent thermal conductivity and pressure heating effects.

Proceedings Eighth Workshop Geothermal Reservoir Engineering
Stanford University, Stanford, California, December 1982
SGP-TR-60

HYDROTHERMAL INJECTION EXPERIMENTS AT THE RAFT RIVER KGRA, IDAHO

W. F. Downs and R. E. McAtee, EG&G Idaho, Inc.
R. M. Capuano and W. Sill, Univ. of Utah Res. Inst.

ABSTRACT

The optimal development and management of a geothermal resource requires a knowledge of the hydrological characteristics of the reservoir. Reservoir engineering analysis techniques for permeable aquifers have been undergoing development for several decades but little attention has been paid to fracture-dominated systems. The Department of Energy funded a joint EG&G Idaho, Inc./Univ. of Utah Research Institute program to test the ability of "Huff-Puff" tests to help characterize a fracture-dominated reservoir. Several series of these injection ("Huff")-backflow ("Puff") tests were conducted at the Raft River KGRA in Southern Idaho. These test series are described and preliminary results and interpretations are discussed.

INTRODUCTION

In early summer 1982, the Department of Energy (DOE) funded a hydrothermal injection project to investigate new and novel techniques which could improve the ability of commercial well field operators to plan development and management strategies for fractured geothermal systems. The objective of the experimental program was to explore the feasibility of acquiring meaningful information from single well tests using a combination of geochemical and geophysical techniques. The Raft River facility was selected for the initial testing because of its immediate availability and extensive monitoring capability. One major limitation, however, was that testing had to be completed by December 1, 1982 in order to allow the facility to be turned over to the U.S. General Services Administration (GSA) for sale. The program was funded as a joint effort between EG&G Idaho, Inc. and the University of Utah Research Institute (UURI).

The proposal that was presented to DOE outlined a series of "Huff-Puff" tests in which the "Huff" phase consisted of injecting a fluid of distinctly different chemical composition down the test well and the "Puff" phase consisted of backflowing the test well and monitoring changes in chemistry. Raft River Geothermal Production well no. 5 (RRGP-5) was chosen as the test well. The production aquifer in RRGP-5 is a fracture system at 1382 m. Due to drilling problems, this aquifer had to be cemented off but was later reopened via a near vertical hydraulically induced fracture from the bottom of the casing (1398 m). The concentrations of dissolved solids in this well is very low for geothermal wells in this area and the specific conductivity is 2700 μmho/cm. Geothermal fluids from RRGP-3 were chosen for injection into RRGP-5. This fluid is the hottest at the well head and will, therefore, be near reservoir temperature at delivery to site five. RRGP-3 fluids also contain higher total dissolved solids (μ = 8000 μmho/cm). This RRGP-3 fluid in the primary tracer in all of our tests.

In addition to the RRGP-3 fluid, selected chemicals were injected into the formation to act as secondary tracers. At least one secondary tracer was added during each test. The chemicals selected as secondary tracers had to meet several criteria: (1) they had to be able to withstand the reservoir temperature (135°C) without decomposing, (2) their reactivity with the formation had to be kept at a minimum, and (3) they had to be inexpensive (<$20.00/lb). This last condition was necessary because of the large mass of water and, therefore, tracer that would have to be injected during long term tests.

EXPERIMENTS

Three series of experiments were conducted at Raft River between early September and early December 1982. Each series was designed to provide information on a different aspect of the Raft River reservoir. The object of each test and parameters that were varied are listed in the summary below. The injection and backflow rates were maintained at 9.46 L/s (150 gpm). This rate was chosen because both RRGP-3 and RRGP-5 can consistently supply this amount by artesian flow.

Baseline data on chemistry and downhole logs were collected on each of the wells previous to its being used for experimentation. The downhole logs included temperature, spinner flowmeter, and conductivity. Well head instrumentation included temperature, pressure, flow rate, pH, conductivity and redox potential. These instruments were either recorded on a strip chart or on a digital printout data logger.

RAFT RIVER INJECTION TEST SUMMARY

Test	Phase Duration			Object(s)
	Injection	Quiescence	Backflow	
2A-1	1 hr. (bore only)	---	1.33 hrs.	o Test downhole T/μ probe (200 ft.). o Determine tracer recovery rates from bore hole.
2A-2	2 hrs.	---	12.4 hrs.	o Test downhole T/μ probe o Determine tracer (I^-) recovery from near well formation.
2C	46.5 hrs.	---	110 hrs.	o Explore a larger volume of the reservoir. o Determine the position in the open bore where the fluid is leaving. o Determine tracer (Mg^{2+}) recovery from a larger volume of the reservoir.
2D	96.5 hrs.	---	237 hrs.	o Explore a larger volume of the reservoir. o Determine the response of the reservoir to multiple injection of tracer slugs. o Clean up reservoir in preparation for test 5.
4A	0.3 hr.	28 hrs.	8.0 hrs.	o Determine whether a natural hydrologic flow system was removing injected solutions from the immediate vicinity of the injection well.
4B	0.3 hr.	2 hrs.	10.5 hrs.	
4C	0.3 hr.	12 hrs.	8.5 hrs.	
4D	0.3 hr.	50 hrs.	48.5 hrs.	
5	min. 432 hrs. max. 504 hrs.	48 hrs.	min. 0 hrs. max. 120 hrs.	o Determine whether breakthrough from RRGP-5 to RRGE-1 can be accomplished in 18 to 21 days. o Determine whether the extent of fluid flow can be traced using spontaneous potential or resistivity surveys. o Determine reservoir pressure recovery as a function of flow rate.

There were two individual experiments in the 2A test. The first experiment, 2A-1, was a training exercise for the operations personnel and consisted of pumping RRGP-2 fluid laced with a tracer cocktail down the cased bore for a period of one hour. This injection was followed by a backflow for 1.33 hrs. Based on the criteria outlined in the previous section and the need for the tracers to provide a contrast with the native reservoir fluids, four tracers were chosen for experimentations: I^-as NaI, Br^-as NaBr, Mg^{2+} as $MgCl_2$ and B^{3+} as borax ($Na_2B_4O_7 \cdot 10H_2O$). In addition, the organic dyes fluorescein and rhodamine B were tested in later experiments. The tracer cocktail injected during experiment 2A-1 had the following concentrations: 20 ppm I^-, 20 ppm Br^-, 20 ppm Mg^{2+} and 10 ppm B^{3+}. The recovery on the I^-, Mg^{2+} and B^{3+} was greater than 96%. Analytical problems were encountered in analysing for Br^- in the high chloride (2200 ppm) geothermal brines using a Br^- selective ion electrode. This problem can be overcome using ion chromatography but this method is time consuming and not conducive to being conducted in the field.

Experiment 2A-2 was the first time that fluid from RRGP-3 was injected into the formation at RRGP-5. Injection time into the formation was two hours. The tracer selected for this experiment was I^- and was injected at a concentration of 150 ppm. The high temperature conductivity/temperature probe was inserted into RRGP-5 at a depth of 1396 m (about 2 m from the bottom of the casing). This instrument performed very well during the short term tests and showed exactly when the injection fluid started entering the formation. Backflow was initiated within a few minutes of the termination of injection. Based on downhole conductivity measurements, the influx of undiluted RRGP-3 fluid into the bottom of the casing lasted less than 4 minutes. Figure 1 is a plot of the tracer concentration and downhole conductivity as a function of time. These plots follow each other very closely and indicate that simple dilution is the major mechanism at work.

Test 2C had a longer term injection period--46.5 hours into the formation--and a different tracer, Mg^{2+}. Figure 2 is a plot of the tracer concentration and conductivity as a function of time for test 2C. The concentration of Mg^{2+} and the uphole conductivity both decrease as soon as the well bore has been cleared. The magnesium concentration, however, decreases much more rapidly than does the conductivity. A plot of the calcium concentration shows a significant increase (20%) at the initiation of backflow and then decreases at a rate less than that of the conductivity. This suggests that ion exchange of Mg^{2+} for Ca^{2+} is the dominate rock-water interaction and that this reaction is superimposed on the dilution curve.

Because dilution is a major effect and it starts immediately without respect to the injection time, it was decided to conduct a series of tests in which there were quiescent periods between injection and backflow. These experiments would help us determine whether or not an overall hydrologic flow was sweeping some of our injected fluids away from the sphere of influence of the test well. This test 4 series consisted of a 20 min. injection into the formation, a variable length quiescent time--2 to 50 hrs--and enough backflow to recover the tracer. Nearly all of the tracer was recovered in these experiments. This led to the conclusion that there was little or no natural hydrologic flow through the RRGP-5 fracture system.

Tracer & Conductivity Plot as a Function of Time: Test 2A-2

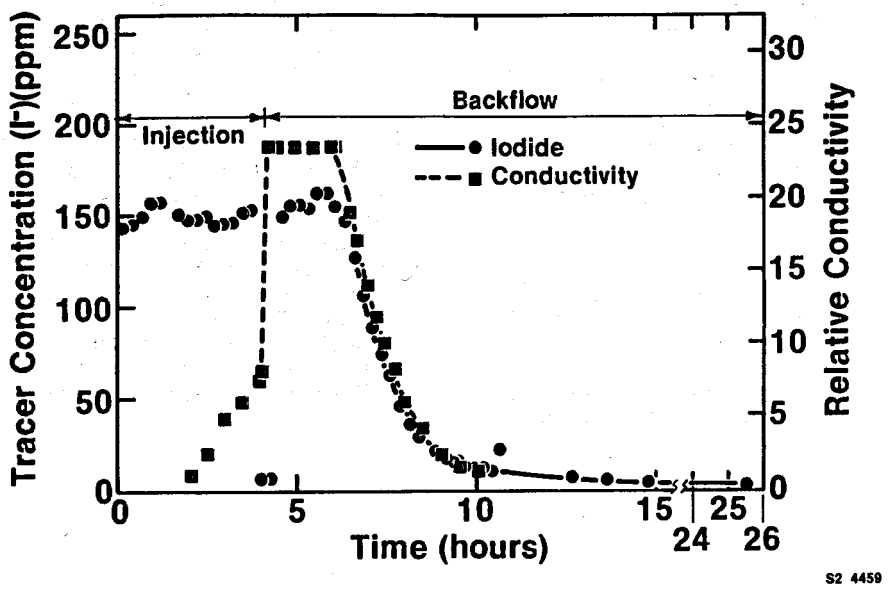

FIGURE 1

Tracer & Conductivity Plot as a Function of Time: Test 2C

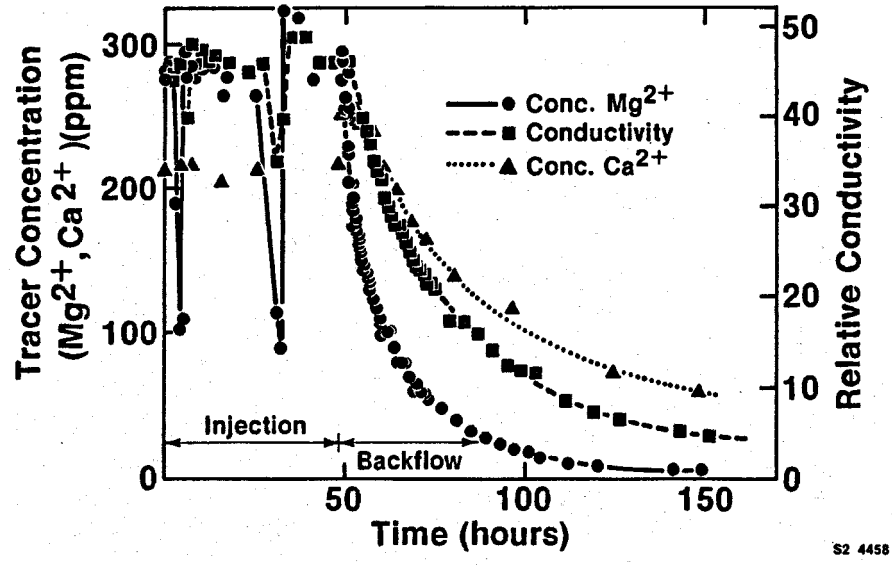

FIGURE 2

Test 2D was the final experiment of the series and had the longest term injection and backflow. Because continuous injection of tracer would require a very large amount of chemical, it was decided to inject slugs of tracer at the beginning of injection, after 24 and 48 hours of injection and just previous to backflow. A 1200 kg slug of either an individual tracer or combinations of chemical tracers or dyes were injected at a rate of 100 kg/min. The tracers started to return almost immediately and all of them reached concentrations well above background levels within the first 20 hours of backflow. Even though some of the tracers were injected as much as 48 hours apart, they all started coming back very soon and show approximately the same bimodal concentration maxima.

Test 5 is the final experiment to be conducted before the Raft River site has to be vacated. Test 5 is a long term (20 day) experiment to determine whether fluid break through could be obtained between two adjacent wells--RRGP-5 to RRGE-1. This test is underway at the time that this paper was submitted and no results will be available until the workshop presentation. In addition to the monitoring for well-to-well break through, Test 5 will be used to determine whether subsurface fluid movement can be detected by geophysical means. A team of geophysicists from UURI will be conducting a spontaneous potential survey during injection and a resistivity survey at the conclusion of injection to try to delineate the interface between the higher conductivity RRGP-3 fluid and the lower conductivity native fluids. Preliminary geophysical results from test 2C showed promise but the short term injection period of that test did not allow sufficient time for a definitive survey.

Proceedings Eighth Workshop Geothermal Reservoir Engineering
Stanford University, Stanford, California, December 1982
SGP-TR-60

Dup

RESPONSE OF RRGI 6 AND RRGI 7 TO INJECTION DURING THE 5MW PLANT OPERATIONS MARCH 25 - JUNE 15, 1982 AT RAFT RIVER, IDAHO

P. A. SKIBA

Geosciences Branch,
Idaho National Engineering Laboratory

ABSTRACT

Injection testing conducted between March 25 and June 15, 1982 at the Raft River Site generated a substantial quantity of non-isothermal and various temperature transient pressure data. Injection pressure build-up measured at the wellhead strongly responds to temperature changes of the injected fluid. An increase in the fluid temperature results in an injection pressure increase while a temperature decrease is followed by an injection pressure decline. Data analyses indicate that changes in fluid viscosity and density due to temperature changes do not explain pressure build-up responses. The pressure build-up behaviors are attributed to the reservoir transmissivity changes. The absolute wellhead pressure values are significantly lower than predicted for the cold fluid injection.

INTRODUCTION

The Raft River Geothermal Injection Wells RRGI 6 and RRGI 7 are 1172 meters deep. The open hole interval (injection zone) is between the 514 meter depth and the bottom of the hole in RRGI 6 and between the 619 meter depth and the bottom of the hole in RRGI 7. Both wells are open hole in the Salt Lake Formation which consists of interbeded siltstones and sandstones. Fractures within the Salt Lake Formation are partially filled with calcite. Rock samples and geophysical logs indicate that intergranular porosity and permeability exist in addition to some fracturing in the Salt Lake Formation Dolenc (1981).

Extensive injection into RRGI 6 and RRGI 7 was performed during testing of the 5 MW(e) Raft River Power Plant. Full scale power production tests of the 5 MW Plant were conducted between March 25 and June 15, 1982. During this testing, a total of 2.372×10^8 liters of fluid were injected into RRGI 6 and 3.135×10^8 liters into RRGI 7. This was the most extensive injection ever conducted at the Raft River Site. Injection rates and fluid temperature were variable during these tests. The injected fluid temperature ranged between 35°C and 80°C. Several tests with periods of relatively isothermal injection conditions provided data for calculation of the reservoir transmissivities for the various injection temperatures. The portions of tests with nonisothermal injection conditions are not suitable for analytical evaluation of reservoir parameters. These nonisothermal injection conditions provided material for the general discussion on the thermal effects on the wellhead pressure behavior.

The pressure fall-off data are not discussed in this paper because of incompleteness, lack of temperature measurements, and complexity created by variable injection rates and partial recovery between tests. This partial recovery also effects pressure build-up during injections. However, for simplicity no corrections were made to eliminate partial recovery effects.

TESTS CONDUCTED

Injection pumping into RRGI 6 and RRGI 7 started on March 25, 1982. Sixteen separate injections in both wells were performed between March 25 and June 15. The injection schedule was irregular, dictated by the shut-downs and start-ups of the 5 MW plant and the geothermal water supply system. Duration of the injection pumping ranged between 200 and 18,000 minutes. The injection rates were dictated by the 5 MW Plant production experiment's need to dispose of geothermal fluid. The temperature changes were related to discontinuous heat extraction by the Power Plant. Spent geothermal fluid was directed into the holding ponds near RRGI 6 and RRGI 7; it was then injected into the wells. This procedure resulted in injection fluid temperatures in the 35° to 80°C range. Injection at RRGI 6 and RRGI 7 was conducted at rates ranging between 32 and 75 lps. Well RRGI 7 generally had higher and steadier injection rates than RRGI 6.

The data recorded during injection include: wellhead pressure readings from the 400 psi digiquartz pressure transducer and from a mechanical Heise gauge, temperature and flow rates continuously recorded on a strip chart (based on platimium RTD and ΔP gauge) and temperature readings from the mercury thermometer. No downhole instrumentation was used during testing.

DISCUSSION ON TESTS RESULTS

Data from eight separate injection tests into RRGI 6 were plotted on semilogarithmic

graph paper. The data plots for most of these tests represent irregular wellhead pressure response due to changing injection rates. One test conducted in RRGI 6 was selected to illustrate pressure response to the injection. Data from this test conducted on May 16 through 28 are presented in Figure 1.

The pressure build-up follows a straight line trend for the first 260 minutes of the test. During this time, the injection rate was steady at 38.3 lps and the temperature was close to isothermal at 67-69°C. The transmissivity value calculated from this first 260 minutes is 4.8 x 10^{-4} m^2/s. Transmissivity values calculated from previous injections are generally less than 2.0 x 10^{-4} m^2/s for injected fluid at 130°C Dolenc (1981).

Between 900 minutes and 4500 minutes, the injected fluid temperature declined from 70°C to 49°C. This temperature decrease resulted in the estimated wellhead pressure decrease of 400 kPa. The estimated pressure decrease is based on the difference between projected and measured wellhead pressure. The density difference between 70°C and 49°C fluid would produce a decrease in wellhead pressure of approximately 90 kPa. This is due to the hydrostatic pressure increase within an 843 meter length of the wellbore. Viscosity of the injected fluid at 49°C is approximately 1.4 times higher than the viscosity of 70°C fluid. This higher viscosity should result in an increase in the wellhead pressure Mangold (1979). It is apparent that the density and viscosity effects do not explain the wellhead pressure responses to the temperature changes.

Relatively steady injection rates and continuous temperature readings provide better data for RRGI-7 than the data collected for RRGI 6. Data from five tests conducted in RRGI are presented in Figures 2 through 6. All the data plots demonstrate similar pattern in the wellhead pressure responses to the temperature changes.

Transmissivity values calculated from these plots are listed in Table 1. The transmissivities for each test were calculated from portions of the data plots where temperature was nearly constant. The fluid temperature during these injections ranged from 48.3°C to 80°C. Transmissivity values plotted against injected fluid temperature are presented in Figure 7. The transmissivity values, as shown in Figure 7, represent both rock and fluid properties. Thus if rock properties remain constant , for lower temperatures, fluid transmissivity values should be lower due to higher viscosity. On the contrary, however, observed transmissivity values are higher for the lower temperature fluid. Apparently, injection of lower temperature fluid results in an increase in the transmitting capacity of the aquifer. The wellhead pressure behavior during the nonisothermal injection conditions follows a pattern described for the RRGI 6 test, discussed previously.

During the injection conducted on May 2-5 (Figure 3), between 300 minutes and 1400 minutes of the test, the temperature decreased from 64°C to 45°C. This temperature decrease resulted in an estimated wellhead decrease of 270 kPa. More examples of the wellhead pressure changes due to injected fluid temperature changes are listed in Table 2.

Further indication of the transmissivity increase due to the cold water injection is demonstrated by the absolute wellhead pressure data. The wellhead pressure of 2585 kPa was predicted for 52°C water and 63 lps injection rate after 3 days of pumping Petty (1980). The recorded pressure was below 1600 kPa for similar injection conditions (Figure 3). The predicted wellhead pressure was based on the viscosity change. Apparently the effects of viscosity changes were overrun by the changes in aquifer properties.

INTERFERENCE BETWEEN RRGI 6 AND RRGI 7

Injection pumping into RRGI 6 and RRGI 7 was conducted simultaneously. Because of this parallel pumping schedule, no interference effects could be detected from well data. Additionally, the frequent changes in the injection rates and temperatures resulted in highly irregular wellhead pressure plots. Any interference effects would be masked by this irregularity.

CONCLUSIONS

The responses of RRGI 6 and RRGI 7 to nonisothermal and variable temperature fluid injection lead to the following conclusions:

1. Decrease in injected fluid temperature results in a significant decrease in the wellhead pressure build-up.
2. The lower temperature fluid injections result in an increase in reservoir transmissivity.
3. The effects of viscosity changes are overrun by the changes in transmitting properties of the rock.
4. Specially designed variable temperature and nonisothermal injection tests and numerical modeling are needed to fully understand the relation between changing properties of fluid and rock.

ACKNOWLEDGEMENT

This work was supported by the U.S. Department of Energy under contract No. DE-AC07-76ID01570.

REFERENCES

1. Dolenc M. R., et al., "Raft River Geoscience Case Study," EG&G, 1981.

2. Mangold D. C., et al., "A study of thermal effects in well test analysis" SPE 8232, 1979.

3. Petty S., "Pressure build-up during cold water injection", Interoffice correspondence, 1980.

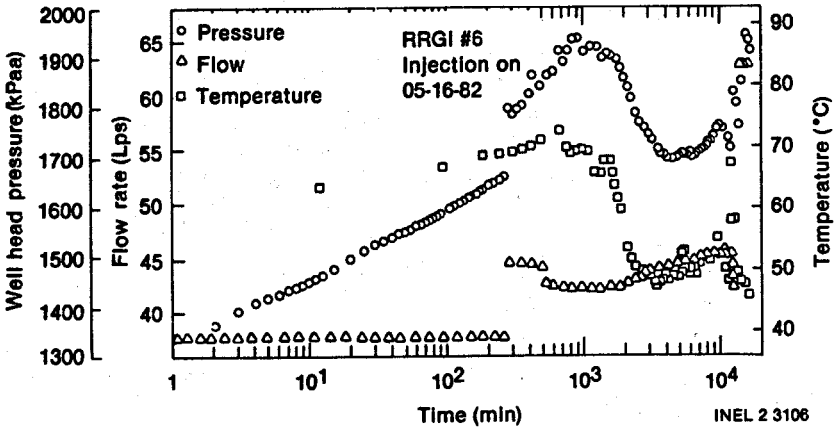

Figure 1. RRGI 6 injection data, test conducted 5/16-5/28, 1982.

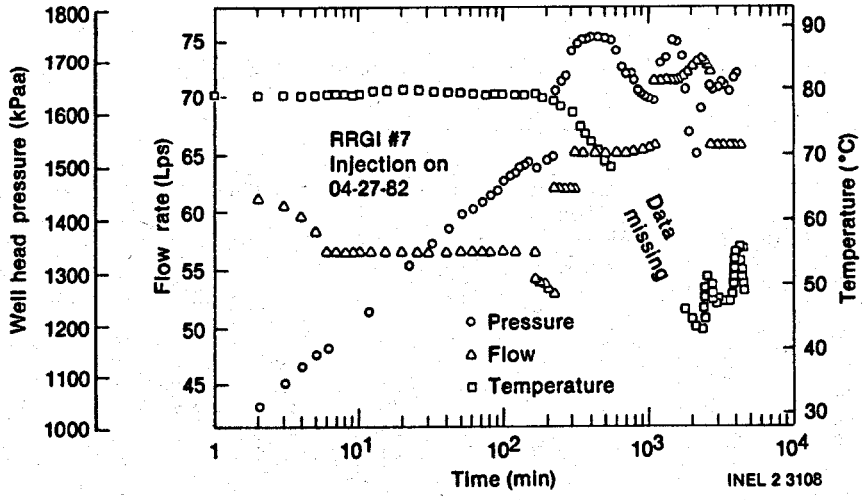

Figure 2. RRGI 7 injection data, test conducted 4/27-4/30, 1982.

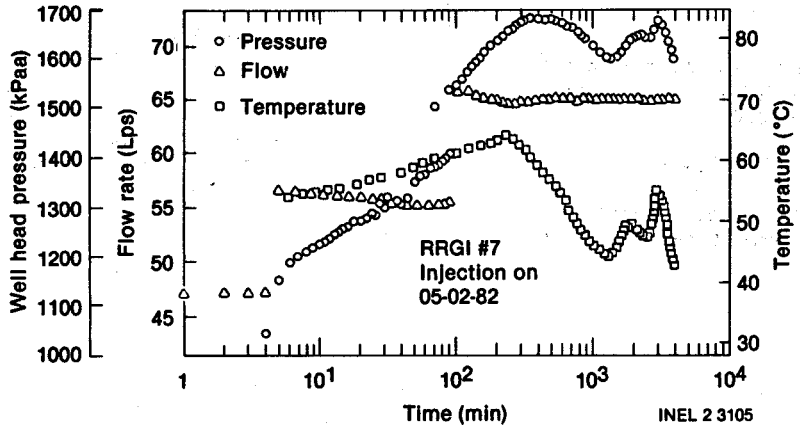

Figure 3. RRGI 7 injection data, test conducted 5/2-5/5, 1982.

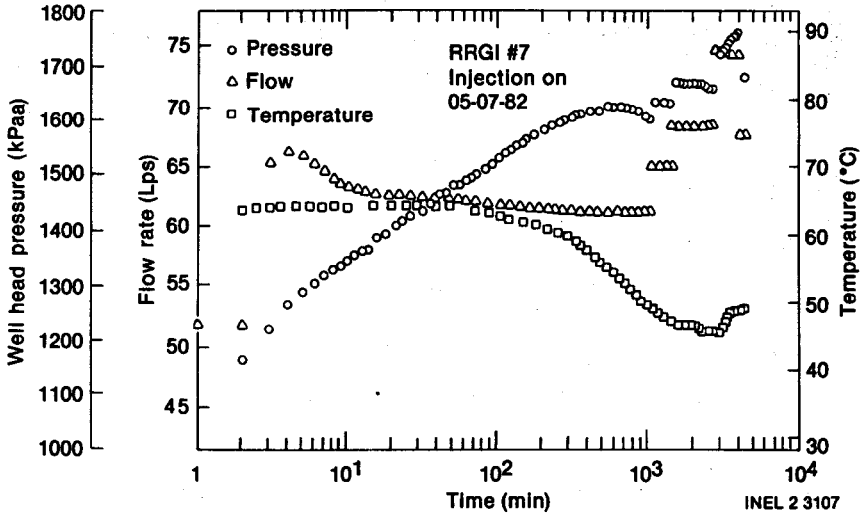

Figure 4. RRGI 7 injection data, test conducted 5/7-5/10, 1982.

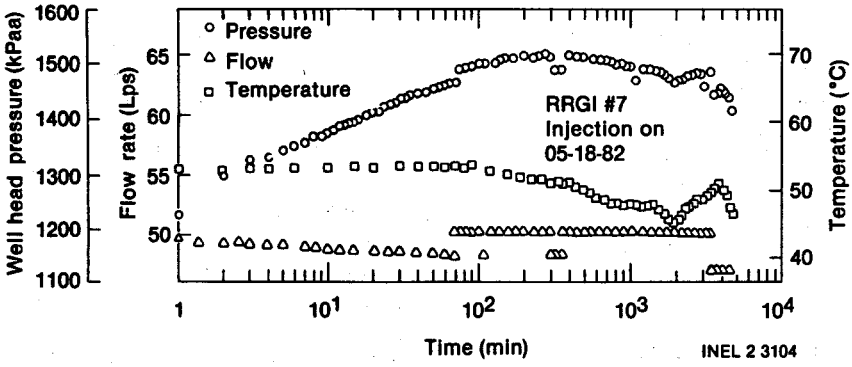

Figure 5. RRGI 7 injection data, test conducted 5/18-5/21, 1982.

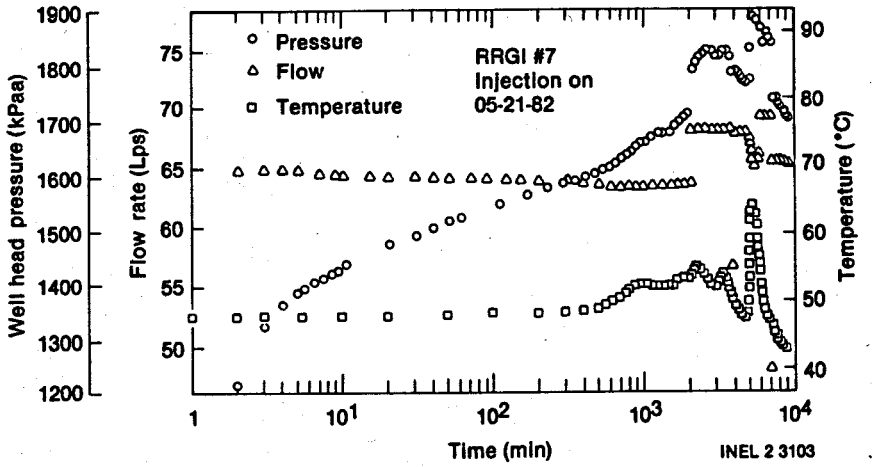

Figure 6. RRGI 7 injection data, test conducted 5/21-5/27, 1982.

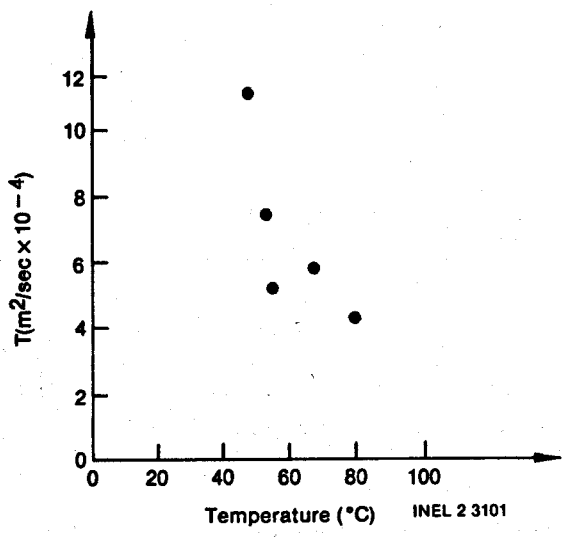

Figure 7. RRGI 7 transmissivity versus temperature

TABLE 1. TRANSMISSIVITY VALUES RRGI-7

Test Date	Injection Rate = Q (Lps)	Q/ΔP (Lps/Pa/log cycle)	Transmissivity (M^2/s)	Temperature (°C)	Remarks
4/27-4/30	56.5	2.40×10^{-1}	4.3×10^{-4}	80.0	Early time, temperature steady
5/02-5/05	55.8	2.93×10^{-1}	5.2×10^{-4}	56 to 59	Early time, temperature increasing
5/02-5/05	65.1	2.32×10^{-1}	4.2×10^{-4}	59 to 64	Temperature increasing flow slightly decreased
5/07-5/10	62.2	3.27×10^{-1}	5.8×10^{-4}	64	
5/18-5/21	49.5	4.13×10^{-1}	7.4×10^{-4}	53.2	Flow slightly decreased
5/21-5/27	64.5	6.45×10^{-1}	1.15×10^{-3}	48.3	Time 20 to 500 min. effected by recovery

*$T = 1.79 \times 10^{-3}$ Q/ΔP
*Units as shown in the Table 1

TABLE 2. WELLHEAD PRESSURE DECREASE DUE TO TEMPERATURE DECREASE

Test	Time Interval (min.)	Temperature change from-to; Δt (°C)	Wellhead pressure change;estimated, density effect, net (kPa)	(kPa)	(kPa)
RRGI 6 May 16-28 RRGI-7	900-4500	70-49, 21	400	90	310
May 2-5	300-1400	64-45, 19	270	85	185
May 7-10	300-1000	60-50, 10	120	40	80
May 8-21	200-2000	525-45, 7.5	180	30	150

Proceedings Eighth Workshop Geothermal Reservoir Engineering
Stanford University, Stanford, California, December 1982
SGP-TR-60

DISPERSION IN FRACTURE NETWORKS

Laurence C. Hull and Karen N. Koslow

Geosciences Branch, Idaho National Engineering Laboratory

Idaho Falls, Idaho 83415

ABSTRACT

A physical model was built to study the relationship between fracture network characteristics and dispersion of solutes. The study was aimed at evaluating dispersion effects due to differences in the orientation of flow to the fracture network. Radial flow injection tests were conducted at three different flow rates (30, 60, 90 cm^3/min.). Solute breakthrough was measured with specific conductance probes at 14 orientations to the major axis of the fracture network. Dispersivity coefficients were calculated from breakthrough curves. Results indicated calculated dispersivity coefficients increased with increasing flow rates and were affected by flow orientation to the orthogonal fracture network.

INTRODUCTION

Dispersion is the result of two processes, molecular diffusion and mechanical mixing. Molecular diffusion is the independent movement of solute particles from the fluid motion, due to thermal kinetic energy of individual solute particles. In this study, we will deal only with the mechanical mixing process, referring to it simply as dispersion. Mechanical mixing is the spreading-out of solutes due to characteristics of the medium, as measured by the dispersivity coefficient (α) and unequal flow velocities through the medium. In porous media the spreading of a tracer front depends only on the distance traveled by the front (Bear, 1961). Dispersivity coefficients depend on flow direction, due to anisotropy in a porous medium (Nuri, 1974), but will be independent of flow velocity.

In fracture networks, contaminant transport is governed by the same processes as in porous media. However, the actual path length along which dispersion occurs and true local flow velocities within fractures are difficult to determine. Application of traditional data collection and analysis techniques for measuring dispersion in the field is complicated by these factors. For example, the actual path water takes through a fracture network will probably be much longer than the straight distance between injection and measurement points. Flow direction in fractured media often departs from the general hydraulic gradient for much longer distances than is found in porous media. This introduces two unknowns into the advection-dispersion equation, which may preclude developing a unique solution. By developing a better understanding of dispersion in fracture networks under controlled conditions, a better method of interpreting field data may be derived. Hence, a physical model was built to study the relationship between fracture network characteristics and dispersion of solutes.

The experimental studies described here are the first in a series to evaluate characteristics of fracture networks; such as fracture spacing, width, and orientation, believed to affect dispersion of solutes. Actual dispersion parameters calculated from these experiments would not be applicable to field situations because of the disparity in scale. However, general concepts concerning the properties of fracture networks controlling dispersion would be determined, and these concepts would be transferable to field situations.

Few laboratory studies describing dispersion in fracture networks are available. Mandel and Weinberger (1972) analyzed the flow of a tagged liquid through an irregular hexagonal lattice structure. Longitudinal dispersion was found to be a function of the flow velocities within the porous media channels and a function of the pore space geometry.

A laboratory study to measure the mixing effects at fracture junctions was carried out by Krizek et al (1972). Tracer breakthrough curves were measured at outlet fractures leading away from a single fracture junction formed in plexiglass. Complete mixing was found to occur at the intersection, as equivalent breakthrough curves were measured in all outlet fractures. As only one inlet fracture was supplying tracer to the junction, results may not be applicable to situations where more than one fracture is feeding a junction and the head drop along outlet fractures is not equal. They incorporated the complete mixing concept into a predictive numerical model for transport in fracture networks. The model, however, was not verified by laboratory or field experiments.

Experiments carried out by Wilson and Witherspoon (1976) indicated little mixing

occured at fracture junctions under laminar flow conditions. Early tests in our fracture network, where tracer solution was observed passing through fracture intersections without mixing, supported this conclusion. The orientation of flow to the major fracture network controls the number of fracture junctions a solute particle will travel through. If the total distance travelled by a solute particle is accounted for, then we should not see any effects of flow orientation to major fracture network on dispersivity coefficients. Therefore, it was hypothesized there would be little difference in dispersion for flow through a fracture network and flow through a single fracture of equivalent length. Hence, orientation of flow direction to fracture network would have little influence on measured dispersivities.

MATERIALS AND METHODS

The physical model was constructed by cutting orthogonal grooves, 0.16 cm wide and 0.95 cm deep, in a sheet of plexiglass (Figure 1). The fracture network consisted of single fractures at right angles to one another, with fracture spacings of 10.2 cm. The network was enclosed in a quarter circle with a radius of 81.28 cm. Therefore, two major fractures compose the boundaries of the model, serving as major axes to flow direction. These two major fractures behave much like single fractures. Actual distance travelled by a solute particle is smallest through these two fractures. Hence, pressure gradient is steepest across these outside fractures and true local velocities within these fractures are greatest.

Radial flow injection tests were selected because data can be collected for a variety of flow orientations to the major fracture axis with a single test. Also, data analysis methodology is well developed for this configuration. Finally, this shape closely simulates configurations often applied in actual field experiments.

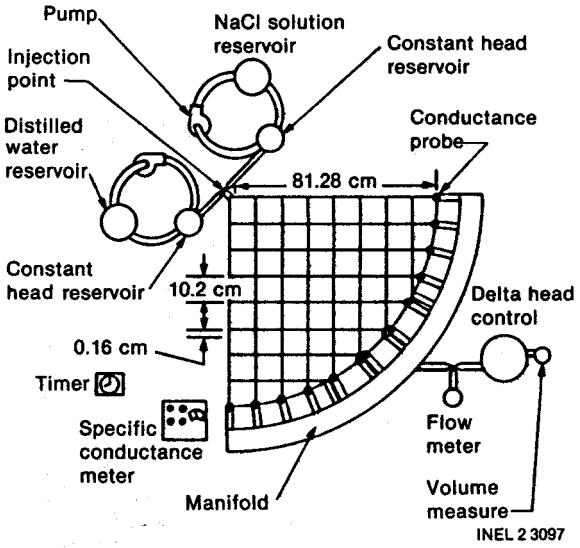

Figure 1. Design of hydrologic model, showing fracture network and support equipment.

Two constant head reservoirs supplied the model with distilled water or a dilute sodium chloride solution (conductance 10 μS). Both solutions were dyed with food coloring, enabling observation of the tracer front. Head drop across the model was controlled by a third constant head reservoir at the outlet. Specific conductance probes were installed at outlets to measure change in solute concentration and determine the resultant breakthrough curves. The laboratory model was designed with the following hydraulic criteria in mind: (1) laminar flow throughout the model (low Reynolds number), (2) advection dominant over diffusion (high Peclet number), (3) discharge on the order of a few liters per hour, and (4) a reasonable headloss (several centimeters) across the model. All tests were run in replicate once with tracer replacing distilled water and once with distilled water replacing tracer solution.

RESULTS

Figure 2 shows representative breakthrough curves for three flow volumes. Under radial flow conditions velocity is not a constant, necessitating the use of volume as the flow parameter. Solute breakthrough was observed to be inversely related to flow volume.

A plot of arrival times, based on the time a concentration of C/Co = 0.5 arrives at the electrode, for electrodes placed at different angles is shown in Figure 3. There is a general increase in arrival times as the angle approaches 45°. The lines in the figure represent the best fit to the data of the equation

$$\Delta t_{0.5} = \frac{81.28\ (\sin\theta + \cos\theta)}{v} \qquad (1)$$

where:

81.28 = radius of model

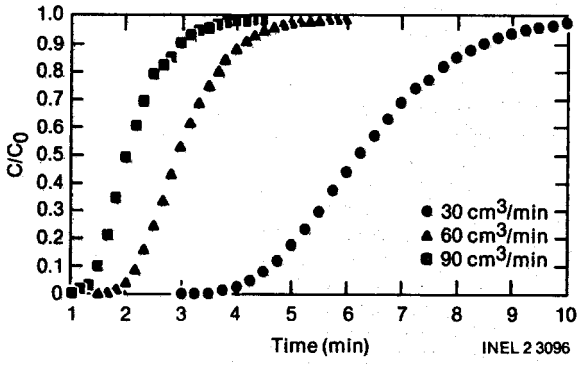

Figure 2. Representative breakthrough curves.

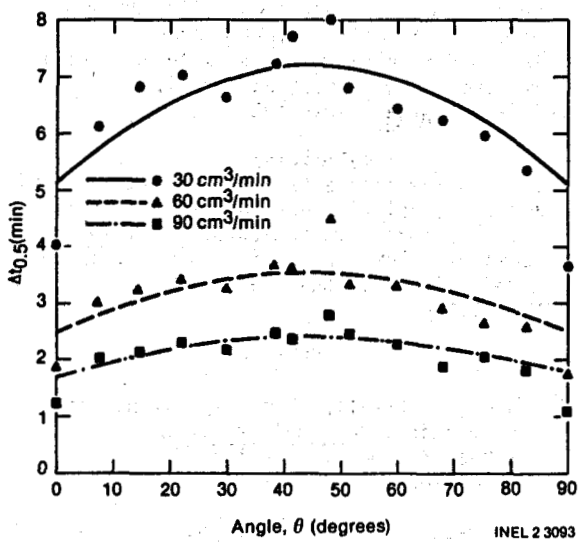

Figure 3. Arrival times versus angle when $C/C_0 = .5$

θ = angle

v = average linear velocity

$\Delta t_{0.5}$ = Arrival time of a tracer concentration equal to 50% of the final value

DATA ANALYSIS

Data were analyzed with the method presented by Hoopes and Harleman (1967). The method is based on the analytical solution to the advection-dispersion equation for radial flow.

$$C/Co = 1/2 \ \text{erfc}\left[\left(1 - \frac{4Qt}{b\pi nr^2}\right)\Big/\left(\frac{16\,\alpha}{3\,r}\right)^{1/2}\right] \quad (2)$$

C/Co = relative tracer concentration

erfc = complimentary error function

Q = discharge (cm^3/min)

b = full fracture width (cm)

n = porosity

r = distance from injection point (cm)

α = dispersivity coefficient (cm)

A factor of 4 was included to account for the quarter symmetry employed in our model.

A plot of relative concentration versus relative flow volume on arithmetic probability paper is shown in Figure 4. Theoretically, dispersion in an idealized system, will yield a straight line for this type of plot. The standard deviation is obtained from the average of the 16th and 84th percentile, and is related to α by the equation:

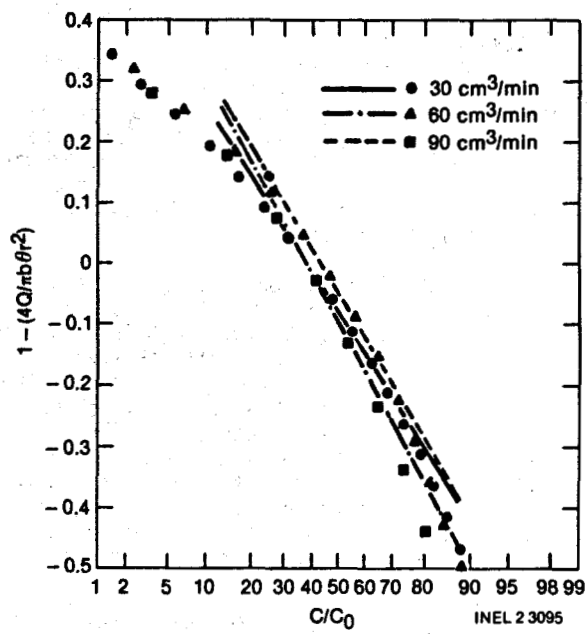

Figure 4. Relative concentration versus relative flow volume.

$$\alpha = 3/8 \ r \ \sigma^2 \quad (3)$$

A straight line was fit to the central data points by eye. Curvature of the plot may be the result of mixing in the conductance electrodes. A new electrode layout, with electrodes imbedded in the fracture walls, is being designed in an attempt to resolve this problem.

Dispersivity coefficients were calculated from breakthrough curves measured at 14 orientations to the fracture network. Because of bilateral symetry about 45°, there are actually two replicate locations at seven orientations. Figure 5 is a plot of α versus orientation.

CONCLUSIONS

The original hypothesis, indicating little difference of dispersion between flow through

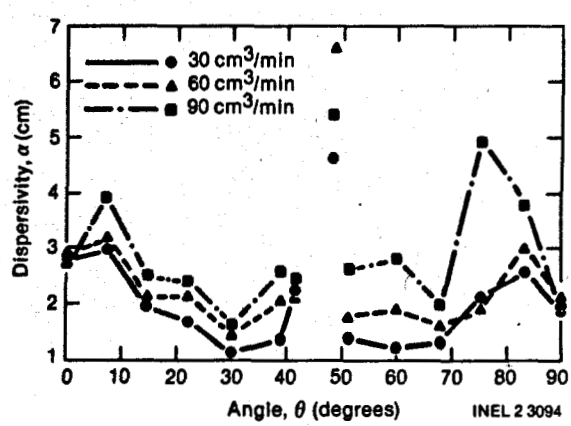

Figure 5. Dispersivity coefficient versus angle.

a fracture network and flow through a single fracture of equal length, was invalid. A relation between dispersivity and orientation of flow direction to the major fracture was observed, with highest dispersivity coefficients occuring at angles near the boundary fracture. The extremely high value measured at 48.59° was not substantiated by the equivalent electrode at 41.41°, and is probably an effect of the individual electrode.

Movement of the tracer front, illustrating rapid solute arrival near boundary fractures is shown in Figure 6. Breakthrough is greatest near boundary fractures and smallest when orientation of flow direction to boundary fractures nears 45°. This delayed passage of the front is due to a lower pressure gradient across fractures orthogonal to the boundary fracture. As orientation of flow direction to the boundary fracture deviates, the number of junctions a solute passes through increases. Hence, solute travel time across the model

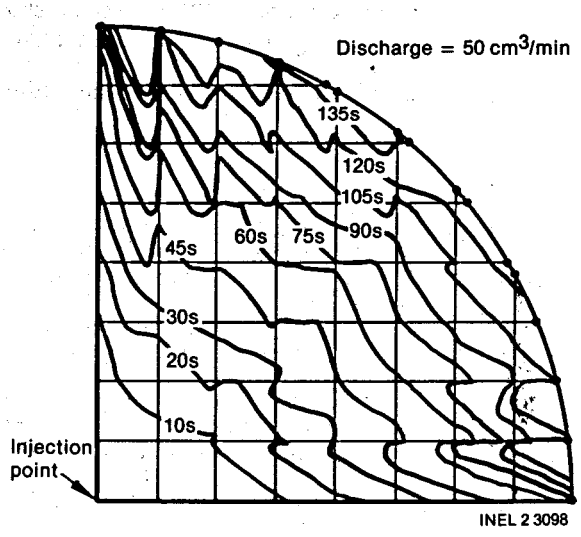

Figure 6. Movement of tracer front over time(s).

increases, as the solute particle encounters more and more orthogonal fractures. Dispersivity coefficients increased with increasing flow rates. The effect was small, but consistent at all orientations.

True local velocities within individual fractures may also affect dispersivity coefficients. Velocity is not constant in radial flow, therefore, evaluation of local velocities is complex. Further testing is required to determine local velocity effects on dispersivity.

REFERENCES

1. Bear, J. (1961), "Some Experiments in Dispersion, "Journal of Geophysical Research, 66, 8, August 1961, pp. 2455-2467.

2. Hoopes, J. A. and Harleman, D. R. F. (1976) "Dispersion in Radial Flow from a Recharge Well "Journal of Geophysical Research 72 (14) pp. 3595-3607, 1967.

3. Krizek, R. J., Kardi, G. M., and Socias, E. (1972) "Dispersion of a Contaminant in Fissured Rock." Proceedings Stuttgart, Symposium on Percolation Through Fissured Rock, International Society of Rock Mechanics, TC3, pp. 1-15.

4. Mandel, S. and Weinberger, Z., (1972), "Analysis of a Network-Model for Dispersive Flow," Journal of Hydrology, 16, 1972, pp. 147-157.

5. Nuri, F. Q. (1974), "Investigation and Verification of a Model for the Dispersion Coefficient Tensor in Flow Through Anisotropic, Homogeneous Porous Media," Ph.D. Thesis, University of Wisconsin, 1974.

6. Wilson, C. R. and Witherspoon, P. A. (1976), "Flow Interference Effects at Fracture Inersections," Water Resources Research, 12, 1, February 1976, pp. 102-104

Proceedings Eighth Workshop Geothermal Reservoir Engineering
Stanford University, Stanford, California, December 1982
SGP-TR-60

RETENTION OF CHEMICAL TRACERS IN GEOTHERMAL RESERVOIRS

Roland N. Horne, Kenneth A. Breitenbach, Martin P. Fossum

Stanford Geothermal Program
Stanford University, CA 94305, USA

ABSTRACT

This paper examines the advantages and disadvantages of chemical tracers for use in geothermal reservoir monitoring. Tracers are used to determine the magnitude of connectivity between injection and production wells in order to estimate the likelihood of premature fluid breakthrough. Even though chemical tracers are generally less environmentally sensitive than radioactivematerials, quantities injected need to be much larger to be distinguishable by chemical analysis. As a result, a non-equilibrium concentration of tracer material is injected into the reservoir, and the tracer is susceptible to retention within the reservoir by ion exchange, diffusion into the solids or immobile reservoir fluid, adsorption or dissolution. These various reactions lead to changes in the tracer concentration as the traced fluid flows through the reservoir, and therefore reduce the capability of the experiment to distinguish concentration changes due to purely mechanical effects. Experimental observations reported here show that substantial fractions of KI tracer were retained under reservoir conditions, even though it appears that the retained material was subsequently released into more dilute fluid. The result is an apparent "storage and release" mechanism that will distort the later response of a tracer breakthrough.

INTRODUCTION

A tracer is an identifiable substance that can be followed through the course of a process providing information on the pattern of events in the process or on the redistribution of the parts or elements involved. A tracer is a simulator. It must be similar in behavior to the substance which it has to trace, yet it must be sufficiently different to be identifiable. These are two contradictory conditions. The selection of a tracer is thus a search for a compromise.

In the management of geothermal reservoirs, tracers have become an important tool. They have provided valuable insight into the problem of short circuiting of waste water between reinjection and production wells Horne (1982a and b). Tracer tests provide a method of evaluating the nature of the fracture system (Fossum and Horne, 1982) and thus the potential for short-circuiting problems.

Tracers which have been used in geothermal reservoirs can be divided into two general groups: (1) chemical tracers; and (2) radioactive tracers. Chemical tracers are those which can be identified and measured quantitatively by general analytical methods such as conductivity, refractive index and elemental spectrometry. Radioactive tracers are detected by their emitted radiation, usually beta or gamma. Radioactive tracers present more severe licensing and safety concerns than chemical tracers and this study, therefore, investigated the use of chemical tracers only.

Tracers can be further subdivided into those which can be made part of the natural system and those which cannot. The first group includes radioisotopes of constituent elements in the reservoir fluids. These tracers only have to achieve equilibrium with their own non-radioactive kind. The second group of tracers includes most chemical tracers. This group has to establish equilibrium with every other kind present in the system. As a result, non-equilibrium processes such as dissolution, ion exchange, diffusion inside solids, and adsorption can occur between tracer and reservoir rock. These non-equilibrium processes will be of great importance in the field. These various types of reactions occur at a microscopic level and lead to changes in tracer concentration as the tracer fluid flows through the porous media.

This investigation was concerned with the characteristics of chemical tracer retention in reservoir rock. In most of the previous work done concerning tracer behavior in reservoirs, the retention parameter was not quantified and thus neglected in the interpretation of the tracer return. This investigation set out, therefore, to examine the magnitude of the retention problem, and to determine how it may affect the interpretation of tracer test results.

PREVIOUS WORK

Strum and Johnson (1950) studied the results of several tracer tests using brine, fluorescein dye, and a surface active compound. Their results verified the existence of directional permeabilities which had already been measured on core samples. Their findings are generally considered the first to illustrate the important use of tracers in verifying reservoir characteristics.

A comprehensive list of information obtainable from tracer tests was presented by Wagner (1974) who studied the results of twenty tracer programs conducted in petroleum reservoirs undergoing waterfloods, gas drives and water solvent injection operations.

The use of tracer tests in evaluating the short-circuiting problem found in geothermal reservoirs undergoing waste water reinjection was summarized in Horne (1982a and b). The nature of the fracture system at Wairakei was estimated by Fossum and Horne (1982) using the results of

tracer tests performed by the Institute of Nuclear Sciences (McCabe, Barry and Manning, 1981).

The macroscopic processes of dispersion, diffusion and convection were considered by Horne and Rodriguez (1981); the present work is primarily concerned with the microscopic processes seen in tracer flow. Microscopic processes include adsorption, ion exchange, dissolution and diffusion inside solids. These processes are due to chemical or physical changes in the tracer and lead to tracer retention in the reservoir.

Vetter (1981) made an attempt to quantify radioactive tracer adsorption in porous media. This paper focuses on chemical tracers and the parameters causing their retention.

THE RETENTION EXPERIMENTS

The experimental apparatus consisted of an air bath, core holder, confining pressure system, water flow system, tracer flow system, temperature recording device, and cooling system. The confining pressure and water flow systems were designed and constructed by A. Sageev (Sageev, 1980). A schematic diagram of the apparatus is shown in Figure 1.

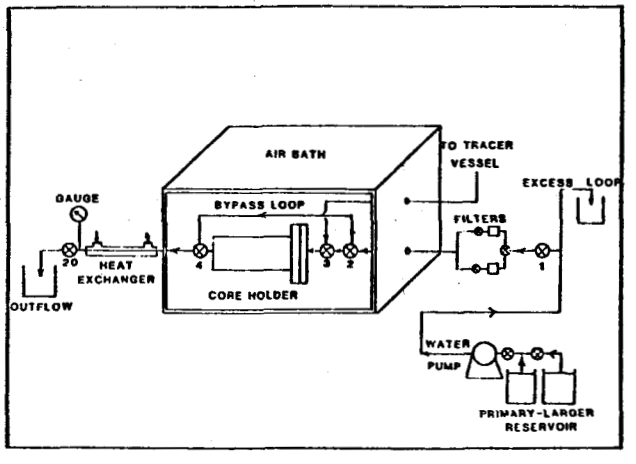

Figure 1 A schematic of the water flow systems

The core material was a volcanic andesite which was taken from the Los Azufres geothermal field, Mexico. Due to the extremely low permeability, the rock was crushed and sieved to various size fractions. A mixture of 40 to 140 mesh size was selected to be used. The mesh range was rinsed and washed several times before packing into the core holder. Porosity measurements were made with a Russell Volumeter.

The air bath houses the core holder which hangs from the ceiling to minimize vibration while the air bath is operating. In addition, the air bath houses the heating coils ahead of the core, the core bypass loop, flow lines, high temperature three-way valves, confining pressure line and thermocouples.

The assembled core holder is designed to withstand a maximum confining pressure of 4000 psig. The core plugs are sealed by "o" rings at both ends. The viton sleeve supporting the core material is rated not to exceed 350°F, setting an upper temperature limit on all the experiments. The viton sleeve is held in an aluminum perforated sleeve between the core plugs.

The viton sleeve is pressurized from the outside by the confining pressure system. A high pressure vessel is located outside the air bath and holds both oil and water. The water outlet is located on the lower end of the vessel while the oil outlet is on the upper end. Water was used in the confining chamber of the core holder to minimize the risk of contamination should a failure occur in the viton sleeve of the core holder. The pressure is applied by an Enerpac hand pump rated at 10,000 psig. The pump is oil operated.

The water flow system is comprised of the intake reservoir, water pump, excess flow loop, filters, and core bypass loop. The pump is capable of producing a maximum flow of about 1150 cc/hr at room conditions.

The core bypass loop was built into the water flow system so that the core could be isolated during specific parts of an experimental run. After tracer has been injected into the system, water flow is diverted through the core bypass loop, cleaning the system of chemical tracer from the down stream core plug to the outflow vessel. The result is that during the displacement of tracer, only tracer that has been in the core, and not the flow tubing, is collected and analyzed.

The tracer flow system consists of a gas system, tracer container, and a high pressure tracer vessel. A 2200 psig nitrogen bottle supplies gas to charge the high pressure tracer vessel. Nitrogen served as the displacement fluid driving chemical tracer through the core. All experimental runs were made with a gas pressure of 250 psig. The high pressure vessel is stainless steel and capable of holding 260 cc of chemical tracer under pressures up to 1000 psig. Before each run, the high pressure vessel is filled with tracers from the tracer container by gravity drainage.

Five thermocouples are scanned once every ten seconds by a Leeds and Northrup Speedomax Recorder which records temperatures in and around the core holder. Downstream of the core holder, outside the air bath, is a heat exchanger, pressure gauge rated to 800 psig, and a needle valve. The needle valve is used to regulate the downstream pressure. It is important to keep the pressure above 100 psig to prevent flash vaporization during the displacement of tracer from the core.

Chemical analysis to obtain tracer concentration was performed with Orion Model 94 single junction reference electrodes. Model 94-53 is iodide specific, and Model 94-35 is bromide specific. Ion specific electrodes allow for ion concentrations to be measured quickly and

accurately. Estimated accuracy is ± 0.2 ppm. Measurements are read off the Orion Model 901 ionalyzer meter.

RESULTS

The core dimensions were taken with a micrometer. The up stream measurements are taken 90° apart, while the down stream measurements are taken 120° apart to ensure accuracy around the core plugs. The porosity was measured with a Russel volumeter. The permeability was measured using pressure taps upstream and downstream of the core. The results are presented below:

Length of sand	=	15.348 cm
Diameter of sand	=	2.596 cm
Area of sand	=	5.293 cm^2
Volume of sand	=	81.237 cc
Weight of sand	=	126.5 g
Sand density (packed)	=	1.557 g/cc
Porosity	=	46.7%
Permeability	=	2.3 md

In order to quantify tracer retention under different conditions, it was necessary to analyze the water before and after it had been in the core for background concentrations of the traced ions (I, Br). The analysis of water before it had been through the core revealed trace amounts (< 0.5 ppm) of iodide and bromide.

The water background was analyzed after a three-day residence in the core at 300°F. The results are as follows:

	Concentration (ppm)
Iodide	0.26
Bromide	1.0
Bicarbonate	70.0
Calcium	19.0
Chloride	9.0
Magnesium	0.0
Potassium	4.5
Sodium	16.0
Sulfate (SO_4)	<4.0
Total Dissolved Solids	210.0

The total of the common salts equals one-half of the total dissolved solids. Some other salt must be present, perhaps silica. The low concentrations of iodide and bromide made it possible to select them as tracers. In addition, the water background analysis made it possible to account for tracer amounts in the material balance calculations.

In each of the experimental runs, complete saturation of the core with tracer was achieved by flowing three pore volumes (114 cc). It was assumed in all the calculations that as long as complete saturation of tracer in the core was achieved, the amount of tracer retained was not dependent upon the amount of tracer injected.

A summary of the experimental runs and results is presented in Table 1. The first three runs (#1, #2, #3) were made with potassium iodide at room temperature with a two-hour residence time. The results from Table 1 show that there was an increase in the amount of retention with an increase in tracer concentration. However, the percentage of tracer retained was so small (0.6% to 4.5%) that for all practical purposes, it can be assumed that retention is negligible under these conditions (two-hour residence, room temperature).

The next series of experimental runs (#4, #5, #6, #7, #8) were made under identical conditions (three-day residence, KI tracer, 300°F) but with the tracer concentration increasing from 10 ppm to 500 ppm. The objective of these runs was to test the effect of increasing tracer concentration on retention. The results expressed as a percentage retention are seen graphically in Figure 2. For the 20 ppm to 500 ppm runs, the percentage retention was quite constant, varying between 61.6% and 69.4%. The 10 ppm run showed a much smaller percentage retention of 30.6%. 10 ppm is much closer to the normal background at Los Azufres, which is around 1 ppm (Iglesias and Hiriart, 1981), and may be less of a perturbation to the iodide equilibrium of the system. The remaining experimental runs with KI were made using 10 ppm concentration of tracer. Run #9 was with potassium iodide for three-day residence at 300°F. This run followed runs #4-#8 which used increasing tracer concentration. The objective of run #9 was to go back to a low concentration of tracer to see if the microscopic processes causing retention were reversible. The pore volume was injected with 0.379 mg of tracer. At the end of the residence time, more tracer was produced (0.59 mg) than had been injected. Assuming that all the tracer had been produced from the previous run (#8), this shows that the retention was reversed.

To study the effect of residence time on tracer retention, runs #10 and #12 were made using 10 ppm potassium iodide at 300°F, but with residence times of one-day and two-hours, respectively. The results of these two runs, together with run #4 (three-day residence) are seen in Figure 3. Tracer retention increases with increasing residence time and appears to reach an equilibrium value given a long enough residence time.

The effect of temperature on retention is seen by comparing run #11 with run #4 and run #1 with run #12. These two comparisons do not show a consistent temperature effect.

The last run (#13) was made using a different chemical tracer, sodium bromide, at 10 ppm for three-day residence at 300°F. The result was that 0.136 mg were retained, representing 35.9% of the amount injected. Comparing this result to potassium iodide (run #4) under identical conditions, the potassium iodide showed 30.6% tracer retention. Thus, it appears that both tracers have

TABLE 1

Summary of Experimental Runs

Run #	Tracer	Concentration (ppm)	Residence Time	Temperature (°F)	Mass of Tracer Into Core (mg)	Mass of Tracer Out of Core (mg)	Tracer Retained (mg)	Tracer Retained (%)
1	KI	10	2 Hour	Room	.379	.368	.011	2.9
2	KI	50	2 Hour	Room	1.895	1.81	.085	4.5
3	KI	500	2 Hour	Room	18.95	18.84	.11	0.6
4	KI	10	3 Day	300	.379	.263	.116	30.6
5	KI	20	3 Day	300	.758	.238	.52	68.6
6	KI	50	3 Day	300	1.895	.616	1.28	67.5
7	KI	100	3 Day	300	3.79	1.16	2.63	69.4
8	KI	500	3 Day	300	18.95	7.28	11.67	61.6
9	KI	10	3 Day	300	.379	.59	—	—
10	KI	10	1 Day	300	.379	.281	.098	25.9
11	KI	10	3 Day	Room	.379	.065	.314	82.8
12	KI	10	2 Hour	300	.379	.315	.064	16.9
13	NaBr	10	3 Day	300	.379	.243	.136	35.9

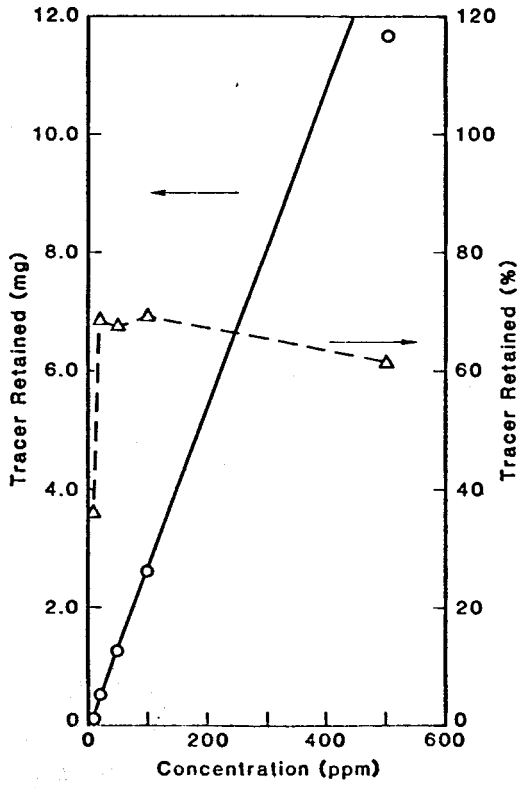

Figure 2 Potassium Iodide, 3 day Residence, 300°F

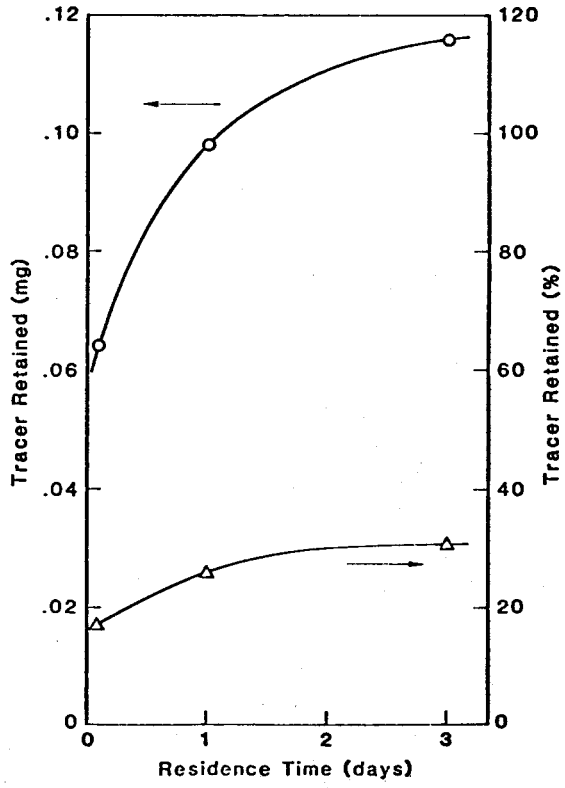

Figure 3 Potassium Iodide, 10 ppm, 300°F

similar degrees of retention under these circumstances.

EFFECT ON FIELD TESTS

Based on the preliminary results of these experiments it appears that about 60% of KI tracer is retained within the Los Azufres andesite sample, but may subsequently be released once the reservoir fluid is depleted of tracer. This "storage and release" mechanism would alter the tracer breakthrough profile such that the trailing edge of the tracer slug would be more dispersed than indicated by the normal dispersion transfer function used in Fossum and Horne (1982). This may account for the unexpectedly large dispersion (small Peclet number) in the analyses of Fossum and Horne (1982) or even for the observation of a double flowpath response. Dr. M. Manning of Institute of Nuclear Sciences, DSIR, Wellington, New Zealand (which conducted the Wairakei tracer tests) analyzed the response of Wairakei well WK 121 which showed a single, very strong response to tracer injection at WK 101, and suggested the holdup mechanism. We examined the response using the fracture flowpath model and confirmed Dr. Manning's results; despite the single, clearly defined peak, it is not possible to match the response with a single flowpath model, see Figure 4. The addition of a second flowpath improves the match (see Figure 5), but it is not until a third flowpath is added that the match becomes acceptable (see Figure 6). Figure 6 also shows the three individual components of the calculated response. Table 2 lists the inferred Peclet numbers and near arrival times for the single, double and triple flowpath models. Also listed are the "apparent" fracture apertures - these generally do not make physical sense since greater flow fraction is allocated to smaller fractures.

The results of this analysis for the WK 121 test are distinctly different from those reported in Fossum and Horne (1982) for WK 116, WK 76 and WK 108. In the latter three analyses the match obtained was satisfactory with only two flowpaths and the larger flow fraction is through the wider fracture (except for WK 76 where the flows are of similar size). In each of the three cases there is an indication of the second peak in the observed data. On the other hand the WK 121 shows a simpler response with a single discernible peak of substantial magnitude. It is therefore unsatisfying to attribute the complex three path model to this response.

TABLE 2

Inferred Flowpath Parameters WK 121

		Flow Fraction	Mean Time (days)	Peclet Number	Apparent Fracture (Aperture (mm)
Primary path	- single	1.00	2.95	9.98	12
	- double	0.63	2.56	20.27	8
	- triple	0.44	2.35	27.83	6
Secondary path	- double	0.38	4.57	6.75	17
	- triple	0.40	3.47	14.48	10
Tertiary path	- triple	0.16	6.97	4.74	26

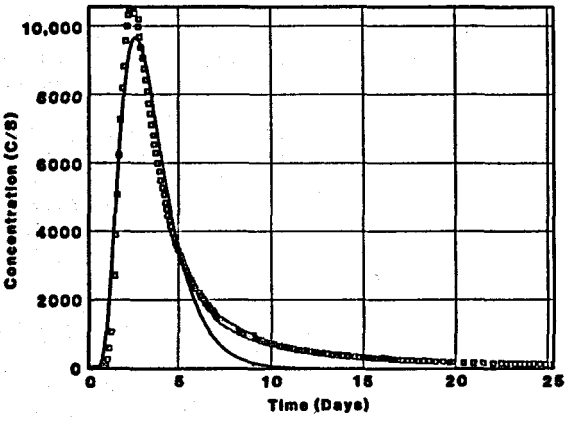

Figure 4 WK 121 response and single flowpath match

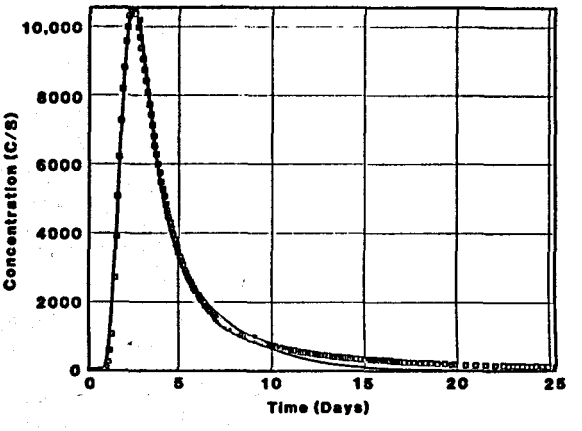

Figure 5 WK 121 response and double flowpath match

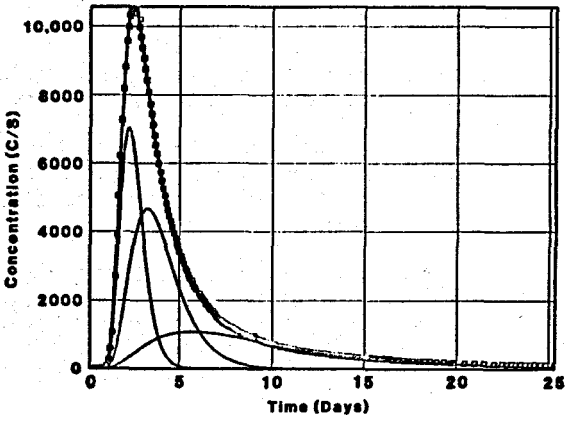

Figure 6 WK 121 response and triple flowpath match, 3 individual components indicated

Another explanation for the high concentrations in the WK 121 tracer response after the peak is the "retention and release" mechanism suggested by the experimental results. This is a more attractive model than multiple paths, particularly since the multiple path analysis results in greater flow through the smaller channels (which is a physically unreasonable result unless the narrowest paths are also the shortest). This "holdup" effect results in an underestimate of the Peclet number, and a consequent overestimate of the fracture aperture.

That WK 121 shows these effects where the earlier analyses did not is not explained, either the more rapid transport in WK 121 (2-3 days mean transport time as compared to 8-20 days for WK 116, 76 and 108) emphasizes the effect or the "second path" in the other three tests are also attributable to holdup. Further work is in progress in an attempt to quantify the process after which more extensive interpretation may become possible. One intriguing aspect of the holdup phenomenon is that it may be dependent on the surface area of the fracture, thus permitting this important parameter to be estimated.

CONCLUSIONS

An experimental apparatus was designed and built to investigate tracer retention on geothermal reservoir rocks at moderate temperature (300°F - 150°C). The effects of tracer type, concentration, residence time and temperature were evaluated. The following conclusions were reached.

1. An increase in tracer concentration produces an increase in retention.

2. An increase in residence time produces an increase in tracer retention.

3. The microscopic processes comprising retention are at least partially reversible.

4. Potassium iodide showed very similar retention values to sodium bromide under identical conditions.

5. The effect of temperature on retention was not consistent in the experiments.

6. Significant amounts of iodide and bromide tracers can be retained in reservoir rocks, and this effect must be considered in designing field tests.

It is not clear exactly where the tracer is retained. These experiments are continuing using a stainless steel core-holder assembly to determine whether the tracer is reacting with the viton sleeve in the present apparatus. This configuration will also permit higher temperatures.

The possible effects of tracer retention and release on field experiment interpretation were considered qualitatively, and this preliminary examination suggests that there is both a need and a significant advantage to quantifying the holdup mechanism. There is a delayed concentration enhancement in the response at well WK 121 which is not convincingly explained with the multiple flowpath model and is apparently the effect of a holdup of some kind.

ACKNOWLEDGEMENT

This research was funded by the U.S. Department of Energy Contract Number DE-AT03-80SF11459.

REFERENCES

Fossum, M. P., and Horne, R. N., (1982), "Interpretation of Tracer Return Profiles at Wairakei Geothermal Field Using Fracture Analysis," Geothermal Resources Council Transactions, 6.

Horne, R. N., (1982a), "Geothermal Reinjection Experience in Japan," Journal of Petroleum Technology, 34, p. 495-503.

Horne, R. N., (1982b), "Effects of Water Injection into Fractured Geothermal Reservoirs - A Summary of Experience Worldwide," in Fractures in Geothermal Reservoirs, Geothermal Resources Council, Davis, Calif.

Horne, R. N., and Rodriguez, F., (1981), "Dispersion in Tracer Flow in Fractured Geothermal Systems," Proceedings, 7th Workshop on Geothermal Reservoir Engineering, Stanford, December 1981, SGP-TR-55, p. 103-108 (also submitted J. Geophysical Research, 1982).

Iglesias, E. R., and Hiriart, G. (1981), "Design of a Tracer Test for the Geothermal Field of Los Azufres, Michoacan, Mexico: Progress Report," Proceedings, 7th Workshop on Geothermal Reservoir Engineering, Stanford, December 1981, SGP-TR-55, p. 41-46.

McCabe, W. J., Barry, B. J., and Manning, M. R., (1981), "Radioactive Tracers in Geothermal Underground Water Flow Studies," Institute of Nuclear Sciences Report INS-R-298, DSIR, October 1981.

Sageev, A., (1981), "Design and Construction of an Absolute Permeameter to Measure the Effect of Elevated Temperature on the Absolute Permeability to Distilled Water of Unconsolidated Sand Cover," SGP-TR-43, Stanford University, Stanford, Calif., December 1980.

Strum, P. W., Johnson, W. E. (1951), "Field Experiments with Chemical Tracers in Flood Waters," Producers Monthly, Vol. p. 11-18.

Wagner, O. R., (1977), "The Use of Tracers in Diagnosing Interwell Reservoir Heterogeneities-Field Results," Journal of Petroleum Technology, 29, p. 1410-1416.

Vetter, O. J., (1981), "Evaluation of Well-to-Well Tracers for Geothermal Reservoirs, " LBL-11500, Earth Sciences Division, Lawrence Berkeley Laboratory, University of California, August 1981.

Proceedings Eighth Workshop Geothermal Reservoir Engineering
Stanford University, Stanford, California, December 1982
SGP-TR-60

FLUID GEOCHEMISTRY APPLICATIONS IN RESERVOIR ENGINEERING (VAPOUR-DOMINATED SYSTEMS) (+)

Franco D'Amore, Romano Celati and Claudio Calore

Istituto Internazionale per le Ricerche Geotermiche
Via del Buongusto 1
56100 PISA, Italy

ABSTRACT

During these last few years fluid geochemistry has proved to be a valid tool for analysing the processes occurring in geothermal reservoirs. Space and time variations in fluid composition have been interpreted as being due to geological setting and reservoir processes, including water recharge, steam condensation and vaporization of liquid water.

The major effort is now invested in developing conceptual and quantitative models for chemical and physical processes that could produce the observed variations in fluid composition.

These models are an effective complement to the classical methods of reservoir engineering in field development and exploitation.

The fields in which the geochemical methods seem to be most effective are:
- individuation of the main zones of steam upflow and of fluid sources in the various parts of the reservoir;
- identification of the main flow paths of the fluid in the reservoir;
- geothermometry;
- estimates of liquid saturation of the reservoir;
- analysis of the processes of natural recharge and reinjection.

Previous work in the field, as well as current development of research conducted by the authors on gas composition, are discussed and reviewed.

INTRODUCTION

It is only recently that some authors have shown that the chemical and isotopic composition of the steam in vapour-dominated geothermal systems can be related to physical and chemical processes occurring in the reservoirs. This composition can be used to develop conceptual models of the reservoirs prior to and during exploitation, and, in some cases, even to provide quantitative information(Celati et al., 1973; Panichi et al.,1974; D'Amore et al.,1977; D'Amore,1977; Truesdell et al.,1977;Truesdell and Frye,1977; D'Amore and Nuti,1977; Truesdell and Nehring,1978; Mazor,1978; D'Amore and Truesdell,1979; Calore et al.,1980; D'Amore et al., 1981). The chemical and isotopic composition of the fluid in vapour-dominated fields has, in fact, been seen to vary areally inside the latter and, in certain areas, undergoes conspicuous and regular temporal variations.

This paper reviews some of the chemical and physical processes that may be responsible for the observed variations and proposes some simple quantitative models.

The belated interest in the geochemistry of the vapour-dominated systems stems from the fact that the fluid produced consists merely of water and a limited number of volatile chemical species, whereas nothing is known of the composition of the liquid phase from which the steam originated. The chemical composition, moreover, can be extremely different from one point to the next within the same field, and from one field to another. In the case of The Geysers and Larderello, for example, the variation in gas/steam ratio exceeds three orders of magnitude, and two orders in the concentration of H_2, H_2S and CH_4 in the uncondensable gas. Nor is it always possible to distinguish between differences in original composition and those deriving from field exploitation, due to the frequent lack of data and to the fact that exploitation itself can produce multiple interactions between the various parts of the system and modify the original flow patterns (D'Amore et al.,1981).

The relations between the reactive gas species

(+) The results from the Larderello field form part of the ENEL-CNR research agreement.

are,moreover, greatly dependent on unknown redox conditions in the reservoir, which, in their turn, are controlled by complex chemical reactions involving oxides, silicates and iron sulphides (Giggenbach,1981).

The geochemical models considered so far are based on the main gaseous species only and are extremely simplified. Very little is known as yet on the kinetics of the chemical reactions involved in the models (Giggenbach,1982; Nehring and D'Amore,1981). A further problem related to the hypothesis of chemical equilibrium concerns fluid components such as CH_4 and CO_2, or N_2 and NH_3, which may have different origins and undergo a mixing within the system under study. We generally have no knowledge of the time required to reach equilibrium.

In the next section we will review previous work in the application of volatile components to the study of some characteristics of vapour-dominated reservoirs.

STATE-OF-THE-ART

One of the most important objectives of the exploration and exploitation phases of a geothermal field is to individuate the upflow areas in the field, characterized by the upward movement of deep high-temperature fluids. Generally these areas have a relatively high permeability down to great depths. During exploitation the fluid characteristics in these areas are:
- relative maxima of temperature, revealed by direct measurements and geothermometric computations;
- positive $\delta^{18}O$ values with respect to nearby areas, as shown at Larderello and The Geysers (Panichi et al.,1974; D'Amore and Truesdell, 1979; Truesdell et al.,1977). These positive values are probably tied to the fact that the steam produced derives from a water that has interacted with the rocks for relatively long periods in a high-temperature environment, without undergoing local condensation or mixing with recent meteoric water;
- local maxima of H_3BO_3 and HCl values, as found in the central areas of the Larderello field (D'Amore et al.,1977);
- low values of NH_3 and gas/steam ratio;
- high concentrations of H_2 and H_2S in the gas.

This composition may be related to a fluid derived from the boiling of a brine with high NaCl and H_3BO_3, and low NH_3 and gas concentrations (D'Amore and Truesdell,1979),moving through prevalently "dry" conduits.

Condensation greatly modifies the composition of the fluid with respect to some apparently non-reactive or poorly reactive species such as CO_2 , H_3BO_3, HCl, NH_3 and Ar.

In 1979 D'Amore and Truesdell proposed a condensation model in which the steam flows laterally from a central area of boiling or upward flow,and releases heat to the surface conductively. This heat loss causes a progressive partial condensation of the steam. The liquid formed is drained downwards to reach the deep liquid-dominated zone, while the residual steam continues its lateral movement towards the edges of the field. On the margins of the vapour-dominated system, where no steam condensation takes place, the temperature decreases considerably. Gravity segregation may result in accumulations of gas in the uppermost parts of the reservoir.

Because of the high gas contents, the wells at Larderello are non-commercial in zones where the fraction of condensed steam exceeds about 80%; at The Geysers, on the other hand, where the gas content is generally at least one order of magnitude lower than at Larderello, the wells are still exploitable in areas in which the condensed fraction reaches 95%.

High condensation areas show relative minima of $\delta^{18}O$ and H_3BO_3, absence of HCl, and high values of gas/steam ratio and NH_3 content.Permeability and temperature frequently decrease on approaching these field boundaries.

The spatial variations in the composition of the steam phase predicted by the condensation model should refer to a two-phase system unaffected by exploitation. During exploitation the concentrations of the different species change as the fluid produced derives partly from the original steam phase and, for the most part, from the boiling of the liquid phase. The composition of the fluid produced then depends on the relative contribution of the two original phases, as the concentrations of each individual species may be very different in these two phases. The variations induced by exploitation are smaller for the more soluble species. With regard to ^{18}O in particular, D'Amore and Truesdell (1979) have shown that the difference in isotopic composition between the steam and condensate phases remains constant in an isothermal condensation process; that is, the condensate has the same gradient

as the steam. The steam produced by vaporization of the condensate will thus have the same ^{18}O gradient as the liquid, and the values will merely be about 2‰ higher(at 230°C).

Relatively negative $\delta^{18}O$ values, low gas/steam ratios, low H_3BO_3 and generally low NH_3 values, absence of HCl and presence of tritium were also noted at Larderello, near the recharge areas on the field margins. These characteristics of fluid composition have been attributed to a mixing between steam of deep origin and steam deriving from the vaporization of locally infiltrated water (Celati et al.,1973; Panichi et al.,1974; Petracco and Squarci,1975; D'Amore et al.,1977). Pressure declines within the reservoir caused by exploitation were shown to increase the contribution of recent meteoric waters to the fluid produced (Calore et al.,1982).

The geochemical and isotopic investigations have also proved particularly useful in the analysis of fluid mixing processes caused by reinjection in the central areas of Larderello. Analysis of gas, ^{18}O and D contents, in particular, have been utilized in a quantitative evaluation of the contribution of reinjected water to production (Nuti et al.,1981; Giovannoni et al.,1981; Cappetti et al.,1982).

An analysis of the long production histories of Larderello (Sestini,1970) revealed that the observed chemical variations could be related with the behaviour of certain physical variables such as well flow-rate and temperature (D'Amore and Truesdell,1979; D'Amore et al., 1981). One model capable of explaining the observed variations assumes that at least three sources of fluid contribute to production, in varying degrees, during exploitation. These three sources coincide with the three different zones of the reservoir (upper condensate, intermediate two-phase and deep brine), hypothesized by White et al.(1971) and Truesdell and White (1973). The temporal evolution of the chemical and physical parameters are interpreted as a gradual modification to the contribution from each of these sources induced by exploitation. Simple quantitative models can, with a good approximation, reproduce the trends in flow-rate, temperature, gas/steam ratio, H_3BO_3 , NH_3 and HCl observed in individual wells (D'Amore and Truesdell,1979).

These models were also used to reproduce the evolution simultaneously observed in all the wells in the Serrazzano area, assuming that the chemical and physical characteristics of the three sources vary from place to place, in accordance with a progressive condensation model (D'Amore et al.,1981).

The only geothermometers applicable to vapour-dominated systems are those based on the ratios of the gaseous components (H_2, CO_2, CH_4, H_2S)(Hulston and McCabe,1962; Truesdell and Nehring,1978; D'Amore and Truesdell,1980;D'Amore and Panichi,1980) and on the distribution of the C,H and O isotopes among the gaseous components (i.e., $\delta^{13}C(CO_2-CH_4)$, $\delta D(CH_4-H_2)$, $\delta D(H_2O-H_2)$, $\delta^{18}O(H_2O-CO_2)$(Craig,1953; Craig, 1975; Hulston and McCabe,1962; Bottinga,1969; Panichi et al.,1977; Hulston,1977; Panichi and Gonfiantini,1978; Panichi et al.,1979). Panichi et al.(1979) applied the isotopic geothermometers to the fluid of numerous wells at Larderello.

The pair CH_4-CO_2 gives, on average, temperature values of the order of 340°C at Larderello. Comparison with the estimated temperatures at the top of the reservoir suggests that the reaction $CO_2 + H_2 = CH_4 + 2H_2O$ is unable to explain the observed isotopic compositions, or, at least, that attainment of isotopic equilibrium must be such a slow process (Giggenbach, 1981) that the high temperature values can only be related to deeper zones of the reservoir far below the horizons exploited at present. It was then proposed that the synthesis reactions for methane and carbon dioxide ($C + 2H_2 = CH_4$ and $C + O_2 = CO_2$), forwarded for Larderello by D'Amore and Nuti(1977),could represent an adequate alternative for reproducing the thermal state of the field. It would,therefore, appear that CH_4 and CO_2 have a separate origin and do not reach isotopic equilibrium in the layers exploited at present. The pair CH_4-H_2 gives an average value of 312°C, and the pair H_2O-H_2 254°C.

The isotopic composition appears to give the temperatures reached by the geothermal fluid in different parts of the system. The various geothermometers equilibrate at different rates; i.e., in decreasing order,CO_2-H_2O, H_2O-H_2, CH_4-H_2, CH_4-CO_2. If the fluid cools during its rise towards the exploited horizons, then comparison of the temperatures provided by the various pairs should give an indication of the thermal history of the fluid.

With the exception of the geothermometer proposed by D'Amore and Panichi(1980), which is based on purely empirical concepts, all the

other geothermometers utilizing the gaseous composition to estimate the temperatures in vapour-dominated reservoirs have two main limitations:

1) the geothermometers are based on the hypothesis that certain chemical equilibria exist in the steam phase, but the composition utilized is actually that of the fluid at wellhead, which derives in part from the vaporization of the liquid phase existing in the reservoir. The chemical equilibria in question do not effectively refer to the fluid produced, but to the steam phase in the reservoir; this phase may be much different in composition from the steam produced. Despite this drawback, a good geothermometer for the vapour-dominated systems has proved to be the $\log(H_2S/CO_2) = 8.92 - 4033.5/T - 0.79 \log T - \frac{1}{2}\log(\text{litres } CO_2 \text{ STP/kg steam})$. This geothermometer was applied by D'Amore and Truesdell (1980) to the computation of the percentage volume of liquid water in the reservoir at The Geysers and Larderello. They assumed that the difference between the geothermometric and bottomhole temperature values in a producing well reflects the cooling produced in the reservoir by vaporization of the liquid phase. Nehring and D'Amore (1981) and D'Amore and Truesdell (1980) have also developed some geothermometers based on the gaseous composition that can be applied to liquid-dominated systems. Again no account was made for the possible two-phase nature of the fluid in the reservoir. Recently Giggenbach (1980) developed and applied to the New Zealand fields a method by which temperature and saturation can be computed simultaneously;

2) with the exception of the geothermometer based on the Fisher-Tropsch equation, all the geothermometers utilize oxygen fugacities obtained from empirical equations, and sulphur fugacities based on simple geochemical models that ignore the real mineralogical composition of the reservoir rocks.

It is only by taking into account the existence of two-phase conditions in the geothermal reservoirs that reasonable solutions can be obtained for the various problems related to gas geochemistry in vapour-dominated systems.

The development of methods for determining the fractions of the two fluid phases is a prerequisite for any quantitative considerations on the composition of the fluids in these geothermal systems. Thus an estimate of liquid saturation in the reservoir is one of the main objectives of current geochemical investigations. These studies are also of considerable interest in reservoir engineering, as they can be used to estimate fluid reserves. The results of the first studies in this field were presented by Grant (1979), Celati et al.(1980),Giggenbach (1980), D'Amore and Truesdell (1980) and D'Amore and Celati (1983). Giggenbach's method, which assumes the existence of two simultaneous equilibria

$$N_2 + 3H_2 = 2NH_3$$

$$CO_2 + 4H_2 = CH_4 + 2H_2O$$

seems inadequate for vapour-dominated fields such as Larderello and The Geysers,as the first reaction is not in equilibrium. D'Amore and Celati (1983) developed a method for calculating the steam/liquid ratio in the reservoir utilizing only the second equation, with an assigned temperature value. The results of the latest developments in this direction are now described.

NEW RESULTS IN RESEARCH ON GASEOUS COMPOSITION

Large temporal variations in the gas/steam ratio had already been observed in the Larderello field(Sestini,1970). D'Amore and Truesdell (1979) and D'Amore et al.(1981) based their interpretation of this temporal evolution on the simple quantitative models outlined earlier in this paper. An attempt was later made to interpret the spatial and temporal variations in the gaseous composition also.

If we exclude those areas of the field in which the chemical evolution is clearly due to water recharge, then a correlation can be observed between the percentages of H_2 and H_2S in the dry gas and the gas/steam ratio. A typical example is shown in Fig.1, where the temporal

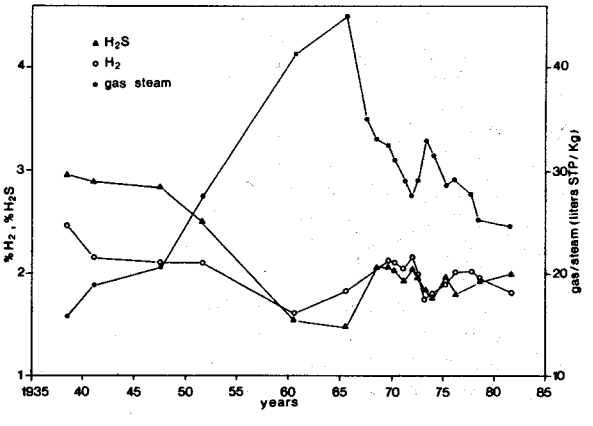

Figure 1. Example of temporal variations in the gas/steam ratio, and ($\%H_2$) and ($\%H_2S$) in the dry gas of one well at Larderello.

variation in the gas/steam ratio is accompanied by an inverse variation in the percentages of H_2 and H_2S in the dry gas.

The type of relationship existing between gas/steam ratio and H_2 and H_2S can be individuated by study of a large number of wells. Figures 2 and 3 show this relationship for wells with reservoir temperatures between 240°C and 270°C.

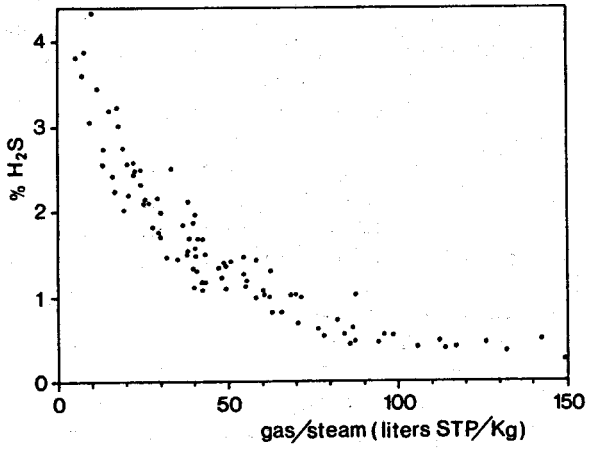

Figure 2. (%H_2S) in dry gas vs gas/steam ratio for Larderello wells with reservoir temperatures between 240° and 270°C.

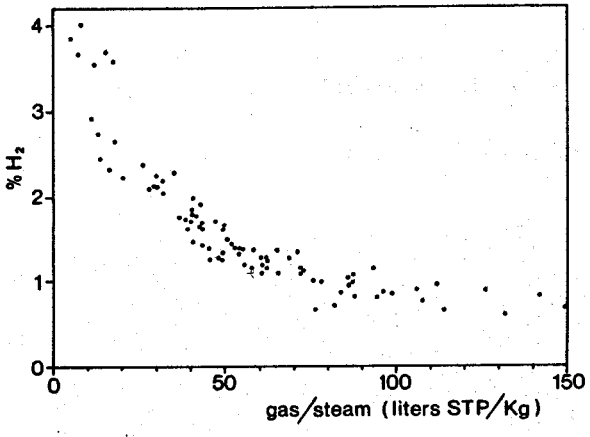

Figure 3. (%H_2) in dry gas vs gas/steam ratio for Larderello wells with reservoir temperatures between 240° and 270°C.

Note that the trend is the same for different wells and for one single well in different periods, whether the gas/steam ratio increases or decreases.

Figures 4 and 5 give the percentages of H_2S and H_2 plotted vs the gas/steam ratio for wells with reservoir temperatures between 180°C and 230°C.

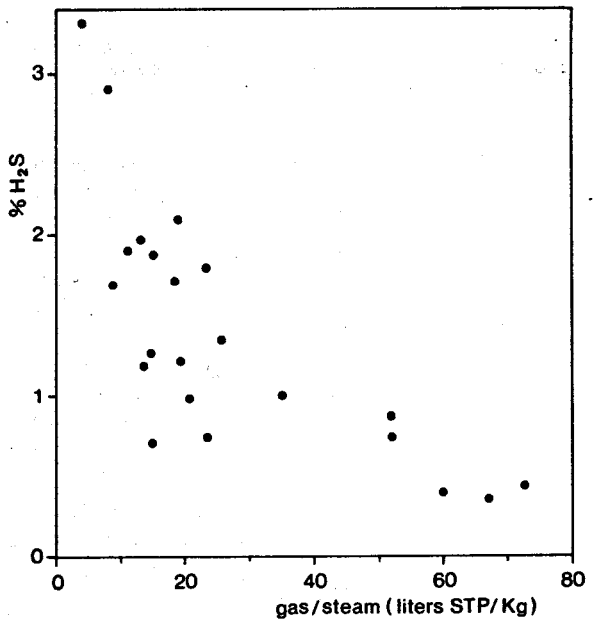

Figure 4. (%H_2S) in dry gas vs gas/steam ratio for Larderello wells with reservoir temperatures between 180°C and 230°C.

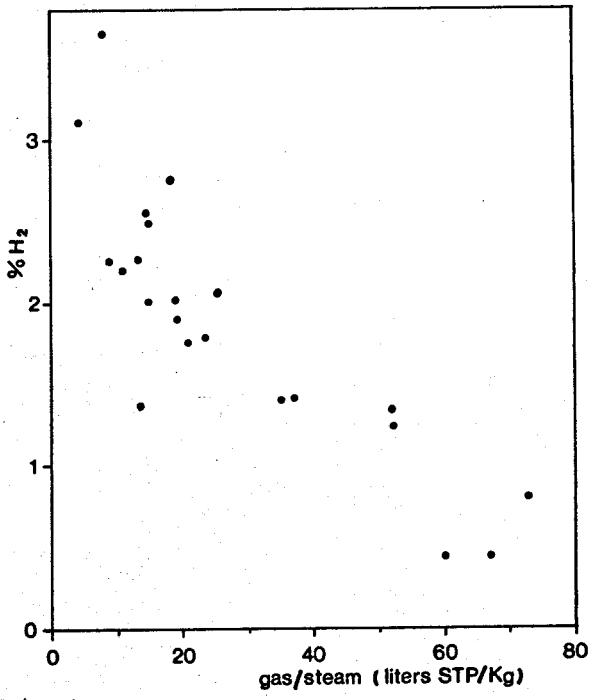

Figure 5. (%H_2) in dry gas vs gas/steam ratio for Larderello wells with reservoir temperatures between 180°C and 230°C.

The estimated reservoir temperatures are based on in-hole temperature logs and bottom-hole

temperature values calculated for the productive wells (Calore,1979; Calore et al.,1979).

Note that an inverse correlation with the gas/steam ratio was also observed for the percentage of H_2 in the dry gas in the superheated fumaroles of the Lassen geothermal system (Truesdell, written comm.,1982) and for the H_2 and H_2S in the fumaroles of Chipilapa area,El Salvador (Martinez, pers.comm.,1982). The approximately hyperbolic trend suggests that the H_2/H_2O and H_2S/H_2O ratios for a given temperature value are almost constant and, therefore, that the H_2 and H_2S contents are controlled by chemical reactions involving water.

Using several data on gas composition from The Geysers it was possible to extend the observed relationship for H_2 and H_2S up to three orders of magnitude for the gas/steam ratio.

Plotting the Larderello and The Geysers data on log-log paper (Figs.6,7), a deviation from a -1 slope straight line is observed, increasing towards the low values of the gas/steam ratio. This corresponds to the fact that, at a given temperature, the H_2/H_2O and H_2S/H_2O ratios do not remain constant as the gas/steam ratio decreases, but decrease continually and with differing trends.

For hydrogen we considered the reaction of water dissociation in the steam phase:

$$H_2O = H_2 + \tfrac{1}{2}O_2 \qquad (1)$$

The equilibrium constant is

$$\log K_H = 2.652 - 12776/T \qquad (2)$$

For this reaction we obtain the following equation:

$$\frac{P_{H_2}}{P_{gas}} = \frac{1}{P_{gas}/P_v} \cdot \frac{K_H}{f_{O_2}^{\frac{1}{2}}} \qquad (3)$$

where P_v is steam pressure and f_{O_2} oxygen fugacity. At first oxygen fugacity was computed from a linear function of 1/T, which is intermediate between those utilized by D'Amore and Panichi (1980) and D'Amore and Truesdell(1980):

$$\log f_{O_2} = 5.29 - 22512/T \qquad (4)$$

At 250°C, for a gas/steam ratio of 200 l/kg (STP) we obtain

$$(\%H_2) = P_{H_2}/P_{gas} \cdot 100 = 0.79$$

This point practically lies on the curve obtained for Larderello field data at that value of gas/steam ratio (Point A in Fig.7).

Assuming that at such high values of gas/steam ratio the reservoir fraction of steam by weight y is about unity, then H_2 and H_2O can be considered in equilibrium in the vapour phase, in accordance with equ.(1). From equ.(3) it then follows that

$$P_{H_2}/P_v = K_H/f_{O_2}^{\frac{1}{2}} \qquad (5)$$

that is, at a fixed temperature and for high steam quality values

$((\%H_2)$in the gas) . (gas/steam) = constant

Thus, if the steam phase alone exists in the reservoir, we should obtain a straight line of

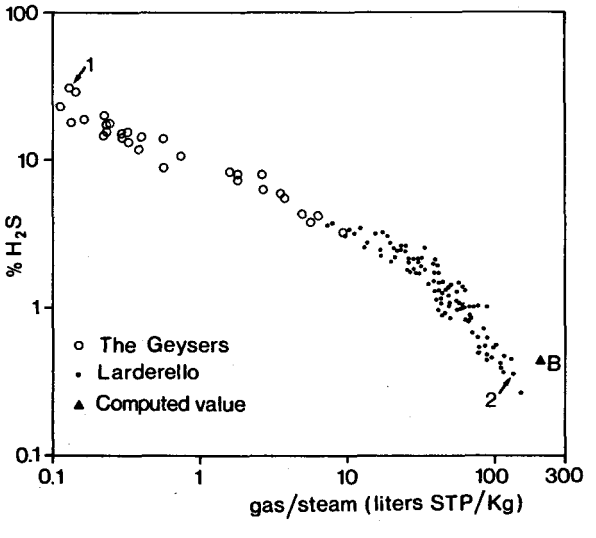

Figure 6. Log-log plot of ($\%H_2S$) in dry gas vs gas/steam ratio for wells at Larderello and The Geysers.

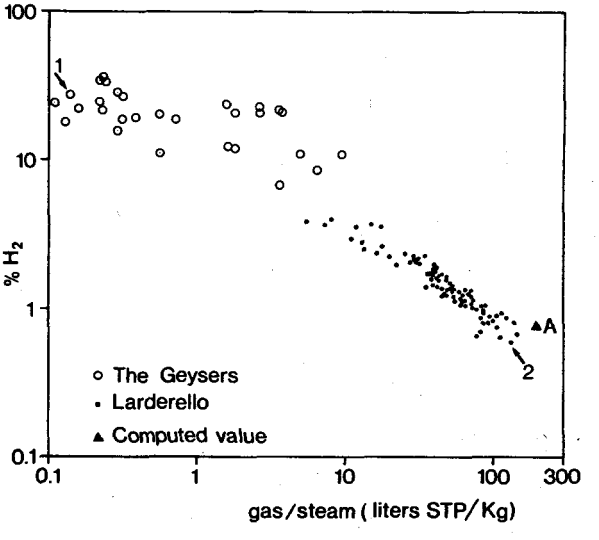

Figure 7. Log-log plot of ($\%H_2$) in dry gas vs gas/steam ratio for wells at Larderello and The Geysers.

slope -1 in the diagram in Fig.7. This is indeed almost the case, with some scattering of points, for the Larderello wells with the highest observed gas/steam ratios.

The slope of the curve in Fig.7 decreases with the decrease in gas/steam ratio until it more or less reaches constant values of ($\%H_2$) for the lowest gas/steam ratios at The Geysers. It is reasonable to assume that such low gas/steam ratios reflect high liquid saturations in the reservoir. We can, therefore, consider reaction (1) still valid for the steam phase in the reservoir, but the deviations from the straight line of slope -1 will depend on the fact that the fluid produced derives from a fluid whose steam quality y in the reservoir is less than 1. Thus, the third parameter, along with temperature and gas/steam ratio, required to explain the trend in Fig.7, is reservoir steam saturation.

Let us now consider the following equations, where n represents number of moles, subscripts v and 1 the steam and liquid phases in the reservoir, WH the fluid at wellhead, y the molar fraction of steam, and B_{H_2} the coefficient of H_2 distribution between the steam and liquid phases, which is a temperature-dependent quantity:

$$n_{H_2O,v} + n_{H_2O,1} = n_{H_2O,WH} \quad (6)$$

$$n_{H_2,v} + n_{H_2,1} = n_{H_2,WH} \quad (7)$$

$$(n_{H_2}/n_{H_2O})_v \; / \; (n_{H_2}/n_{H_2O})_1 = B_{H_2} \quad (8)$$

$$n_{H_2O,v} \; / (n_{H_2O,v} + n_{H_2O,1}) = y \quad (9)$$

From equations (6) and (9) we can obtain:

$$y\left(\frac{n_{H_2}}{n_{H_2O}}\right)_v + (1-y)\,\frac{1}{B_{H_2}}\left(\frac{n_{H_2}}{n_{H_2O}}\right)_v = \left(\frac{n_{H_2}}{n_{H_2O}}\right)_{WH} \quad (10)$$

From equations (5) and (10) we then obtain:

$$\log(\%H_2) = 5.095 - \log(G/V) + \log\frac{K_H}{f_{O_2}^{\frac{1}{2}}} + \log\left(y + \frac{1-y}{B_{H_2}}\right) \quad (11)$$

where the coefficient 5.095 is required if all the species are considered ideal gases and the gas/steam ratio (G/V) is expressed in STP litres/kg. Note that in this equation ($\%H_2$) is a function of the gas/steam ratio, temperature and steam quality. The percentage of hydrogen tends to increase with the decrease in the gas/steam ratio and increase in temperature and steam quality.

An equation similar to (11) can also be obtained for H_2S. We start with the following equation of equilibrium between H_2 and H_2S:

$$H_2S = H_2 + \tfrac{1}{2}S_2 \quad (12)$$

The equilibrium constant is

$$\log K_S = -0.13 - 4394.5/T + 0.79 \log T \quad (13)$$

The strong correlation observed between the values of H_2S and H_2 (Fig.8) in areas of the Larderello geothermal field with comparable temperatures and no local condensation or mixing phenomena supports equ.(12).

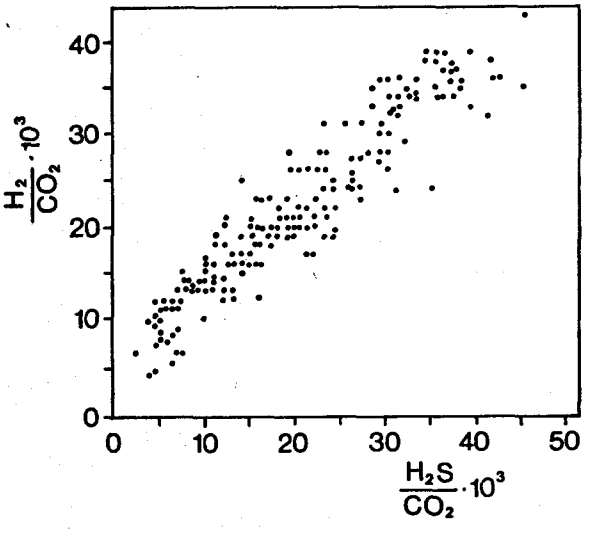

Figure 8. Relationship between H_2 and H_2S for Larderello wells (from D'Amore, 1977).

Let us now consider equations similar to those from (6) to (9) for H_2S, utilizing the distribution coefficient B_{H_2S} :

$$(n_{H_2S}/n_{H_2O})_v \; / \; (n_{H_2S}/n_{H_2O})_1 = B_{H_2S} \quad (14)$$

We then obtain an equation similar to equ.(10):

$$y(n_{H_2S}/n_{H_2O})_v + (1-y)\,\frac{1}{B_{H_2S}}\,(n_{H_2S}/n_{H_2O})_v = (n_{H_2S}/n_{H_2O})_{WH} \quad (15)$$

Combining equs.(12) and (1) we have:

$$P_{H_2S}/P_{H_2O} = (K_H\, f_{S_2}^{\frac{1}{2}})/(K_S f_{O_2}^{\frac{1}{2}}) \quad (16)$$

where f_{S_2} is sulphur fugacity. From equations (15) and (16) we have:

$$\log(\%H_2S) = 5.095 - \log(G/V) + \log\frac{K_H f_{S_2}^{\frac{1}{2}}}{K_S f_{O_2}^{\frac{1}{2}}} + \log\left(y + \frac{1-y}{B_{H_2S}}\right) \quad (17)$$

A simple equation relating the O_2 and S_2 fugacities could be obtained from the magnetite-pyrite equilibrium:

$$1/3Fe_3O_4 + S_2 = FeS_2 + 2/3O_2 \qquad (18)$$

The equilibrium constant is:

$$\log K_{MP} = -4.683 - 3796/T \qquad (19)$$

Although relatively large quantities of pyrite have been found in all the geothermal fields, including Larderello and The Geysers, magnetite shows only a sporadic occurrence. We can thus deduce that the magnetite field is occupied by iron silicates whose thermodynamic data are poorly known at the moment (Truesdell and Henley,1982). Obviously we should consider the real equilibria between iron silicates in the reservoir for oxygen fugacity also, instead of an empirical equation such as (4). However, equ.(18), which has been used by numerous other researchers in the past, could be a useful approximation at high temperatures. For example, from equ.(16), which includes $f_{S_2}^{\frac{1}{2}}$ and $f_{O_2}^{\frac{1}{2}}$, and equ.(18), we obtain:

$$(P_{H_2S}/P_{H_2O}) = \frac{K_H}{K_S K_{MP}^{\frac{1}{2}}} \frac{1}{f_{O_2}^{1/6}} \qquad (20)$$

so that the H_2S/H_2O ratio is dependent on $f_{O_2}^{1/6}$. Uncertainties of one order of magnitude in f_{O_2} thus lead to no serious errors in the computation of P_{H_2S}/P_{H_2O}.

Assuming y = 1 and a gas/steam ratio of 200 l/kg, ($\%H_2S$) becomes 0.46, which agrees with the field data for high gas/steam ratios observed at Larderello (point B in Fig.6). From equ.(20) we can modify equ.(17) to:

$$\log (\%H_2S) = 5.095 - \log (G/V) + \log \frac{K_H}{K_S K_{MP}^{\frac{1}{2}} f_{O_2}^{1/6}} + \log \left(y + \frac{1-y}{B_{H_2S}}\right) \qquad (21)$$

Utilizing equ.(4) for the f_{O_2} at 250°C we obtained the diagrams shown in Figs.9 and 10 for various values of y; the values observed for H_2S and H_2 are also plotted vs gas/steam ratio. In these figures the shift towards low gas/steam ratios corresponds to a regular decrease in steam saturation. Plotting all the field data on the diagram for 250°C is not entirely correct as the reservoir temperatures for the wells considered at The Geysers and Larderello run from 230° to 270°C. The saturation values attainable from the two diagrams, however, are compatible. For example, for samples 1 and 2 of The Geysers and Larderello (at extreme values of the gas/steam ratio), we obtain from the H_2 diagram y(1) = 2.2% and y(2) = 51%; from the H_2S diagram y(1) = 2.0% and y(2) = 51%.

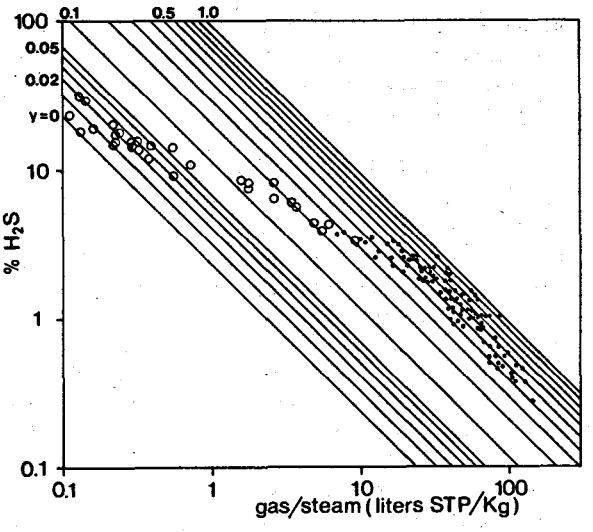

Figure 9. Relationship between ($\%H_2S$) and gas/steam ratio for different values of y at 250°C according to equ.(21), using empirical equ.(4) for f_{O_2}.

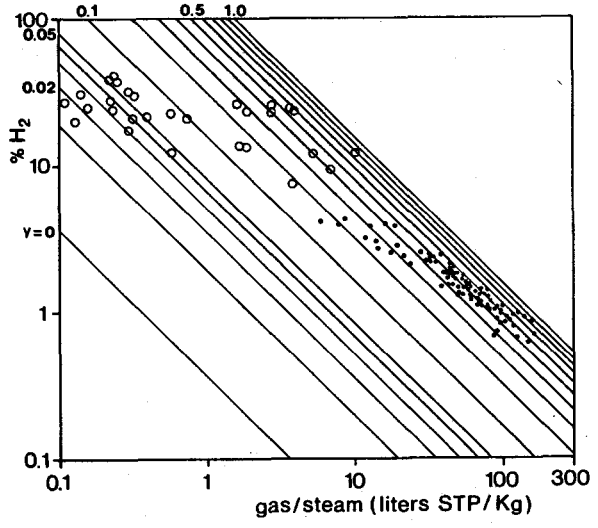

Figure 10. Relationship between ($\%H_2$) and gas/steam ratio for different values of y at 250°C according to equ.(11), using empirical equ.(4) for f_{O_2}.

Utilizing the H_2 and H_2S concentrations, simultaneous evaluations of temperature and saturation in the reservoir can now be obtained, provided that a more accurate f_{O_2} than that given by equ.(4) could be introduced in equs.(22) and (23).

$$\log (H_2/H_2O) = 2.652 - 12776/T - \tfrac{1}{3}\log f_{O_2} + \log \left(y + \frac{1-y}{B_{H_2}}\right) \qquad (22)$$

$$\log (H_2S/H_2O) = 5.124 - 6483/T - 0.79 \log T - 1/6 \log f_{O_2} + \log (y + \frac{1-y}{B_{H_2S}}) \quad (23)$$

Equation (4) is, in fact, not accurate enough for H_2, as (H_2/H_2O) is a function of the square root of f_{O_2}. The y values obtained from H_2 concentrations using equ.(4) for f_{O_2} were generally poorly compatible with those calculated by means of the Fisher-Tropsch equation, according to D'Amore and Celati (1983):

$$CH_4 + 2H_2O = CO_2 + 4H_2 \quad (24)$$

The equilibrium constant is:

$$\log K_C = 10.76 - 9323/T \quad (25)$$

Starting with the total composition of the fluid at wellhead, this method calculates for each temperature the molar fractions of all the gaseous components in the steam phase coexisting with the liquid phase in the reservoir. The calculated values of these concentrations, $X_{v,i}$, are functions of temperature and of the molar steam fraction, y, present in the reservoir. The gaseous species are, in fact, distributed in the two phases in the reservoir. Steam quality y is calculated from $(K_C f_w^2 \gamma_{CH_4} / \gamma_{CO_2} \gamma_{H_2}^4) =$

$$(X_{v,H_2}^4 X_{v,CO_2} / X_{v,CH_4}) P_t^4 \quad (26)$$

where f_w is water fugacity, γ_i the fugacity coefficients for the various species i, and P_t total pressure in the reservoir. The left-hand side of the equation is dependent on temperature alone, but the right-hand side is also a function of y.For each temperature value there will, therefore, be one y value such that the two members of equ.(26) will be equal.

To obtain a value of f_{O_2} for each gas analysis we utilized equ.(24) with equ.(1), so that:

$$\log f_{O_2} = -\tfrac{1}{2} \log(CH_4/CO_2) + 18.014 - 23648.7/T - 4.1521 \log T - \tfrac{1}{2}\left[\log(y + \frac{1-y}{B_{CO_2}}) - \log(y + \frac{1-y}{B_{CH_4}})\right] \quad (27)$$

When calculating f_{O_2} we ignore the term in brackets containing y and the distribution coefficients. This term is in fact less than 0.1 logarithmic units for $y > 0.01$ and temperatures $< 270°C$. By introducing the approximated equ. (27) in equs.(22) and (23) we obtain:

$$\log(H_2/H_2O) = -6.355 - 951.6/T + 2.076 \log T + 1/4 \log(CH_4/CO_2) + \log (y + \frac{1-y}{B_{H_2}}) \quad (28)$$

and

$$\log(H_2S/H_2O) = 2.122 - 2542/T - 0.098 \log T + 1/12 \log(CH_4/CO_2) + \log (y + \frac{1-y}{B_{H_2S}}) \quad (29)$$

where B_{H_2} and B_{H_2S} are known temperature-dependents[2]:

$$\log B_{H_2} = 6.2283 - 0.01403\ t°C \quad (30)$$

$$\log B_{H_2S} = 4.0547 - 0.00981\ t°C \quad (31)$$

Table 1 gives the calculated steam qualities for some wells at Larderello and The Geysers, at fixed temperatures: y (FT) were obtained from the method by D'Amore and Celati (1983), $y(H_2)$ from equ.(28) and $y(H_2S)$ from equ.(29). The temperatures used for Larderello are reservoir values estimated as described above. As the reservoir temperature is not known for each well at The Geysers we assumed a value of 240°C; this leads to some inaccuracy in the calculation of y, as the temperatures may obviously vary from well to well. Figures 11 and 12 are diagrams showing the saturation values obtained by the various methods. A better fitting would be obtained by plotting a temperature of 220°-230°C for some wells at The Geysers, instead of 240°C.

Using both equs.(28) and (29) concomitantly,we can calculate both temperature and saturation, as shown in Fig.13. Plotting the data from Table 1 we can see that the temperatures of The Geysers samples are generally lower than those from Larderello, and the steam quality values much lower.

We must point out that calculation of f_{O_2} with equ.(27) gives an approximate value only,as the CH_4/CO_2 ratio is also a function of steam pressure (P_v) and the latter varies from one part of the reservoir to another.

$$P_{CH_4}/P_{CO_2} = \frac{K_H P_v^2}{K_C f_{O_2}^{\frac{1}{2}}} \quad (32)$$

Instead of P_v we used saturated steam fugacity, which is a function of temperature only. The problem still remains of developing a method capable of evaluating f_{O_2} and f_{S_2} in the various fields, and zones of the same field or reservoir.

The calculated value of steam quality, y, can be used to estimate the drainage volume of each productive well. Let us assume that the steam

Locality	Temp. °C	Gas/steam 1STP/kg	$\log \frac{H_2S}{H_2O}$	$\log \frac{H_2}{H_2O}$	$\log \frac{CH_4}{CO_2}$	y(F.T.) %	$y(H_2S)$ %	$y(H_2)$ %
1) The Geysers	240	0.11	-4.71	-4.67	-0.63	1	1	1
2) The Geysers	240	0.13	-4.72	-4.72	-1.14	1	1	1
3) The Geysers	240	0.18	-4.57	-4.33	-0.39	2	2	2
4) The Geysers	240	0.22	-4.58	-4.21	-1.24	5	2	5
5) The Geysers	240	0.23	-4.55	-4.18	-1.00	5	2	4
6) The Geysers	240	0.32	-4.47	-4.17	-0.89	5	3	4
7) The Geysers	240	0.56	-4.39	-4.31	-1.14	4	4	3
8) The Geysers	240	0.72	-4.21	-3.97	-0.79	7	7	6
9) The Geysers	240	1.6	-4.14	-3.80	-0.61	10	8	8
10)The Geysers	240	1.8	-3.94	-3.51	-0.71	21	15	18
11)The Geysers	240	1.8	-3.98	-3.79	-0.70	11	13	9
12)The Geysers	240	3.8	-3.78	-3.20	-0.53	38	21	33
13)The Geysers	240	4.4	-3.74	-3.15	-0.78	49	32	42
14)The Geysers	240	5.2	-3.49	-3.04	-0.69	45	52	60
15)The Geysers	240	5.6	-3.63	-3.02	-0.48	56	31	48
16)The Geysers	240	9.8	-3.35	-2.84	-0.53	86	61	75
17)Larderello	210	3.6	-4.77	-4.40	-3.27	16	7	15
18)Larderello	240	6.1	-3.83	-3.79	-2.05	23	26	20
19)Larderello	220	8.8	-3.92	-3.80	-2.03	28	23	25
20)Larderello	260	9.5	-3.65	-3.78	-2.32	23	26	19
21)Larderello	270	14.0	-3.46	-3.37	-1.72	37	30	31
22)Larderello	270	18.0	-3.35	-3.33	-1.83	44	40	36
23)Larderello	270	19.0	-3.31	-3.26	-1.77	49	44	41
24)Larderello	260	20.0	-3.48	-3.50	-2.21	41	40	34
25)Larderello	260	20.0	-3.35	-3.14	-1.64	67	49	56
26)Larderello	270	22.0	-3.27	-3.20	-1.76	57	47	48
27)Larderello	250	25.0	-3.41	-3.41	-1.79	44	54	37
28)Larderello	240	28.0	-3.72	-3.64	-2.16	35	35	30
29)Larderello	270	28.0	-3.25	-3.18	-1.67	56	50	46
30)Larderello	260	33.0	-3.35	-3.31	-1.88	52	51	43
31)Larderello	260	44.0	-3.25	-3.24	-2.14	71	68	59
32)Larderello	250	44.0	-3.33	-3.19	-2.11	87	70	74
33)Larderello	240	135.0	-3.42	-3.21	-2.01	87	69	75

Table 1. Steam qualities for some wells at Larderello and The Geysers, at fixed temperatures.

produced by a well from the start of production derives from the total vaporization of the liquid water stored in the volume V:

$$V = \frac{m_1 v_1}{\phi S_1} \qquad (33)$$

where m_1 is the cumulative steam production, v_1 is the specific volume of liquid water at boiling point, ϕ is porosity, and S_1 is liquid saturation

$$S_1 = 1 + (\frac{1}{y} - 1)(v_1/v_v) \qquad (34)$$

Applying equ.(33) to some wells at Larderello, at 250°C, and assuming a porosity of 10%, we can calculate the radius r of a hypothetical spherical volume of the reservoir feeding each well. For wells that have been producing for a few tens of years r is about one kilometre. In the case of recent wells at The Geysers, on the other hand, r proves to be of the order of about 150 m. These values are reasonable if we consider that at the moment at Larderello the liquid water boils far from wellbottom.

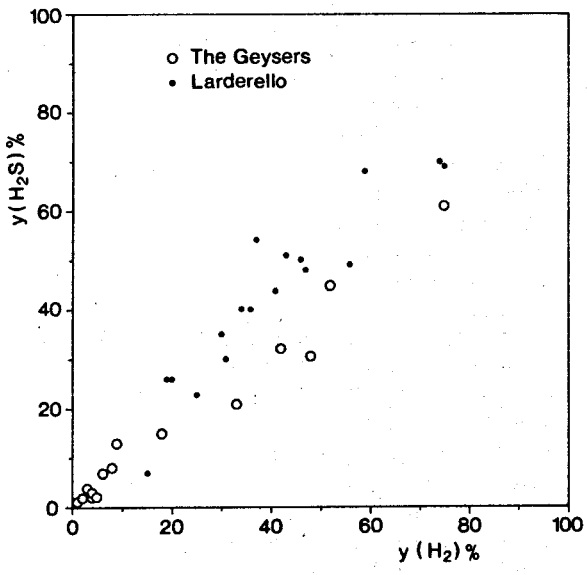

Figure 11. Comparison of y values calculated with equs.(28) and (29) from data given in Table 1, at fixed temperatures.

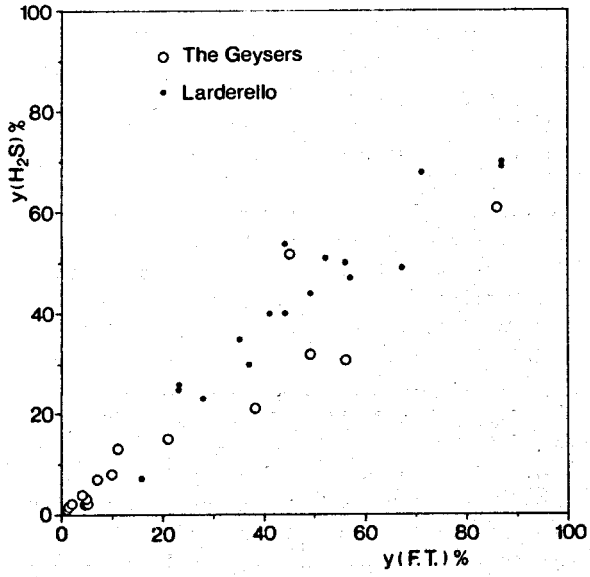

Figure 12. Comparison of y values calculated with equ.(29) and with the Fisher-Tropsch equation (24), using the method of D'Amore and Celati (1983).

REFERENCES

Bottinga,Y. (1969),"Calculated fractionation factors for carbon and hydrogen isotope exchange in the system calcite-carbon-dioxide-graphite-methane-hydrogen-water vapour," Geochim.Cosmochim.Acta, v.33, p.49.

Calore,C.(1979),"Distribution of temperature at the top of the geothermal reservoir at Larderello," CNR unpublished report, in Italian.

Calore,C.,Celati,R.,D'Amore,F. and Noto,P. (1982),"Geochemical evidence of natural recharge in Larderello-Castelnuovo area," this Workshop.

Calore,C.,Celati,R.,D'Amore,F.,Squarci,P.and Truesdell,A.H.(1980,"A geologic, hydrologic and geochemical model of the Serrazzano zone of the Larderello geothermal field," Proc. Sixth Workshop Geothermal Reservoir Engineering, Stanford University,Stanford,CA., 16-18 Dec.,p.21-27.

Calore,C.,Celati,R.,Squarci,P. and Taffi,L. (1979),"Hydrogeological and thermal characteristics of the peripheral zones north and west of the Larderello field," Proc.First Informative Seminar of the Geothermal Research Units of CNR, Finalized Energy Project, Rome,18-21 Dec. 1979, p.248-258. (In Italian).

Cappetti,G.,Calore,C.,Celati,R., Giovannoni,A. and Ruffilli,C.(1982),"Reinjection in the Larderello geothermal field," International Conference on Geothermal Energy, Florence,Italy, 11-14 May, p.395-407.

Celati,R.,Noto,P.,Panichi,C.,Squarci,P. and Taffi,L.(1973),"Interactions between the steam reservoir and surrounding aquifers in the Larderello geothermal field," Geothermics, v.2, p.174-185.

Celati,R.,Marconcini,R.,Neri,G.,Pruess,K., Schroeder,R. and Weres,O.(1980),"Modeling vapour-dominated systems-Serrazzano. Lumped parameter models," Proc.Second DOE-ENEL Workshop for Cooperative Research in Geothermal Energy, Berkeley,p.328-341.

Craig,H.(1953),"The geochemistry of the stable carbon isotopes," Geochim.Cosmochim.Acta,v.3, p.53-92.

Craig,H.(1975),"Isotopic temperatures in geothermal systems," IAEA Advisory Group on the Application of Nuclear Techniques to Geothermal Studies,Pisa, unpublished oral commun.

D'Amore,F.(1977),"Study of the applicability of the geochemistry of gases in geothermal prospection," Seminar on Geothermal Energy, Brussels, 6-8 Dec., EUR 5920,v.II,p.441-454.

D'Amore,F.,Calore,C. and Celati,R.(1981),"Temporal evolution of the composition of the fluid from Serrazzano zone(Larderello)," Proc. Seventh Workshop Geothermal Reservoir Engineering,Stanford University,Stanford,CA,15-17 Dec.,p.91-96.

D'Amore,F. and Celati,R.(1983),"Methodology for calculating steam quality in geothermal reservoirs,"Geothermics,v.12,in press.
D'Amore,F.,Celati,R.,Ferrara,G.C. and Panichi C.(1977),"Secondary changes in the chemical and isotopic composition of the geothermal fluids in the Larderello field,"Geothermics, v.5, p.153-163.
D'Amore,F. and Nuti,S.(1977),"Notes on the chemistry of geothermal gases,"Geothermics, v.6, p.39-65.
D'Amore,F. and Panichi,C.(1980),"Evaluation of deep temperatures of hydrothermal systems by a new gas-geothermometer,"Geochim.Cosmochim.Acta, v.44, p.549-556.
D'Amore,F. and Truesdell,A.H.(1979),"Models for steam chemistry at Larderello and The Geysers," Proc.Fifth Workshop Geothermal Reservoir Engineering,Stanford University, Stanford,CA, 12-14 Dec.,p.283-297.
D'Amore,F. and Truesdell,A.H.(1980),"Gas thermometry for drillhole fluids from vapor-dominated and hot water geothermal fields," Proc.Sixth Workshop Geothermal Reservoir Engineering, Stanford University, Stanford,CA, 16-18 Dec.,p.351-360.
Giggenbach,W.F.(1980),"Geothermal gas equilibria," Geochim.Cosmochim.Acta,v.44,p.2021-2032.
Giggenbach,W.F.(1981),"Geothermal mineral equilibria,"Geochim.Cosmochim.Acta, v.45,p.393-410.
Giggenbach,W.F.(1982),"Carbon-13 exchange between CO_2 and CH_4 under geothermal conditions," eochim.Cosmochim.Acta, v.46, p.159-165.
Giovannoni,A., Allegrini,G.,Cappetti,G. and Celati,R.(1981),"First results of a reinjection experiment at Larderello," Proc.Seventh Workshop Geothermal Reservoir Engineering, Stanford University,Stanford,CA,15-17 Dec., p.77-84.
Grant,M.A.(1979),"Water content of the Kawah Kamojang geothermal reservoir,"Geothermics, v.8, p.21-30.
Hulston,J.R.(1977),"Isotope work applied to geothermal systems at the Institute of Nuclear Sciences,New Zealand," Geothermics,v.5,p.89-96.
Hulston,J.R. and McCabe,W.J.(1962a),"Mass spectrometer measurements in the thermal areas of New Zealand.Part 1.Carbon dioxide and residual gas analyses,"Geochim.Cosmochim.Acta, v.26, p.383-397.
Hulston,J.R. and McCabe,W.J.(1962b),"Mass spectrometer measurements in the thermal areas of New Zealand.Part 2.Carbon isotopic ratios," Geochim.Cosmochim.Acta,v.26,p.399-410.
Mazor,E.(1978),"Noble gases in a section across the vapor-dominated geothermal field of Larderello,Italy,"PAGEOPH,v.117,p.262-275.
Nehring,N.L. and D'Amore,F.(1981),"Gas chemistry and thermometry of the Cerro Prieto geothermal field,"Proc.Third Symp.on the Cerro Prieto Field, 24-26 March,p.178-185.
Nuti,S.,Calore,C. and Noto,P.(1981),"Use of environmental isotopes as natural tracers in a reinjection experiment at Larderello,"Seventh Workshop Geothermal Reservoir Engineering, Stanford University,Stanford,CA,15-17 Dec., p.85-90.
Panichi,C.,Celati,R.,Noto,P.,Squarci,P.,Taffi, L. and Tongiorgi,E.(1974),"Oxygen and hydrogen isotope studies of the Larderello(Italy) geothermal system,"In:Isotope Techniques in Groundwater Hydrology,1974.IAEA,v.2,p.3-28.
Panichi,C.,Ferrara,G.C. and Gonfiantini,R.(1977),"Isotope geothermometry in the Larderello geothermal field,"Geothermics,v.5,p.81-88.
Panichi,C. and Gonfiantini,R.(1978),"Environmental isotopes in geothermal studies,"Geothermics, v.6, p.143-161.
Panichi,C.,Nuti,S. and Noto,P.(1979),"Use of isotopic geothermometers in the Larderello geothermal field,"In:Isotope Hydrology 1978,v.II, International Atomic Energy Agency,Vienna, p.613-630.
Petracco,C. and Squarci,P.(1976),"Hydrologic balance of Larderello geothermal region,"Proc. 2nd U.N.Symp. on the Development and Use of Geothermal Resources,San Francisco,v.1,p.521-530.
Sestini,G.(1970),"Superheating of geothermal steam,"Proc.U.N.Symp. on the Development and Utilization of Geothermal Resources, Pisa. Geothermics,sp.iss.2, v.2,pt.1,p.622-648.
Truesdell,A.H. and Henley,R.W.(1982),"Chemical equilibria in the Cerro Prieto hydrothermal fluid," Proc.Fourth Symposium on the Cerro Prieto geothermal field,Guadalajara,Mexico, 10-12 Aug.
Truesdell,A.H. and Frye,G.A.(1977),"Isotope geochemistry in geothermal reservoir studies," Society Petroleum Engineers n.6533, 6p.
Truesdell,A.H. and Nehring,N.L.(1978),"Gases and water isotopes in a geochemical section across the Larderello,Italy,geothermal field," PAGEOPH, v.117, p.276-289.
Truesdell,A.H.,Nehring,N.L. and Frye,G.A.(1977),"Steam production at The Geysers,California,comes from liquid water near the well-bottom(abs)," Geological Society America Abstracts with Programs,v.9, p.1206.
Truesdell,A.H. and White,D.E.(1973),"Production of superheated steam from vapor-dominated geothermal reservoirs,"Geothermics,v.2,p.154-173.
White,D.E.,Muffler,L.J.P. and Truesdell,A.H.(1971),"Vapor-dominated hydrothermal systems compared with hot-water systems,"Econ.Geol., v.66,p.75-97.

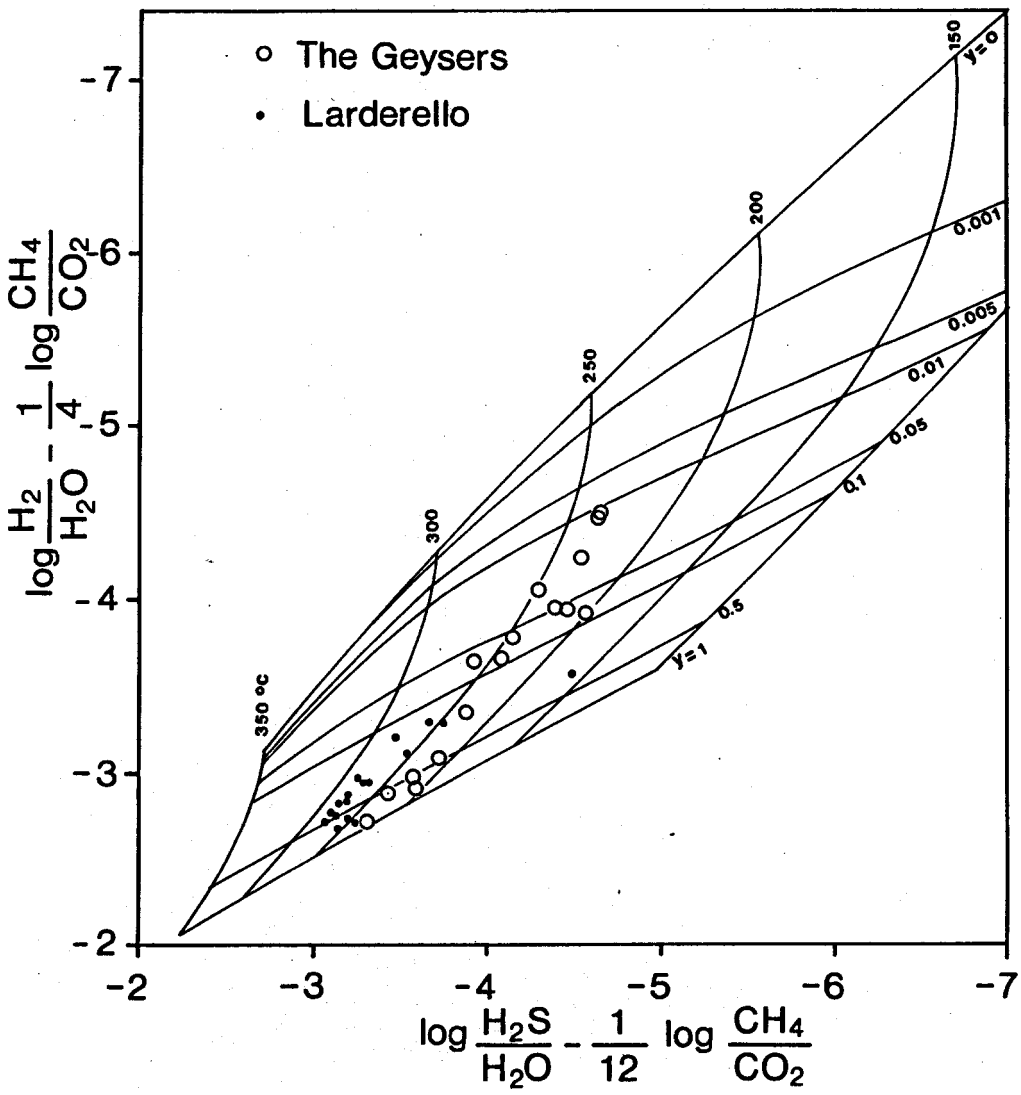

Figure 13. Application of equations (28) and (29) to the simultaneous calculation of temperature and steam quality.

Proceedings Eighth Workshop Geothermal Reservoir Engineering
Stanford University, Stanford, CAlifornia, December 1982
SGP-TR-60

"A Summary of the Chemical Characteristics of the HGP-A Well; Puna, Hawaii"

Donald M. Thomas

Hawaii Institute of Geophysics, Honolulu, Hawaii 96822

ABSTRACT

The HGP-A geothermal well is located on the Lower East Rift Zone of Kilauea Volcano. It was completed in 1976 to a depth of 1966 meters and has a bottomhole temperature of 360°C. Evaluation of the chemistry of the fluids produced indicate that recharge to the reservoir discovered by the HGP-A well is largely fresh meteoric water with smaller amounts of seawater recharge. The changes in fluid chemistry during production suggest that at least two separate aquifers are providing fluids to the well and that silica deposition is occuring in the reservoir formation. Isotopic data indicate that the fluid circulation and residence times in the reservoir are relatively short and that the heat source for this part of the rift zone is either very young or relatively large.

Introduction

HGP-A geothermal well was completed in 1976 on the lower East Rift Zone of Kilauea Volcano. The total depth of the well is 1966 meters and under static conditions has a bottomhole temperature of approximately 360°C. Production testing of the well indicated that it was capable of producing approximately 50,000 kg/hr of a mixed fluid having a steam quality of about 48%. In 1981 a 3 megawatt electrical generator was installed on the well as a "proof of feasibility" project (jointly sponsored by the U.S. Department of Energy, the State and County of Hawaii and Hawaiian Electric Co.) to demonstrate the technical feasibility of generating electrical power from the reservoir discovered by HGP-A. At the present time the wellhead generator is producing a gross output of 2.9 MW.

Well Fluid Chemistry

During the initial testing of HGP-A samples of downhole and production fluids were analyzed for major trace element compositions and noncondensable gas concentrations. More recently, production fluid chemistry has been monitored on an intermittent basis since the generator facility began operations in June 1981. The chemical data acquired during the testing and production from HGP-A have provided a number of insights into the properties of the reservoir as well as the production characteristics of the wellbore itself.

Downhole Chemistry

Downhole sampling in HGP-A was conducted during the periods of wellbore shut-in that were interspersed with short duration production flow testing and thus were able to monitor changes in production formations induced by well flow. Figures 1 and 2 and Table 1 present a selected set of downhole chemistry data collected during the first twelve months of production testing.

The chloride concentrations observed in the wellbore fluids (Figure 1) were relatively uniform at all sampling depths through December 1976. The two subsequent downhole profiles indicate, however, that higher salinity fluids were produced from two intermediate depth aquifers after the December 1976 flow test. These data suggest that the initial production from HGP-A was entirely from a single aquifer but, after repeated testing, higher salinity aquifers began providing fluids to the well. A change in aquifer productivity is supported by engineering data that indicated increased mass flow rates with each flow test performed. On this basis it is suggested that substantial skin damage occurred to the wellbore by lost mud during drilling and completion operations and that repeated thermal and pressure shocks associated with production testing were required in order to clear the damaged aquifers.

It is of note that magnesium ion concentrations (Figure 2) in the downhole samples do not follow the chloride concentrations on a one to one basis. Although there is a substantial increase in magnesium ion associated with the upper saline aquifer, the higher salinity fluids in the deeper production zone have a much smaller change in magnesium concentration. It has been found that magnesium ion is strongly depleted in thermally altered groundwaters in Hawaii (Cox and Thomas, 1979) through the formation of the alteration mineral chlorite. These data suggest that the saline fluids entering the wellbore at depth have come to chemical and thermal equilibrium with the reservoir rocks whereas the fluids entering at shallow depths are relatively unaltered seawater. Thus it is probable that the upper saline aquifer was producing low temperature fluids to the wellbore and thereby reducing the average discharge

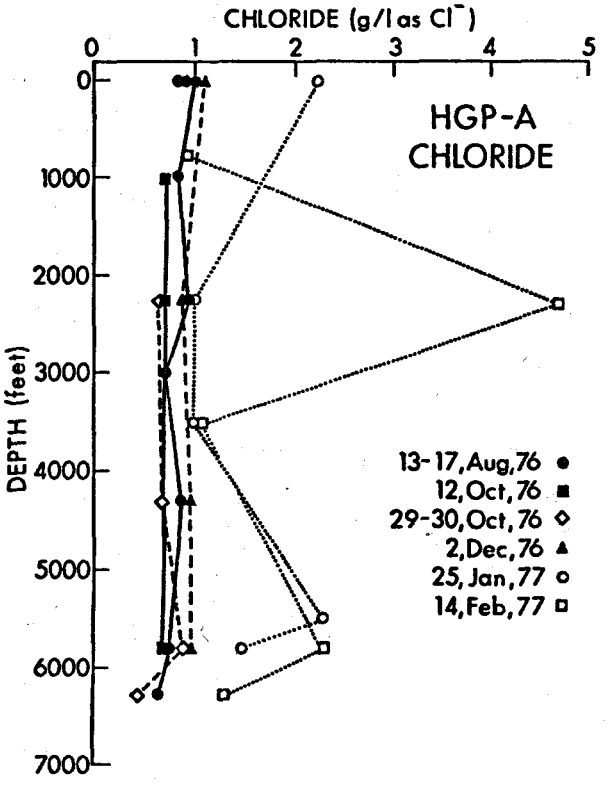

Figure 1 Plot of Chloride Concentration versus depth for downhole profile samples.

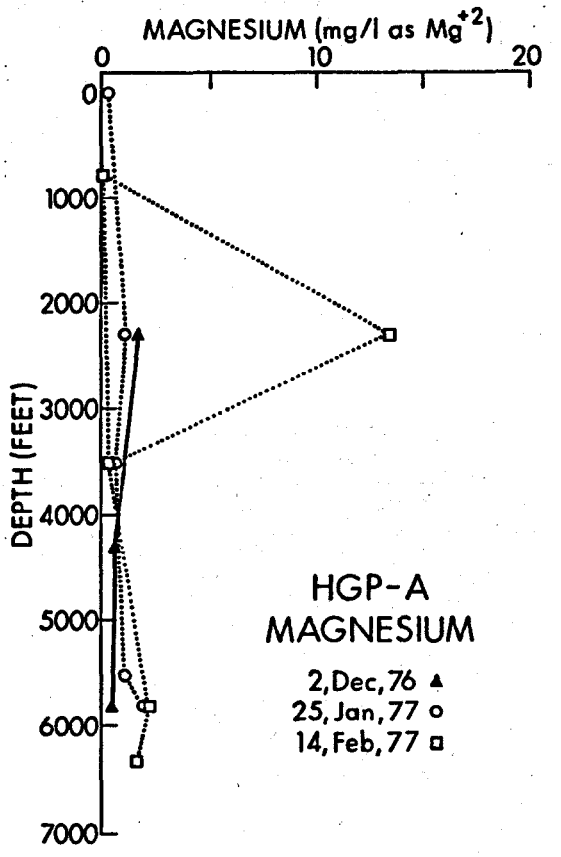

Figure 2 Plot of Magnesium Ion Concentration versus depth for downhole profile samples.

enthalpy from HGP-A. During subsequent operations this upper zone was cased off. However, as a result of the recasing program, damage was sustained to the slotted liner in the deeper wellbore and no further downhole sampling has been possible.

Production Chemistry: Brine

During early flow testing of HGP-A the salinity of the fluids produced (Table 2) was quite low and. even though the salinity has increased during recent production periods, the total dissolved solids content of the reservoir fluids has remained well below seawater abundances. The low salinity of the geothermal fluids was unexpected since the primary production zones in HGP-A are located nearly 1500 meters below the bottom of the Ghyben-Herzber- fresh water lens that was initially thought to be present in this area.

The relatively small amounts of sea water present in the HGP-A reservoir may be the result of the permiability structure of the Kilauea East Rift Zone. The rift system is made up of numerous vertical or near vertical dikes and fractures trending in an east-west direction. The fracturing in the rift system allows rapid recharge and fluid circulation in a vertical and east-west direction but the numerous dikes within the rift zone presents a virtually impermiable barrier to seawater intruding into the system from the south. Thus rapid vertical and east-west circulation of freshwater through the rift system tends to dilute the relatively smaller amounts of intruding seawater present in the deeper parts of the rift zone.

The chloride concentrations in the reservoir fluids suggests that approximately 10% to 20% of the recharge to the reservoir is of seawater origin. However, it is apparent that the cation concentrations in the saline component have been substantially altered from those present in seawater. Both calcium and magnesium have been heavily depleted whereas potassium and sodium have been enriched relative to seawater by about 450% and 5% respectively. Magnesium depletion, as noted above, is probably the result of chlorite formation in the reservoir whereas the retrograde solubility product constant of calcium and sulfate ion may provide the controlling mechanism for the removal of calcium ion from seawater. Both chlorite and anhydrite have been found in cores from the deeper part of HGP-A; ther former as an alteration product and the latter as a vein filling mineral (Stone, 1977). It is of note that anhydrite deposition may also provide a secondary controlling mechanism for the exclusion of

Table 1. Downhole Water Chemistry Data (mg/kg)

Date	Depth (meters)	Cl	Na	K	Mg	Ca
12/2 /76	690	910	500	77.5	1.9	21
12/2 /76	1310	920	480	85	0.7	17.3
12/3 /76	1770	980	500	223	0.6	22.6
2/14/77	690	4800	2160	248	14.7	465
2/14/77	1070	1030	600	82.5	0.4	39.3
2/14/77	1770	2330	1080	160	2.0	161
2/14/77	1920	1310	620	87.5	1.9	95.7

Table 2. Chemical Analyses of HGP-A Brines During Production (mg/kg)

	Cl^-	Na	K	Mg	Ca	SiO_2
11-8 -76	2190	1200	212	<0.5	81.9	
11-17-76	2520	1320	223	0.5	78.8	
1-29-77	2590	1260	225	0.5	78.2	
4-11-77	3050	1460	266	0.1	77.3	710
6-15-78	2420	1500	250	0.08	56.6	
1-14-80	2450	1440	216	0.1	33.2	
6-12-81	1593	806	154	0.02	18.5	1200
9- 4-81	3700	2190	250	0.1	72	800
12-22-81	3261	1745	281	0.04	58.3	1100
3-22-82	5050	2655	431	0.080	121.	
4-19-82	5293	2792	472	0.134	123.	799
5-17-82	5489	3066	508	0.060	124	802
6-14-82	5677	3200	513	0.070	149	818
7-14-82	6044	3300	536	0.073	157.	

seawater from the interior of the rift zone. The enrichment of potassium in the reservoir fluids is largely the result of alteration of small amounts of plagioclase or interstitial glass present in the reservoir basalts (Bischoff and Dickson, 1975).

As noted above, the chloride and total dissolved solids content of the geothermal brines has increased throughout the production history of HGP-A. This increase has been of major concern not only from the engineering aspect of handling higher salinity fluids but also in terms of the possibility that cold seawater is intruding into the reservoir tapped by HGP-A. An evaluation of the major element chemistry changes indicates that the cation to chloride ion rations have remained relatively constant; if cold seawater were entering the reservior we would expect to see a trend of increasing calcium and magnesium to chloride ion ratios. Thus it is likely that, if seawater is entering the HGP-A reservoir, it has come to chemical and thermal equilibrium with the reservoir conditions and may not pose an immediate threat to the enthalpy of the production fluids.

An alternative explanation for at least part of the observed increase in fluid salinity is that steam formation in the production aquifers is gradually mining more heat from the reservoir rock and thereby increasing the overall steam quality. During recent production periods the steam quality of the well discharge has been observed to increase at constant or declining total flow during the first hundred hours of production and thus this may provide one mechanism for increasing the residual fluid salinity. However, the entire change in TDS concentrations during the current production period cannot be accounted for by this mechanism alone: the steam quality has increased by approximately 30% beyond its initial value whereas the total dissolved solids concentrations increased by approximately 300%.

The application of cation geothermometers (Fournier and Truesdell, 1973) to the reservoir fluid compositions have been attempted on a number of occasions. The results of these calculations yield reservoir temperatures that range from 80°C to 120°C below the measured static bottom hole temperature in HGP-A. The lack of agreement between the cation geothermometer and the measured temperature is considered to be largely due to the general deficiency of potassium bearing minerals in Hawaiian basalts. Silica geothermometry calculations have also been attempted with similar results. Although the silica concentrations are quite high in the initial fluids produced, the concentrations drop off rapidly after production begins. This suggests that silica is rapidly reequilibrating in the flashed geothermal brines by deposition of silica in the reservoir formation. Calculation of silica temperatures on the flashed brines using Fournier and Potter's (1982) revised silica geothermometer yield temperatures (345°C) at the upper end of the applicable temperature range of the thermometer and slightly below the maximum measured downhole temperature of 360°C.

The deposition of hydrothermal minerals in the reservoir rock due to steam formation is of major concern for the future productivity of the resource. As noted above, it is highly probable that silica is being deposited from the thermal fluids during the flashing process. However, evaluation of the major element chemistry suggests that deposition of other scale minerals is not presently occurring. Comparison of the cation concentrations to the chloride ion indicates a nearly constant ratio during present production periods even though the individual concentrations have increased by 300%. If deposition were occurring one would expect a gradual decline in the ratio of the cation being deposited to the chloride ion concentration.

Non Condensable Gas Compositions

The concentration and composition of non-condensable gases in the steam phase have been monitored since the completion of HGP-A (Table 3). Preliminary analyses of the gases during short duration testing indicated quite variable compositions and concentrations; more recent intensive monitoring of the steam chemistry during start up operations has indicated that the concentration of non-condensable gases changes quite radically during the first hundred hours of production and then gradually stabilizes. The observed changes are thought to be due in part to the development and migration of the flash front out into the reservoir.

The total concentration of non-condensable gases in the steam phase is not appreciably higher than that observed in other geothermal systems worldwide. However, the composition of the non-condensable gases is quite different: hydrogen sulfide makes up approximately 40% of the total mass and hydrogen is present in a nearly equal molar concentration to nitrogen. In addition, recent analysis of the steam phase for trace volatiles has been unable to detect ammonia, mercury, boron, or arsenic.

Table 3.
Non-Condensable Gas Compositions (mg/kg)

Date	CO_2	H_2S	N_2	H_2
2/09/77	4431	1435	131	46.3
5/08/77	2378	878	375	15.1
7/19/77	445	112.	116.	2.3
1/19/80	1000	750	168	11.0
5/31/82	1238	886	129	11.0

Stable and Radio Isotopic Studies

Analyses of the light stable isotopes of helium, hydrogen, oxygen, and carbon were performed on the fluids from HGP-A during the initial testing of the well. Helium isotopic analyses yielded $^3He/^4He$ ratios of approximately seven times the atmospheric ratio and about half that observed for helium in the Kilauea summit fumaroles. These data suggest that the heat source for the HGP-A reservoir is a relatively young (or large) magma body that has not yet completely outgassed its primordial component of inert gases.

During early production tests, samples of water were analyzed for H/D and $^{18}O/^{16}O$ isotopic ratios. The results obtained indicated that the majority of the recharge to the geothermal well was meteoric water with minor amounts of seawater and hydrothermal (^{18}O shifted) water present. Although this would suggest extremely short recharge and residence times, more complete hydrogen and oxygen isotopic data are required before any firm conclusions can be drawn.

A very limited number of stable carbon isotopic analyses performed on carbon dioxide present in the geothermal fluids have found C-13 ratios ranging from -1.97% to -3.6% versus PDB. These values are considerably heavier than those associated with the expected sources of carbon in the well fluids: biogenic CO_2 at approximately -20% and magmatic carbon at approximately -7%. Although a complete analysis of the carbonate chemistry connot be made with the presently available data, it is highly probable that deposition and remobilization of carbonate is the major controlling factor in the carbon isotopic compositions observed.

Tritium and radiocarbon analyses performed on the brine and gas phase from HGP-A indicate that the age of the recharge water is at least

30 years (no detectable tritium) but is probably less than 12,000 years (carbon-14 approximately 20% of modern). It is of note that the carbon age is considered to be a maximum age in that any contribution by magmatic sources to the biogenic carbon present in the well would yield apparent ages that are older than the true radiocarbon age. Thus the average lifetime of recharge to the portion of the geothermal reservoir tapped by HGP-A is considerably shorter than that observed in most other continental geothermal systems.

Analysis of radon in the geothermal fluids from HGP-A have provided values ranging from 1.16 nanocuries per kilogram (nCi/kg) of steam condensate during early, short period, production testing to 3.7 nCi/kg during longer term production (Kruger, personal communication). The radon concentration calculated for the reservoir fluids from the present data is approximately 1.65 nCi/kg of total fluid. This value is considerably lower than the average observed at The Geysers of 20 nCi/kg (Kruger, personal communication) and is probably the result of the lower uranium concentrations persent in Hawaiian basalts relative to the more silicic volcanic and sedimentary rocks present in continental geothermal fields.

Summary

In summary, the geochemical monitoring conducted at HGP-A has provided information on a number of characteristics of the reservoir discovered by the HGP-A well:

1) seawater intrusion and circulation within the rift zone is severely restricted. It is suggested that the exclusion of seawater is either the result of the permeability structure of the rift zone or by thermal precipitation of alteration and and hydrothermal minerals.

2) Changes in fluid compositions during extended production suggest that multiple aquifers are providing fluids to the well and that these aquifers may have relatively small fluid volumes available.

3) The total non-condensable gas concentrations in the reservoir fluids are within the worldwide range however the concentrations of the individual species are considerably different from those observed in continental environments.

4) Radioisotopic analyses suggest that the recharge-discharge lifetime in the reservoir is relatively short in comparison to those occurring in continental geothermal systems.

References

Bischoff, J. L., and F. W. Dickson (1975) Seawater-basalt interaction at 200°C and 500 bars: implications for origin of seafloor heavy metal deposits and regulations of seawater chemistry, Earth Planet. Sci. Lett., N. 25, p. 385-397.

Cox, M. E., and D. M. Thomas (1979) Chloride/Magnesium ratio of shallow groundwaters as a regional geothermal indicator in Hawaii. Hawaii Institute of Geophysics Technical Report No. 79-9, 51 p.

Fournier, R. O., and R. W. Potter, II (1982) A revised and expanded silica (quartz) geothermometer. Geothermal Resources Council Bulletin, V. II, No. 10, pp. 3-12.

Fournier, R. O., and A. H. Truesdell (1973) An empirical Na-K-Ca geothermometer for natural waters. Geochem. Cosmo. Act., V. 37, pp. 1255-1275.

Stone, C. (1977) Chemistry, petrography, and hydrothermal alteration of basalts from Hawaii Geothermal Project Well-A, Kilauea, Hawaii. Master of Science Thesis, University of Hawaii, 84 p.

Proceedings Eighth Workshop Geothermal Reservoir Engineering
Stanford University, Stanford, California, December 1982
SGP-TR-60

INTERPRETATION OF RADON CONCENTRATION IN THE SERRAZZANO ZONE OF THE LARDERELLO GEOTHERMAL FIELD

Lewis Semprini and Paul Kruger
Stanford Geothermal Program
Stanford University
and
Franco D'Amore
CNR - Istituto Internazionale per le Ricerche Geotermiche
Pisa, Italy

ABSTRACT

Wellhead concentrations of radon were made at 22 wells in the south-west region of the Larderello geothermal fields by two analytical methods, a field measurement as reported by D'Amore and laboratory measurement as reported by Semprini and Kruger. Agreement between the two methods was satisfactory.

The radon concentrations were correlated with average specific volume of superheated steam for each well estimated from available thermodynamic parameters of the reservoir. The correlation was improved by adjusting the specific volume of steam by a mass steam saturation value calculated at the boiling front from chemical fluid composition for each well by a method developed by D'Amore and Celati. A compressible flow model for radon transport developed by Sakakura et al. was also tested.

The results confirm that radon behavior in geothermal systems is characterized by thermodynamic conditions in the reservoir. In the Serrazzano zone, abnormally high values of radon concentration with respect to estimated specific volume in four of the 22 wells were observed an area of proposed low permeability. The high values may also result from higher emanating power or lower porosity in this zone. A cross-section normal to the zone of low permeability between the two basins shows a similar radon profile as noted in a Geysers production zone.

A comparison of these data with the set obtained in 1976 by D'Amore shows relatively constant radon concentration despite several wells having large variations in gas/steam ratios.

INTRODUCTION

Radon concentration measurements in the Serrazzano zone of the vapor-dominated field at Larderello, Italy were examined with respect to thermodynamic and geologic conditions in the reservoir. The thermodynamic relationship was evaluated for reservoir pressure and the geologic parameters included porosity and permeability.

Properties of radon and its use in geothermal reservoir engineering have been discussed by Stoker and Kruger (1975), D'Amore, Sabroux, and Zedwoog (1978), Warren and Kruger (1979), and Semprini and Kruger (1981). Wellhead concentrations of 3.83-day ^{222}Rn reflect reservoir conditions during the preceding 30-day residence of the produced geofluid. This time dependent factor makes ^{222}Rn a useful natural tracer for studying spatial and temporal changes in the reservoir. Radon achieves an equilibrium concentration (nCi/kg pore fluid) when the rate of emanation from the rock matrix equals the rate of decay in the fluid,

$$C_f = \frac{E_m \rho_r}{\phi \rho_f} \qquad (1)$$

where C_f = mass concentration of radon in the pore fluid (nCi/kg)
E_m = emanation power (nCi/kg rock)
ρ_r, ρ_f = rock, fluid density (kg/m^3)
ϕ = porosity (m^3 fluid/m^3 formation)

The emanation of radon from formation rock is dependent on several parameters, e.g., rock type, intrinsic and fracture porosity and permeability, radium content, moisture saturation, and the local thermodynamic conditions. Radon emanation from graywacke rock has been shown by Macias (1981) and Satomi (1982) to increase with temperature. On the basis that rock in the Serrazzano formation has the same emanation properties as graywacke, the change in emanation over the temperature range of 210 to 270°C (Cappetti et al. 1982) could range from 10 to 15%. On the other hand, for a temperature range of 210 to 270°C, the fluid density in a vapor-dominated reservoir would change by a factor of 2.9. Thus radon concentration should be sensitive to changes in fluid density which is related to changes in formation pressure.

Semprini and Kruger (1981) examined the relationship of radon concentration to specific volume in vapor-dominated and liquid-dominated reservoirs. The specific volume for a static two-phase fluid is

$$\bar{V}_f = \frac{x}{\rho_L} + \frac{(1-x)}{\rho_v} \quad (2)$$

where x = liquid mass fraction
$(1-x)$ = vapor mass fraction

The equation is valid for a dynamic system if the phases move with equal velocity. Semprini and Kruger (1982) showed a positive linear correlation (with correlation coefficient, $r^2 = 0.80$) between radon concentration and fluid specific volume at the Cerro Prieto geothermal field in Mexico. Specific volumes were calculated from measured wellhead enthalpies and from geothermometer estimates of reservoir temperatures.

In vapor-dominated reservoirs, fluid specific volume is more difficult to estimate because of greater compressibility factors, larger fracture porosity, and immobile liquid saturation. In such reservoirs, specific volume of the steam can change along the flowpath as pressure decreases, while radon can continuously emanate to the fluid with changes in emanation rate as a function of fracture size distribution. Radon concentration can also be affected by liquid saturation in the reservoir, especially if emanation into the vapor phase is small or residence time for buildup is short.

Radon concentration measurements have been evaluated with respect to reservoir thermodynamic conditions in three ways: (1) an equilibrium model with estimated specific volume, (2) the equilibrium model adjusted for estimated steam saturation, and (3) a compressible flow model adapted from Sakakura et al. (1959).

The specific volume model used a reservoir average pressure and temperature to calculate the equilibrium specific volume around each well. Reservoir temperatures and top pressures for the Serrazzano zone were reported by Cappetti et al. (1982). The average pressure was estimated as a root-mean-square pressure from the pressure at saturated reservoir temperature and the lower pressure at the reservoir top.

$$P = \frac{\left(P^2_{(T_{res})} + P^2_{(top)}\right)^{\frac{1}{2}}}{2} \quad (3)$$

The specific volume of the steam, $\bar{V}_s$, is obtained from superheated steam tables at the estimated reservoir temperature, T_{res}, assuming isothermal flow to the well. On the basis of constant emanation and rock porosity, the volumetric emanation, E_v, is constant, and the radon concentration is given by

$$[Rn]_s = E_v \cdot \bar{V}_s \quad (4)$$

In model 2 steam saturation is incorporated. It is computed by a method proposed by D'Amore and Celati (1983) using gas composition. In this model, the steam saturation is the average value of the calculted reservoir saturation and the steam saturation near the wellbore, assumed to be 100%. The average steam saturation, $\bar{Y}$, represents the $(1-x)$ term in equation (2). Since liquid density is much greater than vapor density, only the steam term is used for fluids of high vapor mass fraction (as in the Serrazzano zone) to calculate equilibrium radon concentation,

$$[Rn]_s = E_v[\bar{Y} \cdot \bar{V}_s] \quad (5)$$

The radon transport model proposed by Sakakura et al. (1959) is based on a flow model for a compressible fluid in radial geometry with a uniform emanation source term. The analytical equations of this model were discussed by Stoker and Kruger (1975) and used to interpret radon measurements at The Geysers vapor-dominated field in California. The model parameters include reservoir pressure, flowing wellhead pressure, flowrate, and estimates of porosity thickness and effective reservoir radius. Sensitivity analysis of the Sakakura et al. (1959) model noted that radon concentration was most affected by reservoir static and wellhead flowing pressures. These parameters are estimated as a lumped parameter, K (in units of m^3/kg) such that the radon concentration is given by

$$[Rn]_s = K \cdot E_v \quad (6)$$

EXPERIMENTAL PROGRAM

The Serrazzano zone of the Larderello geothermal field was selected for evaluation of the three models. The geologic, hydrologic, and geochemical conditions for this reservoir were available from Calore et al. (1980) and D'Amore et al. (1981). The thermodynamic data for the reservoir were obtained from Cappetti et al. (1982). Earlier radon measurements for the Serrazzano zone were reported by D'Amore (1975). The present measurements allow a comparison of the results over a seven-year period of production.

Radon measurements were made by two techniques, one involving field measurements during sampling and the other by laboratory

analysis of wellhead samples. The field measurement method was described by D'Amore (1975). The geofluid is condensed at the wellhead sampling port and separated into measured condensate and noncondensable gas fractions. The noncondensable gas, containing more than 95% of the radon, is transferred to ZnS-lined scintillation flasks for radon measurement. The radon concentration at the wellhead is determined from the gas/steam ratio.

The laboratory measurements were made with the method described by Stoker and Kruger (1975). Adsorption-purified radon is transferred to ZnS-lined scintillation counting flasks for measurement in a single-channel pulse-height analyzer.

RADON MEASUREMENT COMPARISON

Twenty-two wells were sampled for radon in the Serrazzano zone using the field technique. Samples of fifteen of these wells were collected for measurement in the Stanford geothermal laboratories. Agreement of the two sets of results was evaluated by linear regression. The regression line of [Rn] (field) = 21.1+1.24 [Rn] (lab) had a correlation coefficient of $r^2 = 0.90$. The slope value significantly greater than 1.0 shows the field measurements with higher concentrations compared to the laboratory measurements. This factor may result from a too low counting efficiency factor for carbon dioxide as the carrying gas in the field technique. Since the two sets of data differ by a constant factor, use of the 22-well data set should not affect the validity of data interpretation.

TEST RESULTS

Table 1 gives the test data and reservoir parameter values used in the set of model evaluations. The values for reservoir temperature (T_{res}) and top pressure (P_{top}) were obtained from Cappetti et al. (1982). The steam mass saturation (Y) was derived from gas composition data from samples obtained by D'Amore during the radon survey. The saturation pressures based on reservoir temperatures of 210 to 270° C ranged from 19 to 55 bar. Reservoir top pressure ranged from 5 to 25 bar. The average pressure calculated from equation (3) ranged from 14.0 to 42.7 bar. The radon concentration ranged from 41 to 302 nCi/kg.

Results of linear regression analysis of radon and specific volume calculated from average reservoir pressure are shown in Figure 1. The resulting regression equation $\hat{[Rn]} = -2.3 + 1500\ (\bar{V}_{s2})$ nCi/kg has a correlation coefficient of $r^2 = 0.65$. A t-test of the regression shows the intercept value of -2.3 cannot be distinguished from zero, which is predicted by equation (4). For estimated values of radium content of 1.0 nCi/kg, porosity of 5%, and rock density of 2.5 g/cm^3, volumetric emanation represents an emanating power of 3 percent.

To check the regression linearity, analysis was also performed for log-log regression. Results showed the regression form could not be distinguished from linear. The correlation coefficient $r^2 = 0.65$ indicates that about two-thirds of the observed radon concentration can be attributed to the fluid specific volume in the reservoir due to the existing pressure distribution for constant porosity and emanation. The linear relationship with specific volume calculated using the p^2-average pressure given in equation (3) indicates that radon concentration reflects thermodynamic conditions closer to true reservoir pressures than pressures near the wellbore.

The effect of steam saturation on specific volume was also examined by regression analysis. Estimates of steam mass saturation ranged from 0.38 to 0.83 kg/kg. Linear regression of radon concentration with steam mass saturation, $\bar{Y}$, shows little correlation ($r^2 = 0.22$). Linear regression with combined saturation-specific volume, $(\bar{Y} \cdot V_s)$, in equation (5) resulted in a regression line $\hat{[Rn]} = 13.0 + 1646\ (\bar{Y} \cdot \bar{V}_{s2})$ with an improved correlation coefficient, $r^2 = 0.69$. Log-log regression also showed a regression form that could not be distinguished from linear. The improved correlation suggests that vapor saturation may be an important parameter in reservoirs of low steam saturation.

The Sakakura et al. (1959) model of compressible flow was tested with reservoir pressures ranging from P_{top} to P_{res}. The best fit was achieved with a constant value for the effective reservoir radius, r_e, for all wells and for P_{res} approximately equal to the p^2-average pressure obtained from equation (3). The fit of model to observation was rather insensitive to the value of effective radius with r_e varying from 50 to 1000 m. The correlation of radon concentration to the coefficient K derived by the analytical model is shown in Figure 2. The regression line $\hat{[Rn]} = 36.2 + 1600\ (K)$ nCi/m^3 has a correlation coefficient, $r^2 = 0.63$. The slope value, representing the volumetric emanation factor, E_v, is statistically the same as that obtained for the equilibrium model. However, testing of the linearity by log-log regression showed a regression curve $\hat{[Rn]} = 832(K)^{0.65}$, significantly different from linear. The discrepancy may result from incorrect pressure differentials or nonconstant effective reservoir radius.

SPATIAL VARIATIONS

The observed changes in radon concentration may be due to geologic factors which influence the distribution of emanation, porosity, and permeability throughout the reservoir.

Table 1

RESERVOIR AND RADON DATA FOR THE SERRAZZANO GEOTHERMAL FIELD

Well	T_{res} (°C)	P_{top} (bars)	$\bar{P}$ (bars)	Y (kg/kg)	$\bar{V}_s$ (m^3/kg)	$\bar{Y}\,\bar{V}_s$ (m^3/kg)	K* (m^3/kg)	Rn (nCi/kg)
1	270	20	41	0.39	0.052	0.036	0.020	50
2	250	12	30	0.82	0.072	0.066	0.051	95
3	240	5	24	0.58	0.088	0.070	0.054	148
4	230	5	20	0.43	0.105	0.076	0.070	149
5	230	5	20	0.53	0.105	0.081	0.072	132
6	220	5	17	0.63	0.126	0.103	0.092	145
7	230	5	20	0.66	0.105	0.087	0.071	124
8	220	5	17	0.72	0.122	0.105	0.093	166
9	220	5	17	0.64	0.122	0.100	0.091	157
10	210	5	14	0.82	0.147	0.134	0.114	302
11	270	19	41	0.59	0.052	0.042	0.02	136
12	230	16	23	0.49	0.090	0.072	0.065	153
13	240	17	27	0.38	0.079	0.059	0.052	153
14	220	20	22	0.40	0.092	0.064	0.056	127
15	240	25	30	0.80	0.070	0.063	0.031	95
16	240	22	28	0.74	0.074	0.064	0.048	132
17	270	25	43	0.46	0.049	0.036	0.027	41
18	260	20	36	0.42	0.059	0.042	0.037	108
19	260	25	38	0.38	0.056	0.039	0.042	68
20	220	15	20	0.54	0.105	0.081	0.073	129
21	220	9	18	0.83	0.118	0.109	0.089	183
22	220	8	17	0.65	0.118	0.098	0.084	168

*Based on reservoir radius of 500m and porosity-thickness of 25 m.

Figure 3 shows well locations and contours of radon concentration in the Serrazzano zone. During analysis of radon concentration as a function of specific volume, it was noted that the four wells (Nos. 10, 11, 12, and 13) most deviant from the regression line in Figure 1 were located near areas of low permeability. Linear regression analysis of the 22-well data set without the data for these four wells resulted in an improved correlation coefficient, $r^2 = 0.79$. Although sufficient data are not available for quantitative analysis, the higher radon concentrations in these wells with respect to thermodynamic conditions may be due to lower reservoir porosity and higher surface area for radon emanation associated with zones of low fracture permeability. Laboratory experiments reported by Sammis et al. (1981) showed radon concentration in pore fluids in granite cores was inversely related to permeability. The high radon concentrations for these four wells in this zone may be associated with lower porosity. Using equation (1), a 50% reduction in porosity from the field average of 5% could account for the higher observed concentrations.

Three of the wells (Nos. 1, 17, and 19) showed lower radon concentration from the regression line for specific volume. D'Amore et al. (1981) proposed from the observed high reservoir temperatures and high boron and chloride content of the produced fluid that these wells are located in zones of fluid upflow. Reservoir porosity in an upflow zone may be higher than average field values (Celati, personal communication). A porosity of 7.5% compared to a field average of 5% would account, in equation (1), for these lower observed radon concentrations. It is clear that multi-parameter regression analysis when sufficient data on porosity are available would enhance the interpretation of the radon concentration data with respect to thermodynamic behavior in a geothermal reservoir.

TEMPORAL VARIATIONS

Comparison of results from the 1976 and 1982 surveys shows little change in radon concentration in the 22 wells. These results suggest thermodynamic conditions that influence radon concentrations have remained fairly constant during this period. In several wells, radon concentration remained constant in the fluid while the total noncondensable gas content ratio changed. Decrease in gas/steam ratio occured in wells 12, 13, and 14. These wells are located near a reinjection area that started operation between the two survey periods. Reinjection studies in the Larderello field by Giovannoni et al. (1981) have shown a decrease in gas/steam ratio after start of reinjection. The decrease in gas concentration indicates production of a steam mixture containing original reservoir fluid of high gas/steam ratio and reinjection fluid with negligible gas content. The constant radon concentration, however, indicates the thermodynamic conditions near the producing wells. have not changed, even though the produced steam contains vapor from reinjected fluid.

COMPARISON WITH OTHER GEOTHERMAL FIELDS

The correlation of radon concentrations with estimated values of specific volume for three geothermal reservoirs, Cerro Prieto, Mexico, The Geysers, California, and Serrazzano, Italy are shown in Figure 4. The large increase in specific volume from liquid- to vapor-dominated systems is reflected in the respective increase in radon concentrations. The relationships of radon concentration to specific volume cannot be directly compared among fields due to possible variations in radon emanation and formation porosity for the different reservoirs. Regression analysis of radon in relation to specific volume yields a volumetric emanation factor for each reservoir, from which an estimate of the emanating power can be made. Assuming uniform radium content of 1 nCi/kg, rock density of 2500 kg/m^3, and average porosity values of 15% for Cerro Prieto, 7% for The Geysers, and 5% for Serrazzano, the average emanation power is 1%, 1.5%, and 3% respectively. This small variation in emanation power could result from variations in reservoir rock type for the three fields.

Cross sections normal to zones of low permeability show similar trends at both The Geysers and the Serrazzano reservoirs. Figure 5 shows the transect of radon concentration and estimated values of specific volume in the Serrazzano reservoir along the transect A-B given in Figure 3. Radon concentration increases towards zones of lower permeability to a greater extent than predicted by the specific volume relationship. Figure 6 shows a similar relationship for a transect across The Geysers reservoir. Both data suggest a less porous reservoir and/or a higher amount of emanation in these zones. The similar trends in both the Serrazzano and Geysers reservoirs indicate tht radon concentrations are related not only to thermodynamic conditions, but also changes in physical properties of the reservoir.

ACKNOWLEDGMENT

The authors wish to thank ENEL for their permission and cooperation in conducting this study in the Serrazzano Field. The Stanford effort was conducted under support from the U.S. Department of Energy.

REFERENCES

Calore, R., R. Celati, F. D'Amore, P. Squarci, and A. Truesdell. (1980) A Geologic, Hydrologic and Geochemical Model of the Serrazzano Zone of the Larderello Geothermal Field, Proceedings, Sixth Workshop Geothermal Reservoir Engineering, Stanford University.

Cappetti, G., A. Giovannoni, C. Ruffilli, C. Calore, and R. Celati. (1982) Reinjection in the Larderello Geothermal Field, International Conference on Geothermal Energy, Florence, Italy.

D'Amore, F. (1975) Radon-222 Survey in the Larderello Geothermal Field, Italy, GEOTHERMICS, 4: 1-4.

D'Amore, F., J. C. Sabroux, and P. Zedwoog. (1978-79) Determination of Characteristics of Steam Reservoirs by Radon-222 Measurements in Geothermal Fluids, Pageoph, 117: 253-261.

D'Amore, F., C. Calore, and R. Celati. (1981) Temporal Evolution of the Composition of the Fluid from Serrazzano Zone (Larderello), Proceedings, Seventh Workshop Geothermal Reservoir Engineering, Stanford University.

D'Amore, F. and R. Celati (1983) Methodology for Calculating Steam Quality in Geothermal Reservoirs, GEOTHERMICS, (In Press).

Macias-Chapa, L. (1981) Radon Emanation in Geothermal Reservoirs, Engineers Thesis, Dept. of Civil Engineering, Stanford University.

Sakakura, A. Y., C. Lindberg, and H. Faul. (1959) Equation of Continuity in Geology with Applications to the Transport of Radioactive Gas, U.S. Geological Survey Bulletin 1052-1.

Sammis, C., M. Barnerdt, and D. E. Hammond. (1981) Stress Release of Rn^{222} and CH_4 to Percolating Water in Granitic Rock, Proceedings, Seventh Workshop Geothermal Reservoir Engineering, Stanford University.

Satomi, K. (1982) Radon Emanation Mechanism From Finely Ground Rock, Engineers Thesis,

Dept. of Civil Engineering, Stanford University.

Semprini, L. and P. Kruger. (1981) Radon and Ammonia Transects Across The Cerro Prieto Geothermal Field, Proceedings, Third Symposium on The Cerro Prieto Geothermal Field. Baja California, Mexico.

Semprini, L. and P. Kruger. (1982) Relationship of Radon Concentrations to Spatial and Temporal Variations of Reservoir Thermodynamic Conditions in the Cerro Prieto Geothermal Field, Proceedings, Fourth Symposium on the Cerro Prieto Geothermal Field, Baja California, Mexico.

Stoker, A. and P. Kruger (1975) Radon Measurements in Geothermal Reservoirs, Second United Nations Symposium on the Development and Use of Geothermal Resources, San Francisco, CA.

Warren, G. and P. Kruger (1979) Transients in Vapor-Dominated Geothermal Reservoirs, Paper SPE-8000, Proceedings, 1979 SPE California Regional Meeting, Ventura, CA.

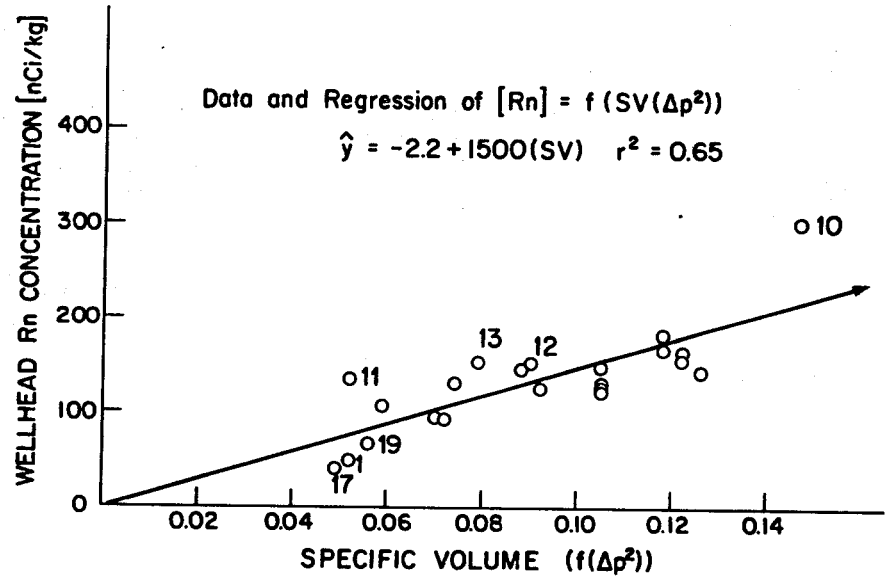

Figure 1. Correlation of radon concentration and specific volume.

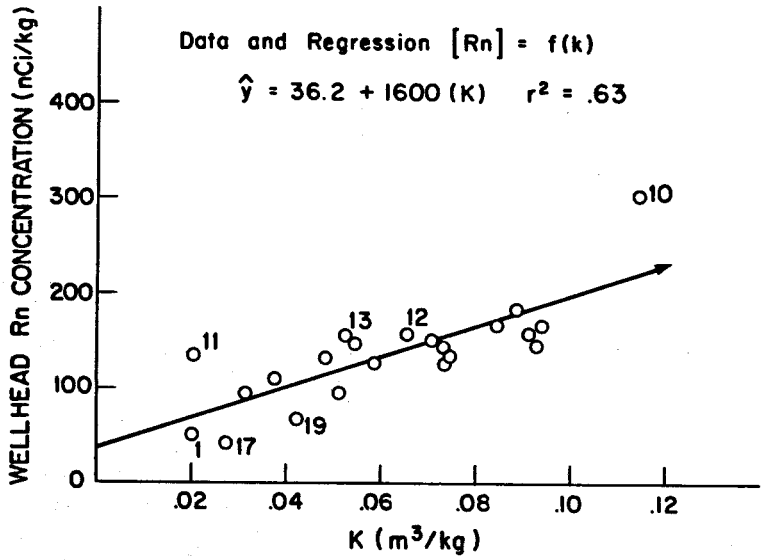

Figure 2. Correlation of radon concen- and the K parameter from Sakakura et al. (1959).

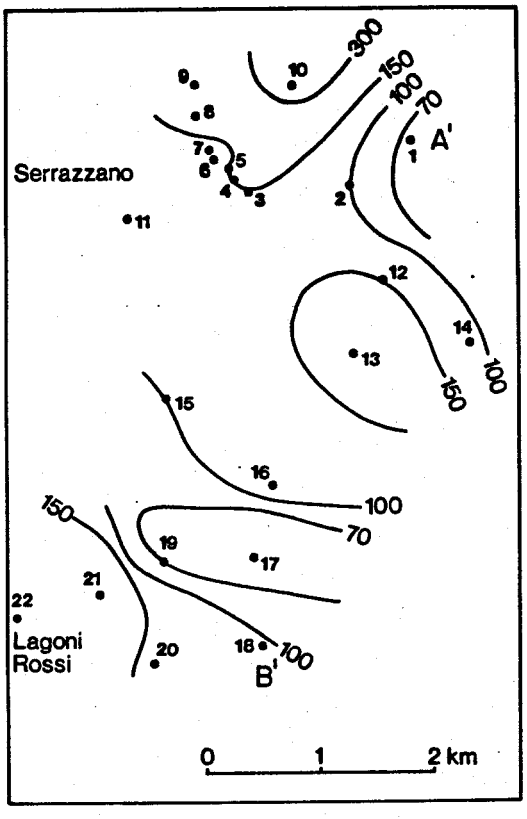

Figure 3. Radon concentration contours in the Serrazzano reservoir.

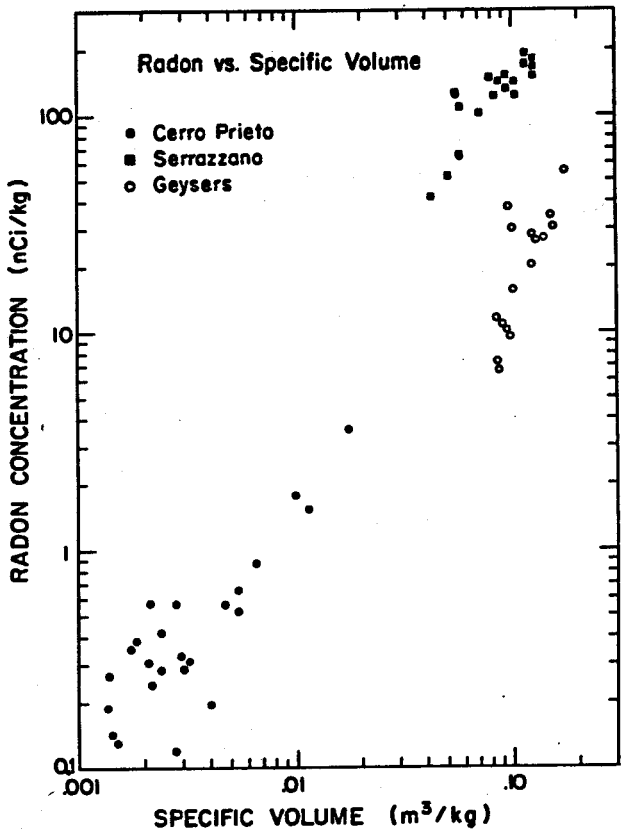

Figure 4. Radon concentration and specific volume for three geothermal reservoirs.

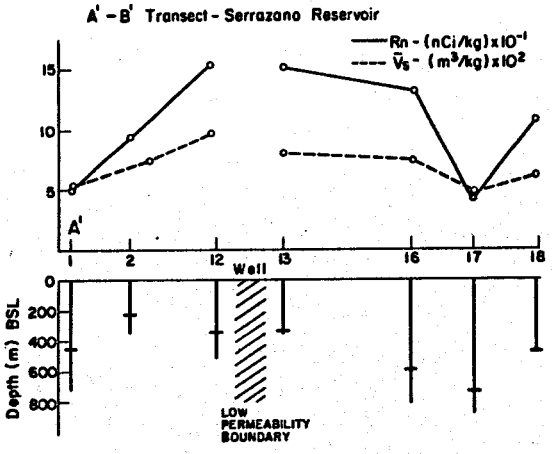

Figure 5. Radon and specific volume across a zone of low permeability in the Serrazzano reservoir.

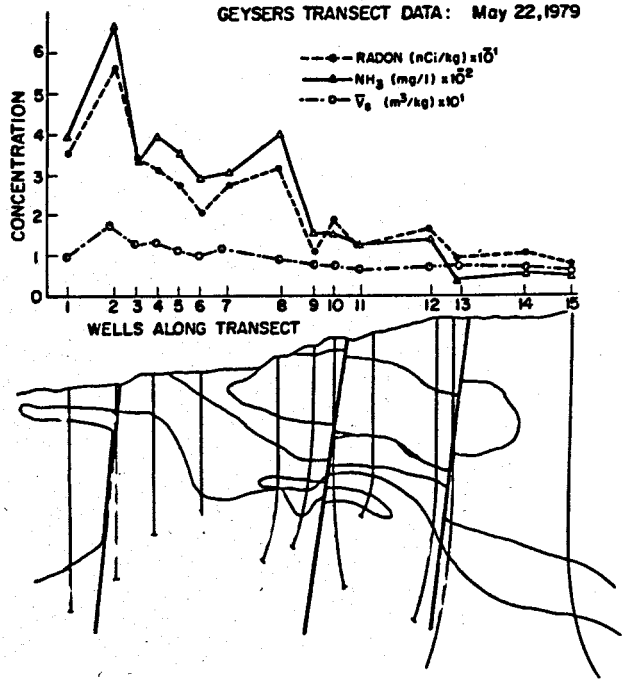

Figure 6. Radon and specific volume transect in The Geysers reservoir.

Proceedings Eighth Workshop Geothermal Reservoir Engineering
Stanford University, Stanford, California, December 1982
SGP-TR-60

GEOCHEMICAL EVIDENCE OF NATURAL RECHARGE IN LARDERELLO AND CASTELNUOVO AREAS (+)

Claudio Calore, Romano Celati, Franco D'Amore and Pietro Noto

Istituto Internazionale per le Ricerche Geotermiche (CNR)
Via del Buongusto 1
56100 PISA, Italy

ABSTRACT

The spatial variations of the isotopic composition of the fluid in Castelnuovo and the southern zone of Larderello were, in the early 1970s, interpreted as the effects of a natural recharge.

It was subsequently noted that this distribution might be the result of the condensation process, at least in areas with no tritium. In order to further investigate this problem a study was undertaken of the spatial and temporal variations in the gas/steam ratio and in the isotopic composition.

Preliminary interpretation of the results of this study confirms that the evolution of fluid composition in this area is due to a mixing between the fluid originally present in the reservoir and recent meteoric waters. The area affected by natural recharge is, moreover, in continual expansion.

INTRODUCTION

The areal distribution of the chemical and isotopic composition of the fluid in the Larderello geothermal field is considered to be governed prevalently by some physical processes occurring in the reservoir, such as steam condensation, vaporization of liquid water and recharge from lateral aquifers (Celati et al., 1973; Panichi et al.,1974; Petracco and Squarci, 1976; D'Amore et al., 1977; Truesdell and Nehring, 1978; Mazor, 1978; D'Amore and Truesdell, 1979; Calore et al.,1980; D'Amore et al., 1981).

D'Amore and Truesdell (1979) observed that the spatial variations in isotopic composition and in some chemical species, in the northern area of the Larderello field, could be ascribed to a lateral flow of steam from central boiling or upflow zones towards the margins of the system. During this movement the steam undergoes a progressive condensation, with enrichment in the more volatile chemical components, depletion in the more soluble, and simultaneous depletion in ^{18}O.

With regard to the south and south-eastern areas of the Larderello field, Celati et al. (1973) and Panichi et al.(1974) suggested that the tritium present in some peripheral wells, and the relatively more negative $\delta^{18}O$ values spread over a wide zone of the field near absorption areas, were due to a mixing between steam of deep origin and steam deriving from recent meteoric waters. Although the influence of recharge was evident in the wells with high tritium contents, the isotopic data alone did not suffice to distinguish between a mixing and condensation model (D'Amore and Truesdell, 1979).

During the period 1980-82 this problem was further investigated by systematic isotopic analysis of samples from the Larderello and Castelnuovo areas, and by study of the spatial and temporal variations in both the gas/steam ratio and isotopic composition.

TEMPORAL VARIATIONS IN $\delta^{18}O$, TRITIUM AND GAS/STEAM RATIO

Figures 1 and 2 show the areal distribution of $\delta^{18}O$ and gas/steam ratio in the periods 1968-72 and 1978-82, for Castelnuovo area and the southern part of the Larderello area. The following considerations can be made:
- the areas with the most negative $\delta^{18}O$ values generally have the lowest gas/steam ratios;
- the gas/steam ratio and $\delta^{18}O$ have decreased greatly during the last 10 years in these same areas. Taking the curves of 10 and 20 l STP/kg

(+) Work conducted as part of the ENEL-CNR research agreement.

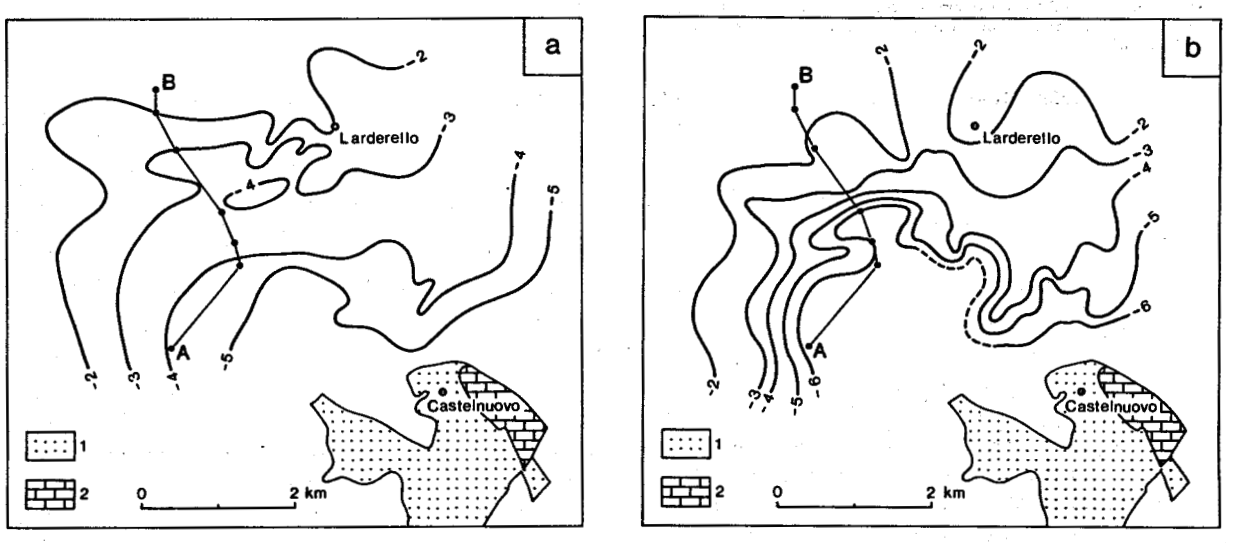

Figure 1. Areal distribution of $\delta^{18}O$ in the Castelnuovo and southern Larderello areas. a) data of 1968-72 period; b) data of 1978-82 period; A-B) section represented in Fig.3; 1) outcrop of "macigno" sandstone; 2) outcrop of prevalently brecciated dolostones.

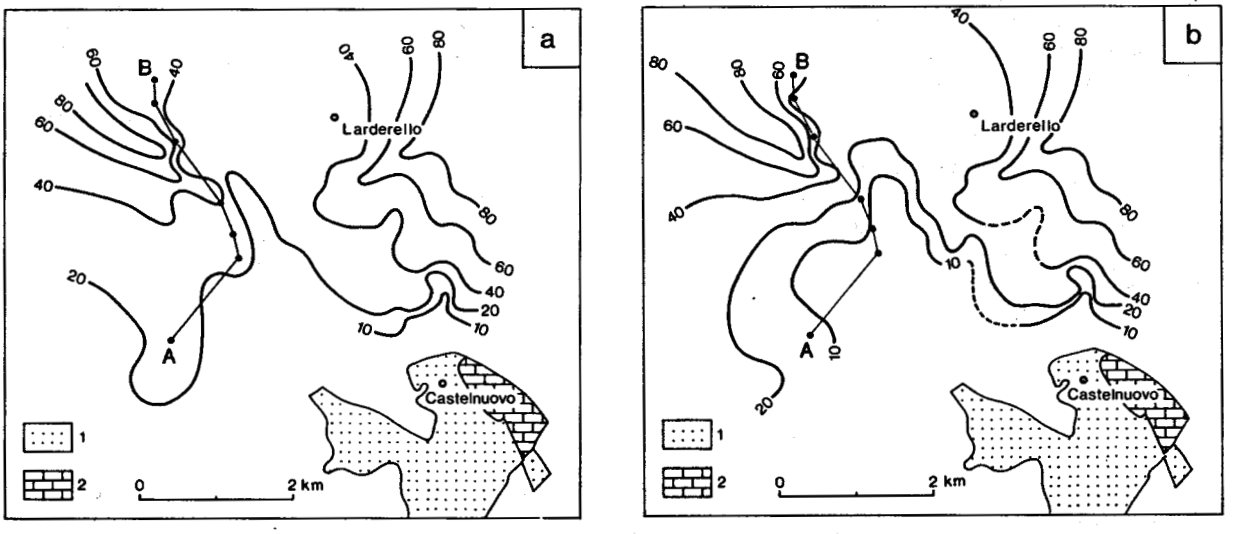

Figure 2. Areal distribution of the gas/steam ratio in the Castelnuovo and southern Larderello areas. For legend see Fig.1.

as reference for the gas/steam ratio, and the -5 and -6 curves for $\delta^{18}O$, it is evident that the maximum variations occur prevalently along a S-N and a SE-NW direction;
- the variations in the same period were not as conspicuous in the areas already characterized by high gas content and relatively more positive $\delta^{18}O$ values.

The temporal variations in $\delta^{18}O$ and gas/steam ratio are more evident in Fig.3, which shows the trends for the two periods in question along the section A-B (Figs.1,2), which passes through wells having gas/steam and $\delta^{18}O$ data for both periods.

Figure 4 shows some typical trends in gas/steam ratio, along with the available $\delta^{18}O$ data, for some wells in the study area of the field. The trend for one well (W6) showing no notable variations in either gas/steam ratio or $\delta^{18}O$ is given for comparison. The different

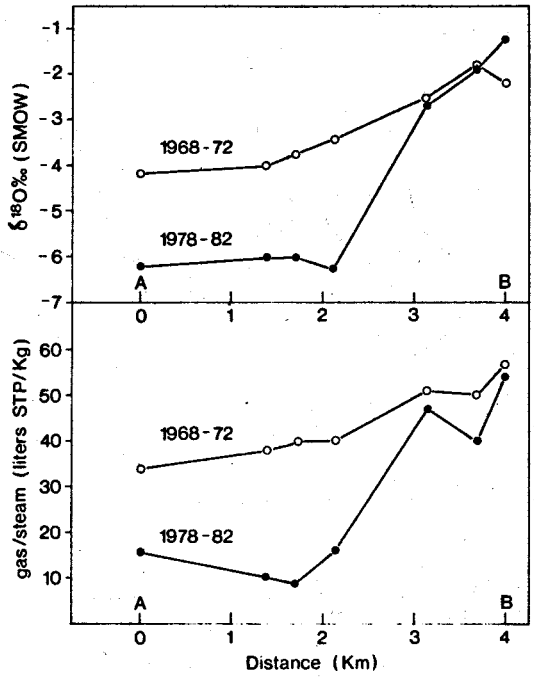

Figure 3. Trend of $\delta^{18}O$ and gas/steam ratio, along the section A-B (Figs.1,2), in the periods 1968-72 and 1978-82.

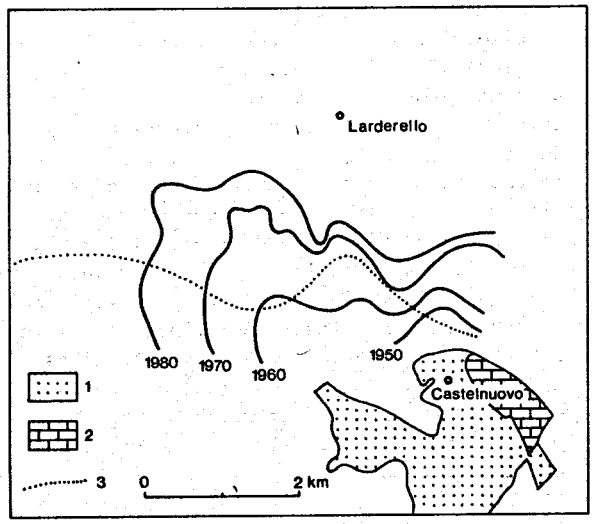

Figure 5. Dates on which a sharp decrease in the gas/steam ratio occurred. 1) and 2) as in Fig.1; 3) boundary of the "macigno" sandstone beneath the flysch cover.

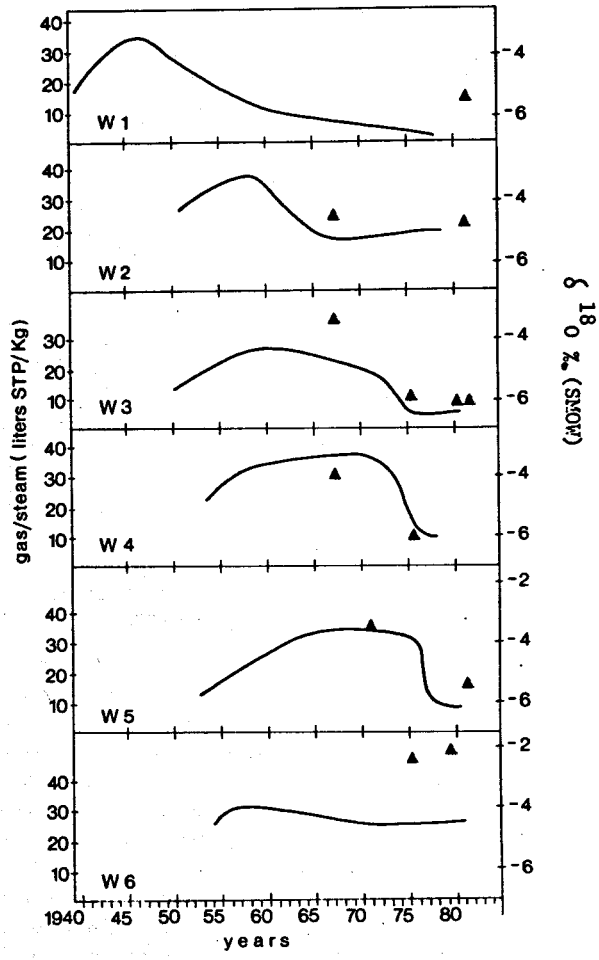

Figure 4. Temporal evolution of the gas/steam ratio (line) and $\delta^{18}O$ (triangles) for some wells in Castelnuovo and Larderello areas.

dates on which the gas/steam ratio decreases correspond to different geographic positions of the wells. The sequence W1 to W6 in Fig.4 corresponds to well locations running SE to NW, indicating that the decrease in gas/steam ratio advances in that direction with time; this phenomenon is more evident in Fig.5, which shows the zones that have gradually become affected from 1950 on.

Figure 6 is a comparison of the areal distribution of the tritium content of the steam during the two survey periods. The following considerations can be made:
- the areal distribution is qualitatively similar in both periods;

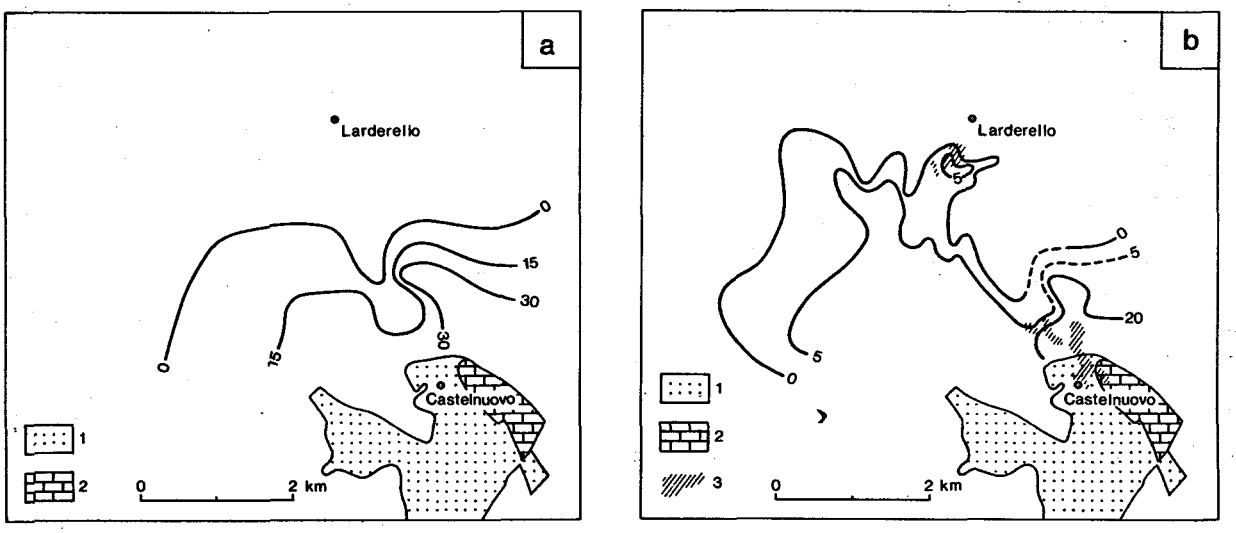

Figure 6. Areal distribution of tritium in the Castelnuovo and southern Larderello areas. a)data of 1968-72 period; b)data of 1978-82 period; 1) and 2) as in Fig.1, 3) natural manifestations.

- the densely drilled area of Castelnuovo has still the highest tritium concentrations even though the absolute values have all shown a decrease. The latter can be ascribed to a depletion of the tritium content of the rainwater (tritium content is now less than half of the 1970 value);
- the area whose steam contains tritium has widened considerably. The largest increases still occur along the same directions observed for $\delta^{18}O$ and gas/steam ratio. In the 1978-82 period, moreover, a relative maximum can be observed in the densely drilled zone of Larderello.

DISCUSSION

Significant tritium concentrations, that were once a characteristic of the more peripheral zones only, can now be found in many wells a few kilometres from the infiltration areas. This fact indicates a contribution of recent waters to production over a wide zone of the field. The maximum tritium values are found in the Castelnuovo area and are probably caused by the proximity of the productive wells to the infiltration area. The largest tritium content at Castelnuovo is observed in front of a small outcrop of carbonate rocks of much higher permeability than the surrounding sandstone. The relative maximum in tritium content in the central area of Larderello could be related to the presence of old manifestations in this area, now exhausted because of exploitation. The area of the manifestations may nowadays act as an infiltration area for surface meteoric waters, as the cover is not totally impermeable.

D'Amore and Truesdell (1979) discussed the temporal variations in gas/steam ratio observed in some wells of the central area of Larderello. The slow declines observed after 10-15 years of production, accompanied by the appearance and gradual increase of HCl, were attributed to an increased contribution to production from boiling of a brine. The declines in gas/steam ratio in the zone now under study differ in some important respects from those considered by D'Amore and Truesdell (1979). The variations are, in fact, usually much larger, occur in periods of a few years only and there is no concomitant appearance of HCl in the steam. Furthermore, the concentrations of H_3BO_3 and NH_3 remained constant as the gas content decreased in the wells studied by D'Amore and Truesdell (1979), whereas these concentrations generally decrease in the wells of the present study. Similar phenomena were also observed in the Larderello field in the areas affected by reinjection (Giovannoni et al.,1981; Cappetti et al., 1982).

The areal distribution of the gas/steam ratio, which decreases from the central zones of the field towards the recharge areas, and its evo-

lution towards low values are compatible with a dilution of the gas in the original fluid, caused by a mixing with recent meteoric waters of negligible gas content. Figure 5 can then be interpreted as a gradual advance of the dilution front.

A simple mass balance of the gas was carried out for some wells, assuming a mixing between original steam, with a gas content equal to that of the steam produced before the effects of dilution became apparent, and a steam with no gas content. The contribution of recharge water results more than 50% in many wells in the study area.

Throughout the study area the dilution front has generally made the greatest progress in correspondence to zones of intense fracturation, tied to particular structural characteristics (Celati et al.,1973; Panichi et al., 1974; Celati et al.,1975). The zone most affected by recharge may also be tied to the presence of a "macigno" sandstone (Fig.5);the latter forms an aquifer overlying the carbonate reservoir and separated from it, discontinuously, by prevalently impermeable shales. The water seeps from the sandstone into the underlying reservoir wherever the shale layer is missing or densely fractured.

The rapidity of the observed variations supports the hypothesis that the current increase in contribution of recharge water to production is mainly the consequence of intense field exploitation (D'Amore and Truesdell, 1979; Calore et al.,1981).

Some lack of correlation between the distributions of the different variables can be referred to other phenomena that, along with recharge, control the present fluid composition in the zone. In the areas on the NE and NW margins of the study area some effects of the lateral flow and condensation described by D'Amore and Truesdell (1979) are still evident. Moreover, recharge has recently begun to affect wells producing fluids of different original composition, and undergoing an evolution tied to variations in the contribution from various steam sources (D'Amore and Truesdell, 1979). The stage reached in their evolution varies according to the duration of production.

The recharge model is adequate for interpreting the situation in the southern part of the field after a long period of production. Pre-exploitation conditions are not known, as drilling was extended to the peripheral areas after tens of years of exploitation in the older part of the field.

D'Amore and Truesdell (1979) noted that the water-calcite and water-feldspar isotopic equilibration rates are rather fast at the reservoir temperatures, whereas the recharge water takes a long time to reach zones with no tritium. In a porous medium, if the rock mass is much larger than the cumulative mass of interacting fluid, and the isotopic composition of the rock is uniform, then the water should equilibrate with the rock and no gradients should appear in the isotopic composition of the fluid.

In order to explain the gradients that did appear, D'Amore and Truesdell (1979) also considered the possibility that, in the period prior to field exploitation, condensation was also present in the area in question. On a geological time-scale this process could have produced $\delta^{18}O$ gradients in the reservoir rock. According to this hypothesis the recharge water, as it gradually flows from the marginal areas to the centre of the field, is now equilibrating with rocks whose $\delta^{18}O$ is progressively more positive. Even in this case, however, assuming a high mass ratio of rock to circulated recharge water, we cannot explain the rapid evolution of the $\delta^{18}O$ to increasingly more negative values.

We must then consider the factors capable of reducing the water-rock isotope exchange or the rock/recharge water ratio.

For the first case we could hypothesize that the circulation of the recharge water mostly takes place in low-temperature rocks and that its vaporization occurs within a rather short distance as it reaches the high-temperature reservoir, then flowing towards the central zones in the steam phase.

We could hypothesize for the second case that, during its circulation, most of the recharge water came into contact with a small part of the reservoir rock only. This could happen if the water were to flow prevalently through a limited number of fractures that also determine the preferential flow-paths.

Another possible concomitant phenomenon is that of a progressive vaporization of the recharge water during its circulation within the reservoir.

Research in future will be directed at further investigating these factors and at conducting isotopic analyses of samples of the reservoir rocks.

ACKNOWLEDGEMENTS

The authors would like to thank their colleagues Costanzo Panichi and Paolo Squarci for their kind assistance and advice.

REFERENCES

Calore,C., Celati,R.,D'Amore,F., Squarci,P. and Truesdell,A.H. (1980),"A geologic, hydrologic and geochemical model of the Serrazzano zone of the Larderello geothermal field," Proc. Sixth Workshop Geothermal Reservoir Engineering, Stanford University, Stanford, CA, 16-18 Dec., p.21-27.

Calore,C., Celati,R., Gianelli,G., Norton,D. and Squarci,P. (1981), "Studi sulla origine del sistema geotermico di Larderello," Proc. Second Informative Seminar of the Geothermal Research Units, CNR- Finalized Energy Project, Geothermal Energy Sub-project, Rome, 16-19 June, p.218-225.

Celati,R., Noto,P., Panichi,C., Squarci,P. and Taffi,L. (1973),"Interactions between the steam reservoir and surrounding aquifers in the Larderello geothermal field,"Geothermics, v.2, p.174-185.

Celati,R., Squarci,P., Neri,G. and Perusini, P. (1975),"An attempt to correlate kh distribution with geological structure of Larderello geothermal field."In:Geothermal Reservoir Engineering, Kruger,P. and Ramey H.J.,eds., Stanford Geothermal Program, Stanford, 15-17 Dec., p.37-41.

D'Amore,F., Celati,R., Ferrara,G.C. and Panichi C. (1977),"Secondary changes in the chemical and isotopic composition of the geothermal fluids in the Larderello field,"Geothermics, v.5, p.153-163.

D'Amore,F. and Truesdell,A.H. (1979),"Models for steam chemistry at Larderello and The Geysers," Proc.Fifth Workshop Geothermal Reservoir Engineering, Stanford University, Stanford,CA, 12-14 Dec., p.283-297.

D'Amore,F., Calore,C. and Celati,R. (1981), "Temporal evolution of the composition of the fluid from Serrazzano zone (Larderello),"Proc. Seventh Workshop Geothermal Reservoir Engineering, Stanford University, Stanford, CA, 15-17 Dec., p.91-96.

Mazor,E. (1978),"Noble gases in a section across the vapour-dominated geothermal field of Larderello, Italy," PAGEOPH , v.117, p.262- 275.

Panichi,C., Celati,R., Noto,P., Squarci,P., Taffi,L. and Tongiorgi,E. (1974),"Oxygen and hydrogen isotope studies of the Larderello (Italy) geothermal system." In: Isotope Techniques in Groundwater Hydrology, 1974. International Atomic Energy Agency, Vienna, v.2, p.3-28.

Petracco,C. and Squarci,P. (1976),"Hydrologic balance of Larderello geothermal region,"Proc. 2nd U.N.Symposium on the Development and Use of Geothermal Resources, San Francisco, 20-29 May 1975, v.1, p.521-530.

Truesdell,A.H. and Nehring, N.L. (1978),"Gases and water isotopes in a geochemical section across the Larderello,Italy, geothermal field," PAGEOPH, v.117, p.276-289.

Proceedings Eighth Workshop Geothermal Reservoir Engineering
Stanford University, Stanford, California, December 1982
SGP-TR-60

THERMAL WATERS AND THE EFFECT OF THEIR USE ON THE ENVIRONMENT

I. M. Dvorov
Scientific Council on Geothermal Investigations of the USSR
Academy of Sciences
and
V. I. Dvorov
Geological Institute of the USSR Academy of Sciences

Geothermal industrial activity disturbs in one way or another the ecological balance in nature. In the USSR, estimation of detrimental environmental effects with rapidly developing world economy is now considered not only in theoretical terms, but also as a complex and urgent problem, which has not been studied enough by scientists. Not very long ago this problem troubled only a small group of technologists. Recently, however, economists have become more experienced in this problem, who rely very heavily upon the results processed by computers. Industry and agriculture are vital for human well-being within a desirable environmental setting and extraction of thermal waters can be of much use within the USSR in reaching such objectives. Against this background we should consider the undesirable effects of the thermoenergetic and chemical use of thermal waters on nature.

What damage does the environment suffer from withdrawing considerable thermal groundwaters to the surface? The answers to this question are as follows:

1) chemical incompatibility between thermal waters and surface species;

2) gas contamination of the atmosphere by noncondensable gas components;

3) thermal pollution;

4) disturbance of water balance on the surface by extra inundation of poorly drained parts of the landscape; and

5) alteration of the landscape and involuntary occupation of land at the expense of drilling, pipeline construction, and plant operation.

Before considering this problem in detail, we shall briefly describe thermal waters as a physical and chemical component of the lithosphere.

Natural water, according to Academician V. I. Vernadsky, is a peculiar mineral with a complex chemical structure. Pure water designated by the symbol H_2O is actually a compound of hydrogen and oxygen atoms in a polymer structure, where water molecules are united into three-dimensional chains. Such ordered structure of the water determines many of its parameters which differ from the properties of other liquids. Among other things, it has a universal ability to solve solid and gas compounds.

All waters contain different salts and gases in solution. The smallest salt content is observed in atmospheric precipitation and in waters of thawing glaciers and snows. Total mineralization (salt content) of such waters usually does not exceed 0.1 g/liter. Groundwaters, associated with salt-bearing sea and continental basins are mineralized most considerably. Their total salt-content can be as large as 500-600 g/l.

The salt concentration of a water determines its properties, both physical and chemical. Increased salinity increases the boiling point of a solution and decreases its freezing point. Saline waters dissolve gases less intensely, but their aggressiveness towards the rocks and minerals is considerably increased, compared to pure water. High chloride brines can dissolve many compounds which are practically insoluble in chemically pure water. For example, the solubility of galenite in distilled water is 0.000001 g/l, while chloride brines with mineralization of 300 g/l can dissolve about 0.9 g/l; i.e., the solubility increases approximately by one million fold. This increased solubility with salinity is especially troublesome for nonorganic lead compounds which generally are toxic.

Thermal waters, as other groundwaters, can be subdivided into three main chemical types determined by the anion composition of their components (4):

1) bicarbonate with predominance of dissolved salts of carbonic acid ($NaHCO_3$, $Ca/HCO_{3/2}$, $Mg/HCO_{2/2}$);

2) sulphate - with predominance of sulphate salts (Na_2SO_4, $CaSO_4$, K_{2SO_4});

3) chloride (NaCl, KCl, $CaCl_2$, $MgCl_2$).
The variety of subtypes is determined by the ratio between cations and alkaline and alkaline-earth metals, and by noncondensable

gas concentration, (e.g., O_2, N_2, H_2S, CH_4, CO_2) which frequently can be related to the chemical environment in the thermal water.

This report examines a few of the many types and quantities of salt and gas components in hydrothermal waters. In successive order, we shall consider the chemical composition of hydrothermal fluids (from fresh water to brines).

Fresh waters are characterized by bulk salt content that does not exceed 1 g/l; mineralized brackish waters in which the salt content varies between 1 and 10 g/l, and saline waters in which the salt content varies between 10 and 35 g/l. Waters with mineralization exceeding 35g/l (the saturation concentration of NaCl), the waters are called saturated brines.

Commercial reserves of fresh thermal waters are not abundant, since in most geological situations, they react with the formation rock and extract various elements. Nevertheless, a few hydrothermal fluids with mineralization below 1 g/l have been found. The small mineralization results from the fact that they circulate in well eluted terrigenous or fractured magmatic rocks. Such formations do not contain easily dissolved minerals. Exceptions are volcanic glass, some types of micas and potash feldspar, which are poorly soluble but still capable of mineralizing water. The results are nitric alkaline fluids with mineralization between 0.5 and 1.0 g/l. Their anion complex contains chloride, bicarbonate and fluoride-ions and cation complex - Na- and K-ions. Such waters also contain undissociated compounds, such as saturation groundwater concentration of silicic acid and boric acid.

The gas composition of nitric alkaline fluids is represented mainly by nitrogen of atmospheric origin and small quantities of carbon dioxide and methane. The absence of oxygen is explained by active reduction processes, usual for the considerable depths where oxygen is absorbed.

Another example of fresh thermal waters is volcanic hydrothermal fluids of near-surface origin. A magmatic body solidifying at considerable depth creates around itself a wide zone of groundwater boiling. The steam initially generated in this zone moves upward along faults and near the surface, where its temperature drops to 100-200°C. At this point, the steam may be condensed and transformed into liquid water. Frequently the steam-bearing fissures heat the formation rock to such a temperature that the initial steam either does not condense at all, or condenses during a cold season. Such steam jets and steam-gas fumaroles are abundant on Kamchatka and the Kuril Islands. In mountains with glaciers and snowbanks condensation of the initial steam is inevitable. In this case, the thaw waters with temperature from 0 to +4°C are saturated with minerals from all near-surface rocks. Secondary heating of glacial waters by hot steam jets can occur with formation of hydrothermal water with the smallest salt concentrations (0.1-0.2 g/l).

Such condensed hydrothermal fluids can have higher mineralization - 1.0-5.0 g/l, as the initial steam can contain aggressive gases, such as carbon dioxide, hydrogen sulphide and sulphur dioxide. The dissolution of these gases in water and interaction between the solution and rocks can increase mineralization and alter the chemical composition of hydrothermal water.

Condensed carbon dioxide bearing steam jets usually form chloride bicarbonate-sodium hydrothermal fluids with the following composition:

$$M_{0.-5.0}\ \frac{Cl^-\ HCO_3}{Na^+} \qquad (8)$$

Sulphur and hydrogen sulphide fumaroles form sulpho-sodium waters with a small amount of chloride and bicarbonate.

$$\text{Composition: } M_{0.1-5.0}\ \frac{SO_4^{2-}(Cl^-,\ HCO_3^-)}{Na^+}$$

While the anion composition of condensed hydrothermal fluid is determined by presence of one or another gas in the initial steam, their cation composition varies in sodium, potassium and calcium content, depending on the type of enclosing rocks.

Brackish and saline hydrothermal waters. Waters of this class are possibly the most abundant. The chemical type of brackish and saline hydrothermal water are very diversified with large ranges of chemical composition.

Thermal waters with mineralization up to 35 g/l are formed both on the platforms and in tectonically active zones with a higher hydrothermal gradient. The enclosing rocks for such fluids are represented, as a rule, by sandy-clayey deposits, and fissured, carbonate and sulphate rocks without spatial contacts with salt-bearing deposits.

This class includes the overwhelming majority of mineral waters: carbonate, sulphuretted, methane-nitric. These fluids are widespread in the young mountain folded regions, in submontane and intermontane troughs, and marginal parts of the platforms.

Thermal brines. Thermal brines are formed during long-term surface evaporation of

saline waters. The 10-20 fold decrease in volume by evaporation creates a solution precipitating sodium and potassium chlorides, thus forming commercial deposits of rock salts, which sooner or later become involved in active sphere of hydrothermal waters. The latter results in formation of thermal brines by leaching.

Thermal brines belong to a class of chloride waters, where chloride is the predominant anion. Numerous studies showed that the chemical composition of thermal brines is determined by the type of their formation (5). In case of concentration of marine waters, the composition of evaporates gradually changes along the following scheme:

$$M_{35-100}\ \frac{Cl^- SO_4^{2-}}{Na^+ Mg^{2+}} \longrightarrow M_{100-150}\ \frac{Cl^-}{Na^+} \longrightarrow$$

$$\longrightarrow M_{150-300}\ \frac{Cl^-}{Na^+ Ca^{2+}\ (K^+)} \longrightarrow$$

$$M_{>300}\ \frac{Cl^-}{Ca^{2+}\ Mg^{2+}(K+)}$$

On the other hand, if the brines are formed by leaching of rock salts, their chemical composition appears to be more stable. As the rock salts consist mainly of NaCl with small amounts of KCl, the leaching brines correspondingly acquire the following composition:

$$M_{250-300}\ \frac{Cl^-}{Na^+}\ ;\ M_{250-300}\ \frac{Cl^-}{Na^+\ K^+}$$

Thermal brines are found in many regions of the USSR and the volume of these waters is very considerable. Among these are several oil- and gas-bearing provinces rich in thermal brines, such as the Fore-Carpathians, Fore-Caucasus and Fore-Urals, the Apsheron peninsula, West and East Turkmenistan, and West Siberia.

Why are thermal waters valuable? It is clear that 30% solutions of NaCl can be hardly used as water for drinking, but they are a valuable industrial raw material. Huge concentrations of their main components - Na, K and Cl can hardly attract interest of the industry as rich commercial deposits of rock salts are still available. However, the brine includes considerable concentrations of microcomponents exceeding tens and hundreds of mg/l. A partial list includes: Li, Rb, Cs, Br, I, U, Ra, Pb, Zn, Cu, Ag, Au. A number of these elements (B, I, Br, rare alkali) are extracted now from thermal industrial brines.

All chemical types of thermal waters, from fresh to brine, contain toxic components dangerous for living organisms.

In volcanic hydrothermal water with low mineralization, they are represented by hydrosulphide-ion, ammonia, boric acid.

In saline thermal waters, usually an associated with oil- and gas-bearing deposits, the most dangerous components, besides those mentioned above, are phenols.

Thermal brines contain all possible complexes of toxic components. Besides, their high salt loading does not permit their discharge into open water systems. If for some reason (an accident at the drilling site, for instance) the brines outburst onto the surface, they can destroy existing vegetation, and transform the landscape into a salt desert covered only by species of plants adapted to high salinity of soil waters.

Some high-temperature geothermal deposits with high discharge, particularly in the North Caucasus - the Daghestan ASSR, Checheno-Ingush ASSR, the Krasnodar district and other regions of the USSR contain high concentrations of phenol. The use of these waters, despite their low mineralization, is hindered by a law prohibiting their discharge into the surface water systems. Poor and expensive technology for removing phenols requires the thermal waters to be discharged back into the same water-bearing horizons. In addition, the reinjection of water will increase the period of exploitation of thermal waters and improve the dynamics of the water head system.

The injection of waste thermal waters back into a water-bearing layer has a decided advantage over other methods of industrial water utilization. However, its application can be restricted both by economic and technological reasons. The economic restrictions cannot be predicted in general form, as they are determined by regional conditions in comparison to expenses of alternative methods of power production (e.g., by traditional fuel). The chemical restrictions can be predicted more concretely.

The first case. Extraction of hot brine fluids and surface flashing (e.g., at the Tarum square, Daghestan) will inevitably result in a fresh water condensate and saturated brine with salt concentration close to a natural brine. The latter is an oversaturated solution bearing suspended crystals of chlorides (halite and salvine), formed after cooling and separation of the distillate. The injection of such a solution back into the water-bearing layer will inevitably cause a gradual colmatage of the filtration zone near the injection hole by chloride salts.

The second case. Injection of waste hydrosulphide-carbon-dioxide waters under

conditions of exploitation by the binary conversion system. Even the most efficient use of thermal waters with applications of heat exchangers does not completely prevent corrosion of drill-pipes, pipe-lines, etc. Herewith, the injected solution will bear a high bulk iron concentration, as compared to the initial solution. Not dwelling upon the ways of iron transport in the solution, we must emphasize that the water intake layer will be closed by a finely dispersed iron sulphide. If part of the heat supply system is exposed to atmosphere, the role of the clogging element will be played by iron hydroxide instead of sulphides.

The third case. Injection of phenol-bearing waters after depletion of thermopotential in the system open to atmosphere. In this case the injected water, will bring atmospheric oxygen into a water collector. If the intake layer contains mineral of ferrous iron, they, in combination with the iron from corrosion, can cause an iron oxide colmatage of this layer. Undoubtedly, it is a rather difficult technological problem, but still it can be solved in each specific case. Therefore, reinjection of waste waters is regarded as the most prospective method of thermal water disposal.

The correct estimation of atmospheric pollution requires a comparison between the gas waste of the geothermal power industry and the power cycle based on the burning of organic fuel. We note that the low potential geothermal heat-transfer medium does not practically affect the composition of the atmosphere.

Let us compare the impact exerted by two power stations, 1000 megawatts each, one of them operating on coal, the other on high-temperature geothermal fluid.

If the sulphur concentration in the coal is 1%, the power station discharges into the atmosphere: 140 tons of SO_2, 20,000 tons of CO_2, considerable amount of nitric oxides, hydrogen and other aerosols.

A hydrothermal power station operating on natural steam similar to that of the Great Geyser of Kamchatka (0.2-1.8% of noncondensable gases; among them CO_2 - 82.5%; CH_4 - 6.6%, NH_3 - 3.8%; H_2 - 4.5%)* emits daily into the atmosphere: 860 tons of CO_2 and about 48 tons of sulphur compounds. Keeping in mind that about 30% of H_2S is absorbed by the condensate, its pollution effect is 4 times lower for the sulphur compounds and 20 times lower for carbon dioxide than a coal-fired steam plant (1, 7). A direct comparison of geothermal and nuclear power stations in respect to atmosphere pollution will show that production of electric energy from nuclear fuel is a "cleaner" process for the environment (2, 3).

A few words about "thermocontamination" (thermal pollution) of the surface water system which can result from considerable discharge of waste thermal waters. The term "thermocontamination" itself presupposes a possible ill-utilization of the heat, when the geothermal technological scheme consists of only one consumer depleting an insignificant thermopotential. For example, the Pauzhetka geothermal power station in Kamchatka discharges waters with a temperature of 100°C into the Pauzhetka river. Some greenhouses, not connected into a system of multiple use of hydrothermal power, "heat" the surface water systems by their waste waters with temperatures 40-50°C. It is not completely clear now what is the effect of such "heating" on the water environments and how far the waste thermal waters flow. One thing is clear, that the majority of fauna and flora species are very sensitive to a thermal change of water environments, and therefore the "thermocontamination" of the surface water systems possibly disturbs their ecological balance.

It may be useless to speak about a control over "thermocontamination", as it is simply a violation of technological rules of using thermal waters as a heat-transfer medium.

Another undesirable effect of recovery of considerable amounts of ground thermal waters on the surface is swamping of poorly drained landscape. A basis for hydrologic calculation for draining such a discharge is needed even for thermal waters with good chemical parameters to permit their discharge into surface water systems. Insufficient drainage of the regions with arid climate may cause an efflux of ground waters and soil salinization, and in the regions with humid climate - swamping, i.e., a reduction of cultivated fields. If the area relief does not permit the total removal of the waste thermal waters, the most practical method is pumping them back into the water-bearing layer.

As a whole, the exploitation of geothermal waters causes minimum damage to nature. Only during drilling and construction (a very short period) compared to exploitation, the natural landscape suffers considerable losses. When these works are over, only

*Pauzhetka thermal waters of Kamchatka have a similar composition: CO_2 - 83.2%, H_2S - 4.4%, NH_3-3.0%, but their power is much lower than that of the Great Geyser of Kamchatka (8).

experienced specialists can estimate that the site is an area of recovery of thermal waters.

It is not so with exploitation of other mineral resources. The world annual production of oil and gas together with transportation from one place to another exceeds 4 x 10^9 tons. The world recovers annually more than 2 x10^9 tons of coal and about 20 x 10^9 tons of rocks in a form of ore and barren material. The reworked fuel, ore and rocks are absorbed into the atmosphere, soil and water (9). Behind these billions of tons stand dozens of millions of hectares of land dug up by quarries covered by waste piles and hole basements; the land crossed by railways and pipelines.

The development of the world industry, whatever "clear" ways it follows, will undoubtfully change the environment. The damage impaired by economically developed countries, due to pollution of the environment, is estimated by considerable figures. For example, in Japan in 1970, it was equal to 23 x 10^9 dollars. In the USA for 1977, it was estimated at 25 x 10^9 dollars (9) for air pollution alone. In contrast for the years 1976-1980, the USSR spent 15 x 10^9 dollars for protection of the environment. Our country established maximum tolerable concentrations in air, fresh and sea waters (6) for more than 2500 deleterious compounds. The protection of environment is included into a system of state measurements, providing a state of environmental conditions appropriate for vital activities of present and future generations.

With respect to the impact of geothermal power engineering on natural environments, we should note one of the most important aspects determining the significance of the Earth's heat compared to other energy resources.

A geothermal complex of any purpose (power-and-heat generation, power generation, etc.) can be regarded as unique, as all parts of the "Thermocycle" are concentrated in one place.

Other power complexes, using organic and nuclear fuel, spread their thermocycles far beyond their boundaries. A broad consideration of the thermocycle (recovery, processing, and transportation of fuel) shows how considerable its effect on the environment is.

The above mentioned correlation shows that the "natural" or reproduced power sources (heat of the Earth, the Sun, the Wind) being produced by the Earth's nature, are the most acceptable and cleanest.

However, the practical approach to the state of the thermopower balance does not give an opportunity to hope for any essential replacement of the traditional organic fuel for the reproduced power sources. The main objective nowadays is the use of environmentally clean power sources wherever possible. The efficiency and reliability of natural "power generator" are confirmed by the long-term use of thermal waters in our country.

BIBLIOGRAPHY

1. Berman, E., Geothermal power. "Mir", (Moscow, 1978) (in Russian).

2. Dvorov, I. M., Abyssal heat of the Earth. "Nauka", (Moscow, 1972) (in Russian).

3. Dvorov, I. M., Geothermal power generation. "Nauka", (Moscow, 1976) (in Russian).

4. Dvorov, I. M. and V. I. Dvorov, Thermal waters and their use. "Prosveshchenie", (Moscow, 1976) (in Russian).

5. Dvorov, V. I., Thermal waters of Cheleken and geochemical properties of their formation. "Nauka", (Moscow, 1975) (in Russian).

6. On protection of environment. Documents of the USSR Communist Party and Government for 1917-1981. Izdat. Politicheskaya literaturea, (Moscow, 1981) (in Russian).

7. Bowen, R. G., Effect of geothermal complexes on the environments. In "Geothermal power","Mir",(Moscow, 1975) (in Russian).

8. Pauzhetka hot waters of Kamchatka. "Nauka", (Moscow, 1965) (in Russian).

9. Sidorenko, A. V., Protection of environments and rational use of natural resources of the USSR, Vestnik Academy of Science SSSR., (Moscow, 1978) (in Russian).

EIGHTH WORKSHOP ON GEOTHERMAL RESERVOIR ENGINEERING

Participants List

Rick Allis
D.S.I.R. (Geothermal Research Center)
Wairakei
Private Bag, Taupo, New Zealand

Paul Atkinson
Union Oil Co. of Calif. - Geothermal Div.
2099 Range Avenue
Santa Rosa, CA 95401

Ben Barker
Union Oil Co. of Calif. - Geothermal Div.
2099 Range Avenue
Santa Rosa, CA 95401

A. S. Batchelor
Camborne Sch. of Mines Geoth. Energy Proj.
Rosemanowes Quarry, Herniss, Longdowns,
PENRYN Cornwall, UK

Sally Benson
Lawrence Berkeley Laboratory
1 Cyclotron Road, Bldg. 90 MS1106
Berkeley, CA 94720

William T. Box, Jr.
Aminoil USA, Inc.
P.O. Box 11279
Santa Rosa, CA 95406

Bill Brigham
Petroleum Engineering Department
Stanford University

Donald W. Brown
Los Alamos National Laboratory
P.O. Box 1663, Mail Stop J979
Los Alamos, NM 87545

Charles G. Bufe
U.S. Geological Survey & DOE
906 National Center
Roston, VA 22092

Claudio Calore
C.N.R.
Instituto Internazionale per le
Ricerche Geotermiche
Via del Buongusto 1, 56100
Pisa, Italy

Regina M. Capuano
UURI/Earth Science Laboratory
420 Chipeta Way, Suite 120
Salt Lake City, UT 84108

Mitchell Che
GeothermEx, Inc.
5221 Central Avenue - S. 201
Richmond, CA 94804

Mario Castaneda
I.I.E.
Cuernavaca, Mor., Mexico
Apdo. Postal #475

Dr. Jim Combs
Geothermal Resources International, Inc.
545 Middlefield Road, Suite 200
Menlo Park, CA 94025

Richard Corbaley
California Div. of Oil & Gas
485-B Broadway
El Centro, CA 92243

John Counsil
Aminoil USA, Inc.
P.O. Box 11279
Santa Rosa, CA 95406

Gene Culver
Geo Heat Center
OIT
Klamath Falls, OR 97601

Franco D'Amore
C.N.R.
Instituto Internazionale per le
Ricerche Geotermiche
Via del Buongusto 1
56100 Pisa, Italy

William DaSie
Chevron Resources Co.
595 Market St.
San Francisco, CA 94119

Alfonso Arenas Diaz
Instituto de Investigaciones Electricas
Interior Internado Palmira Cuernavaca
Morelos - Geotermia Bldg. 24, Mexico

Richard F. Dondanville
Union Oil Geothermal Division
P.O. Box 6854
Santa Rosa, CA 95406

W.F. "Bill" Downs
EG&G Idaho, Inc.
P.O. Box 1625
Idaho Falls, ID 83415

David Dougherty
Princeton University
Princeton, NJ 08544

Andy Drenick
GRI Operator Corporation
2300 County Center Dr., Suite 264
Santa Rosa, CA 95401

Herman Dykstra, Consultant
4180 Treat Blvd., Suite 1
Concord, CA 94518

Michael J. Economides
University of Alaska
Fairbanks, Alaska 99701

Kathleen Enedy
Aminoil USA, Inc.
P.O. Box 11279
Santa Rosa, CA 95406

Steve Enedy
Union Oil Co. of Calif.-Geothermal Div.
2099 Range Avenue
Santa Rosa, CA 95401

Jim Fallon
Union Oil Co. of Calif.-Geothermal Div.
2099 Range Avenue
Santa Rossa, CA 95401

Horacio Ferriz
Applied Earth Sciences
Stanford University

Murray C. Gardner
GeothermEx, Inc.
5221 Central Avenue
Richmond, CA 94804

Gino Giannone
AGIP S.P.A.
P.O. Box 12069
20120 Milano, Italy

Norman Goldstein
Lawrence Berkeley Laboratory
University of California
Berkeley, CA 94720

Keshav Goyal
Phillips Petroleum Company
655 East 4500 South
Salt Lake City, Utah 84107

Malcolm Grant
D.S.I.R.
P.O. Box 1335
Wellington, New Zealand

B. Greider
Geothermal Resources Int'l
545 Middlefield Rd., Suite 200
Menlo Park, CA 94025

Jon S. Gudmundsson
Petroleum Engineering Department
Stanford University

Mohinder S. Gulati
Union Oil Co. of Calif.-Geothermal Div.
2099 Range Avenue
Santa Rosa, CA 95401

Susan E. Halfman
Lawrence Berkeley Laboratory
University of California
Berkeley, CA 94720

Jeffrey Hebein
MCR Geothermal Corp.
10880 Wilshire Blvd.
Los Angeles, CA 90024

Bruce H. Hellier
U.S. Dept. of Interior
Minerals Management Service
432 Arboleda Drive
Los Altos, CA 94022

Keisuke Hibiya
Petroleum Engineering Department
Stanford University

Seiichi Hirakawa
University of Tokyo, Faculty of Engineering
Bunkyo-ku, Tokyo 113, Japan

Yoshikazu Hirakawa
Tokyo 155, Japan

Viet Thai Hoang
Chevron Resources Co.
P.O. Box 7147
San Francisco, CA 94120

Roland N. Horne
Petroleum Engineering Department
Stanford University

Dan Hoyer
MCR Geothemal Corporation
10880 Wilshire Blvd.
Los Angeles, CA 90024

Evan Hughes
EPRI
P.O. Box 10412
Palo Alto, CA 94303
Larry Hull
Idaho National Engineering Lab.
EG&G Idaho, Inc.
P.O. Box 1625
Idaho Falls, ID 83415

Eduardo Iglesias
Instituto de Investigaciones Electricas
Apartado Postal 475, Cuernavaca
Morelos, Mexico

Joe L. Iovenitti
Thermal Power Company
601 California Street
San Francisco, CA 94108

Bill Isherwood
Department of Interior
MS 92, 345 Middlefield Road
Menlo Park, CA 94025

James R. Kelsey
Saudia National Laboratories
P.O. Box 5800 - 9741
Albuquerque, NM 87185

Mary Keskinen
Occidental Research Corporation
2100 S.E. Main Street
Irvine, CA 92713

Paul Kruger
Civil Engineering Department
Stanford University

Mark K. Kumataka
Occidental Geothermal, Inc.
5000 Stockdale Highway
Bakersfield, CA 93309

Phil LaMori
Oxy
P.O. Box 19601
Irvine, CA 92713

Al E. Lewis, Jr.
State Dept. Water Resources
1416 - 9th Street
Sacramento, CA 95819

Donald R. Lindsay
Occidental Geothermal, Inc.
5000 Stockdale Highway
Bakersfield, CA 93309

Steve Lipman
Union Oil Co. of Calif.-Geothermal Div.
2099 Range Avenue
Santa Rosa, CA 95401

Marcelo Lippman
Lawrence Berkeley Laboratory
Berkeley, CA 94720

Enrique A. Contreras Lopez
Instituto de Investigaciones Electricas
Apartado Postal 475, Cuernavaca
Morelos, Mexico

Garth M. Lyon
Union Oil Company
2099 Range Avenue
Santa Rosa, CA 95401

Luis Macias-Chapa
Petroleum Engineering Department
Stanford University

Mark Magers
Union Oil Co. of Calif.-Geothermal Div.
2099 Range Avenue
Santa Rosa, CA 95401

Bryan L. McCulley
Woodward-Clyde Consultants
One Walnut Creek Center
100 Pringle Avenue
Walnut Creek, CA 94596

James R. McNitt
GeothermEx
5221 Central Avenue
Richmond, CA 94804

Philip H. Messer
Union Oil Co. of California
81-711 Highway 111
Indio, CA 92201

Donald E. Michels
Republic Geothermal, Inc.
11823 E. Slauson Ave.
Santa Fe Springs, CA 90601

Frank G. Miller
Petroleum Engineering Department
Stanford University

Mark Miller
Petroleum Engineering Department
Stanford University

Allen Moench
USGS Mail Stop 96
345 Middlefield Road
Menlo Park, CA 94025

Phil Mogen
Union Oil Co. of Calif.-Geothermal Div.
2099 Range Avenue
Santa Rosa, CA 95401

Dr. Martin W. Molloy
U.S. Department of Energy
1333 Broadway
Oakland, CA 94612

Manuel Nathenson
U.S. Geological Survey M/S 90C
345 Middlefield Road
Menlo Park, CA 94025

Gerald Niimi
ThermaSource, Inc.
5721 Brigadoon Way
Santa Rosa, CA 95405

Susan Petty
Well Production Testing
2270 Camino Vida Roble, Suite D
Carlsbad, CA 92008

George Pinder
Princeton University
Princeton, NJ 08540

Al Pingol
Union Oil Co. of Calif.-Geothermal Div.
2099 Range Avenue
Santa Rosa, CA 95401

Lynn Pittinger
Union Oil Co. of Calif.-Geothermal Div.
2099 Range Avenue
Santa Rosa, CA 95401

Lynne Preslo
Woodward-Clyde Consultants
One Walnut Creek Center
Walnut Creek, CA 94596

Karsten Pruess
Lawrence Berkeley Laboratory
Berkeley, CA 94720

Peter M. Pyle
U.C. Berkeley
3 Glen Drive
Fairfax, CA 94930

Greg Raasch
Union Oil Co. of Calif.-Geothermal Div.
2099 Range Avenue
Santa Rosa, CA 95401

F.M. Rago
University of Texas
Austin, Texas

Henry J. Ramey, Jr.
Petroleum Engineering Department
Stanford University

Jack Ramsthaler
EG&G Idaho
P.O. Box 1625
Idaho Falls, Idaho 83401

Marshall Reed
Minerals Management Service
345 Middlefield Road
Menlo Park, CA 94025

T. David Riney
S-Cubed
P.O. Box 1620
La Jolla, CA 92038

Jesus Rivera
University of Mexico and
Aquater Consultant
29 Valle Frio. Valle Del Paraiso
Tlalnepantla, Edo, Mexico 54060

Vasel W. Roberts
EPRI
3412 Hillview Avenue
Palo Alto, CA 94303

Jill Robinson
GRI Operator Corporation
545 Middlefield Road, Suite 200
Menlo Park, CA 94025

Avrami Sageev
Petroleum Engineering Department
Stanford University

Subir Sanyal
GeothermEx, Inc.
5221 Central Avenue, #201
Richmond, CA 94804

Basil V. Savoy
Mono Power Company
P.O. Box 800
Rosemead, CA 91770

Alex Schriener
Union Oil - Geothermal
P.O. Box 6854
Santa Rosa, CA 95406

Ron Schroeder
BGI
2000 Center St., Room 108
Berkeley, CA 94703

Harold R. Sells
San Diego Gas & Electric Co.
P.O. Box 1831
San Diego, CA 92112

Lewis Semprini
Civil Engineering Department
Stanford University

Alan Shenker
GRI Operator Corporation
2300 County Center Drive, Suite 264
Santa Rosa, CA 95401

Piotr A. Skiba
EG&G Idaho
P.O. Box 1625
Idaho Falls, ID 83415

A. A. Soneda
Pacific Gas & Electric Co.
77 Beale Street, Room 1349
San Francisco, CA 94106

Michael L. Sorey
U.S. Geological Survey
345 Middlefield Road
Menlo Park, CA 94025

Valgardur Stefansson
Orkustofnun
Grensasvegur 9
Reykjavik, Iceland

Kenneth F. Stelling
State of California
2904 McBride Lane
Santa Rosa, CA 95401

Sam Sugine
Los Angeles Dept. of Water & Power
111 No. Hope Street
Los Angeles, CA 90012

Stanley S. S. Sun
Minerals Management Service
345 Middlefield Road, M/S 80A
Menlo Park, CA 94025

Masaharu Tachimori
Process Technology R&D Laboratories
Nippon Steel Corporation
1-1-1 Edamitsu, Yawata-Higashi-Ku
Kitakyushu-City, 805, Japan

John Thackston
Woodward-Clyde Consultants
One Walnut Creek Center
100 Pringle Avenue
Walnut Creek, CA

Donald Thomas
Hawaii Institute of Geophysics
2525 Correa Road
Honolulu, HI 96822

Ronald S.H. Toms
U.S. Department of Energy
Geothermal and Hydropower Tech. Div.
Washington, D.C. 20585

Giorgio Tore
AGIP
20097 San Donato Milanese (Milano)
Italia

Alred H. Truesdell
U.S. Geological Survey M/S 18
345 Middlefield Road
Menlo Park, CA 94025

M. J. Umari
U.S. Geological Survey
Western Bank Bldg., Room 703
505 Marquette N.W.
Albuquerque, NM 87102

M. S. Watts
Union Oil Company
P.O. Box 6854
Santa Rosa, CA 95405

E. R. Western
Sunoco Energy Development Co.
12700 Park Central Place, Suite 1500
Dallas, Texas 75251

James Whelan
Naval Weapons Center
China Lake, CA

Donald E. White
U.S. Geological Survey
222 Blackburn Avenue
Menlo Park, CA 94025

Andy Whittome
Chevron Resources
595 Market Street
San Francisco, CA 94120

Ken Williamson
Union Oil Company
P.O. Box 6854
Santa Rosa, CA 95406

Phillip Wright
UURI/Earth Science Laboratory
420 Chipeta Way, Suite 120
Salt Lake City, UT 84108

S. Marc Zand
U.S. Minerals Management Service
345 Middlefield Road, M/S 92
Menlo Park, CA 94025

George Zyvoloski
Los Alamos National Laboratory
Los Alamos, N.M. 87544